THE UNIVERSITY OF HERTFORDSHIRE

Faculty of Engineering and Information Science

Stratified Flow in the Built Environment

Ahmad Salmeh Iial-Awad

A Thesis submitted in partial fulfilment of
the requirements of the University of Hertfordshire
for the Degree of Doctor of Philosophy

The programme of research was carried out in the

School of Aerospace, Automotive and Design Engineering,

Faculty of Engineering and Information Science,

University of Hertfordshire

Hatfield August 2006

Abstract

Stratified flow in an environmental chamber has been investigated. The chamber of dimensions (7.5m long, 5.6m wide and 3.0m) at the University of Hertfordshire has been used. Sets of experiments investigating the effect of the major flow parameters such as airflow rate, jet momentum, flow conditions and height of the air supply device have been conducted. Results have been obtained to evaluate the flow characteristics and thermal stratification mechanism. The study has demonstrated the validity of using smoke visualization to evaluate the stratified flow characteristics such as interface level height, stratified layer thickness, and degree of stratification. The effects of both hot and cold airflow rates in the ranges of (0.0 to 8.0 m^3/min) were investigated. The flow characteristics vary depending on the flow parameters and the experimental conditions.

The effect of supply terminal and extract terminal at various airflow rates on the flow characteristics is experimentally investigated. It has been found that relative influence of inertia and buoyancy forces resolves the stratified flow characteristics. The stratification interface level height and the ventilation flow rates are two main factors in the design of natural ventilation system. The results can be used to obtain a good estimation of the effectiveness of a ventilation system at design stage.

Experimental work was carried out using ceiling jet to supply hot and cold air to a confined space, to investigate the effect of jet momentum in breaking and mixing the stratified layer. The flow of high momentum was supplied downward from the ceiling. The magnitude of momentum needed depends on the degree of stratification, stratified layer interface level height and the stratification conditions. It can be seen that the jet momentum has significant influence on the mixing of the stratified flow characteristics. The results indicated that once the momentum was initiated a mixed flow grew in the occupied zone above the floor. The height of this zone depends on the stratified flow characteristics, and the temperature and momentum of the ceiling jet.

Another area of experimentation was the inversion of input airflow supplies. In this case, the flow of high buoyancy was supplied upward, whilst the flow of high

momentum was supplied downward from the ceiling. The stratified layer lost its stability and broke down due to the drag and tearing of cold air penetrated downward from higher levels. The compound effect of these two conditions will circulate the air in the whole space and disturb the stability of the stratified layer to reach fully mixed flow

A comprehensive definition of the degree of stratification was formulated. Analytical solutions were developed for the stratified layer thickness and location as a function of temperature gradient and airflow ratios. These expressions were calibrated using the experimental results. The critical momentum needed to breakdown the stratified layer also evaluated. Comparisons with previous studies where also carried out.

It was found that the stratified layer interface level height is dependent on the ratio of airflow rate and geometrical effects. If mixed flow is desired then the cold inflow aperture should be located higher than the hot inflow aperture, whiles the interface level height is not located at the exhaust aperture height.

The critical vertical momentum necessary in order to break down a stratified layer has been found to depend on the stratified layer interface level height. A semi-empirical formula based on the present experimental results has been developed to predict the critical vertical momentum for given stratified conditions.

Based on the present experimental results, the effect of momentum is greater than the effect of buoyancy and the time needed to break down the stratified layer is considerable less than the time it takes to stratify.

Experimental data also demonstrate a ventilation method for increasing the occupied zone height without breaking down the stratified layer.

Acknowledgement

It gives me great pleasure to take this opportunity to acknowledge my indebtedness to all those who have helped me in completing my Ph.D. work.

First and foremost, I would like to express my deepest thanks to my principle supervisor, Prof. Arne Eric Holdø, for his help, enthusiastic support, continuous encouragement, and guidance during my research work.

I owe special thanks to my second supervisor, Prof. Omar Badran of Al-Balqa` Applied University, Jordan, for his early guidance and supervision, many helpful discussion, and thorough review of this thesis. Also I am grateful for the assistance of my third supervisor Dr. Raj Calay for her help during my study. Their support and advice over the past three years has been excellent.

I am greatly indebted to Al-Balqa` Applied University in Jordan for their financial support during my Ph.D. work in United Kingdom; also I greatly appreciate the support received from the Faculty of Engineering and Information Science and School of Aerospace, Automotive and Design Engineering, of the University of Hertfordshire, UK, where I did my research.

I am very grateful for the assistance of Mr. Dave Bell for his help in preparing the experimental set up and making the necessary equipment to be available whenever I needed them.

The last but not the least, I would like to thank my parents, my wife, my son and daughters for their continuous support and encouragements. Without their help and patience, it would have been impossible for me to finish my research in a short period of time.

Table of contents

Nomenclature

A, B, C, a, b, c	Constants or coefficients used
A	Cross sectional area (m^2)
AH	Parameter =Ri Re
Ar	Archimedes number ($Ar = g\rho H^2 \Delta\rho/\mu^2$)
B	Width of the chamber (m)
C_p	Specific heat of air (kJ /kg °C)
C_d	Discharge coefficient
D_{hyd}	Hydraulic diameter (m)
DS	Degree of stratification
F	Body forces (gravitational forces)
f	Friction factor (dimensionless)
Fr	Froude number
g	Gravity acceleration (m/ s^2)
g'	Reduced gravity (m/s^2)
Gr	Grashof number ($Gr = \frac{g D_{hyd}^3 \Delta T / T_m}{\nu^2}$)
h	Interface level height (m)
h'	Interface top height (m)
H	Height of the chamber (m)
i,j,k,m,n	Integer numbers in equations
L	Length scale (m)
$\dot{m}$	Mass flow rate of air (kg/ s)
M	Momentum (m^4/s^2)
P	Pressure (Pa)
Pe	P'eclet number
Pr	Prandtl number
$\dot{Q}$	Total rate of heat added (kJ /kg)
q	Absorption heat (kJ /kg)

Q	Volume flow rate (m^3/min)
Q_{out}	Overall Flow rate (m^3/min)
R	Universal gas constant (kJ /kg °K)
Re	Reynolds number ($Re = \frac{U_{ch} D_{hyd}}{\nu}$)
Ri	Richardson number
E	Energy (kJ)
S	Perimeter (m)
t	Time (s)
T	Temperature (°C)
Tm	Mean chamber temperature (°C)
ΔT	Temperature difference (°C)
u,v,w	Local air velocities in x,y,z-directions (m/ s)
U,V,W	Time average velocity in the x,y,z-directions (m/s)
Ur	Equivalent chamber velocity (m/s)
V	Volume (m^3)
x, y, z	Horizontal, transversal and vertical coordinates (m)

Greek symbols

β	Thermal expansion coefficient (1/K).
δ	Stratified layer thickness (m)
∂	Partial derivative.
Δ	Difference between variables.
κ	Von Karman constant (0.41).
ν	Kinematics viscosity ($m^2 \cdot s^{-1}$)
μ	Dynamic viscosity (kg/m s)
ρ	Density (kg/m)
ϕ	General specific dependent variable
τ	Characteristic time (s)
τ_c	Conversion time period (s)
τ_s	Steady state time period (s)

Γ	Source term of ϕ
S_ϕ	General specific dependent variable

Superscript

$'$	Fluctuation

Subscript

c	Cold
ch	Chamber
ex	Exhaust
h	Hot
j	Jet
i,j,k,m,n	Index number, 1,2,3
global	Global
local	Local
loss	Loss
w	Wall
0	Ambient condition
1	Bottom of the chamber
2	Top of the chamber

Abbreviations

CFD	Computational Fluid Dynamics
$k-\varepsilon$	$k-\varepsilon$ Turbulence model

Keywords:

Experimental Study, Fluid Mechanics, Stratified Flow, Stratified Layer, Ventilation.

Chapter 1

Chapter 1

Introduction

1.1 Introduction

In general, ventilation is the method used to remove the heat and contaminants in buildings and workplaces, by delivering air of high quality and right quantity to the ventilated space. Rapid dilution for removal of contaminants from the workplace in a safe and reliable manner is the aim of good ventilation. It is the process of providing fresh air to the building occupants, rather than the building itself, in order to sustain a healthy air quality with minimum capital cost and environmental impact, [Awbi (1998)].

A large percentage of our time is spent indoors, and the work performance is negatively affected by unsuitable indoor temperatures and by indoor pollution [Wargocki et al. (1998)]. Furthermore, the greatest component of energy consumption, in modern buildings, is probably for ventilation, and it is usually in the range of 30-60% of the building energy consumption, [Awbi (1998)]. The environment should be designed for comfort to satisfy the requirements of health, and to increase our productiveness.

The present focus on energy efficiency, environmental public health and high quality work output, means that it is essential to design good ventilation systems, which fulfil the requirements of low energy consumption and good air quality in buildings.

1.2 Ventilation Techniques

Ventilation can be achieved by natural ventilation, mechanical ventilation or mixed ventilation (natural and mechanical). The study of ventilation and environmental

phenomenon is strongly supported by theoretical models such as the analytical techniques and the use of Computational Fluid Dynamics (CFD). The latter has been widely used [Lun (1995)]. Experimental methods are caring out for the understanding of ventilation.

In the past, ventilation was mainly used to remove smoke and excess heat from the buildings to the outside, rather than providing fresh air for comfort. This was done during the natural movement of air through any apertures connecting the inside of the building to the external environment. Over the years, the main purpose of ventilation systems is to achieve the best indoor environment, in order to sustain a healthy air quality with minimum capital cost and environmental impact, [Awbi, 1998].

1.3 Stratification

1.3.1 Problem Definition Description

Stratification is an interesting area of fluid mechanics and heat transfer. It is complex, but has many important applications. It depends on the transient behaviour of the fluids as they start to layer. Layering that occurs, mainly in the warm environment is called thermal stratification, during which a warmer, less dense layer overlies a colder denser layer. Between these two layers is a third called the stratified layer, where strong vertical differences (gradients) in temperature, and therefore, density exist. It is a process driven by density differences; therefore, it is a buoyancy driven phenomenon. [Dagestad (1991)].

Temperature and density are the main parameters influencing the physical creation of stratified layers. Promoting stratification is a key factor to minimize supply airflow requirements, in design and operation, where the degree of stratification has to be balanced with comfort consideration. In other words, it aims to minimize energy use (reduce room air flow) while maintaining comfort (acceptable temperature and stratification in the occupied zone). [Webster et al. (2002)].

1.3.2 Practical Examples of Stratification

Figure 1.3.2 shows a layer of Mediterranean Sea as it enters the Atlantic Ocean and moves, horizontally, several hundred kilometres into the Atlantic before stabilizing at a depth of about 1000 meters with its own warm, saline, and less dense characteristics. It is stratified under the effect of density difference, where the buoyancy forces are sufficient to stratify the flow.

The hot buoyant cloud (thermal) in a stratified environment is established when rising in an incompressible neutrally stratified medium. After a period of time, the water motion becomes self-controlled due to buoyancy forces, and the vertical coordinate of the water may increase until it reaches the point of stability, where the degree of stratification is high enough to maintain on the layer, [Makhviladze et. al., (1996)].

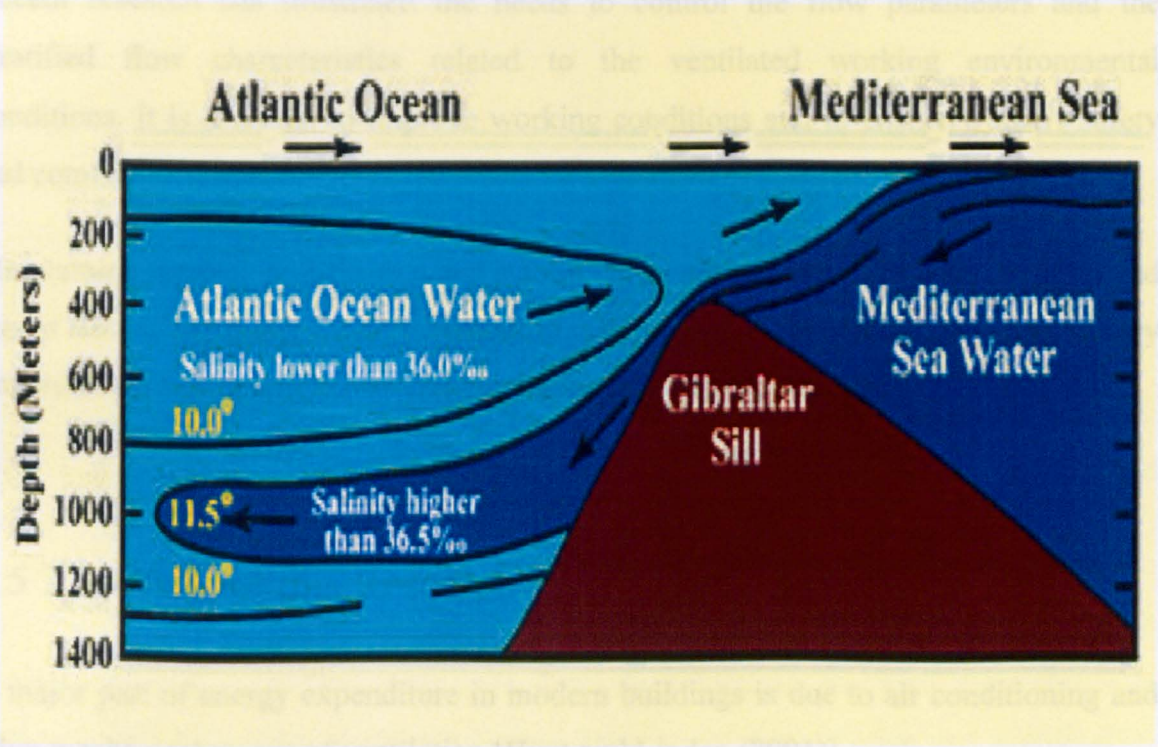

Figure 1.3.2: The Mediterranean Sea water as it enters the Atlantic over the Gibraltar (Marine Geology, Kuenen, p. 43).

1.4 Importance of the Problem

The present work is expected to increase our understanding of the processes of stratification and mixing in the mediums of vertical temperature gradient or sharp

density interfaces. Stratification is considered a significant factor in heat and mass transfer due to the variations in density and temperature. It finds applications in solar heating systems, polymer technology, industrial reservoirs, atmosphere, cumulus clouds, oceans and lakes, producing water, oil and gas in hydro cyclones. Stratification due to concentration difference also arises in several chemical processes and systems in industry.

In ventilation applications, the working environment is influenced by a large number of variables such as input airflow rate, openings heights, temperature differences and surroundings fluctuations. These variables should be changed individually or collectualy to produce significant change in flow characteristics. This change is required to maintain a safe environment with high quality ventilation, and efficient removal of pollutants.

Recent research has illustrated the needs to control the flow parameters and the stratified flow characteristics related to the ventilated working environmental conditions. It is essential to improve working conditions and to ensure workers safety and comfort.

Maintaining thermal stratification and stability are very important for both stratified and mixed flow. Controlling inside temperature difference and ventilation flow rates is very important for both energy costs and ventilation systems efficiencies.

1.5 The Aims of this Research

A major part of energy expenditure in modern buildings is due to air conditioning and other mechanical means of ventilation [Hunt and Linden (2001)].

Temperature and density are the main parameters influencing the physical creation of stratified layers. Promoting stratification is a key factor to minimize supply airflow requirements, in design and operation, where the degree of stratification has to be balanced with comfort consideration. In other words, it aims to minimize energy use (reduce room air flow) while maintaining comfort (acceptable temperature and air velocity in the presence of stratification). [Webster et al. (2002)]

The global aims of the project are:

- To investigate the phenomenon of stratification in the built environment.
- To study the parameters that affect the stratified flow such as input airflow rates, input heights and output vertical locations.
- To evaluate the stratified flow characteristics such as stratified layer thickness, stratified layer interface level height and the degree of stratification as a function of flow parameters.
- To study the effect of jet momentum of inlet airflow and the inverting of input locations on the stratified flow characteristics.

These targets can be achieved using experimental methods to describe the flow characteristics.

1.6 Thesis Outline

During the course of the research project, a wide-ranging series of literature reviews have been conducted. It was to provide both knowledge background and skills building to achieve the aims of the work with good qualitative results that can be considered in ventilation applications. The report consists of eight Chapters and related Appendices.

Chapter 1 provides an introductory view of the phenomenon of stratification, the purpose of air modelling techniques and introduces the project scope, framework, and general argument structure.

Chapter 2 presents an overview of the development of experimental, analytical and computational methods and highlights methods related to stratified flow that still encountered. This review provides a general background to ventilation and stratification techniques that can be applied to obtain high-quality results. In addition, it examines the fluid mechanics principles, which are required to investigate ventilation problems, its solutions and applications, and upon which the predicted results are based. Chapter 2 also includes an overview of theoretical background and a brief summary of the major conclusions drawn from the research investigations identified by literature surveys.

Chapter 3 explains the analytical developments of stratified flow characteristics, and the experimental set-up, experimental tests, and measuring methods used in the present investigations. It also explains the measuring procedures, uncertainty and smoke visualisation.

Chapter 4 studies the effect of time and spatial variations on the stratified flow. It summarises the results of experimental and visualisation data to be analysed, compared and discussed. The comparative performance of a number of visualisation methods and experimental output data is conducted. In this chapter a number of different experiments were proposed to clarify the effect of input location (input height), exhaust location (exhaust height), airflow rates, and to provide high quality data to be studied and analyzed. Details of the experimental results obtained are given and discussed in this chapter.

In chapters 5, some results are presented on a number of experiments on mixing across a stratified layer interface when the turbulence is produced by an air jet located at the ceiling level in the middle of the environmental chamber. The effect of momentum in destroying the stratified layer and mixing the flow using cold and warm jet flow has been studied. In this chapter, cases explained in chapter 4 using the recent modelling technique are repeated. Smoke and temperature visulisations are also used to validate the experimental work and to indicate the effect of air jet flow on the stratified flow chracteristics. Chapter 5 also studies the effect of inverting input locations on the stratified flow characteristics and the usage of the inversion technique to destroy the stratified layer and mix the flow. Both temperature and smoke visualisation are carried out.

Chapter 6 presents a general discussion of the results compared with existing work, to classify the agreements and to identify gaps between the present model and the others. In Chapter 7 are the key conclusions drawn during the present work and in Chapter 8 are the suggestions for future work.

Appendices (A1 to A4) include explanation data, published work and supporting details for the main lines of argument in chapters 3 through 6. Reference information for the technical literature and other source documents are in the body of the report.

The schematic models proposed by [Skistad (1998)] and [Calay et al. (2000)] for selective ventilation in large enclosures were the basis for the experimental models used in this study (Chapter 3). The models were applied, in the environmental chamber, to study the parameters that affect the stratified flow and the stratified flow characteristics, and are given in chapter 4. In chapter 5, the physical process proposed by [Calay et al. (2000)] for momentum jet flow was the basis for the experimental model used to de-stratify the flow. A different smoke and temperature visualisation techniques are used to clarify the phenomenon of stratification in the environmental chamber, and to compare with the values obtained from the experiments.

The thermocouples, which were type K, had resolution within ± 2.5% of the temperature range of the tests. However, the repeatability of measurements indicates that the real error is less than this. Repeated experiments and measurements give consistent results, and consequently confidence that this error and its value are meaningful.

Chapter 2

Literature Review and Theoretical Background

2.1 Introduction

Thermal stratification is often a dominant feature of the flow characteristics within ventilated buildings. There may be many heat sources such as occupants and equipment within a room so that a thermal plume develops around them resulting in a vertical temperature gradient. These sources may develop pure buoyancy driven plumes or mixed convection jets as in the supply of hot air in mechanical heating systems. Generally such jets or plumes propagate entraining air from ambient to a height where the temperature within the jets becomes equal to the ambient temperature. At this height the flow becomes stratified and there may be a zone above or below the stratified zone where flow is mixed i.e. the temperature profile is uniform, [Calay et. al. (2000)]

Theoretical and experimental work has established that the location where flow becomes stratified is influenced by ventilation system parameters in relation to the geometric size and shape of the enclosure and the power of the heat sources. Most studies investigated stratification in enclosures due to isolated heat sources approximated as point sources. Normally buildings have many openings, there might be mechanical supply or extraction of air by a fan which means that ventilation in buildings is often due to the combined effects of pressure and temperature acting simultaneously. Analytical solutions can only be obtained for idealised simple cases such as natural ventilation for two identical openings. There is no analytical solution to predict flow characteristics or ventilation rates for real condition as results strongly depend upon the relative positioning of the openings for inflow and outflow, shape and aspect ratio of the openings.

2.2 Governing Equations

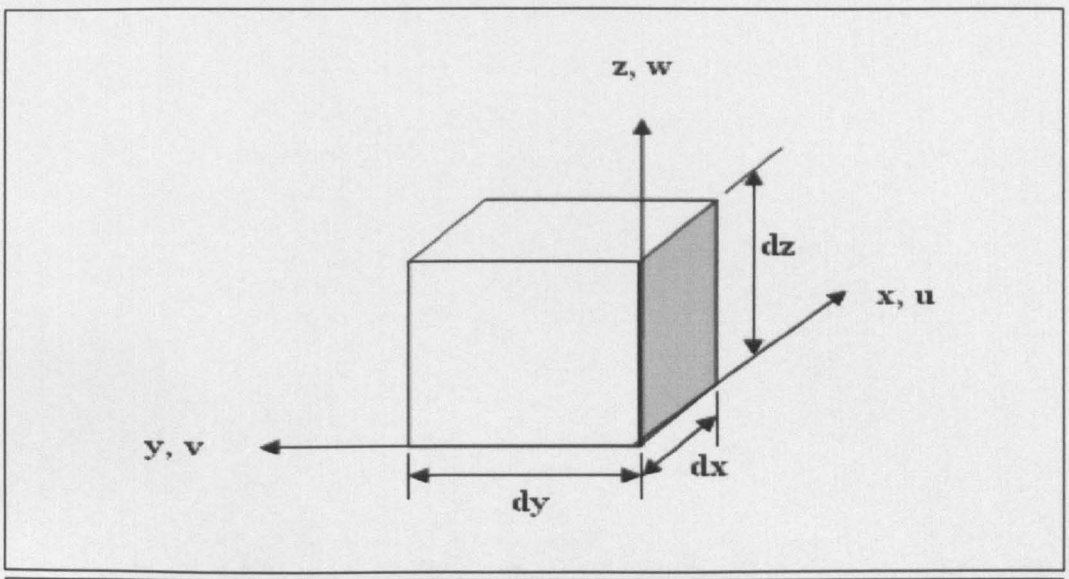

Figure 2.2.1: The unit volume representation.

For general understanding of stratification in ventilation and air conditioning problems, the fundamental principles and laws of physics are applied and analysed. The governing equations commonly used for the problem under consideration are based on the continuity equation for mass transfer, the Navier–Stokes equations for momentum transfer and the thermal energy equation.

- Conservation of mass.

$$\frac{\partial \rho}{\partial t}+\frac{\partial(\rho u)}{\partial x}+\frac{\partial(\rho \upsilon)}{\partial y}+\frac{\partial(\rho w)}{\partial z}=0 \qquad (2.2.1)$$

- Conservation of momentum.

X- Momentum

$$\frac{\partial(\rho u)}{\partial t}+\frac{\partial\left(\rho u^{2}\right)}{\partial x}+\frac{\partial(\rho u \upsilon)}{\partial y}+\frac{\partial(\rho u w)}{\partial z}=-\frac{\partial p}{\partial x}+\mu\left(\frac{\partial^{2} u}{dx^{2}}+\frac{\partial^{2} u}{dy^{2}}+\frac{\partial^{2} u}{dz^{2}}\right)+F_{x} \qquad (2.2.2)$$

Y- Momentum

$$\frac{\partial(\rho v)}{\partial t}+\frac{\partial(\rho u v)}{\partial x}+\frac{\partial(\rho v^2)}{\partial y}+\frac{\partial(\rho v w)}{\partial z}=-\frac{\partial p}{\partial y}+\mu\left(\frac{\partial^2 v}{dx^2}+\frac{\partial^2 v}{dy^2}+\frac{\partial^2 v}{dz^2}\right)+F_y \qquad (2.2.3)$$

Z- Momentum

$$\frac{\partial(\rho w)}{\partial t}+\frac{\partial(\rho u w)}{\partial x}+\frac{\partial(\rho v w)}{\partial y}+\frac{\partial(\rho w^2)}{\partial z}=-\frac{\partial p}{\partial z}+\mu\left(\frac{\partial^2 w}{dx^2}+\frac{\partial^2 w}{dy^2}+\frac{\partial^2 w}{dz^2}\right)+F_z \qquad (2.2.4)$$

• Conservation of energy.

$$\rho\left(\frac{\partial E}{\partial t}+u\frac{\partial E}{\partial x}+v\frac{\partial E}{\partial y}+w\frac{\partial E}{\partial z}\right)=-p\left(\frac{\partial u}{\partial x}+\frac{\partial v}{\partial y}+\frac{\partial w}{\partial z}\right)+\alpha\left(\frac{\partial^2 T}{\partial x^2}+\frac{\partial^2 T}{\partial y^2}+\frac{\partial^2 T}{\partial z^2}\right)+\dot{Q} \qquad (2.2.5)$$

In the above equations, u, v and w are the local air velocities in x, y and z-directions, ρ is the fluid density, p is the pressure, μ is the dynamic viscosity, T is the temperature, F_x, F_y and F_z are the body forces (gravitational forces), E is the energy rate, $\dot{Q}$ is the total rate of heat added, and $\alpha = k/\rho c_p$ is the thermal diffusivity in which k is the effective thermal conductivity and c_p is the specific heat of the fluid at constant pressure.

Assuming that the stratified flow characteristics across the direction of the flow (y-direction) are uniform, the flow is assumed to be two dimensional. In ventilation applications, the flow is assumed to be steady, Newtonian, incompressible and Boussinesq. The fluid properties are constants in a limited temperature range, except for the buoyancy term where the density is allowed to vary, which is known as the Boussinesq approximation $[\rho = \rho_\infty(1-\beta(T-T_\infty))]$. As a result of buoyancy forces, the body forces (gravitational force) are proportional to the density gradient, and so to the temperature gradient.

- Conservation of mass becomes:

$$\frac{\partial u}{\partial x}+\frac{\partial w}{\partial z}=0 \qquad (2.2.6)$$

For two dimensional flows, the flow of the $\frac{\partial v}{\partial y}=0$ component is neglected.

- Conservation of momentum becomes:

$$u\frac{\partial u}{\partial x}+w\frac{\partial u}{\partial z}=\nu\left(\frac{\partial^2 u}{\partial x^2}+\frac{\partial^2 u}{\partial z^2}\right)+g\beta(T-T_\infty) \tag{2.2.7}$$

- Conservation of energy becomes:

$$u\frac{\partial T}{\partial x}+w\frac{\partial T}{\partial z}=\alpha\left(\frac{\partial^2 T}{\partial x^2}+\frac{\partial^2 T}{\partial z^2}\right) \tag{2.2.8}$$

In the above equations ν is the kinematic viscosity, T_∞ and ρ_∞ are the reference temperature and density, and $\beta=-\frac{1}{\rho}\frac{\partial\rho}{\partial T}=-\frac{1}{\rho}\frac{(\rho_\infty-\rho)}{(T_\infty-T)}$ is the volumetric thermal expansion coefficient.

In order to solve the governing equations for a stratified flow, they must be simplified on the basis of acceptable assumptions. For an incompressible medium the density depends only on the temperature T. In environmental problems, the range of temperature variations is comparatively small. As long as the temperature variation is not large the temperature variations obeys the equation of state, and the Boussinesq approximation is applicable.

Chamber scales are employed for non-dimensionalisation. Therefore, all distances are normalized by chamber height, H, and velocities by chamber equivalent velocity, U defined by $U=\frac{Q_c+Q_h}{BH}$ where B is the chamber width.

$$u^*=\frac{u}{U} \qquad \upsilon^*=\frac{\upsilon}{U} \qquad x^*=\frac{x}{H}$$

$$z^*=\frac{z}{H} \qquad Re=\frac{UH}{\nu} \qquad Pr=\frac{\nu}{\alpha}$$

$$T^*=\frac{(T-T_1)}{(T_2-T_1)} \qquad Gr=\frac{g\beta(T-T_1)H^3}{\nu^2} \qquad Ri=\frac{g\beta\left(\frac{dT}{dz}\right)}{\left(\frac{du}{dz}\right)^2}\approx\frac{g'H}{U^2}$$

where T^* is the dimensionless temperature, in which T_1 and T_2 are the reference temperatures chosen as the measured temperatures at the bottom and the top of the environmental chamber, Re is the Reynolds number, Pr is the Prandtl number, Ri is the Richardson number, and Gr is the Grashof number.

Using the non-dimensional scheme and dropping the stars (*) for convenience, the governing equations may be written as follows:

- Conservation of mass:

$$\frac{\partial u}{\partial x}+\frac{\partial w}{\partial z}=0 \tag{2.2.9}$$

- Conservation of momentum.

$$u\frac{\partial u}{\partial x}+w\frac{\partial u}{\partial z}=\frac{\nu}{UH}\left(\frac{\partial^2 u}{\partial x^2}+\frac{\partial^2 u}{\partial z^2}\right)+\left[\frac{(g\beta(T-T_\infty))H^3}{\nu^2}\frac{\upsilon^2}{(UH)^2}\right]T \tag{2.2.10}$$

or

$$u\frac{\partial u}{\partial x}+w\frac{\partial u}{\partial z}=\frac{1}{Re}\left(\frac{\partial^2 u}{\partial x^2}+\frac{\partial^2 u}{\partial z^2}\right)+Ri\,T \tag{2.2.11}$$

or

$$u\frac{\partial u}{\partial x}+w\frac{\partial u}{\partial z}=\frac{1}{Re}\left(\frac{\partial^2 u}{\partial x^2}+\frac{\partial^2 u}{\partial z^2}\right)+\left[\frac{Gr}{Re^2}\right]T \tag{2.2.12}$$

- Conservation of energy (2.2.8) becomes.

$$u\frac{\partial T}{\partial x}+w\frac{\partial T}{\partial z}=\frac{\alpha}{\nu}\frac{\nu}{UH}\left(\frac{\partial^2 T}{\partial x^2}+\frac{\partial^2 T}{\partial z^2}\right) \tag{2.2.13}$$

or

$$u\frac{\partial T}{\partial x}+w\frac{\partial T}{\partial z}=\frac{1}{Pr}\frac{1}{Re}\left(\frac{\partial^2 T}{\partial x^2}+\frac{\partial^2 T}{\partial z^2}\right) \tag{2.2.14}$$

In order to apply the results obtained by small-scale to correspond with the natural situation, the sources of buoyancy must be scaled" [Linden et al (1990)]. Therefore, the main conserving ventilation factors applied to attain the similarity between buoyancy-driven flows at small-scale model to that at full-scale model [Hunt and Linden (1999)] are the Re, Pe and Fr number:

$$\frac{Re_{model}}{Re_{full-scale}} = \left(\frac{g'_{model}}{g'_{full-scale}}\right)^{\frac{1}{2}}\left(\frac{H_{model}}{H_{full-scale}}\right)^{\frac{3}{2}}\left(\frac{\nu_{full-scale}}{\nu_{model}}\right) = 1 \qquad (2.2.15)$$

$$\frac{Pe_{model}}{Pe_{full-scale}} = \left(\frac{g'_{model}}{g'_{full-scale}}\right)^{\frac{1}{2}}\left(\frac{H_{model}}{H_{full-scale}}\right)^{\frac{3}{2}}\left(\frac{\kappa_{full-scale}}{\kappa_{model}}\right) = 1 \qquad (2.2.16)$$

And

$$\frac{Fr_{model}}{Fr_{full-scale}} = \left(\frac{U_{model}}{U_{full-scale}}\right)\left(\frac{g'_{full-scale}}{g'_{model}}\right)^{\frac{1}{2}}\left(\frac{H_{full-scale}}{H_{model}}\right)^{\frac{1}{2}} = 1 \qquad (2.2.17)$$

Where U_{model} denotes the speed of the fluid driven by the model and $U_{full-scale}$ denotes the speed in the full scale, g' is the reduced gravity defined as $g' = g\frac{\Delta\rho}{\rho} = g\frac{\Delta T}{T}$

The dimensionless parameters are the Reynolds numbers, $Re = \frac{UH}{\nu}$, the Peclet number $Pe = \frac{UH}{\kappa}\cdot$ and the Froude number $Fr = \frac{U^2}{gH}$.

In the above equations, the velocity U scales for flow driven by a reduced gravity is given by $(g'H)^{1/2}$, $Re = \frac{(g'H)^{1/2}H}{\nu}$ and $Pe = \frac{(g'H)^{1/2}H}{\kappa}$ in which ν is the kinematic viscosity κ is the coefficient of molecular diffusivity, β is the coefficient of expansion and H is a typical vertical scale.

For modelling of natural ventilation in small-scale laboratory experiments, [Hunt and Linden (1999)] characterized the reduced gravity g' with the dimensions of lt^{-2} , so that, $\frac{g'_{model}}{g'_{full-scale}} = \frac{(lt^{-2})_{model}}{(lt^{-2})_{full-scale}}$ (2.2.18)

from which,

$$\frac{t_{model}}{t_{full-scale}} = \left(\frac{g'_{model}}{g'_{full-scale}} \times \frac{l_{full-scale}}{l_{model}} \right)^{\frac{1}{2}} \tag{2.2.19}$$

and,

$$\frac{U_{full-scale}}{U_{model}} = \left(\frac{lg'_{full-scale}}{lg'_{model}} \right)^{\frac{1}{2}} \tag{2.2.20}$$

The source of buoyancy scaled by [Linden et al (1990)] is

$B = \frac{g\beta W}{\rho c_p}$, where β is the thermal coefficient of expansion, W is the heat flux and c_p is the specific heat capacity at constant pressure. The dimensions of B are $l^4 t^{-3}$ and so equivalent scaling can be introduced for the laboratory scale.

For air, where the density differences were created using heat, the Reynolds and Peclet numbers at the small-scale were reduced by $\left(\frac{H_{model}}{H_{full-scale}} \right)^{\frac{3}{2}}$. For laboratory models of height ratios from 1: 20- 1: 100, the Reynolds and Peclet numbers were reduced by two or three orders of magnitude. By using fresh water as a working fluid and salt water to produce density differences in the system, the decrease in the magnitude of the dimensionless groups due to the change in scale is counteracted as $\nu_{air} \succ\succ \nu_{water}$ and $\kappa_{heat} \succ\succ \kappa_{salt}$ where κ_{heat} and κ_{salt} denote the diffusivities of heat in air and salt in water respectively[Linden et al (1990)]. A considerably larger density differences can be achieved experimentally using fresh water and salt water, than density difference in air due to temperature change, hence $g'_{model} \succ\succ g'_{full-scale}$. Dynamical similarity is then achieved at small-scale in the laboratory as $g'_{model} \succ\succ g'_{full-scale}$ and $U_{model} \prec\prec U_{full-scale}$.

2.3 Previous Work Related to Stratified Flow

2.3.1 Review of Analytical Work

During spray painting of objects, stratification occurs due to over-spray and solvent vapours. These layers may cause an explosion source or fire hazards. It may cause toxicity by absorption or inhalation of solvent vapours and fine over spray particles, in the place of work [Wander (2002)]. As a result, ventilation is used to remove particles of over spray to protect the texture of the surfaces already painted and those yet to be painted. This can be done by removing over-spray and solvent vapours by ventilation stream to the external environment to be exhausted [Wander (2002)].

Skistad (1998) and Calay et al (2000) introduced the concept of selective ventilation, which utilises the principle of "selective withdrawal". In this ventilation method the upper part of the room is divided into different regions using temporary walls whilst the air is exhausted at the height of stratification where the extracted heat or contaminant concentration is highest.

Thermal stratification is very important for efficient ventilation, fire exhaust, and solar heating. It affected by the flow and the heat transfer parameters that can be improved by controlling of these parameters, [Hahne and Chen, (1998)].

Mathematical and experimental investigations were done by [Hunt and Linden (1999)]. The study was to describe the natural ventilation using combined effects of buoyancy and wind. They derived a mathematical model for stratified layer interface height based on wind speed and openings heights.

Analytical study on the enhancement of natural ventilation in a solar house was presented by [Dai et al. (2003)]. They found that a solar adsorption cooling effectiveness, using solar house natural ventilation, could attain a value of 0.12 for COP (coefficient of performance), which increases ventilation effectiveness and provides cooling to the room without any change in humidity.

The position of neutral buoyancy, (the position where pressure in the room equals that in the exterior), was investigated by [Andersen (2003), Li et al. (2000), Fitzgerald and Woods (2004)]. [Li and Delsante (2001)], and [Chen and Li (2002)] investigated the

effect of both wind and thermal buoyancy on the position of neutral buoyancy. They used vents at multiple levels, and applied mass, energy and momentum equations. It was found that the position of neutral buoyancy can be related to the ratio of the upper and lower vent areas depending on the nature of the heat source. The analyses of [Li, et al. (2000)] for neutral height and pressure lines are shown in Figure 2.3.1.

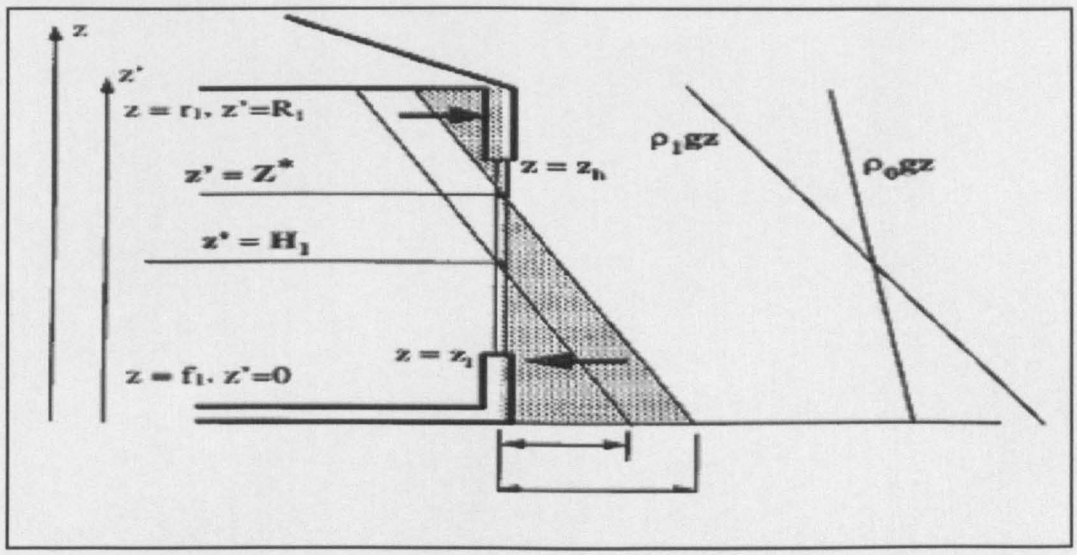

Figure 2.3.1: Pressure profiles across an opening in a single-zone building [Li et al (2000)].

Chen and Li (2002) studied the effects of buoyancy source, opening sizes and locations of a single zone building on displacement ventilation. The investigations were for three level openings. They found that the ventilation mode is a function of buoyancy source and geometries. Also they found that the location of the stratification interface level height is a function of the geometrical parameters and independent of the strength of buoyancy source. The results of [Chen and Li (2002)] were in an agreement with [Linden et al. (1990)] that the stratification within a space depends on the entrainment produced by buoyancy sources upon the geometry of the sources and the openings rather than the source strength while the strength of stratification however depend on the source strength.

A relationship between neutral height of air distribution and ventilation load was investigated by [Xing and Awbi (2002)]. Their results were obtained for a ventilated room, under several activities, using displacement ventilation. The neutral height above the heat source versus ventilation load based on mean temperature investigated by [Xing and Awbi (2002)] is shown in Figure 2.3.2.

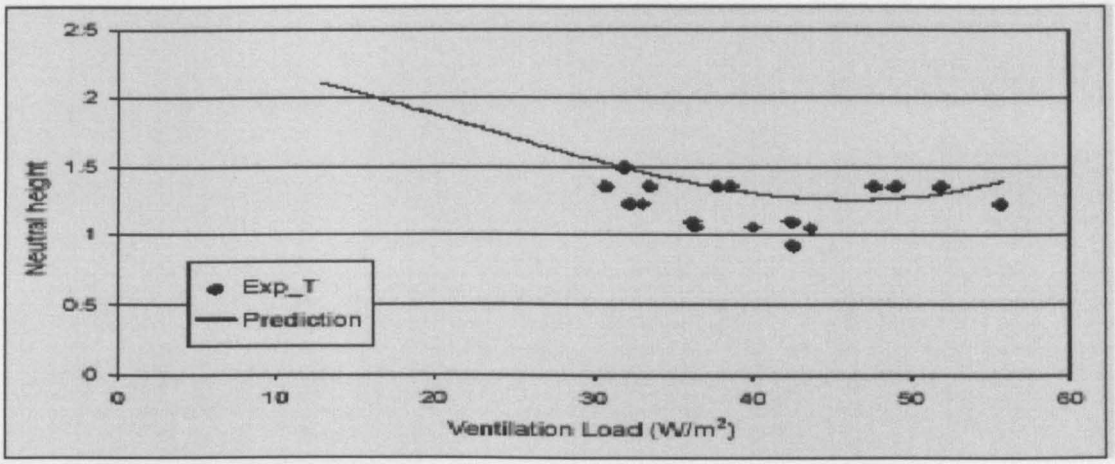

Figure 2.3.2: Neutral height versus ventilation load (based on mean temperature) in ventilated room, [Xing and Awbi (2000)].

Mundt (1994) found that the pollutants could be locked in at different levels (layers of pollutants). The distribution of pollutants is very sensitive to disturbances; that can cause a great decrease in the local ventilation effectiveness. "In spite of this, or perhaps because of this, a person can obtain a good air quality in the breathing zone, even if this zone is in a polluted layer. The convective plume around a body breaks through the polluted layers very rapidly" [Mundt (1994)].

The temperature gradient in a room is always positive (or zero) and increases up to the ceiling, while the contaminant concentration might have another form with a maximum somewhere in the middle of the room. The temperature gradient is very much dependent on the ventilation flow rate and not so much on the position of the heat sources [Mundt (1995)]. The contaminant removal effectiveness (the system's ability to remove contaminants from the space.), in displacement ventilation, was found to be related to the ventilation flow rate, and very sensitive to the level of the source and its position, [Mundt (2001)]. However, [Hagstrom et al. (2000)] found that it was a function of both the location and the power of the sources in relation to the supply and exhaust openings.

Heat loss in solar storage tanks was basically the main (destructive) item among several loss factors, investigated by [Al-Najem (1993)]. [Al-Najem and El-Refaee (1997)] made a comparison study for prediction of a turbulent mixing factor (eddy conductivity) at the inlet and outlet of a thermal storage tank, also the performance of thermal stratification in that tank. The model showed a good agreement with the experimental data of [Loehke et al. (1978)]. The analysis of [Alizadeh (1999)] can be used to link the flow

parameters in the stratified layer using the properties of flow in the lower and upper zones. Figure 2.3.3 shows the vertical temperature distribution inside the tank at the end of the simulation of [Alizadeh (1999)]. As seen in Figure 2.3.3, the temperature distribution of the storage tank is in a well stratified state

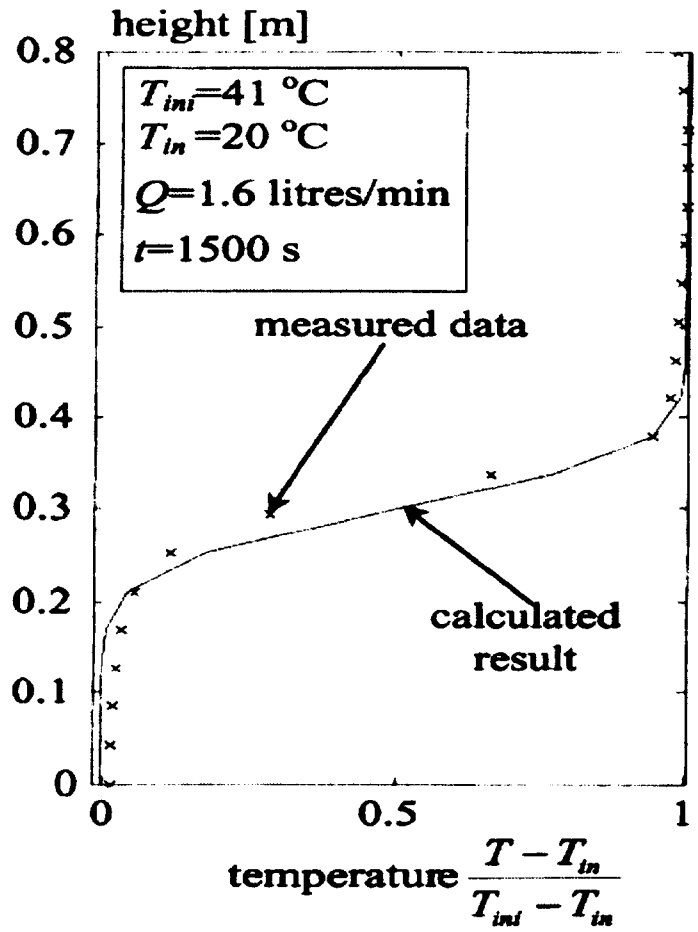

Figure 2.3.3 shows the vertical temperature distribution inside the tank at the end of the simulation resuts evaluated by [Alizadeh (1999].

2.3.2 Review of Experimental Work

Behne (1999) investigated the combination of cold ceiling and mixing ventilation system in the test chamber. Both displacement and mixing flow systems were studied and compared directly. Both were evaluated under the same conditions. He evaluated both the contaminant removal efficiency and the vertical air temperature rise. His results showed that the buoyant airflow rate is much higher than the supply airflow of about $400\,m^3/h$. The variation was due to the re-circulation that takes place in the test chamber.

Slater et al. (2003) studied the breathing zone, and the concentration levels generating during Gas Metal Arc Welding (GMAW) of mild steel within a defined working environment. They found that the use of ventilation techniques to control welder exposure from hazardous fumes could aid in reducing consideration to meet occupational exposure standards. Also, the most effective method of reducing operator exposure of welding fumes was the local extraction ventilation, which produces concentration levels below the recommended threshold of $5mg/m^3$.

Kikuchi et al. (2003) evaluated the effectiveness of local ventilation for industrial workplaces. The effectiveness was evaluated using the ratio of the average contaminant concentration in the occupied zone to the concentration of completely mixed indoor air. Lee and Awbi (2004) studied the effect of interior partitions and the gap under the partitions on indoor air quality. Their results showed that the gap under the partitions has more significant effect than the partition height. This was due to the cause of dividing the supply airflow into two parts above and below the partition.

Karimipanah (1999) studied the deflection of wall-jets in ventilated enclosures. The experiments were described by pressure distribution using a full-scale test room with varying room length. In the same manner, [Jeremy et al (2004)] presented a laboratory experiment to study the transient filling of a room with a buoyant dense fluid. They found that the steady two-layer stratification was established in the room. The height of the interface between the cold incoming air and the warm overlying air was dependent on the aspect ratio of the doorway to door height.

Wood et al. (2003) established a two-layer stratification and steady displacement flow in a room of turbulent plume originating from the top. The results showed that, the interface location is not only dependent of the opening geometry but also the source conditions, such as location and direction (upward or downward).

2.3.3 Review of Numerical Work (CFD)

A series of experimental tests were carried out by [Jaluria et al. (1998)] to identify the basic nature of the transport across a horizontal vent in a compartment, driven by pressure and density differences. By [Karimipanah and Awbi (2002)] to evaluate the

performance of impinging jet ventilation system compared with a wall displacement ventilation system. Also by [Allocca et al. (2003)] to determine the effects of buoyancy and wind on ventilation airflow rates whilst [Bertin et al. (2002)] studied the wall-fire behaviour in a ventilated room. The results of [Bertin et al. (2002)] are shown in Figure 2.3.4.

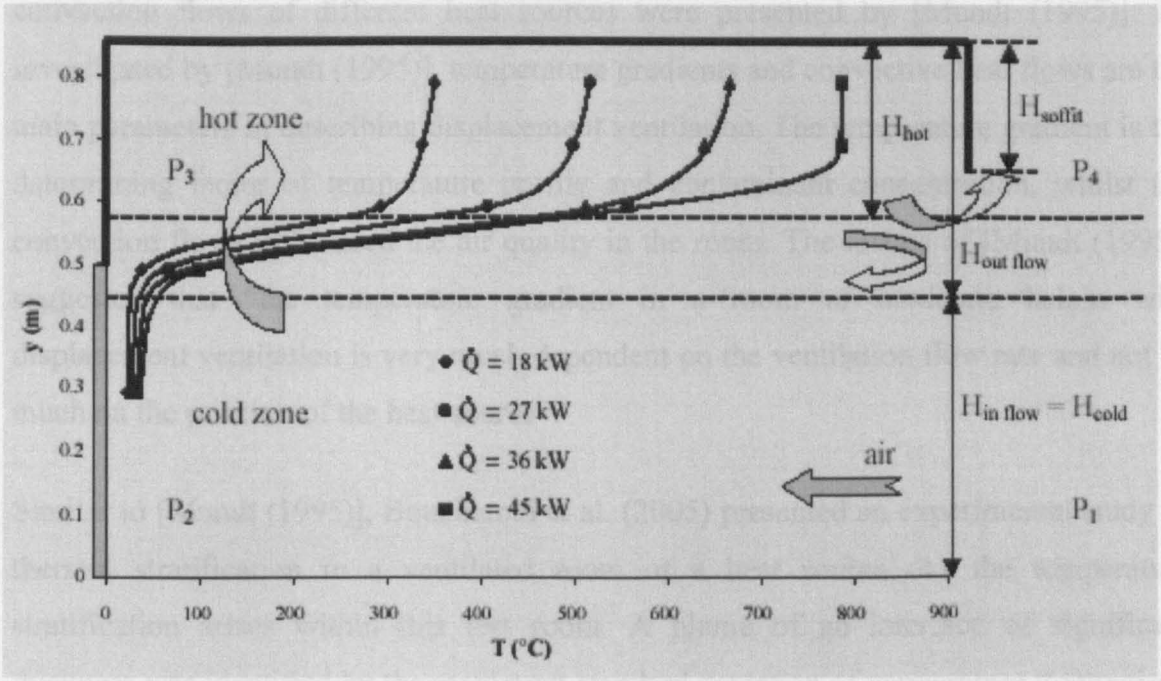

Figure 2.3.4: Evaluation of the mean temperature after thermal stabilization (under strong stratification) and for various height values (X_{th}=0.59 m and z_{th}=0.205 m). [G. Bertin et al. (2002)].

Further series of computational and experimental studies were done by [Holford and Hunt (2003)] to provide a prediction for thermal stratification and airflow rates, by extending the theory of displacement flow developed by [Linden et al. (1990)]. The experiments of [Holford and Hunt (2003)] were done on atrium buildings, using zones and field models. An atrium is a central feature of many modern naturally ventilated building designs. [Poreh and Trebukov (2000)] studied ventilation in a atrium under wind effects (speed and direction), and warmed atrium ventilation by direct solar heating as studied by [Joanne et al (2003)] .

Various numerical studies were used to predict ventilation efficiency. However, the quality of such predictive models on the numerical methods and appropriate turbulence models were investigated by [Woodburn and Britter (1996)], [McGrattan et al. (1996)], [Chow (1996)], [Kunsch (2002)], [Holford and Hunt (2003)], [Karimipanah (1999)],

[Murakami and Kato (1989)], [Gan (2000)], [Fukuhara and Tsuji (2003)], [Nagasawa (2003)], and that of [Dewan et al. (2003)] who showed the numerical techniques can provide a very good prediction of the stratified flow behaviour using effective parameters.

An experimental model (Figure 2.3.5) for the calculation of temperature gradients and convection flows of different heat sources were presented by [Mundt (1995)]. As investigated by [Mundt (1995)], temperature gradients and convective heat flows are the main parameters in describing displacement ventilation. The temperature gradient is the determining factor of temperature profile and contaminant concentration, whilst the convection flows influenced the air quality in the room. The results of [Mundt (1995)] suggested that "the temperature gradient in a room of moderate height with displacement ventilation is very much dependent on the ventilation flow rate and not so much on the position of the heat source".

Similar to [Mundt (1995)], Bouzinaoui et al. (2005) presented an experimental study of thermal stratification in a ventilated room of a heat source. As the temperature stratification arises within this test room. A plume of an interface of significant thickness was identified by the maximum standard deviation of temperature fluctuations as shown in Figure 2.3.6, where C is the fluorescent concentration (mol/m^3), T is the temperature (°C) and σ is the slandered deviation of temperature variations (°C).

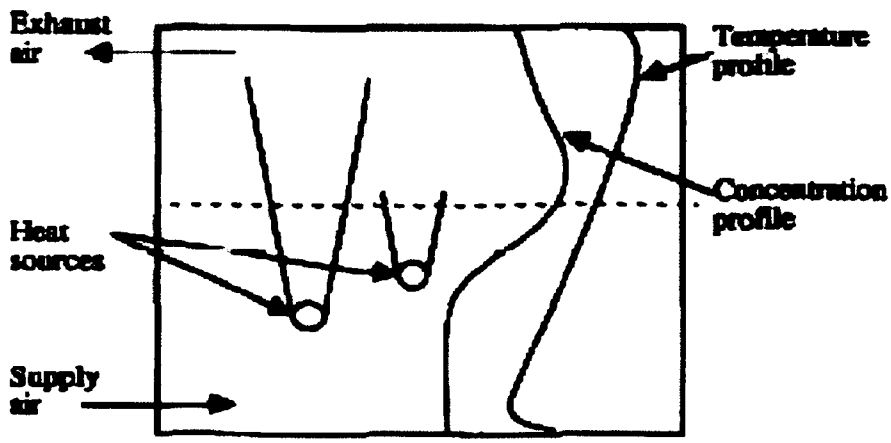

Figure 3.3.5: The principle of displacement ventilation showing temperature and contamination concentration profiles, as presented by [Mundt (1995)].

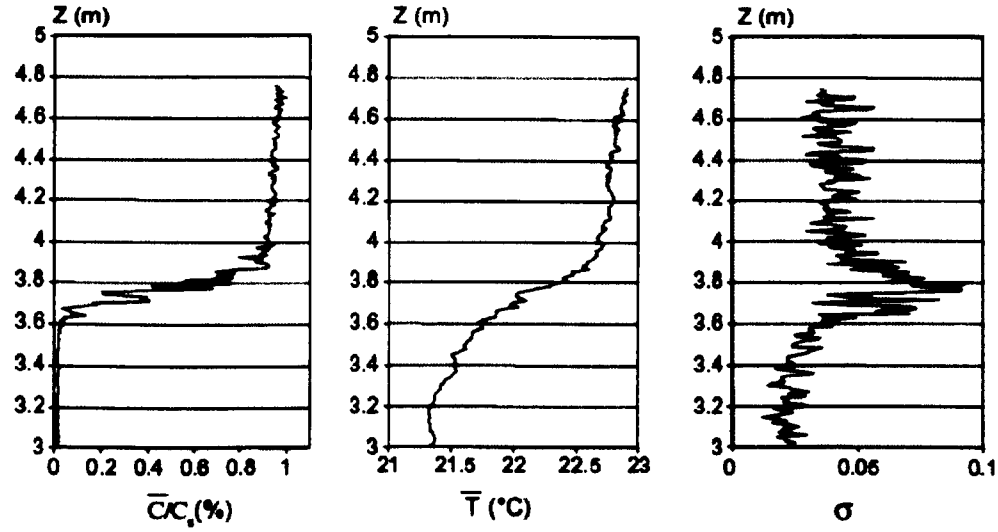

Figure 2.3.6: Vertical profiles of normalized tracer gas mean concentration, mean temperature and temperature fluctuation standard deviation, as presented by [Bouzinaoui et al. (2005)].

2.3.4 Turbulence in Stratified Flow

Laminar layers of stratified flow are stable with small perturbations. For large values of Ri number where the flow is still stratified, turbulence may exist in the stratified flow due to the local instabilities of concentrated vertical motion, [Calay et al. (2000)].

Subbarao and Muralidhar (1997) studied the effect of turbulence in isothermal and stably stratified flows. They investigated the effect of shear in promoting the growth of turbulence in isothermal flow. Their experimental results showed the vertical profiles of temperature with significant fluctuations. The temperature fluctuations were comparatively high in the experiment of strongest stratification. They related these fluctuations to the local temperature of the flow, where the sign of gradient of temperature fluctuation was the same as the sign of mean-temperature gradient.

Yam et al. (2003) provided an analytical technique using the fluctuation of both indoor and outdoor temperatures. The instantaneous temperature was the mean and the fluctuating component. They showed that, the magnitude of the indoor air temperature fluctuation is always smaller than that of the outdoor air temperature, Figure 2.3.7. Also they found that, for large time constant, the fluctuation of indoor air temperature with time becomes small, Figure 2.3.8.

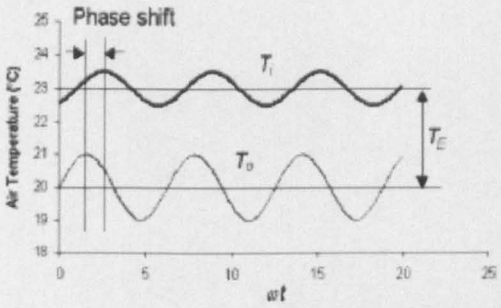

Figure 2.3.7: A sketch of the periodic indoor and outdoor air temperature profiles in a simple building when the ventilation flow rate is constant, Yam et al. (2003).

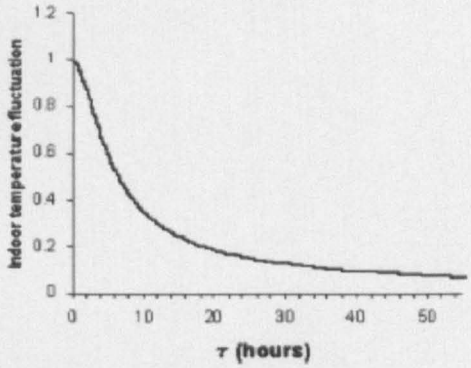

Figure 2.3.8: The non-dimensional indoors air temperature fluctuation $\Delta\widetilde{T}_i$ (normalized by the outdoor air temperature fluctuation $\Delta\widetilde{T}_0$) as a function of the time constant, Yam et al.

2.3.5 Stratified Flow by Salt-Baths and Smoke Visualisation

Salt-baths and smoke visualisation are used as a simple process to display the results in an easier form of observation. The salt-baths of easy experimental set-up can scale the flow characteristics in ventilated areas, where the variations of density are proportional to the variations of temperature. This technique was developed by [Linden et al. (1990)] for the fluid mechanics of natural ventilation in buildings. The technique used salt as a medium to increase the density of examined flow. This allows the effect of buoyancy to be made much greater than those in the real experiment, and so long, the reduced gravity. On the other hand larger buoyancies reduce the test time such that measurements were difficult to take.

Salt-bath laboratory techniques have been used in a number of ventilation studies. [Holford and Hunt (2003)] mentioned that the low value of the kinematic viscosity of water, and the large buoyancy of saline solution, give an approximate dynamical similarity between airflows in buildings and the flow of saline in salt-baths, where the non-dimensional variables are defined in the same manner for both flows. On the contrary, [Howell and Potts (2001)] presented an experimental temperature stratification established within a full-scale enclosure to confirm the salt-bath model of [Linden et al. 1990]. They found that an agreement has been reported when neglecting the mechanism of thermal radiation and diffusion because the salt-bath technique also neglects it,

"Whilst the kinematics viscosity of water is only about one-tenth that of air, the diffusivity of salt in water is less than one ten-thousandth that of heat in air (Lane-Serff, 1989). The salt-bath technique is, therefore, only suitable for modelling flows where diffusion of heat is insignificant, since salt diffuses too slowly in water to represent the diffusion of heat".

In water experiments, the radiative heat transfer is not significant; so that the temperature and concentration stratifications are coincide. In full-scale air modelling experiments, the concentration shows larger stratification than the temperature, where radiation is reducing the temperature gradient. Whilst the first technique is popular; the second is given little attention, [Li et al, (1993)].

"There are two main advantages of modelling flow ventilation using small-scale models in water. The first is that the flow visualisation is very straight forward, and complex flow patterns can be easily determined. The second advantage is that it is possible to use large values of reduced gravity $g' = \frac{g\,\Delta\rho}{\rho}$ (much larger values than is possible in air models) so that realistic Reynolds numbers and Peclet numbers (Re and Pe) may be realized. Thus direct similarity is achieved. In addition it is possible to make quantitative measurements of velocity and temperature (salt concentration) distribution" [Linden et al. 1990].

Using dyed saline solution, [Jermy and Woods (2004)] classified the flow and mixing produced by exchange processes in displacement ventilation and mixing ventilation. The results are illustrated in Figure 2.3.9. It was observed that for some flow, steady two-layer stratification was established with a certain interface height under a finite source of buoyancy in the room, whilst the others leaded to a well-mixed interior.

Small-scale modeles by [Linden et al, (1990)], [Linden (1995), (1999)], [Hunt and Linden (1999)] and others were used by many researchers to display the flow characteristics of ventilated enclosures. [Chenvidyakarn and Woods (2005)] concluded that "the using of small scale was not an exact replica of the full-scale, while it replicates its key ventilation features". As developed by [Linden et al. (1990)] and written by [Holford and Hunt (2003)], the low value of the kinematic viscosity of water, and the large buoyancy of saline solution, give an approximate dynamical similarity between airflows in buildings and the flow of saline in salt-baths, where the non-

dimensional variables are defined in the same manner for both flows. [Hunt and linden (1999)] simulated the combined effect of buoyancy and wind in natural-displacement ventilation. Using small-scale technique, the experimental observations and the mathematical model developed showed a good agreement over a wide range of density differences and wind speeds.

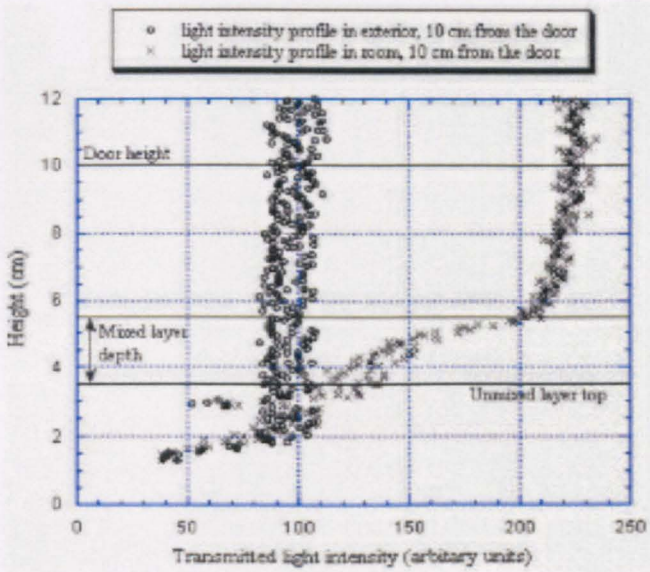

Figure 2.3.9: Vertical profiles of transmitted light intensity measured during a transient experiment of (10 cm high doorway, 90 seconds after opening), [Phillips and Woods (2003)].

In the research by [Linden et al. (1990)], the stratified layer interface level height was predicted as a sharp interface between two layers of air of differing temperature, clean and polluted zone, which were in opposition to the results of [Mundt (1995)]. Also, the mathematical model of [Linden et. al. (1990)] didn't explain the temperature distribution within the test-room. Both diffusion of heat and thermal radiation were neglected, while the remaining mechanism for heat transfer is convection. Therefore, two layers of air of differing temperatures can coexist in the same confined space without any diffusion over the sharp interface, [Howell and Potts (2001)].

Despite its capability to represent the flow of air in rooms, enclosures and buildings, and the quantitative agreement between the temperature stratified experiments and the salt stratified experiments, the small-scale technique has some disadvantages. [Howell and Potts (2001)] confirmed that the salt-bath modelling technique and related

mathematical model of [Linden et. al. (1990)] was not appropriate for the prediction of natural displacement ventilation flow driven by a source of buoyancy at floor level.

From Figure 2.3.9, the behaviour of air and water flow shows that the viscosity of liquids and gases is strongly affected by the temperature. The viscosity of gases used for the calculation is the power law of temperature difference, which is given by:

$$\frac{\mu}{\mu_0} = \left(\frac{T}{T_0}\right)^{0.7} \tag{2.3.1}$$

Whilst the empirical fit for the viscosity of liquids is given by:

$$\ln\frac{\mu}{\mu_0} = a + b\left(\frac{T_0}{T}\right) + c\left(\frac{T_0}{T}\right)^2 \tag{2.3.2}$$

where η_0 is the value of viscosity at a reference temperature T_0, which is $273^\circ K$, a, b and c are constants ($a = -1.94$, $b = -4.8$ and $c = 6.74$) and T is the temperature in $^\circ K$.

Figure 2.3.10 shows that the viscosity of water strongly decreases if the water temperature is increased. On the contrary, the viscosity of air slightly increases by increasing the air temperature.

The variation in the behaviour of the fluid is referred to the cohesive and intermolecular forces within the fluid. Therefore, it is reflected on the behaviour of liquids and the degree of agreement between the results obtained using small-scale technique and that of using full-scale technique.

The thermal diffusivity, which is related to the steady state thermal conductivity through the equation

$$\kappa = \frac{k}{\rho c_p} \tag{2.3.3}$$

where, κ is the thermal diffusivity, k is the thermal conductivity, c_p is the constant pressure specific heat and ρ is the density. It is a measure of the ability of a certain body to change its temperature.

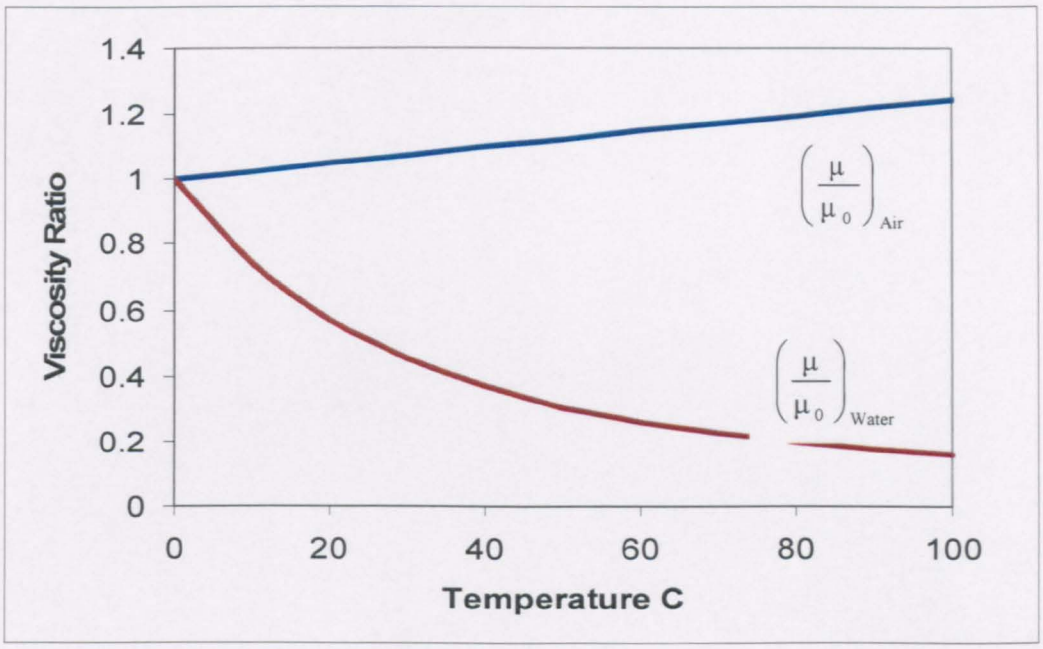

Figure 2.3.9: The viscosity ratio for air and water as a function of temperature (aerodynamics for students 2006).

From the verification of [Howell and Potts (2001)] and [Howell and Potts (2002)] the salt-bath modelling technique and related mathematical model of [Linden et. al. (1990)] have limited applications in natural and displacement flows. Therefore the salt-bath technique is not appropriate to model the ventilation flows in full-scale where both radiation and molecular diffusion coexist. While the temperature profiles shows a significant layer between upper and lower zones in the full-scale test-room, the model of Linden showed a sharp interface between two layers of different temperatures [Howell and Potts (2002)].

From the above analysis, it is confirmed that the small-scale modelling technique is not suitable for studying the stratified flow where effects of radiative and diffusive heat transfer are significant. In order to overcome this, the air modelling technique more realistically describe the temperature distribution within the full-scale chamber, and the full-scale technique is more appropriate to model the stratified flow in the built environment. Where the full-scale environmental chamber is used for testing realistic temperature-stratified flow, the full scale model can predict the flow behavior in a more realistic way concerning diffusivity and interpret the stratified flow behavior naturally more than the salt method.

A series of visualisation tests were conducted by many experimental researchers. Ventilation with heat transfer inside a ventilated enclosure using temperature measurements, flow visualisations and numerical simulations have been done by [Dubovsky et al. (2000)]. The visualisation technique was performed using smoke sticks. The comparisons of smoke visualisation results with numerical results were in agreement. The results of [Dubovsky et al. (2000)] are shown in Figure 2.3.11.

Figure 2.3.11: Results for the ventilated steady state: (a) by smoke visualization; (b) by numerical simulation; (c) the simulated temperature field, [Dubovsky et al. (2000)].

performed by [Ziskind et al. (2002)]. They studied the natural convection using a hot plate at the top of the building. They found that the effective ventilation could be achieved by means of natural convection heat transfer from the hot element at the top of the building heated by solar radiation. The experimental results of [Ziskind et al. (2002)] are shown in Figure 2.3.12.

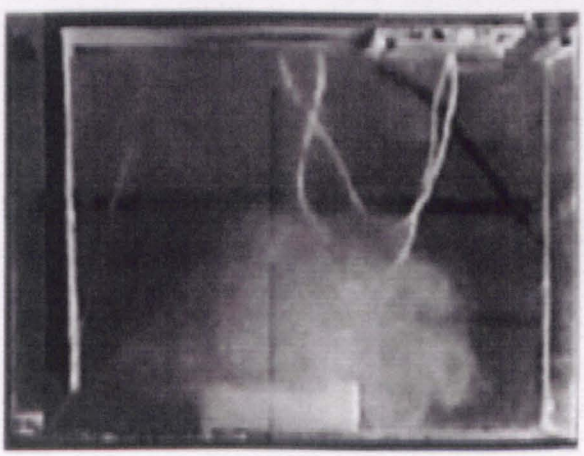

Figure 2.3.12: Experimental results of Ziskind et al. (2002), using smoke visualisation approach.

2.4 Previous Work on the Effect of Input and Exhaust Duct Locations

The location of the interface or the stratified layers and the strength of stratification are depending on the location of the exhaust and the temperature and momentum differential across the enclosure [Calay et al (2000]:

A ventilation of air supplied to both occupied and unoccupied spaces within buildings is necessary in order to replenish the oxygen supply to act as a fluid to dilute the carbon dioxide, odours and process emissions. It also necessary to prevent the build-up of potentially explosive vapour mixtures in the unoccupied plant spaces to provide air movement as a constituent part of comfort, and to control airborne contamination in industrial ventilation. Inside the enclosures, ventilation is used to remove pollutants, harmful gases and particulates from the multipurpose space, where different levels of pollutants are produced during different activities such as, welding, assembling and painting that take place side by side in one big hall, where ventilated air must conform to standards to ensure workers safety. It must be supplied into the hall until the contaminant concentration decreases below the harmful levels, [Calay et al 2000].

The configurations of building rooms and especially the location of inlet and outlet openings in relation to dominant wind direction at the site have major effects on the ventilation rates in buildings. Locating inlet openings near high-pressure surfaces of a building, and exit openings at low-pressure ones produces higher flow rates through windows [Ayad (1999)].

The thermal stratification generated by a localised source of heat at floor level in a confined space is of considerable interest to building ventilation. Many sources of heat generated in building may be regarded as being localised e.g. computers, occupants etc., and knowledge of the developing vertical temperature profile produced by these sources is required before air quality and occupant comfort levels can be determined. In general, these sources may be classified as either a 'pure' buoyancy source, e.g. an electric fire or a radiator in a hot water heating system, or as a 'forced' buoyancy source which characterised by non-zero momentum fluxes, e.g. in a heating system in which warm air is injected into space, [Hunt and Linden (1999)].

Teitel and Tanny (1999) developed a theoretical model to study the effect of openings height and wind speed in green houses. It was based on non-dimensional mass and energy conservation equations. The model was calibrated against experimental results. The results showed that ventilation, in greenhouses, was increased by increasing the height of the openings, the wind speed, and by decreasing the solar radiation

Sinha et al. (2000) discovered, numerically, the velocity and temperature distribution of warm air introduced in a room at high values of Gr/Re^2. Solutions were presented for various locations of inlets and outlets, and for different values of Gr and Re numbers. The results of [Sinha et al. (2000)] showed that when the location of the outlet was at higher level than the inlet the location led to a better temperature distribution. When the location of the outlet was at a lower level than the inlet;

1. Increasing Gr number made the warm jet almost horizontal to flow downwards towards the exit.
2. Increasing Gr number increased the intensity of recirculation and yielded uniform temperature distribution.

Chen et al. (2001) studied the displacement ventilation in a single-zone building using a simple multi-layer stratification model. The flow rate was driven by a heat source distributed uniformly over a vertical wall. Experiments were carried out using a fine hydrogen bubbles generated by electrolyses in a water tank. Theoretical expressions were obtained for the stratification interface height and ventilation flow rate. As concluded by them, the theoretical and experimental results of [Chen et al. (2001)] compared with those obtained by an existing model available in the literature were in agreement, while the upper and lower layers were might be different from those of other layers.

The location of the interface of the stratified layers and its strength is dependent on the location of exhaust opening, and the temperature and momentum differential through the enclosure [Calay et al (2000)]. The sizes and locations of the room openings must be chosen to get the balance between the depth and the temperature of the warm layer in the upper zone. The depth must be sufficient to drive the required airflow, while the temperature of the warm zone is in the range, and the warm layer is above the level of occupied zone, [Hunt and Linden (2001)].

2.5 Previous Work of Mixed Flow and Air Jets

Mixing ventilation is widely used in offices and commercial buildings [Yue (1999)]. In mixing ventilation, the fresh air is introduced to mix through the ventilated space. The openings are arranged so that the relatively cool air enters at high level, while the relatively warm air enters at low level. In this case, mixing ventilation will produced due to buoyant convection of flow, [Linden et al. (1990)].

In this type of ventilation, the air is supplied from the ceiling with a speed much higher than these accepted in the occupied zone. Due to the air entrainment, both jet speed and temperature differences become smaller, which dilute the contaminant to an amount acceptable in the occupied zone [Yue (1999)].

"A jet of air is the flow resulting from the interaction of the fluid issuing from an opening with the surrounding fluid. This process is called entrainment of the secondary fluid (fluid surrounding the jet) by the primary fluid (the fluid issuing from the opening)" [Awbi (1998)].

Plumes are defined as "buoyant jets where the initial jet momentum is not significant, or has become completely dominated by the buoyancy force" [Baines P. G. (2002)].

A plume generated by a heat source will go upward. During its rising towards the ceiling, the volumetric flow rate will increase by entrainment of surrounding air. Therefore, a circulation of polluted air is formed in the upper region, while another large circulation flow is also created in the lower region. In between a momentum based separation was yielded and a stratified layer was established since each circulation contains its regional properties with little momentum interaction, [Hee-Jin and Dale (2001)]. Hence, "the strength and size of those circulation flows are main factors in characterising the stratification level". [Hee-Jin and Dale (2001)]

Linden et al. (1990) found that when the room's upper opening size was smaller than the lower one, the fluid flows through the small opening is high enough to work as a jet. The jet introduced will cause an entrainment buoyant fluid across the interface. Because of the high-density gradient above and below the interface, the interface descends faster. When the output is somewhere down the ceiling, the amount of mixing is much greater and the interface is diffuse. In natural ventilation under the effect of both buoyancy and

wind driven velocity, [Hunt and Linden (1999)] found that the amount of mixing was increased as the initial Froude number increased, and so the momentum of the incoming buoyant jet is increased.

The flow pattern in a large enclosure is dominated by convection currents and thermal stratification. Stratification is very common in buildings with a single large open space. Warm air rises under the influence of buoyancy forces, which cause a positive temperature gradient between the floor and the ceiling. Activities such as heating and welding act as additional heat sources and contribute to already existing temperature gradients across the space.

However, in other buildings where indoor air quality load are important, stratification effects can be desirable. Stratification in cooling seasons can reduce the cooling loads because the warm stratified layer below the ceiling acts as an insulating buffer, which reduces the roof and lighting heat gain components. An additional reduction in cooling load is achieved by locating the outlet extract at the height of stratification because heat extracted per unit of mass flow would be significantly higher than if the extract was positional below the stratified layer. There are many experimentalists and theoreticians who have investigated the effect of jets or plumes on the stratified layer characteristics, [Hung et al (1999)], [Shy (1999)], [Al-Najem and Al-Refaee (1997)], [Redondo et al (1996)], [Cardoso et al (2001)], [Karimipanah (1999)], [Murakami et al (1996)] and [Bloomfield and Kerr (1999)].

[Hung et al (1999)] showed that the thermal stratification reduces the heat transfer rate from vertical surface. They also found that non-Darcian and thermal dispersion effects have significant influences on velocity and temperature profiles as well as the local heat transfer rate.

Shy (1999) investigated experimentally the mixing processes involving large-scale motion and chaotic small-scale motions across a sharp density interface using a pH-sensitive, laser induced fluorescence technique in a water tank. He used a turbulent round jet impinging from above on the sharp density interface over a flow Reynolds number of ($2500 < Re < 25{,}000$) and a flow Richardson number of ($0 < Ri < 5$) based on the local jet scales at the interface. He found that at large Re, molecular mixing first occurs at the perimeter of the jet front, forming a mixed layer, in contrast to the case of a jet in a uniform environment.

Al-Najem and Al-Refaee (1997) studied numerically the transient behaviour of thermal stratification in storage systems using a computer code based on Chapeau-Galerkin integral formulation. Their results showed that the turbulent mixing (or eddy conductivity) factor caused by hydrodynamic disturbances at inlet and outlet ports of storage tank plays an important role in the performance of thermal stratification storage tanks.

Redondo et al (1996) used detailed flow visualisation as well as density measurements in zero-mean-flow laboratory experiments involving grid-stirred turbulent mixing across a density interface and bubble-induced mixing. They found that the overall mixing efficiency of the processes depends on the local Richardson number as well as on the local vorticity.

Cardoso et al (2001) found that when small particles sediment from a surface current generated by an axisymmetric turbulent plume, the concentration of particles in the environment surrounding the plume is larger at higher levels compare with that at lower levels. This distribution of particles in the environment results in an unstable density stratification and as a result, convection in the environment may result.

Karimipanah (1999) conducted measurements of the pressure along the perimeter of a slot ventilated room for different room sizes. He found that the momentum of the jet at the end of the room is decreased with increasing room length. They could not predict the corner flows by their CFD simulation using the linear eddy viscosity or standard stress models. However they suggested that these effects may be captured by using a second moment closure turbulence model with a new near wall approach.

Awbi (1998) used an experimental environmental chamber to compare the effectiveness of both mixing and displacement ventilation. He found that using displacement ventilation is more energy efficient than mixing technique. In mixing process, the air was normally supplied from high levels causing a flow jet mixing the injected air with the domain. [Awbi (1998)] found that the process of removing heat and contaminant from the room involves both diffusion and convection. Therefore, it is influenced by the characteristics of both the air supply and the room geometries, such as jet speed and momentum, temperature difference between air injected and the domain, position and type of air supply, distribution of heat and contaminant sources, etc.

Laboratory experiments of a jet impinging on a stratified interface were done by [Cotel et al. (1997)]. The entrainment of both vertical and inclined (15°) jets was studied using water tank experiments. At Ri<10, [Cotel et al. (1997)] found that the entrainment of vertical jet was proportional to $Ri^{-1/2}$, while the inclined jet was proportional to $Ri^{-3/2}$. At Ri>10, the results of [Cotel et al. (1997)] show the entrainment rate was independent of Ri, where the interface is effectively flat, according to their experimental model.

Bloomfield and Kerr (1999) preformed an experimental and theoretical investigation of the flow and density distribution arising from the upward turbulent injection of a dense fluid into a stratified environment of finite extent. They found that as more dense fluid is added through either a point or line source, both fountain and the environment evolve with time. They applied their results into two problems: the replenishment of magma chambers and the heating or cooling of a room.

Using a ceiling jet, it is possible to ventilate the working zone without destroying the stratified layers. This can happen by injecting the air of low momentum through a large diameter jet or plume, where the entrainment per unit area of jet is inversely proportional to its perimeter. This type of ventilation is very useful in many applications like in theatres and television studios, where the inlets can't be fixed close to the floor or changeable decorations [Calay et al. (2000)].

Auban et al. (2001) described an experimental study of thermal plume in confined stratified environment, where the ventilation at a given flow rate was designed to maintain the height of this stratification. The experiments were performed in a square-base tank using light fluid, fluorescent tracer and Laser Doppler. The stratified layer interface level and thickness were determined based on the concentration and fluctuations of the injected fluid.

A simple multi-layer stratification model using a fine bubble technique was proposed by [Chen and Mahony (2001)]. The studied parameters were the stratification interface level height and ventilation flow rate using heat source distributed uniformly over a vertical wall. The data obtained were compared with the results of [Linden et al. (1990)], and good agreement was achieved. [Chen and Mahony (2001)] results showed the entrainment behaviour of fluid flow near the high ranges of interface level heights and the entrainment at the low level of each stratification layer.

2.6 Summary and Objectives

In this chapter, the literature reviews of the theoretical, analytical, computational and experimental modelling were used as the base for the design of the experimental work and test matrices. It is also used to give an indication for the various parameters that affects the stratified flow, which are to be highlighted in details. While the analytical and schematic models proposed by [Skistad (1998)] and [Calay et al. (2000)] for selective ventilation in large enclosures are the motivation for the present experimental study.

This section summarizes numbers of findings of the literature review and identifies research needs. There is literally a wide agreement on the importance of best applications for stratification control; hence the factors that impact ventilation and confer significant energy savings through the applications. Another issue meriting attention is the positive benefit of using stratified flow to maintain ventilation rates at design levels to reduce contaminant concentration and energy consumption, which indicates the urgent need for more research on these issues.

The general characteristics of flow in ventilated areas have been reviewed. The main studies in ventilation and stratification areas were also covered. The studies of [Dagestad (1991)], [Mundt (1995)], [Skistad (1998)], [Hunt and Linden (1999)], and [Xing and Awbi (2002)] were outlined with the development of different applications in ventilation systems. Ideas have been introduced, results have been evaluated and conclusions have been discussed.

Despite numerous investigations of the effect of flow parameters on ventilation systems and techniques, such as [Behne (1999)], [Chen and Li (2002)], [Dubovsky et al. (2001)] and [Holford and Hunt (2003)], there are a few investigations regarding the stratified flow and stratification phenomenon, [Dagestad (1991)], [Mundt (1995)], [Skistad (1998)] are not fully explained. Whilst the experimental investigations using salt baths have been popular [Linden (1979)], [Linden et al. (1990)], [Jermy and Andrew (2004)], the investigations using air modelling in experimental tests to date have been limited. In ventilation there are needs for further experimental work to understand the role of the stratified layer.

In order to provide comfort and healthy environment, it is difficult to generalize the stratification effects in a built environment. The conclusion offered by a review of the literature is that attention must be paid to maximising the advantages effects of stratification and minimizing the disadvantages..

From the literature review, stratification describes a situation of temperature or density gradient. In this situation, fluids of less density are lying above that of higher density. Stratification exists because the vertical density gradients are always positive. Stratification exists because the fluids of high density gradients do not mix easily. While the vertical density gradient is mainly determined by the vertical temperature gradient, stratification is determined by the degree of vertical temperature gradient.

There is some confusion in the literature regarding the terms stratified layer interface level height, stratified layer thickness and the degree of stratification. More analysis and clean definitions would be helpful and significant research in this area is still needed.

The degree of stratification is a measurement of flow condition. In weakly stratified situation, the degree of stratification is so low that the stratified situation is easily broken by small amount of momentum. In strongly stratified situations, the degree of stratification is so high that it requires a large amount of momentum to break down the stratified situation.

No exact definition or mathematical equation exists that can accurately define a degree of stratification for a given stratified situation. It is therefore not possible to quantify the stratified flow by its degree of stratification or predict the stratified flow situation by the estimated degree of stratification without a clear definition for the term "Degree of stratification". Therefore, a theoretical approach is needed to establishing an effective verification to determine the degree of stratification.

In general, the literature presents three scientific procedures that are relevant to the stratified flow. It has covered case studies conducted through computer simulation (CFD), small-scale model using the salt-bath technique, and some analytical and experimental full-scale air modelling technique.

As demonstrated in the literature review, it would still be extremely useful to carry out more experimental work using air modelling technique.

In summary, the key objectives involved to be studied in this work are:

- The stratified flow parameters, such as airflow rate, flow direction and input and output duct locations.
- The stratified flow characteristics, such as stratified layer interface level height, stratified layer thickness, temperature gradient and degree of stratification.
- The mixing of stratified flow using both jet momentum and inversion of input duct locations.

Chapter 3

Experimental Design and Analytical Developments

3.1 Introduction

Most experimental studies, such as [Linden (1979)], [Linden et al. (1990)], [Hunt and Linden (1999)], [Jeremy and Andrew (2004)], and others concentrated on modelling the ventilation flows using salt-bath techniques. The thermal properties of air are very different from salt solutions, especially the viscosity and molecular diffusion. The diffusivity of salt in water is less than that of heat in air. The salt-bath technique is not appropriate for modeling the ventilation flow through the full-scale test rooms or buildings, where all mechanisms of thermal transport coexist, [Howell and Potts (2002)]. Despite its high construction and operation costs, air modelling systems using air, instead of salt promise to provide the most accurate and reliable information.

Sets of experiments investigating the stratification in an environmental chamber were conducted. The experimental set-up used to support these models is presented. The flow parameters such as input airflow, temperature, openings heights and other parameters were used to model the stratified flow patterns interactions. programming, analysis and discussion of the results are explained in details.

The analytical models proposed by [Skistad (1998)] for selective ventilation in large enclosures is the basis for the present study. A schematic diagram of selective withdrawal of a polluted layer of air-"Select-vent" presented by [Skistad (1998)], with the adefinition sketch of temperature profile, stratified layer interface level height h, stratified layer thickness δ and stratified layer top height h' are shown in figure 3.1.1.

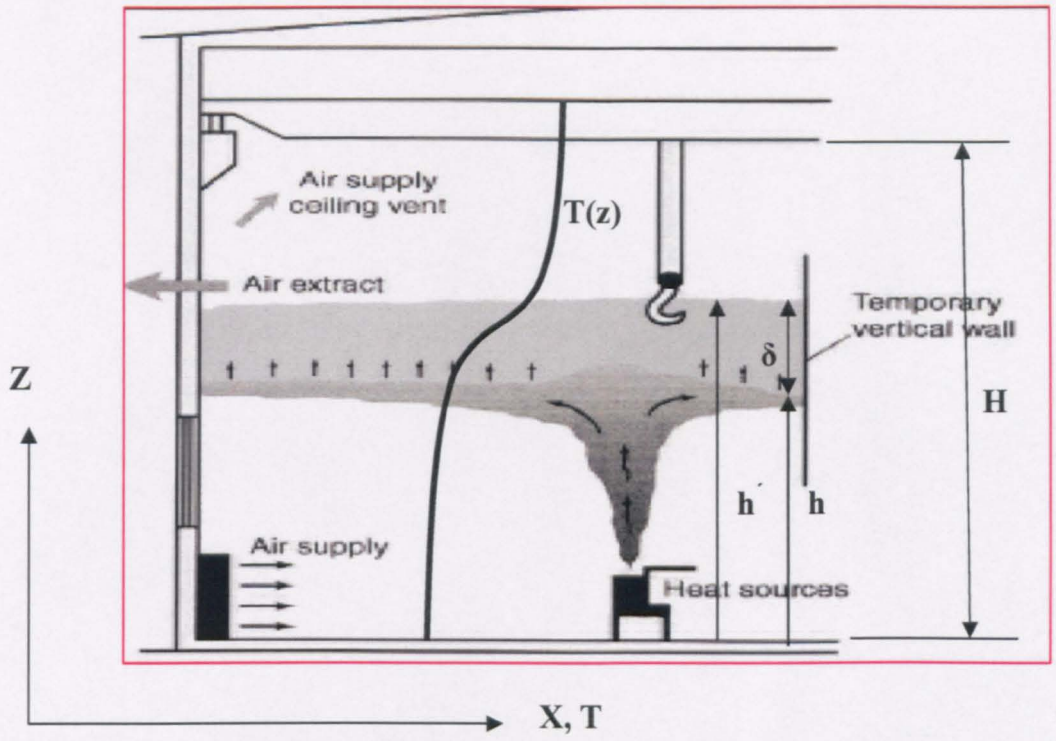

Figure 3.1.1: A schematic diagram of selective withdrawal of a polluted layer of air-"Select-vent" presented by [Skistad (1998)], with a definition sketch of temperature profile, stratified layer interface level height h, stratified layer thickness δ and stratified layer top height h′.

3.2 Analytical developments

It was shown in chapter 2 that there exist no formal definitions for the following parameters:

- Stratified layer thickness δ
- Stratified layer interface level height h
- Stratified layer top height h′
- Degree of stratification DS

These are, in most instances, undetermined characteristics that greatly influence the stratified layer and the prediction of stratification situation. A complete analysis of the stratified flow parameters and characteristics is required to provide a suitable determination of stratification situation.

However, it is clear from the literature that these parameters need to be defined in a comprehensive manner so that it is possible to measure the parameters.

3.2.1 Definition of δ, the stratified layer thickness

A formal definition for the temperature profile is employed to predict the stratified flow in a built environment. A stratified region is a region in which mixing levels are low. It consists of convectively mixed homogeneous zones separated by stably stratified layer, in which the vertical temperature gradient is sharply increased. This sharp increase takes place over a finite distance called the interface or stratified layer thickness. Formal definition of stratified layer thickness is significant because, as well as being a good estimation for the stratified layer thickness, this allows us to define the relevant parameters h, h′ and DS easily.

To give a formal definition for stratified layer, the change in temperature gradient of the stratified flows is taken into account. Figure 3.2.1 show the vertical profile of air temperature in the environmental chamber, T(z). The function T(z) has three critical points: (h, T(h)), (h′, T(h′)) and (h+δ/2, T(h+δ/2)). At these points, the analytical definitions of stratified layer interface level height h, stratified layer interface top height h′ and the stratified layer thickness δ are created.

From the temperature profile T (z) and the sign of the first derivative T′(z) = +ve along the vertical height, the temperature profile is always linear in the upper and lower zones. In between, the stratified layer is bounded by the sharp changes in temperature gradient. This layer is established in the region of maximum temperature gradient defined by the direction of the second derivative T″ (z), where the temperature profile is concave down. From which, the neutral height of the stratified layer is defined by the vertical height at which. T″ (z) =0.

From this definition, the neutral height of the stratified layer is define by the characteristic height at which,

$$\left.\frac{d^2T}{dz^2}\right|_{z=h+\frac{\delta}{2}} = 0 \qquad (3.2.1)$$

From the definition of the neutral height, the stratified layer thickness δ is the stabilized-layer thickness between the stratified layer interface level height h and the stratified layer top height h′. It is started with sharp increase in temperature profile and ended when the temperature profile decrease sharply.

$$\delta = h' - h \qquad (3.2.2)$$

Equations 3.2.1 and 3.2.2 give both the height and the thickness of the stratified layer. The thickness of the stratified layer primarily depends on the input airflow rates and the geometrical dimensions of the whole space.

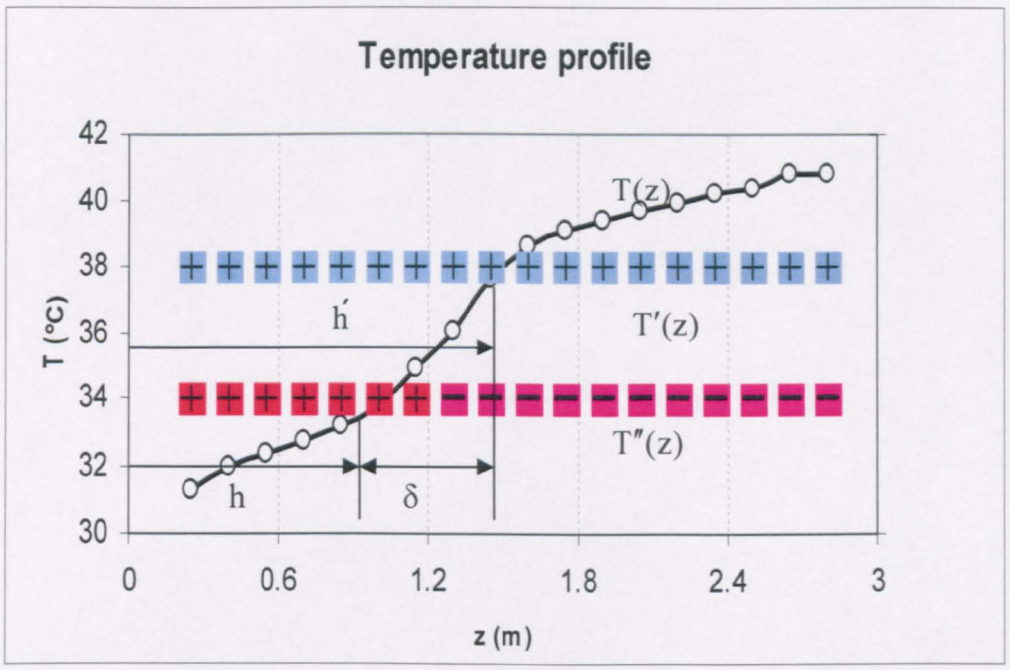

Figure 3.2.1 Temperature profile T (z), and the sign of the first derivative T′ (z) and the second derivative T″ (z) showing the line of maximum temperature gradient (z=1.2 m) where the stratified layer is located and the smoke is concentrated.

3.2.2 Definition of h, the Stratified Layer Interface Level Height

As shown in Figure 3.2.1, the stratified layer established in the chamber divides the domain into two zones (upper and lower). Each zone is having its own properties. The lower zone, below the stratified layer, has low temperature gradient and is close to mixed flow. The upper zone, above the stratified layer, is characterized by hot airflow producing a fairly well-mixed flow. The height of the stratified layer is h is a dependents of the input airflow ratio Qc/Q_h, and the input and output vertical heights.

From this definition, the interface level height h is define by the characteristic height at which,

$$\left.\frac{d^2T}{dz^2}\right|_{z=h} = \text{Maximum} \qquad (3.2.3)$$

3.2.3 Definition of h', the Stratified Layer top Height

From the establishment of zones in stratified flow, stratification will typically take place over a range of $0.1 \le z/H \le 0.9$ within the chamber height, otherwise, the flow may stratify but without zone establishment. In which, z is the height of the temperature sensor (thermocouple) and H is the height of the chamber.

As shown in Figure 3.2.1, h is the height of the lower zone whilst h′ is the height of the upper zone. From the same definition of h, the stratified layer top height h′ is define by the characteristic height at which,

$$\left.\frac{d^2T}{dz^2}\right|_{z=h} = \text{Minimum} \qquad (3.2.4)$$

3.2.4 Definition of DS, the Degree of Stratification

Based on previous studies, there is no exact definition or mathematical equation that can accurately define a degree of stratification for a given stratified situation. To quantify the stratified flow situation by its degree of stratification, a scientific definition for the degree of stratification is needed. From temperature distribution and smoke visualisation, the degree of stratification depends on the temperature gradient across the stratified layer relative to the overall temperature gradient. In other words, the degree of stratification of a stratified flow is based on the temperature gradient of the stratified layer within the stratified region.

From this definition the degree of stratification DS is given by:

$$DS = \frac{\left.\frac{dT}{dz}\right|_{h}^{h'}}{\left.\frac{dT}{dz}\right|_{0}^{H}} \approx \frac{\frac{\Delta T|_{\text{across the stratified layer}}}{\delta}}{\frac{\Delta T|_{\text{overall temperature difference}}}{H}} \qquad (3.2.5)$$

3.3 Experimental Apparatus

The experimental apparatus is described in two parts: the test chamber with its heating and cooling systems and the instrumentations. Both the experimental apparatus and procedures take into account the [Skistad (1998)] model and the definitions of the stratified flow characteristics as defined in the previous section.

3.3.1 Test Chamber

All tests were conducted in the environmental chamber at the University of Hertfordshire that is presented in figure (3.3.1). The physical dimensions of the chamber were large enough so that the walls did not affect the flow, and the height was sufficient for the build up of the stratified layer. The dimensions of the identical rectangular chamber were (7.5m long, 5.6m wide and 3.0m height) with two windows (double glazed) isolated from an enclosed space. The walls of the test chamber were insulated. The walls as well as the roof were 12.5 cm thick, with white polyester outer finish and polyurethane foam interior made. The floor included a layer of 10 cm thick concrete, and below it a layer of 10 cm thick Styrofoam.

Environmental flow variables were controlled by the means of airflow systems. The test chamber vent supply airflow up to $14\,m^3/min$ of hot air, and up to $12\,m^3/min$ of cold air. The hot air supply temperature was fixed at 40 and 45°C using the chamber heating and cooling system as shown in figure (3.3.2). The system can supply air at temperatures ranging from –40°C to +50°C. The cold air supply temperature was the ambient temperature. It was varied according to the surroundings and weather fluctuations. The volume flow rate is being assumed to be the same at the inlet and

outlet. The walls were assumed to be adiabatic and well sealed, so that the chamber was, practically, insulated. The internal surfaces were painted white, so that the inside of the chamber is visible from the outside. The radiative heat transfer between the surfaces could be assumed insignificant due to the low heat conditions.

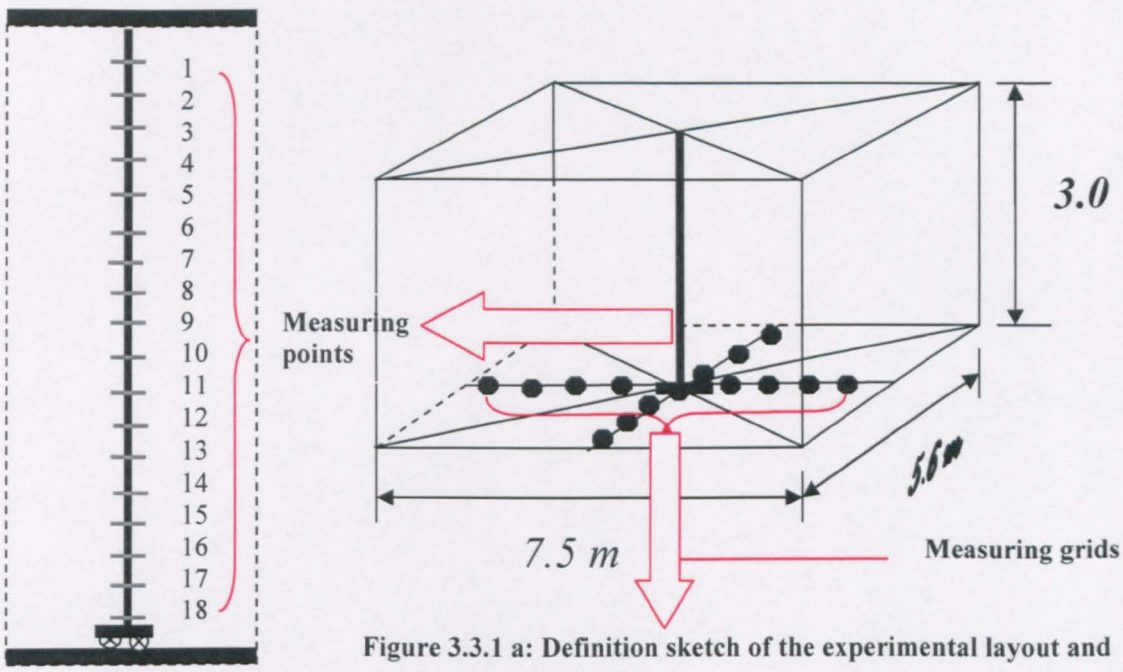

Figure 3.3.1 a: Definition sketch of the experimental layout and the thermocouples stand.

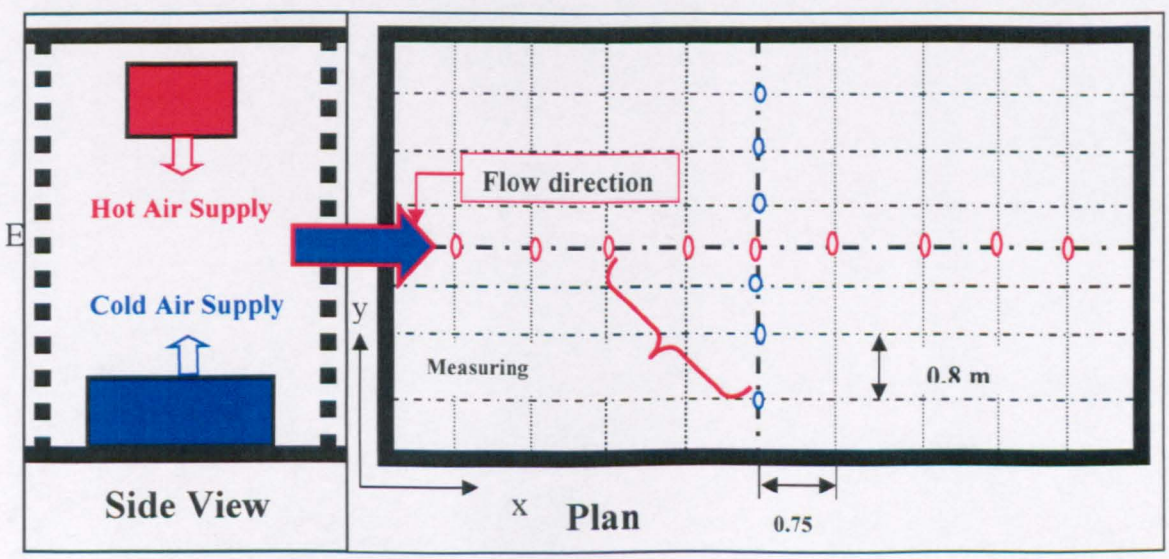

Figure 3.3.1 b: Definition sketch of the environmental chamber showing a diagrammatic representation of the input airflow supplies, flow direction and measuring locations.

The temperature distributions for the flow inside the chamber were measured using eighteen K-type thermocouples. The thermocouple stand was inserted vertically on a multidirectional movable base located at the centre of the chamber as shown in figure 3.3.1. The junctions of the thermocouples were located at the centres of eighteen equal distances on the thermocouple stand. Three thermocouples were placed at the hot inlet airflow, cold inlet airflow and the outlet. Another was located outside the chamber to measure the ambient temperature. All of these are located to give continuous monitoring of all required temperatures.

Concerning the measurements, the test chamber was equipped with sensors to determine the air temperatures (thermocouples), as well as the input air velocities and flow rates (A rotating vane anemometer LC6000). A procedure was allowed by distributing the temperature sensors to cover the essential vertical and horizontal planes within the chamber. This was done by using thermocouple stand in the vertical direction, and by moving the base in both directions on the horizontal plane. As a result, the measurement points were represented at 15 cm grid in vertical plane, and 75 cm x 80 cm grid in each directions of investigated horizontal plane.

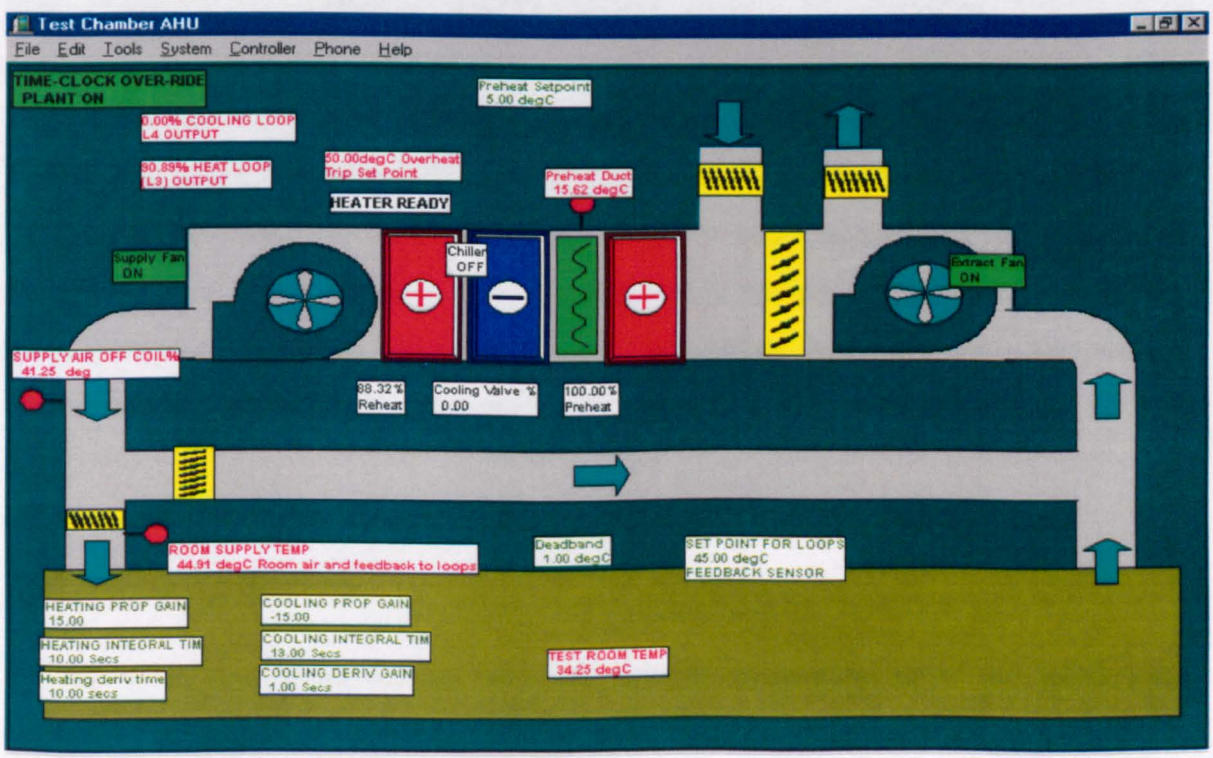

Figure 3.3.2: Schematic diagram of the experimental set-up cooling and heating system.

The present experimental methodology showed complete descriptions for the boundary conditions (supply air temperature and flow rate, inside temperatures and chamber boundaries). Field measurements will facilitate the comparisons with the analytical and numerical data based on our model. The conditions were based on the assumptions that the walls of the test chamber were insulated, the exhaust air was leaving the room through the exhaust opening (negligible infiltrations through the walls) and all measurements were made under steady-state conditions.

To obtain the best possible stratifying airflow, the temperature difference must be high enough, the entire hot airflow temperature ought to be fixed at large values (45 °C), and the ambient temperature must be low. If this cannot be done, the stratification of air might not of get good quality at all times and points, where the air quality in the occupied zone will vary according to flow parameters.

3.2.2 Instrumentation

To get quantitative and qualitative results, the inputs of our modeling technique must truly represent the conditions that the model assumes it represents. The level of accepting the data from a measuring system is identifying by the instrument errors. When each measuring device is well calibrated and working properly, the measurement system as a whole can be providing a realistic observation, where the quality of the row data is a dependent of both measuring property and confounding environmental conditions. The instrumentation and data acquisition devices are contained within the instrumentation apparatus. It includes two groups of measurements, the airflow measurements and the temperature measurements.

3.2.2.1 Airflow Measurements

To determine the inputs airflow rates, air velocity measurements at the inlets were carried out using a rotating vane anemometer LC6000 (manufactured by Airflow, 2001, approved to BS EN ISO 9001). It was used to measure both cold and hot airflow rates. It was suitable for most applications where the air stream was large enough, and the air velocity was ranging from 0.25-30m/s. Its resolution at 20°C and 1013mb is better than

±2% for the readings from 5-30 m/s, and ±0.1m/s for the readings between 0.25-4.99 m/s as mentioned in the published manual (Appendix A3.4). To give the best readings, the measurements were taken using a tube of 0.11m in diameter at the entrance of the airflow ducts, where calculations based on airflow rates, like velocity, mass flow rate and heat capacity could be calculated. The inflow rate was within the resolution, of the device approximately, within ± 5.7%, as listed in Appendix A3.4. The overall accuracy was a function of the overall parameters that affect the flow and the instruments used at certain boundaries and the experimental conditions.

3.2.2.2 Temperature Measurements

A total of 21 copper-constantan thermocouples (K-type) were used to measure the temperature distribution in the environmental chamber (figure 3.3.1). A rake of 18 thermocouples was to measure the vertical temperature distribution at the centre of the chamber, while the others were to measure the temperature at the inlets and the outlet openings. The thermocouples were distributed vertically along the chamber height using metal stand. The stand was located in the centre of the chamber in order to capture the temperature gradients in the stratified region. Thermocouples that placed at the inlets and outlets were used for monitoring the inflow and outflow temperatures. All the thermocouples are connected to the data logger by individual channels. The signals received by the data logger are converted into the corresponding temperatures respectively. All the thermocouples have been calibrated and the calibration results are presented in Appendix A3.2. The thermocouples were calibrated against a platinum resistance thermometer. The precision of the measured temperatures (using a K-type thermocouple) was within 1.0 °C, as listed in the published catalogue. The calibration was used at ranges of 10 to 55 °C which brought the estimated uncertainty of type K thermocouple down to ± 2.5% based on the calibration data.

3.3.3 Data Acquisition and Logging

The analog output signals from all of the sensors are received by a data logger (34970A bench link Figure 3.3.3). The data recording system used in this study has taken the data

from all temperature sensors at a rate of one reading per second. The data logger has three building blocks of 60 channels. The system can be plugged into the existing network to send data directly to a personal computer. Signals from all the sensors are analog DC voltages configured on the different output scales for each measurement. For each experiment large amounts of temperature data are generated. The signals sent to the data logger from each sensor are:

- Input hot air temperature
- Input cold air temperature
- Output temperature
- Ambient temperature
- All eighteenth internal temperatures at the thermocouple stand.

Figure 3.3.3 a): The bench link data logger 34970A.

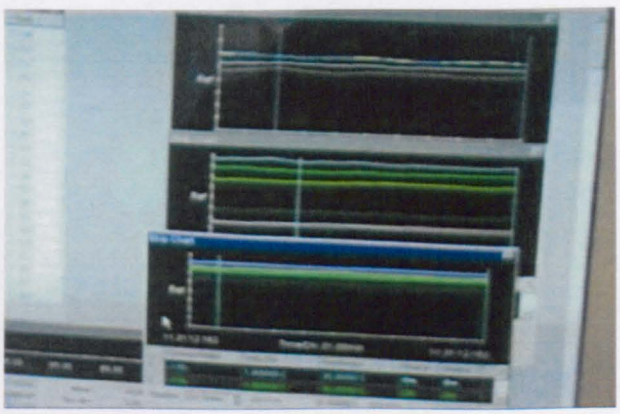

Figure 33.3 b): An isothermal temperature lines as shown on the Strip Chart Window of the bench link data logger software.

The temperature measurements have been monitored and stored in the data logger software. When a scan is started, the instrument scans the data of the required channels. It stores the resulting time-stamped data in a scan record. The data logger obtains scan records from the instruments and logs the data into files of the computer. Each scan record written in the data file consists of the time and the temperature values for the computed channels. The temperature data was written to data files for further

processing. The temperature distribution was estimated by averaging the readings of 5 successive measurements at steady state conditions.

3.4 Measuring Procedures

3.4.1 Theoretical Framework

In practical experiments, the measuring methods are the ways of gathering data obtained correctly. It is based on both analytical background and flow observations. It is used to represent the flow characteristics and reaching the experimental objectives. The measuring methods used in this work were listed:

1. The temperature difference in the vertical direction was measured according to the absolute difference between the temperatures in the top and the bottom of the chamber over the entire air column.
2. The temperature distribution in the vertical direction was measured at several stations along the vertical column (all stations were measured at the centre of the chamber between the inlet and the outlet).
3. Input airflow rates for both cold and hot airflow were measured at the duct entries.
4. The readings were taken at the centre of the environmental chamber, so that the walls would not have any significant effect on the measurements such as mixing and heat transfer.
5. The location of thermocouple stand was varied in both directions along and across the direction of the flow.

3.4.2 Scanning Frequency

There are three important keys affects scanning measurements, the start, the end and the interval of scanning. The default setting was to scan every minute using a 34970A bench link data logger shown in figure (3.3.3 a). The method used was to wait until the system reaches the steady state, then the required number of readings were selected.

During the scanning the preliminary results were observed on the Strip Chart Window for all channels as shown in figure (3.3.3 b). When the system reached the steady state, and the required measurements were obtained, scanning was stopped and the data stored in the Bench link software database to be analyzed and discussed.

At stratified zones the streamlines will be diverge from one another. The distance between these streamlines is a result of stratification, where the temperature profiles are in gradient. At mixed zones the temperature streamlines will be close to one another because the profiles are close to vertical (less stratification). The change of jet speed does not impact only the shape of the profile, but also its position on the temperature scale.

Before each series of tests, the facilities were setup and all instruments calibrated. The holes in the walls were all sealed to eliminate wall leakages as an uncontrolled variable. Profile measurements were made at a number of locations to study the uniformity of the stratified layer in both x-direction and y-directions. The tree locations were adjusted at the middle of the environmental chamber as necessary, to maintain a large clearance from the input and the output where the momentum was too high.

As a result, the stratification profiles presented here implies the temperature conditions in the chamber away from the direct influence of the supply diffusers. The temperature profiles shown are the average of measurements taken with the thermocouple stand at five time steps in the environmental chamber.

Tests were normally run for a long time of 2 hours to achieve steady state. Tests were conducted several times to study the effect of one variable while other variables and conditions were held constant. Temperature values were measured every 60 seconds. The period of scanning (60 seconds) is sufficient to capture the temperature variations, where the test time is so long (2 hours) and the variations are so small. The measured temperature information was automatically recorded to a data acquirement unit. It, automatically, sampled the output from all thermocouples and stored the data on a personal computer connected to the device.

3.4.3 Measuring Stations:

1. In the middle of the environmental chamber, to measure the vertical temperature gradient from 0.2m to 2.8m above the floor (18 points in total). This was done to evaluate the stratified layer characteristics (interface level height, stratified layer thickness, temperature profiles and the degree of stratification).
2. At nine locations in the flow direction (x-axis) and six locations across flow direction. Each station measured the vertical temperature gradient from 0.2m to 2.8m above the floor (18 points in total). This was done to study the influenced length, uniformity of the stratified layer and the validity of measurements in station1.
3. At different inlet and outlet opening heights. Each station measured the vertical temperature gradient from 0.2m to 2.8m above the floor (18 points in total). The measurements were taken to evaluate the effect of these heights on stratified flow. It can be used to destratify the flow by supplying cold air from the top of the chamber and the hot air from the bottom.

3.4.4 Creation of Stratified Flow

Based on the previous reported analytical, numerical and experimental observations in chapter 2, and preliminary experiments, we predicted the following:

- Based on "ASHRAE 62 Standard" developed by the American Society of Heating, Refrigerating, and Air Conditioning Engineers, the specified airflow rates supplied to a room within a building is (15 to 60 CFM/person), depending on the activities that normally occur in that room. Using this guideline and assuming occupancy of (2 to 8 persons), the total typical ventilation rate would be in the range of (0.85 to 13.6 m^3/min)
- From the establishment of zones in stratified flow, stratification takes place at ranges of $0.1 \le \bar{h} \le 0.9$, otherwise, the flow may stratify but without zone establishment. $\bar{h} = \frac{z}{H}$ and z is the height of the temperature sensor (thermocouple) and H is the height of the chamber.

- From the definition of Richardson number (Ri), which is the ratio of potential energy to kinetic energy, the best stratification can occur at large values of temperature difference ΔT and low values of momentum airflow.
- To study the stability of the flow, the flow rate values must cover the ranges of Richardson numbers based on the input conditions (airflow rates and temperatures) ranging (from 0.08 to Max.), and indicate the stability and the type of the stratified flow.
- Stratification interface level height, stratified layer thickness and stability of the stratified flow must be studied at full ranges of opening heights ranging (from 0.5m to 2.0m).

According to the above specifications, following are the design sets of experiments. The technique used to evaluate the stratified flow characteristics was air modelling. Four sets of experiments were carried out. Both cold and hot airflow rates were entered at different inputs and outputs heights. Cold air was entered at the bottom of the environmental chamber with five different values whilst the hot airflow was entered the top of the chamber with five different values. Both hot and cold airflow were supplied using rectangular diffusers of 0.5 x 0.5 m for hot air and 1.0 x 0.5 m for cold air. The diffusers help in admitting the flow with minimum disturbance to establish the stratification in the flow and maintain the stratified layer. The experimental data must give the indication of the stratified flow characteristics such as stratified layer interface level height, stratified layer thickness, degree of stratification and stability.

The first set of experiments was to study the distribution of the thermal stratified layer in the whole space. This was done through the moving of thermocouple stand in both directions along and across the flow. Experiments were carried out for many inflow rate at certain inlet and outlet heights. The purposes of this set of experiment are:

- To study the symmetry of the stratified layer in both directions along and across the flow direction.
- To study the effect of walls on the stratified flow, where both heat transfer and disturbances were high compared with that at the centre of the chamber.
- To study the stratified layer near the openings, where both temperature difference and momentum were varied.

- To estimate the approximate shape of the stratified region to be used in analytical solutions.
- To validate the measurements obtained at the centre of the chamber, where the stand was located.

These purposes were supported by [Howell and Potts, (2002)]. They mentioned that most of the predictive techniques neglected both thermal radiation and diffusion as mechanisms of thermal transport. [Howell and Potts, (2002)] come to this conclusion, for large spaces it has an insignificant effect on the temperature stratification at steady state conditions.

The second set of experiments was to study the effect of input airflow rate on stratified flow characteristics. Both input and exhaust heights were fixed, while the hot airflow rates were varied. These experiments were carried out for hot airflow rates from 1.0 ~ $5.0\,m^3/min$ at 45°C, and cold airflow rates from 0.0 ~ $8.0\,m^3/min$ at the ambient temperature. The purposes of this set of experiments were:

- To study the effect of both hot and cold airflow rates on the stratified flow characteristics.
- To classify the stratified flow characteristics by the inputs airflow rates.

The third set of experiments was to study the effect of input hot airflow height on stratified flow. Both cold airflow and the exhaust heights were fixed, while the hot airflow height was varied. This was done for four different heights 1.0, 1.5, 2.0m. The hot air supply was then activated to produce stratification. These experiments were carried out for hot airflow rates from 1.0 ~ $5.0\,m^3/min$ at 45°C, and cold airflow rates from 0.0 ~ $8.0\,m^3/min$ at the ambient temperature. The purposes of this set of experiments were:

- To study the effect of input height on the stratified flow characteristics.
- To study the effect of both hot and cold airflow rates on the stratified flow characteristics in the presence of various input heights..

The fourth set of experiments was to study the effect of exhaust height on stratified flow. It was similar to the third set, except that both hot and the cold airflow heights were fixed at certain heights, while the exhaust height was varied for five different

heights 0.5, 1.0, 1.5, 2.0, and 2.5 m. The hot air temperature for this case is 45°C and the experiments were carried out for hot airflow rates of 1.0 to 5.0 m^3/min. The cold inflow temperature for this case was the ambient and the experiments were carried out for cold airflow rates of 0.0 to 8.0 m^3/min. The purposes of this set of experiments were:

- To study the effect of exhaust height on the stratified flow characteristics and contaminant removal.
- To study the effect of both hot and cold airflow rates on the stratified flow at various exhaust heights.
- To evaluate the best exhaust height be used in ventilation applications.

3.4.5 Mixing of Stratified Flow

In the first part of this work, laboratory experiments were done to investigate the effect of jet flow on the stratified flow characteristics. The experiments were performed in the same setup described in the previous section 3.3. The new experiments were presented using both cold and warm air jet flow. The jet of 0.11m diameter was used to inject air vertically downward to destroy the stratified layer or flow through it. The injected momentum was increased gradually by increasing the jet speeds from (0.0 ~ 15.0m/s). The injected air has an efficient momentum to disturb the surrounding air, and hence the temperature distribution in the environmental chamber. With combined effects of buoyancy and momentum, the degree of stratification and the flow characteristics are being a complement of both the buoyancy and the momentum of injected flow. The experiments were done over various degree of stratification (weak, intermediate and strong stratification). During the experiments the position of the interface and the motion through the layers were monitored visually.

The jet is located at the center of the chamber to minimize the effect of sidewalls on the determination of the amount of entrainment. A separate rotational fan was used to supply the jet with both hot and cold airflow. The 0.11 m diameter nozzle was directed vertically, and supplies the air with an adjustable flow rate. It is possible to go from the stratified case to the mixed case by changing jet airflow rate, thus changing the relative

magnitudes of the buoyancy and momentum fluxes. The thermocouples were vertically distributed on the stand. The stand was located in the middle of the chamber in order to capture the temperature gradients in the stratified region. A data logger was interfaced to a personal computer to collect the flow of temperature signals arriving from the test chamber. Pictures were recorded onto a videotape and simultaneously to computer hard disk.

To study the behavior of the stratified flow characteristics under the effect of jet momentum airflow, wide temperature and smoke visualisation images were taken besides the quantitative and qualitative measurements for both stratified and mixed flow.

The experiments were performed according to the following procedure:

When a steady state is reached and a stratified layer is established between the upper and the clear lower zones, the source of momentum (the jet) located at the center of the chamber is turned on. Whiles the injected air is increased, the stratified layer starts to translate up or downward depends on the initial situation of stratification and the amount of momentum. The experiments are done for both cold and warm jet flow according to the test matrix showing in table (3.4.1).

Jet Type	Q_{hot} (m^3 / min)	Q_{cold} (m^3 / min)		
Cold Jet	**1.0**	**2.0**	**4.0**	**6.0**
=	**2.0**	**2.0**	**4.0**	**6.0**
=	**3.0**	**2.0**	**4.0**	**6.0**
Warm Jet	**1.0**	**2.0**	**4.0**	**6.0**
=	**2.0**	**2.0**	**4.0**	**6.0**
=	**3.0**	**2.0**	**4.0**	**6.0**

Table 3.4.1: Details of experimental tests used to mix the stratified layer of hot and cold airflow rates listed in the table with a resolution of ±5.7%. For each test, the jet speed was increased gradually from (0.0 ~ 15.0 m/s).

For the sequence of jet experiments, the only parameter was changed from one run to the next was the flow rate, whilst during the run the jet speed was changed gradually in

the ranges from 0.0 to15 m/s. The thermocouple readings were taken every 10 seconds. The criterion used to reach a steady state condition was based on 0.2 °C variations.

A last set of experiments is done to study the stratified flow characteristics and the usage of the inversion technique to destroy the stratified layer and mix the flow. It is used to investigate the mixing process that takes place inside the environmental chamber and the growth of the mixed layers. This can be done by the inversion of input airflow suppliers. In this case, the buoyant cold layer in the lower zone will loose its buoyancy forces while being heated with the hot airflow penetrated at lower levels in the environmental chamber.

The temperature and smoke visualisation is carried out. Two cases of relatively strong stratification are studied using the experimental set-up presented in this chapter. The purpose of this technique is to remove the polluted and hot gases from the occupied zone and to mix the air to a reasonably uniform temperature, yet satisfying the requirements of comfort. This type of experiment must be done after complete stratification to investigate the effect of inversion of air suppliers on the stratified flow. The experiments were carried out for 2 to $6\,m^3/min$ cold airflow rates and 1 to $3\,m^3/min$ hot airflow rates.

3.5 Smoke Visualization

Smoke visualisation was used as an easy method to display the results in simple form being to the human observer. Smoke, as a form of pollutant source was presented by introducing the smoke into the environmental chamber using smoke generator unit photographed in figure (3.5.1). Photographic flow visualisation records were also prepared using digital camera with default shutter speed. A series of visualisation tests were conducted using the smoking unit. The tests were to study the stratification flow characteristics such as thickness, interface level height, and degree of stratification.

The maximum heater voltage of the unit is limited by 25 volts, while the oil flow rate is adjusted by 10 steps. The oil flow rate and heater voltage were adjusted to suit prevailing conditions as necessary. The smoke device produces a non-toxic, non-corrosive, dense white smoke suitable for observation and photography. Oil was heated

inside the smoke machine. An electrical resistance heated the oil to introduce a vapor of small visible particles. As there is no entraining gas, the smoke exit velocity is due only to effects of thermal expansion.

The recommended oil is Shell "Ondina EL" or its exact equivalent. It is medicinal quality white oil approved for use in environmental applications. The thermal and chemical specifications of the oil are listed below (See Appendix A3.3):

Specific Gravity	**0.86 at 20 °C.**
Viscosity	**14.3 centistokes at 40 °C**
Flash Point	**159 °C**
Auto-ignition Temp	**Above 250 °C**
Combustibility	**as for hydrocarbons with this flash point**
Extinguishing Media	**CO2, dry chemical powder or foam**

The smoke was initiated with high momentum and exhibited turbulent mixing. It mixed with the air through the lower zone at the centre of the environmental chamber. On reaching the interface level height, the smoke started to spread out steadily along the interface in the stratified region, where it was seen easily in this case.

Figure (3.5.2) shows a real view of stratified flow. During the experiments, the smoke was seen ascending and coming to rest in a stratified region to form a layer of certain thickness. This thickness was dependent on flow parameters. After that the smoke was evacuated through the exhaust opening.

Figure 3.5.1: A photograph of smoking machine used to penetrate smoke for visualisation.

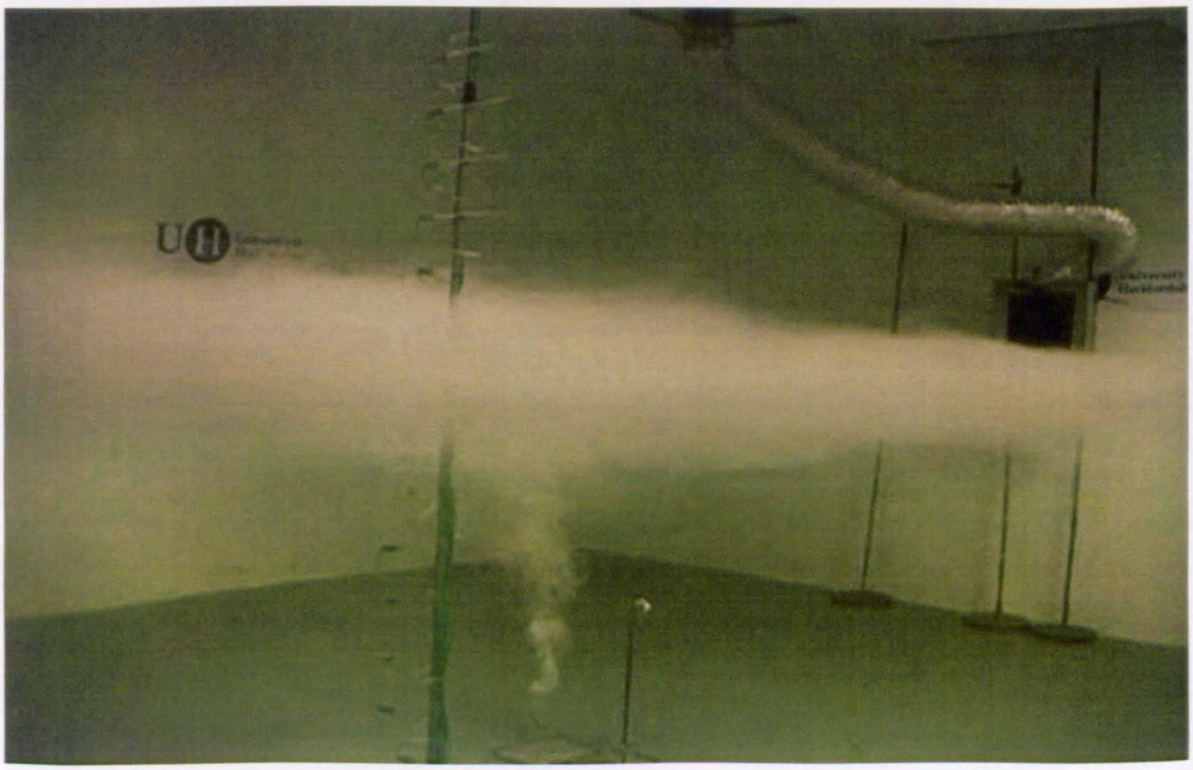

Figure 3.5.2: A video-recorded picture of stratified flow induced by smoke rise in the environmental chamber at steady state conditions.

Chapter 4

Effect of Ventilation Aperture Location and Inflow outflow Rate on the Stratified Flow

---

4.1 Introduction

4.1.1 Experimental Conditions (Test Matrix)

It was necessary to plan several scenarios of tests that cover a wide range of flow rates, at different input and output heights. The test sequences for the experiments are shown in Tables 4.1.1, 4.1.2 and 4.1.3. These test matrices were designed to take optimum advantages of the stratified flow conditions. The airflow rates are based on "ASHRAE 62 Standard", where the specified airflow rates supplied to a room within a building is (15 to 60 ft^3/min/person), depending on the activities that normally occur in that room. Using this guideline and assuming occupancy of (2 to 8 persons), the total typical ventilation rate would be in the range of (0.85 to 13.6 m^3/min).

Measuring locations along the direction of the flow (X-axis) in m								
0.75	1.50	2.25	3.00	3.75	4.50	5.25	6.00	6.75
Measuring locations across the direction of the flow (Y-axis) in m								
0.80	1.60	2.40	3.20	4.00	4.80			

Table 4.1.1: Details of experimental trials for fifteen experimental tests included the studied locations: nine locations were along the direction of the flow, and six locations were across the direction of the flow.

H_{exit}(m)	H_{hot} (m)	Q_{hot}(m^3 / min)	Q_{cold} (m^3 / min)				
1.5	2.0	1.0	0.0	2.0	4.0	6.0	8.0
=	=	2.0	0.0	2.0	4.0	6.0	8.0
=	=	3.0	0.0	2.0	4.0	6.0	8.0
=	=	4.0	0.0	2.0	4.0	6.0	8.0
=	=	5.0	0.0	2.0	4.0	6.0	8.0
=	1.5	1.0	0.0	2.0	4.0	6.0	8.0
=	=	2.0	0.0	2.0	4.0	6.0	8.0
=	=	3.0	0.0	2.0	4.0	6.0	8.0
=	=	4.0	0.0	2.0	4.0	6.0	8.0
=	=	5.0	0.0	2.0	4.0	6.0	8.0
=	1.0	1.0	0.0	2.0	4.0	6.0	8.0
=	=	2.0	0.0	2.0	4.0	6.0	8.0
=	=	3.0	0.0	2.0	4.0	6.0	8.0
=	=	4.0	0.0	2.0	4.0	6.0	8.0
=	=	5.0	0.0	2.0	4.0	6.0	8.0

Table 4.1.2: Details of experimental trials for a number of experimental tests included the studied flow parameters in the environmental chamber, and the runs in which the release mechanisms and measurement setup were tested. The tests were for variable input heights. The measurements of air flow rate are within a resolution of ±5.7%.

To analyse the data, ranges of input output airflow rates are classified into three levels. Table 4.1.4 shows the ranges of hot and cold airflow rates related to the level of flow (low, moderate and high). The calculations were based on, hot air diffuser area of 0.25 m^2 and cold air diffuser area of 0.50 m^2.

H_{hot}(m)	H_{exit}(m)	Q_{hot}(m^3/min)	Q_{cold} (m^3/min)				
2.0	2.5	1.0	0.0	2.0	4.0	6.0	8.0
=	=	2.0	0.0	2.0	4.0	6.0	8.0
=	=	3.0	0.0	2.0	4.0	6.0	8.0
=	=	4.0	0.0	2.0	4.0	6.0	8.0
=	=	5.0	0.0	2.0	4.0	6.0	8.0
=	2.0	1.0	0.0	2.0	4.0	6.0	8.0
=	=	2.0	0.0	2.0	4.0	6.0	8.0
=	=	3.0	0.0	2.0	4.0	6.0	8.0
=	=	4.0	0.0	2.0	4.0	6.0	8.0
=	=	5.0	0.0	2.0	4.0	6.0	8.0
=	1.5	1.0	0.0	2.0	4.0	6.0	8.0
=	=	2.0	0.0	2.0	4.0	6.0	8.0
=	=	3.0	0.0	2.0	4.0	6.0	8.0
=	=	4.0	0.0	2.0	4.0	6.0	8.0
=	=	5.0	0.0	2.0	4.0	6.0	8.0
=	1.0	1.0	0.0	2.0	4.0	6.0	8.0
=	=	2.0	0.0	2.0	4.0	6.0	8.0
=	=	3.0	0.0	2.0	4.0	6.0	8.0
=	=	4.0	0.0	2.0	4.0	6.0	8.0
=	=	5.0	0.0	2.0	4.0	6.0	8.0

Table 4.1.3: Details of experimental trials for a number of experimental tests included the studied flow parameters in the chamber, and the runs in which the release mechanisms and measurement setup were tested. The tests were for variable exhaust heights. The measurements of air flow rate are within a resolution of ±5.7%.

Type of flow\Class of flow	Low	Moderate	High
Cold airflow rate, m^3/min	0.0, 2.0	4.0, 6.0	8.0, 10.0
Hot airflow rate, m^3/min	0.0, 1.0	2.0, 3.0	4.0, 5.0

Table 4.1.4: shows the ranges of hot and cold airflow rates that be classified into three classis low, moderate and high. The calculations were based on, hot air diffuser area of 0.25 m^2 and cold air diffuser area of 0.50 m^2. The measurements of air flow rate are within a resolution of ±5.7%.

4.1.2 Preliminary Experiments

A number of preliminary experiments were carried out to test the experimental set-up. The first round of results allowed us to approximate the flow parameters that influence the stratified flow and the experimental set up. It provides an additional recalibration to reduce the errors that may occur during the experiments.

Figures 4.1.1 to 4.1.3 display a number of representative data. Figure 4.1.1 shows steady state results of temperature distribution at the thermocouple stand with different values of cold airflow rates $Q_c = 0, 2, 4, 6, 8\,m^3/min$ and fixed moderate hot air flow rate $3\,m^3/min$. The results give an indication of the stratified flow characteristics such as stratified layer interface level height, stratified layer thickness and degree of stratification defined by h, δ and DS respectively.

Figure 4.1.2 shows the results of vertical temperature profile in dimensionless form with the dimensionless height at moderate hot air flow rate $2\,m^3/min$, and moderate cold airflow rate $4.0\,m^3/min$. The results are for steady state conditions ($dT/dt \approx 0$) and higher degree of stratification DS= 4.0. The phenomenon of stratification and the stratified flow characteristics are observed clearly.

.

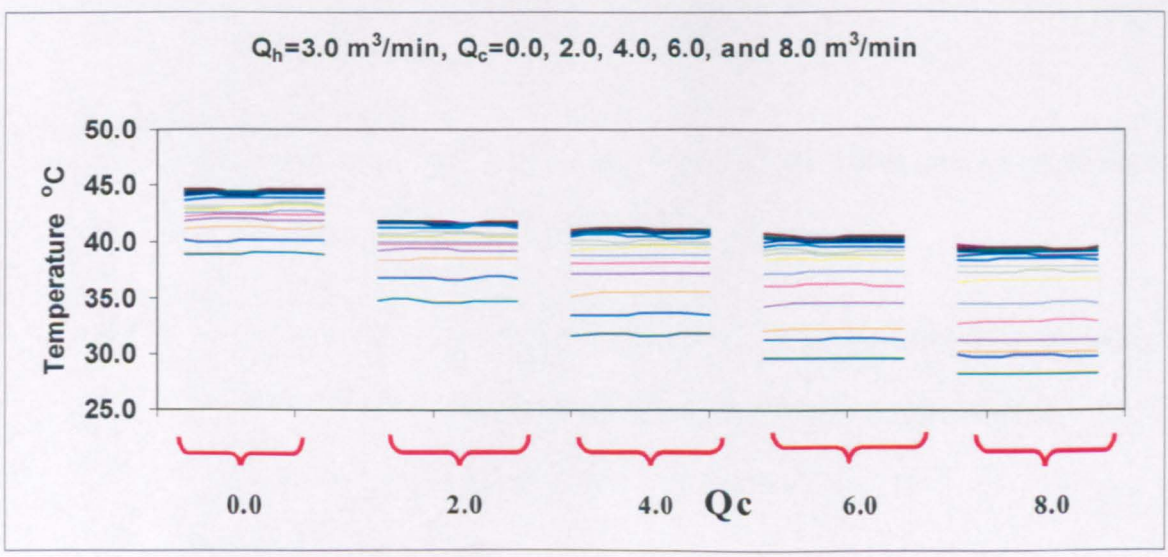

Figure 4.1.1: Temperature distribution across the chamber at a fixed axial location of (3.75, 2.8) m of ($Q_h = 3.0\,m^3/min$) for different cold flow rates ($Q_c = 0, 2, 4, 6, 8\,m^3/min$) at fixed input and output heights of (2.0 and 1.5) m in the environmental chamber.

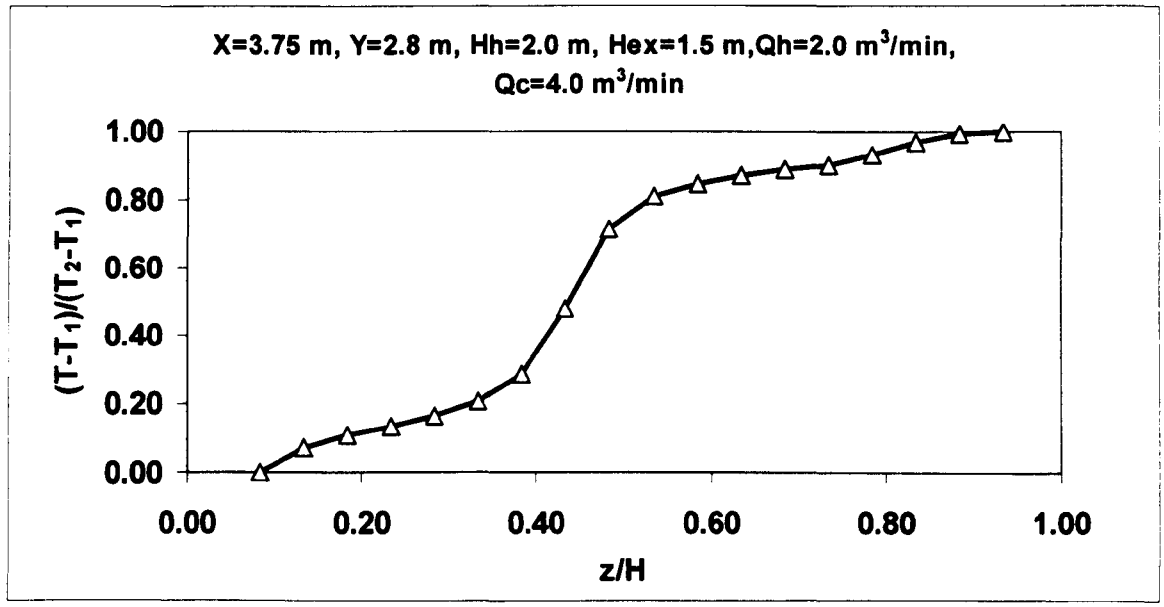

Figure 4.1.2: Dimensionless temperature profile along vertical centreline with dimensionless height across the chamber at a fixed axial location of (3.75, 2.8) m, ($Q_h = 2.0\,m^3/min$) and ($Q_c = 4.0\,m^3/min$) for different temperature readings of 1min time step.

The results shown in Figure 4.1.3 are the vertical temperature profile in dimensionless form with dimensionless height for different values of cold airflow rates. The preliminary analysis shows the effect of increase in cold airflow rate on the stratified flow characteristics. It increases the stratified layer interface level height (h) and the degree of stratification until it reaches the peak value of DS=4.0 at $Q_c = 4.0\,m^3/min$, it decreases the stratified layer thickness

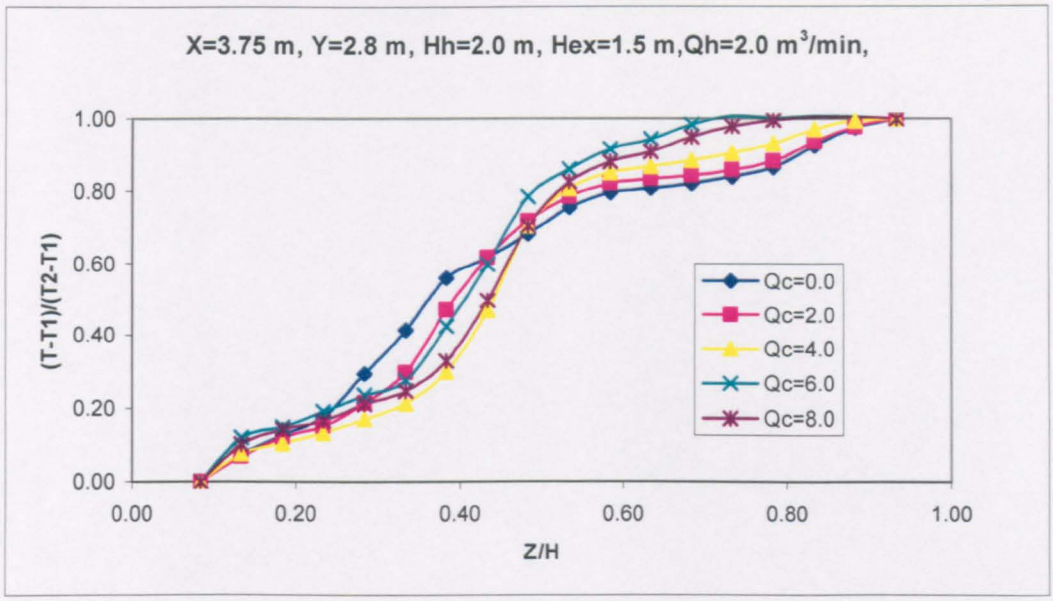

Figure 4.1.3: Dimensionless temperature profile along vertical centreline with dimensionless height across the chamber at a fixed axial location of (3.75, 2.8) m and fixed hot air flow rate ($Q_h = 2.0 m^3/min$) for different cold flow rates ($Q_c = 0, 2, 4, 6, 8 m^3/min$) in the environmental chamber.

4.2 Smoke Visualisation

The distribution of contaminants in workrooms is dependent on both clean-air volumetric flow rates and the characteristics of the contaminants, [Raisanen and Niemela (1997)]. Contaminants in the environmental chamber are introduced as a smoke in the lower zone. The smoke rises until it reaches the stratified layer interface level height h. Then it starts to spread horizontally at the level of this height. A digital camera was used to take pictures of the smoke flow visualisation under steady state conditions. The flow visualisation photographs displayed in Figures 4.2.2 to 4.2.8 correspond to the experimental test matrix (i.e. tables 4.1.1 to 4.1.3). The figures show the results in a clear and simple form.

Figure 4.2.1 shows the variations of isothermal temperature lines with time for input airflow height $H_h = 2.0$ m, exhaust height $H_{ext} = 1.5$ m, hot airflow rate $Q_h = 2.0 m^3/min$ and cold airflow rate $Q_c = 8.0 m^3/min$ at steady state conditions as obtained from thermocouple readings ($dT/dt \approx 0$). For this test case, Figure 4.2.2 shows the same results. The figure visualises the stratified layer thickness δ and interface level height h.

The smoke visualisation shows the location of the stratified layer, and at a Ri =27 and $dT/dz = 3.25\ ^{\circ}C/m$, it confirms that there are stable conditions as the smoke does not move.

Comparison between these Figures 4.2.1 and 4.2.2 shows the agreement between these different techniques, the validity of the experimental results, and the validity of smoke visualisation to investigate the stratified flow characteristics. Analysing stratified flow using temperature profiles or smoke flow gives the same results in terms of δ, h and dT/dz, the advantages of smoke visualisation are listed below:

- Gives an approximate shape for the stratified layer in the whole space.
- Gives the indications for the stratified flow characteristics at all points in chamber while the temperature isothermal lines give these indications at the stand location.
- Could be used to indicate the type and velocity of the flow, the diffusion between the zones, the particles movement and so the convection through the stratified layer.

While the temperature gradient dT/dz is always positive and reaches its maximum values across the stratified layer boundaries, the concentration of smoke should be in the stratified layer. It is in agreement with [Mundt (1995)] who conducted both temperature and contaminant profiles in ventilated room, where the results showed that the contaminants has been concentrated somewhere in the middle of the room, where the source of heat was located and the higher temperature gradient was evaluated.

Figures, 4.2.3 to 4.2.6 show smoke visualisation for two values of hot airflow rates $Q_h = 1$ and $2\ m^3/min$ and four different values of cold air flow rates $Q_c = 2, 4, 6$ and $8 m^3/min$. The smoke concentration gives an indication of the effect of cold airflow rates with increasing h, δ and dT/dz. The flow streamlines of penetrated smoke in lower and upper zones give an indication to the momentum forces and the amount of mixing in each zone.

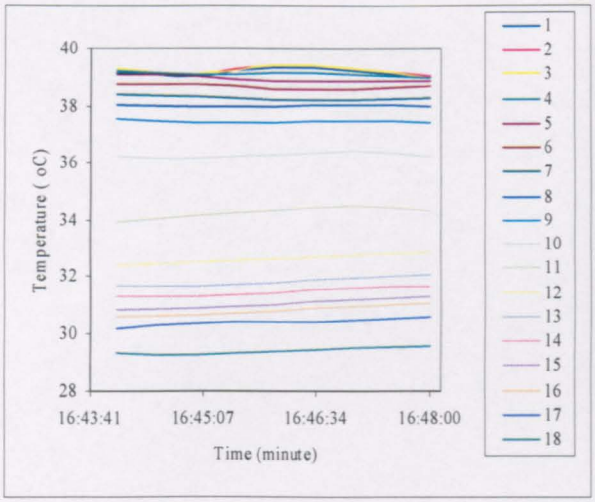

Figure 4.2.1: The temperature lines, at the 18th thermocouples stand, for $Q_h = 2.0\,m^3/min$ and $Q_c = 8.0\,m^3/min$, DS = 6.7.

Figure 4.2.2: A video-recorded picture showing stratification induced by smoke visualization, for $Q_h = 2.0\,m^3/min$ and $Q_c = 8.0\,m^3/min$, DS = 6.7.

From smoke visualisation shown in the Figures 4.2.3 and 4.2.4, it is seen that increasing the cold airflow rates (from $Q_c = 2\,m^3/min$ to $Q_c = 4\,m^3/min$ at fixed low hot airflow rate ($Q_h = 1\,m^3/min$) leads to an increase of δ, due to contrary changes in momentum and buoyancy forces. The overall Ri changes from 200 to 75 and the Re changes from 7000 to 14000. Comparison between Figures 4.2.3 and 4.2.4 shows that the stratified layer across the direction of the flow (Figure 4.2.3) is more uniform compare to the stratified layer along the direction of the flow (Figure 4.2.4), where the momentum fluxes is higher(Re=14000) and buoyancy fluxes is lower (Ri=75) .

Figures 4.2.3 shows a visible jet flow above the source of smoke, which is due to the vertical momentum of smoke flow issuing from the smoking machine. This jet causes an entrainment of buoyant smoke above the stratified layer. Locally, this causes an increase in the smoke layer thickness due to relatively high density of smoke above the interface

From smoke visualisation shown in Figures 4.2.5 and 4.2.6, increasing the cold airflow rate from intermediate to comparatively higher values (6.0 to $8\,m^3/min$) at fixed hot airflow rate of ($Q_h = 2\,m^3/min$) leads to decrease the smoke concentration, and the

smoke layer thickness, due to the increase in momentum (the overall Re increases from 19000 to 24000).

Figure 4.2.3: A video-recorded picture showing stratification induced by smoke visualization, across the direction of the flow for $H_h = 2.0\,m$, $H_{ext} = 1.5\,m$, $Q_h = 1.0\,m^3/min$ and $Q_c = 2.0\,m^3/min$, Ri ~ 200 , Re ~ 7000 and ΔT= 4.8 °C) .

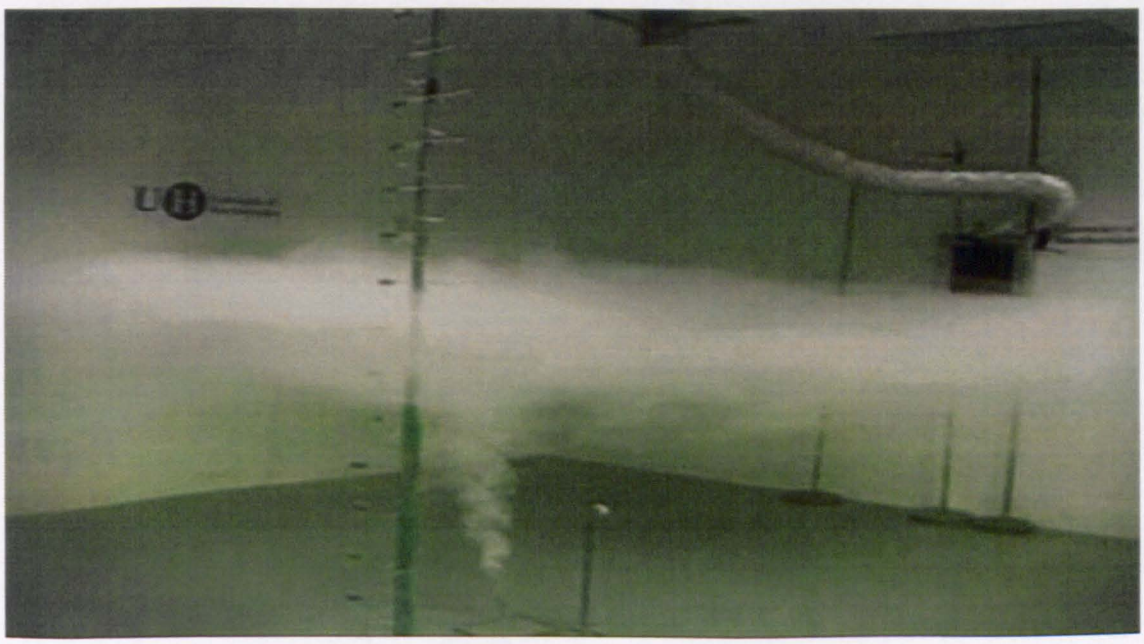

Figure 4.2.4: A video-recorded picture showing stratification induced by smoke visualization, along the direction of the flow for $H_h = 2.0\,m$, $H_{ext} = 1.5\,m$, $Q_h = 1.0\,m^3/min$ and $Q_c = 4.0\,m^3/min$, Ri ~ 75 , Re ~ 14000, and ΔT= 6.68 °C.

Figure 4.2.5: A video-recorded picture showing stratification induced by smoke visualization, for $H_h = 2.0\,m$, $H_{ext} = 1.5m$, $Q_h = 2.0\,m^3/min$ and $Q_c = 6.0\,m^3/min$, at steady state conditions, Ri ~ 133 , Re ~ 19000, ΔT= 11.9 °C, DS=3.4.

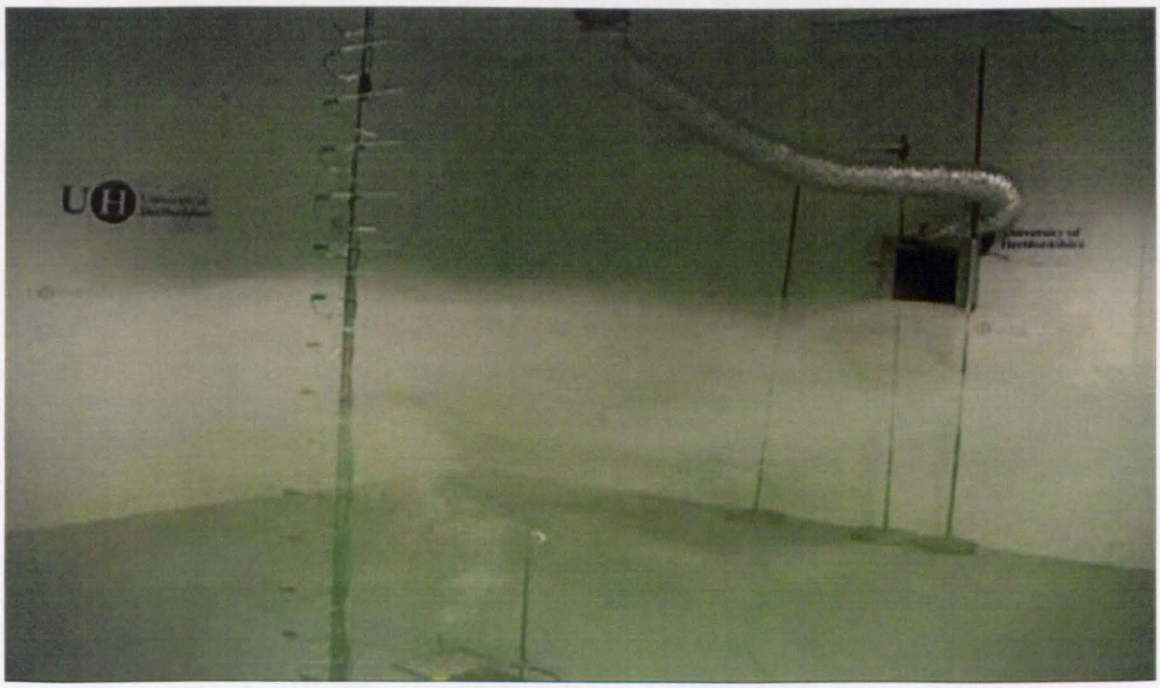

Figure 4.2.6 A video-recorded picture showing stratification induced by smoke visualization, for $H_h = 2.0m$, $H_{ext} = 1.5m$, $Q_h = 2.0\,m^3/min$ and $Q_c = 8.0\,m^3/min$, at steady state conditions, Ri ~ 27 , Re ~ 24000 and ΔT= 9.76 °C, DS=3.27.

Figures 4.2.3 to 4.2.6 gives an indication of the combined effect of increasing hot and cold airflow rates ($Q_h = 1$ *to* $2\,m^3/\min$) and ($Q_c = 2$ *to* $8\,m^3/\min$).

- The smoke visualisation in Figures 4.2.3 and 4.2.5 show an increase in the smoke layer thickness, it confirms the increase in the stratified layer thickness δ as the smoke layer thickness is increased. As discussed earlier, it is due to the decrease of buoyancy to momentum ratio (Ri/Re) despite the increase in temperature difference ΔT, where the flow is changed from relatively low to relatively moderate airflow. The comparative momentum fluxes are higher (Re=19000) and buoyancy fluxes are lower (Ri=133).
- At the same manner, from the smoke visualisation shown in Figures 4.2.4 and 4.2.6, the increase in both input airflow rates (hot and cold) decreases the degree of stratification and increases smoke layer thickness. It is due to the decrease in buoyancy to momentum ratio Ri/Re despite the increase in ΔT, where the flow is translated from relatively moderate to relatively high airflow.

Figures 4.2.3 to 4.2.6 represent video-recorded pictures for different tests conditions. The video-recorded pictures display the results in simple form. The results demonstrate [Skistad (1998)] suggestion, where the relatively small amount of smoke has a very large effect on the results.

Figure 4.2.7: A video-recorded picture for the upper zone of stratified flow induced by smoke rise at steady state conditions.

Figure 4.2.8: A video-recorded picture for the lower zone stratified flow induced by smoke rise at steady state conditions.

From Figures 4.2.7 and 4.2.8, the stratified region is classified by three zones, with respect to smoke visualisation.

- Above the stratified layer there is a smoke free zone. If the source of smoke is close to the stratified layer interface or already exceeded, the smoke penetrates into the upper zone and go upward to reach the ceiling, as shown in Figure 4.2.7. Despite of penetration into the upper zone the flow remains stratified.
- A stratified layer of interface level height, stratified layer thickness and degree of stratification depend on the parameters affecting the flow. It can consider as a thermal barrier that decelerates the smoke penetration and increases both, the temperature in the upper zone, and the smoke concentration along the interface. In this case exhaust openings should be at the level of stratification where smoke is concentrated.
- Below the stratified layer there is a smoke free zone. This zone is free from smoke hazards as shown in Figure 4.2.8. It should be taken in consideration especially for tunnels and buildings designs, where stratified flow is important in fire control and smoke management.

At the source of smoke, as the smoke develops from ignition, oil and entrained air rise as a buoyant flux over the source of smoke release. During penetration of smoke, ambient conditions begin to affect the smoke, and relatively cool ambient air is entrained with the plume gases to decrease the temperature of the smoke, [Qin et al (2006)]. The smoke velocity of the upper part decreases due to the decrease in the buoyancy forces and heat losses, [Lee and Ryou (2005)]. The warm smoke would initially have lower density than the surrounding. It continues to rise freely until it becomes as cool (as dense) as the surrounding air. Once it reaches this stage of equilibrium at which its temperature equals that of the surrounding environment.

In the presence of stratification, while the buoyancy and momentum forces cause the smoke to flow in the downstream direction, the stratification deflects the upward smoke motion by entrainment of ambient air. The primary variables characterizing a smoke penetration are the smoke characteristics and the stratification characteristics. The smoke characteristics like the kinematic buoyancy and momentum are comparable with the stratification characteristics like the strength and interface level height of the

stratified layer. Depending on these parameters, the smoke motion exhibited a range of behaviors:

Case 1: When the stratified layer interface level height, is much less than the smoke penetration height. In this case, the smoke reaches the stratified layer before loosing its buoyancy force, so it will go through the stratified layer to stratify at the level of neutral buoyancy. In this case, strong stratified layer can work as a thermal barrier against the smoke penetration due to the higher temperature gradient in the stratified layer and the entrainment of hot air. While the smoke buoyancy flux above this level being negative, the smoke will then descend back towards the stratified layer height and to stratify horizontally at the level of stratification, with a bulb shape as shown in Figure 4.2.4.

Case 2: when stratified layer interface level height is much greater than the smoke penetration height. In this case, the increase in the volumetric flux due to the entrainment of cold air will decrease the reduced gravity in order to preserve the conservation of buoyancy flux. Therefore the smoke will reach its neutral buoyancy before reaching the stratified layer, and start to stratify at a height of neutral buoyancy rather than the interface level height. In this case, [Lee and Ryou (2005)] considered the smoke interface height would be a position of a zero velocity.

Case 3: when the smoke penetration height is at the level of stratification. In this case, the smoke temperature equals that of the surrounding environment (have equal densities), the buoyancy of the smoke is zero, and the neutral buoyancy height is at the level of stratification. In which, the smoke will stratify at the neutral buoyancy height without significant effect for the stratified layer height.

The stratified flow can be characterized by Reynolds number Re, which represents the importance of the inertial forces to the viscous forces, the Grashof number Gr, which represents the importance of the buoyancy forces to the viscous forces and the Richardson number Ri which represents the importance of the buoyancy forces to the inertial forces.

A series of visualisation tests using Aero-tech™ smoke machine were recorded. It displays the results in a clear and simple form.

4.3 Tests Conditions

The study of stratified flow characteristics as a function of time and space (locations) with the other parameters such as airflow rate, input and output vertical locations can be used for ventilation purposes, where the time, height and spacing variations of the built environment are significant.

4.3.1 Time Variations of Temperature

Creation of stratified flow takes a considerable time. After the chamber heating system is on, one should allow sufficient time for the temperature to stabilize, particularly if the chamber has been at ambient temperature. Since a data logger is installed in the chamber, the temperature is continuously monitored. All the measurements were taken at steady state conditions. The time needed to reach this condition varied from experiment to experiment. It depends, mainly, on the weather fluctuations, measuring situations and flow conditions. The typical time to reach steady state in our case was about (2-hours).

To display the variation of stratified flow as a function of time, Figure 4.3.1 shows the relations between the temperature isothermal lines and the time variations for a specific period of time (140 minutes). A steady (isothermal) temperature lines are shown in Figure 4.3.1. It shows the measuring temperatures of thermocouples on the stand as time advances. Figure 4.3.1 shows the changes of the typical temperature distribution with time.

As can be seen in the figure, the changes in temperature are visible near the top and bottom of the chamber, and non visible in between. Over a period of time (90 minutes from 16:20 to 17:50), it can be shown that the isothermal line degradation $dT/dt = Min$. The changes were large near the ceiling and the floor due to heat transfer, heat loss to the ambient, thermal radiation and mixing. The observed changes are too small compared with the accuracy in the temperature measurements of 2.5%. From the observations it is seen that a steady state condition ($dT/dt \approx 0$) is reached after 2 hours.

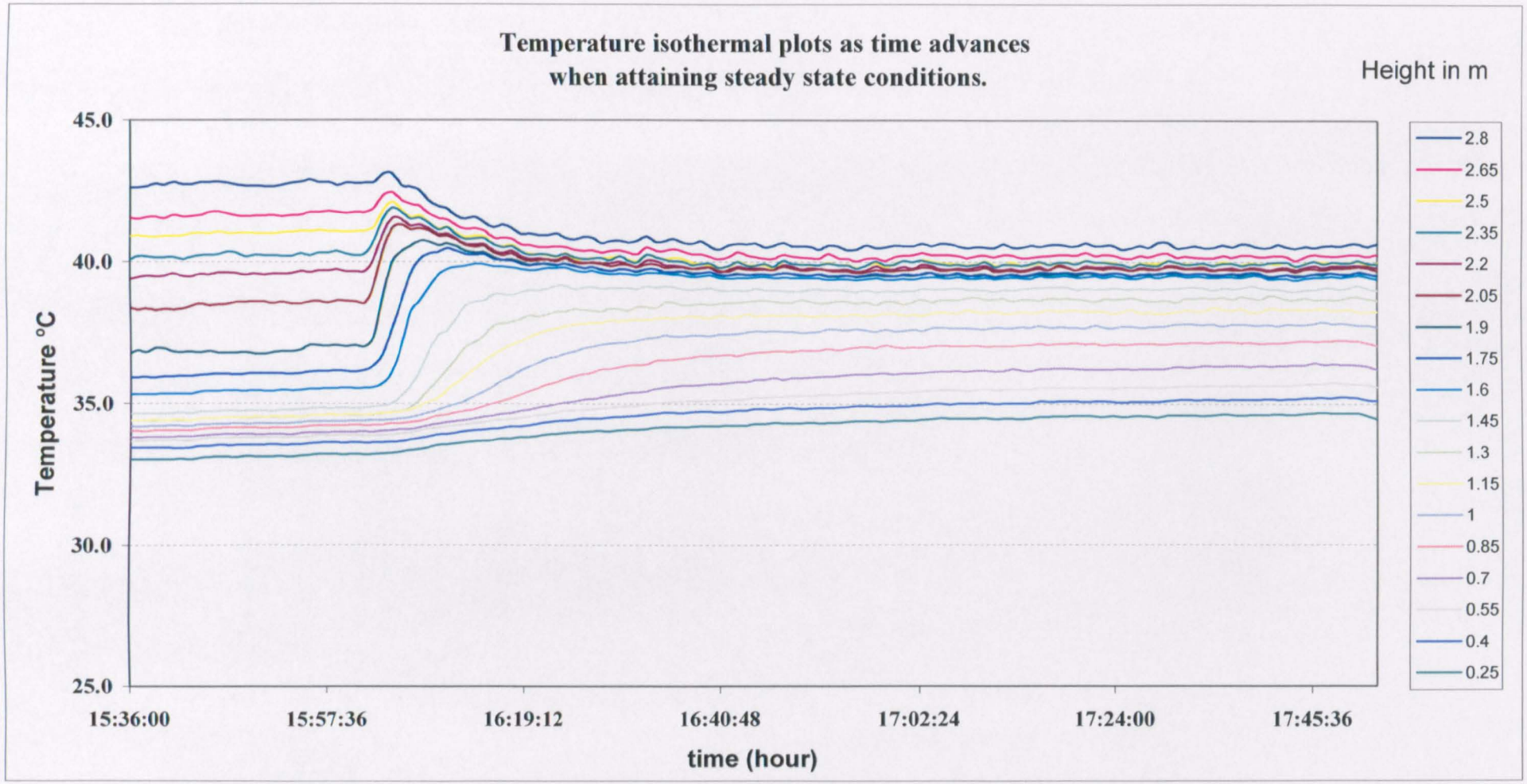

Figure 4.3.1: gives an isothermal temperature lines as time advances when attaining steady state conditions.

The variations of vertical temperature profiles for long period of time (10 hours) under the effect of increasing airflow rates are shown in Figure 4.3.2. The first three curves in Figure 4.3.2 show the initial vertical potential temperature profile, whereas the sequence curves illustrate the monitory reordered potential temperature profile. Figure 4.3.2 shows all the temperature profiles from mid of the day to the mid of the night, successively offset by 2 °C to see how the depth of the layers varies with time. The temperature profiles close to the walls show small fluctuations that resulted from velocity disturbances and local heat transfer by the walls. While every single profile from this sequence is only representative of the temperature at the given time, the formation of the stratified flow shown in the figure was achieved through the following stages:

1. Before activating airflow rate (before 12:00:46), the flow is steady and fully mixed, where the vertical temperature profile is always uniform ($dT/dt \approx 0$ and $dT/dz \approx 0$).
2. For the period of (12:00:46 to 14:15:46), while the hot airflow was on and the cold air flow was of the flow started to stratify in the upper zone $dT/dz \succ 0$. In the lower zone the flow was fully mixed $dT/dz \approx 0$, while the stratified layer was yet to be established.
3. For the period of (14:15:46 to 16:00:46), a stratified layer has appeared in the upper zone, and started to translate downwards. The temperature profile in the lower zone is approximately linear i.e. $dT/dz \approx 0\ ^\circ C/m$.
4. Further time step of 15 minutes at time (16:15:46), a dynamical significance full-scale stratified layer was formed with (h=1.0 m, δ=0.6 m and $dT/d\delta = 8\ ^\circ C/m$). Both vertical temperature profiles above and below the stratified layer was quite linear ($dT/dz \approx 0\ ^\circ C/m$), with two separate homogeneous layers in the upper and lower zone.
5. For the period of (16:15:46 to 18:15:46), while the cold airflow was still not activated, the stratified layer thickness δ has become thicker and dilute. Interface level height h has reduced. The degree of stratification dT/dz is going down, and the temperature profile in the upper zone is quit linear ($dT/dz \approx 0\ ^\circ C/m$).

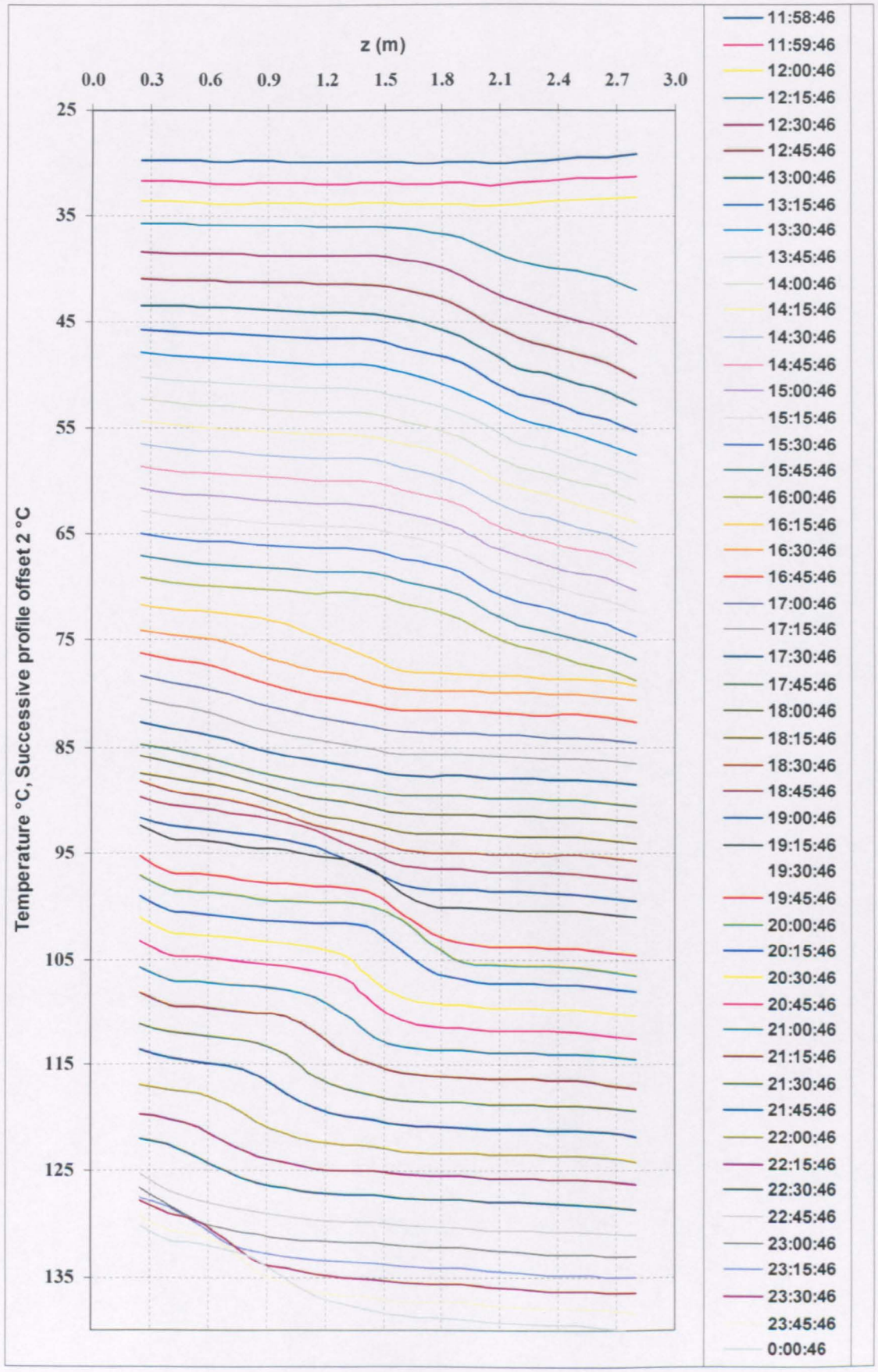

Figure 4.3.2: Vertical temperature profiles, each successive profile is offset by 2.0 °C and separated initially by a minute and lately by 15 minutes intervals. The successive profile plot was used by [(Lorke et al. (2004)] and others.

6. For the period of (18:15:46 to 20:45:46), the cold airflow was activated; the stratified layer thickness δ has become thinner and more concentrated. Interface level height h has gone up. The temperature profile in the upper and lower zones is quit linear ($dT/dz \approx 0\ ^{\circ}C/m$).
7. Further time step of 15 minutes at time (19:15:46 to 20:15:46), a full-scale stratified layer was formed with (h=1.4 m, δ=0.3 m and $dT/d\delta = 15\ ^{\circ}C/m$). Both vertical temperature profiles above and below the stratified layer was quite linear ($dT/dz \approx 0\ ^{\circ}C/m$), with two separate homogeneous layers in the upper and lower zone.
8. For the period of (20:45:46 to 00:00:46), while the hot airflow was increased, the process was continuing as in step 3 with the same loop.

Figures 4.3.3 to 4.3.5 show steady state temperature visualisation for three different values of hot airflow rates ($Q_h = 1.0, 3.0, 5.0\ m^3/min$), and various values of cold airflow rates ($Q_c = 0.0 - 8.0\ m^3/min$). Both hot and cold airflow rates were supplied to the top and bottom of the chamber respectively using rectangular cross section diffusers. The diffusers help in admitting the flow with minimum momentum to maintain the stratified layer. The data obtained gives an indication of the stratified flow characteristics such as, interface level height h, stratified layer thickness δ, degree of stratification DS and stability defined by Ri. The results show the measured vertical temperature distribution along with the thermocouple stand. The highest degree of stratification DS of ($dT/d\delta = Max$) occurred at low and moderate hot airflow rates, whilst the weakest stratification of ($dT/d\delta = Min$) occurred at comparatively high hot airflow rates.

The effect of increasing cold airflow rate is to:

1. Increase the temperature difference, ΔT.
2. Increase interface level height, h.
3. Improves degree of stratification defined by DS
4. Decrease the stratified layer thickness, δ.

Figures (4.3.3 to 4.3.5) show that low cold airflow rates are insufficient to preserve a thermally stratified temperature distribution, especially with the presence of

comparatively high hot airflow rates ($Q_h = 4$ and $5\ m^3/min$). In the case of comparatively low hot airflow rate ($Q_h = 1$ and $2\ m^3/min$), Figure 4.3.3 show no significant effect due to cold airflow on the temperature of the upper zone, whilst a significant effect was visible in the temperature of the lower zone. However, increasing the cold airflow rates will increase the amount of cold air in the lower zone, which increase the temperature difference, and the density in the lower zone. Thus increase the center of mass and buoyancy forces, which thrust the hot air toward the ceiling and push the stratified layer interface higher.

Figure 4.3.3 shows that at low hot airflow $Q_h = 1.0\ m^3/min$, increasing cold airflow rates propagate the flow to stratify at high values of cold airflow rates. In this case, the flow is stratified under the effect of high cooling loads rather than comparatively insufficient heating loads. Whereas the cold air supply is ambient air, the flow is stratified under the effect of ambient conditions. In other words, for stratification at low hot air supply, the effect of surrounding conditions and ambient external fluctuations is significant.

The results in Figures 4.3.3 to 4.3.5 show the effect of hot airflow rates on the stratified flow characteristics. Increasing the hot airflow from $Q_h = 1.0\ m^3/min$ to $Q_h = 5.0\ m^3/min$ at fixed cold airflow will:

1. Decrease the temperature difference, ΔT.
2. Decrease the interface level height, h.
3. Extended the stratified layer thickness, δ
4. Decrease the degree of stratification DS.
5. And in the result it destratified the flow.

It should be due to two reasons:

- The first reason is due to increase in the upper zone temperature, which increases the heat transfer between the zones due to temperature differences. Therefore, it increases lower zone temperature, so decreases the buoyancy forces. This condition may generate downward flows that incline the upper zone towards the bottom of the chamber.
- The second reason is due to increase in the velocity of air in the upper zone of the chamber, which increases the shearing forces through the interface.

Therefore, it increases mixing that promotes the flow to be destratified. Similar to third effect has been observed by [Linden (1979)] that mixing produced by the mean turbulent shears increases the thickness of the stratified layer.

Figur 4.3.4 shows the strongest stratification of the conditions tested ($dT/d\delta = Max$). The results are due to increase in bouyancy forces and temperature gradient hence Ri number is also increased.

Figures 4.3.3 to 4.3.5 show the isothemal temperature lines with small fluctuations with time. The temperature fluctuations are visible in the stratified layer. These fluctuations may be related to flow parameters such as density and velocity, where these parameters are the key factors of buoyancy and momentum forces. These observations are in agreement with [Subbarao and Muralidhar (1997)]. It may be due to small disturbances near the measurement stand and thermocouples nodes, or small perturbations that described by [Turner (1973)]. [Turner (1973)] analysis showed that the flow could stabilize with small perturbations for all flow of $Ri \succ 1/4$. It is also in agreement with [Linden et al. (1990)] that "ventilation flows are turbulent, unsteady and three-dimensional".

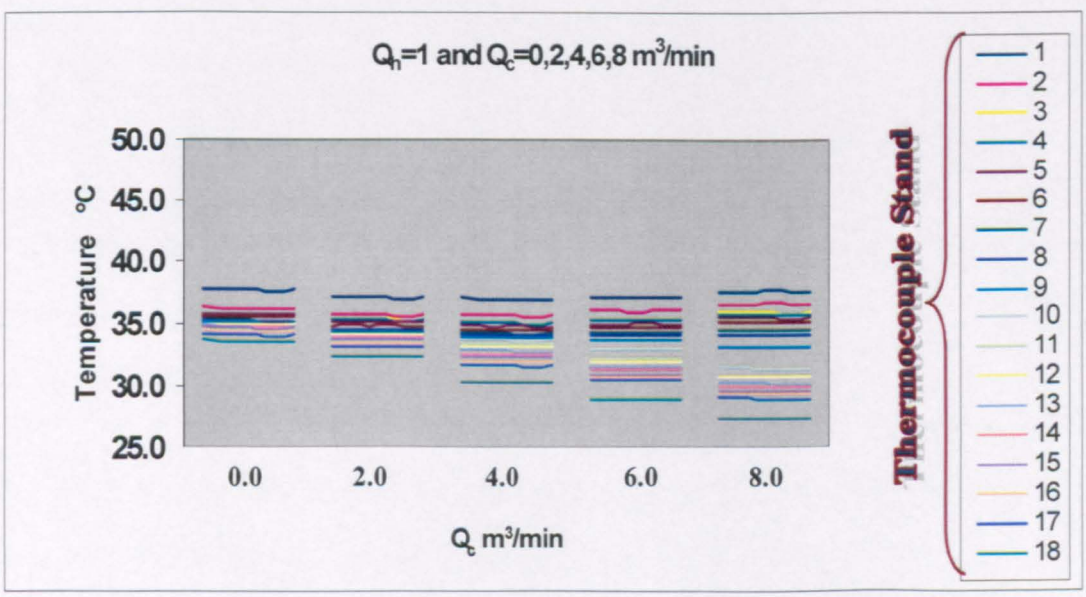

Figure 4.3.3: Temperature distribution across the chamber at a fixed axial location of (3.75, 2.8) m and fixed hot air flow rate ($Q_h = 1.0\ m^3/min$) for different cold flow rates ($Q_c = 0, 2, 4, 6, 8\ m^3/min$) in the chamber.

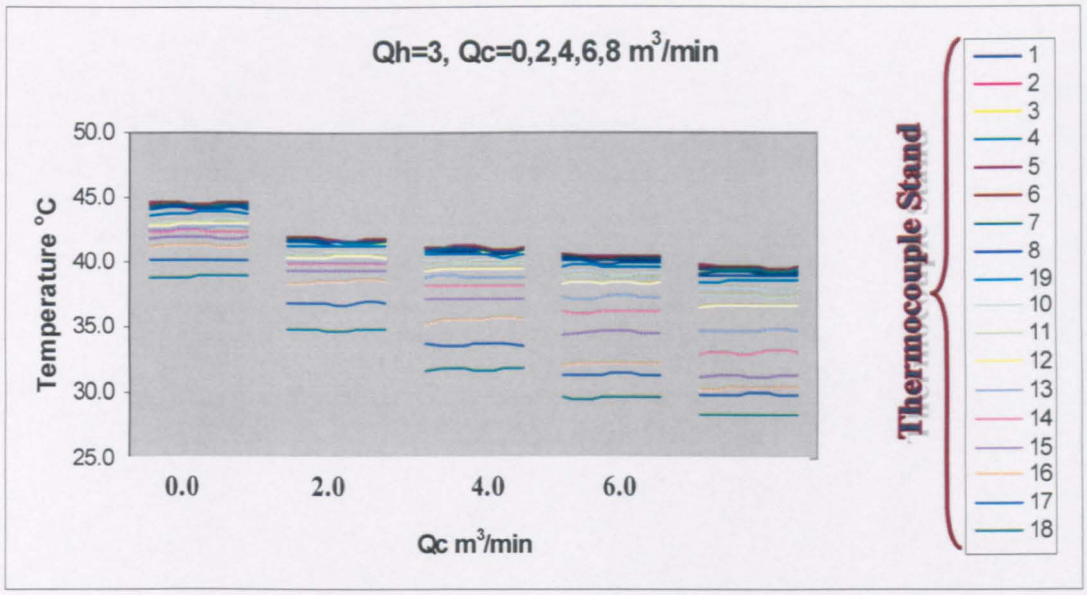

Figure 4.3.4: Temperature distribution across the chamber at a fixed axial location of (3.75,2.8) m and fixed hot air flow rate ($Q_h = 3.0 m^3/min$) for different cold flow rates ($Q_c = 0, 2, 4, 6, 8 m^3/min$) in the environmental chamber.

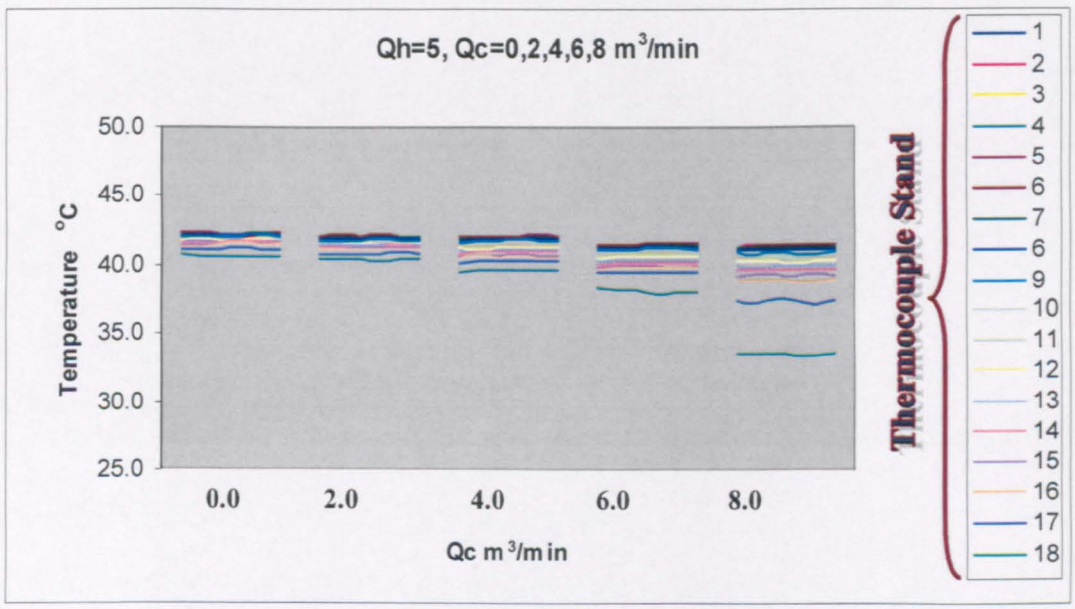

Figure 4.3.5: Temperature distribution across the chamber at a fixed axial location of (3.75, 2.8) m and fixed hot air flow rate ($Q_h = 5.0 m^3/min$) for different cold flow rates ($Q_c = 0, 2, 4, 6, 8 m^3/min$) in the environmental chamber.

4.3.2 Spatial Variations of Temperature

Uniform stratified flow in the environmental chamber is an important factor in predicting and calculating the flow characteristics. Fifteen locations were tested, nine locations along the stream-wise direction (x-axis), and six locations across the stream-wise direction (y-axis). The tests were done to estimate the approximate shape of the stratified layer, and to validate the choosing of the chamber centre as a reference location for stratified flow calculations. The schematic diagram for these locations is shown in Figure 4.3.6.

The variations of temperature profile in both along and across the stream-wise direction have been measured. Figures (4.3.7) to (4.3.8) shows an agreement between the measured air temperatures in the middle of the chamber to that measured at a number of locations.

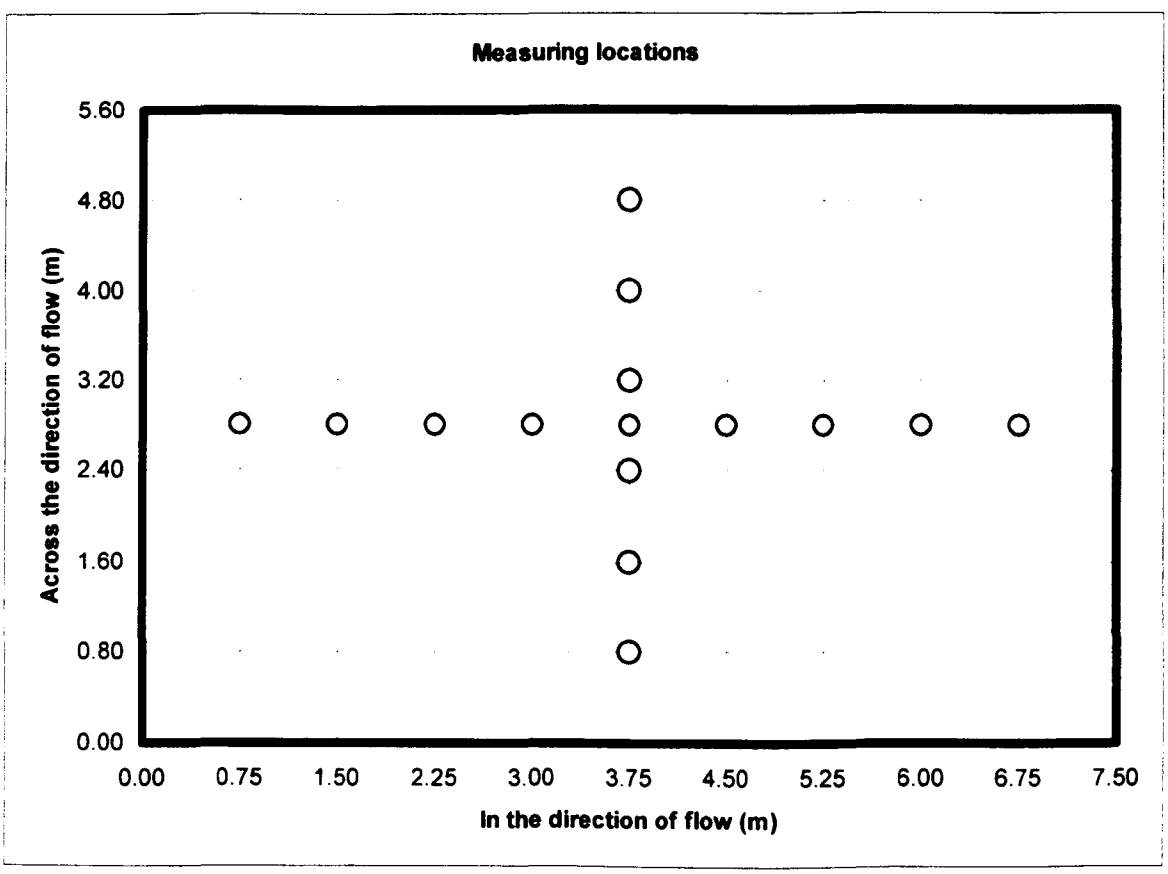

Figure 4.3.6: Definition sketch of the environmental chamber plan view showing a diagrammatic representation of measuring locations listed in table 4.1.1.

The measured transitional temperature profiles at various stream-wise locations (x = 0.75, 1.5, 2.25, 3.0, 3.75, 4.5, 5.25, 6.0, 6.75 m) along the longitudinal line of symmetry are shown in Figures 4.3.7 and 4.3.8. It shows the temperature profile for a grid of 0.75 m along the distance between the inlet airflow rate and the outlet. Figures (4.3.7: a to h) show comparisons of eight experimental temperature profiles at the entire locations along the flow direction. The data is for the case of (DS=3.4) to show the stratified layer distribution and the interface level height in the flow direction. The temperature profiles appear to be independent of the x-direction, while the flow direction does, however, influence the temperature difference.

Combinations of these profiles are shown in Figure 4.3.8. The Figure shows the normalized temperature profiles against the normalized height in the stream-wise direction. The comparison is based on the measured vertical temperature distribution in the middle of the chamber. The results show that the vertical temperature profile variation in the environmental chamber is near symmetrical in the x-direction. The variations in the vertical values are small over the entire chamber. Whilst, near the inlets, the temperature difference is maximum, and the momentum of inflow is so high, which increase mixing in the region close to the flow sources.

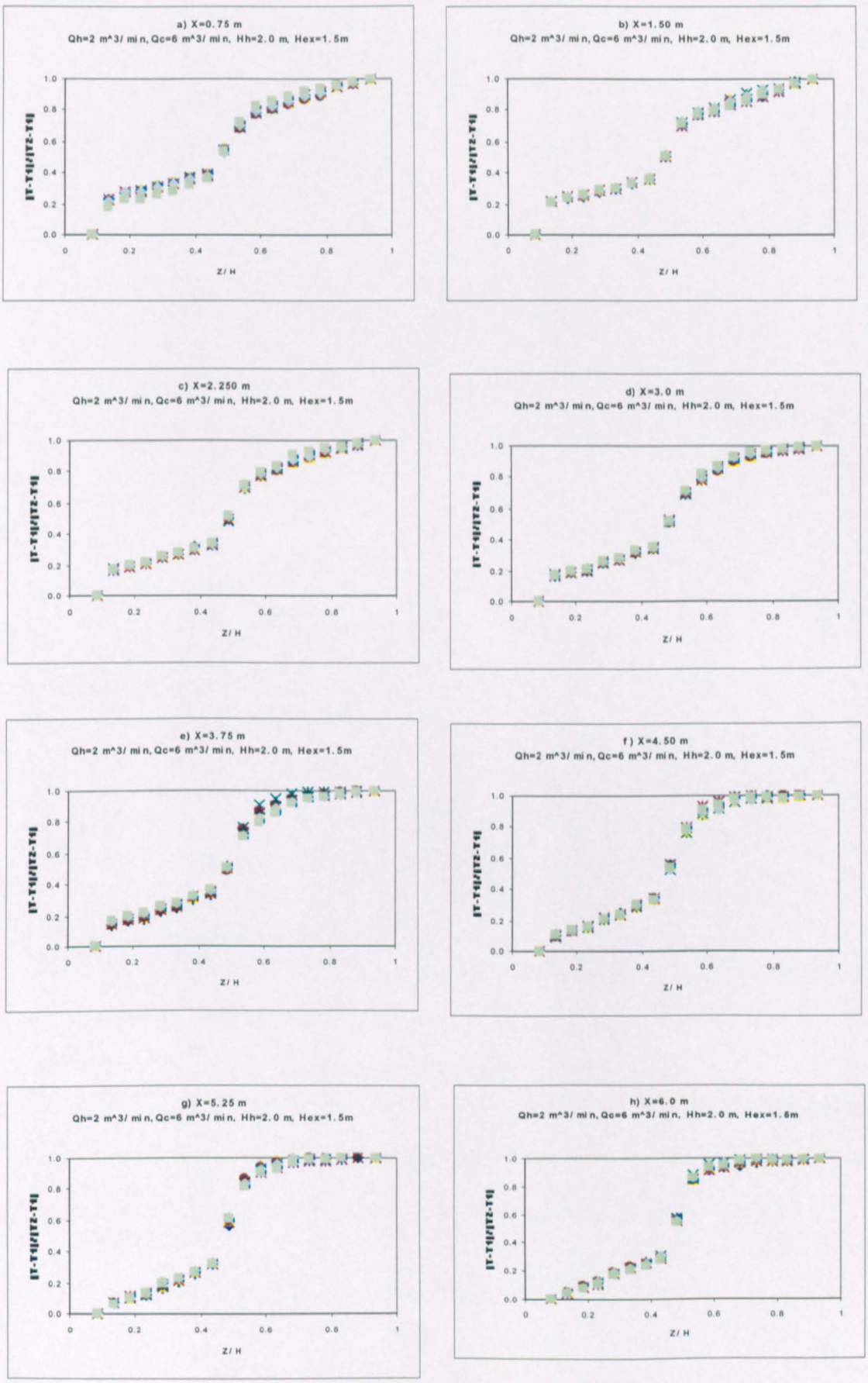

Figure 4.3.7 (a) to (h): Dimensionless temperature profile along vertical centreline with dimensionless height for a number of locations along the direction of the flow, where ($Q_h = 2.0 m^3/min$) and ($Q_c = 6.0 m^3/min$).

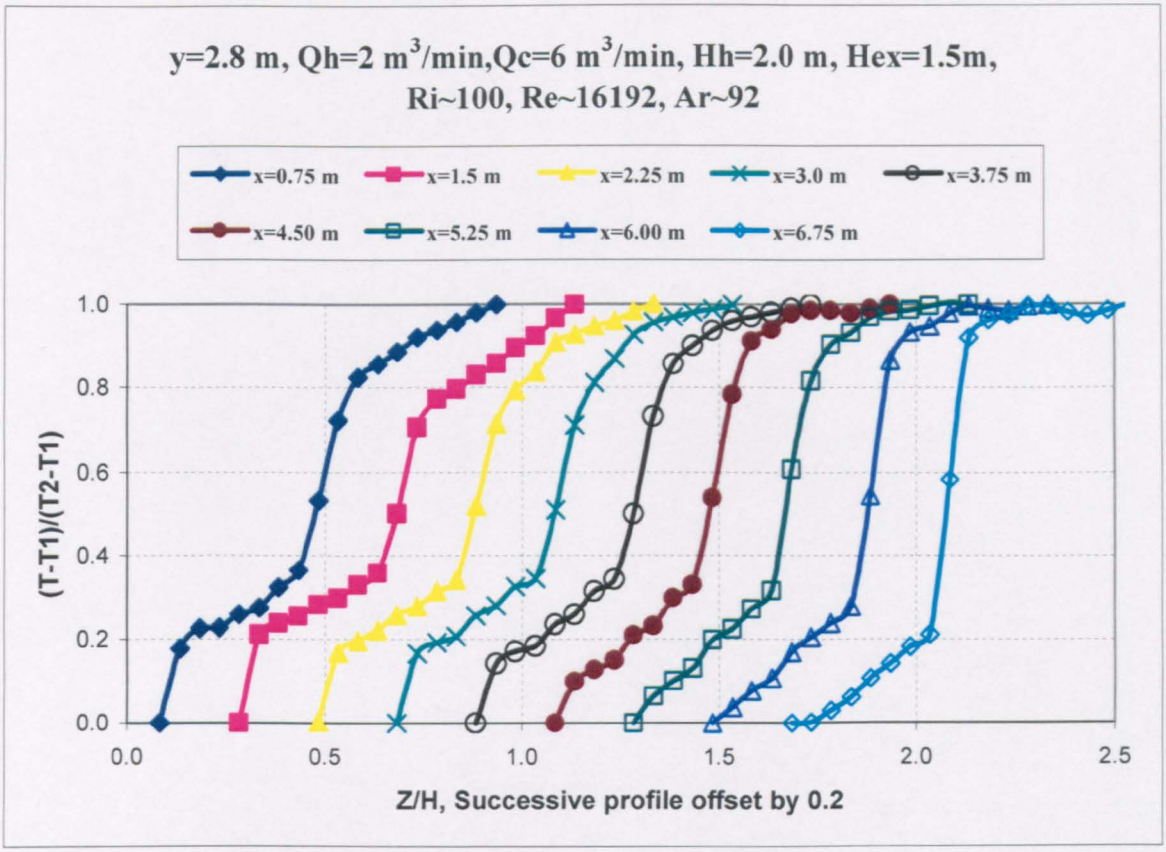

Figure 4.3.8: Dimensionless temperature profile along vertical centreline with dimensionless height for a number of locations along the direction of the flow, where ($Q_h = 2.0 m^3/min$) and ($Q_c = 6.0 m^3/min$), with successive profile offset by 0.2 in z-direction.

The measured transitional temperature profiles across the stream-wise direction in the locations of (y = 0.8, 1.6, 2.4, 3.2, 4.0, 4.8 m) across the line of symmetry are shown in Figures 4.3.9 and 4.3.10. Figures 4.3.9 (a) to (f) show a comparison of six temperature profile for a grid of 0.8 m from wall to wall across the direction of flow. The results show that the temperature profile in the chamber is precisely symmetrical in the y-direction. The variations in the vertical values are insignificant at the entire locations. Whilst, at the walls, the temperature difference and momentum are comparatively high due to heat transfer and disturbances near the walls.

Combinations of these profiles are shown in Figure 4.3.10. The Figure shows the temperature profiles at six measuring locations across the stream-wise direction (y-direction). The result shows that for large-sized environmental chamber, the flow characteristics are uniform.

Comparing the results of temperature profiles across the direction of flow (Figures 4.3.9 and 4.3.10) with that along the direction of flow (Figures 4.3.7 and 4.3.8), shows insignificant variations across the flow direction compared with the variations along the flow direction. The degree of stratification appears almost the same. It is considered, possibly, due to the relatively decrease in flow temperature, and wall effect on both temperature and velocity. As shown in the figures, as the distance from the center increases, the degree of stratification lowered slightly due to the increase of heat transfer and wall disturbances.

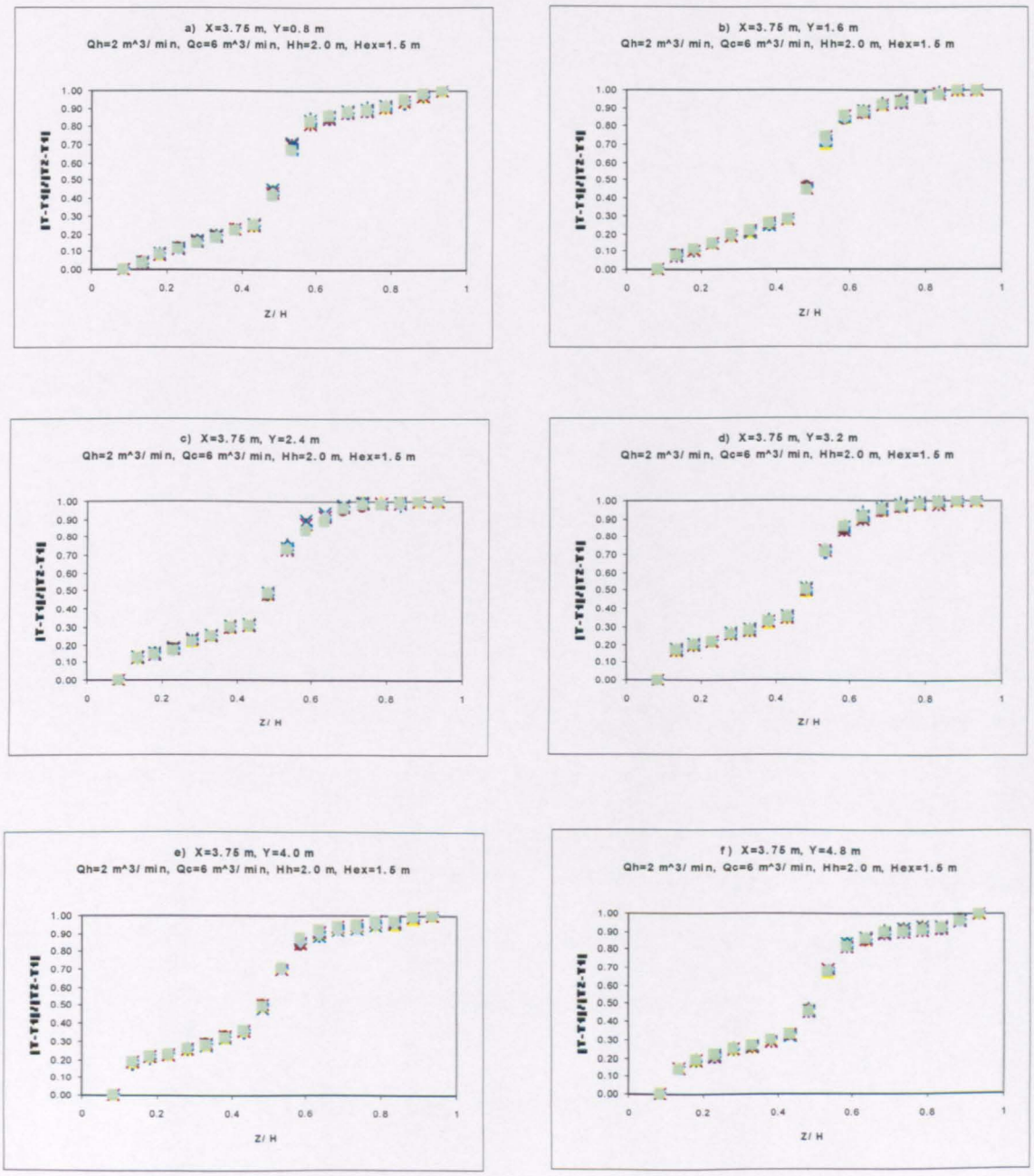

Figure 4.3.9 (a) to (f): Dimensionless temperature profile along vertical centreline with dimensionless height for a number of locations across the direction of the flow for hot airflow rate ($Q_h = 2.0 m^3/min$) and cold airflow rate ($Q_c = 6.0 m^3/min$) in the chamber.

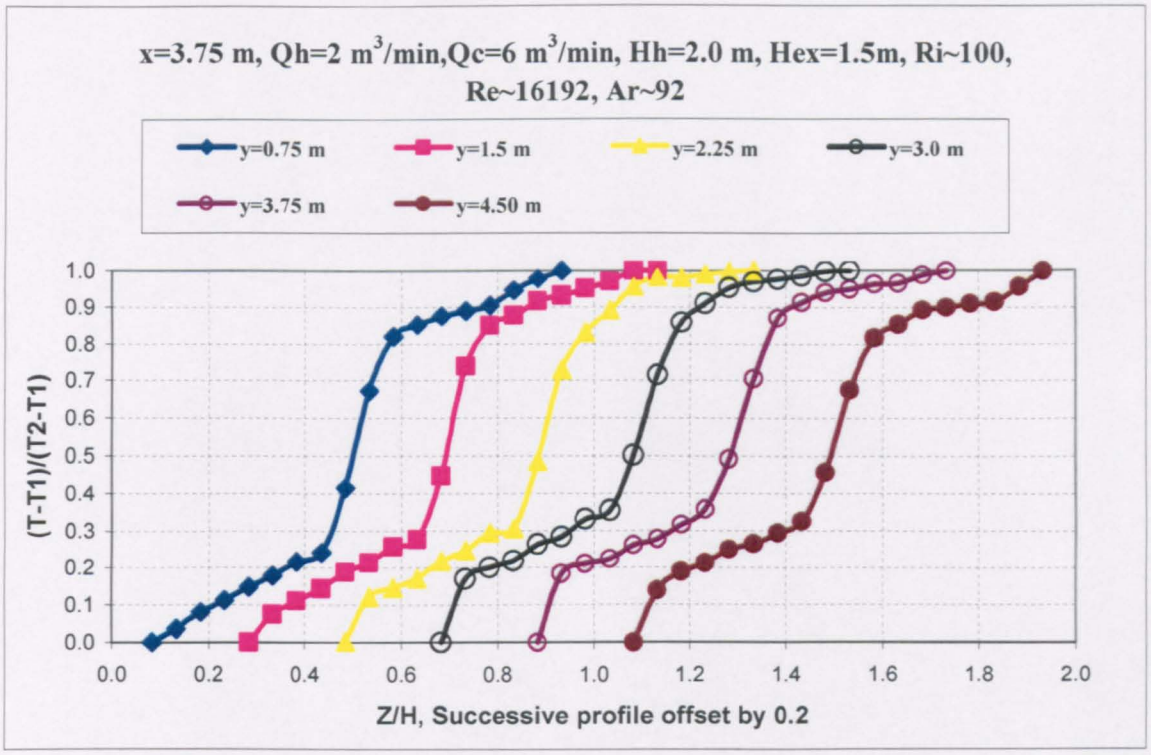

Figure 4.3.10: Dimensionless temperature profile along vertical centreline with dimensionless height for a number of locations across the direction of the flow for hot airflow rate ($Q_h = 2.0 m^3/min$) and cold airflow rate ($Q_c = 6.0 m^3/min$), with successive profile offset by 0.2 in z-direction.

4.4 Effect of Input Airflow Rate

The effect of input airflow rate on stratified flow was studied. Different values of inflow were tested, experimentally, along with several flow parameters inside the chamber. The flow rates studied were in the ranges of $Q_h = 1.0 - 5.0\ m^3/min$ and $Q_c = 0.0 - 8.0\ m^3/min$. These ranges could be useful for studying both stratified and mixed flow. It covers all ranges of Ri (from 0.67 to 200).

The temperature profiles for various values of hot and cold airflow rates, at fixed input and output locations, are plotted in Figures 4.4.1 and 4.4.2 respectively. The results are in terms of the dimensionless temperature $(T - T_1)/(T_2 - T_1)$ with the dimensionless

height z/H, where T_1 and T_2 being respectively the temperatures at the bottom and the top of the chamber, and H is the chamber height.

For both cases shown in Figures 4.4.1 and 4.4.2, it is observed that the temperature distribution is affected by the input airflow rates. While the effect of hot airflow rate on temperature profiles is significant (Figure 4.4.1), the effect of cold airflow rates is smaller (Figure 4.4.2).

Figure 4.4.1 shows the results of various values of hot airflow $Q_h = 1.0 - 5.0\,m^3/min$ at comparatively high cold airflow $Q_c = 4.0\,m^3/min$. The Figure shows that for low values of hot airflow ($Q_h = 1.0\,m^3/min$), the heat released is not efficient to stratify the flow. For high values of airflow ($Q_h = 3.0 - 5.0\,m^3/min$), the momentum is high enough to cause weak stratification or mixed flow, while the strongest stratification is found for moderate values of hot airflow ($Q_h = 2.0\,m^3/min$). For this case, the flow characteristics are h = 1.2m, δ = 0.6m, $dT/d\delta = 15\,^{\circ}C/m$ and DS=7.6.

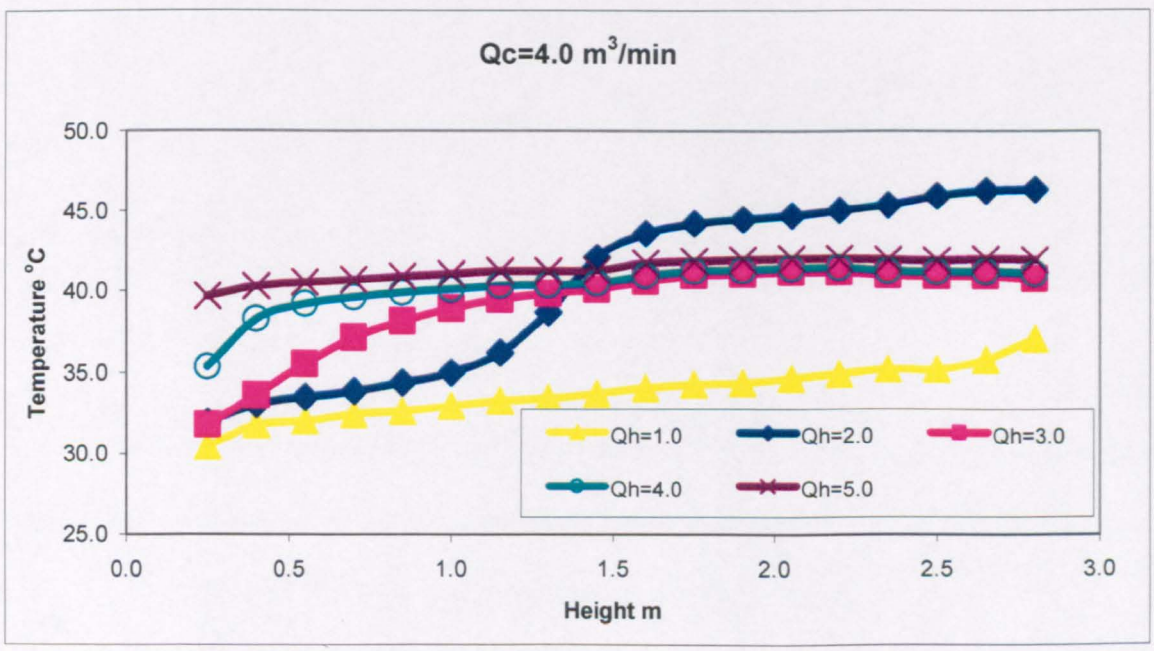

Figure 4.4.1: Comparison of temperature profile along vertical centreline with the height across the chamber at a fixed axial location of (3.75, 2.8) m and fixed cold air flow rate ($Q_c = 4.0m^3/min$) for different hot airflow rates ($Q_h = 1, 2, 3, 4, 5m^3/min$) in the environmental chamber.

Figure 4.4.2 shows the results of temperature profiles at comparatively low $Q_h = 2.0\,m^3/min$ with various values of $Q_c = 0.0 - 8.0\,m^3/mir$. The temperature profiles show a visible change. For both low and moderate cold airflow rate, increasing the flow rate increases the temperature difference and so affect the degree of stratification DS. On the contrary, high levels of cold airflow rates cause a decrease in temperature difference and so $dT/d\delta$. In general, the results show that the profiles are more stratified in the interior regions (stratified region) than for exterior regions

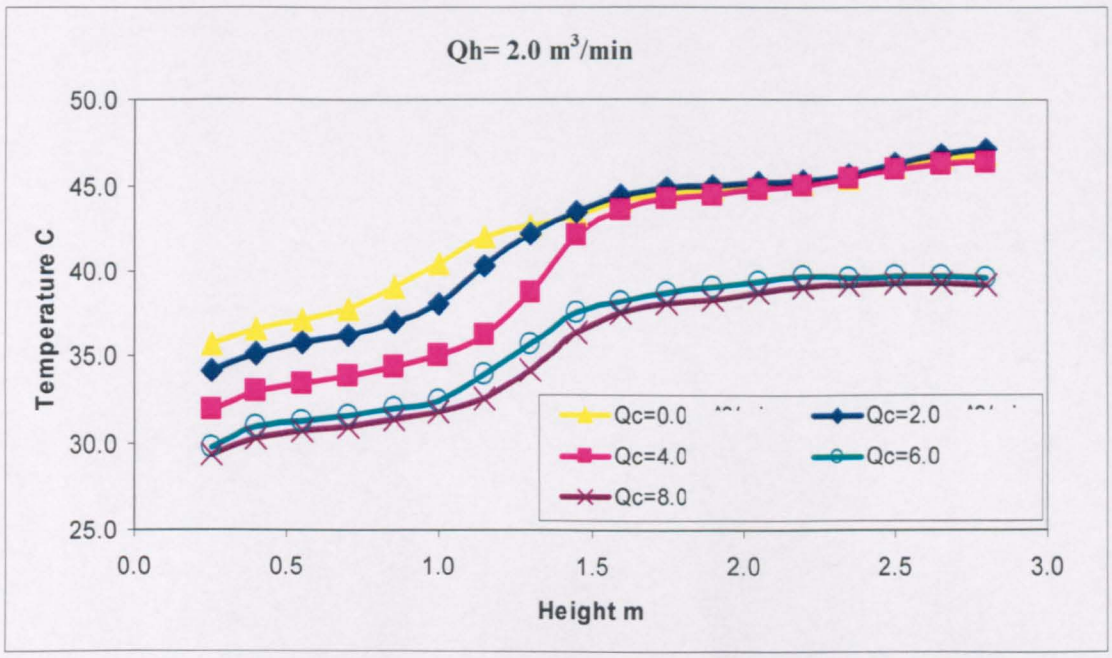

Figure 4.4.2: Comparison of temperature profile along vertical centreline with the height across the chamber at a fixed axial location of (3.75, 2.8) m and fixed hot air flow rate ($Q_h = 2.0 m^3/min$) for different cold flow rates ($Q_c = 0,2,4,6,8 m^3/min$) in the environmental chamber.

Comparison between Figures 4.4.1 and 4.4.2 shows that the effect of increasing hot airflow rate on the stratified flow characteristics, at fixed cold airflow rate, is more significant than the effect of increasing cold airflow rate at a fixed value of hot airflow rate. In other words, hot air flow rate has more significant effect on the stratified flow characteristics than that of cold airflow.

Figure 4.4.3 (a) to (e) presents the vertical temperature gradient dT/dz with the vertical height. The results are displayed as a function of hot airflow rates. It can be seen that, the increase in the amount of hot airflow rate propagates stratification to occur at low values of cold airflow rate, and the interface level height h descends to attain the

ground. By the definition of Richardson number in equation (4.4.2) it decreases the stability of the flow by decreasing the Ri, and so destabilize the flow.

$$Ri = g\,\beta\,\frac{\left(\frac{dT}{dz}\right)}{\left(\frac{du}{dz}\right)^2} \qquad (4.4.2)$$

where, β is the volumetric expansion coefficient for air.

Therefore, related to the present set-up, to provide good thermal stratification, the hot airflow has to be moderate, and the momentum must be low. This could be done when the hot air supply is distributed vertically over a large area.

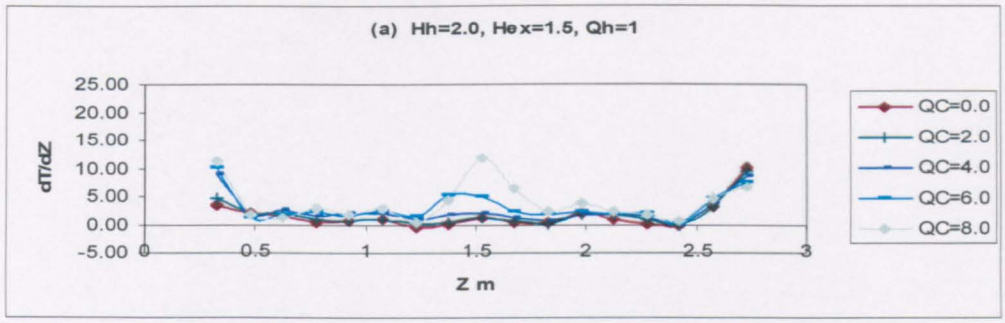

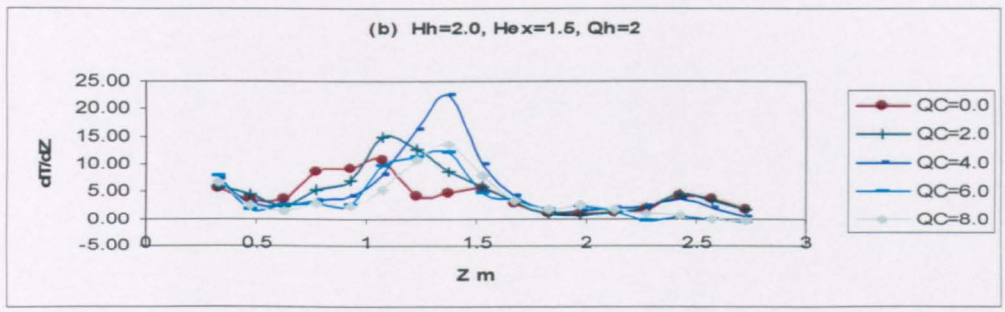

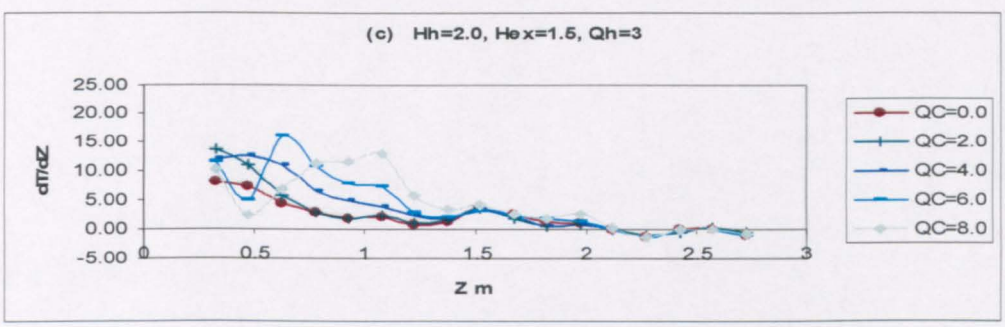

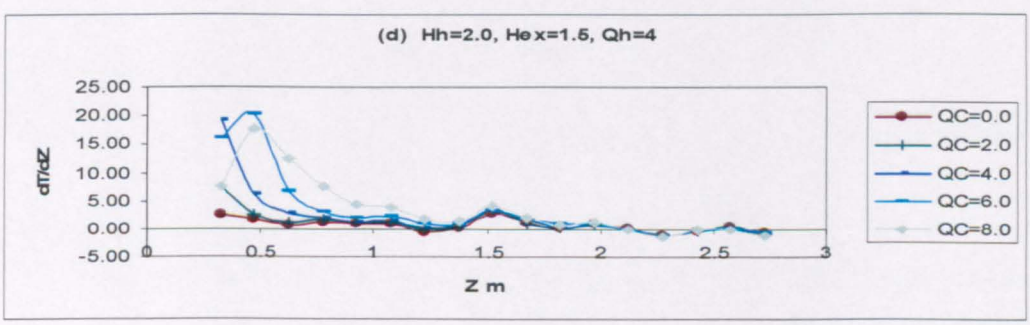

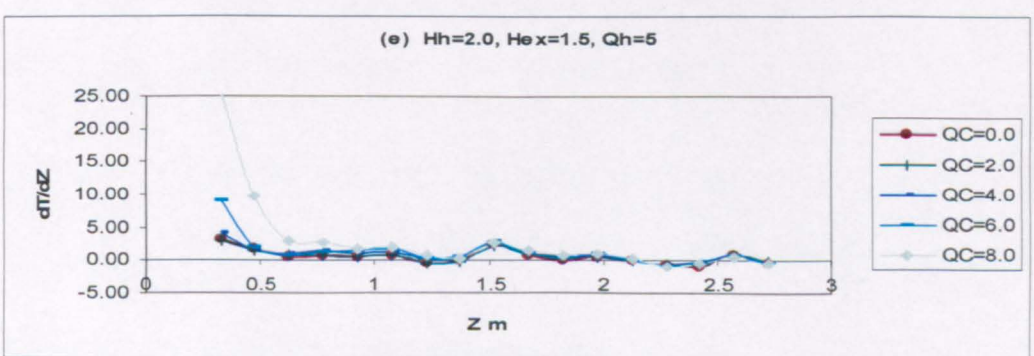

Figure 4.4.3 (a) to (e): Temperature gradient dT/dz with vertical height across the chamber at a fixed axial location of (3.75,2.8) m and certain values of hot air flow rate for different cold airflow rates ($Q_c = 0,2,4,6,8 m^3/min$) in the chamber.

Figure 4.4.4 (a) to (e) presents the vertical temperature gradient dT/dz with the vertical height for various cold airflow rates. It can be seen from the Figure, for low and moderate cold airflow rates, increasing of cold airflow rate will increase the interface level height h and dT/dz. It increases the interface level height h due to the increase in buoyancy forces. For high cold airflow rates ($Q_c = 8.0 m^3/min$), the flow starts to destabilize. The instability can be related to two causes:

- Mixing due to high momentum induce a strong fluid motion that sufficient to mix the flow and destroy thermal stratification.
- Increase in radiative energy absorbed by water vapor in the lower zone, as investigated by [Teodosiu et al. (2003)]. This could happen due to the radiative heat transfer between the upper zone boundaries and the water vapor in the lower zone. In our case, using ambient air as a cold air supply, with high relative humidity, can cause this effect. This cause was supported by [Mundt (1995)]. [Mundt (1995)] related the reason to the radiation from warmer ceiling to the cold floor, then the convection heat transport to the air from the floor in the lower zone.

Therefore, to provide good thermal stratification, the cold airflow rate has to be moderate, and the momentum must be low. It is in agreement with [Hejazi and Siren (1997)] results that high cold airflow rates caused problems occurred in air distribution and control of ventilation systems.

In conclusion, weak stratification is often due to mixing, and poor ventilation is the cause of many factors, which leads to poor distribution of the air in the working space, [Chung et al. (1997)].

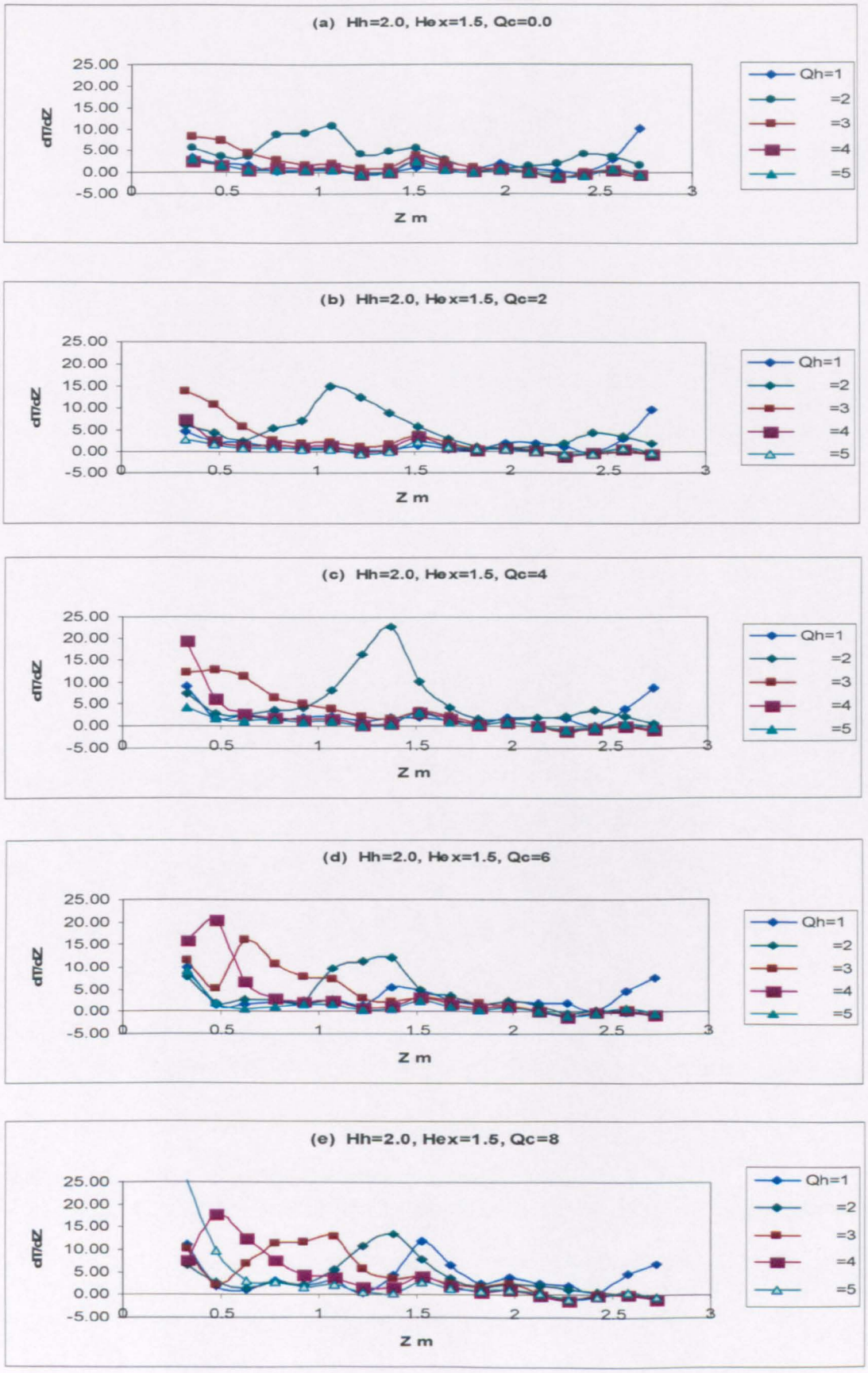

Figure 4.4.4 (a) to (e): Temperature gradient dT/dz with vertical height across the chamber at a fixed axial location of (3.75,2.8) m and certain values of cold airflow rates for different values of hot airflow rates ($Q_h = 1.0 - 5.0 m^3/min$).

The effect of input airflow rates on the stratified flow characteristics h, h′ and δ are shown in Figure 4.4.5. Figure 4.4.5 shows the effect of increasing cold airflow rate to decrease both h′ and δ, whiles it increase the stratified layer interface level height h. The figure shows the decrease of the stratified layer thickness δ, due to the momentum transfer from the cold airflow to the stratified layer according to the momentum equation, which specifies the density variations effect. The decrease is not significant at lower flow rates. When the cold airflow is comparatively high, there were higher decrease in the stratified layer thickness and height, while the interface level height increases. Increasing the source momentum leads to increase mixing, due to energy transfer, and as a result the stratified layer thickness and the stratified layer height decreased more rapidly than for low and moderate cold airflow rates.

Figure 4.4.6 shows the effect of increasing hot airflow rate to decrease both the stratified layer top height h′ and the stratified layer interface level height h, whiles it increase the stratified layer thickness δ. The Figure shows that the decrease of both h and h′ is rapid whilst the increase of δ is small. The effect is due to the increase of temperature difference, heat transfer, and as a result the stratified layer is extended, which should therefore lead to a low degree of stratification DS.

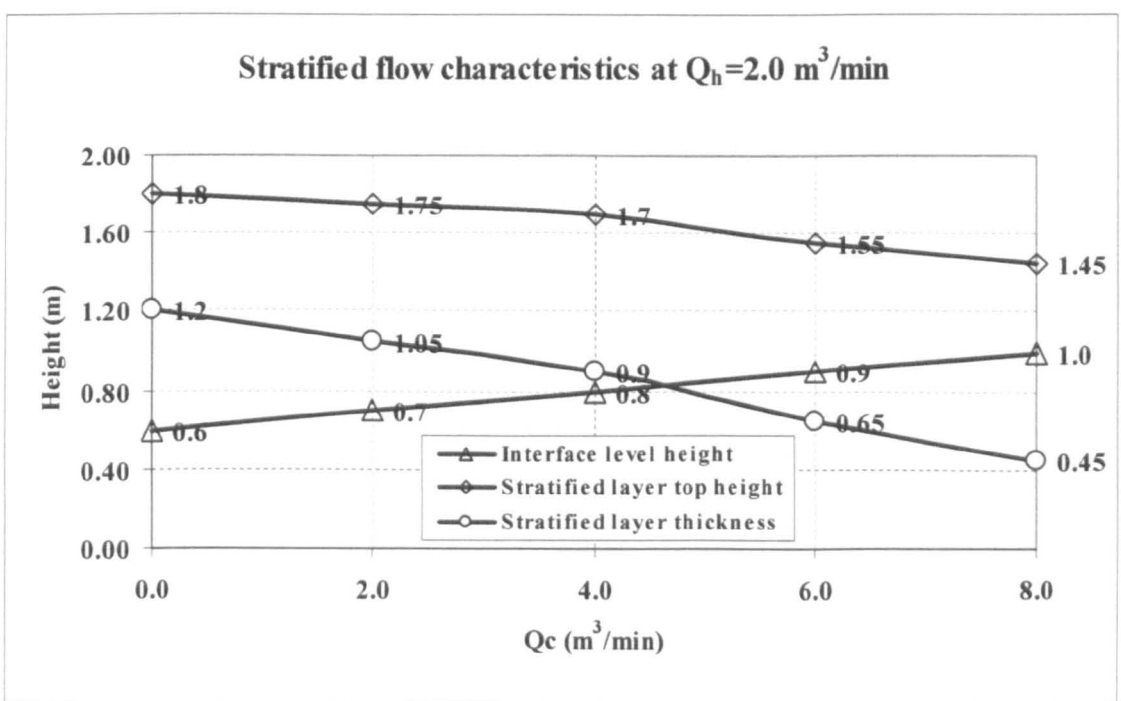

Figure 4.4.5: The stratified layer interface level height, the stratified layer height and the stratified layer thickness with cold airflow rate for intermediate hot airflow rate. (Values on graph are heights in m).

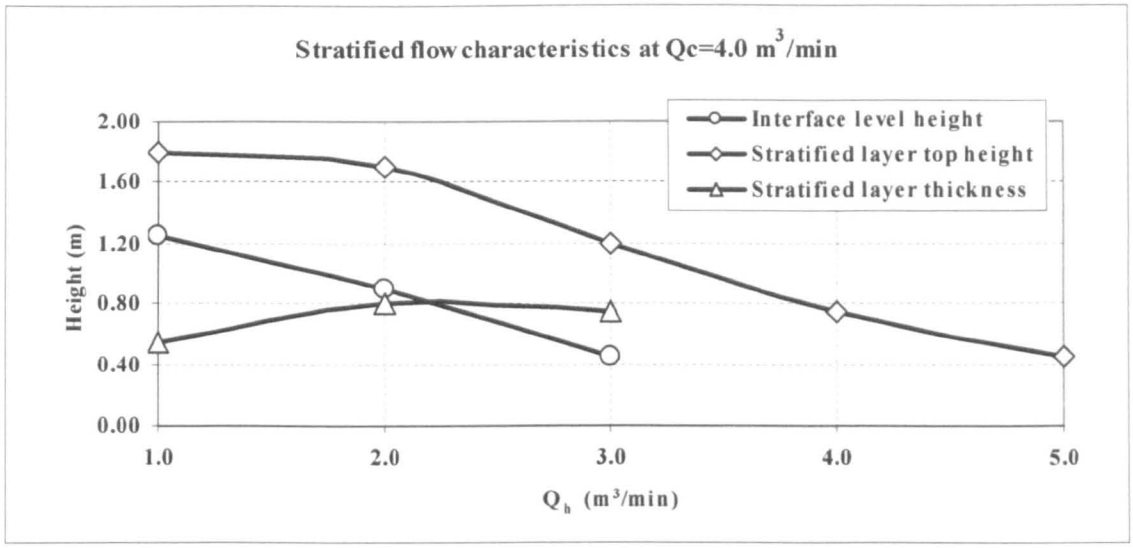

Figure 4.4.6: The stratified layer interface level height h, the stratified layer height and the stratified layer thickness with hot airflow rate for intermediate cold airflow rate.(In this case, h reaches the ground before Q_h reaches the value $4.0\ m^3/min$ so δ, while the interface top height h' is still over).

Figure 4.4.7 shows the temperature gradient across the stratified layer $dT/dz|_{z\to\delta}$ and the strongest degree of stratification DS with cold airflow rates at an intermediate values of hot airflow rates ($Q_h = 2.0, 3.0\ m^3/min$). The results show that the strongest degree of stratification DS=7.6 and 4.0 are for intermediate values of cold airflow rates ($Q_c = 4.0$ and $6.0\,m^3/min$) as listed in table 4.1.4. It is at an airflow ratio ($Q_c/Q_h = 2$), where the buoyancy and momentum forces are in balanced. Compared with the lower and higher cold airflow rates. For comparatively low airflow rates the buoyancy forces is sufficient to stabilize the flow. For comparatively high airflow rates the momentum is high enough to overcome the stabilizing influence of the buoyancy forces.

The best results are for moderate airflow rates of sufficient buoyancy forces and low kinetic energy to overcome the stabilized case. There are overcoming forces between the buoyancy tending to stratify the interior and the momentum tending to mix it. Thus with a forced plume it is possible to go from the stratified case to the mixed case by changing the relative magnitudes of the buoyancy and momentum fluxes. [Hunt et al (2002)].

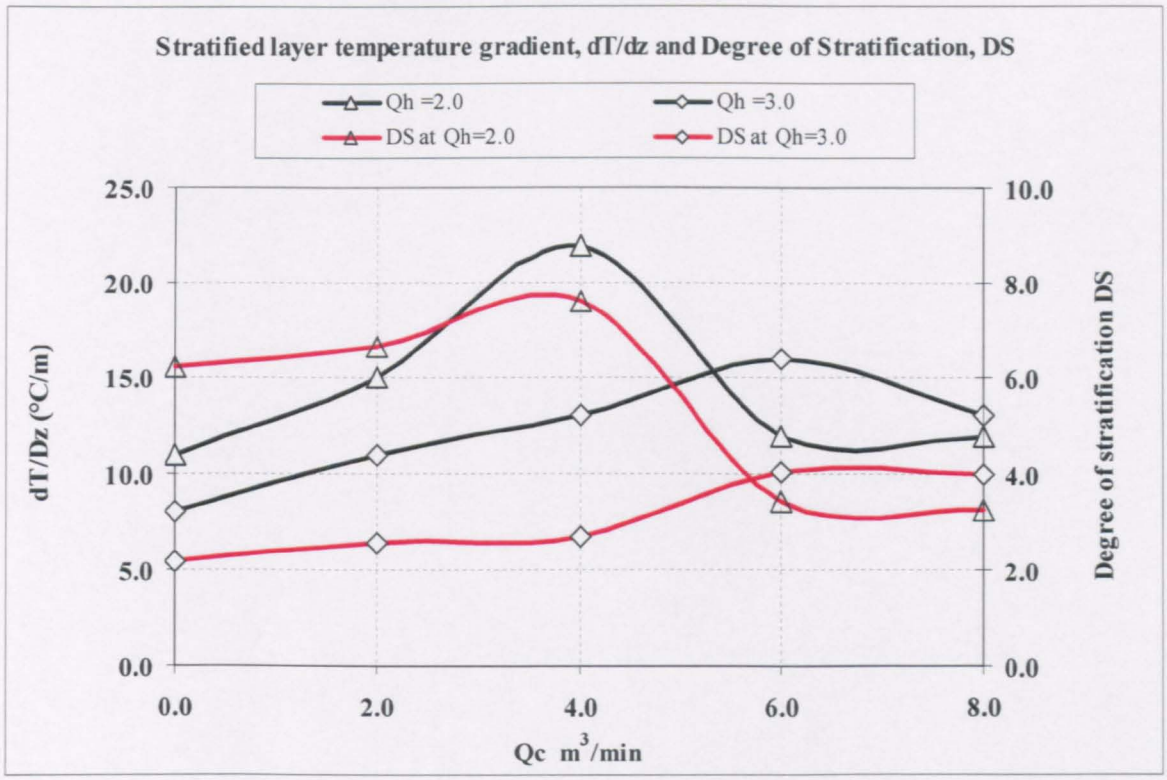

Figure 4.4.7: The stratified layer temperature gradient dT/dz (°C/m) and the degree of stratification DS in stratified flow with various values of cold airflow rates (Q_c = 0,2,4,6,8 m^3 / min) for intermediate values of hot airflow rates (Q_h = 2, 3 m^3 / min).

The effects of input airflow rates on the reduced gravity g' are shown in Figures 4.4.8. Figure 4.4.8 shows the effect of increasing cold airflow on the reduced gravity g':

- At low and moderate hot airflow rates, increasing cold airflow rate with comparatively low values shows rapid increase in g', whiles more increase in cold airflow rate results in rapid decrease.
- At comparatively high hot airflow rates, increasing cold airflow rates shows a small decrease in the values of g' at the full ranges of cold airflow rates.
- The maximum value of g' is at moderate values of input airflow rates, due to moderate balance between buoyancy and momentum.

Figure 4.4.8 shows the effect of increasing hot airflow rate on the reduced gravity g'. It shows the increase of g' with increase of hot airflow rates due to the increase in

temperature difference. It also shows the maximum value of g' is at comparatively low cold airflow rate.

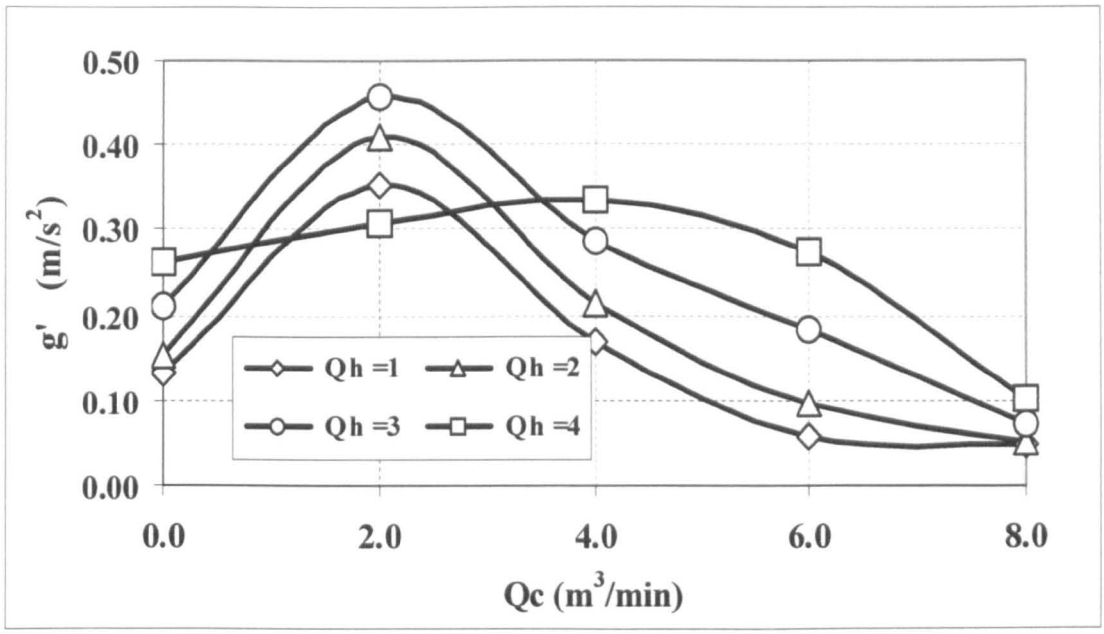

Figure 4.4.8: Reduced gravity g' m/s^2 with various values of cold airflow rates ($Q_c = 0,2,4,6,8 m^3/min$) for hot airflow rates ($Q_h = 1,2,3,4 m^3/min$) in the environmental chamber.

In summary, controlling of airflow rates can be used for controlling the degree of stratification and stratification interface level height to maintain on stratified layer. It is in agreement with the results of [Linden (1979)]. [Linden (1979)] identified the needs for input flow rates to remove the mixed fluid from the stratified region in order to keep its thickness constant.

4.5 Effect of Vertical Inflow and Outflow Location

4.5.1 Effect of Input Vertical Location

Noting that, for our case, the input location was the source of heat release in the chamber where hot air was penetrated. This location was considered as a useful parameter to be investigated. Various input locations were tested, experimentally, along with several flow parameters inside the chamber. The locations studied were (1.0, 1.5,

2.0 m). The experiments were carried out for different ranges of flow rates of both hot and cold air corresponding to different ranges of Ri (0.67 to 200). The temperature profiles for various values of cold airflow rates ($Q_c = 0.0 - 8.0\,m^3/mir$) and input locations ($H_h = 2.0\,m$ and $H_h = 1.5\,m$), at fixed exhaust location ($H_{ext} = 1.5\,m$) at hot airflow rate ($Q_h = 2.0\,m^3/min$), are plotted in Figures 4.5.1 and 4.5.2 respectively. The results were in terms of the dimensionless temperature $(T - T_1)/(T_2 - T_1)$ with the dimensionless height z/H, where T_1 and T_2 being respectively the temperatures at the bottom and the top of the chamber, and H is the total height of the chamber.

For both cases shown in Figures 4.5.1 and 4.5.2, it is observed that the temperature distribution is affected by both the input location and the cold airflow rate. While the effect of input location on temperature profiles is significant the effect of cold airflow rates is smaller, especially for input location of 1.5 m. The effect of cold airflow rate was much stronger for the 2.0 m input location than that of 1.5 m.

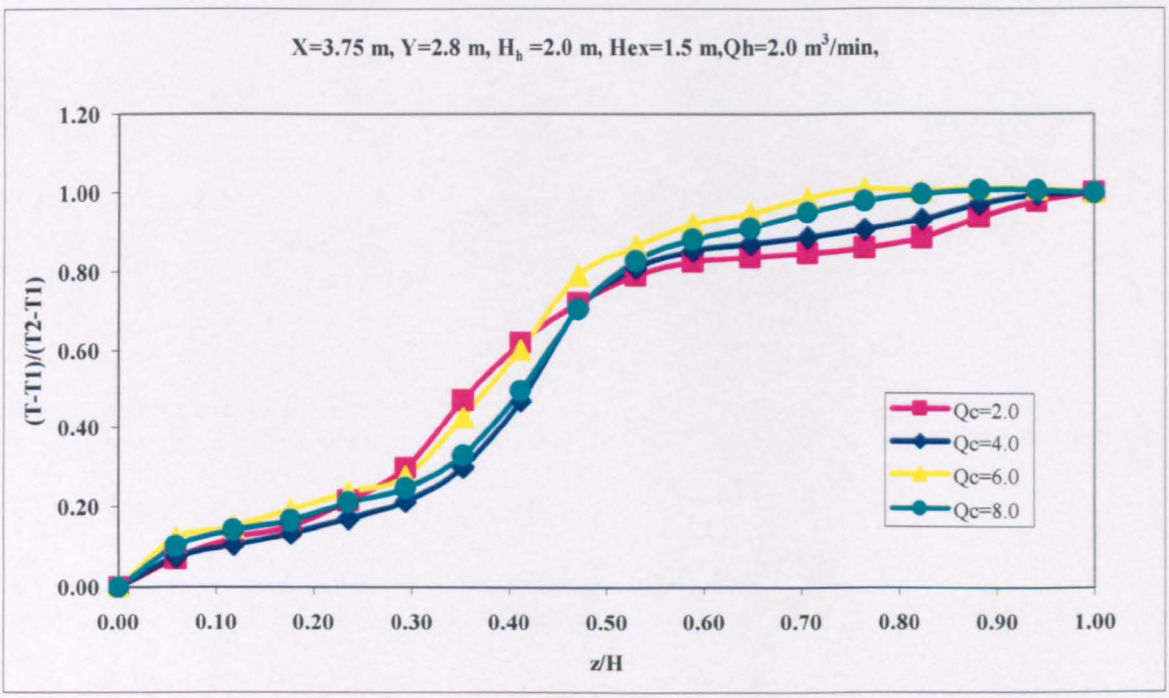

Figure 4.5.1: Comparison of dimensionless temperature profile along vertical centreline with dimensionless height across the chamber at a fixed axial location of (3.75, 2.8) m and fixed hot air flow rate (Q_h = 2.0m^3 / min) for different cold flow rates (Q_c = 0,2,4,6,8m^3 / min) in the environmental chamber for 2.0 m input location.

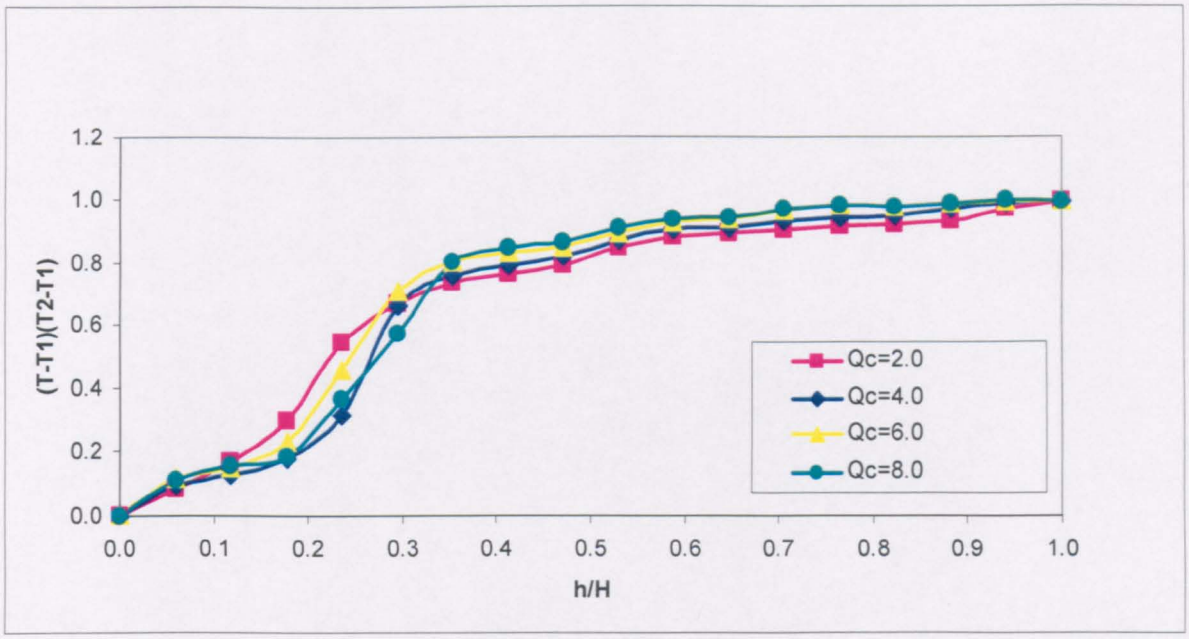

Figure 4.5.2: Comparison of dimensionless temperature profile along vertical centreline with dimensionless height across the chamber at a fixed axial location of (3.75,2.8) m and fixed hot air flow rate ($Q_h = 2.0 m^3/min$) for different cold flow rates ($Q_c = 0,2,4,6,8 m^3/min$) in the environmental chamber for 1.5 m input location.

Comparison between Figures 4.5.1 and 4.5.2 shows the effect of increasing input location of hot airflow rate from 1.5 m to 2.0 m (i.e. 30% height increase) on the stratified flow characteristics:

1. It increases the stratified layer interface level height h.
2. It increases the temperature variations in the upper zone.
3. It reinforces the effect of cold airflow rates on the stratified flow characteristics.

Firstly, the higher of the input location yields a higher interface level height; the effects were due to the height shift of hot air flow rate (ΔH_h) that shifted the stratified layer upward in response to the change in the level of the supply diffuser, so the interface level height h. From the Figures, the increase in h was more than the height shift, which is due to both: the height shift (ΔH_h) and the height difference between hot and cold airflow rates ($H_h - H_c$) that decreases the amount of heat transfer between the zones and the amount of mixing and so propagates the flow to stratify.

Secondly, as input location H_h increases, larger circulation flows are generated in the upper region, whereas; minor ones are formed for low H_h . This change of flow fields was related to plume strength, which results in different levels of stratification, [Hee-Jin and Dale (2001)]. When input location is located at 1.0 m, no visible stratification level is observed because the hot airflow is ascended directly into the floor before it yields a stratified layer, where the spread of hot air beneath the low input location is dependent on the input location, as one would expect. Because the penetration distance is decreased then the small height is sufficient to prevent hot air reaching the ground. In this case it can also be observed that the flow is completely mixed where the penetration distance and the interface level height are both found to decrease with decreasing input location, [Abdulkarim and Yogesh (1996)].

Thirdly, when the vertical location of the heat source is at lower levels, a convective heat gain from the heat source to the lower zone is increasing. The lower zone is originally cold, this will increase the temperature in the lower zone leading to decrease it in the upper zones, so a reduction in the average temperature of the work zone will result, [Sinha et al.(2000)]. Thus, the cold airflow rates have a wide domain to affect the flow, especially in both the stratified layer and the upper zone.

From the Figures 4.5.1 and 4.5.2, it can be seen that, when input location is reduced by 25% (from $H_h = 2.0\,m$ to $H_h = 1.5\,m$), the shape of temperature profile showed less sensitivity to the change in cold airflow rate. It also can be seen that, the decrease of H_h affects the flow to stratify at lower height while the interface level height descends to attain the ground.

It can be noted that, in the stratified layer, the temperature profiles is more mixed close to the upper zone than that close to the lower zone, while it is more mixed in lower zone than that in the upper zone. However, as the input location increases or the amount of cold airflow rates increases, the interface tends upwards towards the ceiling, and therefore extends the stratified layer thickness δ. As a result, the flow becomes more dilute and the stratified layer more diffused.

As a heat source supply, the results showed that the input location has a significant influence on the flow characteristics. Figures 4.5.2 to 4.5.4 illustrates that as the hot airflow rate increases, the amount of heat in the upper zone, and the interface level

height migrates downwards from the top of the chamber to reach the ground, even though the input location is increasing. It also showed that the interface level height h seen to increase with increase the H_h , and to decrease with increase in the hot airflow rate.

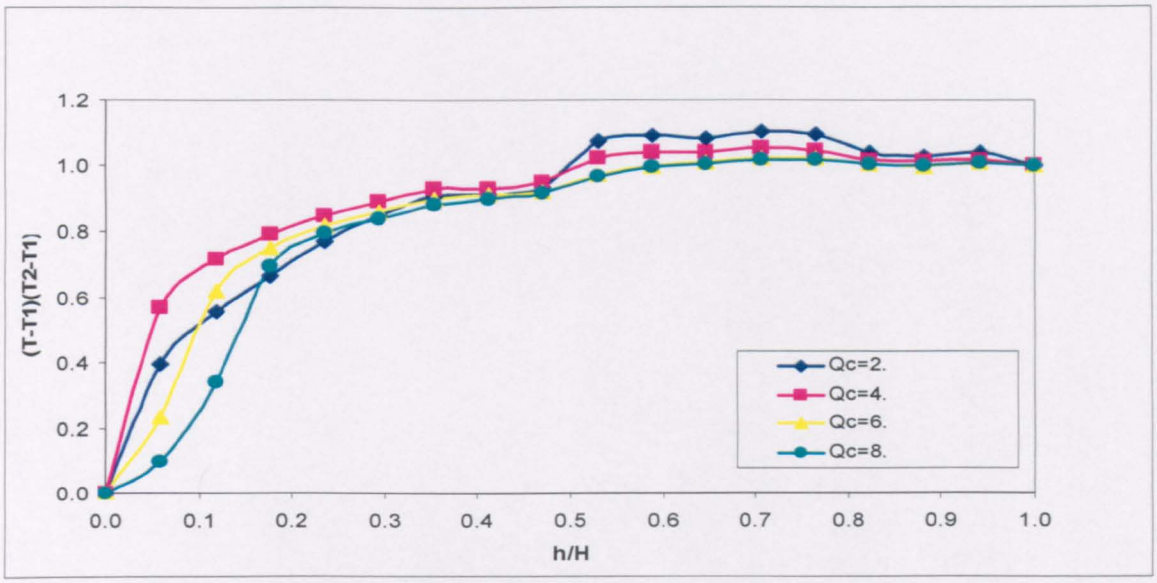

Figure 4.5.3: Comparison of dimensionless temperature profile along vertical centreline with dimensionless height across the chamber at a fixed axial location of (3.75,2.8) m and fixed hot air flow rate ($Q_h = 3.0 m^3/min$) for different cold flow rates ($Q_c = 0,2,4,6,8 m^3/min$) in the environmental chamber for 1.5 m input location.

The results show that higher input location offer a stable stratified flow in which the layer is built up and becomes strong enough to overcome mixing forces. For this case, increasing the hot airflow rates will increase the temperature in the upper zone, and then the hot air in the upper region pushes the stratified layer downward. More increase in flow rate will make the layer to lose its buoyancy. In this case, only one type of flow would be observed in whole space. It is deduced that when the source is at low location, a large circulation is created yielding a lower stratification level. The reverse is applied to the case of higher locations of the heat source where momentum based stratification is to form at a higher level.

Typical temperature profiles are shown in Figures 4.5.5 and 4.5.6 for input location of heights 1.0, 1.5 and 2.0 m. The flow rates were varied for these tests. The temperature distributions were for cases of mixing flow. The Figures show the flow was fully mixed for both modes of low and high airflow rates.

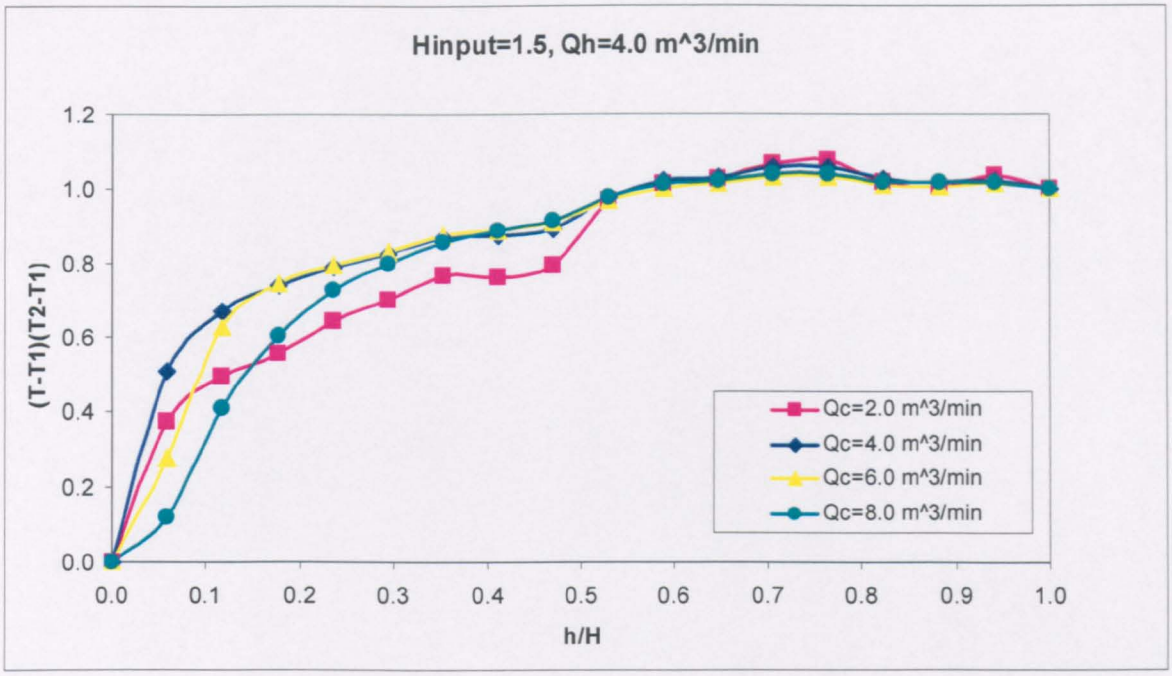

Figure 4.5.4: Comparison of dimensionless temperature profile along vertical centreline with dimensionless height across the chamber at a fixed axial location of (3.75,2.8) m and fixed hot air flow rate ($Q_h = 4.0 m^3/min$) for different cold flow rates ($Q_c = 0,2,4,6,8 m^3/min$) in the environmental chamber for 1.5 m input location.

Figure 4.5.5 show the input locations of no significant effect on the shape of temperature profile for constant given flow rate, whiles airflow rates has a significant effect on the temperature difference. At low mode of hot and cold airflow rates (1&2 m^3/min), the flow has insufficient buoyancy forces required to stratify the flow. At high values of hot and cold airflow rates (5&6 m^3/min), the flow has a maximum momentum that is sufficient to break down the stratified layer and mix the flow. The comparatively high energy introduced by the hot air supply will increase the temperature difference between these modes.

Figure 4.5.6 shows the temperature profiles for moderate airflow rates, with a significant effect of input locations. When the input location is increased vertically, a larger temperature gradient is created (compared to lower location) in the lower zone. The flow becomes stratified in different degrees of stratifications. Two reasons are suggested for this:

1. There is an increase in buoyancy forces to stratify the flow compared with low airflow rate. On the other hand, there is a decrease in momentum forces that break the stratified layer and mix the flow compared with the high airflow rate.
2. As the hot airflow rate reduces, the volumetric flow rate is increased by entrainment of surrounding air, and a circulation flow is formed in the region under the input location. It is observed that when the input location is low both hot and cold air will mix together. This increases the temperature in the lower zone. When the input location is lifted further, the hot air is circulated in the upper region, while the cold air is circulated in the lower region yielding a stratified layer in between [Hee-Jin and Dale (2001)].

From the analysis, the input location affects both the generation of stratified layer and the flow characteristics. Therefore, the strength and size of those circulation flows are main factors in characterizing the stratification level [Hee-Jin and Dale (2001)].

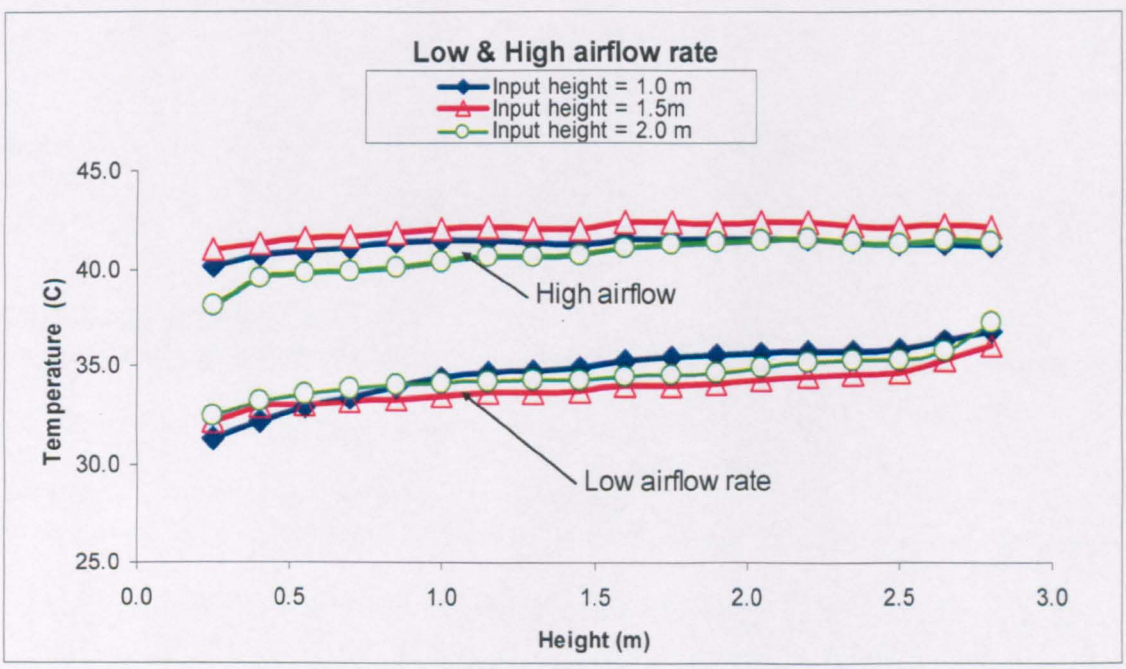

Figure 4.5.5 Comparison of temperature profile along vertical centreline with chamber height at low (Q_h, Q_c=1, 2 m^3/min) and high (Q_h, Q_c=5, 6 m^3/min) modes of air flow rates in the environmental chamber for different input locations.

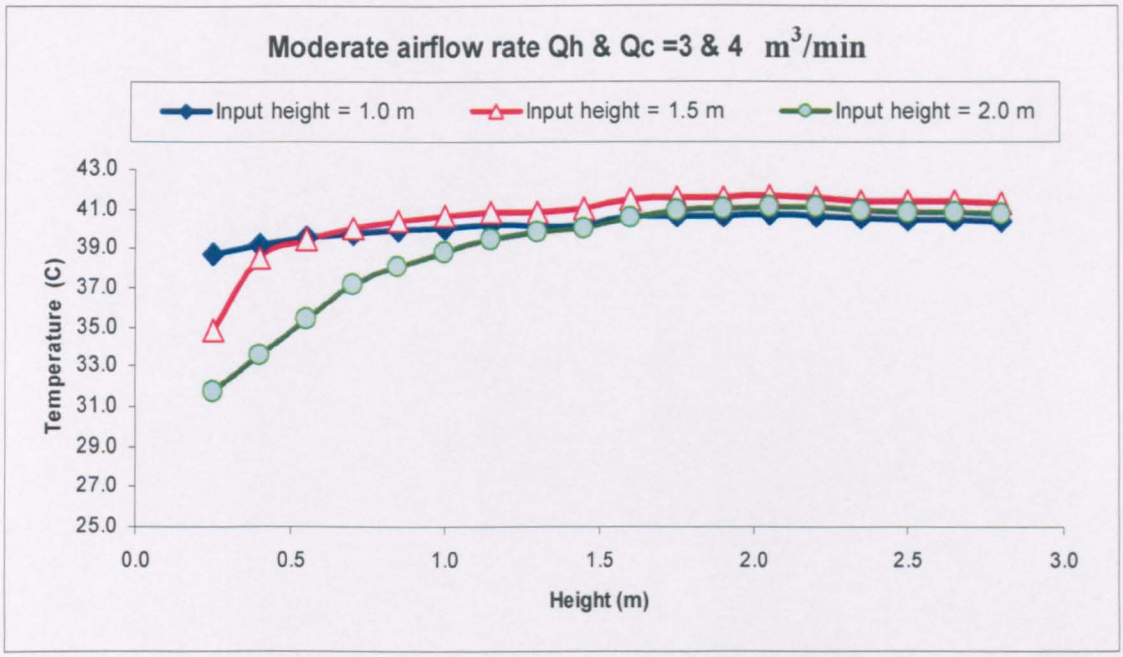

Figure 4.5.6: Comparison of temperature profile along vertical centreline with chamber height at intermediate airflow rates (Q_h, Q_c= 3, 4 m^3/min) in the environmental chamber for different input locations.

4.5.2 Effect of Output Vertical Location

Exhaust location is another parameter that has been investigated. Compared with the previous results for the effect of input location, the flow characteristics are affected considerably by the exhaust location as seen from the results. The dimensionless temperature profiles for various values of hot and cold airflow rates, at fixed input location and large values of exhaust locations were plotted in Figures 4.5.7 to 4.5.10. The Figures shows that at exhaust location 2.5m, the temperature distribution is affected by the input airflow rates with significant values for hot airflow rates, and in smaller values for cold airflow rates.

These Figures also show that the exhaust location does not alter the position of the interface level height. It is to be found in the location above or below the interface level height. Note that the exhaust location does influence the flow rate and the level of the interface. In order to improve the effectiveness of ventilation and to save heating energy costs, the exhaust location must be where "the exhaust temperature should not exceed the temperature in the occupied zone" [Hagstrom et al. (2000)].

Comparisons between Figures 4.5.7 to 4.5.10 show that the flow can stratify at certain heights below the exhaust location depending on the flow boundary conditions. For this the opening geometries must be designed to overcome the phenomenon and exhausted the contaminants and unneeded gases with high removing efficiency. However, when the exhaust location is not at the stratified layer height, but at some way below or above, the removing efficiency becomes low. In other words, fixed exhaust location is ineffective to exhaust the contaminant. The following points are also reported.

1. If the exhaust location is below the stratified layer height. In this case, the cold air flows out through the exhaust opening, while the stratified interface level height becomes smaller.
2. If the exhaust location is at the stratified layer position. In this case, the stratified flow is not established and the transition to mixing flow is observed. This was due to the airflows from the stratified layer through the exhaust opening.
3. If the exhaust location is above the stratified layer. In this case, the hot air flows out through the exhaust opening while the stratified interface level height moves to reach the top of the chamber.

It is seen that the degree of stratification DS for case 1 is considerably higher than that for case 3. Where a higher exhaust location will tends to higher level of stratification. On the other hand, a lower location may result in lower levels of stratification. For these three cases, the stratified interface level height will move up and down to maintain on the stratified layer. It could be fixed by distributing the exhaust location vertically.

From figures 4.5.7 to 4.5.10, the exhaust location is a key factor in stratification phenomenon thus in ventilation process. It is important in the evaluation of the flow characteristics in ventilated rooms. When the exhaust location is situated in the upper zone, while the warm air is supplied at higher level in two zone environment, the warm, fresh air will spread under the ceiling due to buoyancy. It will be extracted when it reaches the outlet. Thus the large amount of fresh air will short circuit into the outlet, while small amount of fresh air will reach the occupied zone. In this case, the exhausting of fresh air is large and the concentration of contaminants in the lower zone is too high. On the contrary, when the exhaust location is situated in the lower zone or close to the stratified layer interface, the contaminant removal effectiveness is larger.

Very similar suggestion was obtained by Mundt (2001) that the source of contaminant must be in the upper zone to be exhausted at large effectiveness.

The increase in hot air flow rates increases the degree of stratification $dT/d\delta$, but further increases in hot air flow rate produce little further increase in degree of stratification $dT/d\delta$. Whatever the explanation for these observations, the results of Figures 4.5.7 to 4.5.10 could provide a useful indication for this case.

From the effect of input airflow rates, while the hot and cold airflow rates decline each other, the input and exhaust locations reinforce each other.

Comparison between Figures 4.5.7 to 4.5.11 shows the effect of increasing exhaust location on the stratified flow characteristics. However, for this case:

1. It increases the stratified layer height, due to the height shift, and decreases the temperature difference $dT/d\delta$ so DS, due to the evacuation of fresh hot air from the upper zone.
2. It increases the significant effect of cold airflow rate due to the wide domain in the lower zone where both the mixing and the influence length will increase.

The analysis above shows that increasing the exhaust vertical location results in an extended stratified region with small temperature difference. The degree of stratification becomes smaller and the flow will tend towards mixed conditions. It is similar to the results obtained by Linden et al. (1990), using filling boxes, and demonstrated when the output location is high, the amount of mixing was increases and the interface was mixed.

Figures 4.5.7 and 4.5.11 shows how the dimensionless temperature distribution varies depending on exhaust locations. The figure shows that the temperature does not vary linearly over the chamber height and it can be divided into three zones. While the height of the lower zone is changing with the source location, the upper zone is fixed for a number of source locations. While temperature remains constant in the lower and upper zones, (except at 2 m case) temperature in the stratified zone changes linearly.

In ventilation applications, stratification interface level height and ventilation airflow rates are the two main factors in the design of natural ventilation system [Chen and Li

(2002)]. Both input and exhaust vertical locations have a significant effect on the flow characteristics, and reinforce each other. In Linden's and Skistad's models there are no more explanations for the effect of these parameters on the stratified flow characteristics.

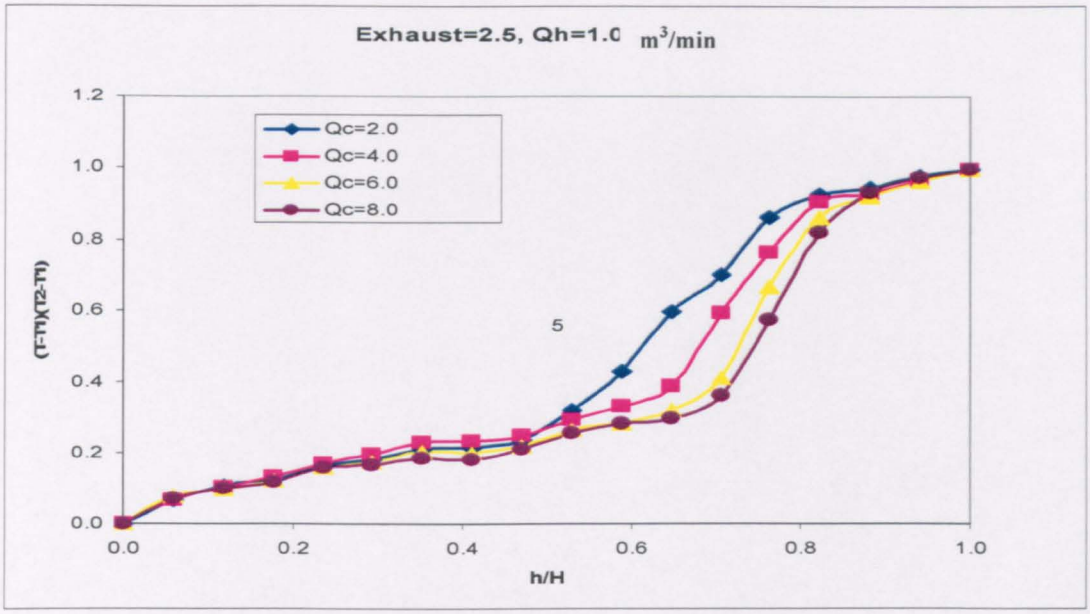

Figure 4.5.7: Comparison of dimensionless temperature profile along vertical centreline with dimensionless height across the chamber at a fixed axial location of (3.75,2.8) m and fixed hot air flow rate ($Q_h = 1.0 m^3/min$) for different cold flow rates ($Q_c = 0,2,4,6,8 m^3/min$) in the environmental chamber for 1.5 m input location.

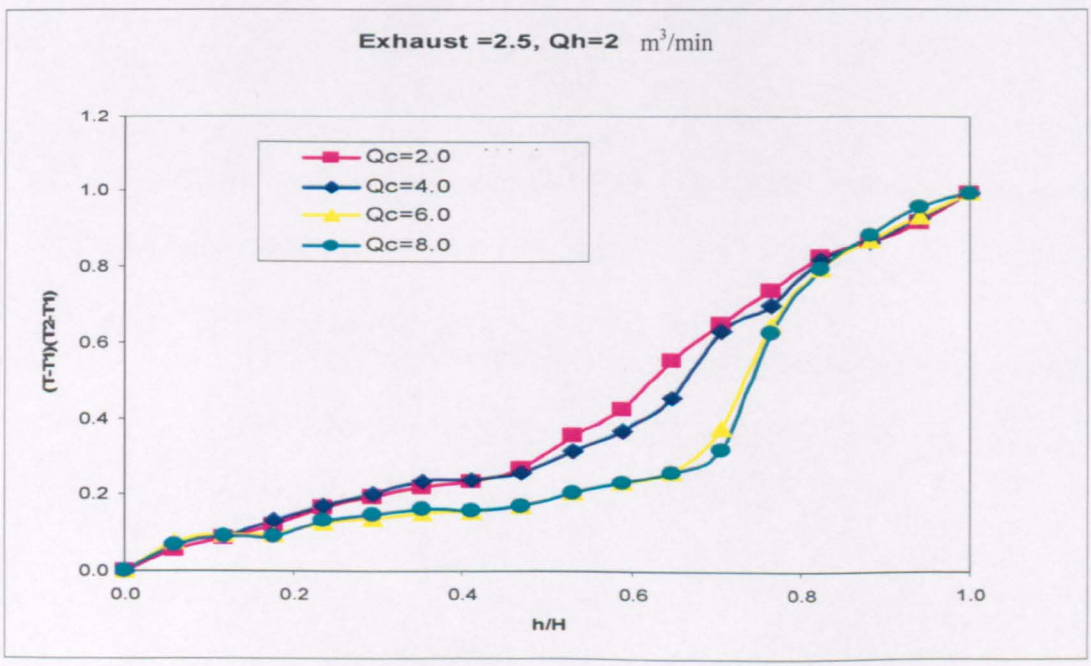

Figure 4.5.8: Comparison of dimensionless temperature profile along vertical centreline with dimensionless height across the chamber at a fixed axial location of (3.75,2.8) m and fixed hot air flow rate ($Q_h = 2.0 m^3/min$) for different cold flow rates ($Q_c = 0,2,4,6,8 m^3/min$) in the environmental chamber for 1.5 m input location.

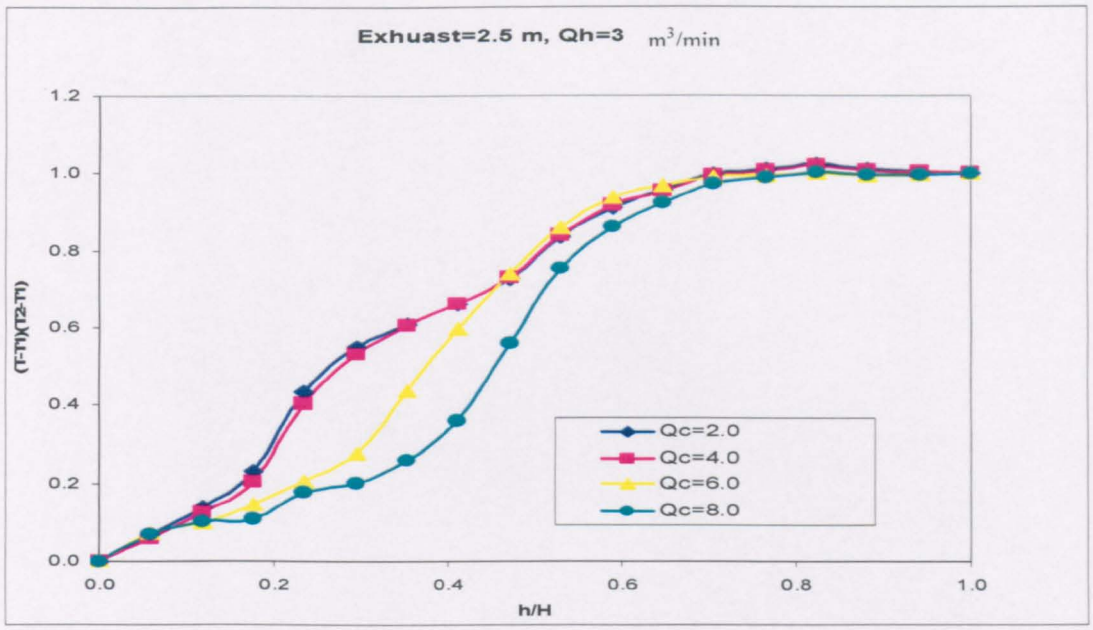

Figure 4.5.9: Comparison of dimensionless temperature profile along vertical centreline with dimensionless height across the chamber at a fixed axial location of (3.75,2.8) m and fixed hot air flow rate ($Q_h = 3.0 m^3/min$) for different cold flow rates ($Q_c = 0,2,4,6,8 m^3/min$) in the environmental chamber for 1.5 m input location.

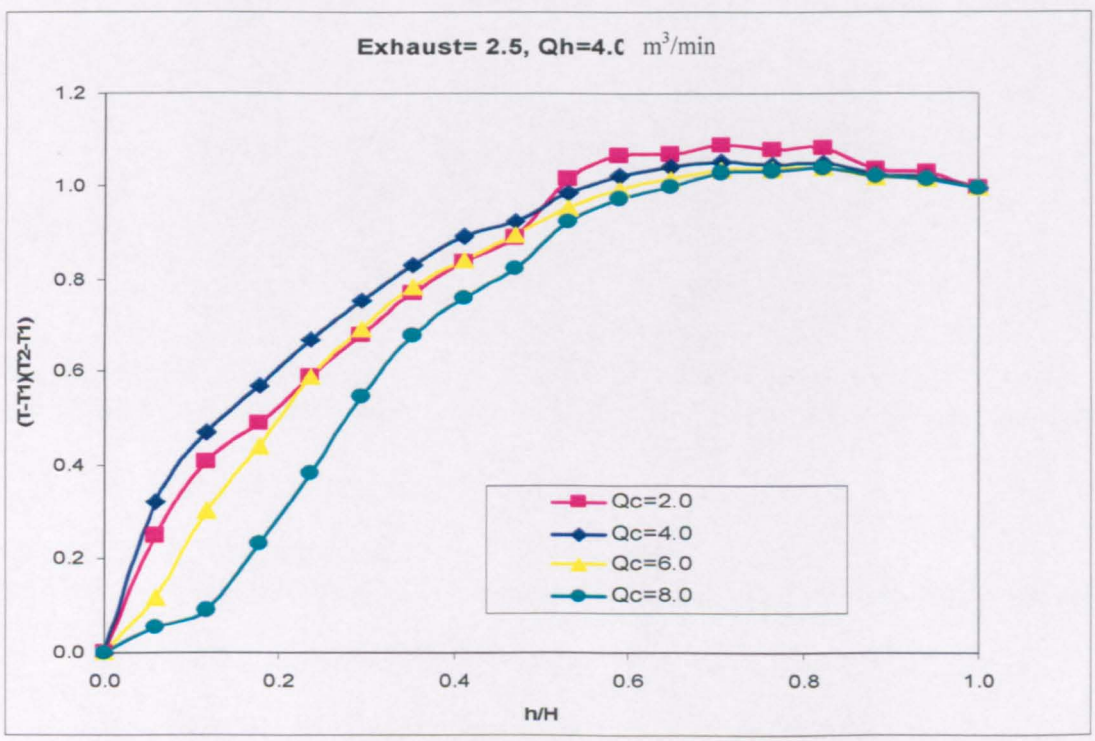

Figure 4.5.10: Comparison of dimensionless temperature profile along vertical centreline with dimensionless height across the chamber at a fixed axial location of (3.75,2.8) m and fixed hot air flow rate ($Q_h = 4.0 m^3/min$) for different cold flow rates ($Q_c = 0,2,4,6,8 m^3/min$) in the environmental chamber for 1.5 m input location.

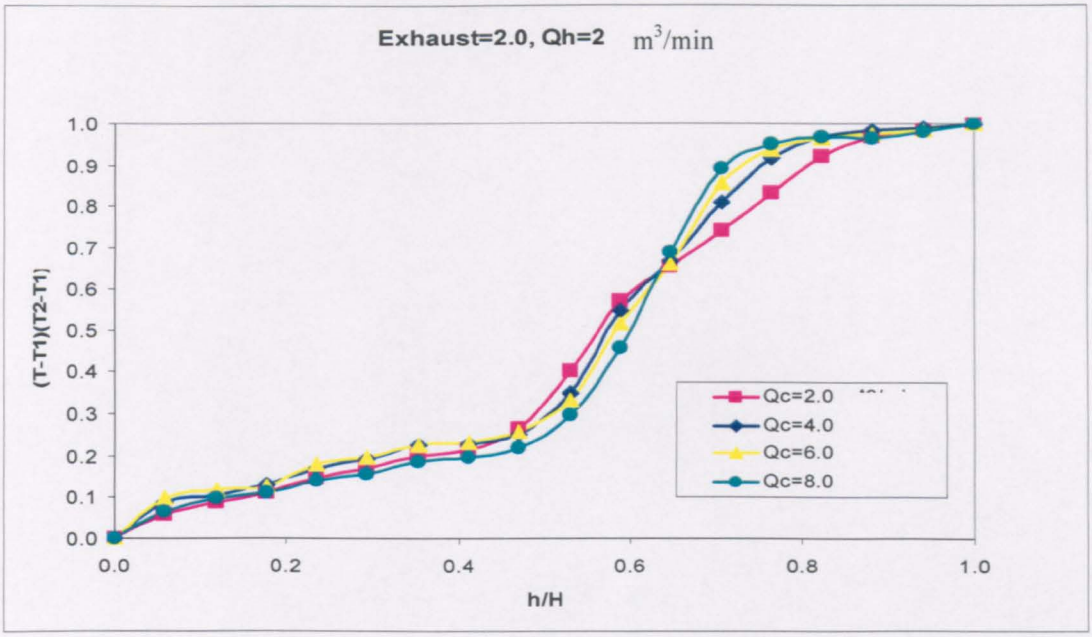

Figure 4.5.11: Comparison of dimensionless temperature profile along vertical centreline with dimensionless height across the chamber at a fixed axial location of (3.75,2.8) m and fixed hot air flow rate ($Q_h = 2.0 m^3/min$) for different cold flow rates ($Q_c = 0,2,4,6,8 m^3/min$) in the environmental chamber for 2.0 m input location.

As presented earlier, the higher the input vertical location, the higher the interface level height. Different heights of input vertical locations will result in different levels of stratification as evaluated by [Hee-Jin and Dale (2001)]. From the experimental results detailed in Chapter 4, it was found that the input vertical location could control the stratified interface level height and mixes the flow. The penetration distance and the interface level height are both found to decrease with decreasing input location, [Abdulkarim and Yogesh (1996)].

The flow characteristics of the input location were found to be affected considerably by the exhaust location. As discussed earlier, Skistad's model related the stratified layer thickness to the extract air flow rate rather than the input and exhaust height. In the present work we found that the exhaust vertical location does not alter the position of the interface level height. It could be in the locations above or below the interface level height. It must be controlled in order to save energy in buildings, where the designers have to take the advantages of thermal stratifications to ventilate the occupied zone rather than the whole space [Calay et al (2000)]. Consequently, the exhaust location must be where "the exhaust temperature should not exceed the temperature in the

occupied zone" [Hagstrom et al. (2000)]. On the contrary, fixed exhaust location is ineffective to extract the contaminant rather than the fresh air from the occupied zone.

The results of temperature profiles and smoke visualisation are in agreement, where both models can give the same indications for the flow characterstics of various values of exhaust locations. The present investigations have shown that there are many important parameters that affect the stratified flow characteristics in contrast to [Skistad (1998)] observations and relations that related the stratified layer thickness to flow and geometrical parameters without considering the input and output locations.

The input and output ducts locations are important for the air quality at the breathing zone. Eexhaust vents or outlets should be located across the room and at high level above inlets to maximize stack effect on the leeward side as high as possible in the building, where the vertical distance between the inlet and exhaust openings should take the advantages of the stack effect.

4.5.3 Smoke Visualisation of Exhaust Locations

smoke visualisation was also used to evaluate the stratified flow characteristics with variable exhaust locations. The results of temperature profiles and smoke visualisation show that both models can give the same indications for the flow characterstics of various values of exhaust locations. The results of smoke visualisation were shown in the Figures 4.5.12 to 4.5.15.

In Figures 4.5.12 and 4.5.13, it is seen that when the exhaust height was comparatively low, the flow stratifies at comparatively lower levels, while the smoke penetrates and emerges in the stratified layer. There are two reasons for this:

Firstly, when the stratified layer interface level height is low enough then the smoke will emerge in the stratified layer under the effect of high upward buoyant forces, where smoke is still warm compare with the relatively cool lower zone, cross temperature differences did, however, provide a source of potential energy which drive the smoke to rotate downward.

Secondly, when the stratified interface level height is low, the entrainment air from the lower zone to the smoke plume will be at minimum, for this case, the smoke velocity

occupied zone" [Hagstrom et al. (2000)]. On the contrary, fixed exhaust location is ineffective to extract the contaminant rather than the fresh air from the occupied zone.

The results of temperature profiles and smoke visualisation are in agreement, where both models can give the same indications for the flow characterstics of various values of exhaust locations. The present investigations have shown that there are many important parameters that affect the stratified flow characteristics in contrast to [Skistad (1998)] observations and relations that related the stratified layer thickness to flow and geometrical parameters without considering the input and output locations.

The input and output ducts locations are important for the air quality at the breathing zone. Eexhaust vents or outlets should be located across the room and at high level above inlets to maximize stack effect on the leeward side as high as possible in the building, where the vertical distance between the inlet and exhaust openings should take the advantages of the stack effect.

4.5.3 Smoke Visualisation of Exhaust Locations

smoke visualisation was also used to evaluate the stratified flow characteristics with variable exhaust locations. The results of temperature profiles and smoke visualisation show that both models can give the same indications for the flow characterstics of various values of exhaust locations. The results of smoke visualisation were shown in the Figures 4.5.12 to 4.5.15.

In Figures 4.5.12 and 4.5.13, it is seen that when the exhaust height was comparatively low, the flow stratifies at comparatively lower levels, while the smoke penetrates and emerges in the stratified layer. There are two reasons for this:

Firstly, when the stratified layer interface level height is low enough then the smoke will emerge in the stratified layer under the effect of high upward buoyant forces, where smoke is still warm compare with the relatively cool lower zone, cross temperature differences did, however, provide a source of potential energy which drive the smoke to rotate downward.

Secondly, when the stratified interface level height is low, the entrainment air from the lower zone to the smoke plume will be at minimum, for this case, the smoke velocity

will be high enough to reach the maximum height at an elevation above the interface level height. However, if the exhaust is in the upper zone, then the velocity reaches its minimum value at an elevation below the exhaust location as seen in Figures 4.5.14 and 4.5.15.

Comparisons between Figures 4.5.12 to 4.5.15 show the effect of increasing exhaust height in increasing of the stratified layer interface level height. As shown in the Figures, the smoke concentration is very high in the stratified layer, due to the high temperature gradient. In the lower and upper zones, the smoke concentration is invisible due to circulations and the high mixing of air in these zones.

At the source of smoke, oil and entrained air rise as a buoyant flux over the source of smoke release. During penetration of smoke, ambient conditions begin to affect the smoke. The lifted smoke would first become warmer (less dense) than the surrounding. It continues to rise freely until it becomes as cool (dense) as the surrounding air. Once it reaches this stage at which its temperature equals that of the surrounding environment it starts to stratify.

In the presence of stratification, while the buoyancy and momentum forces cause the smoke to flow in the downstream direction, the stratification deflects the upward smoke motion by entrainment of ambient air. The primary variables characterizing a smoke penetration are the smoke characteristics and the stratification characteristics. The smoke characteristics like the kinematic buoyancy and momentum are comparable with the stratification characteristics like the strength and interface level height of the stratified layer. Depending on these parameters, the smoke motion exhibited a range of behaviors:

Case 1: When the stratified layer interface level height, is much less than the smoke penetration height. In this case, the smoke reaches the stratified layer before loosing its buoyancy force, so it will go through the stratified layer to stratify at the level of neutral buoyancy. In this case, strong stratified layer can work as a thermal barrier against the smoke penetration due to the higher temperature gradient in the stratified layer and the entrainment of hot air. While the smoke buoyancy flux above this level being negative, the smoke will then descend back towards the stratified layer height and to stratify horizontally at the level of stratification, with a bulb shape as shown in Figure 4.5.13.

Case 2: when stratified layer interface level height is much greater than the smoke penetration height. In this case, the increase in the volumetric flux due to the entrainment of cold air will decrease the reduced gravity in order to preserve the conservation of buoyancy flux. Therefore the smoke will reach its neutral buoyancy before reaching the stratified layer, and start to stratify at a height of neutral buoyancy rather than the interface level height.

Case 3: when the smoke penetration height is at the level of stratification. In this case, the smoke temperature equals that of the surrounding environment (have equal densities), the buoyancy of the smoke is zero, and the neutral buoyancy height is at the level of stratification. In which, the smoke will stratify at the neutral buoyancy height without significant effect for the stratified layer height.

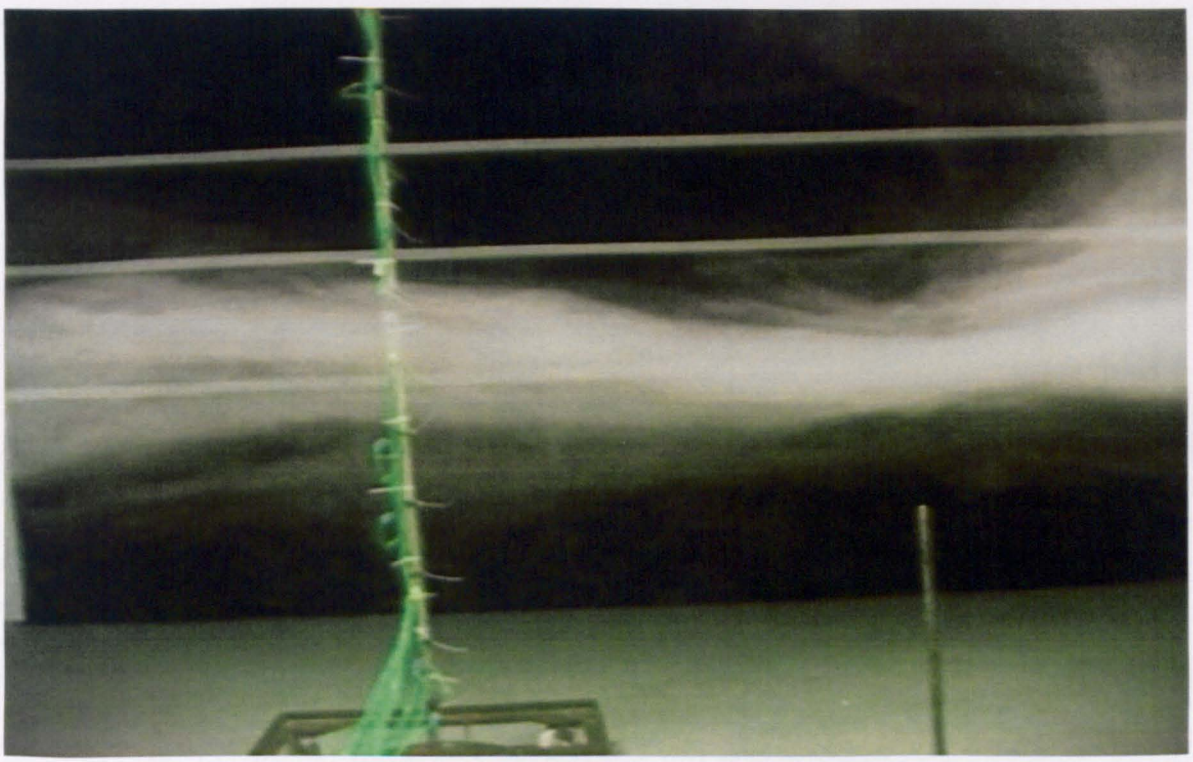

Figure 4.5.12: A video-recorded picture showing stratification induced by smoke visualization, at steady state conditions, for opening vertical locations of $H_h = 2.0\,m$, $H_{ext} = 1.0\,m$ and input airflow rates of $Q_L = 2.0\,m^3/min$ and $Q_U = 6.0\,m^3/min$.

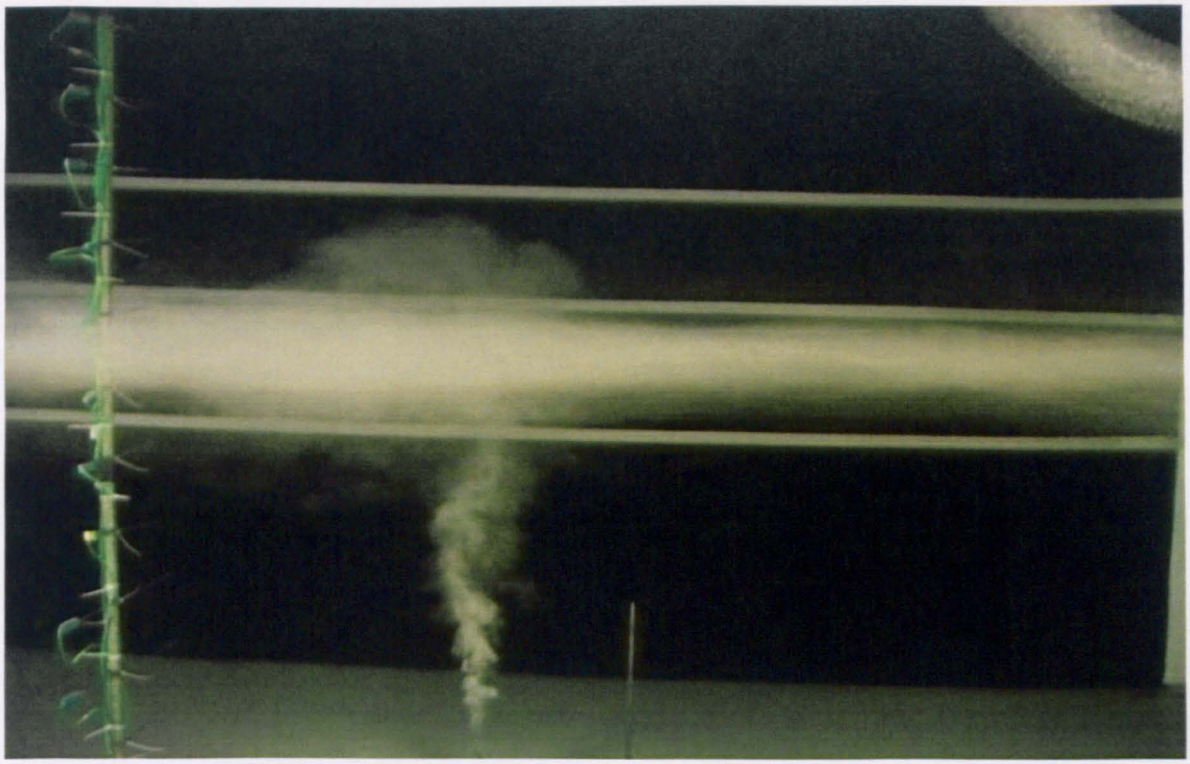

Figure 4.5.13: A video-recorded picture showing stratification induced by smoke visualization, at steady state conditions, for opening vertical locations of $H_h = 2.0\,m$, $H_{ext} = 1.5\,m$ and input airflow rates of $Q_h = 2.0\,m^3/min$ and $Q_c = 6.0\,m^3/min$.

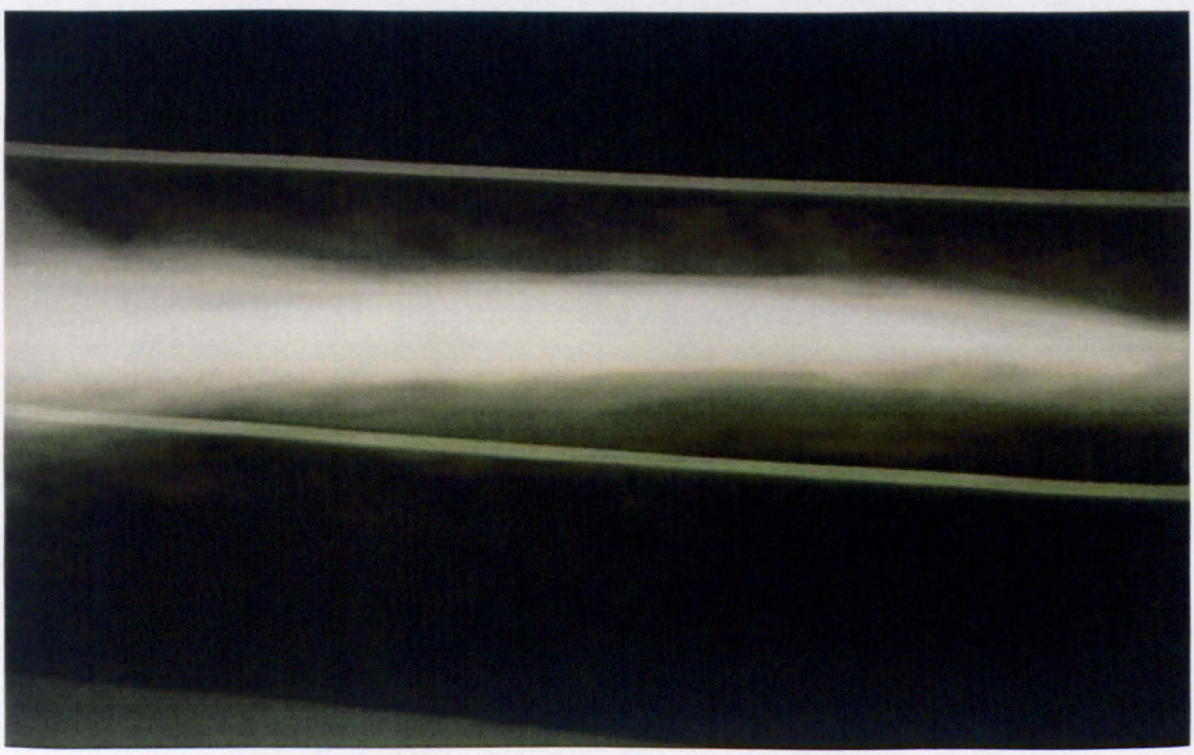

Figure 4.5.14: A video-recorded picture showing stratification induced by smoke visualization, at steady state conditions, for opening vertical locations of $H_h = 2.0\,m$, $H_{ext} = 2.0\,m$ and input airflow rates of $Q_h = 2.0\,m^3/min$ and $Q_c = 6.0\,m^3/min$.

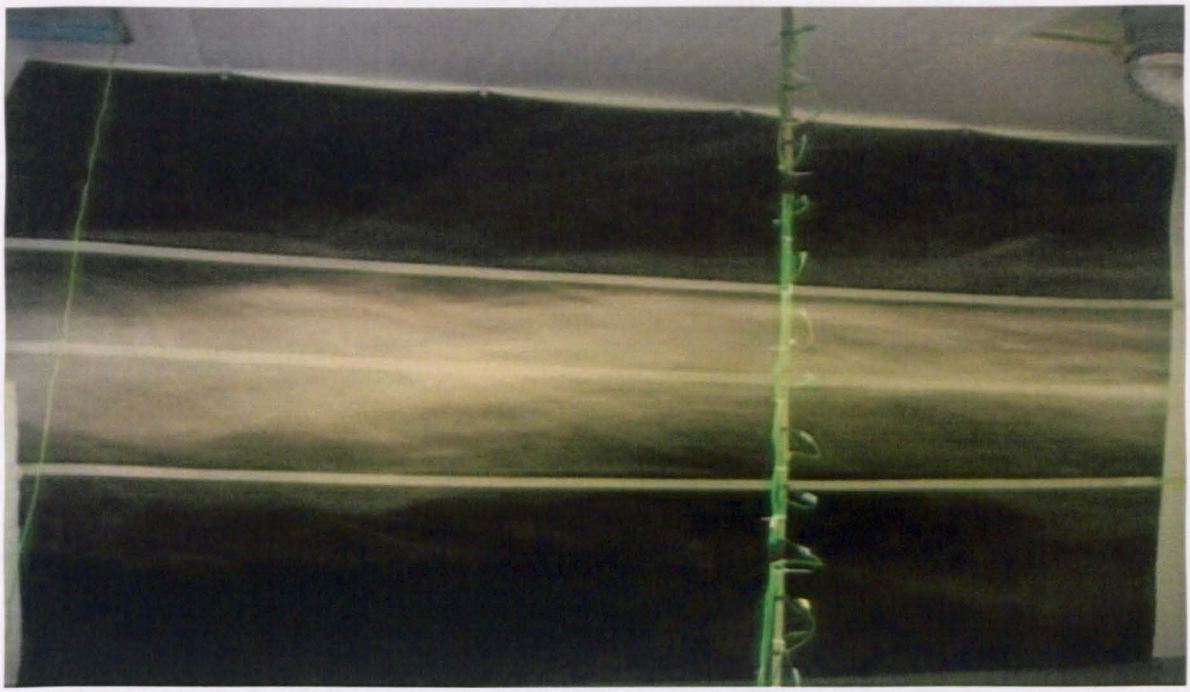

Figure 4.5.15: A video-recorded picture showing stratification induced by smoke visualization, at steady state conditions, for opening vertical locations of $H_h = 2.0\,m$, $H_{ext} = 2.5\,m$ and input airflow rates of $Q_h = 2.0\,m^3/min$ and $Q_c = 6.0\,m^3/min$.

4.6 Summaries and Conclusion

The distribution of the stratified flow along and across the flow direction was investigated. The effect of input airflow rates on the stratified flow was conducted. Both effects of hot and cold airflow rate variations were studied. The experiments were done using the recent experimental air modeling technique explained in Chapter 3. Both temperature and smoke visualisation were compared. Data was analysed, results were discussed and the concluding remarks were given and discussed.

The study has involved a number of exercises that can be used in ventilation research and applications. It was found that for certain ranges of input airflow rates, stratification could occur for all conditions. While the hot airflow rate has more significant effect on the stratified flow than that of cold flow rate the moderate airflow rates show better performance of thermal stratification with respect to thermal energy. Thus, controlling airflow rate may control the degree of stratification, and stratification interface location.

It should be noted that the stratification interface level, the total ventilation flow rate and the geometry of the space are, generally, the major concerns for the design of ventilation systems with most efficiently. The stratification level height must be above the occupied zone, and the ventilation flow rate within the requirements of space occupants.

For large dimensional environmental chamber, the space variations have no significant effect on thermal stratification. Strong stratified layer stand as a thermal barrier to decelerate the smoke motion, which increases both the temperature in the upper zone and the concentration of the smoke along the surface in the occupied zone.

The effects of both input and exhaust locations on the stratified flow characteristics were also investigated. When the aperture of input location is higher, the buoyancy forces are increased and the flow becomes more stratified. On the contrary, the decrease in the aperture of input location decreases the interface level height leading to a mixed flow in both zones.

In terms of interface level height, while the input and exhaust locations are reinforcing each other, the increase in hot and cold airflow rates does not cause a corresponding increase in interface level height.

Chapter 5

Chapter 5

Mixing of Stratified Flow

5.1 Introduction

The purposes of this part of the work were to investigate the momentum required to break down a stratified layer in a ventilated room using an air jet. Two methods of air supply were used. The first method uses cold and warm jet flow. For cold jet supply, the temperature of injected air was the ambient. For warm ceiling jet, the temperature of injected air was the hot air supply. The second method was by inverting the supplier vertical locations. The purpose of these methods was to break or translate the stratified layer according to flow applications. In the first method, the momentum was increased gradually at a downward right angle to intersect the stratified layer despite the degree and the level of stratification. In the second method the flow of high buoyancy was supplied upward, while the flow of high momentum was supplied downward. The momentum required is a dependant of flow characteristics such as h, δ DS and $dT/d\delta$ and the flow conditions.

Figure 5.1.1 shows a general representation for different scenarios of selective ventilation using ceiling jet [Calay et al (2000], where the flow characteristics can be controlled by adjusting the jet temperature and momentum:

1. A high momentum ceiling jet breaks through the stratified layers; circulates the air in the lower zone, and produces full mixing in the occupied zone, as indicated in Figure 5.1.1a.
2. A low momentum ceiling jet increases the interface level height and ventilates the occupied area without destroying the stratified layer (Figure 5.1.1b).
3. A low momentum ceiling cold jet with insufficient momentum fluxes to break through the stratified layer. In this case the interface must be at higher levels

otherwise the injected air will stratify at certain level in the space between the interface level height and the ceiling, as indicated in Figure 5.1.1c.

4. A warmer ceiling jet ventilated the chamber with positive momentum and negative buoyancy (Figure 5.1.1d). In this case, both momentum and buoyancy weaken each other. The momentum initiates the flow to go downward, whilst the buoyancy forces tend to turn the jet upwards.

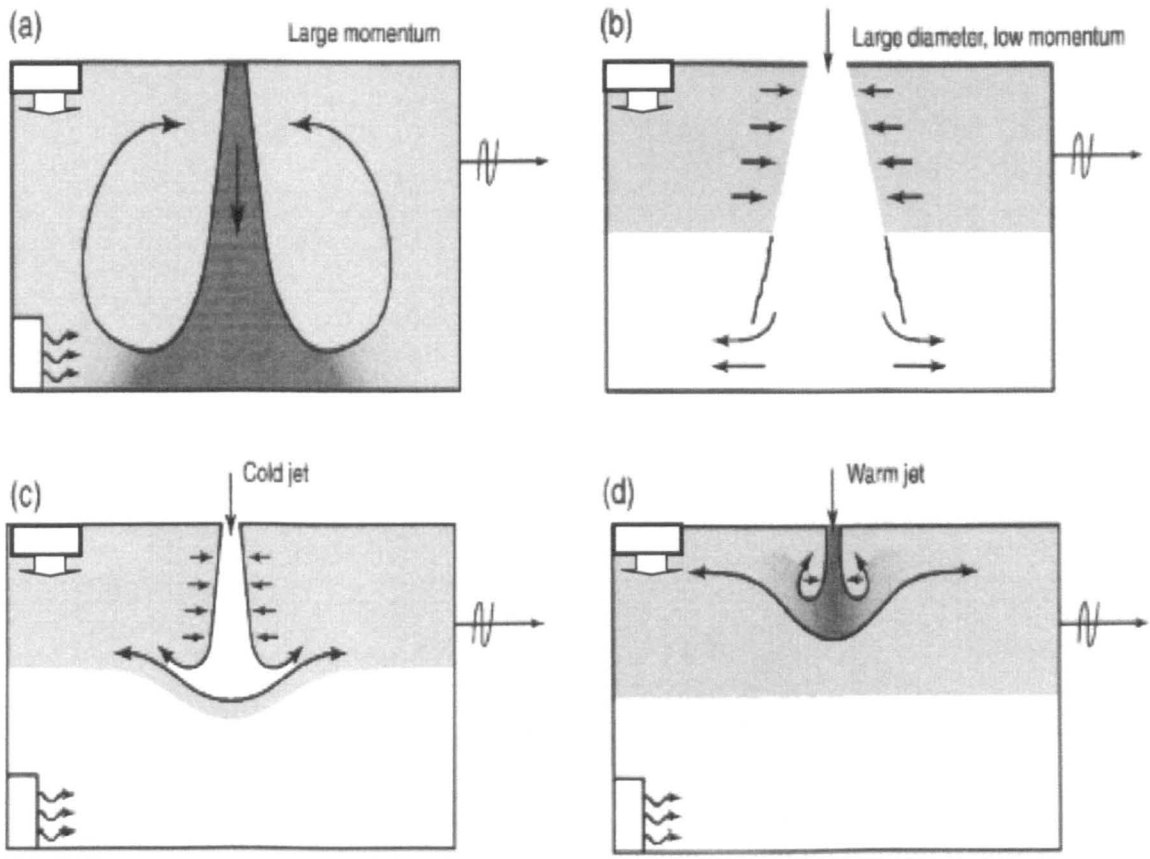

Figure 5.1.1: Typical settings of supply and exhaust locations used in selective ventilation [Calay et al (2000)]: a) High jet momentum, supplies air through the stratified layers and generates full mixing; b) low jet momentum, supplies air without destroying the stratified layer; c) low momentum cold jet stratifies in the upper zone; d) low warm jet provides additional temperature difference to improve the stratification characteristics.

5.2 Flow Specifications and Preliminary Tests

The breaking up of a stratified layer using both a cold and a warm vertical jet was studied. The momentum was introduced by injecting the air from the ceiling using a jet source. The source of the injected air was the ambient for a cold jet while it was the hot

air supply for a warm jet flow. The jet opening size was 0.11 m diameter and the specific momentums were in the ranges of 0.0 to $2.17\,m^4/s^2$ (equation 5.1)

$$M_j = \frac{M}{\rho_j} = Q_j V_j \tag{5.1}$$

Figure 5.2.1 shows a geometric sketch of the environmental chamber with a diagrammatic representation of the input airflow supplies, exhaust, plume, and ceiling jet. The flow specifications (velocity, volumetric flow rate and specific momentum) are listed in table 5.2.1.

Using the jet momentum, the stratified flow was mixed to a achieve uniform vertical temperature distribution, while the stratified layer was translated to higher levels depending on the momentum flux introduced by the jet and the flow conditions. Smoke visulisation was used to validate the experimental work and to indicate the effect of vertical jet flow on the stratified flow characteristics.

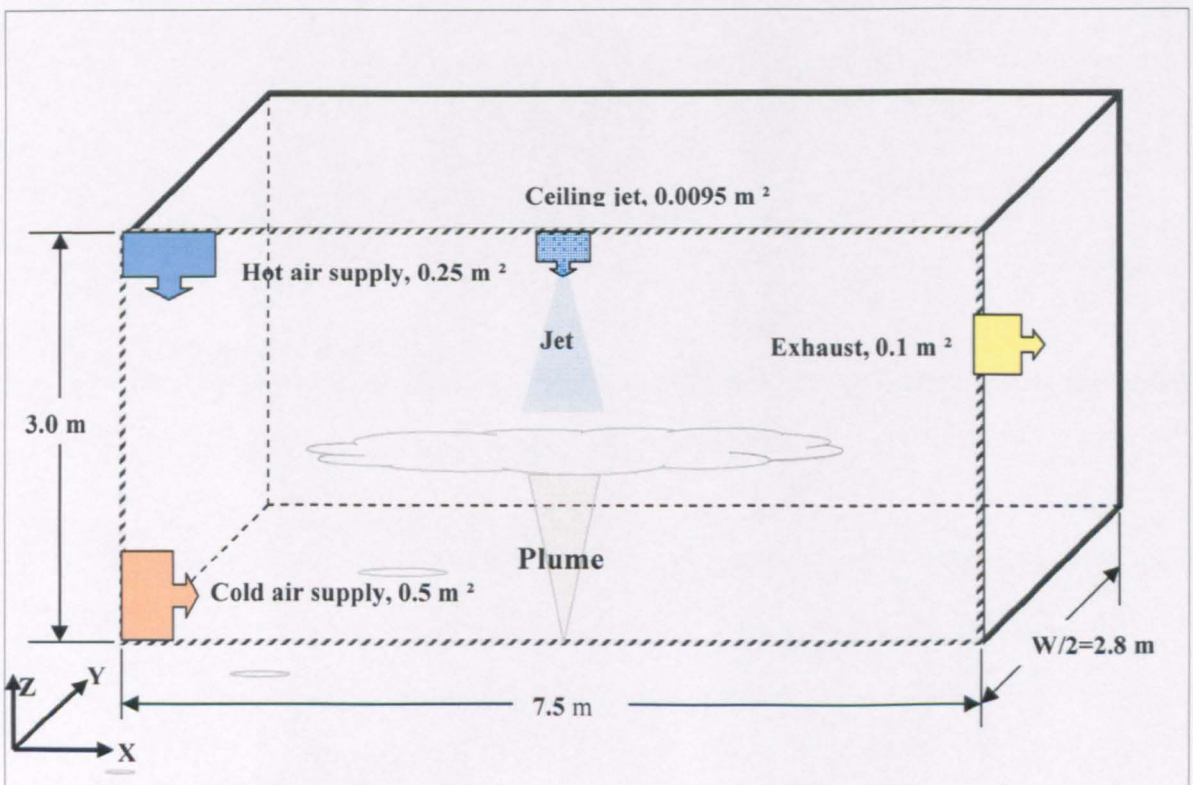

Figure 5.2.1 Definition sketch of the environmental chamber showing a diagrammatic representation of the input airflow supplies, exhaust, and ceiling jet.

V_j (m/s)	Q_j (m^3/min)	$M_j/\rho = Q_j V_j$ (m^4/s^2)
0.000	0.000	0.000
0.378	0.215	0.001
0.756	0.431	0.005
1.133	0.646	0.012
1.511	0.862	0.022
2.267	1.292	0.049
3.022	1.723	0.087
4.533	2.585	0.195
6.044	3.446	0.347
7.555	4.308	0.542
9.066	5.169	0.781
10.577	6.031	1.063
12.088	6.893	1.389
13.599	7.754	1.757
15.110	8.616	2.170

Table 5.2.1: Listed the jet speed (V_j), volumetric flow rate (Q_j) and specific momentum (M_j) used in the experiments.

Figure 5.2.2 shows preliminary experimental results of mixing using both plumes and jets of $3.0\,m/s$. Both cold and hot jet flows were tested. The results are shown in terms of temperature visualization technique. From the preliminary results, we have seen that once the flow was stratified at certain level in the middle of the chamber, the momentum mixed the stratified layer while a new stratified layer was established in the domain. At mixed zones, the temperature isothermal lines were close to one another because the profiles become more vertical (less stratification). The change of jet speed impact on the shape of the profiles and its position on the temperature scale.

Figure 5.2.2 (a) shows the effect of heat source (hot plume) on the stratified flow. The temperature isothermal lines illustrated the effect of hot plume on the stratified flow. It increases the temperature in the lower zone and stratifies at the level of stratification. The buoyant plume has a significant effect on the flow in the lower zone, while it has a small effect on the flow in the upper zone. It is in agreement with the results of [Mundt (1994)] that a person can attain a good air quality in the breathing zone, even if it is in a polluted layer, where the convective plume around the body breaks down through the polluted layers.

Figures 5.2.2 (b) and (c) show the temperature isothermal lines of both cold and hot (warm) jet flow. The results were for the same conditions and modes of jet flow (3.0 m / s), and referring to different flow conditions.

Figure 5.2.2 (b) shows that the effect of hot jet (40 °C) was to increase the temperature in the lower zone, to break down the stratified layer in the middle zone and to stratify the flow in the upper zone. As a result a hot layer was established near the ceiling.

Figure 5.2.2 (c) shows the effect of cold jet (ambient temperature) was to mix the flow in the lower zone, push the stratified interface level height upward to reach the ceiling with no significant effect in the upper zone. For this case, the dense incoming air will flow downwards into the space under the effect of both jet momentum and buoyancy.

Comparisons between Figures 5.2.2 (a) and 5.2.2 (c) shows that the effect of hot plume and the cold jet injecting air downward on a stratified flow are opposed. On the contrary, the effect of hot jet was as a plume in the lower zone and as a cold jet in the upper zone with completely different effects in the middle zone (stratified layer).

Figure 5.2.3 shows the experimental results of both cold and warm jet for the same boundary conditions, whilst the modes of jet flows are referred to different temperature distributions. Figure 5.2.3 shows the stratified flow characteristics of (h = 1.4 m, δ = 0.85 m and $dT/d\delta$ = 13 °C/m) is mixed by using both cold and warm jet flow. The results show the temperature profile of hot jet is always linear, the stratified layer thickness is diffused with dT/dz = 1.7 °C/m, while the temperature profile of cold jet has a significant stratified layer of (h = 2.0 m, δ = 0.3 m and $dT/d\delta$ = 17 °C/m). As seen from the results, while the effect of warm jet is more significant on the flow characteristics δ and $dT/d\delta$, the cold jet has a significant effect on the stratified layer interface level height h, and so the height of the lower zone.

For warm jet, the density of injected air is increased by the entrainment air from the surrounding. On reaching the bottom of the space, the air spreads across the bottom of the space; a circulation is thus set up within the space leads to a mixed the flow. However when the amount of mixing is greater the interface is more diffuse

Figure 5.2.2: Effect of mixing modes on a stratified flow at ($Q_h = 3.0\ m^3/min$) hot airflow rate and ($Q_h = 6.0\ m^3/min$) cold airflow rate, at the centre of environmental chamber. a) Hot plume. b) Hot jet of 0.11m diameter and speed of $V_j = 3.0\ m/s$, c) Cold jet of 0.11m diameter and speed of $V_j = 3.0\ m/s$, (Different colours denote vertical height of temperature sensor from 0.25 to 2.8 m, as shown on thermocouple stand figure 3.3.1).

For relatively cold jet, the dense incoming air will flow into the space descending to the floor as a curved plume. For low specific momentum, the interface descends significantly faster because of the greatest density of the fluid above the interface. The large velocity (momentum) of cold jet inflow caused the entrainment of buoyant fluid from the lower zone to push up the interface to reach the ceiling. Once the front of dense air reaches the stratified layer, the stratified layer breaks down and the flow becomes fully mixed.

.

From the preliminary tests, when the jet momentum is not large enough, or the temperature of air injected is greater than that of the pre-stratified layer, the injected air cannot reach the stratified layer. In this situation, the jet cannot activate the mixing in the domain and may stratify at certain levels above the floor. These levels of stratification depend on both the momentum and the temperature of injected air, and the stratified layer interface level height. The balance between momentum and buoyancy forces in the injected air must be adjusted.

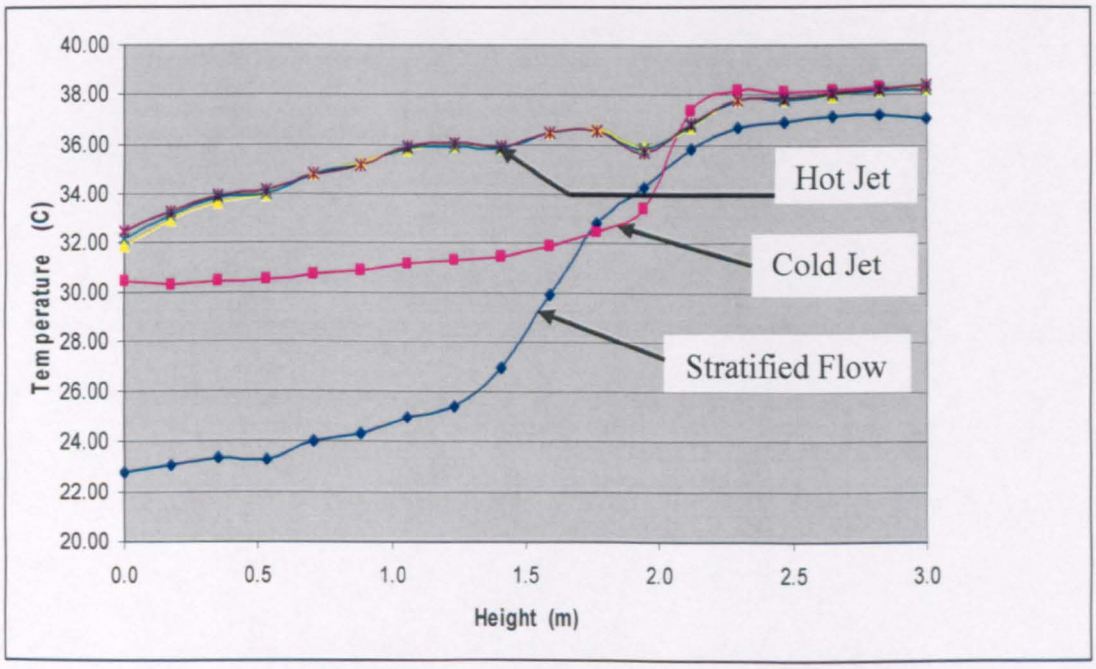

Figure 5.2.3: Effect of both cold and hot ceiling jet of (3.0 m/s) on a stratified flow at (Q_h = 3.0 m^3 / min) hot airflow rate and (Q_h = 6.0 m^3 / min) cold airflow rate with a locations of 2.0 and 1.5 m respectively at the centre of environmental chamber.

5.3. Time Variations of Temperature

While the formation of stratified flow needs long period of time, the breaking down of the formed layer needs less time depending on the method of destruction. Figure 5.3.1 shows a time variations from stratified flow to mixed flow. It shows the relations between the temperature isothermal lines and the time variations for a specific period of time (115 minutes). By inversion the ducts vertical locations, the destruction of the stratified layer occurred within 10 minutes of time (13:22 to 13:32).

Our extensive investigations in Chapter 4 have shown that generally two distinct stratified layers of air form, an upper zone containing warm air and a lower zone containing cooler air separated by a boundary stratified layer with thickness δ. The transformation from stratified flow to mixed flow takes place over a specific period of time depends on both mixing method and flow conditions. Figure 5.3.2 show the variations of vertical temperature profiles for a period of time (5 hours) under the effect of warm jet momentum:

The first three curves in Figure 5.3.2 show the initial conditions of stratified temperature profiles with a degree of stratification value (of DS=2.4), whereas the sequential curves illustrate the measured temperature profiles successively offset by 2 °C.

At beginning of transformation, the temperature profile is very similar to that for a stratified flow. As one goes forward, the temperature profiles become linear, thus indicating a mixed flow development. This is expected since, at the beginning of the transition period, the flow is nearly stratified and is fully mixed at the end of transition period.

It can be seen in 5.3.2 that the degree of stratification DS changes from the near stratified value (of DS=2.2, at time 17:02:55) to the nearly fully mixed value (of DS=1, at time 23:45:05) within the transition period.

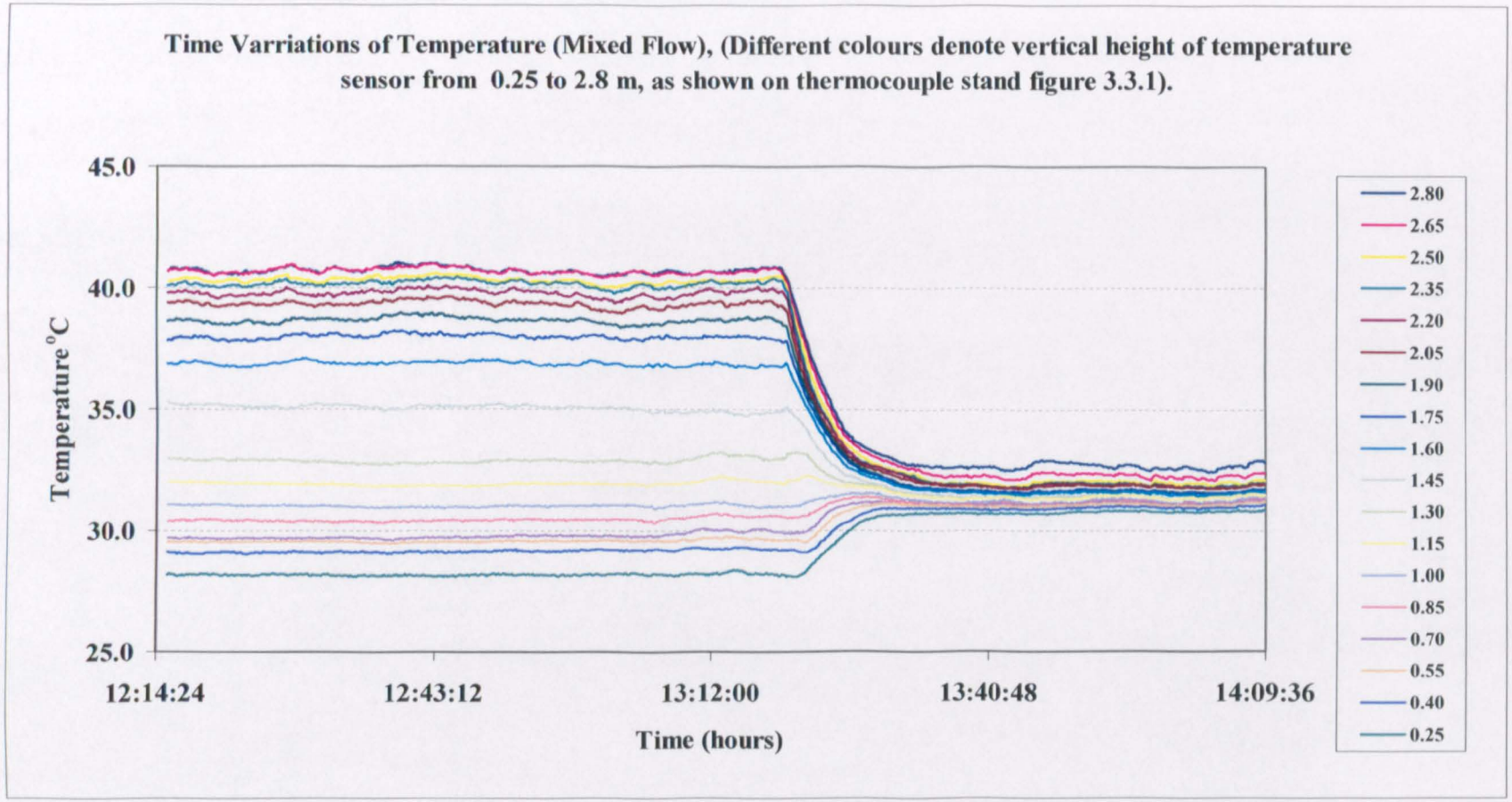

Fig 5.3.1: Time variations of Temperature (Mixed Flow), (Different colours denote vertical height of temperature sensor from 0.25 to 2.8 m, as shown on thermocouple stand Figure.3.3.1.

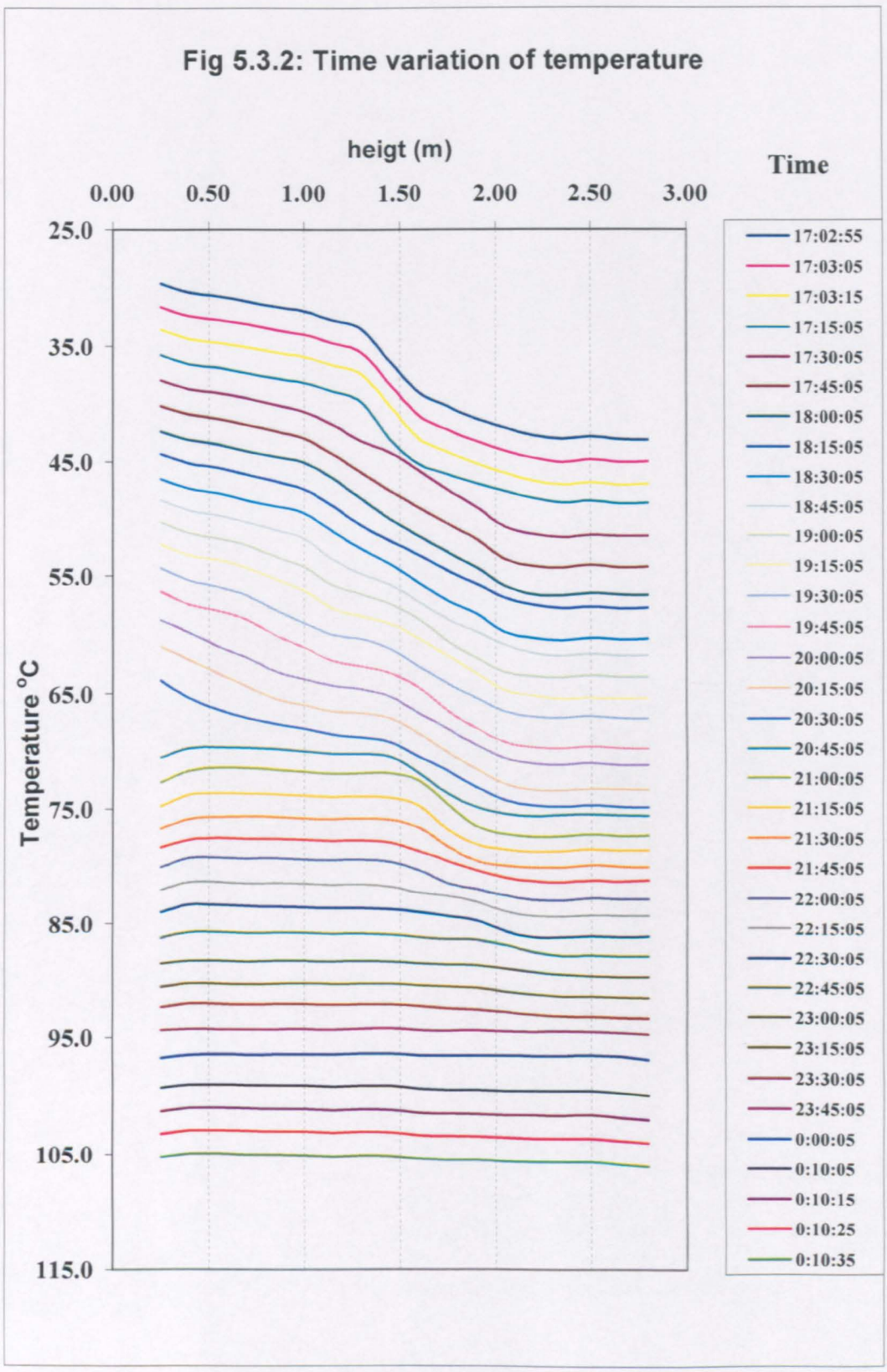

Figure 5.3.2: Vertical temperature profiles, each successive profile is offset by 2.0 °C and separated initially by a minute and lately by 15 minutes intervals. The successive profile plot was used by [(Lorke et al. (2004)] and others.

5.4 Mixing Flow Using Cold Jet

Experimental results using cold jet (i.e. local ambient air) of 0.11 m diameter shown in Figure 5.2.1 were carried out. The effect of momentum, on the mixing of stratified flow for a various air flow rates, was studied. The presented data reveal the effect of varying speeds of the cold vertical jet as illustrated in table 5.2.1 and Figure 5.2.1 on the stratified flow characteristics. Comparisons of fifteen experimental temperature profiles in entire locations will be discussed. The temperature profiles appear to be dependent of jet speed.

For the analysis, the mode of flow is classified according to the stratified layer interface level height. Table 5.4.1 shows the classification of the flow with the airflow rate ratio (Q_c/Q_h).

Mode of flow	Qc / Q_h	2.00	4.00	6.00
High airflow ratio	1.00	2.00	4.00	6.00
Moderate airflow ratio	2.00	1.00	2.00	3.00
Low airflow ratio	3.00	0.67	1.33	2.00

Table 5.4.1: The ranges of airflow ratios as classified to analyze mixing modes, both Q_h and Qc are in m^3/min.

5.4.1 Case 1: Stratified Flow for High Airflow Ratio.

In this case, the airflow ratio is comparatively high (Q_c/Q_h =2.0, 4.0 and 6.0). The flow was stratified at lower hot airflow rate ($Q_h = 1 m^3/min$). The interface level height is relatively high. Figures 5.4.1 to 5.4.3 show how the momentums influence the stratified flow characteristics and the stratification interface level height. By increasing the momentum, the Figures illustrate the growth and the vertical transport of the stratified layer interface level height. In comparisons between the temperature profiles of different momentum airflows, it is seen that the mixing is higher and faster for high momentum.

As expected for weak stratification the mixing will be faster. Since the degree of stratification is low, the stratified layers are easily destroyed. Furthermore, the transformation of kinetic to potential energy has no efficient domain to yield a stratified layer before reaching the stratified region and flows through the stratified layer.

As the injected air goes downward, the volumetric flow rate of the injected air is increased by entrainment of surrounding air in the upper zone. With more increase in momentum flow rate, the descending air impinges upon the ground and circulates in the lower zone. The circulating airflow will push the stratified layer upward to reach the ceiling, (Figures 5.4.1 to 5.4.3).

From Figures 5.4.1 to 5.4.3, it is observed that more momentum air flow yields a stratified layer near the ceiling with different properties such as different density grades. The stratified layer developed near the ceiling was due to the reverse jet flow that ejects backward from the floor. While the strength of this stratified layer is increased by the momentum, the thickness is decreased. Therefore, the momentum is not only a main factor in mixing the flow but also a main factor in stratifying the flow and characterizing the stratification level, [Hee-Jin and Dale (2001)].

Weak stratification occurred due to the unbalance between hot and cold airflow rates. For low hot airflow rates and high cold airflow rate, the flow will stratify at higher levels in the upper zone. In this case, the injected air will flow through the stratified layer to mix with the flow in the lower zone and push the stratified layer upward to reach the ceiling. More increase in jet air momentum will increase the mixing in the lower zone and increase the degree of stratification near the ceiling.

For more detail of data analyzed in Figures 5.4.1 to 5.4.3, see Figures (A2.4.1 to A2.4.3) in Appendix A2.

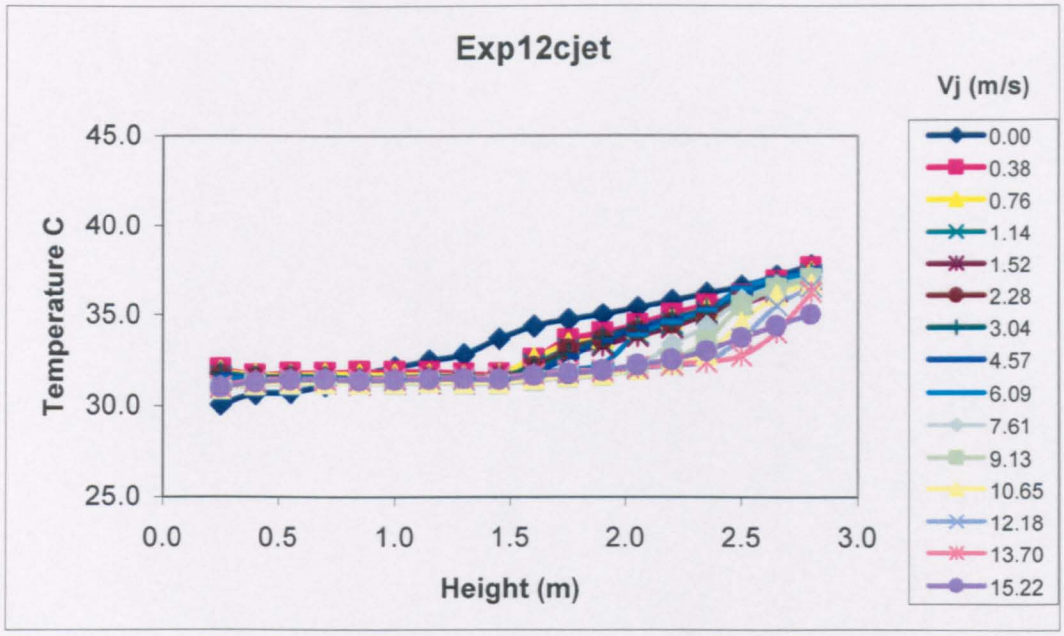

Figure 5.4.1: Vertical temperature profiles for various cold jet speed of 0.11 m diameter, while the flow was stratified at (Q_h = 1.0 m^3 / min) hot airflow rate and (Q_c = 2.0 m^3 / min) cold airflow rate at locations of 2.0 and 1.5 m respectively at the centre of environmental chamber.

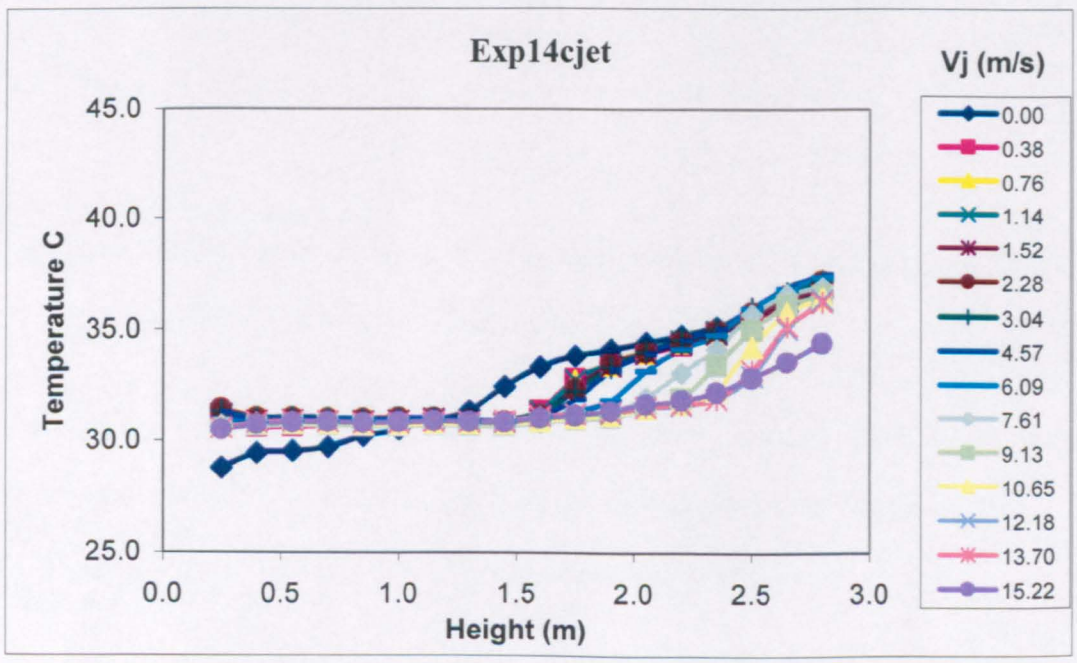

Figure 5.4.2: Vertical temperature profiles for various cold jet speed of 0.11 m diameter, while the flow was stratified at (Q_h = 1.0 m^3 / min) hot airflow rate and (Q_c = 4.0 m^3 / min) cold airflow rate at locations of 2.0 and 1.5 m respectively at the centre of environmental chamber.

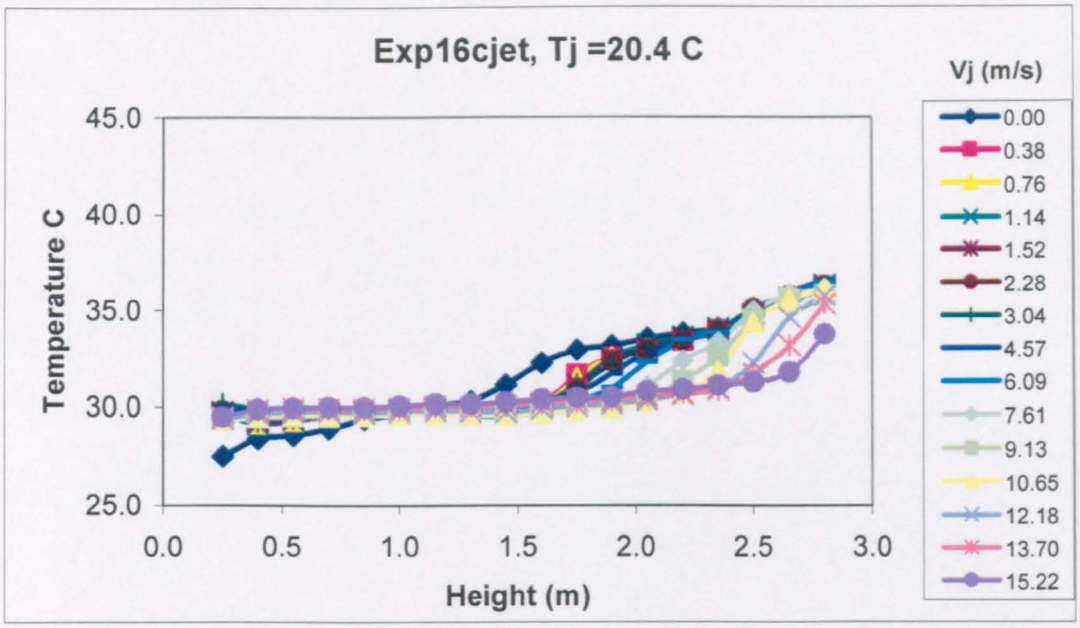

Figure 5.4.3: Vertical temperature profiles for various cold jet speed of 0.11 m diameter, while the flow was stratified at (Q_h = 1.0 m^3 / min) hot airflow rate and (Q_c = 6.0 m^3 / min) cold airflow rate at locations of 2.0 and 1.5 m respectively at the centre of environmental chamber.

5.4.2 Case 2: Stratified Flow for Low Airflow Ratio.

In this case, the airflow ratio is comparatively low (Q_c/Q_h =0.67, 1.33, and 2.0), the interface level height is at lower levels. The flow was stratified at higher hot airflow rate ($Q_h = 3 m^3/\min$). The breakdown of the stratified layer occurs with three possible configurations:

1. When the stratified layer interface level height was much lower (near the ground) as shown in Figures 5.4.4, where the flow was stratified at higher hot airflow rate and lower cold airflow rate ($Q_h = 3 m^3/\min$ $Q_c = 2.0\ m^3/\min$). In this case, the momentum will destroy the stratified layer and mix the flow sooner. It is observed that the flow temperature stream lines turned over in the lower zone due to the horizontal movement of injected air when impingement with the floor. This occurred with no significant effect for jet momentum on the mixing of the upper zone.
2. When the stratified layer interface level height was above the ground with wide domain. The flow was stratified at higher hot airflow rate and intermediate cold

airflow rate ($Q_h = 3m^3/\min\ Q_c = 4.0\ m^3/\min$). The stratified layer interface level height h is enough for the injected air to go through and flows horizontally under the stratified layer, as shown in Figures 5.4.5. In this case, the injected air of low momentum impingement on the stratified layer leading to push it downward. Increasing the momentum leading to lower interface level height, which leading to destroy the stratified layer as well as in case 1.

3. The flow was stratified at higher value of hot and cold airflow rate ($Q_h = 3m^3/\min\ Q_c = 6.0\ m^3/\min$, as shown in Figures 5.4.6. The stratified layer interface level height was above the ground with certain distance that enough for the injected air to go through and stratify. In this case, the injected air through the stratified layer will mix the flow in the lower zone and push the stratified layer upward to reach the ceiling. Increasing the jet momentum will increase the stratified layer interface level height. More increasing will increase the mixing in the lower zone and destroy the stratified layer before reaching the ceiling.

Figures (5.4.4 to 5.4.6) show that when the jet momentum is not strong enough to reach the ground, the stratification is formed at a lower level. On the other hand, when the momentum is high, a large circulation is created yielding a higher stratification level height. Increasing of momentum will destroy the stratified layer before reaching the ceiling level, where a one large mixed zone is observed in whole space.

Comparing Figure 5.4.4 with the Figures 5.4.5 and 5.4.6, it was found that the interface level height was at lower levels where ($Q_c/Q = 0.67$). As can be seen in the Figure, with the increase of momentum; the stratification interface level descends downward with rapid decrease compared with that in Figures 5.4.5 and 5.4.6.

At low jet velocity (V_j= 0.38 to 3.0 m/s), it was observed that the injected air has a significant effect on the temperature profile in the lower zone, while it has no significant effect on the temperature profile in the upper zone despite the decrease in the average temperature of the upper zone. This may occur due to the following:

- While the initial velocity of injected air is low, the injected air needs more time to cross the distance between the jet and the stratified layer. Therefore, the heat transfer from the upper zone to the injected air is increased, while the injected

air temperature is increased. This will decrease the average temperature in upper zone and increase the average temperature in the lower zone.

- While a large part of the air flows out the upper zone reaching the lower zone without mixing with the hot air in the upper zone. This may result in a mixed hot air in the upper zone and a lower stratification interface level height leading to lower height of working zone.
- Also, at low momentum, the influence of the slip velocity between the injected air and the air in the upper zone becomes relatively significant. This may result in large access of injected air to the lower zone, which increases the temperature variations in the lower zone.

As shown in Figures (5.4.4 to 5.4.6), by increasing the jet momentum, the thickness of the upper zone is increased, while the interface level height h is decreased significantly faster to reach the ground due to the comparatively cooled air above the interface. It is similar to the results of [Linden et al (1990)] that small size of opening results in high amount of inflow that works as a jet caused the entrainment across the interface and because of the greater density of the fluid above the interface, the interface descends faster.

At high jet momentum, the impingement of the injected air against the ground converge the direction of injected air to flow horizontally. This type of horizontal flow leads to vertical pressure drop above and below the stratified layer may results in a lower interface level height, and a negative velocity gradient leading to a low value of Ri number and so mixed flow.

Figures (5.4.4 to 5.4.6) show that since the jet momentum is higher, the air penetrating the stratified layer will reach the floor. The entrainment volume flux is large and thus the circulation flow velocity in the lower zone will also be large. The stratified layer becomes dilute, and the mixing in the lower zone becomes larger. This leads to destabilization of the flow.

For more detail of data analyzed in Figures 5.4.4 to 5.4.6, see Figures (A2.4.4 to A2.4.6) in Appendix A2.

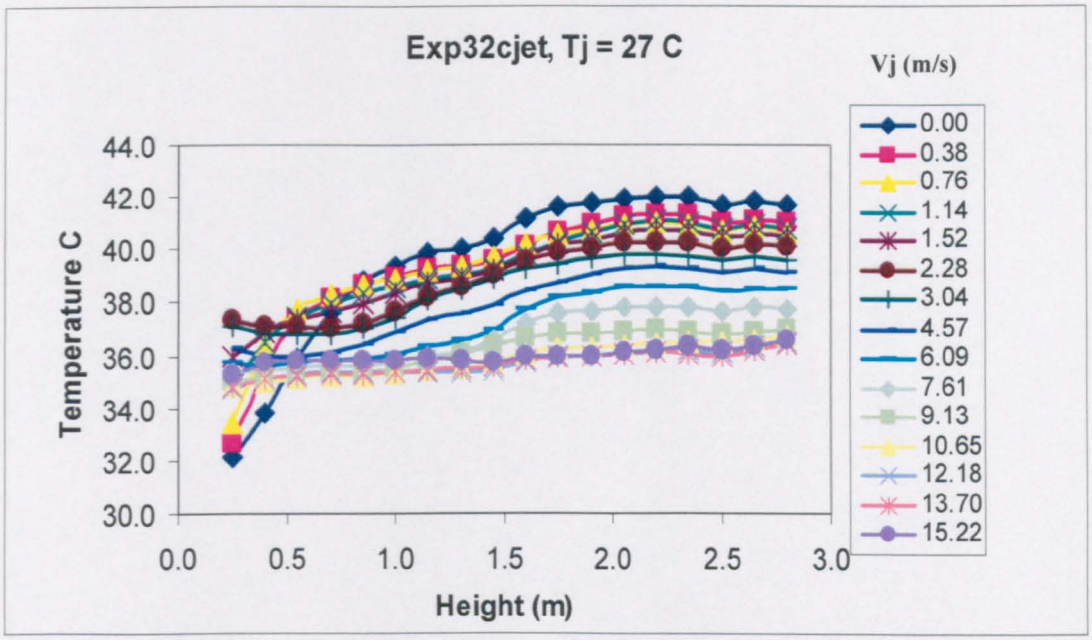

Figure 5.4.4: Vertical temperature profiles for various cold jet speed of 0.11 m diameter, while the flow was stratified at (Q_h = 3.0 m^3 / min) hot airflow rate and (Q_c = 2.0 m^3 / min) cold airflow rate at locations of 2.0 and 1.5 m respectively at the centre of environmental chamber.

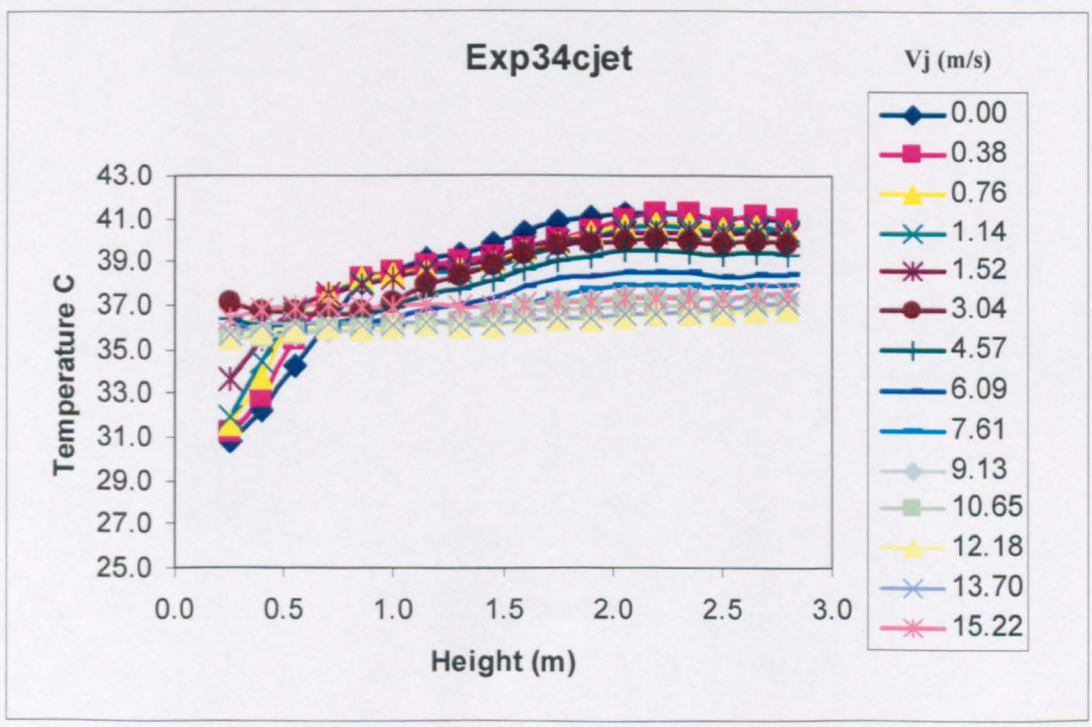

Figure 5.4.5: Vertical temperature profiles for various cold jet speed of 0.11 m diameter, while the flow was stratified at (Q_h = 3.0 m^3 / min) hot airflow rate and (Q_c = 4.0 m^3 / min) cold airflow rate at locations of 2.0 and 1.5 m respectively at the centre of environmental chamber.

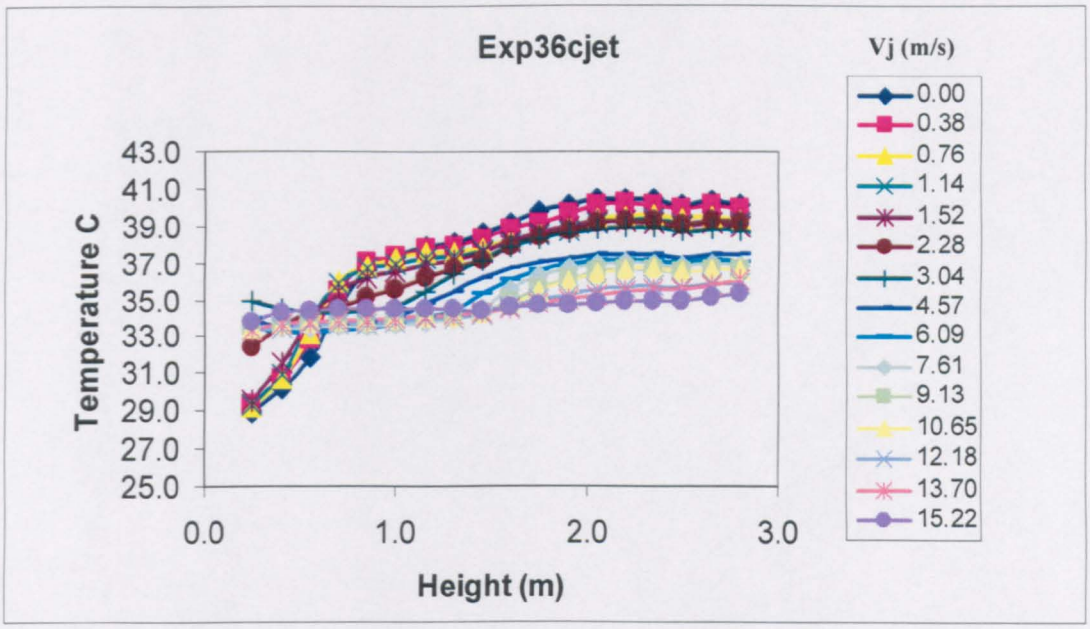

Figure 5.4.6: Vertical temperature profiles for various cold jet speed of 0.11 m diameter, while the flow was stratified at ($Q_h = 3.0\ m^3/\min$) hot airflow rate and ($Q_c = 6.0\ \ m^3/\min$) cold airflow rate at locations of 2.0 and 1.5 m respectively at the centre of environmental chamber.

5.4.3 Case 3: Stratified Flow at Intermediate Airflow Ratio.

In this case, the airflow ratio is intermediate (Q_c/Q_h =1.00, 2.0, 3.0), the interface level height is at mid height of the chamber. The flow was stratified at intermediate hot airflow rate ($Q_h = 2\,m^3/\min$). In this case, strong stratification was occurred where the complement of momentum and buoyancy forces was in balance. The injected air will flow through the stratified layer or mix it depending on the amount of momentum. Increasing the momentum will pick it up toward the ceiling before it destroyed at high momentum and the whole space becomes fully mixed.

Figure 5.4.7 to 5.4.9 show how the average temperatures profiles change with the change in momentum. In the lower zone, the temperature is increased to reach the average temperature of the whole space, while it decreases in the upper zone. The temperature of the stratified layer is a complement of both temperatures in the lower and upper zones. The results reveal the effect of momentum on the flow temperature profiles. As the jet momentum increases, the average temperature in the upper zone is gradually decreasing due to the entrainment volume flux, while in the occupied zone the increasing is more rapidly as discussed in the case 2.

Figures 5.4.7 to 5.4.9 show the effect of increasing jet speed on the temperature profiles. It illustrates the growth and the vertical transport of the stratified layer interface level height with increasing jet momentum. As seen in the Figures, the decrease in the temperature of the lower zone is initially faster due to the smaller thickness of the stratified layer, where the injected air can flow through without destroying the stable layers as presented in Figure 5.1.1 (b). With further increase in jet speed, thermal stratification decays and the stratified layer fades away until the temperature of the air becomes uniform, while the average temperature is decreasing steadily to approach the inlet ones. This is much similar to the results of [Hegazy and Diab (2002)] for the stratified flow in electrical water heaters.

Also by increasing the airflow rates, comparisons indicated that since the momentum is higher, the layer becomes thicker and the mixing in the lower zone becomes larger

As the increase in jet speed continues the interface moves upward. This is due to two reasons:

Firstly, it is due to the high temperature difference through the stratified layer boundaries (8 °C). This will increase the diffusion and radiation heat transfer to the lower zone, while the injected air stratify in the lower zone as a new source of cold airflow rate. This will increase the ratio of Q_c/Q_{out} so the interface level height h (as evaluated in Chapter 4).

Secondly, it is due to the circulation of flow in the lower zone, while the air in the upper zone is static. In this case, the difference in velocity generates a shearing force through the stratified layer. This will tear out the cold air to the upper zone, and increase mixing in the flow. This is similar to the mixing in water tank by heating process [Kang (2002)]

Figures 5.4.7 to 5.4.9 illustrate the effect of increasing jet momentum on the stratified flow characteristics. It decreases the temperature difference ΔT, the temperature gradient dT/dz and so the degree of stratification DS . It shows the translation of the stratified layer interface level height h with the jet speed, while the stratified layer thickness δ is decreased.

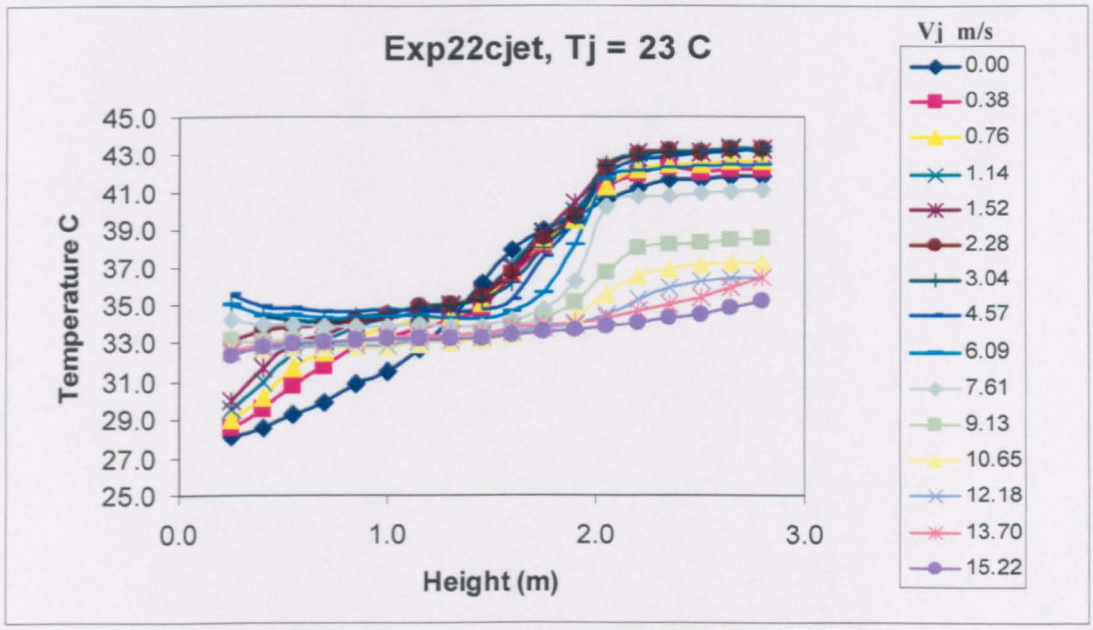

Figure 5.4.7: Vertical temperature profiles for various cold jet speed of 0.11 m diameter, while the flow was stratified at (Q_h = 2.0 m^3 / min) hot airflow rate and (Q_c = 2.0 m^3 / min) cold airflow rate at locations of 2.0 and 1.5 m respectively at the centre of environmental chamber.

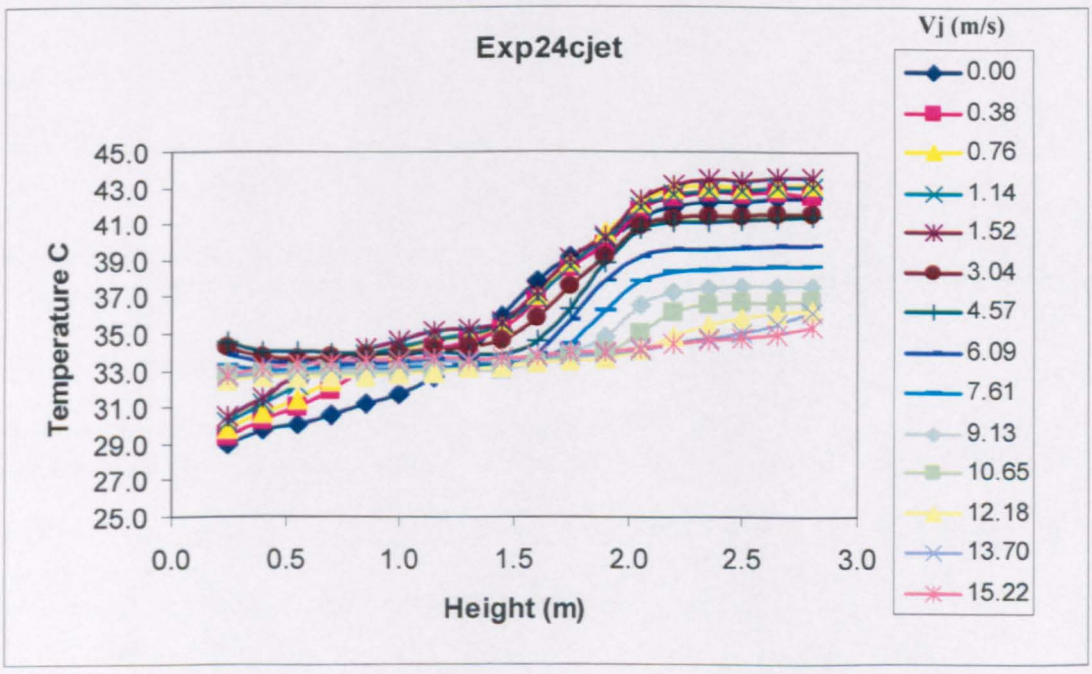

Figure 5.4.8: Vertical temperature profiles for various cold jet speed of 0.11 m diameter, while the flow was stratified at (Q_h = 2.0 m^3 / min) hot airflow rate and (Q_c = 4.0 m^3 / min) cold airflow rate at locations of 2.0 and 1.5 m respectively at the centre of environmental chamber.

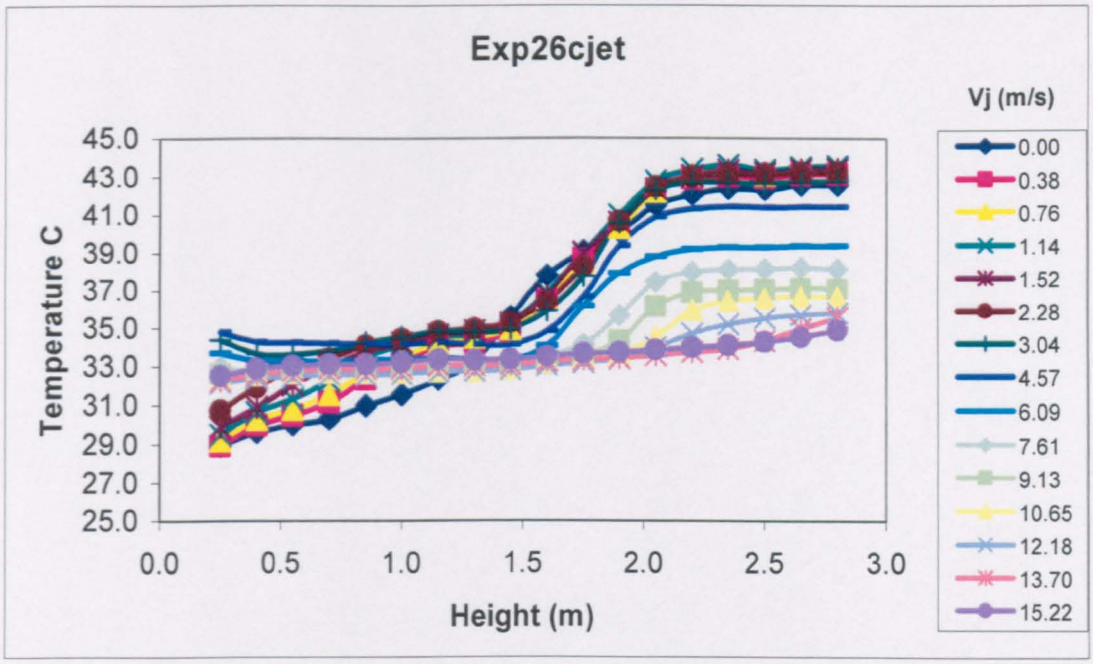

Figure 5.4.9: Vertical temperature profiles for various cold jet speed of 0.11 m diameter, while the flow was stratified at (Q_h = 2.0 m^3 / min) hot airflow rate and (Q_c = 6.0 m^3 / min) cold airflow rate at locations of 2.0 and 1.5 m respectively at the centre of environmental chamber.

Comparisons between these figures show no significant effect for the cold airflow rates on mixing. It is due to the insignificant effect of cold air flow rate on stratifying the flow as discussed in Chapter 4, and so on de-stratifying or mixing it. Also the mixing of a stratified flow is based on the stratified flow situation when the momentum jet starts to mix the flow rather than the initial conditions carried the flow to reach this situation.

Figures 5.4.7 to 5.4.9 show the decrease in temperature gradient by increasing the momentum until it reaches steep values. Therefore, the injected air is flowing directly towards the bottom of the chamber, which tends to circulate the flow in the lower zone. Since it has a negative buoyant force relative to the chamber domain, the mixing of low momentum will establish above the stratified layer, pushing it downward. Increasing the momentum will increase the depth of the injected air to flow through the stratified layer. It increases the buoyant forces in the lower zone under the stratified layer to pick it up until it reaches a stable stratification in the upper part of the chamber. This will increase

the height of occupied zone whilst the hot zone becomes thin. More increase in momentum will overcome the stability of stratified flow to becomes fully mixed flow.

For the case of strong degree of stratification and low momentum, on reaching the interface, the injected air will flow and stratify above the stratified layer for a certain distance depending on the jet momentum, degree of stratification and interface level height. However, for low degree of stratification the injected flow will go through the stratified layer or destroying it, while for high degree of stratification, the stratified layer will stand against the injected flow of low momentum as a solid surface.

Comparing the results of this case with those in case 1 and case 2, it can be noted that:

- For injected cold air at high level from the ceiling, the effect of hot airflow rate compared with cold airflow rate was much higher. As it is expected, the injected air is the ambient. It is injected downwards where the domain is the hot zone rather cold zone. Thus, the entrainment volume flux from the upper zone is large, which results in the significances of the hot air flow rates.
- The results show how the momentum influences the stratified flow of strong characteristics, as shown in Figures 5.4.7 to 5.4.9, with no significant influence on the stratification interface level height. In comparisons with the other cases, it is seen that the mixing is higher and faster for both weak stratification and high momentum.

After it was injected, the jet air flow usually stratified at certain levels when it lost its momentum and negative buoyancy. Based on the level of stratification, there are three different flow configurations. The following is a detailed analysis of these configurations:

Firstly, the flow stratifies at low values of hot airflow rates and high values of cold airflow rates (Qc/Qh = Max). In this case, the flow will stratify at high levels in the upper zone. Therefore, the injected air can flow through the interface without destroying the weak stable layers of competitively low Ri. It mixes the flow in the lower zone, and pushes the stratified layer upward to reach the ceiling.

Secondly, the flow stratifies at high values of hot airflow rates and low values of cold airflow rates (Qc/Qh = Min). In this case, the flow will stratify at levels somewhere in

the lower zone. On reaching the stratified layer, the injected air has no space to flow through the stratified layer of competitively low Ri without destroying or pushing it downwards to reach the ground. The behavior of the flow is a dependence of both the momentum and the interface level height

Thirdly, the flow stratifies at intermediate values of both hot and cold airflow rates (Qc/Qh = Intermediate). This type of flow has a high Ri, where the balance between buoyancy forces and momentum forces are the main parameters to control the flow (Chapter 4). In this case, the flow will stratify near the middle of the chamber. The injected air will flow through the interface without destroying the stable layers.

For more detail of data analyzed in Figures 5.4.7 to 5.4.9, see Figures (A2.4.7 to A2.4.9) in Appendix A2.

5.4.4 Combined Effect of Airflow Rates and Momentum Induced by Cold Jet on Stratified Flow

Effect of both hot and cold airflow rates on the stratified flow was studied and discussed in Chapter 4. The effect of hot airflow rates was more significant. Experiments on mixed flow with different airflow rates were done. In this section, the effect of both hot and cold airflow rates with the presence of momentum, using cold jet, is analyzed and discussed.

Interface level height for various values of hot and cold airflow rates with the jet momentum, at fixed input and output locations, are plotted in Figures 5.4.10 to 5.4.15. The plotted data show that stratified layer interface level height is affected by the input airflow rates. While the effect of hot airflow rate on temperature profiles is significant (Figures 5.4.13 to 5.4.15), the effect of cold airflow rates is smaller (Figure 5.4.10 to 5.4.12).

Figures 5.4.10 to 5.4.12 show the effect of cold jet speed on the interface level height. The results are for various values of hot and cold airflow rates (Q_h = 1.0, 2.0, 3.0 m^3 / min and Q_c = 2.0, 4.0, 6.0 m^3 / min). The results show the effect of cold airflow rate is insignificant for the cases of low and intermediate hot air flow rate, where the stratified

layer interface level height is cooperatively high. The effect of cold airflow rate was significant at high hot air flow rate where the initial stratification was occurred at low interface level height. The results show that the effect of cold airflow rates on the interface level heights is more significant for high jet momentum than for low jet momentum.

Figure 5.4.12 shows that, at high hot airflow rate ($3.0\ m^3/s$) and low and moderate cold airflow rates ($2.0\ m^3/s$ and $4.0\ m^3/s$), the flow is fully mixed at lower momentum ($0.5\ m^4/s^2$). In this case, the interface level height h was at lower levels (case 2). On the contrary, the figure shows that to reach fully mixed flow with high cold airflow rate of ($6.0\ m^3/s$), more than triple times of this momentum will be in needed ($1.75\ m^4/s^2$).

Figures 5.4.13 and 5.4.14 show that, the flow will be not fully mixed at hot airflow rates of (1.0 and $2.0\ m^3/s$) using low momentum jet of ($<0.5\ m^4/s^2$). But the stratified layer interface level height h goes upward to reach 80% of the chamber height at a momentum of ($1.5\ m^4/s^2$). With more jet momentum, the flow never be fully mixed for low hot airflow rate of ($1.0\ m^3/s$), while it is fully for hot airflow rate of ($2.0\ m^3/s$), with better results for the second case.

Comparison between Figures 5.4.10 to 5.4.12 and Figures 5.4.13 to 5.4.15 shows that, the effect of increasing hot airflow rates to mix the flow using cold jet flow is more significant than the effect of increasing cold airflow rates, especially for the cases of high values of cold and hot airflows. This was due to three reasons:

- The comparatively significant effect of hot airflow rates, as discussed in Chapter 4, where the source of heat in our case was the hot air supply (Chapter 5).
- The injected cold air was the ambient. Due to the temperature difference between the injected cold air and the penetrated hot air, the large part of air entrainment to negative buoyancy injected air was the hot air.
- The flow was injected vertically from the ceiling to reach the stratified layer. At high hot air flow rate, the stratified layer was near the ground (Case 2), while the injected air needs long time to cross the distance between the jet and cold air, which increase heat transfer and the entrainment of hot air.

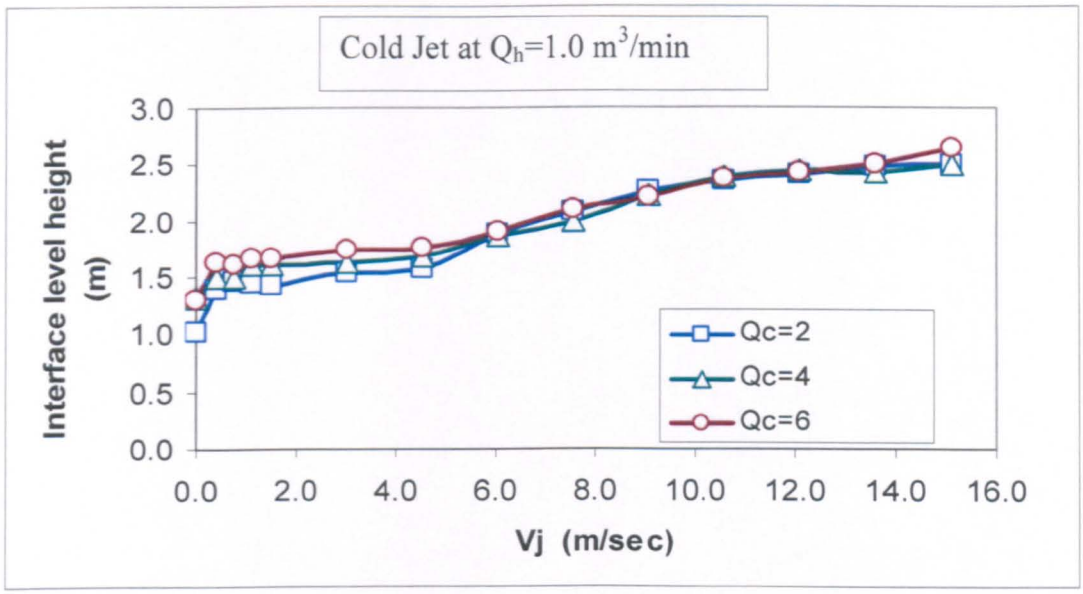

Figure 5.4.10: Comparison of interface level height with the jet speed, at hot airflow rate of $Q_h = 1.0\ m^3/min$ and different cold airflow rates ($Q_c = 2, 4$ and $6\ m^3/min$) in the environmental chamber.

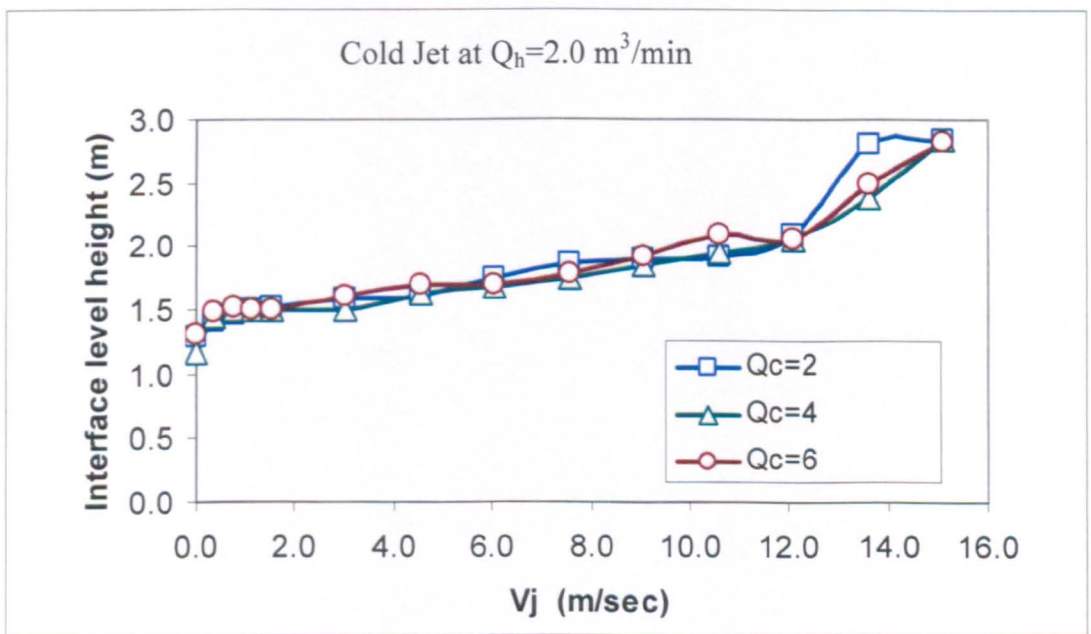

Figure 5.4.11: Comparison of interface level height with the jet speed, at hot airflow rate of $Q_h = 2.0\ m^3/min$ and different cold airflow rates ($Q_c = 2, 4$ and $6\ m^3/min$) in the environmental chamber.

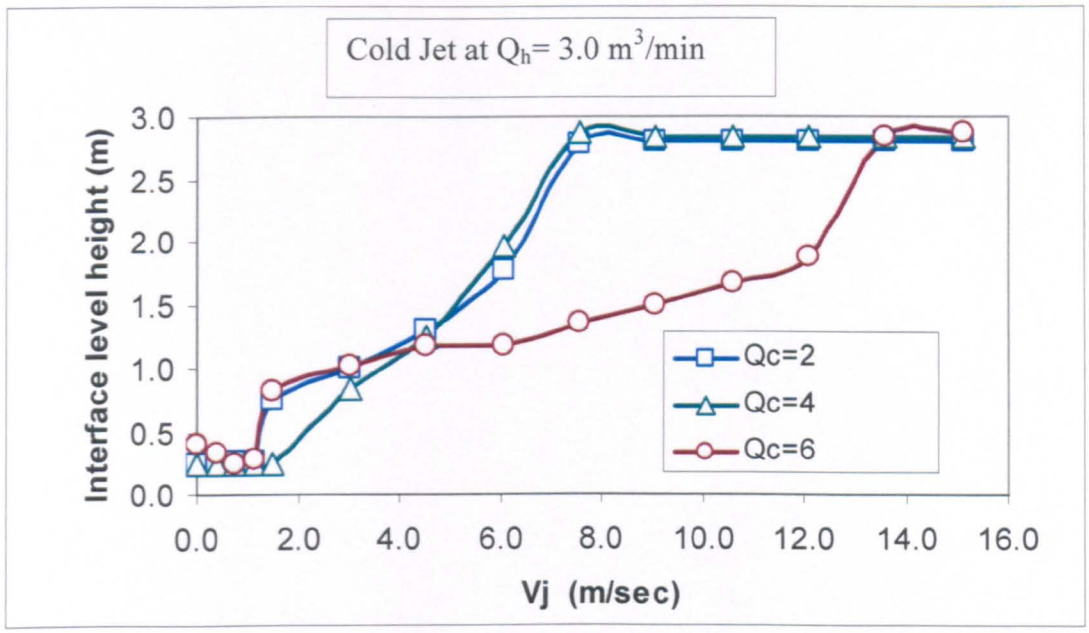

Figure 5.4.12: Comparison of interface level height with the jet speed, at hot airflow rate of Q_h = 3.0 m^3 / min and different cold airflow rates (Q_c = 2, 4 and 6 m^3 / min) in the environmental chamber.

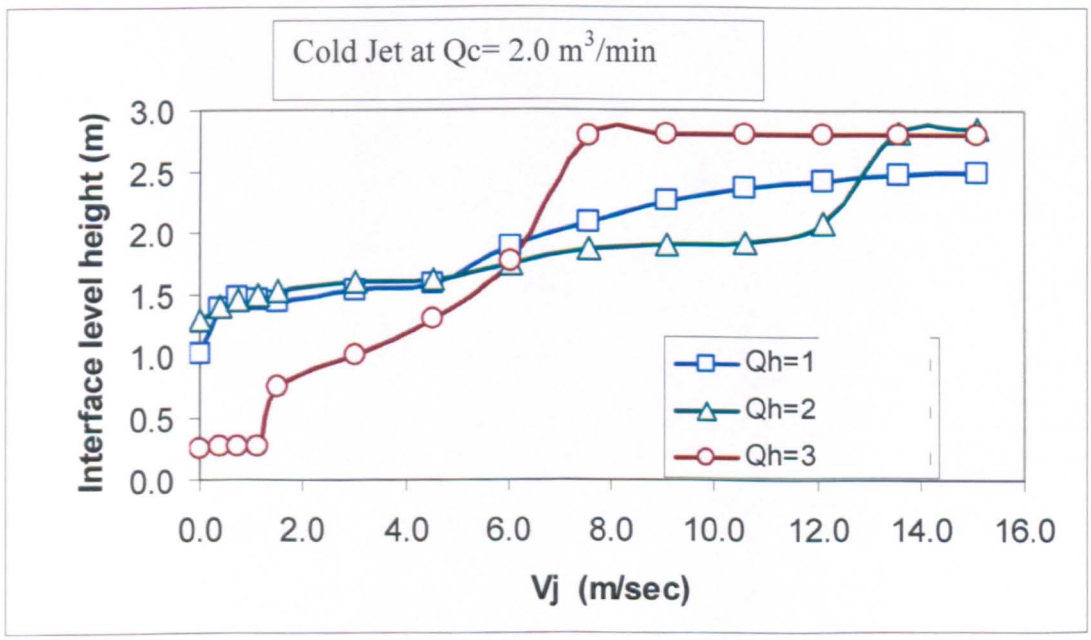

Figure 5.4.13: Comparison of interface level height with the jet speed, at cold airflow rate of Q_c = 2.0 m^3 / min and different hot airflow rates (Q_c = 1, 2 and 3 m^3 / min) in the environmental chamber.

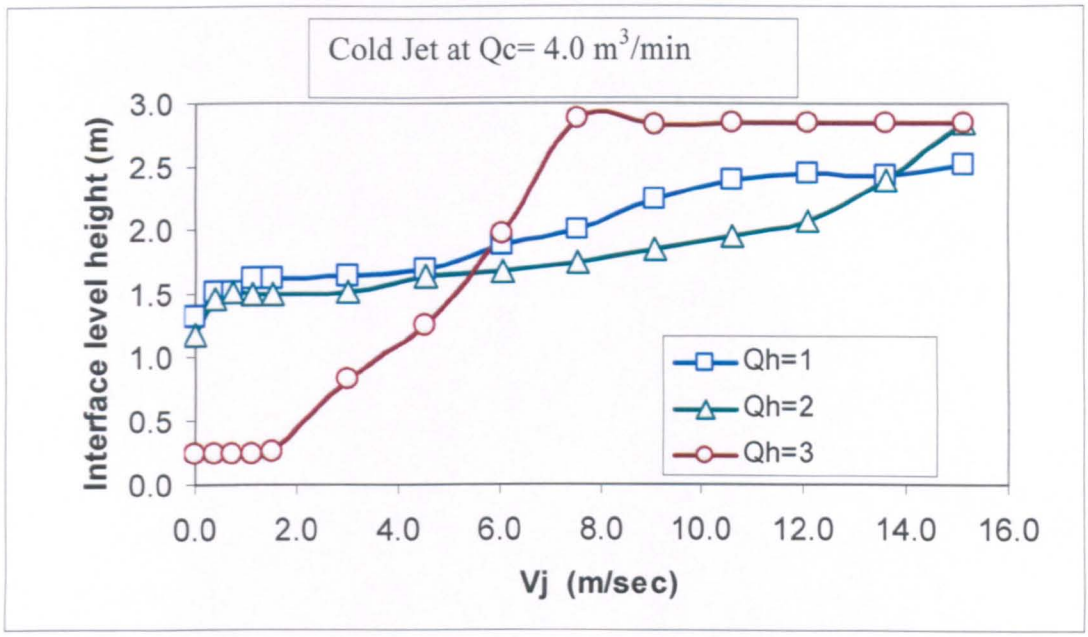

Figure 5.4.14: Comparison of interface level height with the jet speed, at cold airflow rate of Q_c = 4.0 m^3 / min and different hot airflow rates (Q_c = 1, 2 and 3 m^3 / min) in the environmental chamber.

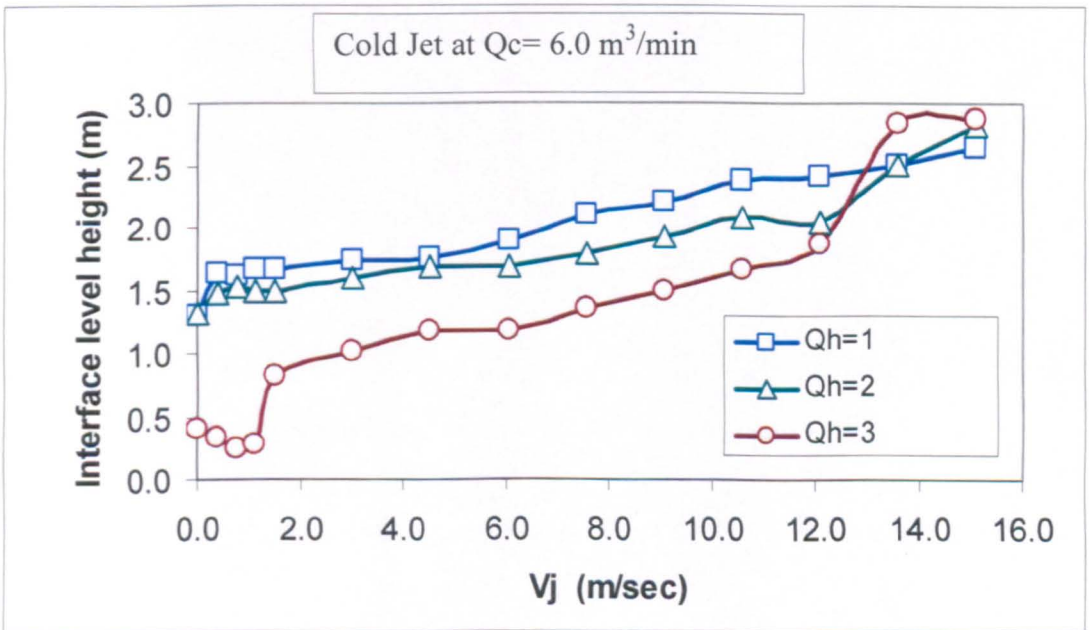

Figure 5.4.15: Comparison of interface level height with the jet speed, at cold airflow rate of Q_c = 6.0 m^3 / min and different hot airflow rates (Q_c = 1, 2 and 3 m^3 / min) in the environmental chamber.

5.4.5 Smoke Visualization of Cold Jet Tests

In this section smoke visualization is included for comparison with the experimental results. Figures 5.4.16 to 5.4.20 are a momentum sequence photographs of a stratified and mixed flow with initial hot and cold airflow rates of (2 and $6\,m^3/min$), Richardson number of 200 and Reynolds number of 9700. The flow has been mixed using a jet of 0.11m in diameter. The injected air was in the range of ($V_j = 0.0$ to $15.0\,m/sec$). The sequence in the Figures shows the effect of cold jet flow on the stratified flow characteristics.

Comparisons between the sequence figures illustrate the effect of momentum on the stratified flow characteristics. As the momentum is increasing, the smoke pictures indicate a more mixed flow in the lower zone and an upward translation of the stratified layer interface level height. Increasing the momentum causes a fully mixed flow at $V_j = 15.0\,m/sec$.

The results are so important to design ventilation systems considering the pollutants to be above the heads of the occupants in the working zone. This will allow the occupants to run away in the case of fire hazards to be safe from highest temperatures.

Unfortunately, it was difficult to get good-quality images for mixed cases of high momentum jet flows. At high jet flows, difficult flow phases, perturbations and fluctuations were introduced, while the flow is more mixed. For this case, the stratified layer is more dilute and the interface as well as the deviation of smoke refraction became so complicated to capture the images.

In general, the experimental and visualization results obtained in this work are in good agreement considering that different modeling technique, different surrounding conditions, complex flow patterns and turbulent dissipations in the domain were found in these experiments. Despite these discrepancies between the experimental and visualized techniques, the results are accepted.

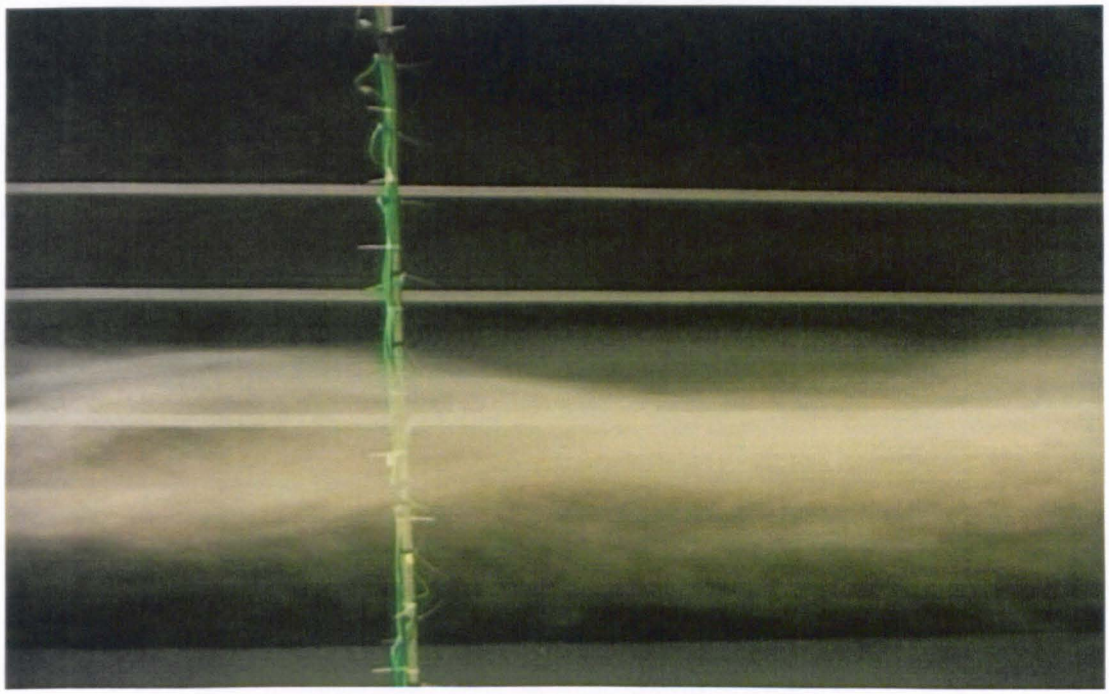

Figure 5.4.16: Video-recorded picture showing the stratified flow with initial cold and hot airflow rates of **2 and 6 m^3/min**, Richardson number of 2.0 and Reynolds number of 2008, with no jet flow (**$V_j = 0.0$ m/sec**).

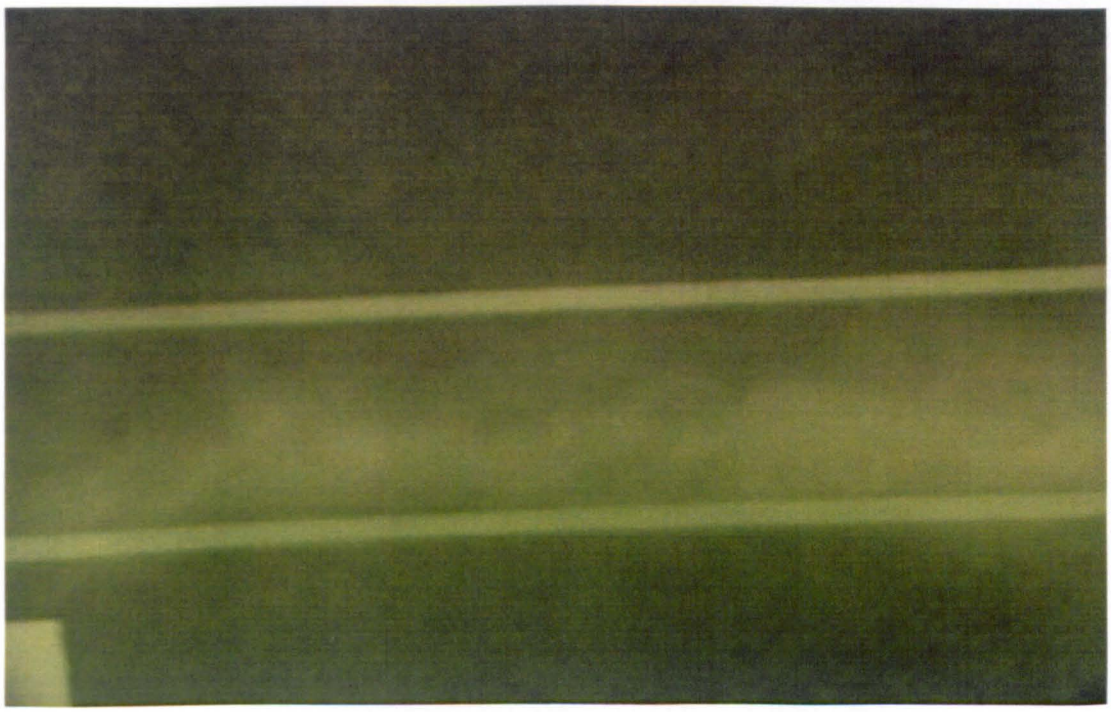

Figure 5.4.17: Video-recorded picture showing the stratified flow with initial cold and hot airflow rates of **2 and 6 m^3/min**, Richardson number of 2.0 and Reynolds number of 2008, with a jet flow of (**$V_j = 3.0$ m/sec**).

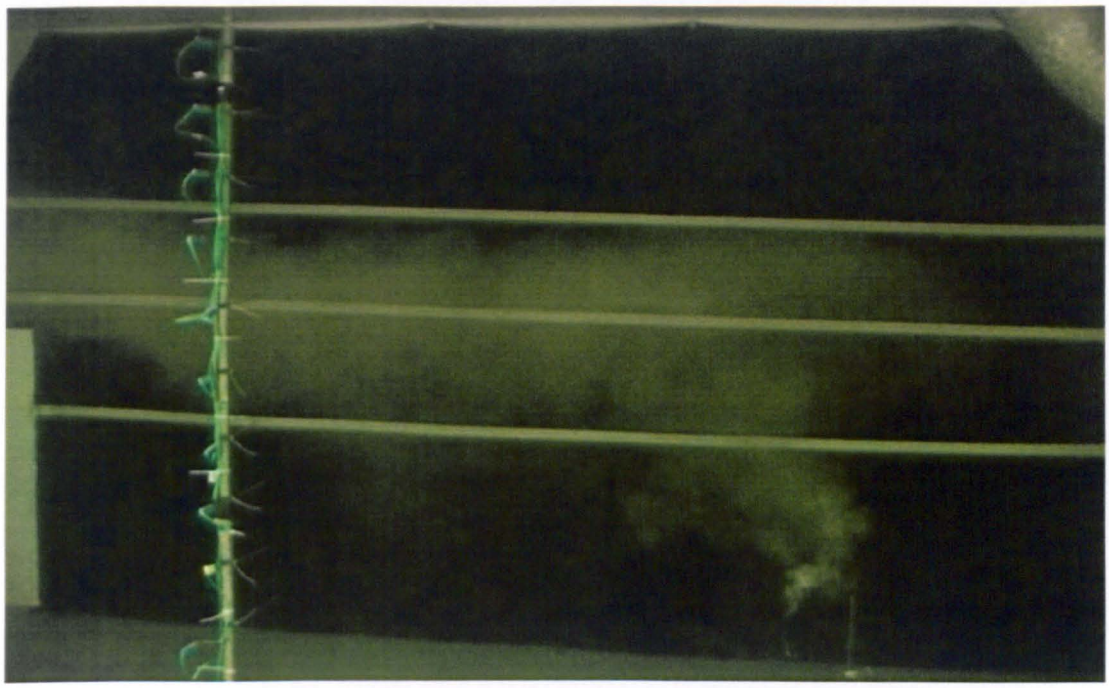

Figure 5.4.18: Video-recorded picture showing the stratified flow with initial cold and hot airflow rates of 2 and $6\,m^3/min$, Richardson number of 2.0 and Reynolds number of 2008, with no jet flow ($V_i = 6.0\ m/sec$).

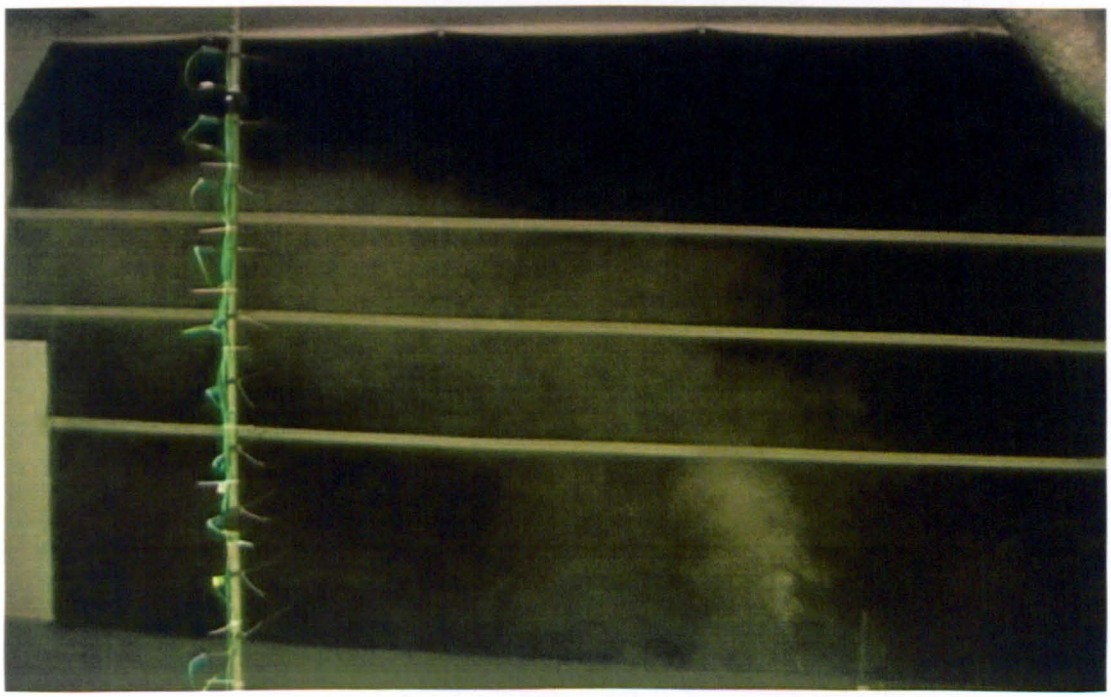

Figure 5.4.19: Video-recorded picture showing the mixed flow with initial cold and hot airflow rates of 2 and $6\,m^3/min$, Richardson number of 2.0 and Reynolds number of 2008, with no jet flow ($V_j = 9.0\ m/sec$).

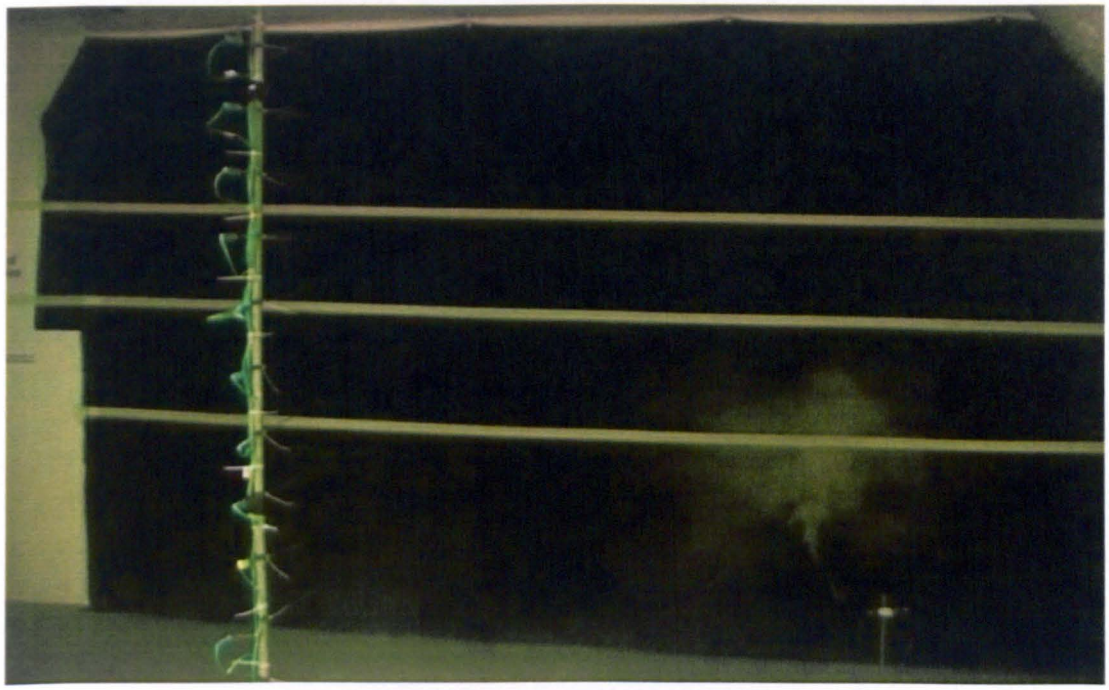

Figure 5.4.20: Video-recorded picture showing the stratified flow with initial cold and hot airflow rates of 2 and $6\,m^3/min$, Richardson number of 2.0 and Reynolds number of 2008, with no jet flow ($V_j = 15.0\ m/sec$).

5.5 Mixing Flow Using Warm Jet

5.5.1 Case 1: Stratified Flow for High Airflow Ratio.

In this case, the airflow ratio is comparatively high (. Q_c/Q_h =2.0, 4.0 and 6.0 m^3/min). The flow was stratified at lower hot airflow rate ($Q_h = 1\,m^3/min$). The interface level height is relatively high. The effect of warm jet on the flow characteristics is shown in Figures 5.5.1 to 5.5.3. Figures 5.5.1 to 5.5.3 show the mixing behaviour under the compound effect of both jet momentum and cold airflow rate. From the comparison between the figures, the mixing was faster and more effective for both low and high cold airflow rates (Q_c/Q_h =2 and 6 m^3/min) (Figures 5.5.1 and 5.5.2). At maximum values of warm jet flow, the situation of fully mixed flow was reached as in the case of low cold airflow rate, while there is hot stratified layer near the ceiling in the cases of intermediate and high values of cold airflow rates(Q_c/Q_h =4 and 6 m^3/min).

Figures 5.5.1 to 5.5.3 show a sequence of temperatures profiles for various jet speeds. From the figures, it can be seen that increasing the momentum leads to stratified the

flow in lower zone, whereas the initial stratified layer is translated upward to reach the ceiling. It is observed that an increasing of both cold airflow rate and warm jet momentum will mix the flow in the domain with two exceptions:

1. A hot stratified layer near the ceiling due to the reverse jet flow that ejects backward from the floor.
2. An overturns near the floor due to the horizontal movement of warm injected air when impingement with the floor.

As shown in the figures, the interface level height is increasing by the jet momentum, while the thickness of the stratified layer is decreasing. Therefore, the warm jet flow should propagate stratification due to temperature difference and buoyancy forces, while it destroys the stratified layer due to high momentum airflow and high mixing process. It also characterizes the stratification level height, [Hee-Jin and Dale (2001)].

For more detail of data analyzed in Figures 5.5.1 to 5.5.3, see Figures (A2.5.1 to A2.5.3) in Appendix A2.

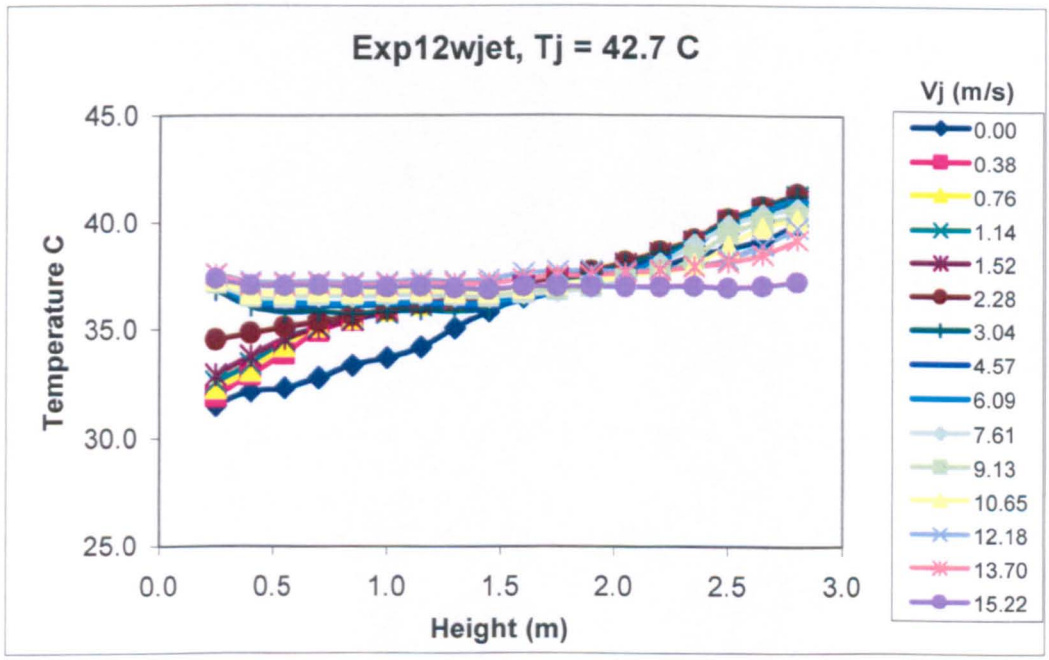

Figure 5.5.1: Vertical temperature profiles for various cold jet speed of 0.11 m diameter, while the flow was stratified at (Q_h = 1.0 m^3 / min) hot airflow rate and (Q_c = 2.0 m^3 / min) cold airflow rate at locations of 2.0 and 1.5 m respectively at the centre of environmental chamber.

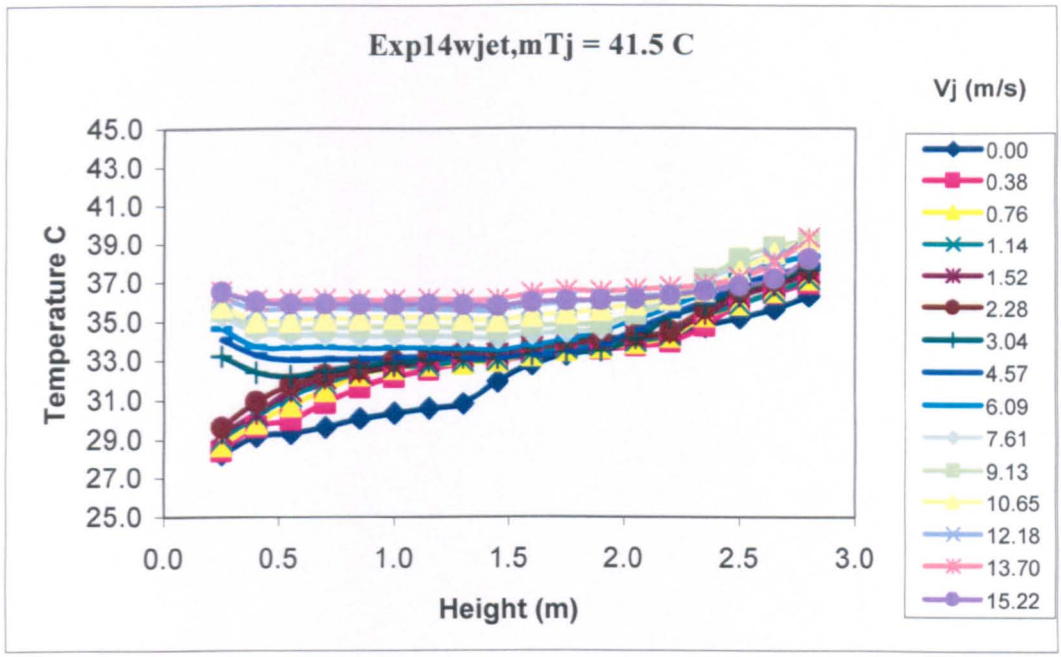

Figure 5.5.2: Vertical temperature profiles for various cold jet speed of 0.11 m diameter, while the flow was stratified at (Q_h = 1.0 m^3 / min) hot airflow rate and (Q_c = 4.0 m^3 / min) cold airflow rate at locations of 2.0 and 1.5 m respectively at the centre of environmental chamber.

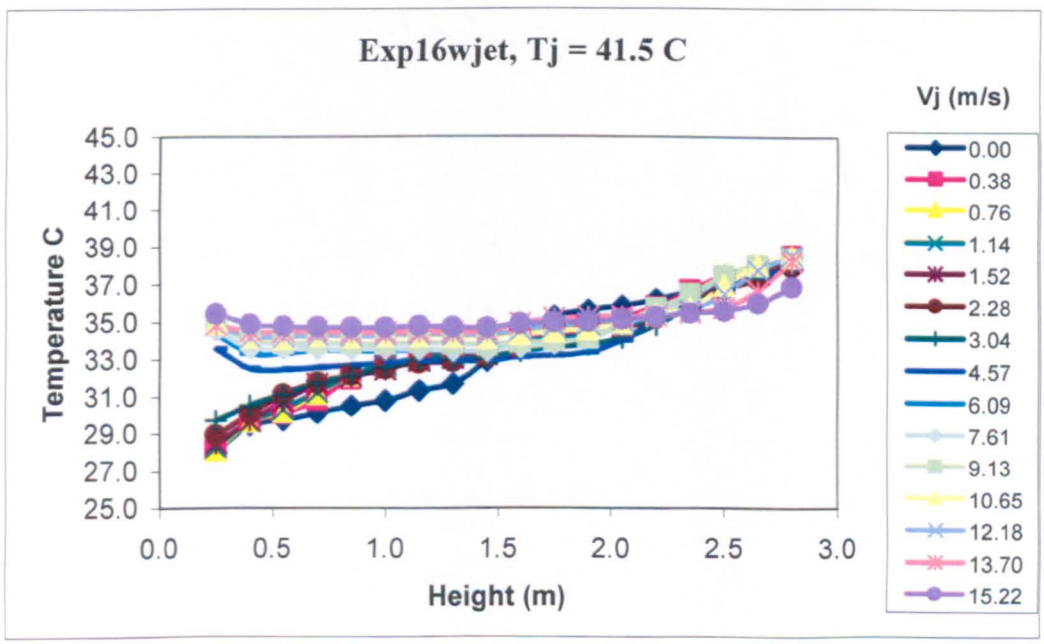

Figure 5.5.3: Vertical temperature profiles for various cold jet speed of 0.11 m diameter, while the flow was stratified at (Q_h = 1.0 m^3 / min) hot airflow rate and (Q_c = 6.0 m^3 / min) cold airflow rate at locations of 2.0 and 1.5 m respectively at the centre of environmental chamber.

5.5.2 Case 2: Stratified Flow for Low Airflow Ratio.

As mentioned earlier (case 2, section 5.4.2), the airflow ratio is comparatively low ($.Q_c/Q_h$ =0.67, 1.33, and 2.0). The flow was stratified at higher hot airflow rate ($Q_h = 3m^3/min$). The stratification is relatively weak ($dT/d\delta$= Min). Interface level height is at lower levels near the floor.

Figures 5.5.4 to 5.5.6 shows the temperature profiles of stratified flow with a sequence of jet speeds. As shown in the figures, injected air has a significant effect on the temperature profile in the lower zone, while it has no significant effect on the average temperature in the upper zone. This was due to:

1. The initial velocity of the injected air pushes the air to reach the lower zone, without mixing exchange.
2. The initial temperature of the injected air flow through the upper zone with out exchanging heat with the hot air in the upper zone.
3. Also, at low momentum, the influence of the slip velocity between the injected warm air and the air in the upper zone is relatively significant. This may result in large access of injected air to the lower zone, which increases the temperature variations and the mixing in that zone.

Furthermore, the negative buoyancy of the injected air is increased in the lower zone. It is due to the temperature difference between the injected hot air and the relatively cold air in the lower zone. This will increase the entrainment volume fluxes through the wide domain, which increases the thickness of the lower zone, while the interface ascends significantly faster because of the comparatively hot air below the interface level. This pushes the interface level height upward to reach the ceiling, (Figures A2.5.4 to A2.5.6). More increase in warm jet flow will result in a fully mixed flow in the whole space. This is due to the decrease in temperature difference between the layers, which leads to weak stratification and so high mixing. In the same manner, high momentum will result in high circulation of mixing velocity in the space, which leads to destabilize the flow.

Figures A2.5.4 to A2.5.6 show sequences of temperature profiles for various jet speeds. The results demonstrate the stratified layer height as a function of initial jet momentum over a wide range of flow rates. As discussed before, despite different types and values

of jet flow, the results show the interface level height is approximately proportional to the momentum jet flow, for the ranges over $0.22 - 2.17\ m^4/s^2$. The proportional degree is more significant in the case of warm jet flow compared with the cold jet flow. This was due to the comparatively high amount of energy dissipation and energy transformation (from potential to kinetic) in the case of cold jet flow compare to the case of warm jet flow.

In the presence of warm jet, the warm air flows downward under the effect of jet momentum while the negative buoyancy decelerates the flow velocity. Therefore, it needs much momentum to reach the stratified layer. When it reaches the stratified layer; it repeats the same configurations mentioned earlier by the using of cold jet:

Firstly, when the hot airflow rate is relatively high and the cold airflow rate is relatively low (Q_c/Q_h = 0.67). In this case, the stratified layer interface level height is low enough (near the floor) as shown in Figures 5.5.4 and A2.5.5. Thus the warm air injected from the ceiling needs much high momentum to reach the stratified layer. On reaching the stratified layer, the momentum will destroy the layer and mix the flow.

As shown in Figures A2.5.4 and A2.5.5, in the lower zone, the temperature distributions illustrate a layering overturn at the lowest sensors. The overturns in temperature profiles occurred at a jet speed of (4.57 m/s). This overturn is due to the horizontal movement of injected air impinge near the floor. It is higher compared with the same case of cold jet, where it was occurred at lower jet speed of (3.04m/s). The difference is due to the negative buoyancy of injected air. In the other zones, the jet momentum has no significant effect, but more mixed flow.

Secondly, when the stratified layer interface level height is above the floor with wide enough for the injected air to go through and flow horizontally under the stratified layer. In this case the flow was stratified at intermediate cold airflow rate (Q_c/Q_h = 1.33), as shown in Figures 5.5.5 and A2.5.5. In the lower zone, the injected air of low momentum impinged at the stratified layer leading to push it downward. Increasing the momentum is leading to a lower interface level height. Thus destroys the stratified layer as well as case 1. An overturn in temperature profile was occurred at lower momentum at a jet speed of 1.52 m/s compare with the last case of warm jet. This was due to the long

distance needed to reach the stratified layer. In the other zones, the jet momentum shows more mixed flow.

Thirdly, when the flow was stratified at higher values of cold airflow rate(Q_c/Q_h = 2.0)., as shown in Figures 5.5.6 and A2.5.6, while the stratified layer interface level height is above the floor with certain level be enough for the injected air to go through the stratified layer. In this case, the injected air will flow through the stratified layer leads to translate the stratified layer interface level height upward to reach the ceiling. Increasing of jet speed leads to increase the mixing in the lower zone and destroy the stratified layer before reaching the ceiling, while the large circulation is created in the whole space.

For more detail of data analyzed in Figures 5.5.4 to 5.5.6, see Figures (A2.5.4 to A2.5.6) in Appendix A2.

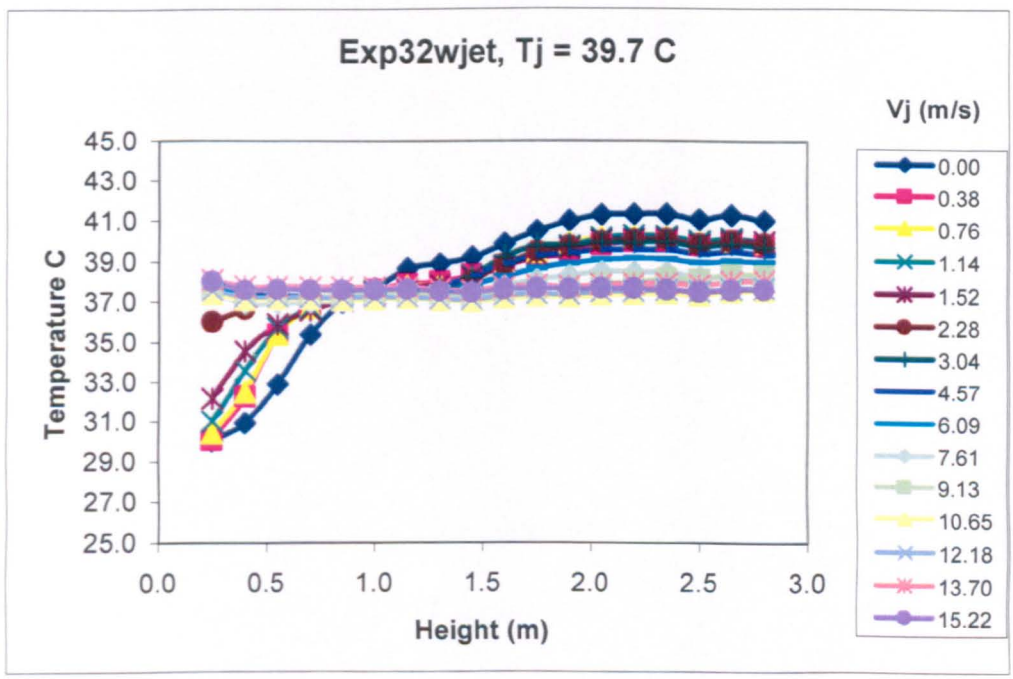

Figure 5.5.4: Vertical temperature profiles for various warm jet speed of 0.11 m diameter, while the flow was stratified at (Q_h = 3.0 m^3 / min) hot airflow rate and (Q_c = 2.0 m^3 / min) cold airflow rate at locations of 2.0 and 1.5 m respectively at the centre of environmental chamber.

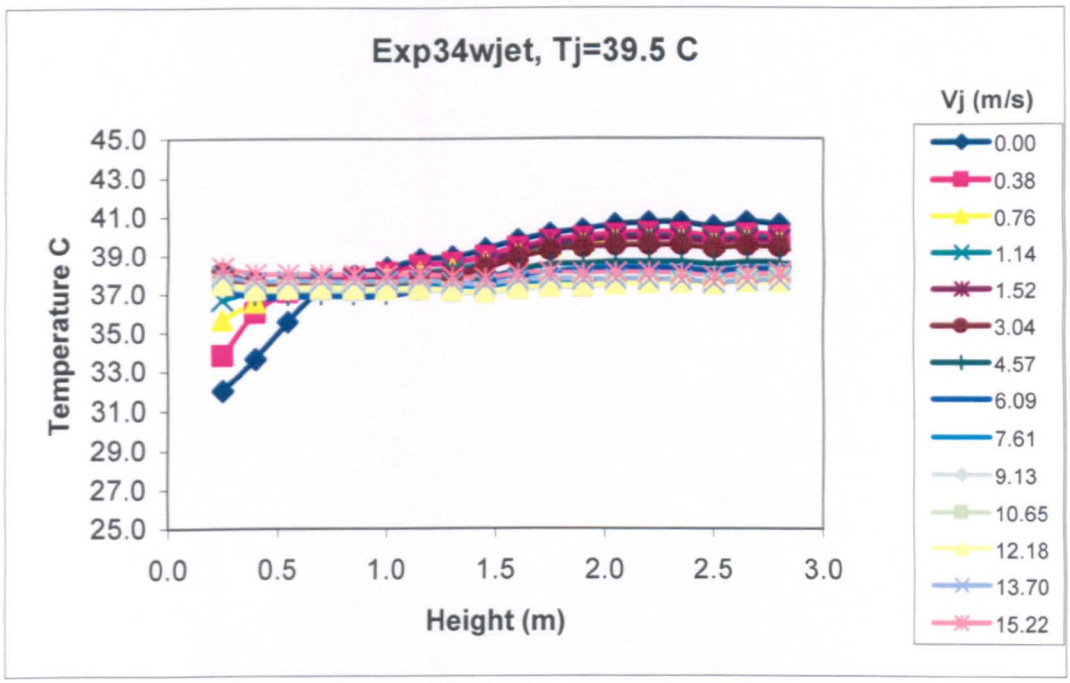

Figure 5.5.6: Vertical temperature profiles for various warm jet speed of 0.11 m diameter, while the flow was stratified at (Q_h = 3.0 m^3 / min) hot airflow rate and (Q_c = 6.0 m^3 / min) cold airflow rate at locations of 2.0 and 1.5 m respectively at the centre of environmental chamber.

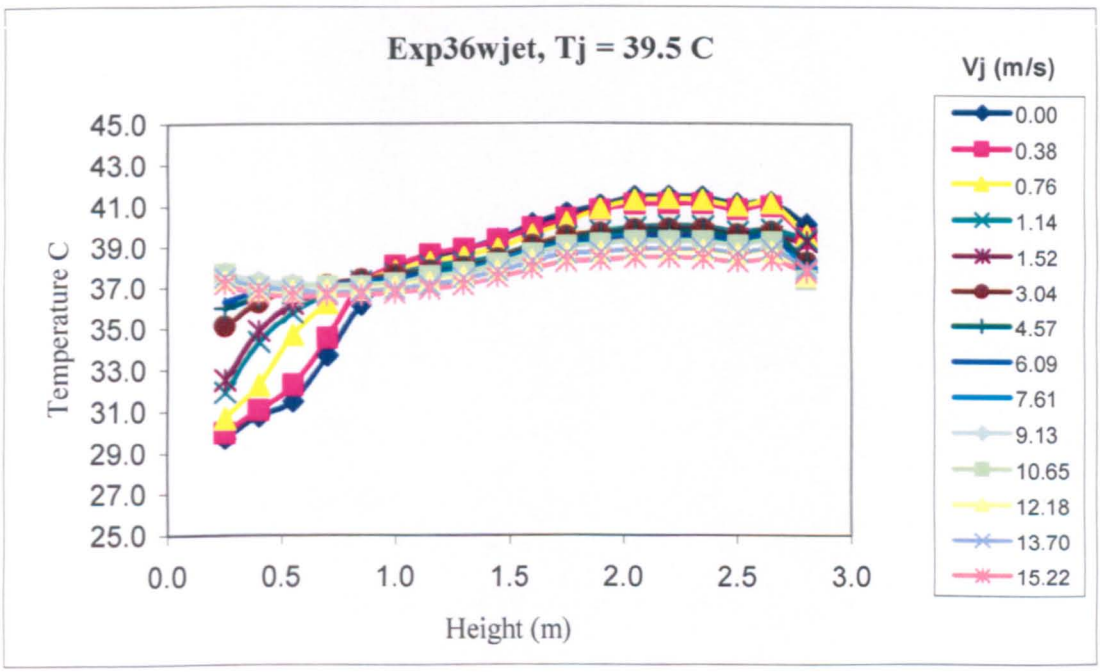

Figure 5.5.5: Vertical temperature profiles for various warm jet speed of 0.11 m diameter, while the flow was stratified at (Q_h = 3.0 m^3 / min) hot airflow rate and (Q_c = 4.0 m^3 / min) cold airflow rate at locations of 2.0 and 1.5 m respectively at the centre of environmental chamber.

5.5.3 Case 3: Stratified Flow at Intermediate Airflow Ratio.

In this case, the airflow ratio is intermediate (Q_c/Q_h =1.00, 2.0, 3.0), the interface level height is at mid height of the chamber. The flow was stratified at intermediate hot airflow rate ($Q_h = 2\,m^3/min$). The results show the momentum influencing the stratified flow, as shown in Figures 5.5.7. In this case, the injected air is pushing up the stratified layer towards the ceiling before it is destroyed at high jet momentum. As a result, the whole space becomes fully mixed. In comparisons with the other cases, it is seen that the mixing is higher and faster for the other cases, of weak stratification, compare with this case.

Figure 5.5.7 to 5.5.9 show the average temperature profiles change with jet momentum. In the lower zone, the temperature is increasing to reach the average temperature of the whole space. The change was higher in the case of warm jet compare with the cold jet. It was due to the temperature difference between the injected air and the relatively cold air in the lower zone, and the entrainment volume flux. In the upper zone the temperature was decreasing with the momentum until it reaches the average temperature of the whole space. The change was higher in the case of cold jet compare with the warm jet. Based on the above, the temperature of the stratified layer is a complement of the temperatures in both zones.

Increasing in jet momentum will increase the dilution (dT/dz= Min) and the height of the stratified layer until it becomes fully mixed. It is due to the decrease in the temperature difference between the layers due to the increase in the temperature of lower zone. The increase in circulated air due to the increase of momentum leads to mixing the flow in the whole space.

For high values of cold airflow rates(Q_c/Q_h =3.0), the stratified interface level height rises up due to bouyancy effect near the oposite wall, which forms a recircultion near the ceiling leads to mixing the flow in the upper zone.

As observed in cases 1 and 2, Figures A2.5.7 to A2.5.9 shows the temperature profiles at the thermocouple stand with negative temperature gradient in the lower zone. It occurred after certain value of jet speed (4.57 m/s) when the injected air reaches the floor. It indicates for the layers overturn that results in a negative bouyancy and more

disturbances accelerates the mixing near the floor. The negative temperature gradient is due to the comparatively hot air impengement on the floor surface and flows horizontally at the surface. The disturbances, where due to the injected-air movement against the floor surface. In these cases, there are three regions of:

1. Warm mixed air near the ceiling due to the recirculation of hot air in the uppper zone.
2. Warm air near the floor due to the impenigment of hot air injected from the ceiling against the floor surface and its recirculation in the lower zone.
3. Stratified layer in between, shifted upward and diluted with the increase of jet momentum.

For moderate air flow rate, where the flow is more stable and the interface level height is at the middle of the test chamber. The increase of cold jet speed leads to a horizontal air flow near the ground, which causes the height of the interface raise up. For the case of low or high air flow rate, where the interface level height is near the vertical boundaries of the environmental chamber (floor or ceiling), the increases in cold jet speed results in a high momentum air flow, which results in earlier fully mixed flow.

For warm jet, the density of injected air increases due to the entrainment air from the surrounding. On reaching the lower levels in the chamber the warm air flows from the jet will expand across the bottom of the chamber and display denser air downwards. A natural circulation is thus set up within the space, [Hee-Jin and Dale (2001)].

It is found that the warm jet flow is more effective than that of cold jet, and the mixing of warm jet is faster.

For more detail of data analyzed in Figures 5.5.7 to 5.5.9, see Figures (A2.5.7 to A2.5.9) in Appendix A2.

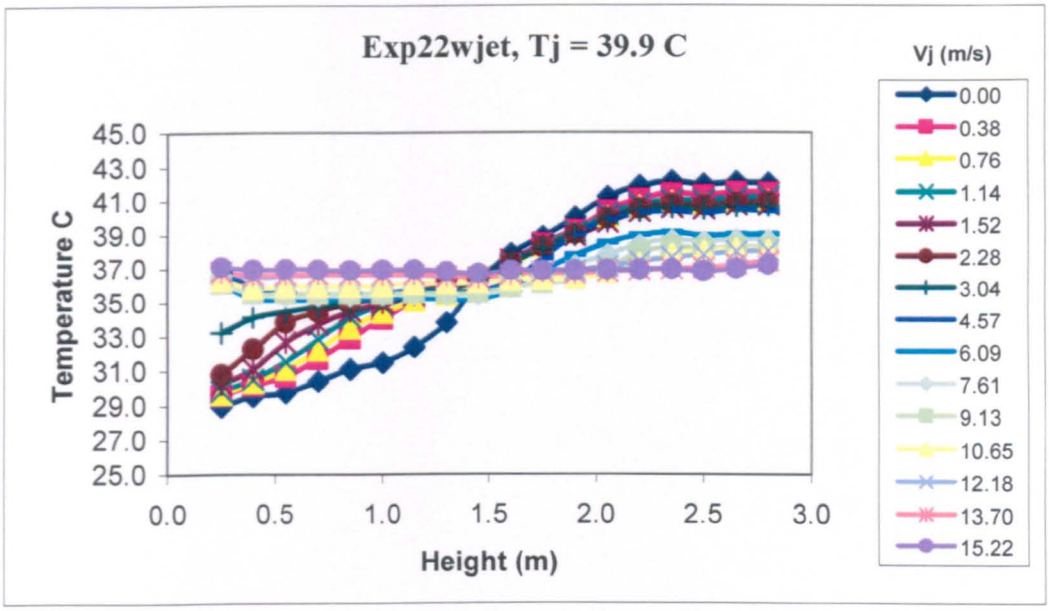

Figure 5.5.7: Vertical temperature profiles for various warm jet speed of 0.11 m diameter, while the flow was stratified at (Q_h = 2.0 m^3 / min) hot airflow rate and (Q_c = 2.0 m^3 / min) cold airflow rate at locations of 2.0 and 1.5 m respectively at the centre of environmental chamber.

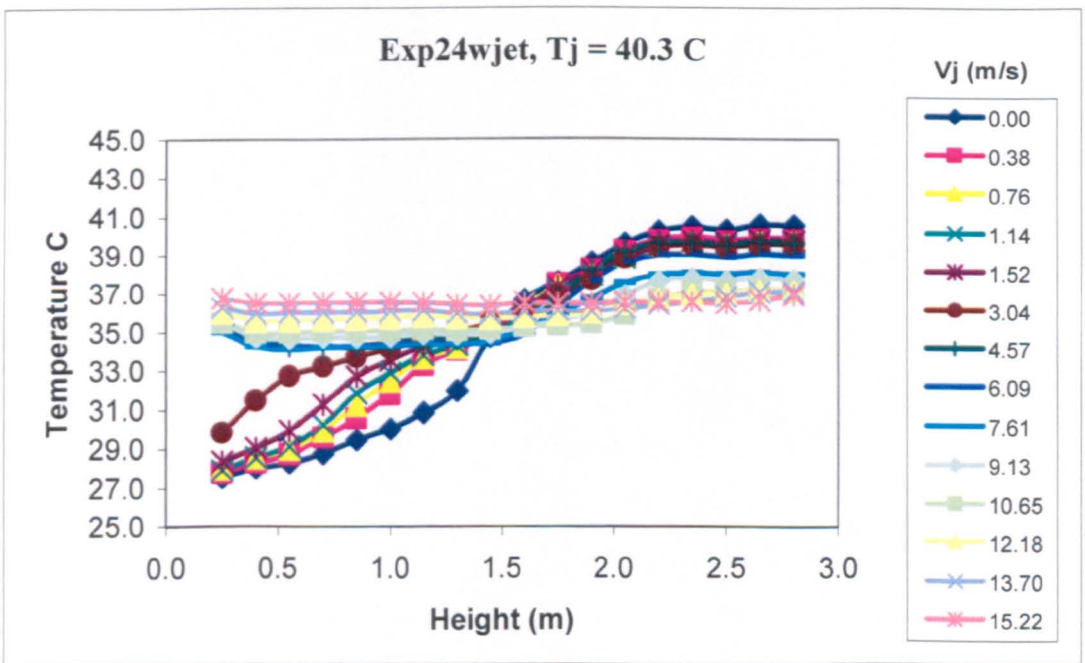

Figure 5.5.8: Vertical temperature profiles for various warm jet speed of 0.11 m diameter, while the flow was stratified at (Q_h = 2.0 m^3 / min) hot airflow rate and (Q_c = 4.0 m^3 / min) cold airflow rate at a locations of 2.0 and 1.5 m respectively at the centre of environmental chamber.

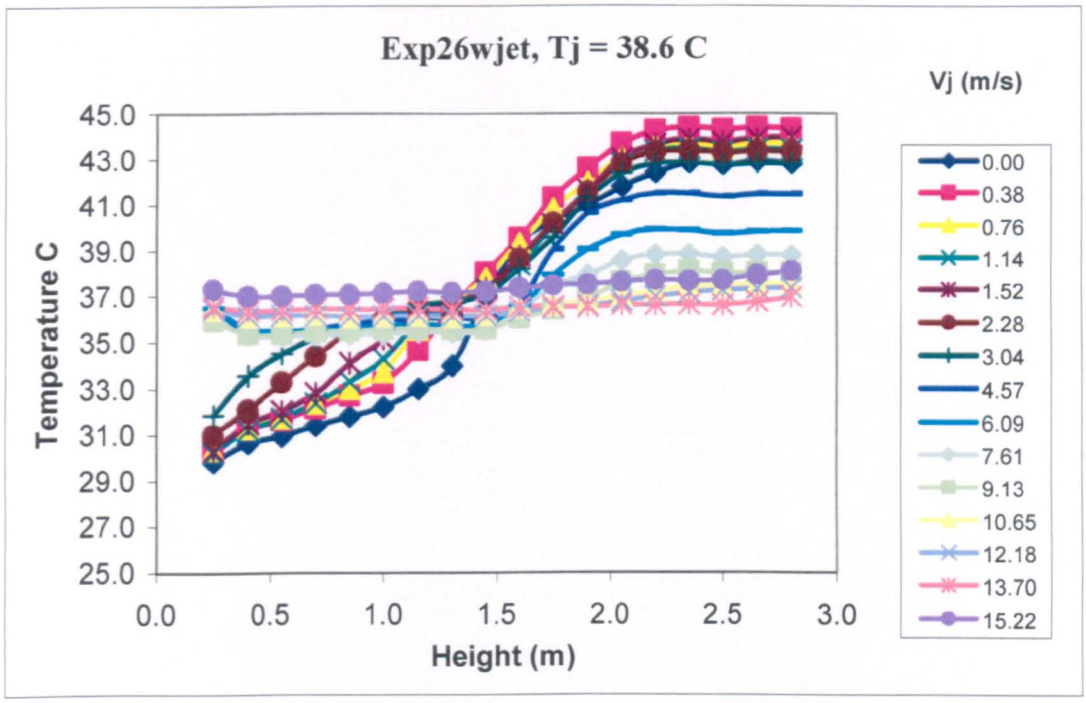

Figure 5.5.9: Vertical temperature profiles for various warm jet speed of 0.11 m diameter, while the flow was stratified at (Q_h = 2.0 m^3 / min) hot airflow rate and (Q_c = 6.0 m^3 / min) cold airflow rate at a locations of 2.0 and 1.5 m respectively at the centre of environmental chamber.

5.5.4 Combined Effect of Airflow Rates and Momentum Induced by Warm Jet on Stratified Flow

In this section, the effect of both hot and cold airflow rates with the presence of momentum using warm jet is analyzed and discussed.

Interface level height for various values of hot and cold airflow rates with the jet momentum, at fixed input and output locations, are shown in Figures A2.5.10 to A2.5.15. The plotted data shows that the stratified layer interface level height is affected by the input airflow rates. While the effect of hot airflow rate on temperature profiles is significant (Figures A2.5.13 to A2.5.15), the effect of cold airflow rates is smaller (Figure A2.5.10 to A2.5.12).

Figures A2.5.10 to A2.5.12 show the effect of warm jet speed on the interface level height. The results are for various values of hot and cold airflow with

$Q_h = 1.0, 2.0, 3.0\ m^3/min$ and $Q_c = 2.0, 4.0, 6.0\ m^3/min$. The results show that the effect of cold airflow rate was insignificant for the cases of low and intermediate hot air flow rate, where the stratified layer interface level height is competitively high. The effect of cold airflow rate was significant at high hot air flow rate where the initial stratification was happened at low interface level height as explained earlier. In general, the results show that the effect of cold airflow rates on the interface level heights is more significant for high jet momentum than for low jet momentum.

Comparison between Figures A2.5.10 to A2.5.12 and Figures A2.5.13 to A2.5.15 shows that, the effect of increasing hot airflow rates in mixing the flow using warm jet is more significant than the effect of increasing cold airflow rates, especially for the cases of intermediate values of warm jet flow and hot airflow rate. This was due to three reasons:

1. The comparatively significant effect of hot airflow rates as a source of heat used in our case.
2. The warm injected air and the hot airflow supply are from the same source, with an equal temperature. In the lower zone, the warm injected air works as a plume. With intermediate air flow ratio (Q_c/Q_h = 1 to 3), the plume has its complement between buoyancy and momentum. Any variation in hot airflow rate is seen clearly on the temperature scale.
3. The warm air was injected vertically from the ceiling to flow downwards. At higher values of hot air flow rates (Q_c/Q_h = Min), the flow is stratified at lower levels (case 2). In this case, the injected air needs long time to cross the distance between the jet and the stratified layer. During this time, the variations of the injected air due to the hot air layering in the upper zone are significant.

Figure A2.5.12 shows that, at comparatively high hot airflow rate, the flow will be fully mixed at a momentum of $0.35\ m^4/s^2$ with an intermediate cold airflow rates. It is also ($0.55\ m^4/s^2$) for the case of low cold airflow rate. For this case, the interface level height was at lower points (case 2). On the contrary, the figure shows that, to reach fully mixed flow in the presence of high cold airflow rate of ($6.0\ m^3/s$), less than half of this momentum will be in needed ($0.2\ m^4/s^2$), while it was three times for the case of cold jet,.

Figures A2.5.13 and A2.5.14 shows that, the flow will never be fully mixed at lower value of hot airflow rate of ($1.0\ m^3/s$). In this case, the stratified layer interface level height goes upward to reach more than 80% of the chamber height despite the higher jet momentum. On the contrary, it reaches a fully mixed flow in the case of higher value of hot airflow rates ($3.0\ m^3/s$), with better results for the higher values of cold airflow rate of ($6.0\ m^3/s$). In this case, the flow is completely mixed at lower momentum of $0.2\ m^4/s^2$.

5.5.5 Smoke Visualization of Warm Jet Tests

Smoke visualization was used to observe the behavior and the characteristics of the stratified flow. Different modeling techniques, various surrounding conditions, complex flow patterns and turbulent dissipations in the required domain were established for all the experiments. Both temperature and smoke visualization are included for comparison purposes. The experimental and flow visualization results obtained in this work are in good agreement. In this work, it became extremely difficult to get clear images for mixed cases of higher momentum jet flow, as mentioned in section 5.4.5.

Figures A2.5.16 to A2.5.25 represents the temperature isothermal lines and photographs of smoke distribution before and after the warm air was injected. The stratified flow was initiated at cold and hot airflow rates of 2 and $6 m^3/min$, Richardson number of 200 and a Reynolds number of 9700. It is classified as strong stratified flow.

Figures A2.5.16 to A2.5.19 are a sequence of temperature visualization showing the effect of warm jet flow on the stratified flow characteristics. The sequence images are covering different temperature distributions and mixing stages. The sequence temperature images are compared with the photograph images of smoke visualization.

Comparing the right and left half of each Figures of A2.5.16 to A2.5.19, the effect of momentum mode of flow on the stratified flow is clearly shown. The figures show the mixed zones of temperature isothermal lines were close to one another because the profiles become more vertical (less stratification). It shows that the stratified zones of temperature isothermal lines were open to one another because the profiles become

more inclined (more stratification). From the figures, the change in jet momentum is not only impacted on the shape of the profiles, but also its position on the temperature scale.

Figures A2.5.20 to A2.5.25 are a momentum sequence photographs for a six stages of mixed flow. The results are for smoke visualization, and the sequence of smoke images is referring to different temperature distribution. The flow was stratified at initial conditions of (2 and $6 m^3/min$) for hot and cold airflow rates respectively. The injected air was in the ranges of ($V_j = 0.0$ to $15.0 m/sec$). The sequence images visualize the effect of warm jet flow on the stratified flow characteristics.

Comparisons between the sequence figures illustrate the effect of momentum on the stratified flow characteristics. As the momentum increases, the smoke images indicate a more dilute of smoke concentration. Increasing the momentum causes a fully mixed flow. Figure A2.5.25 show a fully mixed flow with the presence of high momentum. In this case, a fully mixed flow, of large turbulent circulations, is strong enough to transform the laminar layers of smoke streamlines to turbulent ones at the smoke source.

Both groups of temperature and smoke visualization are included for comparison. In general, the results obtained in this work are in good agreement, considering that different techniques were used. The sequence of temperature profiles gives the values of the temperature measurements at the thermocouple stand, while the sequence of smoke photographs gives the approximate geometries of the stratified layer in the whole space. The results are important in the design of pollutants flow in the working zone, and smoke managements.

5.5.6 The Effect of Warm Jet Compare With the Cold Jet Momentum.

It has seen that the jet momentum has significant influence on the mixing of the stratified flow characteristics. The results indicated that once the momentum was initiated a mixed flow grew in the occupied zone above the floor. The height of this zone is dependent on the stratified flow characteristics, and the temperature and momentum of the ceiling jet.

In the case of warm jet, the injected air is lighter; therefore, the momentum and buoyancy forces are opposed. In this case, the momentum forces will decrease to zero before the injected air looses its buoyancy. Thus, the flow will stratify at certain heights depending on the initial amount of momentum.

In this case, it has seen two layers of stratification at the same time, mainly for the cases of low momentums ($M_j \leq 0.087 m^4/s^2$). In the case of the cold jet, the injected air is heavier than its domain. With initial momentum vertically downward, the momentum and buoyancy forces are reinforcing one another. In this case, the negative buoyancy can reach minimum values before the momentum is decreased to zero. It is due to the hot air entrainment from the upper zone. Thus the flow will stratify at certain level depending on the initial amount of momentum.

Comparing the effects of cold and warm specific jet momentums on the interface level height, Figure 5.5.10 and 5.5.11 show the following:

Firstly, at low hot airflow rate ($Q_h = 1.0\ m^3/min$), the results show that variation of the cold airflow has small effect for both cold and warm jet flow (Figure 5.5.10). While the effect of cold momentum on the stratified flow interface level height is high, the effect of warm momentum is higher. This is visible in the presence of low momentum. It can be related to the following reasons:

1. Insignificant temperature difference between the injected-warmed air and the hot air in the upper zone. Therefore, the injected air is flowing down under the effect of its initial momentum. When it reaches the lower zone:
    - It looses its momentum due to the long time needed to cross the distance between the jet and the lower zone.
    - It looses its negative buoyancy due to the entrainment of cold air from the lower zone.
    - It increases the temperature and the amount of the air in the lower zone, and the thickness of that zone, thus shifted the stratified layer interface level height upwards to reach the ceiling.
2. For the cold jet, the injected air is flowing down under the effect of both momentum and negative buoyancy. Comparing with warm-jet flow, the effect of cold momentum was smaller, which is related to the following reasons:

- The cold jet looses its momentum through the long distance needed to travel before reaching the lower zone. Compare with the warm case, the momentum loss is smaller because it needs less time to cross the distance due to its negative buoyancy and comparatively high slip velocity.
- The cold jet looses its negative buoyancy due to the entrainment of hot air from the upper zone, and the entrainment of cold air from the lower zone. Due to low temperature difference the entrainment is lower than the warm jet.
- It increases the temperature and the amount of air in the lower zone. The increase in temperature is lower compare with the warm jet. Thus the height of the occupied zone is increasing and the stratified layer interface level height is correspondingly shifted.

From the above analysis, the use of warm jet is more effective, compared with the cold jet flow.

Secondly, at higher values of hot airflow rate ($Q_h = 2.0\ m^3/min$), the results show the cold airflow rate with a significant effect for both cold and warm jet flow (Figure 5.5.11). While the effect of cold momentum on the stratified flow interface level height is high, the effect of warm momentum is nearly higher. For higher values of cold airflow rate ($Q_c = 6.0\ m^3/min$), the effect of momentum produced by cold jet is not effective compare with the other cases. This was due to the following reasons:

1. At high cold airflow rate, the flow was stratified at higher interface level height. Therefore, the distance for the injected air to reach the lower zone is comparatively short, so less amount of hot air entrainment from the upper zone. In this, the injected air looses less momentum and reaches the lower zone with comparatively low temperature. Thus, increase the amount of cold air in the lower zone and act as a cold air supply.
2. As discussed latter, more increase in momentum will increase the circulation in the lower zone leading to raise the stratified layer upward and mix the flow.

At lower values of hot airflow rate ($1.0\ m^3/s$), Figures 5.5.10 and 5.5.11 show that the flow will never be fully mixed. In this case, the stratified layer interface level height goes upward to reach more than 80% of the chamber height at higher momentum, while

it reaches the fully mixed case for higher values of hot airflow rates ($2.0\ m^3/s$) with better results for the higher values of cold airflow rate ($6.0\ m^3/s$). In this case, the flow is completely mixed at lower momentum of $0.2\ m^4/s^2$.

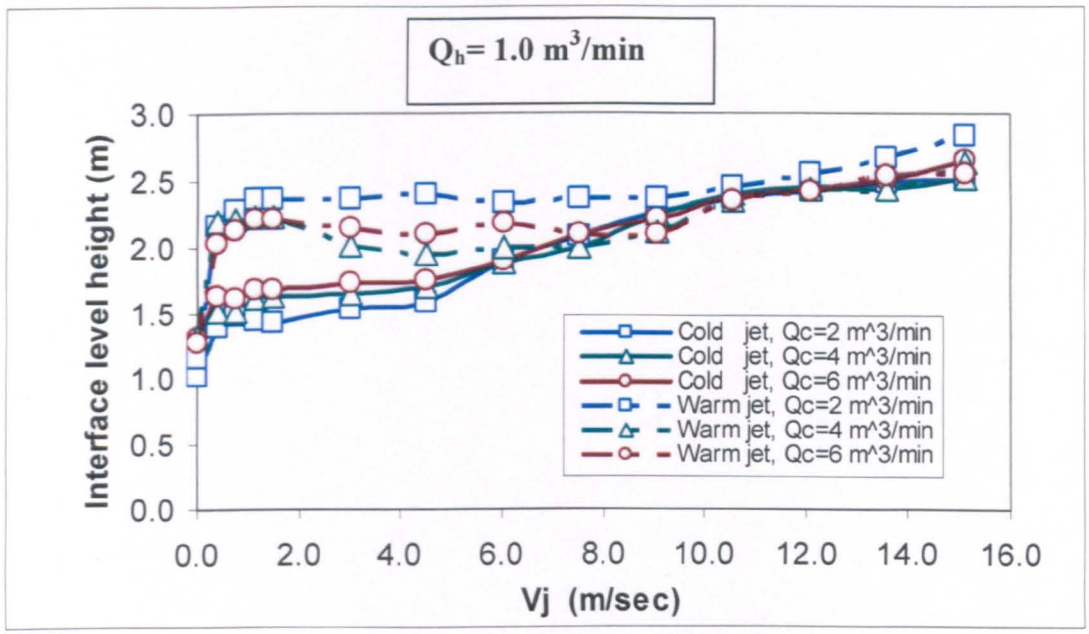

Figure 5.5.10: Comparison of interface level height with the jet speed, at hot airflow rate of $Q_h = 1.0\ m^3/min$ and different cold airflow rates ($Q_c = 2, 4$ and $6\ m^3/min$) in the environmental chamber.

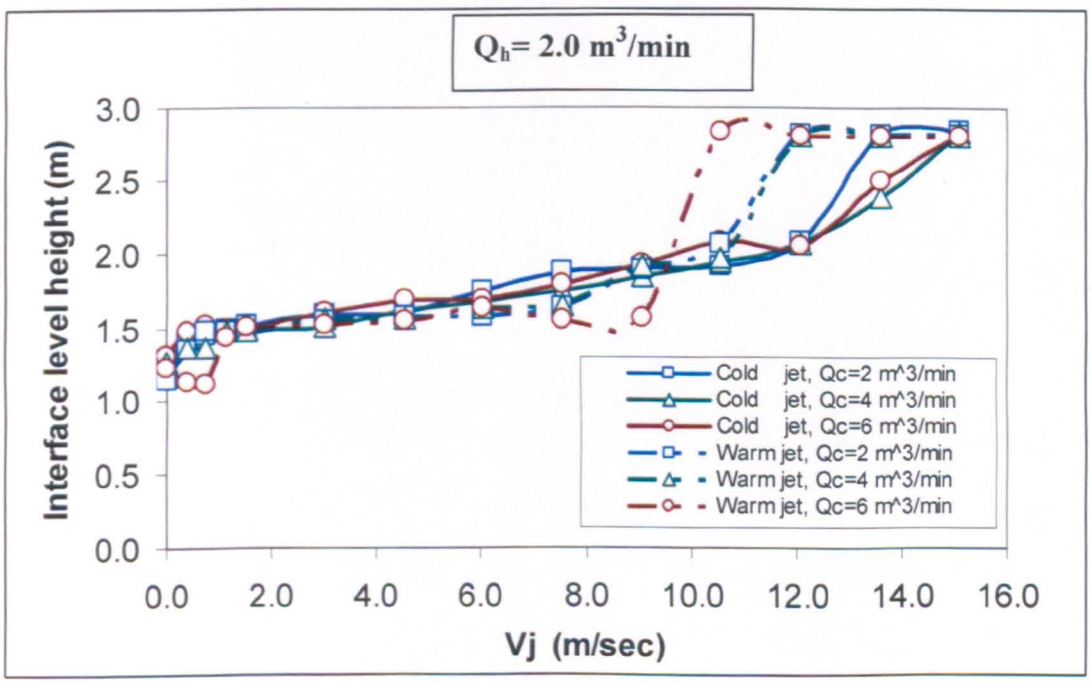

Figure 5.5.11: Comparison of interface level height with the jet speed, at hot airflow rate of $Q_h = 2.0\ m^3/min$ and different cold airflow rates ($Q_c = 2, 4$ and $6\ m^3/min$) in the environmental chamber.

5.6 Mixing Flow Using Inversion of Input Vertical Locations

5.6.1 Inversion Technique

Experiments were done to study the stratified flow characteristics using inversion technique to destroy the stratified layer and mix the flow. The temperature and smoke visualization have been carried out. Two cases of relatively strong stratification were studied using the experimental set-up presented in Chapter 3. The purpose of this technique was to remove the polluted and hot gases from the occupied zone, and to mix the air to a reasonably uniform temperature, yet satisfy the requirements of comfort environment in confined places.

Chapter 4 presented the effect of opening locations on the stratified flow characteristics. The effect of input vertical location was obtained in section 4.4. Similar analyses were carried out to investigate the effect of inversion of input locations on the stratified flow characteristics. A fully mixed flow can be reached when the cold air flows through the upper location, while the hot air flows through the lower ones. In other words, mixing will be introduced under the effect of inputs overturns (inversion of input locations) despite the presence of momentum and buoyancy sources.

In these types of flows, the source of hot air flow rate was the source of both buoyancy and momentum fluxes. While the direction of the flow is upward, the momentum and buoyancy were acting in the same direction. For the cold air supply, the direction of the flow was downward, so both momentum and buoyancy acted in the same direction. As classified by [Hunt et al. (2001)] the flow was of two categories:

1. Warm air forced upwards, where the resulting flow is a forced plume.
2. Cold air blown downwards, where the resulting flow is buoyant jet.

In this case, there are influences between the buoyancy tending to stratify the interior and the momentum tending to mix it. Thus with a forced plume it is possible to go from the stratified case to the mixed case by changing the relative magnitudes and directions of the buoyancy and momentum fluxes.

Figures 5.6.1 and 5.6.2 show the mixing of stratified flow using inversion technique. The results were for two cases of different flow rates. The results show how the

inversion of input locations influences the stratified flow characteristics despite the degree of stratification and the temperature difference. From the comparison between Figure 5.6.1 and 5.6.2, the temperature profiles show that the effect of hot airflow rate in stratified flow is clearly significant, while it disappears in the presence of inversion flow (in mixed flow).

These results, regardless of different initial conditions and different values of airflow rates, showed that the stratified layer was broken down rather than translated to higher levels as shown in the case of jet flow. Refrigerators and big meat stores use similar technique (defrost). In this technique, the refrigeration cycle is reversed for few minutes to remove the ice concentrated in the refrigerator due to the condensation of water vapor inside these stores.

As presented in Chapter 4, the change in the location of heat source was leaded to a change in the characteristics of the circulation flows formed, and so the characteristics of the stratified flow in the domain. In the same manner, the inversion of input supplier's locations will change the circulations formed above and below the stratified layer and so affect the stratified flow characteristics.

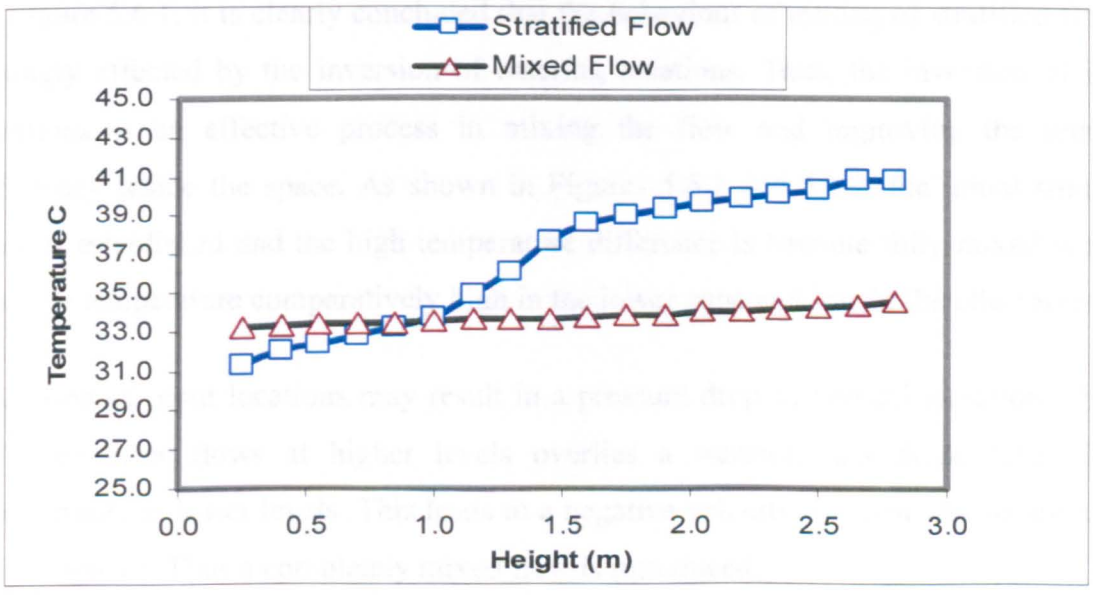

Figure 5.6.1: Temperature profile showing the translation from fully stratified flow to fully mixed flow, using inversion technique. The flow was translated from initial situation (Q_h = 2.0 m^3/min at H_{hot} = 2.0 m and Q_c = 4.0 m^3/min at H_{cold} = 0.5 m) to a new situation of (Q_h = 4.0 m^3/min at H_{hot} = 0.5 m and Q_c = 2.0 m^3/min at H_{cold} = 2.0 m) where the exhaust height was fixed (H_{ex} = 1.5 m).

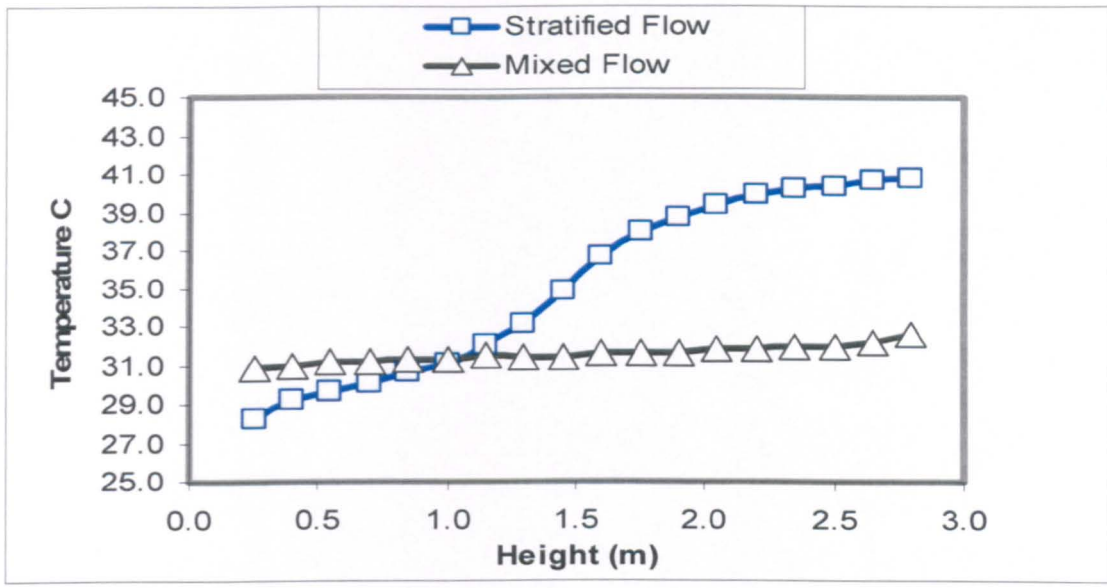

Figure 5.6.2: Temperature profile showing the translation from fully stratified flow to fully mixed flow, using inversion technique. The flow was translated from initial situation (Q_h = 2.0 m^3/min at H_{hot} = 2.0 m and Q_c = 6.0 m^3/min at H_{cold} = 0.5 m) to a new situation of (Q_h = 6.0 m^3/min at H_{hot} = 0.5 m and Q_c = 2.0 m^3/min at H_{cold} = 2.0 m) where the exhaust height was fixed (H_{ex} = 1.5 m).

In Figure 5.6.1, it is clearly concluded that the behaviour of mixing of stratified flow is strongly affected by the inversion of entering locations. Thus, the inversion of input locations is an effective process in mixing the flow and improving the removal efficiency inside the space. As shown in Figures 5.6.1 and 5.6.2, the initial stratified flow is established and the high temperature difference is become fully mixed with an average temperature comparatively high in the lower zone and low in the other zones.

Inversion of input locations may result in a pressure drop in vertical direction when a cold air layer flows at higher levels overlies a warmer, less dense layer flows horizontally at lower levels. This leads to a negative velocity gradient and so low value of Ri number. Thus a completely mixed flow is introduced.

From the results, changing the input location (for constant flow rates) does not change the temperature distribution of the stratification profiles, but change the level of stratified layer and the interface level height. It moves to higher or lower depends on the openings locations (Chapter 4). On the contrary, inversion of input airflow suppliers

gives a complete change in temperature profile and flow situation. It converts the flow from fully stratified flow to fully mixed flow, as shown in the figures.

5.6.2 Smoke Visualization of Inversion Technique Tests

Temperature visualization shows how the vertical temperature distribution changes with inversion of input locations. Comparing the right and left half's of various stratified flow conditions (Figures 5.6.3 and 5.6.6) shows the effect of inversion of input locations on the temperature isothermal lines. It shows a complete change for the distribution of temperature isothermal lines from the case of stratified flow to a case of mixed flow.

In the left half of both figures, the flow was stratified with strong degree of stratification. It shows the stratified layers of temperature isothermal lines were open to one another because the profiles become more inclined (stratified flow). While the inversion was impact both the shape of the profiles and its position on the temperature scale. The smoke visualizations of this case, for different airflow rates, were shown in Figures 5.6.4 and 5.6.7 In this case the smoke is concentrated into the stratified layer above the lower zone rather than shorting up to reach the ceiling, as discussed in Chapter 4.

In the right half, the temperature distribution does not show any variation with height over the full period of time. It shows the mixed zones of temperature isothermal lines were close to one another because the profiles become more vertical (mixed flow). In this case, the whole space becomes one zone, and the temperature distribution shows the same profiles (like an isothermal flow) even though initial situations changes furthermore. Also, the temperature distribution is somewhat independent of the flow situation. The smoke visualizations of this case, for different airflow rates, were shown in Figures 5.6.5 and 5.6.8. In this case, the smoke is rising up due to buoyancy, and shorting up to reach the ceiling rather than concentrating in the stratified layer over the lower zone.

Figures 5.6.3 and 5.6.6 shows how the average temperature changes. It ascends in the lower zone, while it descends in the other zones with steeper descending in the upper one. It should be accepted due to the following reasons:

1. Fully mixed flow will result in large values of disturbances and turbulences leading to fully circulated flow in the whole domain. When reaching steady state, an isothermal flow in the chamber will introduce.
2. Fully mixed flow will improve the effectiveness of hot gas removing from the chambers, which result in increasing of output temperature. Thus, the average temperature in the whole space regardless of the of the stratification degree.
3. When a location of the heat source is at lower level, the convective heat gain from the heat source to the lower zone is increasing. While the lower zone is originally cold, this will result in an increase of its temperature, so that the temperatures in the upper zones are decreasing. As a result, a reduction in the average temperature of the whole domain is occurred, as discussed in Chapter 4.

These observations were similar to the numerical observations of [Sinha et al. (2000)] for hot air inlet located near the floor level, while the exhaust located in the opposite wall or the ceiling. In their case, the buoyancy forces accelerate the penetrated hot air towards the exhaust. This enhances the secondary re-circulation around the path of the penetrated air, which increases the average temperature in most of the occupied zone. As discussed in Chapter 4, where the level of stratification is changed depending on the source location, because of the re-circulation flows generated in the mixed layers was changing with source location.

As shown in Figures 5.6.3 to 5.6.8, the results indicate a close agreement between temperature and smoke visualization. While the stratified layer was broken down rather than translated to higher levels before reaching fully mixed flow, the flow was mixed without any needs for a new air supply, more airflow rates and more energy consumption. Also mixing the stratified flow and improving the pollutant removal efficiency inside the space was so better. So for low ventilation air flow rates and no additional airflow to be used, mixing by inversion technique will be preferable.

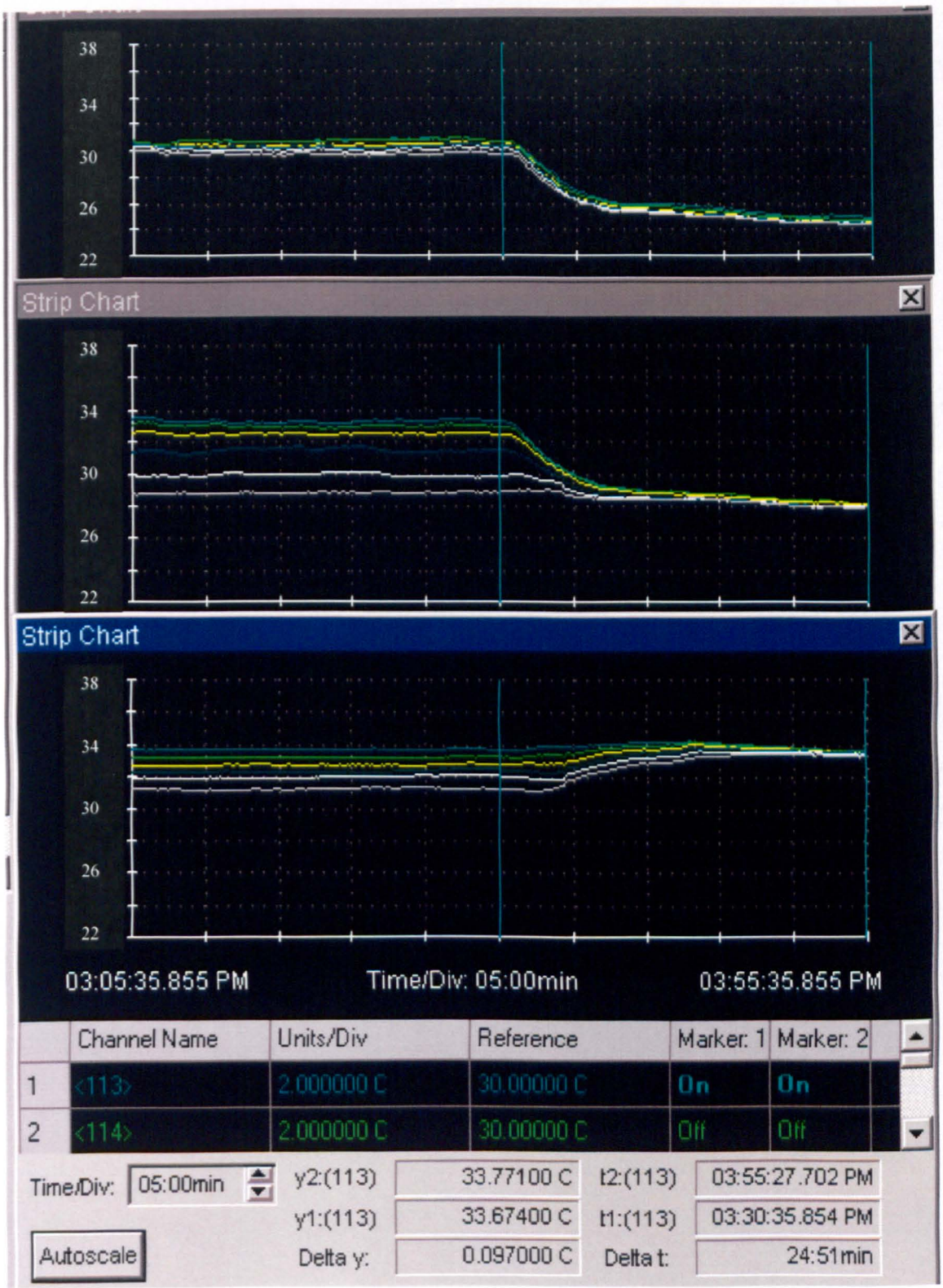

Figure 5.6.3: Temperature visualization showing the mixing of stratified flow of initial situation ($Q_h = 2.0\ m^3/min$ at $H_{hot} = 2.0\ m$ and $Q_c = 4.0\ m^3/min$ at $H_{cold} = 0.5\ m$) to a new situation of ($Q_h = 4.0\ m^3/min$ at $H_{hot} = 0.5\ m$ and $Q_c = 2.0\ m^3/min$ at $H_{cold} = 2.0\ m$) where the exhaust height was fixed ($H_{ex} = 1.5\ m$).

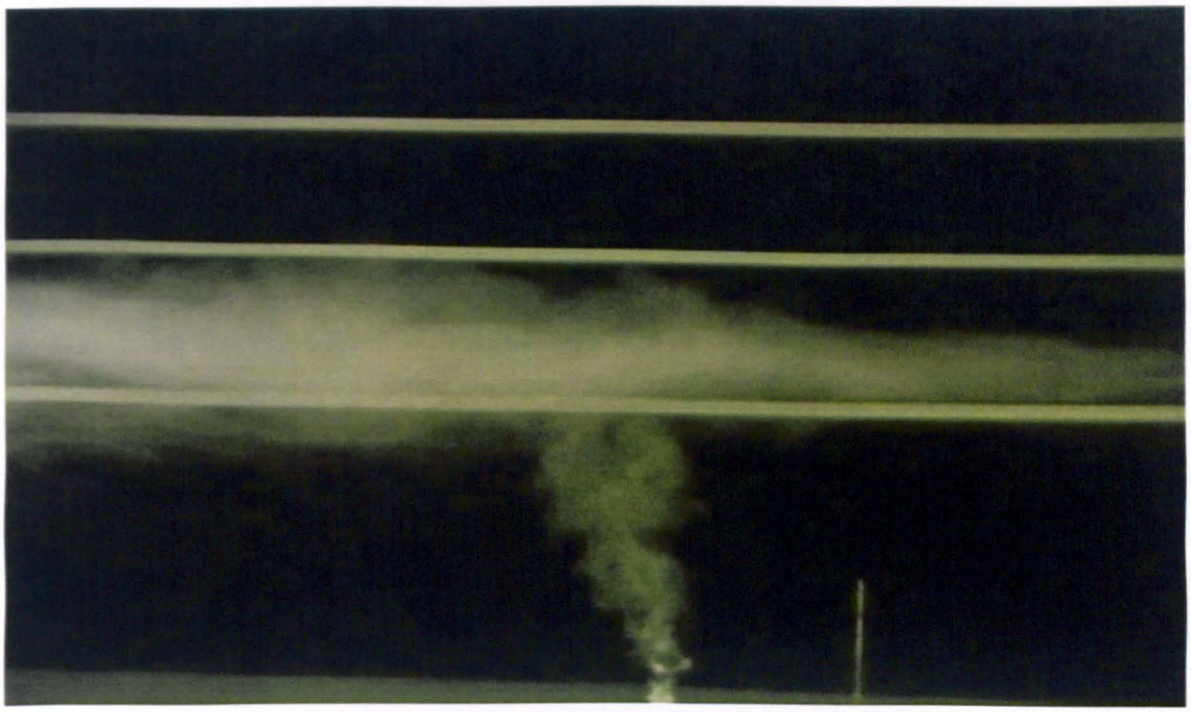

Figure 5.6.4: Smoke visualization showing the stratified flow at the initial situation of $Q_h = 2.0\ m^3/min$ and $Q_c = 4.0\ m^3/min$ and locations heights of $H_{hot} = 2.0\ m$ and $H_{cold} = 0.5\ m$ respectively, at fixed $H_{ex} = 1.5\ m$.

Figure 5.6.5: Smoke visualization showing the mixing of stratified flow of initial situation ($Q_h = 2.0\ m^3/min$ at $H_{hot} = 2.0\ m$ and $Q_c = 4.0\ m^3/min$ at $H_{cold} = 0.5\ m$) to a new situation of ($Q_h = 4.0\ m^3/min$ at $H_{hot} = 0.5\ m$ and $Q_c = 2.0\ m^3/min$ at $H_{cold} = 2.0\ m$) where the exhaust height was fixed ($H_{ex} = 1.5\ m$).

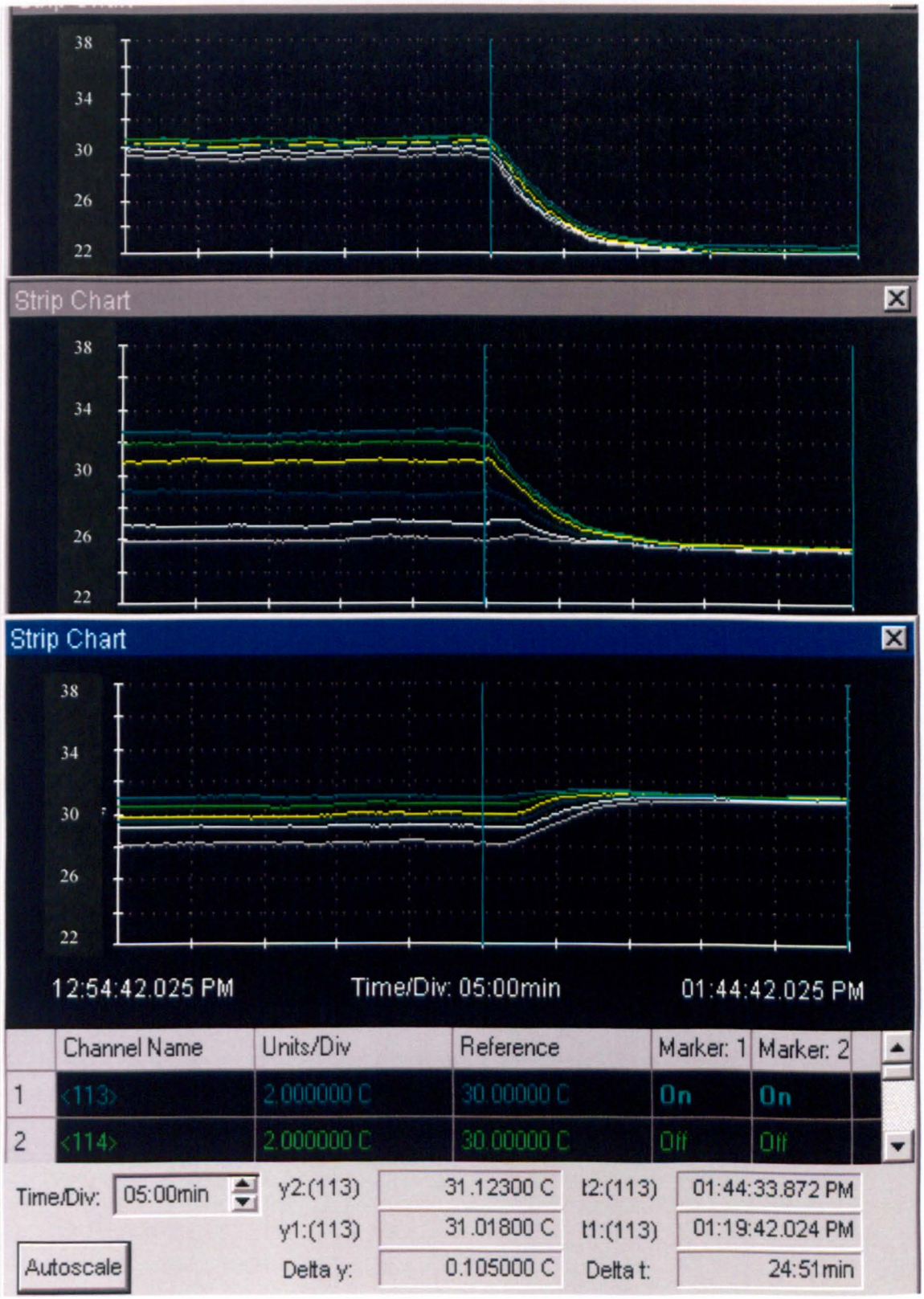

Figure 5.6.6: Temperature visualization showing the mixing of stratified flow of initial situation of ($Q_h = 2.0\ m^3/min$ at $H_{hot} = 2.0\ m$ and $Q_c = 6.0\ m^3/min$ at $H_{cold} = 0.5\ m$) to a new situation of ($Q_h = 6.0\ m^3/min$ at $H_{hot} = 0.5\ m$ and $Q_c = 2.0\ m^3/min$ at $H_{cold} = 2.0\ m$) where the exhaust height was fixed ($H_{ex} = 1.5\ m$).

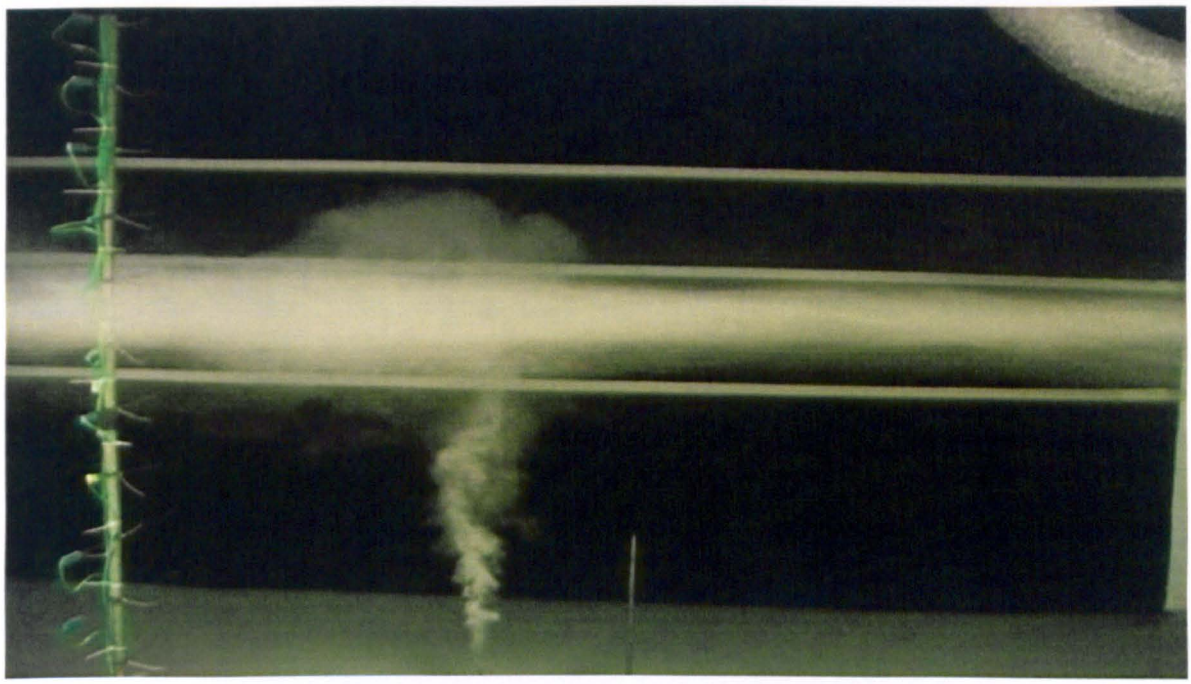

Figure 5.6.7: Temperature visualization showing the mixing of stratified flow of initial situation of (Q_h = 2.0 m^3/min at H_{hot} = 2.0 m and Q_c = 6.0 m^3/min at H_{cold} = 0.5 m) where the exhaust height was fixed (H_{ex} = 1.5 m).

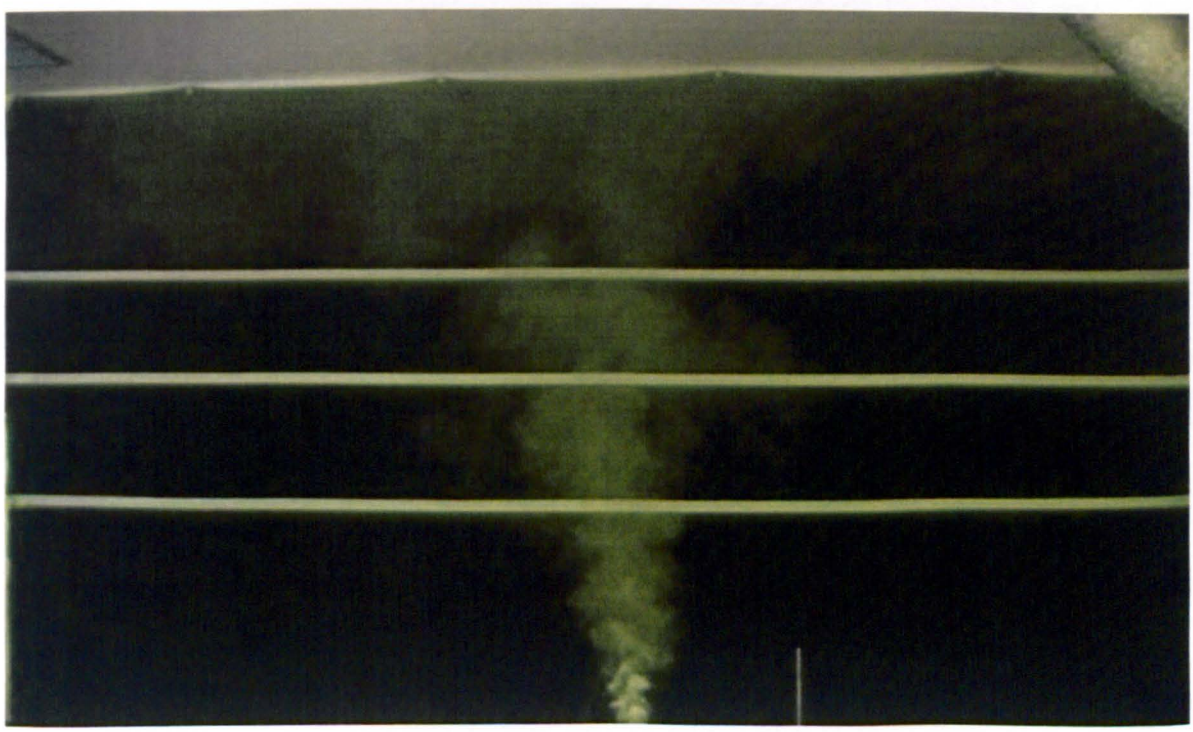

Figure 5.6.8: Smoke visualization showing the mixing of stratified flow of initial situation (Q_h = 2.0 m^3/min at H_{hot} = 2.0 m and Q_c = 6.0 m^3/min at H_{cold} = 0.5 m) to a new situation of (Q_h = 6.0 m^3/min at H_{hot} = 0.5 m and Q_c = 2.0 m^3/min at H_{cold} = 2.0 m) where the exhaust height was fixed (H_{ex} = 1.5 m).

5.7 Summaries and Conclusions

Mixed ventilation is where air is supplied into the space with relatively high momentum flux, in order that, the air in the space will be mixed to a reasonably uniform temperature, yet satisfying the requirement for air speeds. Thus is usually achieved by supplying air at high level within the space. For low jet momentum, the flow unable to reach the floor due to the stronger stratification layer that generated in the lower zone [chow (1996)].

Mixing of stratified flow was carried out using full-scale air-modeling technique, and by two technical methods:

- By increasing the momentum forces to break the balance between buoyancy and momentum. This was carried out using both cold and warm jet flow.
- By inversing the inputs vertical locations.

The effect of initial jet momentum airflow on mixing the stratified flow was investigated by using experimental techniques. When a momentum of the jet is higher, a momentum turbulence gain from the momentum source to the lower zone increases, which results in change in the average temperature and in an increasing in the occupied zone by increasing the stratified layer level height.

It can be concluded that the jet momentum has significant influence on the mixing of the flow and the stratified flow characteristics. The results indicated that once the momentum was initiated a mixed flow grew in the occupied zone above the floor. The height of this zone is a dependent of the stratified flow characteristics, and the temperature and momentum of the ceiling jet.

Also the results showed that the stratified layer height is a function of the initial jet momentum over a wide range of flow rates. These results, despite of different types and values of jet flow, showed that the interface level height was approximately inversely proportional to the momentum in the case of cold jet, at least over the range of $0.22 - 2.17\ m^4/s^2$, and as expected for weak stratification the mixing was more effective and faster.

5.8.1 Cold Jet

It is seen that increasing the momentum will increase the stratified layer interface level height, and more increase in jet momentum will increase the mixing in the lower zone and destroy the stratified layer before reaching the ceiling. From the three cases, it can be concluded that, for the case of strong degree of stratification and low momentum, on reaching the interface, the injected air will flow and stratified above the stratified layer for a certain distance depending on the degree of momentum, degree of stratification and interface level height. However, for low degree of stratification the injected flow will go through the stratified layer or destroying it, while for high degree of stratification, the stratified layer will stand against the injected flow of low momentum as a solid surface.

Comparing the results of this case with those in case 1 and case 2, it can be noted that, the effect of hot airflow rate compare with cold airflow rate was much higher. For relatively cool jet injected air at high level from the ceiling, the entrainment volume flux from the upper zone is large enough. While the hot air domain of penetration is the upper zone, the significant effect of hot airflow rates should be comparatively. From the comparisons, it is seen that the mixing is higher and faster in case 1 and 2 since the temperature gradient and the degree of stratification is not strong enough as shown in this case.

5.8.2 Warm Jet

The effect of momentum of warm jet airflow on mixing the stratified flow was investigated. Extensive experimental measurements providing temperature profiles of various jet speeds of (0.0 to 15.0 m/s) are presented. The experiments were done using air-modeling technique.

It is seen that the jet momentum has significant influence on mixing of stratified flow and flow characteristics. The results showed that the effect of warm jet is more significant especially in the lower and at low jet momentum.

Comparisons between cold and warm jet flow show that the translation of the stratified flow level height and the mixing effectiveness are changed depending on the jet

temperature and momentum. Using warm jet airflow, the mixing of stratified flow was faster while the removing efficiently was higher. Using warm jet, the higher values of momentum will destroy the stratified layer and mix before the interface level height reaches higher levels like that of cold jet flow.

The results demonstrated the stratified layer height as a function of the initial jet momentum over a wide range of flow rates. These results, with respect to different types and values of jet flow, showed that the interface level height was approximately proportional to the momentum in the case of warm jet, at least over the range of $0.22 - 2.17\ m^4/s^2$.

5.8.3 Inversion of Input Vertical Locations

Another area of experimental techniques used to mix the stratified flow is the inversion of input airflow suppliers. In this case, the buoyant cold layer in the lower zone will loose its buoyancy forces while being heated with the hot airflow penetrated at lower levels in the environmental chamber. Also the stratified layer will loose its stability and break down due to the drag and tearing of cold air penetrated downward from higher levels. The compound effect of these two situations will circulate the air in the whole space and disturb the stability of the stratified layer to reach fully mixed flow

From the results, it is concluded that the behaviour of mixing of stratified flow is strongly affected by the inversion of entering locations (i.e. input hot air placed near floor and cold air flow near ceiling). The flow was being fully mixed without any needs for a new air supply, more airflow rates and more energy consumption. Thus, the inversion of input locations is an effective process in the mixing process of the flow and improving the pollutant removal efficiency inside the space. Also the results show that the initial stratified flow and the high temperature difference is becoming fully mixed with an average temperature comparatively low in the whole space.

Comparing with mixing by momentum jet mixing by inversion technique, the latter will be comparatively preferable.

Chapter 6

Chapter 6

General Discussion of Stratified Flow

6.1 Introduction

This Chapter provides a discussion of the results presented in Chapters 4 and 5. Comparisons of the results obtained from the present experiments with the previous studies as well as the small-scale results are discussed. Implications of flow measurements, resolution and uncertainty are examined to identify the key similarities of these results.

The analytical and schematic models proposed by [Skistad (1998)] and [Calay et al. (2000)] for selective ventilation in large enclosures were the basis for a full-scale experimental model used in this study (i.e. Chapter 3). The model of [Skistad (1998)] was set up for the environmental chamber to study the flow parameters and stratified flow characteristics as explained in Chapter 4. In Chapter 5, the physical process proposed by [Calay et al. (2000)] for jet momentum was the bases for the model used to destratify the flow.

A series of experiments were carried out using full-scale air modeling technique. Different smoke and temperature visualization techniques were used to investigate the phenomenon of stratification in the built environment to compare latter with the results of the present work.

In Chapter 4, the effect of flow parameters such as airflow rates, ducts vertical locations and direction of flow were studied. In Chapter 5, both cold and warm jet momentum were introduced to mixing the flow of different stratification conditions. An inversion technique has been used in order to overturn the momentum buoyancy phase flow inside the chamber to break down the stratified layer and mixing the flow.

6.2 Comparison with Other Published Work

The purpose of this section is to present related experimental data from previous studies in comparison with the present work. The results of full-scale air-modeling technique are compared with the related small-scale models. These comparisons are made to identify the similarities of flow parametric, therefore illustrating the similarities between a real full-scale technique and a small-scale one.

Figure 3.1.1 showed a schematic process related to ventilation in rooms with a stratified flow situation. It shows a schematic drawing of selective withdrawal for a polluted layer of air-"Select-vent" presented by [Skistad (1998)]. The proposed work was to achieve three goals using the suggested model where the method of selective ventilation is still subject to research and a number of questions have not yet been answered.

Firstly, to study the effect of flow parameters such as relative input and output airflow rates, which was an important parameter in the technical work of [Skistad (1998)], where the stratified flow characteristic δ (the stratified layer thickness) is a function of extract airflow rate as evaluated by [Skistad (1998)] equation (6.2.1)

$$\delta = k\left(\frac{Q_{out}}{B}\right)^{\frac{1}{2}}\left(\frac{g}{T}\frac{\partial T}{\partial z}\right)^{-\frac{1}{4}} \qquad (6.2.1)$$

where k is a constant =2.0, Q_{out} is the extract airflow rate in m^3/s, B is the width of the withdrawal layer, g is the acceleration of gravity, T is the air temperature in °K, z is the height coordinate and δ is the half thickness of withdrawal layer.

Secondly, to achieve a significant saving of energy by zoning the space, above and below the stratified layer, to a working zone of clean-cool air and an upper zone of clean-hot air, while the pollutants are concentrated at the level of stratification to be extracted.

Thirdly, to study the significance of inlet and outlet duct locations as a key factor in the stratification phenomenon and so in the ventilation process. It is necessary to characterize the exhaust height to be in the right location. Otherwise, when the exhaust location is situated in the upper zone, the extraction of fresh air is higher; hence the concentration of contaminants in the lower zone is higher. On the contrary, if the

exhaust location is situated in the lower zone or close to the stratified layer interface, the contaminant removal effectiveness is better.

To answer the question of Skistad (1998) "How thick will the withdrawal layer be?" The stratified withdrawal layer is a very important component in stratified flow characteristics. It works as a thermal barrier between upper and lower zones from which the temperature difference and the degree of stratification are evaluated.

Consequently, in comparing with the schematic model suggested by Skistad, the experimental observations in this work support the present model. Both models predicted the stratified flow characteristics using full-scale technique with several major differences between the present model and the schematic model of Skistad (figures 3.1.1 and 6.2.1):

- Whilst Skistad's model is a simplified analytical model, the present study is based on full scale experiments.
- The results show that the stratified flow characteristics are affected by different flow parameters. The Skistad's model concerned with the stratified flow characteristics in terms of the stratified layer thickness, and related this parameter to the extract airflow and the geometry of the enclosure (equation 6.2.1).
- According to Skistad's analysis, the flow must stratify at the level of extraction (exhaust height), while in the present model it stratifies at the level of stratification between the bottom and the top of the full-scale height. It can also stratify at the level of neutral buoyancy when the level of stratification is higher, which depends on smoke density and extraction air flow rate.
- According to Skistad's analysis, the stratified layer thickness gives the same results before and after inverting the input locations, which is in disagreement with the present results (Chapter 5), and the results of [Hunt et al. (2001)].
- According to Skistad's analysis the variation of temperature in the enclosure is linear which is in disagreement with the present results and the results of [Mundt (1995)], where the temperature distribution is non linear, and the temperature gradient is maximum somewhere below the ceiling where the contaminants concentrated.

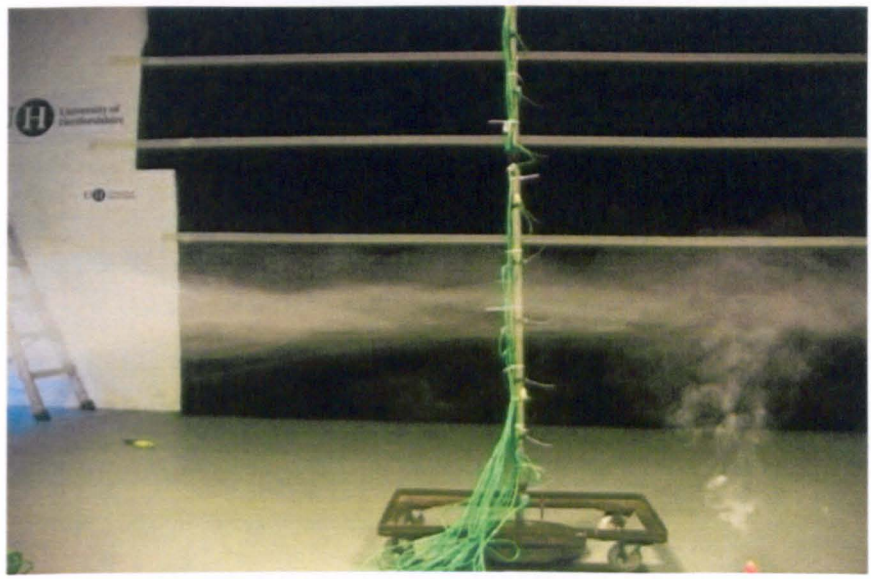

Figure 6.2.1: Temperature visualization showing the stratified layer and zones of (Q_h & Q_c = 3 & 6 m^3/min, $H_{exhaust}$ = 1.5 m).

In ventilation applications, some of the heat source is placed at higher locations. In this case an amount of cold airflow rate is generated through the low level openings. Both Skistad and Linden models relates the stratified flow characteristics to the overall airflow rate (Q_{out}), and ignore the effects of cold airflow rate. In our case, the mass flow rate was varied according to weather fluctuations, where the cold air supply is the ambient, so that the overall airflow rate Q_{out} defined by equation 6.2.2 was used.

$$Q_{out} = Q_c + Q_h \tag{6.2.2}$$

From equation 6.2.1, the stratified layer thickness δ is a power function of overall flow rate Q_{out}. An estimate for stratified layer thickness δ at certain overall airflow rate Q_{out} is described by equation 6.2.3, and shown in Figure 6.2.2.

$$\delta = A(Q_{out})^b \tag{6.2.3}$$

where A and b are constants obtained from the best fit of the experimental results. Figure 6.2.2 shows the relationship between δ and the total airflow rate, as evaluated for different types of cold and hot airflow rate.

With the constants: A = 0.8 and b = -0.25, equation 6.2.3 becomes

$$\delta = 0.8(Q_{out})^{-0.25} \qquad (6.2.4)$$

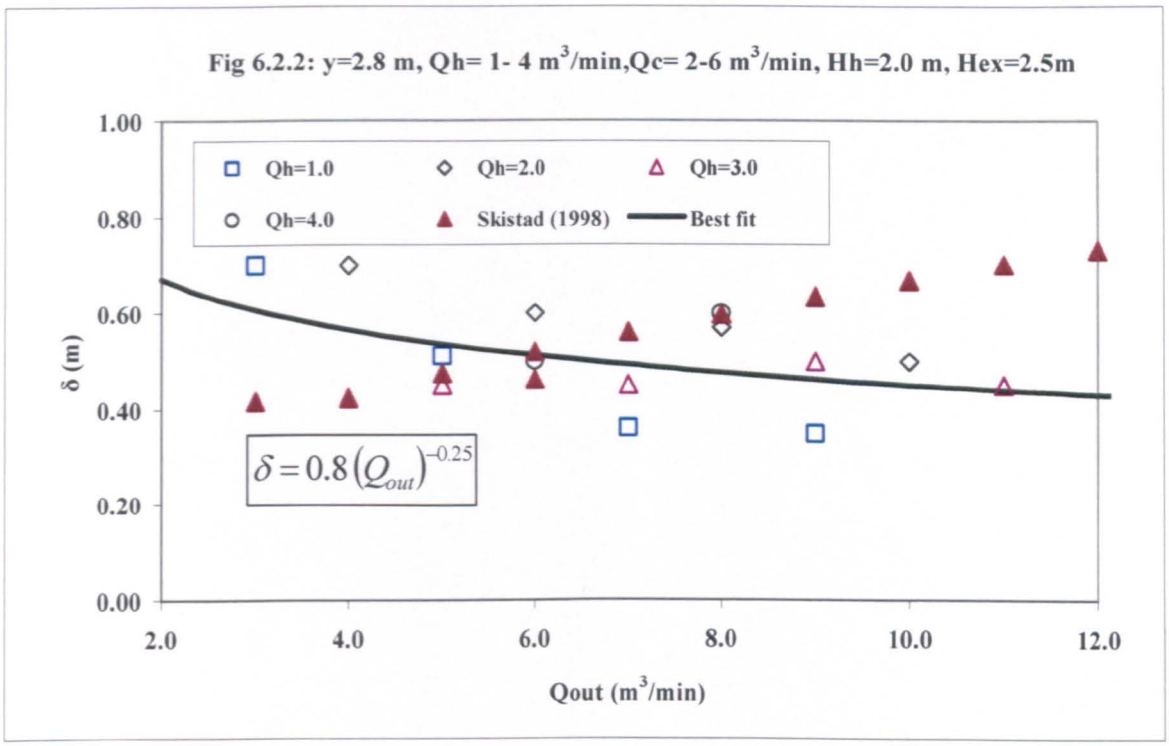

Fig 6.2.2: The stratified layer thickness δ with the overall airflow rate Q_{out} for various values of hot airflow rate Q_h = 1.0, 2.0, 3.0 and 4.0 m^3 / min compare with the results of [Skistad (1998)]. The line represents the prediction of equation 6.2.4.

Table 6.2.1 summarizes the stratified layer thickness δ calculated by [Skistad (1998)], equation (6.2.1) and the present results, along with the variations of input airflow rates. Compared with the present results, there is no statistical agreement between these results. Skistad equation 6.2.1 was based on the withdrawal airflow rate $Q_{ext} = Q_{out} = Q_h$ and the geometry of the enclosure, where the exhaust height is the height of stratification. Some of the variation in stratified layer thickness evaluations can be attributed to the methods used to estimate δ. As previously discussed, there is no mathematical equation that can identify the stratified layer thickness or pinpoint the location of its interface. For these reasons, the results summarized in table 6.2.1 and shown in figure 6.2.2, show an agreement for the cases of high airflow rate while for moderate and low flows the deviations is about 5-30%. In general, it is to be expected

that an agreement between the prediction of [Skistad (1998)] and the present measured data would improve as the reasons mentioned above are solved.

Q_h (m^3/min)	Q_c (m^3/min)	Q_h/V ($hour^{-1}$)	Q_c/V ($hour^{-1}$)	δ (m) (Equation 6.2.1)	δ (m) (Measured)
1	2	0.48	0.95	0.42	0.7
1	4	0.48	1.90	0.47	0.51
1	6	0.48	2.86	0.56	0.36
1	8	0.48	3.81	0.63	0.35
2	2	0.95	0.95	0.42	0.7
2	4	0.95	1.90	0.46	0.6
2	6	0.95	2.86	0.6	0.57
2	8	0.95	3.81	0.67	0.5
3	2	1.43	0.95	0.47	0.45
3	4	1.43	1.90	0.56	0.45
3	6	1.43	2.86	0.63	0.5
3	8	1.43	3.81	0.7	0.45
4	2	1.90	0.95	0.52	0.5
4	4	1.90	1.90	0.6	0.6

Table 6.2.1: The stratified layer thickness calculated by Skistad (1998) equations compared with the present evaluated values for several typical of experiments with several values of airflow rates.

As discussed in Chapter 2, the outputs of small-scale models are displayed by two zones of stratified flow, while the stratified layer is a sharp interface between these zones. Therefore, the temperature difference is determined from the average temperatures above and below the interface. In practice, the interface between these zones is of significant height occurs are over a finite distance within the room called stratified layer.

Despite the flow conditions and weather fluctuations, the stratified layer established using full-scale air modeling technique is still better than that of using small-scale models (model of Linden) as discussed in Chapter 4. The model of Linden may be appropriate to evaluate the stratified flow characteristics, by conserving the dimensionless parameters as reviewed in Chapter 2.

The experiments performed by Linden's model are different at some points from the set-up used in this research:

In the research by Linden:

1. Small-scale experiments were made in a salt-baths set-up to predict the natural displacement ventilation in combination with a wind stack. Both diffusion and radiation were assumed negligible, while the convective heat transfer cannot be neglected.
2. The values of heating or cooling loads were varied through the density difference between the supplied liquid and the domain.
3. The direction of the flow was vertical. The fluid flow driven only by density differences and solute transports. The stratification situation involved buoyancy forces is dependent on the solute concentration.

Whereas in present research:

1. Full-scale experiments were made in the environmental chamber with a mechanical mixing ventilation system. The temperature variation along the vertical height is evaluated. The influence of different flow parameters on the stratified flow characteristics was investigated.
2. The change in the air heating or cooling temperature fraction results from the change of supply airflow rate (Q_c or Q_h) rather than the supply temperature.
3. The flow direction was differing due to the differences in the acting stream forces. The stratification situation was implicated by a coupling of buoyancy and momentum forces.

As shown in figures 6.2.3 and 6.2.4, the results performed by Linden's model disagree at some points from the results evaluated in this research.

In the research by Linden:

1. The stratification occurs at a certain height between the ceiling and the floor, while the stratified layer is the layer between the clean zone and the ceiling, where the liquids layering behavior is to stratify the lighter liquid above the heavier ones.

2. The stratified layer interface level height was predicted as a sharp interface between two layers of air of differing temperature, clean and polluted zone, which in opposing to the results of [Mundt (1995)]. In the same time, this imply that a natural implementation of the stratification occur in our case. While in case of Linden model they made an artificial condition of experiments with totally different densities.
3. The mathematical model of [Linden et. al. (1990)] did not explain the temperature distribution within the test-room. Both diffusion of heat and thermal radiation were neglected, while the remaining mechanism for heat transfer is convection. Therefore, two layers of air of differing temperatures can co-exist in the same confined space without any diffusion over the sharp interface. [Howell and Potts (2001)].
4. The mathematical model of [Linden et. al. (1990)] was in good agreement with the salt-bath technique, where the salt-bath technique also neglects the mechanisms of thermal radiation and diffusion [Howell and Potts (2001)].

Whereas in the present research:

- The stratification can occur at any level inside the chamber, where the gases behavior is lighter and can be stratified at different heights.
- The stratified layer interface level height was the line of maximum degradation of temperature profile with vertical height, while the ventilated space was divided into two clean zones with a polluted-stratified layer in between, which is in agreement to the results of [Mundt (1995)].
- The temperature distribution within the test-chamber is realistically explained, while both diffusion of heat and thermal radiation during the stratified layer coexisted. Therefore, two clean zones of air of differing temperatures can coexist in the same confined space, and a stratified layer of significant thickness was in between, this naturally occurs in real environment.
- The results of temperature measurements and smoke visualization were in good agreement with the results of [Mundt (1995)], where thermal stratification occurs, and both thermal radiation and diffusion were present.

An estimate for the stratified layer interface level height h at a certain effective opening ratio can be obtained from the present results and compared by the work of [Linden

(1990)], who estimated the sharp interface level height with the effective opening ratios A^*/H^2 and A^*L/H:

$$A^* = \frac{a_1 a_2}{\left(\frac{1}{2}\left(a_1^2/c + a_2^2\right)\right)^{\frac{1}{2}}} \qquad (6.2.5)$$

where a_1 *and* a_2 are the input and outlet opening areas, and c=1 is the value of discharge coefficient used by [Linden (1990)] for calculating A^*.

Linden (1990) used equation 6.2.5 to estimate the actual airflow rate. In our case the effective opening area can be estimated from the measured values of airflow rate, assuming the chamber is fully insulated:

$$A^* = \frac{Q_{out}}{v_{out}} \qquad (6.2.6)$$

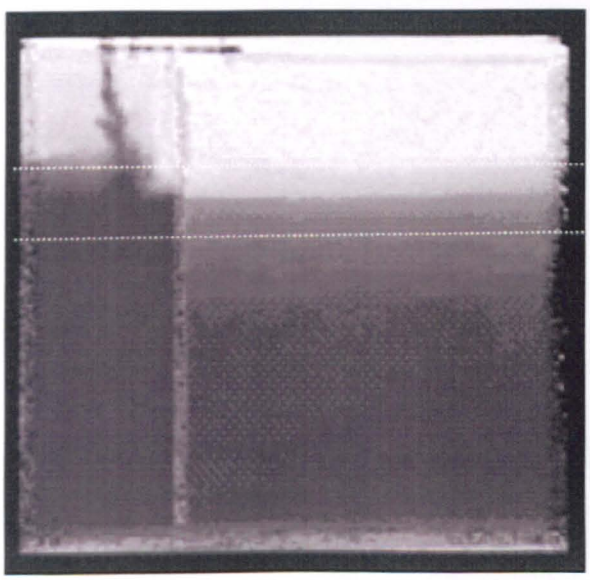

Figure 6.2.3: Shadowgraph images shows the region of sharp density gradient (between the white lines), and the zones at t=470 s. [Lin and Linden (2002)].

Figure 6.2.4: Temperature visualization showing the stratified layer, lower and upper zones of (Q_h & Q_c = 2 & 6 m^3/min).

Figures 6.2.5 and 6.2.6: show the stratified layer interface level height with the effective opening ratios A^*/H^2 and A^*L/H for different airflow rates. The figures show that with an increase in effective openings ratio, the stratification interface level height

remains constant. Good agreement has been reported between the present results, using air modeling technique, and the predictable and experimental data using the salt-bath technique (Linden et. al., 1990).

According to the stratification scheme shown in Figures 6.2.5 and 6.2.6, poor quantitative agreement is reported at high hot airflow rate of (3.0 m^3/min). The poor agreement is due to conditions and assumptions of Linden work, where the airflow rate of natural ventilation is comparatively low compared with 3.0 m^3 /min hot airflow rate.

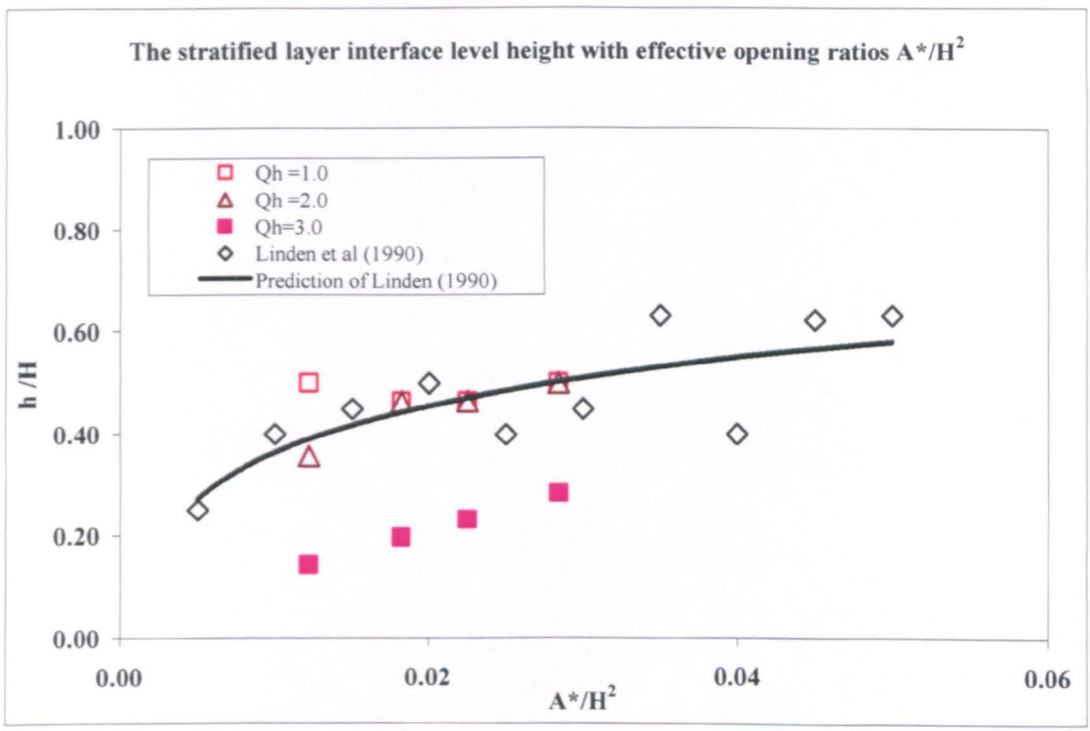

Fig 6.2.5: The stratified layer interface level height h/H with the effective opening ratio A^*/H^2 for various values of hot airflow rate $Q_h = 1.0, 2.0$ and $3.0\ m^3/min$ compare with the results of Linden (1998). The line represents the prediction of Linden (1998).

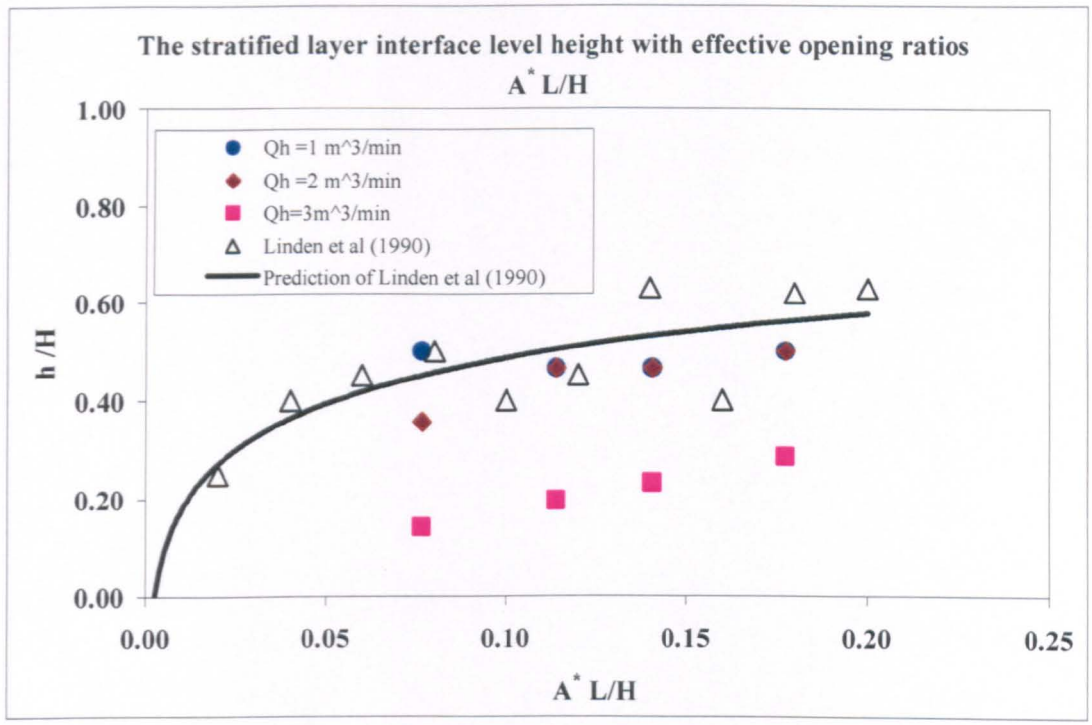

Fig 6.2.6: The stratified layer interface level height h/H with the effective opening per unit length A*L/H for various values of hot airflow rate $Q_h = 1.0, 2.0$ and $3.0\,m^3/min$ compare with the results of Linden (1998). The line represents the prediction of Linden (1998).

6.3 Discussion on Findings

6.3.1 Effect of Space/ Time Variations

As discussed in Chapter 3, measurements were taken at several locations inside the environmental chamber. The scale of these experiments was in both space and time variations. It was designed to address the consequences of variations in time and space of flow conditions that affect stratified flow characteristics.

As discussed in Chapter 4, in the presence of stratification, the parameters characterising the stratified layer deformation are the stratified layer interface level height (h), stratified layer top height (h′), stratified layer thickness (δ), the degree of stratification DS and the temperature gradient inside the stratified layer $dT/d\delta$. The relatively uniform distribution of flow along and across the direction of flow is shown in Figures 6.3.1 and 6.3.2. Figure 6.3.1 and 6.3.2 show the stratified flow characteristics with relatively fixed heights, which support the suggestions mentioned earlier for the governing equations, where the flow is assumed to be uniform.

Despite the variations of temperature profiles in both along and across the direction of the flow, the results demonstrated three dimensional stratified flows with a stratified layer characteristics almost uniform in both along and across the direction of the flow.

Figure 6.3.1 shows the plot of flow characteristics h'/H, h/H and δ/H against the dimensionless length of x/H. The results shows that the temperature profile in the environmental chamber is precisely symmetrical in the x-direction and the flow characteristics are uniform with small variations in the stratified flow characteristics as presented earlier.

Figure 6.3.2 shows the plot of flow characteristics h'/H, h/H and δ/H against the dimensionless width of y/H. The results shows that the temperature profile in the environmental chamber is precisely symmetrical in the y-direction and the flow characteristics are uniform. As presented earlier (Chapter 4), the variations in the vertical values are insignificant at the entire locations. Whilst, at the walls, the temperature difference and momentum are comparatively high which decreases the degree of stratification due to disturbances of the walls.

Comparing the results shown in Figures 6.3.1 and 6.3.2 with that in Figures 4.5.13 and 4.2.3 gives a good agreement between results obtained by temperature sensors and that by smoke visualisation.

As a result, the vertical temperature profile variation in the environmental chamber is near symmetrical. Thus the flow characteristics are uniform, and the stratified flow is assumed two dimensional.

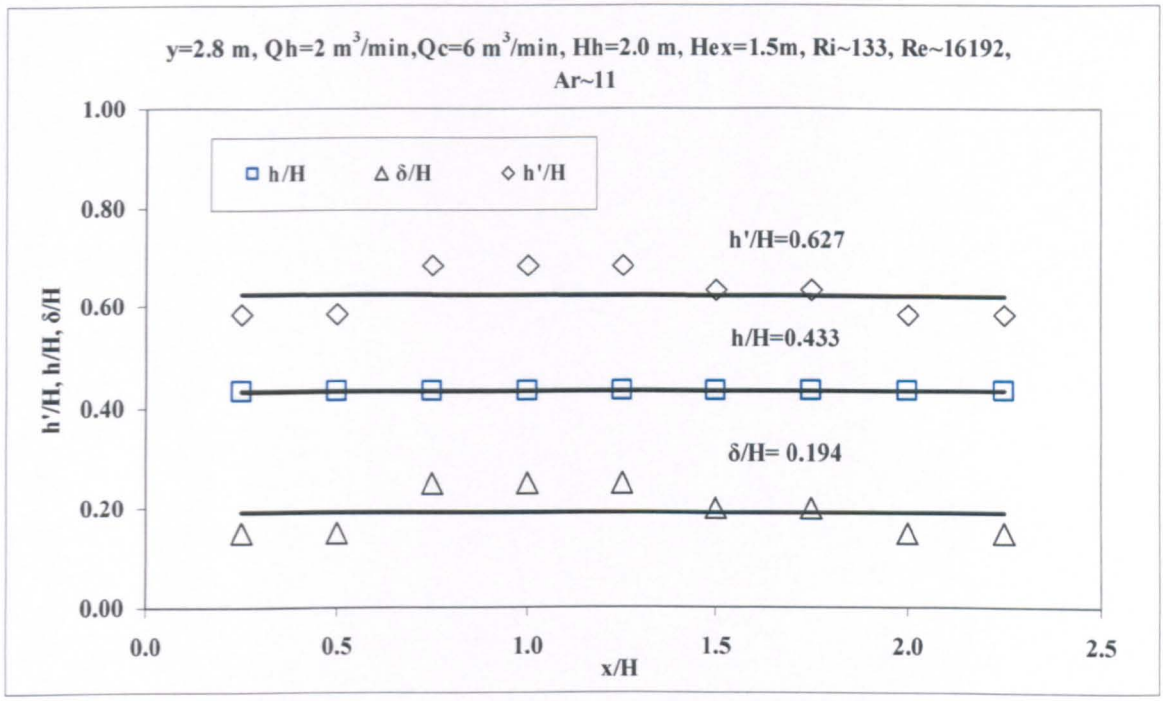

Figure 6.3.1: Stratified flow characteristics h'/H , h/H and δ/H against the dimensionless length of x/H for a number of locations along the direction of the flow, where ($Q_h = 2.0 m^3/min$) and ($Q_c = 6.0 m^3/min$).

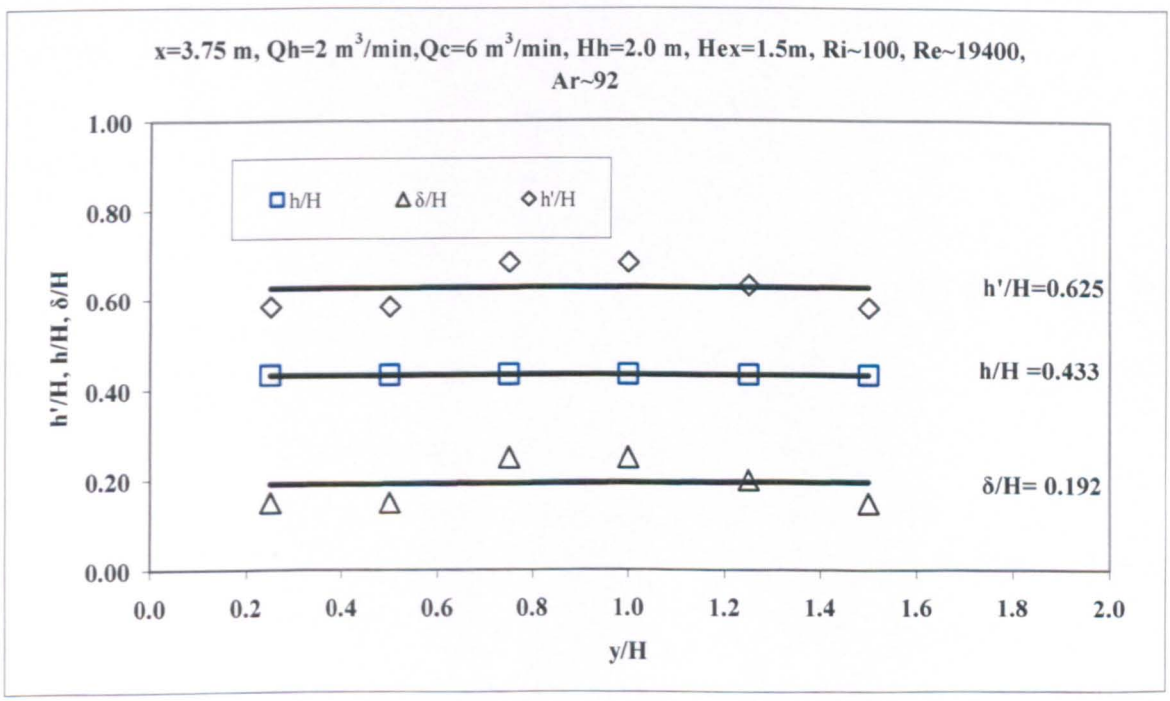

Figure 6.3.2: Stratified flow characteristics h'/H , h/H and δ/H against the dimensionless width of y/H for a number of locations across the direction of the flow, where ($Q_h = 2.0 m^3/min$) and ($Q_c = 6.0 m^3/min$).

In built environment, the flow is typically stratified. The degree of stratification DS depends on the geometry of the space and the flow conditions. When the degree of stratification reaches unity (DS=1), the flow becomes homogenous (pure mixed flow). When a stratified flow changes to mixed flow, its mechanical properties will change. The change from a stratified to a mixed flow takes place over a period of time called conversion period τ_C. The period of time is characterised by space and time variations. It is affected by the stratified flow characteristics, the technique used in mixing and the characteristic time τ.

Based on the continuity equation, the change in airflow rate across the chamber ΔQ is:

$$\Delta Q = \frac{V}{\tau} \tag{6.3.1}$$

where V is the volume of the environmental chamber and Q_{in} and Q_{out} are the input and output airflow rates, the estimate characteristic time is given by:

$$\tau = \frac{\Delta Q}{V} \tag{6.3.2}$$

Creation of stratified flow by increasing the hot airflow rate was shown in Figure. 4.3.1. In this case the characteristic time given by equation 6.3.2 is τ =126 minutes. By increasing the hot airflow rate by 1.0 m^3, the conversion period was (τ_C=10 minutes) [16:01 to 16:11], while the time needed to reach the steady state condition is τ_S=100 minutes.

The time at which mixed flow occurs should be the total of the conversion time and the steady state periodic time. In the same manner, it is the characteristic time needed to maintain the stratified case and go over the flow variations. Thus, the characteristic time and the time needed to reach the steady state condition are always equals.

$$\tau = \tau_C + \tau_S \tag{6.3.3}$$

Time classification	τ_C	τ_S	$\tau_C + \tau_S$	τ	$(\tau_C + \tau_S)/\tau$
Values in minutes	10	100	110	126	87%

6.3.2 Effect of Airflow Rates

As investigated by [Li and Delsante (2001)], [Chen and Li (2002)] and [Fitzgerald and Woods (2004)], the vertical position of the interface was related to the ratio of the upper and lower vent areas depending on the nature of the heat source. As discussed in Chapter 4, both hot and cold airflow rates were adjusted to maintain on the stratified layer and the stratified flow characteristics. Therefore, the control on a stratified layer interface level height, up or downward, is achieved by adjusting the airflow ratio $R = Q_c/Q_h$ as a key parameter of input conditions.

Figure 6.3.3 shows the change in the stratified layer interface level height h/H with respect to airflow rate ratio Q_c/Q_h .

It is identified that the stratification interface level height increases with the airflow ratio for several amounts of hot and cold airflow rates. From the results shown in Figure 6.3.3

$$\left.\begin{array}{l} \dfrac{h}{H} \propto Q_c \\ \dfrac{h}{H} \propto \dfrac{1}{Q_h} \end{array}\right\} \Rightarrow \quad \frac{h}{H} = O\left(\frac{Q_c}{Q_h}\right)$$

or,

$$\frac{h}{H} = A\left(\frac{Q_c}{Q_h}\right)^n + B \qquad (6.3.4)$$

with the boundary condition $\frac{h}{H}(0) = 0$, $B = 0$

Figure 6.3.3 shows the data points measured and the best fit line for the data, which was obtained with A=0.2 and n=0.5 and described by equations 6.3.5

$$\frac{h}{H} = 0.2\left(\frac{Q_c}{Q_h}\right)^{0.5} \qquad (6.3.5)$$

The region above the curve is thus dominated by the contaminant zone, and clean zone dominates the region beneath the correlation curve.

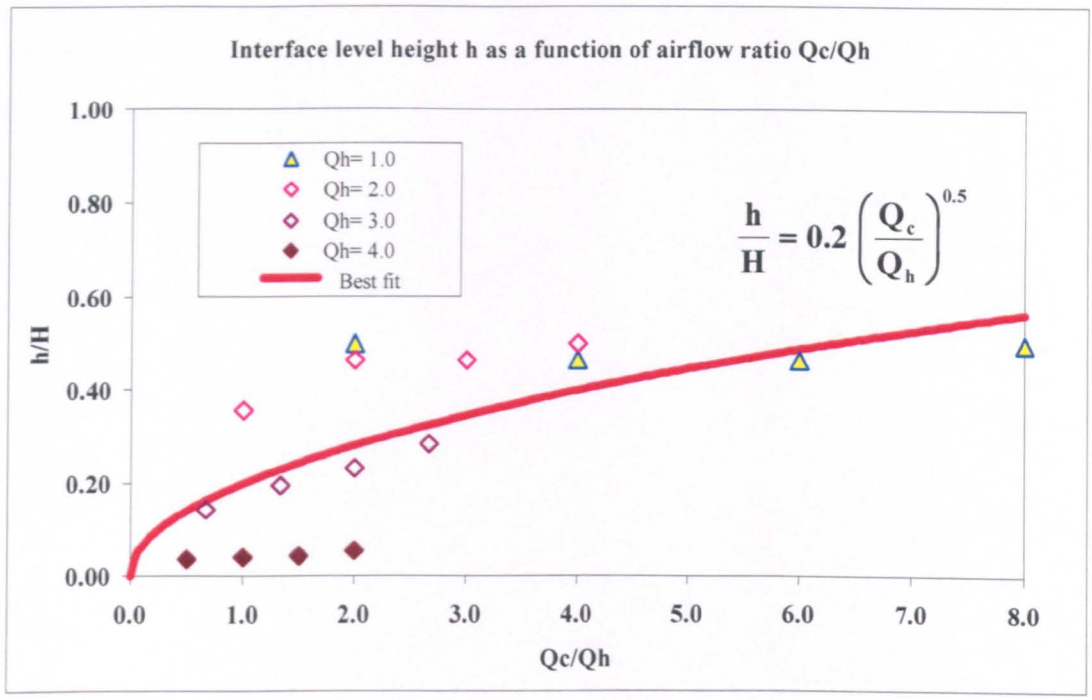

Figure 6.3.3: Variation of the stratified layer interface level height h/H with the ratio of input airflow rate Qc/Qh for various values of hot airflow rate $Q_h = 1.0, 2.0, 3.0$ and $4.0\ m^3/min$. The line represents the prediction of h/H as a function of Qc/Qh, (equation 6.3.5).

As a balance indicator, the stratified layer interface level height h revealed the ratio of buoyancy to momentum forces. As a function of overall airflow out Q_{out}, Figure 6.3.4 shows no specific relation between h and Q_{out}. Observation of Figure 6.3.3 and 6.3.4 once again shows that the stratified layer interface level height h is related to the ratio of airflow rate Q_c/Q_h rather than the overall airflow rate $Q_{out} = Q_h + Q_c$.

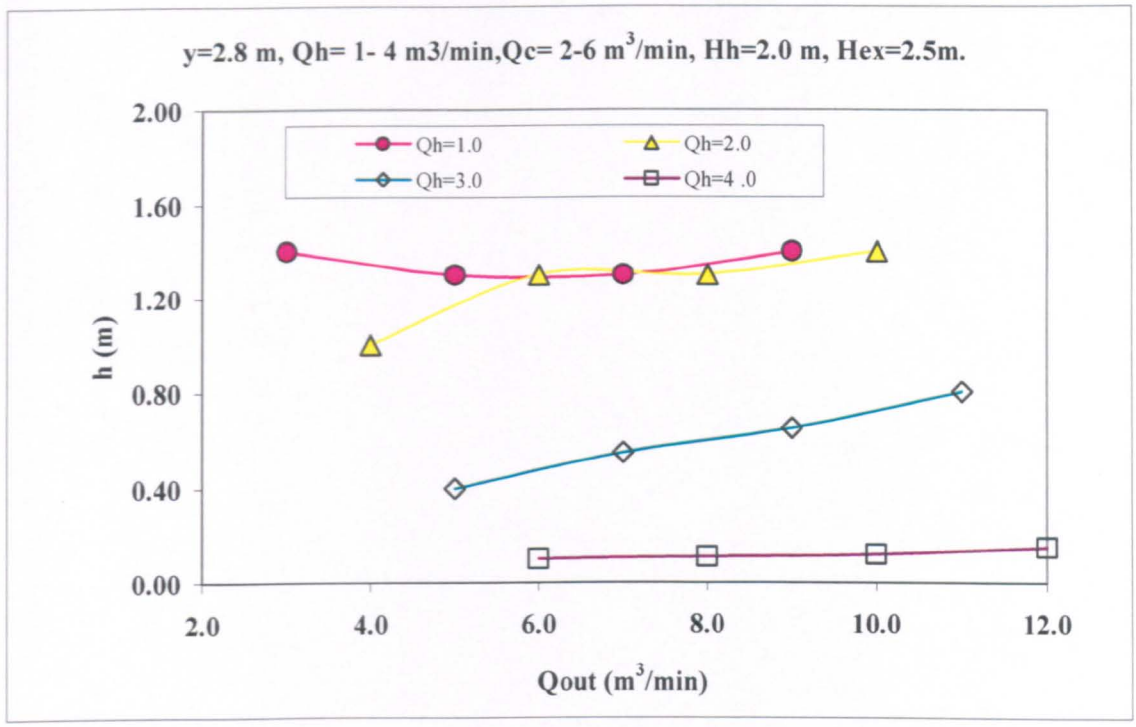

Figure 6.3.4: Variation of the stratified layer interface level height h/H with the overall output airflow rate for various values of hot airflow rate Q_h = 1.0, 2.0, 3.0 and 4.0 m^3 / min .

Figure 6.3.5 shows the change in the stratified layer thickness δ with respect to airflow rate ratio Q_c/Q_h . As shown in Figure 6.3.5, the stratified layer thickness δ is decreased by increasing Q_c/Q_h . The results are in agreement with [Linden (1979)], which identified the needs for input flow rates to remove the mixed fluid from the stratified region in order to keep its thickness constant.

$$\frac{\delta}{H} = f\left(\frac{Q_c}{Q_h}\right)$$

with the boundary condition $\frac{\delta}{H}(\infty) = 0$,

$\Rightarrow$

$$\frac{\delta}{H} = A\, e^{b\left(\frac{Q_c}{Q_h}\right)} \qquad (6.3.6)$$

where A and b are constants obtained from experimental results using the best fit of the data points measured. Since A=0.2, and b=-0.0627, the best fit shown in Figure 6.3.5 is described by equations 6.3.7

$$\frac{\delta}{H} = 0.2\, e^{-0.0627\left(\frac{Q_c}{Q_h}\right)} \qquad (6.3.7)$$

Using equations 6.3.5 and 6.3.7, it possible to obtain an estimate for the flow characteristics δ and h of stratified flow for various airflow rate Q_h and Q_c.

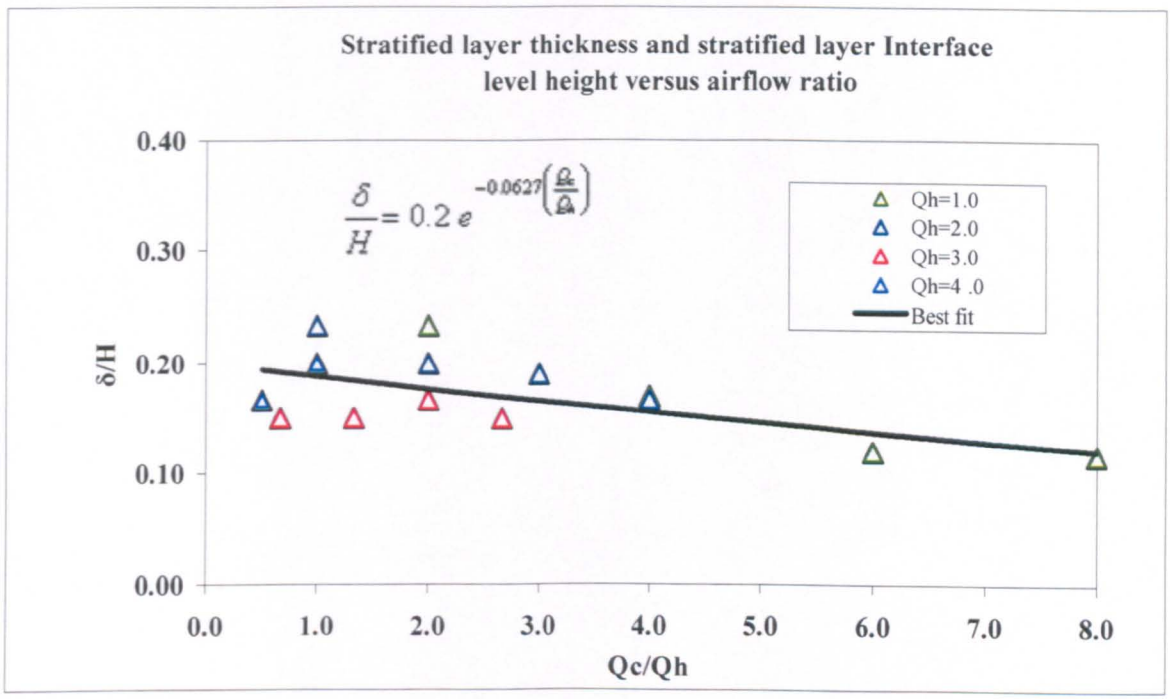

Figure 6.3.5: Variations of the stratified flow thickness δ with the input airflow rate ratio Q_c/Q_h for various values of hot airflow rate Q_h = 1.0, 2.0, 3.0 and 4.0 m^3/min. The line represents the prediction of (6.3.7).

6.3.3 Effect of Buoyancy to Momentum Fluxes

Let us consider the Richardson number to characterise the stratified flow since it is the ratio of the buoyancy to the momentum forces, which are the main forces in completion to determine the stratified layer thickness δ. Figure 6.3.6 shows the change in the stratified layer thickness δ with the stratified flow Richardson number Ri. The value of Ri was varied between 3.8 to 200, which very much spans over a wide range of operating conditions. For high values of Ri = 200, the stratified layer thickness is shown

to be with significant effect. As the value Ri decreases to 3.8, δ is decreased. Thinner stratified layer thickness is expected to form upon further decrease in Ri value. This is referred to the decrease in the ratio of the Ri physical definition (buoyancy to momentum forces), which causes a steep temperature gradients in the vertical direction of the thermocouple stand.

Figure 6.3.6 shows the correspondence between stratified layer thickness δ/H with Ri number. Using the best fit line, it is possible to obtain an estimate for the stratified layer thickness δ for flow Ri number. This line is described by the form:

$$\frac{\delta}{H} = A\, Ri^{b} \qquad (6.3.8)$$

where A and b are constants obtained from experimental results. Since A=0.1217, b=0.0837, the fitted curve shown in Figures 6.3.6 is described by equation 6.3.9.

$$\frac{\delta}{H} = 0.1217\, Ri^{0.0837} \qquad (6.3.8)$$

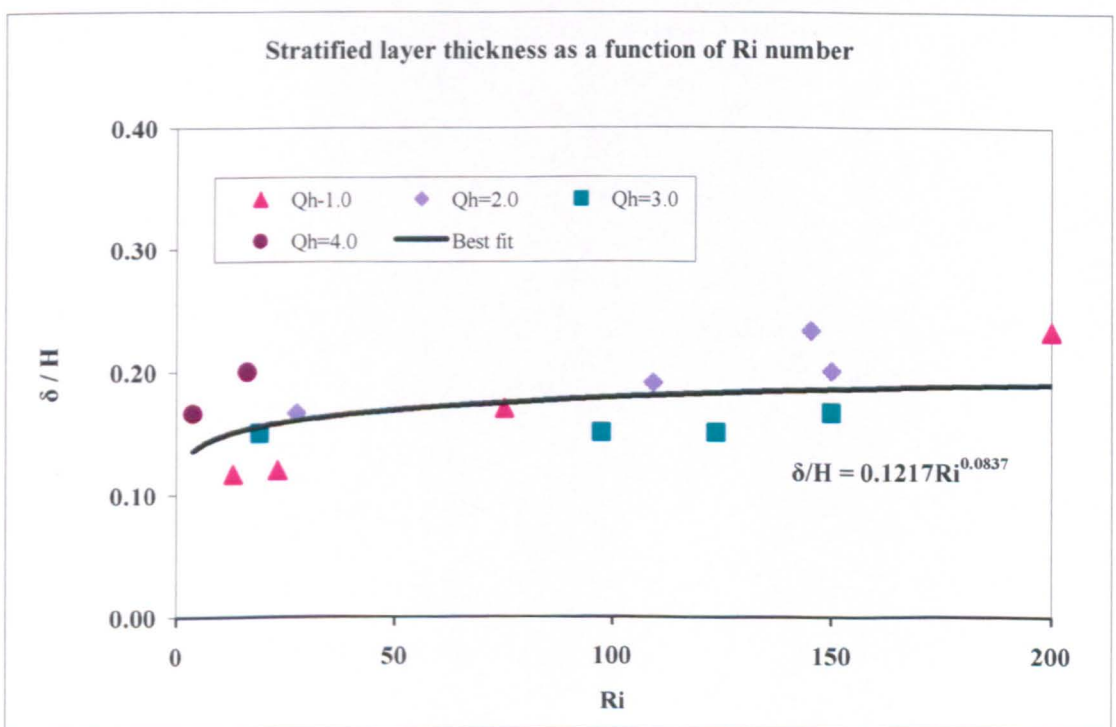

Figure 6.3.6: Variations of the stratified flow layer thickness δ/H with the stratified flow Ri number for various values of hot airflow rate Q_h = 1.0, 2.0, 3.0 and 4.0 m^3 / min . The line represents the prediction of (6.3.8).

The variation of stratified layer thickness with the Reynolds number is displayed in Figure 6.3.7. The Reynolds number was varied between 7000 and 30000. The results show significant variations in the flow characteristics due to the increase in momentum forces upon the increasing of Reynolds number. Thinner stratified layers are shown to form with the increase in Re values.

The fitted curve shown in Figure 6.3.7 is the correspondence between stratified layer thickness δ and flow Re number. It is described by equation (6.3.10). Using the best fit line, it is possible to obtain an estimate for the stratified layer thickness for flow Re number.

$$\frac{\delta}{H} = A\,Re^{b} \qquad (6.3.10)$$

where A and b are constants obtained from experimental results. The fitted curve shown in Figure 6.3.7 is described by equations 6.3.11

$$\frac{\delta}{H} = 3.6757\,Re^{-0..3181} \qquad (6.3.11)$$

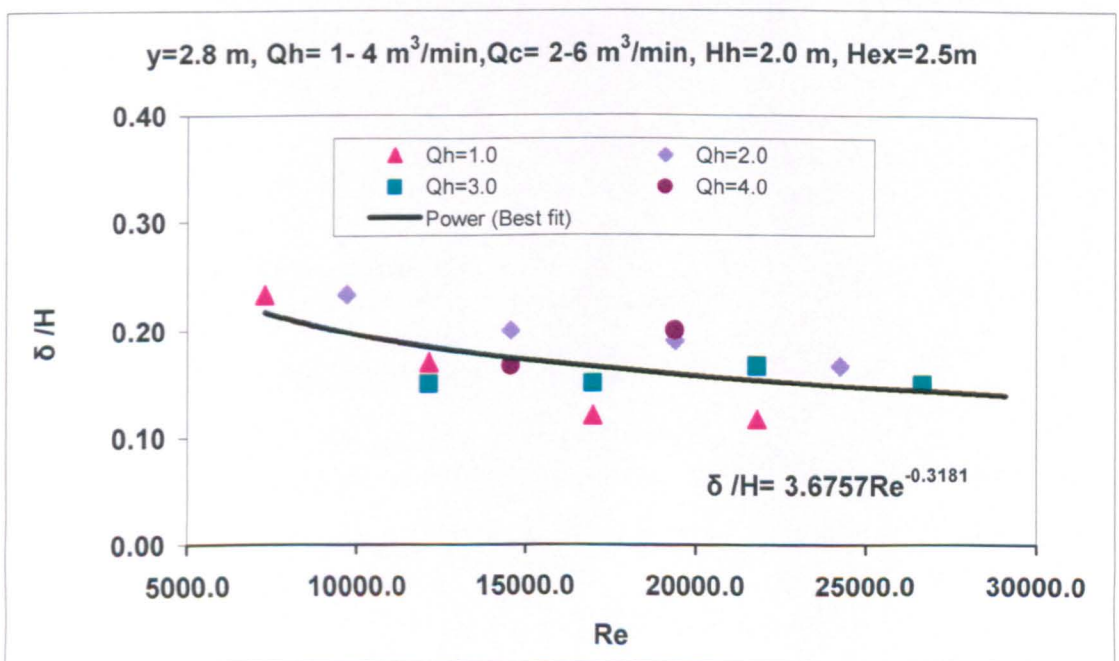

Figure 6.3.7: Variations of the stratified flow layer thickness δ/H with Re number for various values of hot airflow rate $Q_h = 1.0, 2.0, 3.0$ and $4.0\ m^3/min$. The line represents the prediction of (6.3.11).

The study has involved a number of concepts introducing additional governing parameters. The Richardson number is a measure of stratification but with the stratified layer thickness δ and other characteristics, its variation is slight (Figure 6.3.6). An overall Richardson number Ri can be considered to relate buoyancy effects to momentum effects but can't be used to measure the buoyancy effects. The Reynolds number is a measure of stratification (Figure 6.3.6). It can be considered to relate momentum effects to viscous effects and can be used to measure the momentum effects.

Let us consider the ratio $R = \frac{Ri}{Re}$ to characterise the stratified layer thickness δ since it is also the ratio of the buoyancy to the momentum forces. Figure 6.3.9 shows the change in the stratified layer thickness δ with the ratio R. The value of R was varied from 0.0 to 0.027. The low values of R indicate the low values of flow characteristics where the buoyancy forces become diluted, while the momentum forces become concentrated. With more decrease in the ratio R, the flow becomes further weakened. When R~ 0.0, the stratified layer is diminished and the flow changed to a pure mixed flow. As R increases, the stratified layer thickness becomes thicker and stronger.

Figure 6.3.8 show the values of the stratified layer thickness δ at different ratios of $R = Ri/Re$ within the ranges of 0.0-0.027. The relation between δ and R is approximately correlated by:

$$\frac{\delta}{H} = 0.2874\left(\frac{Ri}{Re}\right)^{0.092} \qquad (6.3.12)$$

The variation in the profile indicates that the stratified layer thickness is increased by increasing the ratio R and δ becomes thicker.

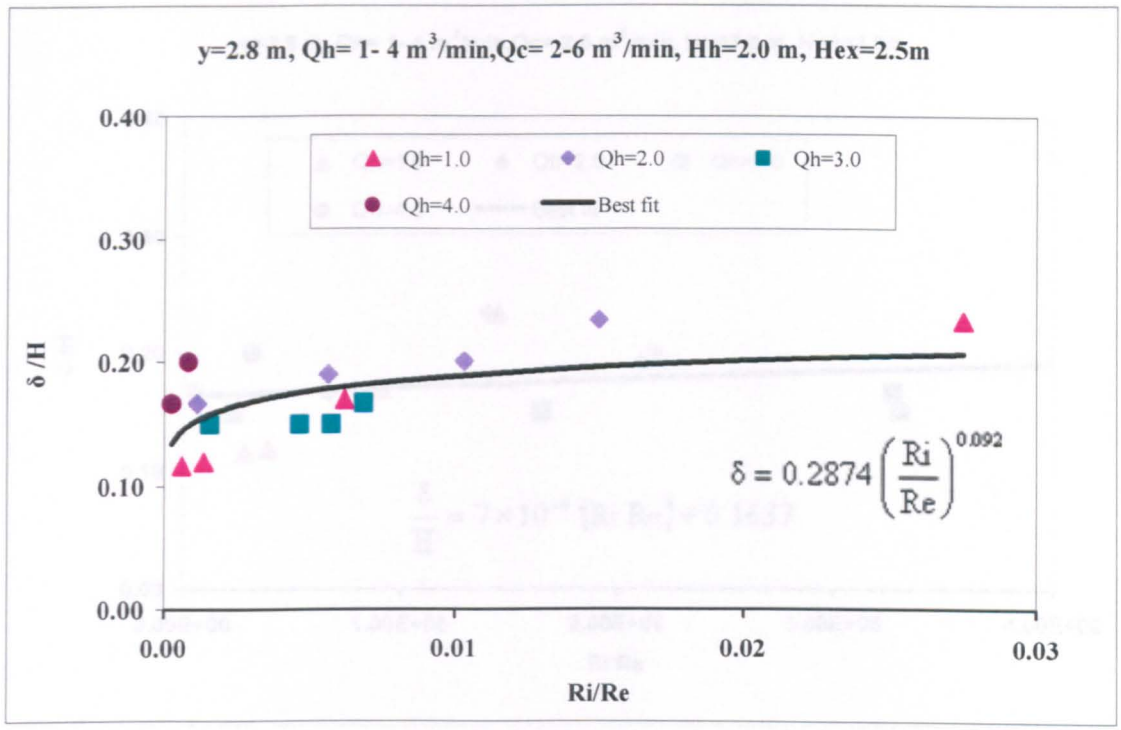

Figure 6.3.8: The variation of stratified layer thickness with the mmomentum-buoyancy ratio R=Ri/Re for various values of hot airflow rate Q_h = 1.0, 2.0, 3.0 and 4.0 m^3/min. The line represents the prediction of equation 6.3.13.

To evaluate the main effective force in stratification mechanism, the relation between stratification and buoyancy must be define and evaluated to investigate the importance of buoyancy. Let us consider a non-dimensional parameter $AH = Ri\,Re$ .It measures the ratio of buoyancy forces to viscous forces. The parameter AH can be evaluated for examining the variations of a stratified flow characteristics under the effect of buoyancy forces.

Figure 6.3.8 shows the change in the stratified layer thickness δ with the parameter AH. The value of AH was varied from 0.0 to $4\times10^{+6}$. The relation between δ and AH, shown in Figure 6.3.9, is approximately correlated by:

$$\frac{\delta}{H} = 7\times10^{-9}\,(Ri\,Re) + 0.1637 \qquad (6.3.13)$$

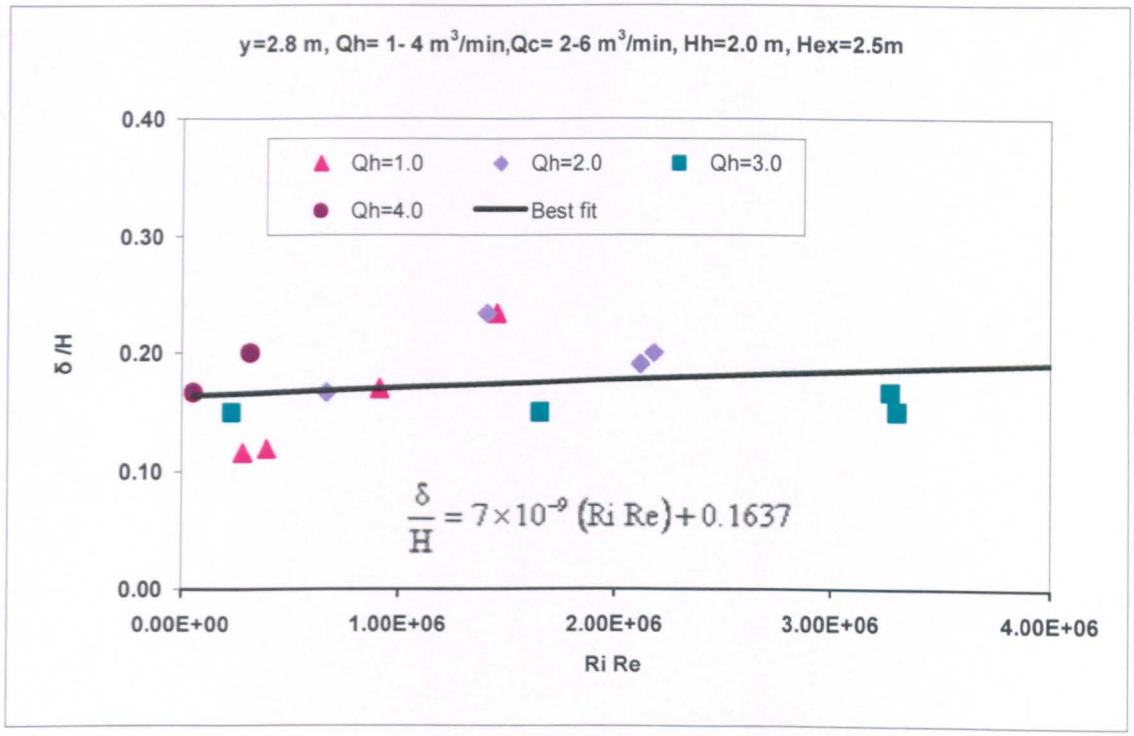

Figure 6.3.9: The variation of stratified layer thickness with the buoyancy-viscous ratio AH=Ri Re for various values of hot airflow rate $Q_h = 1.0, 2.0, 3.0$ and $4.0\,m^3/min$. The line represents the prediction of equation 6.3.12.

From equation 6.3.13 and Figure 6.3.9, $\frac{\delta}{H} \cong 0.1637$ and the variations of the stratified layer thickness δ with the parameter AH is small whilst the variations of δ with the Re is higher (i.e Figure 6.3.7). Thus:

"The effect of Re number on the stratified layer thickness δ is greater than the effect of AH"

$$\text{Effect of}\,[\mathrm{Re}] \succ \text{Effect of}\,[\mathrm{AH}]$$

$$\Downarrow$$

$$\text{Effect of}\left[\frac{\mathrm{M}}{\mathrm{V}}\right] \succ \text{Effect of}\left[\frac{\mathrm{B}}{\mathrm{V}}\right]$$

$$\Downarrow$$

$$\text{Effect of}\,[\mathrm{M}] \succ \text{Effect of}\,[\mathrm{B}]$$

⇓

"The effect of Momentum forces on the stratified layer thickness is greater than the effect of Buoyancy"

In which, B is the Buoyancy forces, M is the momentum forces and V is the Viscous forces.

6.3.4 Effect of Exhaust Height

Several tests were performed to investigate how the opening height affects the stratified flow characteristics in the stratified flow. These tests were conducted by changing both input and exhaust height while keeping both the cold and hot airflow constant. As presented in Chapter 4, the higher the vertical input location, the higher the interface level height. The exhaust vertical location does not alter the position of the interface level height. It could be in the locations above or below the interface level height.

It has been found that the interface level height h is directly proportional to the exhaust height i.e. the height where flow becomes stratified. Therefore by modifying the exhaust position the removal of contaminated air from a multipurpose industrial space can be selectively achieved as proposed by [Calay et al (2000)].

Figure 6.3.10 shows vertical temperature profiles for exhaust aperture locations h_{ext} varied from 1.0 to 2.5m, for a flow of Ri= 40-200 and Re~2500 -32600. By increasing h_{ext} the flow becomes more stratified, the interface level height is ascending and the average temperature inside the chamber is decreasing down, which improve the effectiveness of ventilation, heat removing and energy saving.

Figure 6.3.11 shows that the location of the interface level height h is directly changed with the change in the exhaust height. It increases by increasing the exhaust height. This pattern agrees with the findings of [Calay et al (2000)]. However, the stratified layer thickness is decreased by increasing the exhaust height. This is not so for all cases as observed from Figure 6.3.11, where the sharper interface δ is at $h_{ext} = H/2$, where the

degree of stratification is higher as shown in Figure 6.3.12. In this Figure, the stratified layer temperature gradient $\Delta T/\delta$ shows a higher value of $(12\ ^{\circ}C/m)$.

The exhaust location does not alter the position of the interface level height when the momentum forces dominate the flow, the interface level height was below the exhaust position when the momentum forces at the floor are high compared to the global buoyancy forces (Qc/Qh is low). When momentum is increased at the floor level, this also changes the buoyancy forces; however, the combined effect of inertia and buoyancy forces yields into the development of a mixed zone close to the floor and the stratified layer is pushed upwards. The interface forms between 0.25H-0.3H, which is below exhaust location at 0.5H.

The exhaust location does influence the level of the interface but the interface can form above or below the exhaust height depending upon the relative magnitude of the momentum and buoyancy forces. In order to improve the effectiveness of ventilation and for energy efficiency, the optimum location for exhaust is at the interface or where the temperature reaches its maximum above the occupied zone. When the exhaust position is above the interface level and within the stably stratified zone, the contaminants are extracted efficiently, and the age of air at the breathing zone is higher

However, when the exhaust location is not at the stratified zone and being either below or above this zone, the removal efficiency becomes low. For example when the extract point is below the stratified zone, excess fresh air from the occupied zone can be removed. When the exhaust location is situated in the upper zone the concentration of contaminants in the lower zone may get too high. Therefore the positioning of exhaust must be designed as a significant part of the building HVAC system.

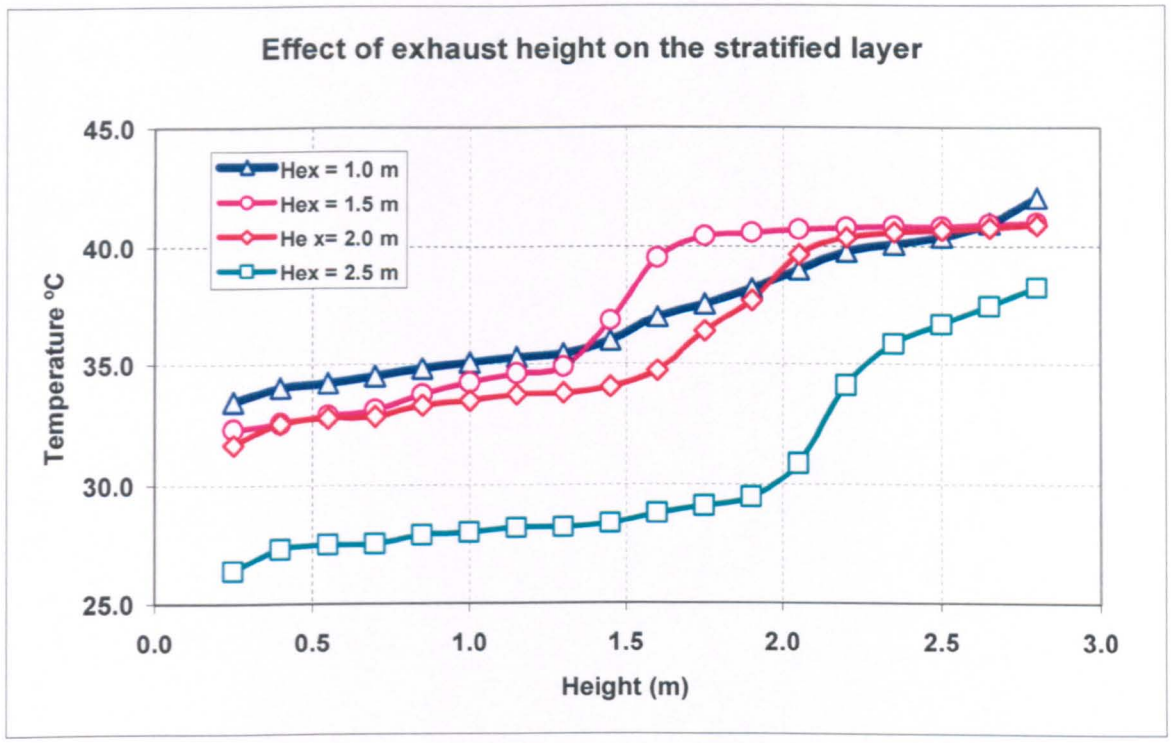

Figure 6.3.10: The stratified layer temperature profile along the vertical axis for different exhaust heights (1.0, 1.5, 2.0, 2.5 m) at hot airflow rate $2.0\ m^3/min$ and cold airflow rate $4.0\ m^3/min$.

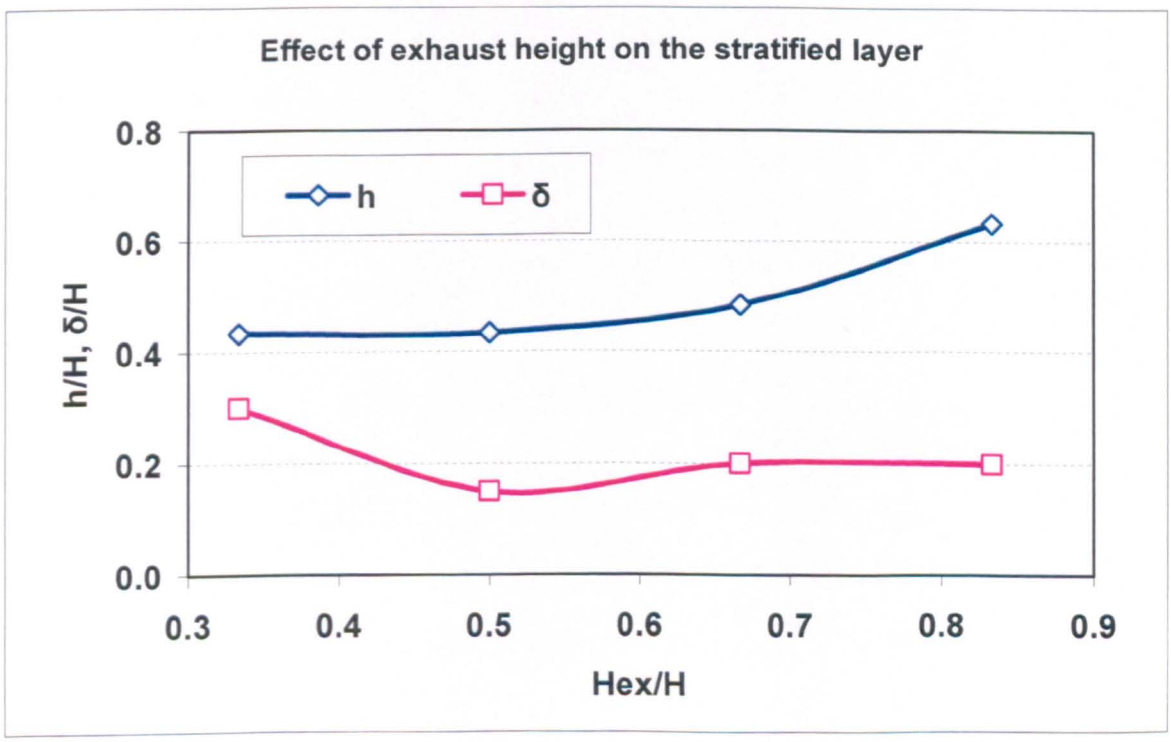

Figure 6.3.11: The stratified flow characteristics h/H and δ/H as a dimensionless form with the exhaust height Hex/H at hot airflow rate $2.0\ m^3/min$ and cold airflow rate $4.0\ m^3/min$.

The sensitivity of both temperature gradient $\Delta T/dz$ and degree of stratification DS patterns to varying the exhaust height Hex has been investigated. Figure 6.3.12 shows that the temperature gradient and the degree of stratification are sensitive to the exhaust vertical location. As discussed in Chapter 4, the higher degree of stratification is at intermediate values of input airflow rates. The height of the exhaust vertical location and the higher degree of stratification shown in Figure 6.3.12 are reflected by the location and amplitude of the highest point on the (DS – $H_{ex)}$ plot, respectively. In this Figure, the stratified layer temperature gradient $\Delta T/\delta$ shows a higher value of $(12\ ^{\circ}C/m)$, while the degree of stratification DS shows a higher value of (4.26). The results conclude that the degree of stratification DS exhibits a sharp decrease at a critical Hex = 0.5H. For flows greater than or less than this critical height DS is decreased, while the stratification gradually disappeared.

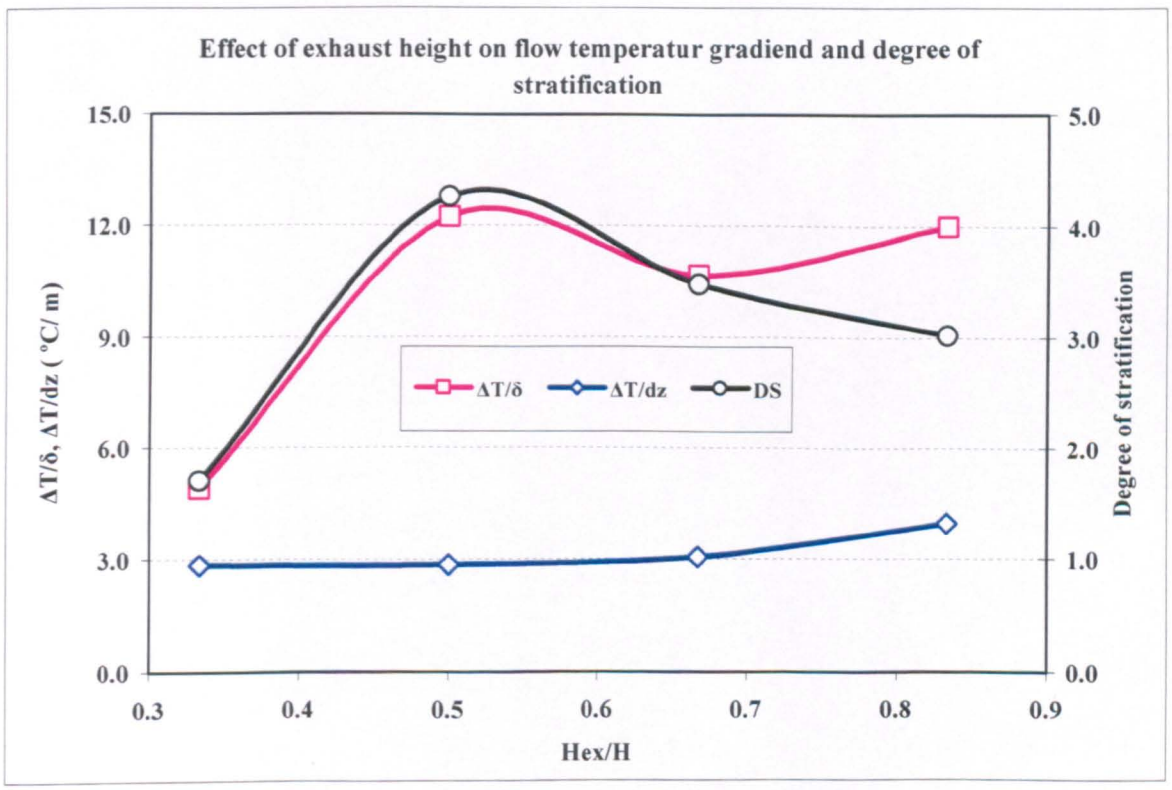

Figure 6.3.12: The stratified flow temperature gradients defined by $\Delta T/\Delta\delta$ and $\Delta T/dz$ and the degree of stratification DS with the exhaust height Hex at hot airflow rate $2.0\ m^3/min$ and cold airflow rate $4.0\ m^3/min$.

6.3.5 Determination of Critical Momentum

Both buoyancy and momentum can influence the room air movement [Awbi (1998)]. While the flow of high buoyancy was introduced in the chamber, the flow of high momentum was supplied downward from the ceiling jet. As discussed in Chapter 5, the magnitude of momentum needed is depending on the degree of stratification, stratified layer interface level height and the stratification conditions. It can be seen that the jet momentum has significant influence on the mixing of the stratified flow characteristics. The results indicated that once the momentum was initiated a mixed flow grew in the occupied zone above the floor. The height of this zone is dependent on the temperature and momentum of the ceiling jet as well as the stratified flow characteristics h, δ ad DS.

The variations of jet speed V_j and jet momentum M_j with interface level height for both hot and cold jet flow are shown in figures 6.3.13 and 6.3.14. The critical jet momentum required to break down the stratified layer is proportional to the stratified layer interface level height. The stratified layer interface level height is translated to reach the ceiling since the injected air is supplied directly into the occupied zone. However for all experimental airflow rates, the critical jet momentum required to breakdown the stratified layer is increased with the growth of the stratified layer height for both cold and warm jet. When a high air flow rate is injected (Vj =max), figure 6.3.13 and 6.3.14 shows that the stratified layer is broken and completely destroyed by the strong momentum despite the stratified flow characteristics.

As discussed earlier, figure 6.3.13 shows that stratified layer interface level h is a very important factor since it plays an important role in breaking and destroying the stratified layer.

In the case of warm jet, the high jet momentum directed to floor level raise the interface level height upward and combined with the cold air in the occupied zone. This increases the temperature in the occupied zone and produced high temperature near the ceiling in the upper zone whilst in the case of low jet momentum, the injected air supplied close to the ceiling did not have sufficient momentum to go through the stratified layer and achieve acceptable mixing. Thus it is stratified in the upper zone producing high temperature layer near the ceiling.

In order to explain the variation of momentum jet with h, the stratified layer potential energy due to gravity is equals to jet kinetic energy.

$$(\Delta\rho)g\,h(A\,\delta)=\frac{1}{2}\rho_j(C_d\,A_j\,V_j)V_j^2 \qquad (6.3.14)$$

$$\Rightarrow$$

$$V_j = C\,h^{\frac{1}{3}} \qquad (6.3.15)$$

and

$$M_j = Q_j V_j = A_j C^2 h^{\frac{2}{3}} \qquad (6.3.16)$$

Where A is the chamber area, A_j is the jet area and C_d is the jet discharge coefficient, here C is a coefficient of flow density, spatial geometry and given by equations (6.3.17).

$$C=\left[\frac{2(\Delta\rho)g\,A\,\delta}{\rho_j C_d A_j}\right]^{\frac{1}{3}} \qquad (6.3.17)$$

Where $\Delta\rho$ is the density difference across the stratified layer, δ is the stratified layer thickness, C_d is the discharge coefficient, ρ_j is the density of the injected air and A_j is the jet cross sectional area.

Hence $T_{Cj} \approx 15\,^{\circ}C$, $T_{wj} \approx 45\,^{\circ}C$, $A_j = 9.5\times10^{-3}\,m^2$, $A=126m^2$, and assuming the temperature difference across an average of $\bar{\delta}=1.5m$ is $\Delta T|_{across\,\delta} \approx 7\,^{\circ}C$ and a discharge coefficient $C_d = 3/4$, the value of the coefficient C given by equation 6.3.17 is $C_{Cj} \approx 12.5$ for cold jet and $C_{wj} \approx 12.82$ for warm jet.

Figures 6.3.13 and 6.3.14 show the relationship between h and both jet velocity V_j and jet momentum M_j, as predicted by equations 6.3.15 to 6.3.17 for both types of jet flow.

.

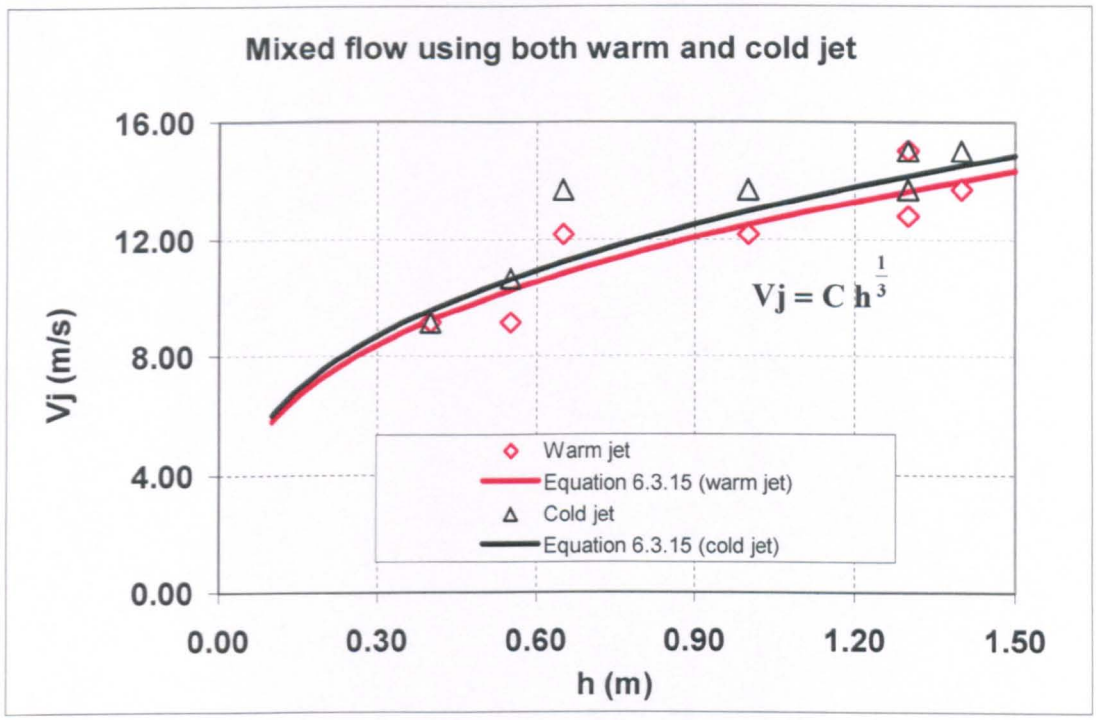

Figure 6.3.13: Critical jet velocity needed to break down the stratified layer with the interface level height for both warm and cold jet flow. The line represents the prediction of (6.3.15).

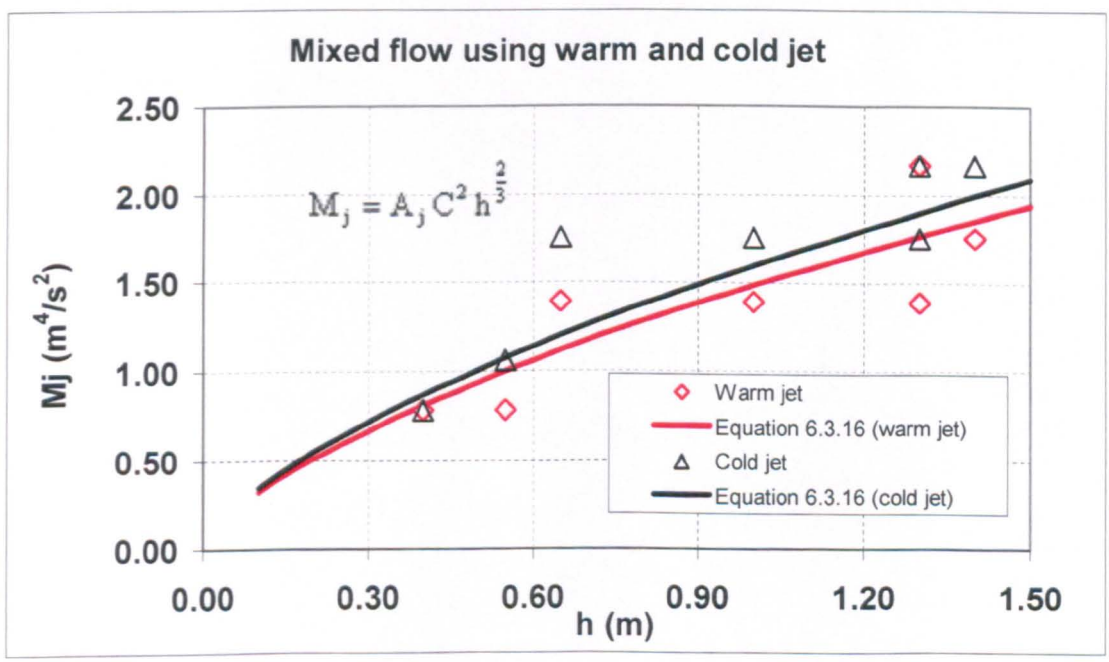

Figure 6.3.14: Critical jet momentum needed to break down the stratified layer with the interface level height for both warm and cold jet flow. The line represents the prediction of (6.3.16).

For different values of Re numbers used in the experiments, and by using the momentum jet, figure 6.3.15 shows the critical momentum jet (The minimum initial jet momentum required to breakdown the stratified layer) needed to break down the stratified layer as a function of Re number. The results show that the momentum flux decreases with Re number. A direct comparison between cold and warm jet flow shows a lag in the interface level height owing to the temperature difference, whereas the results indicated higher values of interface level heights for warm jet.

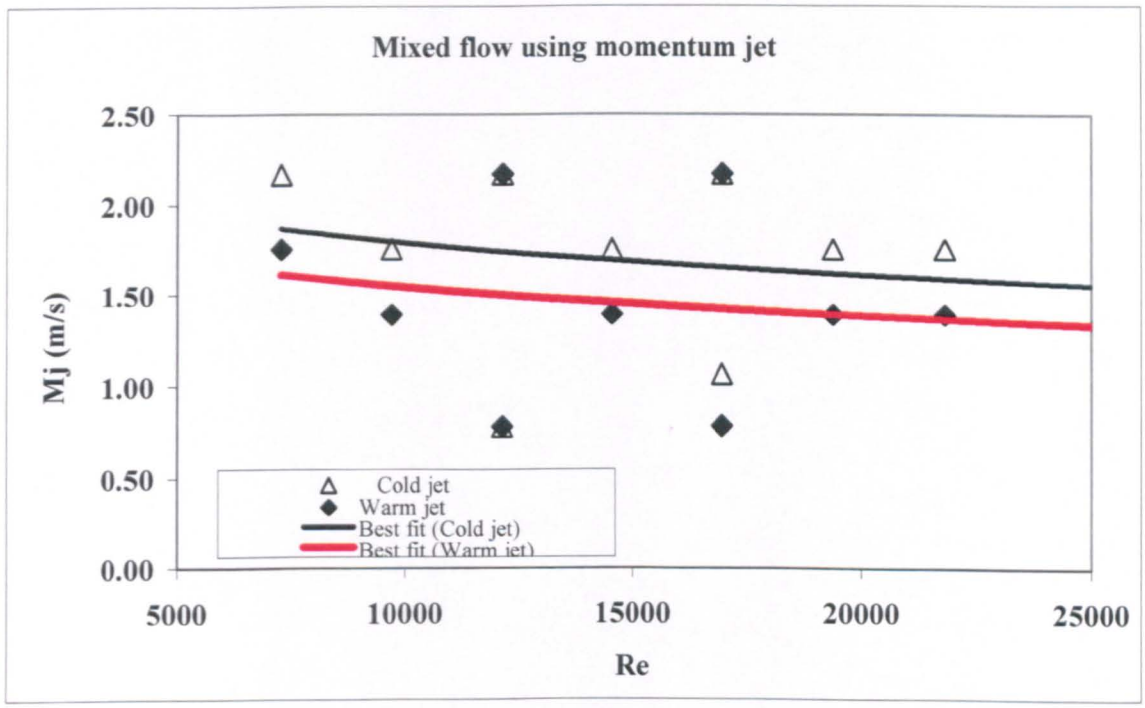

Figure 6.3.15: Critical jet momentum needed to break down the stratified layer with Re number for both warm and cold jet flow.

The experiments have shown that a stratified flow persists in the chamber for a range of initial Re numbers from 7000 to about 22000. The initial stages of typical stratified flows were shown in (Chapter 5). The incoming jet airflow was injected on downwards for a certain distance into the stratified layer. On increasing the initial jet momentum above the critical value, there was a flow transition from a stratified flow to a mixed. During this transitional period, which occurred in the ranges $0.0 \prec M_j \prec (M_j)_{critical}$ the stratified layer interface level height h was observed to be translated upward to reach the ceiling. The translation of h from downwards to upwards is affected by the initial characteristics of stratified flow.

For initial jet momentum greater than the critical values, the jet momentum caused a gradually diluted stratified layer leading to an overturning of the layers in the chamber, and a mixing mode of flow was observed. This mode of mixing is dependent on the relative strength of the initial momentum and the initial flow characteristics. From the results in Figures 6.3.13 to 6.3.15, a significant difference between warm and cold jet flow is observed. For the same flow conditions, the results show the effectiveness of using warm jet to mix the flow is higher than that of cold jet, where the forces of momentum and buoyancy are opposed.

The velocity of the injected air inside the stratified layer is less than that induced inside the lower zone due to the high temperature difference so high reduced gravity. Thus, the velocity of the injected air decreases quickly when it enters the stratified layer. The results show that the critical jet momentum increases with the Buoyancy/momentum ratio (Ri/Re). Figure 6.3.16 shows the critical jet momentum required to breakdown the stratified layer as a function of Ri/Re numbers.

The power efficiency of breaking the stratified layer in this case is decreased by increasing the buoyancy forces of the stratified layer defined by Ri, whilst it is increased by increasing the momentum energy of injected air. We can therefore say that the stratified layer is easily broken and destroyed by high jet momentum.

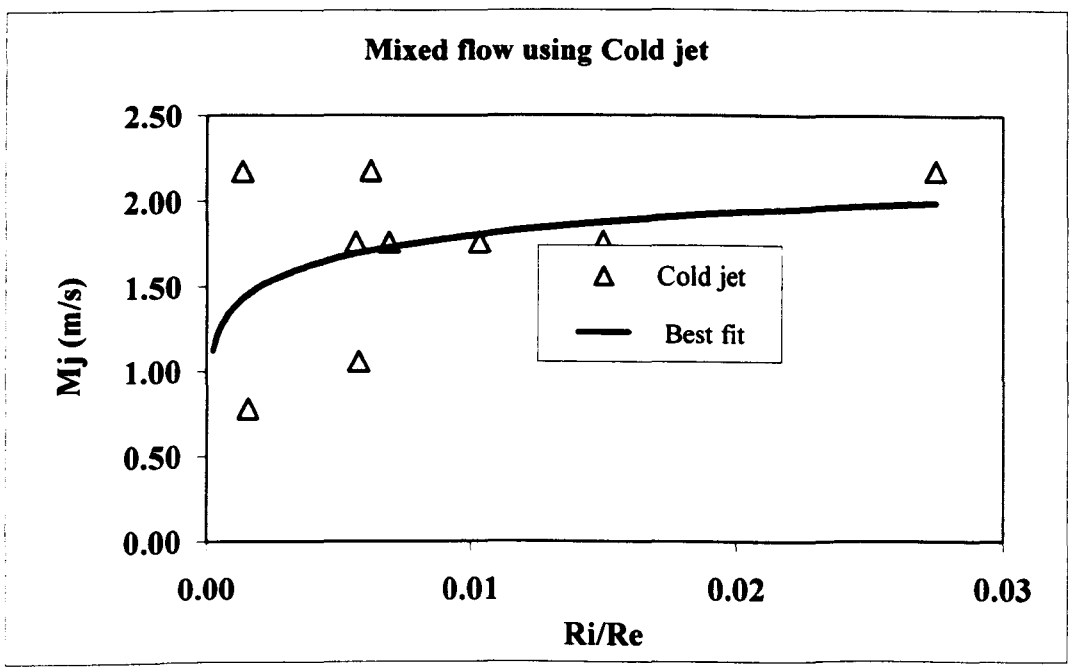

Figure 6.3.16: Critical jet momentum needed to break down the stratified layer with buoyancy to momentum ratio Ri/Re for both warm and cold jet flow.

6.3.6 Mixing the Stratified Flow using Inversion Technique

In reverse cycle air conditioners, "to protect the evaporator from freeze damage, it must occasionally run in a defrost cycle where the flow of refrigerant is reversed, so that heat from the interior of the house will melt accumulated ice deposits in the outdoor coil. This results in uncomfortably cold air being circulated throughout the home during the cycle". [PATH (2005)]

From the above explanation, the definition of stratification phenomenon presented in Chapter 1, and the introduction of [Dagestad (1991)] that the flow has stable stratification when $\Delta\rho/\Delta y \prec 0$, while it has unstable stratification when $\Delta\rho/\Delta y \succ 0$, the inversion technique was revealed and used in the present work. In this technique the stratified flow was mixed by inverting the input airflow suppliers. In this case, the buoyant cold layer in the lower zone will loose its buoyancy forces while being heated with the hot airflow penetrated at lower levels in the environmental chamber. Also the stratified layer will loose its stability and break down due to the drag and tearing of cold air penetrated downward from higher levels. The compound effect of these two situations will circulate the air in the whole space and disturb the stability of the stratified layer to reach a fully mixed flow.

The analysis carried out to investigate the effect of inversion at input locations on the stratified flow characteristics were presented in Chapter 5. A fully mixed flow was reached despite the degree of stratification and the temperature difference when the cold airflow enters through the upper location, while the hot airflow enters through the lower ones. In other words, mixing will be introduced under the effect of inputs overturns (inversion of input locations) despite the presence of momentum and buoyancy sources.

Comparing with the mixing by jet momentum flow, the inversion technique shows several major differences:

In the mixing by momentum jet:

1. The stratified layer was translated to higher levels before broken down to reach fully mixed flow.
2. Mixing process was introduced by an additional air supply, and so additional airflow rates, and more energy consumption.

3. Improving pollutant removal efficiency inside the occupied zone occurred by increasing the stratified layer interface level height so the height of the occupied zone.
4. For these three purposes, mixing by momentum jet is preferable

Whereas in the mixing by inversion technique:

1. The stratified layer was broken down rather than translated to higher levels before reaching fully mixed flow.
2. The flow was mixed without any needs for new air supply or more airflow rates with more energy consumption.
3. Mixing the stratified flow and improving the pollutant removal efficiency inside the space was so better.
4. For these purposes, mixing by inversion technique is preferable.

Figure 6.3.20 shows the variation of temperature T and temperature gradient dT/dz along the vertical height z for two cases of stratified and mixed flow. For stratified case, stratification of air causes a vertical temperature gradient dT/dz reaches 4.4 °C/m along the vertical height of the chamber whilst it reaches a maximum value of 20°C/m in the stratified layer. The degree of stratification for this case is DS= 4.54, (very high degree of stratification).

For mixed flow, Figure 6.3.20 shows an average vertical temperature gradient $dT/dz = dT/d\delta = 0.4\ ^{\circ}C/m$. For this case, the degree of stratification is DS=1.0, (homogenous fully mixed flow). The drop in the temperature gradient is estimated:

$$\frac{\left[\frac{dT}{dz}\right]_{Stratified\ flow}}{\left[\frac{dT}{dz}\right]_{Mixed\ flow}} = 11 \qquad (6.3.19)$$

$$\frac{\left[\frac{dT}{d\delta}\right]_{Stratified\ flow}}{\left[\frac{dT}{d\delta}\right]_{Mixed\ flow}} = 50 \qquad (6.3.20)$$

This low degree of stratification results in a fully mixed flow, where the degree of stratification decreases by 11 times through the vertical height and 50 times through the stratified layer. In this case, the buoyancy forces of low temperature difference (0.4 °C/m) are not efficient to maintain on the stratified condition. Therefore zones disappeared, and a fully homogenous mixed zone is established. In this zone, the air is fully mixed and therefore the air temperature and pollutant concentrations are uniform throughout the space.

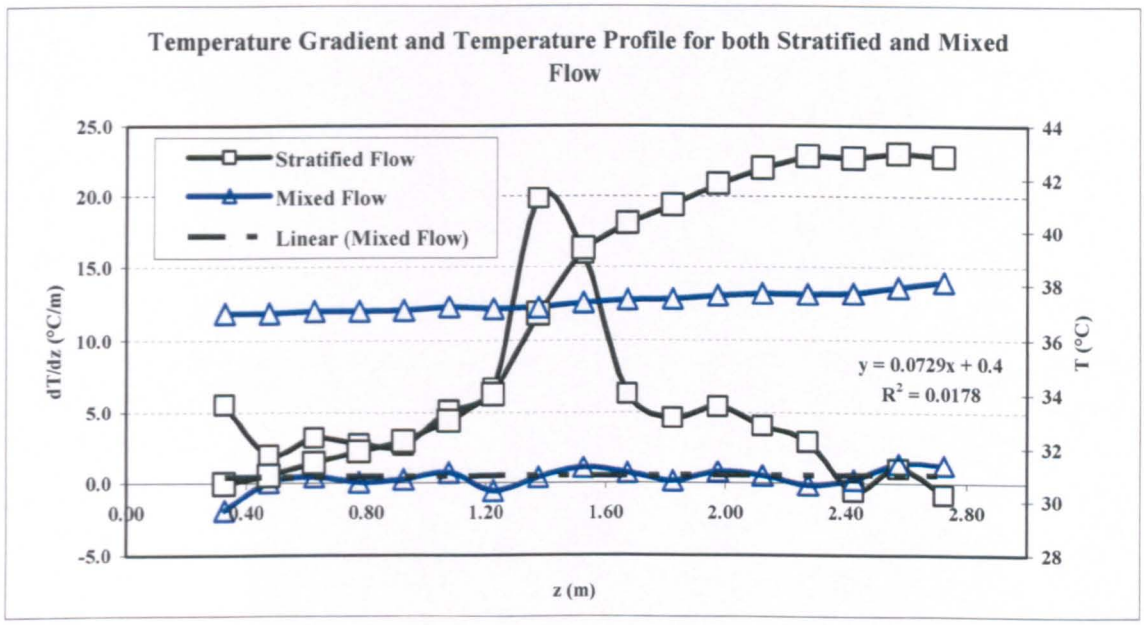

Figure 6.3.20: The temperature profile and temperature gradient for both stratified and mixed flow (figure 5.6.1). In this case, the break down of the stratified layer was introduced by inversion the input vertical locations.

6.4 Implication of Measurement Resolution

The data analysis in the present study emphasized the time dependence for temperature vertical distribution. For stratified flow, the methodology used in the present work focused on short duration releases of (60 s). For mixed flow where the variation is faster, the time resolution of concentration measurements was 10 s. This resolution allowed analysis of the time sequence of temperature distribution.

Table 4.1.4 shows the average airflow rates for different flow configurations. The increase in airflow rates between low and high flow rates were by factors of 1 and 2 m^3/min. The minimum and maximum measured airflow rate for different configurations varied from 1m^3/min for hot airflow rate to 2m^3/min for cold airflow rate. Comparing to the whole volume (126 m^3), the effects of variations in chamber ventilation rates were by factors 0.48 to 0.95 hour $^{-1}$. These values show that the air age inside the chamber is mostly less than an hour.

Figure 4.4.1 showed the sensitivity of the flow characteristics to the varying of input hot airflow rate. In comparison with figure 4.4.2, the sensitivity of the flow to changes in cold airflow rate and so the ambient conditions were smaller. The inflow rate was within the resolution, of the device approximately, within $\pm$ 5.7%, as listed in appendix A3.4.

Using temperature profile as a means to determine the flow characteristics h, δ, DS and dT/dz estimates for the stratified flow experiments will no doubt include errors which cannot be quantified due to the number of uncontrollable flow variables. This method is the only means of evaluating. The accuracy becomes better for stratification of higher temperature gradient over well controlled experiments, so that the flow characteristics could be observed clearly.

Incoming heat loads can create stratification inside the chamber. To understand this process, the standard practice is to measure the air temperature at many intervals along the chamber height and around the stratified layer where the rate of change of temperature is higher. Eighteen temperature sensors, with a multi-channel data logger is used tto record the temperature profile. In these measurements, sensor matching is more important than sensor accuracy, whilst the rate of temperature change with depth is most interest, not the temperature value itself. The highest quality thermocouples temperature sensors are matched to 2.5%.

6.5 Implication on Ventilation Designs

Although a great deal of literature on ventilation implications exists, much of these are technical writing concerned with the mixing of stratified flow to improve the

mechanical and removal efficiency. There have been very few studies conducted on the implications of ventilation in the presence of stratification.

As discussed in Chapter 2, studies of energy saving potential in buildings addressing the need for the implementation of such an energy efficient system. By determining the ways in which the stratified layer can be established and suggesting ways in which this stratification can be overcome, the present work has provided the information needed to promote the implementation of stratified and mixed flow in ventilation systems. It has provided pointes view from which it can develop strategies to increase use of stratification applications and to design the ventilation systems with most benefits.

The purposes of the present work were to investigate the stratified flow characteristics perceived by designers and decision makers in the implementation of ventilation systems in enclosures and buildings. Taking in consideration the effect of stratification on ventilation, heating, and cooling of a building is more efficient and significantly reduce energy use. This is important for many reasons:

- It can save significant amounts of money and energy when used to provide enough comfort.
- It improved the effectiveness of the ventilation system to remove the contaminant and heat from the occupied zone and provide the zone with fresh air.

In ventilation applications, stratification interface level height and ventilation airflow rates are the two main factors in the design of natural ventilation system [Chen and Li (2002)]. Both input and exhaust vertical locations have a significant effect on the flow characteristics, and reinforce each other. In Linden's and Skistad's models there are no further explanations for the effect of these parameters on the stratified flow characteristics.

From the results, the flow can stratify at certain heights below the exhaust location depending on the flow boundary conditions. For this the opening geometries must be designed to overcome the phenomenon and exhausted the contaminants and unneeded gases with high removal efficiency. However, when the exhaust location is not at the

stratified layer height, but at some way below or above, the removal efficiency becomes low. In other words, fixed exhaust location is ineffective to exhaust the contaminant.

The results show that the exhaust location does not alter the position of the interface level height. It could be in the location above or below the interface level height. Note that the exhaust location does influence the flow rate and the level of the interface. In order to improve the effectiveness of ventilation and to save heating energy costs, the exhaust location must be where "the exhaust temperature should not exceed the temperature in the occupied zone" [Hagstrom et al. (2000)].

The inversion of input duct locations is much more efficient in the removal of heat and contaminant than the jet momentum. Ventilation strategies employ this vertical temperature gradient by maintaining the lower occupied zone at comfort conditions while the hotter gases in the upper zone to be exhausted.

6.6 Summary and Concluding Remarks

For efficient design and estimation of optimal operating conditions in ventilation systems, a series of experimental investigations have been performed to study the flow characteristics and the thermal stratification mechanism. The review of previous investigations on the stratified flow, revealed the need for more experimental work using air-modeling technique. In the research work we have examined the stratified flow, in steady state conditions, under the effect of the different major flow parameters. The effect of influence of different flow parameters of air supply, such as airflow rate, jet momentum and temperature, flow conditions, and the vertical location of input and output air flow were investigated. Also the influences the space characteristics, such as geometry of the chamber, type of the walls, and distribution of the heat and smoke sources were also investigated. The combination of all of these factors will lead to the development of tools that aid in designing efficient ventilation systems.

The kind of information that is typically extracted from the experimental results is shown and discussed in Chapters 4, 5 and 6. The results are for the cases mentioned in Chapter 3, where the inlet hot and cold flow rates, input and outlet vertical locations are the main parameters used to stratify the flow, while the momentum of cold and warm jet

flow and the inversion of input locations are the main parameters used to mix the stratified flow. The comparisons between experimental results and visualisation are analyzed in the present work, also the Richardson number and stratification thicknesses calculations were presented to highlight the stratification boundaries and for the comparison purposes with other researchers such as [Mund (2001)] and [Skisdad (1998)]. The general conclusions obtained are discussed, and the areas of special attentions are highlighted and the recommended for future work are suggested.

From the experimental data investigated in the present research work, and the discussions and analysis conducted through out the thesis, the following can be concluded:

6.6.1 Effect of Input Airflow Rates and the Direction of Flow

The effect of input airflow rates on the stratified flow has involved with a number of exercises that can be used in ventilation designs and applications. The results and conclusions remarks concerned with this will be presented in the following:

- It was found that for certain ranges of input flow rates, stratification could occur for all conditions.
- It was seen that the hot flow rate has more significant effect on the stratified flow than that of cold flow rate.
- Controlling airflow rate may slightly control the degree of stratification, and stratification interface thickness.
- The moderate airflow rates show better performance of thermal stratification.

It should be noted that the stratification interface level, the total ventilation flow rate and the geometry of the space are, generally, the major concerns in the design of ventilation systems with most efficiently. So that the stratification levels must be above the occupied zone, and the ventilation flow rate must be within the requirements of space occupants.

A strong stratified region can work as a thermal barrier to decelerate the contaminant motion and increase both the temperature in the upper zone and the concentration of the smoke along the surface in the occupied zone. Also it could be concluded that there is a

slight effect of the flow rate on the stratified layer thickness which can be advantageous or disadvantageous to the occupied regions.

6.6.2 Effect of Input Vertical Locations

The effects of both input and exhaust locations on the stratified flow characteristics were investigated. When the input location is at higher levels (2.0 m), the buoyancy forces is increased with a sufficient amount to stratify the flow, whilst for the decreasing of input location from 2.0m to 1.0 m, the interface level height is decreasing downward to reach the ground, yielding a mixed flow in both zones. The temperature distribution in the upper zone is somewhat independent of the location of input location unlike the lower zone. The results also show that the level of stratification is increased by the increasing of exhaust location.

From the results it can be seen that the input and exhaust vertical locations reinforce each other, while the hot and cold airflow rates do not always reinforce each other, but in fact be against each other, due to the buoyancy differences created due to unbalance effect of both layers of the stratified region .

It can be concluded that the stratified flow characteristics are dependent upon the flow parameters and the geometry of the space (opening locations). The designing of opening heights can be used for controlling the flow characteristics such as mixing or maintaining the flow of the stratified layer.

6.6.3 Effect of Momentum Jet Flow

The effect of momentum jet airflow on mixing the stratified flow was investigated by using an experimental air modelling technique. It is seen that the jet momentum has significant influence on the mixing of the flow and the stratified flow characteristics. The details indicated that once the momentum was initiated a mixed flow grew in the occupied zone above the floor. The height of this zone is a dependent of the stratified flow characteristics, and the temperature and momentum of the ceiling jet.

Comparisons between cold and warm jet flow show that the translation of the stratified flow level height and the mixing effectiveness are changed depending on the jet

temperature and momentum. Using warm jet airflow, the mixing of stratified flow was faster while the removing efficiently was higher. By using warm jet flow, the higher values of momentum will destroy the stratified layer and mix it before the interface level height reaches higher levels like that of cold jet flow.

Chapter 7

Conclusions

The main conclusions of the present study are:

1. Stratified layer interface level height is not located at the exhaust aperture height. This finding is contrary to the predictions by Skistad (1998) and Linden (1995) and others.
2. Stratified layer interface level height is dependent on the ratio of airflow rate and geometrical effects.
3. Based on the present experimental results a definition for degree of stratification is proposed. This definition gives a measure of the stratified layer within the stratified flow. A definition of the degree of stratification has not been previously published.
4. The critical vertical momentum necessary in order to break down a stratified layer has been found to depend on the stratified layer interface level height. A semi-empirical formula based on the present experimental results has been developed to predict the critical vertical momentum for given stratified conditions.
5. Experimental data also demonstrate a ventilation method for increasing the occupied zone height without breaking down the stratified layer.
6. If mixed flow is desired then the cold inflow aperture should be located higher than the hot inflow aperture.
7. Small-scale models, such as those used by Linden (1995) are insufficient for predicting stratified layer thickness. The present work demonstrates that the air within the stratified layer constitutes the region of contaminants. This contradicts the work of Linden (1995), which suggests that the upper layer is the region of the contaminants. Consequently the prediction of stratified layer thickness is important.

8. Based on the present experimental results, the effect of momentum is greater than the effect of buoyancy. The time needed to break down the stratified layer is considerable less than the time it takes to stratify.

The experimental work has also demonstrated a number of flow features of stratified flow. The features are as follows:

1. The present results of different airflow rates and different input exhaust locations showed that the temperature difference and the degree of stratification can be controlled by controlling the flow parameters.
2. The different findings between the Skistad's and the present model, showed that Skistad's model predicted that the flow will stratify at the level of extract air (exhaust height), while in the present model it has seen that the stratification can occur at any level between the bottom and the top of the full-scale height. Also in the present work it was found that the exhaust vertical location does not alter the position of the interface level height. The present investigations have shown that there are many important parameters that affect the stratified flow characteristics in contrast to [Skistad (1998)]. Linden's model predicts the interface level height as a sharp transition between clean and polluted zone, which in opposing to the results of [Mundt (1995)]. The present model predicted the ventilated space as two clean zones with a polluted-stratified layer in between, while the interface level height is suggested to be at the level of maximum gradient of temperature profile.
3. The higher of the input vertical location the higher of the interface level height, where different heights of input vertical locations will results in different levels of stratification as evaluated by [Hee-Jin and Dale (2001)].
4. In the case of cold jet, the injected air is heavier than its domain. With initial momentum vertically downward, the momentum and buoyancy forces are reinforced one another. In some cases, the negative buoyancy can reach minimum values before the momentum decreased to zero. It is due to the hot air entrainment from the upper zone.
5. The using of warm jet is more effective, compared with the cold jet flow, because of the effect of bouncy variations on the stratified layer.
6. More increase in momentum will increase the circulation in the lower zone raising the stratified layer upward and mixing the flow.

7. The inversion of input locations is an effective process in mixing the flow and improving the pollutant removal efficiency inside the space.
8. At the walls, the temperature difference and momentum are comparatively high which decreases the degree of stratification due to disturbances of the walls.
9. The present results are in agreement with the findings of Linden (1979) which identified the needs for input flow rates to remove the mixed fluid from the stratified region in order to keep its thickness constant, with a clearer phenomenon in the present study.
10. The results showed that the decrease of the stratified layer thickness, due to the momentum transfer from the cold air flow to the stratified layer according to the momentum equation, which specifies the density variations effect. The decrease is not significant at lower rates. When the cold airflow rate is comparatively high, there were higher decrease in the stratified layer thickness and height, while the interface level height increases. The reason is: Increasing the source of momentum leads to increase mixing due to energy transfer, and as a result the stratified layer thickness and the stratified layer height decreased more rapidly than for low and moderate cold airflow rates.
11. Also the results showed that the strongest degree of stratification is for moderate airflow rate ($Q_h = 2.0\,m^3/min\, Q_c = 4.0\,m^3/min$), as compared with the comparatively low and high airflow rates. For low airflow rates the buoyancy forces is sufficient to stabilize the flow. For comparatively high airflow rates the momentum is high enough to overcome the stabilizing influence of the buoyancy forces.
12. From the comparison with the schematic model suggested by [Skistad (1998)], the experimental observations in this work support the Skistad model. Both models predicted the stratified flow characteristics using full-scale technique with several major differences between the present model and the schematic model of Skistad.
13. According to Skistad's analysis the variation of temperature in the enclosure is linear which is in disagreement with the present results and the results of [Mundt 1995], where the temperature distribution is a function of height, and the temperature gradient is maximized under the ceiling where the different flow rates of different flow supplies. According to the heat transfer phenomena, the

temperature differences always occur due to the heat flux variations inside the enclosure.

14. From the stratified layer interface level height with the effective opening ratios A^*/H^2 and A^*L/H for different airflow rates, it is concluded that good agreement has been reported between the present results, using air modeling technique, and the predictable and experimental data using the salt-bath technique of [Linden et al.(1998)].
15. The Richardson number provides a measure for the buoyancy forces related to the momentum forces effect. The value of Ri was varied between 3.8 to 200, which very much spans over a wide range of operating conditions. For high values of Ri = 200, while the typical temperature profiles are shown to be characterized by the flow parameters, the stratified layer thickness is shown to be with significant effect. Upon decreasing the Ri value to 3.8, both δ and dT/dz were decrease. Moreover, the overall flow characteristics remain quite the same. The variation of dT/dz with Ri is more significant. Also, thinner stratified layer thickness is expected to form upon further decrease in Ri value. This is referred to the decrease in the ratio of Ri physical mechanism (buoyancy to momentum flow ratio), which causes steep temperature gradients in the vertical direction of the thermocouple stand near the bottom of the environmental chamber.

Chapter 8

Recommendations for Future Work

In this research, we have established a framework for understanding important parameters that affects the stratified flow and its relationships with ventilation developments. The work also illustrates how various factors such as input airflow rate, openings vertical locations, both cold and warm jet flow and the inversion of input locations influenced the characteristics of the stratified flow.

The work done in this research has opened up a wide range of experimental researches in studying the stratified flow, and improving the ventilation systems. In general the results obtained can be used as an important tool for the validation of analytical and numerical predictions, and to the design of ventilation systems and also it can broaden more understanding of flow problems.

As we mentioned earlier, there are many parameters influencing the stratified flow and the degree of stratification and its interfaces. Some of these parameters have been studied extensively in this research, such as the effects of input airflow rates, flow direction, input and outlet vertical locations on the stratified flow were investigated. Also, the effect of momentum jet flow and inversion of input locations on the stratified flow characteristics are performed. The combined effect of all these factors was also indicated.

From the review and comparison of previous investigations with the present experimental investigations, and from conclusions detailed in this Chapter 7, a number of suggestions and recommendations were made regarding further development of this research as following;

- Initial analysis has shown that the effects of these factors are significant and must be encountered when dealing with ventilation design. The results are encouraging the experimentalists and the theoretician to study these parameters extensively in their future work.
- The need for a CFD simulation models to evaluate the flow parameters especially for environmental hazards is necessary. It is therefore essential that further additional simulations can be used to be validated with the present experimental results, within future work.
- It is important to study the effect of input flow temperature, diffuser type and the grill angle on the stratified flow phenomena.
- The evaluation of the type of flow and the perturbations, fluctuations and the shear stress in the stratified layer can be useful for the stratification phenomenon.
- The effect of exhaust height in the presence of stratified flow on energy consumption and contaminant removing efficiency can be studied for predicting of the outlet locations for the ventilation systems.

References

Abdulkarim H. A. and Yogesh J., 1995, Penetrative convection in a stably stratified enclosure , International Journal of Heat and Mass Transfer, Volume 38, Issue 13, September, Pages 2489-2500.

Aerodynamics for students, 2006, http://www.aeromech.usyd.edu.au/aero/fprops/propso -ffluids/ node4.html, 11/5/2006.

Alizadeh Sh., 1999,Experimental and numerical study of thermal stratification in a horizontal cylindrical solar storage tank, Solar Energy, V 66, No 6, August, PP. 409-421.

Allocca C., Chen Q. and Glicksman L.R., 2003, Design analysis of single-sided natural ventilation, Energy and Buildings, Volume 35, Issue 8, September, Pages 785-795.

Al-Najem N., 1993, Degradation of stratified thermocline in solar storage tanks, Int. J. Energy Res. 17, PP. 183-191.

Al-Najem NM; El-Refaee MM, 1997, A numerical study for the prediction of turbulent mixing factor in thermal storage tanks, Applied Thermal Engineering, Volume 17, Number 12, pp. 1173-1181.

Andersen K.T., 2003, Theory for natural ventilation by thermal buoyancy in one zone with uniform temperature, Building and Environment, Volume 38, Issue 11, Pages 1281-1289.

Auban O., Lemoine F., Vallette P. and Fontaine J.R., 2001, Simulation by solutal convection of a thermal plume in a confined stratified environment: application to displacement ventilation, International Journal of Heat and Mass Transfer, Volume 44, Issue 24, Pages 4679-4691.

Awad A. S., Badran, O.O., Holdo, January A.E. and Calay R.K., 2006, Experimental study of stratified flow in a built environment. Proceeding of World Renewable Energy and Environment Conference (WREEC2006), Tripoli-Libya.

Awbi H.B., 1998, Chapter 7, Ventilation, Renewable and Sustainable Energy Reviews, vol. 2, Issu 1-2, pp. 157-1888.

Ayad, S. S., 1999, Computational study of natural ventilation. J. Wind Eng. Ind. Aero. Vol.82, pp 49-68.

Baines Peter G., 2002, Two-dimensional plumes in stratified environments, J. fluid Mech., vol. 471, pp. 315-337.

Behne M., 1999, Door air quality in rooms with cooled ceilings: Mixing ventilation or rather displacement ventilation, Energy and Buildings, Volume 30, Issue 2, Pages 155-166.

Bertin G., Most J.M. and Coutin M., 2002, Wall fire behavior in an under-ventilated room, Fire Safety Journal, Volume 37, Issue 7, Pages 615-630.

Bloomfield, L.J. & Kerr, R.C., 1999 Turbulent fountains in a confined stratified environment. J. Fluid Mech. 389, 27-54.

Bouzinaoui A., Vallette P., Lemoine F., Fontaine J. and Devienne R., 2005, Experimental study of thermal stratification in ventilated confined spaces, International Journal of Heat and Mass Transfer, 48, Pages 4121–4131

Calay R.K, Holdø E. and Hammond G.P., 1998, Natural convective heat transfer rates in rectangular enclosures, Energy and Buildings, Volume 27, Issue 2, Pages 137-146 .

Calay R.K., Borresen B.A. and Holdø E., 2000, Selective ventilation in large enclosures, Energy and Buildings, Volume 32, Issue 3, Pages 281-289.

Cardoso J., Z. Luo J. Miller A. Sheth and K. Kochut, 2001. Survivability Architecture for Workflow Management Systems, Proceedings of the 39th Annual ACM Southeast Conference, Athens, GA. Pages, 207-216.

Celik, I., Umbel, M., and Wilson, W., 1999, "Computations of turbulent mixing at the interface of a density stratified, shear layer", Proceedings of the 3rd ASME/JSME Joint Fluids Engineering Conference, July 18-23, San Francisco, CA.

Chen M.H. and Cardoso S.S.S., 7, 2000, The mixing of liquids by a plume of low-Reynolds number bubbles, Chemical Engineering Science, Volume 55, Issue 14, Pages 2585-2594.

Chen Z.D. and Li Y., 2002, Buoyancy-driven displacement natural ventilation in a single-zone building with three-level openings, Building and Environment, Volume 37, Issue 3, Pages 295-303.

Chen Z.D., Li Y. and Mahoney J., 1, 2000, Experimental modelling of buoyancy-driven flows in buildings using a fine-bubble technique, Building and Environment, Volume 36, Issue 4, Pages 447-455.

Chen Z.D., Li Y., Mahoney J., 2001, Natural ventilation in an enclosure induced by a heat source distributed uniformly over a vertical wall, Building and Environment, vol.36, pp. 493-501.

Chenvidyakarn, T. and Woods, A.W., 2004, The control of pre-cooled natural ventilation, Bldg Services Eng. Science and Technology, 15, Pages127-140.

Chow W.K., 1996, Simulation of tunnel fires using a zone model, Tunnelling and Underground Space Technology, Volume 11, Issue 2, Pages 221-236.

Chung K.Ch., Chen Y.K, Yeh W.Y., Su Y.J., Fu M.H. and Chen B.T., 1997, Experimental validation of the airborne contaminant prediction model in a multizonal workplace, Proceedings of the 5th International Symposium on Ventilation for Contaminant Control, Ottawa, Canada, Pages 289-298.

Cooper P. and Hunt H., 1999,Ventilation and stratification in naturally ventilated spaces driven by heated internal vertical surfaces, Presented at the First International One day Forum on Natural and Hybrid Ventilation, HybVent Forum'99, Sydney, Australia.

Cotel A., Gjestvang J., Ramkhelawan N. and Breidenthal R, 19997, Laboratory experiments of a jet impinging on a stratified interface, Experiments in Fluids, vol. 23, pp. 155-160.

Dagestad S., 1991, Numerical simulation of stratified flows with different K-ε turbulence models, PhD thesis, The Norwegian Institute of Technology, University of Trondheim, Norweg.

Dai Y.G., Sumathy K., Wang R.Z. and Li Y.G., 2003, Enhancement of natural ventilation in a solar house with a solar chimney and a solid adsorption cooling cavity, Solar Energy, Volume 74, Issue 1, Pages 65-75.

Dewan A., Kalita K. and Dass AK., 2003, Comperison of three buoyancy extended version of the $k-\varepsilon-\overline{t'^2}$ model in predicting turbulent plane plume, Applied mathematical modelling, PP. 1-14.

Dubovsky V., Ziskind G., Druckman S., Moshka E., Weiss Y. and Letan R., 2001 Natural convection inside ventilated enclosure heated by downward-facing plate: experiments and numerical simulations, International Journal of Heat and Mass Transfer, V.44, PP. 3155-3168.

Fitzgerald Sh.D. and Woods A.W., 2004, Natural ventilation of a room with vents at multiple levels, Building and Environment, Volume 39, Issue 5, Pages 505-521.

Fukuhara I. and Tsuji K. , 2003, Capture efficiency of push-pull ventilation systems, The 7th International Symposium on Ventilation for Contaminant Control, A meeting to ventilate minds proceeding, Sapporo, Japan, Pages 73-78.

Gan G., 2000, Effective depth of fresh air distribution in rooms with single-sided natural ventilation, Energy and Buildings, Volume 31, Issue 1, Pages 65-73.

Hagström K., Sandberg E., Koskela H. and Hautalampi T., 2000, Classification for the room air conditioning strategies, Building and Environment, Volume 35, Issue 8, Pages 699-707.

Hahne E. and Chen Y., 1998, Numerical study of flow and heat transfer characteristics in hot water stores, Solar Energy, Vol. 64, No. 1-3, pp 9-18.

Haslavskya V., Tannya J.,_, Teitelb M., 2005, Interaction between the mixing and displacement modes in a naturally ventilated enclosure Building and Environment, Available online, , pp 1-7.

Hee-Jin P. and Dale H., 2001, The effect of location of a convective heat source on displacement ventilation: CFD study, Building and Environment, Volume 36, Issue 7, Pages 883-889.

Hegazy A. and Diab M. R., 2002, Performance of an improved design for storage-type domestic electrical water-heaters , Applied Energy, Volume 71, Issue 4, Pages 287-306.

Hejazi M.G. and Siren K.E., 1997, a field study of cold airflows through doorways of industrial buildings, Proceedings of the 5th International Symposium on Ventilation for Contaminant Control, Ottawa, Canada, Pages 299-306.

Helmig D., Boulter J., David D., Birks J.W., Cullen N.J., Steffen K., Johnson B.J. and Oltmans S.J., 2002, Ozone and meteorological boundary-layer conditions at Summit, Greenland, during 3–21 June 2000, Atmospheric Environment, Volume 36, Issues 15-16, Pages 2595-2608,

Holford J.M. and Hunt G.R., 2003, Fundamental atrium design for natural ventilation, Building and Environment, Volume 38, Issue 3, Pages 409-426.

Hoseon Y., Kim C-J, Wook C., 1999, Approximate analytical solutions for stratified thermal storage under variable inlet temperature, Source: Solar Energy, v 66, n 1, p 47-56

Howell S.A. and Potts I., 2001, On the natural displacement ventilation flow through a full scale enclosure, driven by a source of buoyancy at floor level, Seventh International IBPSA Conference, Rio de Janeiro, Brazil.

Howell S.A. and Potts I., 2002, On the natural displacement flow through a full-scale enclosure, and the importance of the radioactive participation of the water vapour content of the ambient air, Building and environment, 37, pp. 817-823.

Hung C.I, Chen C.H and Chen C.B, 1999, Non-Darcy free convection along a non-isothermal vertical surface in a thermally stratified porous medium, International Journal of Engineering Science, Volume 37, Number 4, pp. 477-495.

Hunt G. and Linden P, 2002, Steady state flows in an enclosure ventilated by buoyancy forces assisted by wind, J. Fluid Mechanics, vol. 426, pp. 355-386.

Hunt G.R. and Linden P.F., 1999, The fluid mechanics of natural ventilation—displacement ventilation by buoyancy-driven flows assisted by wind, Building and Environment, Volume 34, Issue 6, Pages 707-720.

Jaluria Y., Lee S.H.K., Mercier G.P. and Tan Q., 1998, Transport processes across a horizontal vent due to density and pressure differences, Experimental Thermal and Fluid Science, Volume 16, Issue 3, Pages 260-273

Jeremy C. Phillips and Andrew W. Woods, 2004, On ventilation of a heated room through a single doorway, Building and Environment, Volume 39, Issue 3, Pages 241-253.

Joanne M. Holford and Gary R. Hunt, 2003, Fundamental atrium design for natural ventilation, Building and Environment, Volume 38, Issue 3, Pages 409-426.

Kang M.G., 2002, Thermal Mixing in a Water Tank. during Heating Process, International. Journal of Heat and Mass Transfer 45, 4361.

Karimipanah M.T., 1998, Deflection of wall-jets in ventilated enclosures described by pressure distribution, Building and Environment, Volume 34, Issue 3,, Pages 329-333.

Karimipanah T. and Awbi H.B., 2002, Theoretical and experimental investigation of impinging jet ventilation and comparison with wall displacement ventilation, Building and Environment, Volume 37, Issue 12, Pages 1329-1342.

Kikuchi S., Ito K. and Kobayashi N., 2003, Numerical analysis of ventilation effectiveness in occupied zones for various industrial ventilation systems, The 7th International Symposium on Ventilation for Contaminant Control, A meeting to ventilate minds proceeding, Sapporo, Japan, Pages 103-108.

Kunsch JP., 2002, Simple model for control of fire gases in a ventilated tunnel, Fire Safety Journal, Volume 37, Issue 1, Pages 67-81.

Lane Serff, G. F., 1989, "Heat flow and air movement in buildings", Ph.D. thesis, Cambridge Univ., UK.

Lee H. and Awbi H.B., 2004, Effect of internal partitioning on indoor air quality of rooms with mixing ventilation- basic study, Building and Environment, Volume 39, Issue 2, Pages 127-141.

Lee S. R. and Ryou H. S., 2005, An Experimental Study of the Effect of the Aspect Ratio on the Critical Velocity in Longitudinal Ventilation Tunnel Fires, Journal of Fire Sciences, Vol. 23, No. 2, 119-138.

Li Y. and Delsante A., 2001, Natural ventilation induced by combined wind and thermal forces*1, Building and Environment, Volume 36, Issue 1, Pages 59-71.

Li Y., Delsante A. and Symons J., 2000, Prediction of natural ventilation in buildings with large openings, Building and Environment, Volume 35, Issue 3, Pages 191-206.

Li Y., Sandberg M. and Fuchs L., 1993, Effects of thermal radiation on air flow with displacement ventilation: an experimental investigation, Energy and Buildings, vol. 19, pp. 263-274.

Linden P.F., 1979, Mixing in stratified fluids, Geophys. Astrophys. Fluid dynamics, Vol. 13, pp. 3-23.

Linden P.F., Lane-Serff G.F. and, Smeed D.A., 1990, Emptying filling boxes: the fluid mechanics of natural ventilation. Journal of Fluid Mechanics, Vol. 212, pp 309–335.

Loehke R., Gari H., Sharp M., Haberstroh R., 1978, Apassive technique for enhancing thermal stratification in liquid storage tanks, ASME, Paper No 78-HT-50.

Makhviladze G.M., Roberts J.P. and Yakush S.E., 1996, Turbulent buoyant thermal in a density stratified atmosphere, International Journal of Heat and Mass Transfer, Volume 39, Issue 7, Pages 1453-1462.

McEvoy M.E., Southall R.G. and Baker P.H., 2003, Test cell evaluation of supply air windows to characterise their optimum performance and its verification by the use of modelling techniques, Energy and Buildings, Volume 35, Issue 10, Pages 1009-1020.

McGrattan KB., Baum HR. and Rehm RG., 1996, Numerical simulation of smoke plumes from large oil fires, Atmospheric Environment, Volume 30, Issue 24, Pages 4125-4136.

Mundt E., 1994, Contamination distribution in displacement ventilation—influence of disturbances, Building and Environment, Volume 29, Issue 3, Pages 311-317.

Mundt E., 2001, Non-buoyant pollutant sources and particles in displacement ventilation, Building and Environment, Volume 36, Issue 7, Pages 829-836.

Mundt El., 1995, Displacement ventilation systems- Convection flow and temperature gradients, Building and Environment, Volume 30, Issue 1, Pages 129-133.

Murakami Sh. and Kato Sh., 1989, Numerical and experimental study on room airflow 3-D predictions using the k-ε Turbulence model, Building and environment, vol. 24, No. 1, pp. 85-97.

Nagasawa Y., Kondo Y., Ogita Sh. and Yoshino H., 2003, Numerical simulation of direct capture efficiency for local ventilation systems, The 7th International Symposium on Ventilation for Contaminant Control, A meeting to ventilate minds proceeding, Sapporo, Japan, Pages 79-84.

PATH (Partnership for Advancing Technology in Housing) 2005, {http://www.-toolbase.org/techinv/techDetails.aspx?technologyID=238}, November 26,2005

Poreh M. and Trebukov S., 2000, Wind effects on smoke motion in buildings, Fire Safety Journal, Volume 35, Issue 3, Pages 257-273.

Qin T.X., Guo Y.C., Chan C.K. and Lin W.Y, 2006, Numerical investigation of smoke exhaust mechanism in a gymnasium under fire scenarios, Building and Environment 41, Pages 1203–1213.

Raisanen J. and Niemela R., 1997, The use of fortable spectrometer for the simultaneous measurements of solvent vapours and tracer gas, Proceedings of the 5th

International Symposium on Ventilation for Contaminant Control, Ottawa, Canada, Pages 269-276.

Redondo J.M, Sanchez M.A. and Cantalapiedra I.R., 1996, Turbulent mechanisms in stratified fluids, Dynamics of Atmospheres and Oceans, vol. 24, pp. 107-115.

Shy S.S., 1999, Mixing dynamics of jet interaction with a sharp density interface, Experimental Thermal and Fluid Science, vol. 10, pp. 355-369.

Sinha S.L., Arora R.C. and Roy S., 2000, Numerical simulation of two-dimensional room air flow with and without buoyancy, Energy and Buildings, Volume 32, Issue 1, Pages 121-129.

Skistad H., 1998, Utilizing, selective withdrawal in the ventilation of large rooms; select-vent, Room Vent Conference, Stockholm.

Slater G., Cooper P. and Norrish J., 2003, Gas metal arc welding fume dispersion and ventilation, The 7th International Symposium on Ventilation for Contaminant Control, A meeting to ventilate minds proceeding, Sapporo, Japan, Pages 219-224.

Subbarao P.M. and Muralidhar K., 1997,Experimental study of turbulence in isothermal and stably stratified homogeneous shear flows: Mean flow measurements, Fluid Dynamics Research, 21, PP. 431-454.

Teitel M. and Tanny J., 1999, Natural ventilation of greenhouses: experiments and model, Agricultural and Forest Meteorology, Volume 96, Issues 1-3, Pages 59-70.

Teodosiu C., Hohota R., Rusaouën G. and Woloszyn M., 2003, Numerical prediction of indoor air humidity and its effect on indoor environment, Building and Environment, Volume 38, Issue 5, Pages 655-664.

Turnuer J.S., 1973, Buoyancy effects in fluids, Cambridge University Press., Cambridge, UK, pp. 367.

University of Minnesota, Duluth, Large Lakes Observatory, 2001, (www.d.mn.edu/llo), Year 2001 Report, U.S.A.

Wander, J. D., 2002, Cost-effective ventilation for large spray-painting operations, Metal Finishing, Volume 100, Issue 3, Pages 23-24.

Wargocki and Wyon D., 1998, Individual control at each workplace for health, comfort and productivity, Environment, 4, 1, pp 3-6

Webster T., Bauman F. and Reese J., 2002, Under floor air distribution: Thermal stratification, ASHRAE Journal, v 44, n 5, p 28-30+32+34+36.

Wood A.W., Caulfield C.P., Phillips J.C., 2003, Blocked natural ventilation: The effect of a Source mass flux, J. Fluid Mech., Volume 495, pp 119 – 133.

Woodburn PJ. and Britter RE., 1996, CFD simulations of a tunnel fire—Part I, Fire Safety Journal, Volume 26, Issue 1, Pages 35-62 .

Xing H. and Awbi H.B., 2002, Measurement and calculation of the neutral height in a room with displacement ventilation, Building and Environment, Volume 37, Issue 10, pp 961-967.

Yam J., Li Y. and Zheng Z., 2003, Nonlinear coupling between thermal mass and natural ventilation in buildings, International Journal of Heat and Mass Transfer, Volume 46, Issue 7, Pages 1251-1264.

Yue Z., 1999, Air jet velocity decay in ventilation application, Building Services Engineering, Royal Institute of technology, Stockholm, Sweden, pp 1-51.

Ziskind G., Druckman S., Moshka E., Weiss Y. and Letan R., August 2001, Natural convection inside ventilated enclosure heated by downward-facing plate: experiments and numerical simulations, International Journal of Heat and Mass Transfer, Volume 44, Issue 16. Pages 3155-3168.

Ziskind G., Dubovsky V. and Letan R., 2002, Ventilation by natural convection of a one-story building, Energy and Buildings, Volume 34, Issue 1, PP. 91-101.

Appendices

A1: Analytical Approach and Steady State Conditions.

A2: Details of data.

A3: Measuring Instrumentations and Calibration.

A3.1:Agilent 34970A Data Acquisition/Switch Unit.

A3.2:Calibration of the Instrumentation used for the Flow and Temperature Measurements.

A3.3:Smoke Generator for Flow Visualization.

A3.4:Rotating Vane Anemometer LC6000.

A4: Published Work.

A4.1: An Approximate analytical solution to flame length in a ventilated room.

A4.2: A model to predict stratification in two-phase flow in horizontal pipes.

A4.3: The effect of momentum jet air flow on the stratified layer characteristics.

A4.4: Experimental study of stratified flow in a built environment.

A4.5: The effect of input supply and flow rate on stratified flow characteristics inside enclosure.

Appendix A1

Analytical Approach and Steady State Conditions

The approach used to analyze results is mentioned below. The analysis and the detailed results will be reported with the parametric study of the stratified flow. Identifications of the parameters affecting the thermal stratification in the environmental chamber are listed:

1. To give a complete study for the stratified flow in ventilated chamber, a number of flow parameters affecting thermal stratification have been tested in the present work:
    - Hot airflow rate.
    - Cold airflow rate.
    - Input and output heights.
    - Heat loss.
2. To investigate the results, the following values and ranges for the parameters affecting the thermal stratification are considered.

Hot air temperature	From 40-45°C.
Cold air temperature	The instantaneous ambient temperature
Hot air diffuser area	0.25 m^2.
Cold air diffuser area	0.50 m^2.
Hot air input heights	1.0 m to 2.5 m in steps of 0.5 m.
Cold Air input height	0.25 m.
Exhaust height	0.5 m to 2.5 m in steps of 0.5 m.
Thermocouple distribution	As presented in chapter 3
Thermocouple heights	As listed in table A1.1
Hot and cold flow rates	As listed in table A1.2.

$$Ri = g\beta H\frac{(T_h - T_c)}{(U_h - U_c)^2}$$

As listed in table A1.3

$$Fr = \frac{|U_h - U_c|}{\sqrt{g\beta(\Delta T)H}}$$

As listed in table A1.4

$$Re_{global} = \frac{\frac{(U_h + U_c)}{2} H_{hyd}}{\nu}$$

As listed in table A1.5

$$H_{hyd} = (H_h - H_c)$$

$$Re_{local} = \frac{U_{ch}\, D_{hyd}}{\nu}$$

Based on the equivalent chamber velocity and hydraulic diameter as listed in table A1.6

$$D_{hyd} = \frac{B\,H}{\frac{B+H}{2}}$$

Based on B=5.6 m, H=3.0 m are the width and height of the chamber respectively.

$$U_{ch} = \frac{(Q_h + Q_c)}{B\,H}$$

Ranging from 0.001 to 0.013 m/s

$$Gr = \frac{g\, D_{hyd}^3\, \Delta T / T_m}{\nu^2}$$

As listed in table A1.7

T_m

Chamber mean temperature

$$Ar = \frac{Gr}{Re^{2.5}}$$

Based on the hydraulic diameter as listed in table A1.8

ΔT

As listed in table A1.9

g'

As listed in table A1.10

Thermocouple No.	Height (m)	Thermocouple No.	Height (m)	Thermocouple No.	Height (m)
1	2.80	7	1.90	13	1.00
2	2.65	8	1.75	14	0.85
3	2.50	9	1.60	15	0.70
4	2.35	10	1.45	16	0.55
5	2.20	11	1.30	17	0.40
6	2.05	12	1.15	18	0.25

Table A1.1: The thermocouples numbers and heights on the measuring stand as presented in chapter 3, (figure 3.3.1).

Class of flow	Low	Moderate	High
Cold airflow rate, m^3/min	0.0, 2.0	4.0	6.0, 8.0
Hot airflow rate, m^3/min	1.0, 2.0	3.0	4.0, 5.0

Table A1.2: shows the ranges of hot and cold airflow rates that be classified into three classis low, moderate and high. The calculations were based on, hot air diffuser area of 0.25 m^2 and cold air diffuser area of 0.50 m^2.

	Qc\Qh m^3/min	1.00	2.00	3.00	4.00	5.00
Ri	0.00	46.72	31.24	6.65	1.25	0.67
	2.00	200.00	145.21	19.00	3.80	1.14
	4.00	75.20	150.00	97.60	16.18	2.89
	6.00	23.10	133.96	150.00	97.71	9.09
	8.00	12.88	27.47	123.83	140.00	86.45

Table A1.3: shows the ranges of Ri number based on the input velocities, input temperatures and based on hot air diffuser area of 0.25 m^2 and cold air diffuser area of 0.50 m^2.

	Qc\Qh m^3/min	1.00	2.00	3.00	4.00	5.00
Fr	0.00	0.1463	0.1789	0.3877	0.8936	1.2250
	2.00	0.0707	0.0830	0.2294	0.5128	0.9367
	4.00	0.1153	0.0816	0.1012	0.2486	0.5883
	6.00	0.2080	0.0864	0.0816	0.1012	0.3317
	8.00	0.2786	0.1908	0.0899	0.0845	0.1075

Table A1.4: shows the ranges of Fr number based on the input velocities, input temperatures and based on hot air diffuser area of 0.25 m^2 and cold air diffuser area of 0.50 m^2.

	Qc\Qh m^3/min	1.00	2.00	3.00	4.00	5.00
Re	0.00	7813	15625	23438	31250	39063
	2.00	23438	31250	39063	46875	54688
	4.00	39063	46875	54688	62500	70313
	6.00	54688	62500	70313	78125	85938
	8.00	70313	78125	85938	93750	101563

Table A1.5: shows the ranges of Re number based on the input velocities based on hot air diffuser area of 0.25 m^2, cold air diffuser area of 0.50 m^2, and the hydraulic height of 1.5m

	Hydraulic diameter (m)	3.91				
	Qc\Qh m^3/min	1.00	2.00	3.00	4.00	5.00
Re	0.00	2424	4849	7273	9697	12122
	2.00	7273	9697	12122	14546	16970
	4.00	12122	14546	16970	19395	21819
	6.00	16970	19395	21819	24244	26668
	8.00	21819	24244	26668	29092	31517

Table A1.6: shows the ranges of Re number based on the equivalent velocity and hydraulic diameter in the environmental chamber.

	Hydraulic diameter (m)	3.91				
	Qc\Qh m^3/min	1.00	2.00	3.00	4.00	5.00
Gr	0.00	2.05E+11	5.49E+11	2.63E+11	8.80E+10	7.32E+10
	2.00	2.37E+11	6.38E+11	3.34E+11	1.50E+11	8.01E+10
	4.00	3.30E+11	7.12E+11	4.29E+11	2.84E+11	1.14E+11
	6.00	4.06E+11	5.88E+11	5.19E+11	4.29E+11	1.60E+11
	8.00	5.09E+11	4.83E+11	5.44E+11	4.61E+11	3.80E+11

Table A1.7: shows the ranges of Gr number based on the reduced gravity $g'\,m/s^2$ listed in table A1.10 and the chamber hydraulic diameter.

	Hydraulic diameter (m)	3.91				
	Qc\Qh m^3/min	1.00	2.00	3.00	4.00	5.00
Ar	0.00	709.12	335.29	58.32	9.50	4.52
	2.00	52.62	68.88	20.63	5.89	2.14
	4.00	20.42	27.90	11.43	5.43	1.62
	6.00	10.82	11.23	7.38	4.69	1.38
	8.00	7.24	5.27	4.68	3.20	2.15

Table A1.8: shows the ranges of Ar number based on the definition of Archimedes number $Ar = \frac{Gr}{Re^{2.5}}$, and the values of Re and Gr were listed in tables A1.6 and A1.7 respectively.

	Qc\Qh m^3/min	1.00	2.00	3.00	4.00	5.00
Temp. Diff.	0.00	4.15	11.10	5.32	1.78	1.48
	2.00	4.80	12.90	6.75	3.04	1.62
	4.00	6.68	14.40	8.67	5.75	2.31
	6.00	8.21	11.90	10.50	8.68	3.23
	8.00	10.30	9.76	11.00	9.33	7.68

Table A1.9: Temperature difference, at the measuring stand across the chamber at a fixed axial location of (3.75,2.8) m and different values of hot and cold air flow rates.

g' m/s^2	Qc\Qh m^3/min	1.00	2.00	3.00	4.00	5.00
	0.00	0.13	0.35	0.17	0.06	0.05
	2.00	0.15	0.41	0.21	0.10	0.05
	4.00	0.21	0.46	0.27	0.18	0.07
	6.00	0.26	0.38	0.33	0.28	0.10
	8.00	0.33	0.31	0.35	0.30	0.24

Table A1.10: Reduced gravity $g' m/s^2$ at the centre of the chamber for various values of cold and hot airflow rates, and based on the temperature difference listed in table A1.9.

3 To evaluate the effect of flow parameters mentioned above on the stratified flow characteristics. The results are analyzed along with the following lines.

- Average temperature difference was estimated from the difference between the floor and ceiling temperature readings rather than the hot and cold air temperatures, because of different experimental input temperatures.
- Stratification temperature profiles were plotted in terms of the dimensionless temperature $\frac{(T - T_1)}{(T_2 - T_1)}$ along a vertical height (with T_1 and T_2 being respectively the temperatures at the floor and the ceiling of the chamber) and a dimensionless height $\frac{z}{H}$.
- Interface level height was the point on the height axis at which the temperature profile has a maximum gradient. [Bouzinaoui et al (2005)]
- Stratified layer thickness was the height difference between the start of concave up and start of concave down on the plot of temperature profile.
- Degree of stratification was estimated from Ri or the degradation of temperature profile with the vertical axis, $\frac{dT}{dz}$.
- Uniformity of the stratified region was estimated through a number of tests were done at different locations in the direction along and across the direction of the flow.

4 To get good quality results, the flow was characterized by both temperature and smoke visualization, and the measurements were taken over a period of time when the flow attaining steady state conditions.

5 The above parametric numbers and the values listed in tables: A1.1 and A1.2 were selected based on theoretical background explained in chapter 2 and preliminary tests done in the environmental chamber, using air modeling techniques explained in Chapter 3.

A1.3 Steady state conditions

All the measurements were taken at steady state conditions. The time needed to reach this condition was varied from experiment to experiment. It depends, mainly, on the surroundings settings, weather fluctuations, measuring situations and flow conditions The typical time to reach steady state in our case was about (2-hours).

A steady (isothermal) temperature lines are shown in Figure A1.1. It shows the measuring temperatures of thermocouple stand as time advances. It is for the last five readings after the flow reaches the steady state conditions. The measured temperature used, in investigations, was the average of these five readings.

Figure A1.1 shows the deviations of the typical temperature distribution lines with time comparing with ideal steady state lines that can't be reached in labs. As can be seen in the figure, the deviations are visible near the top and bottom of the chamber, and non visible in between. Over a period of time (4 minutes), it can be shown that the isothermal line degradation $\theta = \frac{dT}{dt}$ is limited to 0.1°C/min. The deviations were large near the ceiling and the floor due to heat transfer, heat loss to the ambient, thermal diffusion and mixing. The deviation obtained is too small compare with the accuracy in the temperature measurements of 0.3 °C. For this, the measurements are found acceptable for steady state.

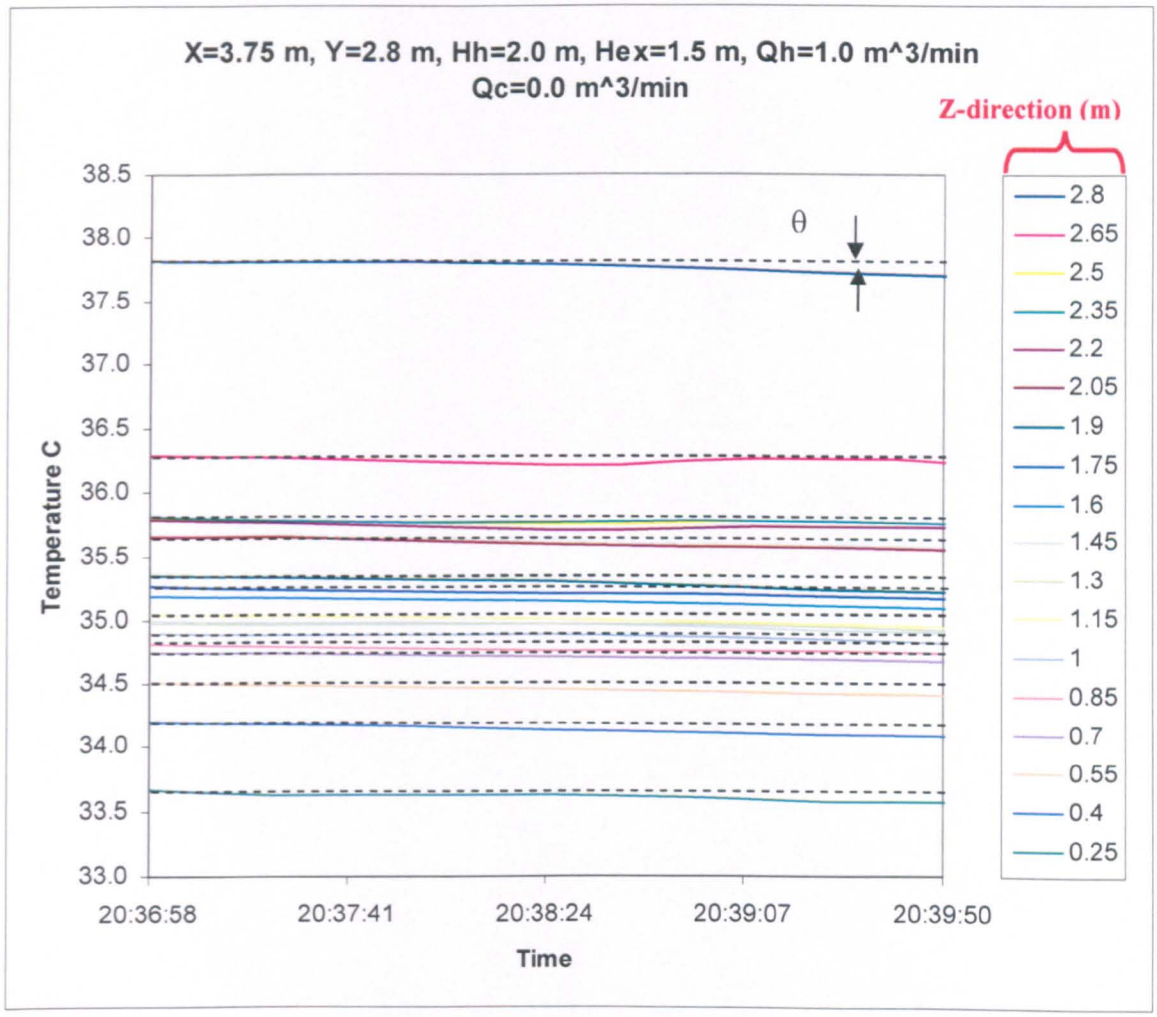

Figure A1.1: gives the isothermal plots as time advances when attaining steady state conditions.

Appendix A2

Details of data

For the cases listed in Chapter 5 and studied in sections 5.4 and 5.5,

Appendix A2 listed the details of data shown in

Figures A2.4.1 to A2.4.9 and Figures A2.5.1 to A2.5.25

that discussed in

Chapter 5.

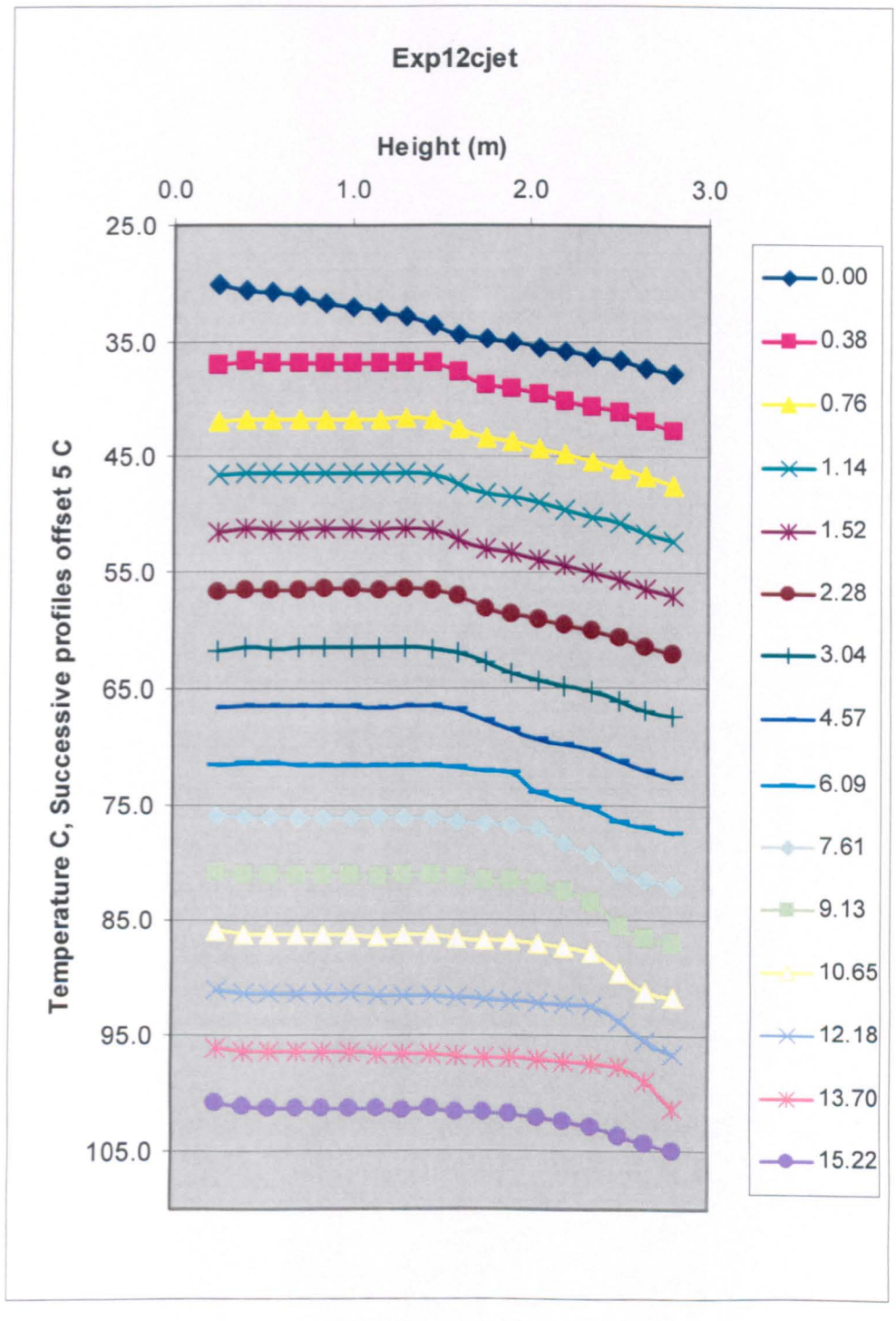

Figure A2.4.1: Illustrates vertical temperature profiles for various cold jet speeds. The flow was stratified at (Q_h = 1.0 m^3 / min) hot airflow rate and (Q_c = 2.0 m^3 / min) cold airflow rate at a locations of 2.0 and 1.5 m respectively at the centre of environmental chamber.

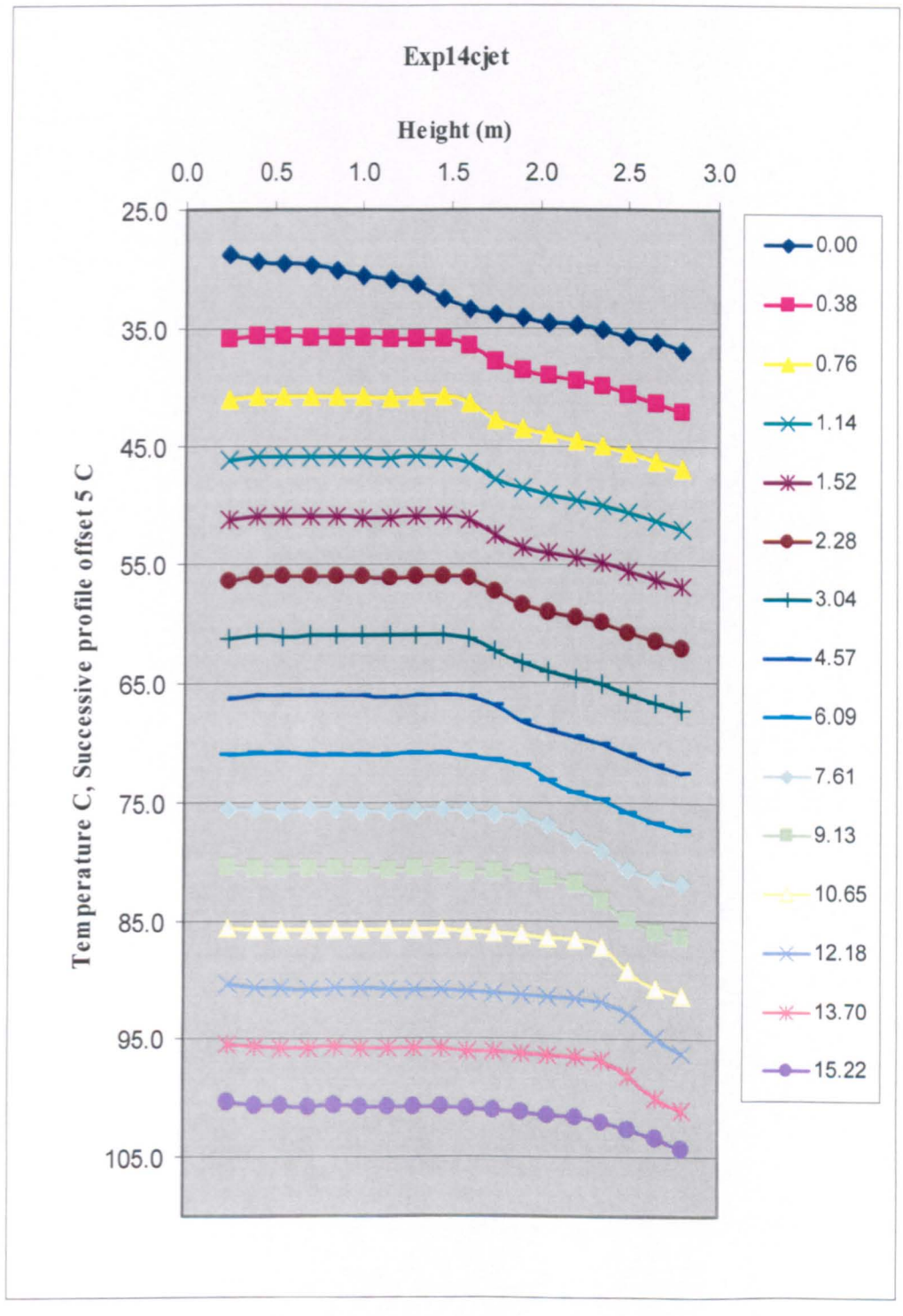

Figure A2.4.2: Illustrates vertical temperature profiles for various cold jet speeds. The flow was stratified at (Q_h = 1.0 m^3 / min) hot airflow rate and (Q_c = 4.0 m^3 / min) cold airflow rate at a locations of 2.0 and 1.5 m respectively at the centre of environmental chamber.

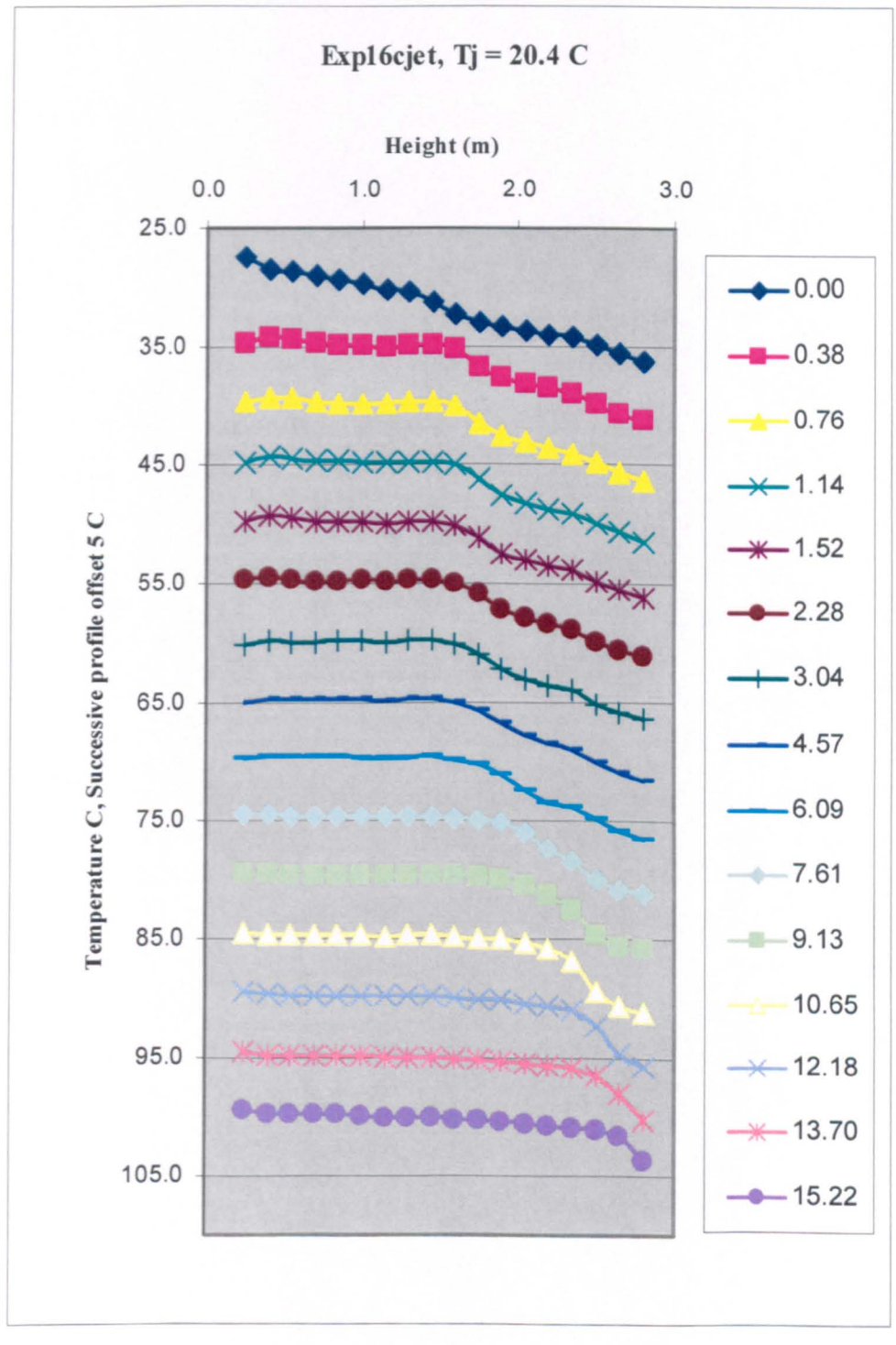

Figure A2.4.3: Illustrates vertical temperature profiles for various cold jet speeds. The flow was stratified at (Q_h = 1.0 m^3 / min) hot airflow rate and (Q_c = 6.0 m^3 / min) cold airflow rate at a location of 2.0 and 1.5 m respectively at the centre of environmental chamber.

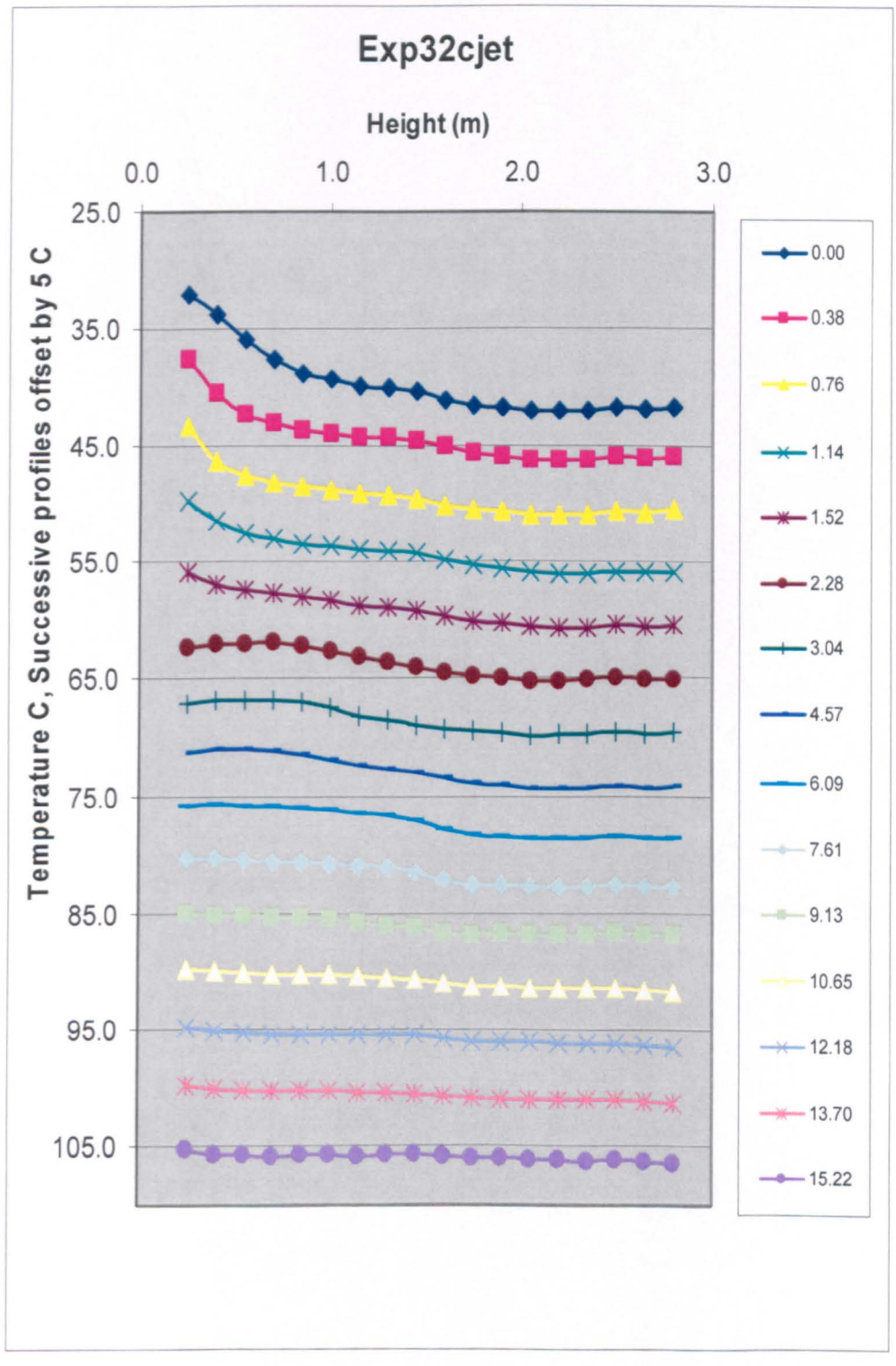

Figure A2.4.5: Illustrates vertical temperature profiles for various cold jet speeds. The flow was stratified at (Q_h = 3.0 m^3 / min) hot airflow rate and (Q_c = 4.0 m^3 / min) cold airflow rate at a location of 2.0 and 1.5 m respectively at the centre of environmental chamber.

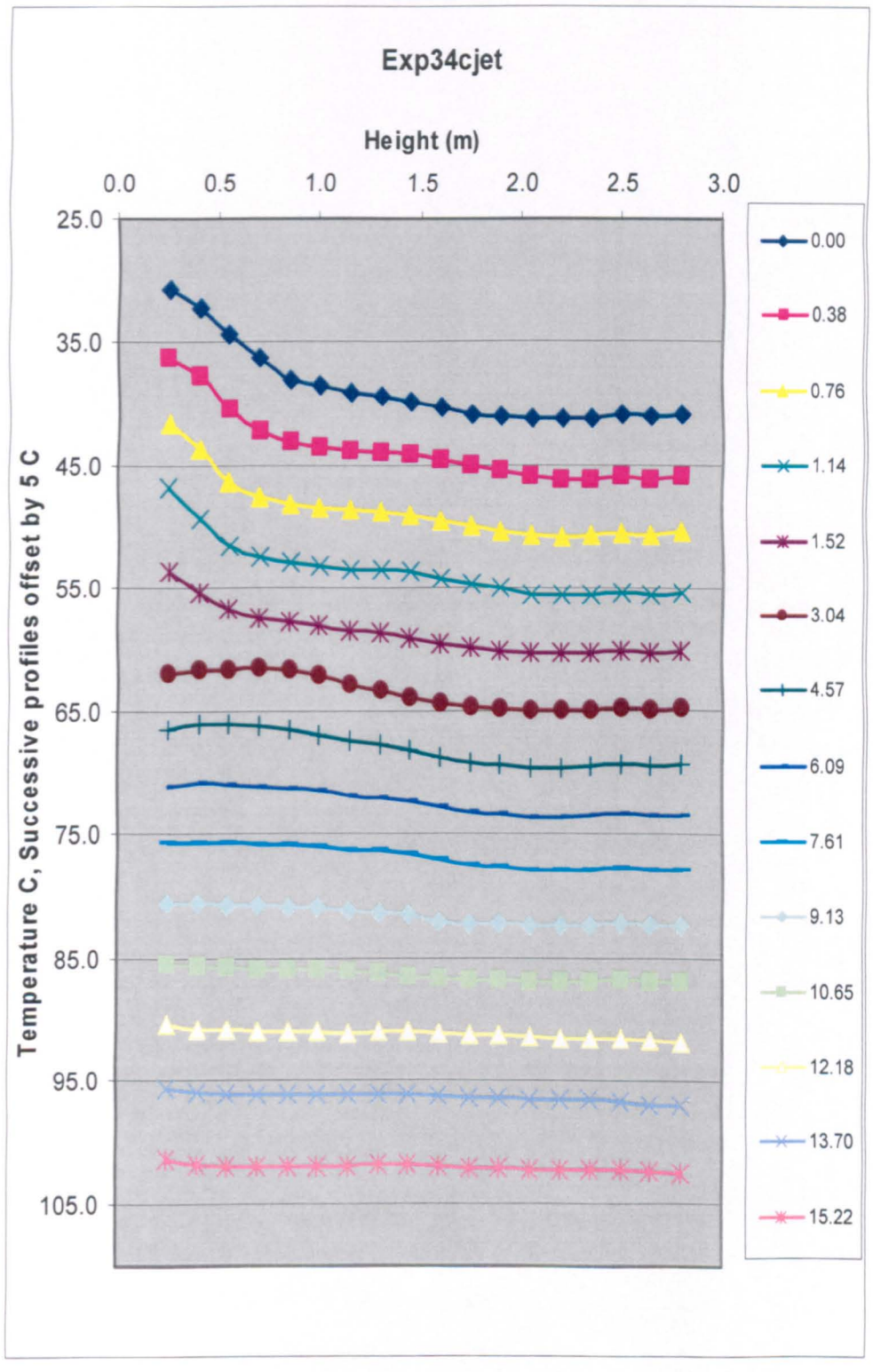

Figure A2.4.5: Illustrates vertical temperature profiles for various cold jet speeds. The flow was stratified at (Q_h = 3.0 m^3 / min) hot airflow rate and (Q_c = 4.0 m^3 / min) cold airflow rate at a location of 2.0 and 1.5 m respectively at the centre of environmental chamber.

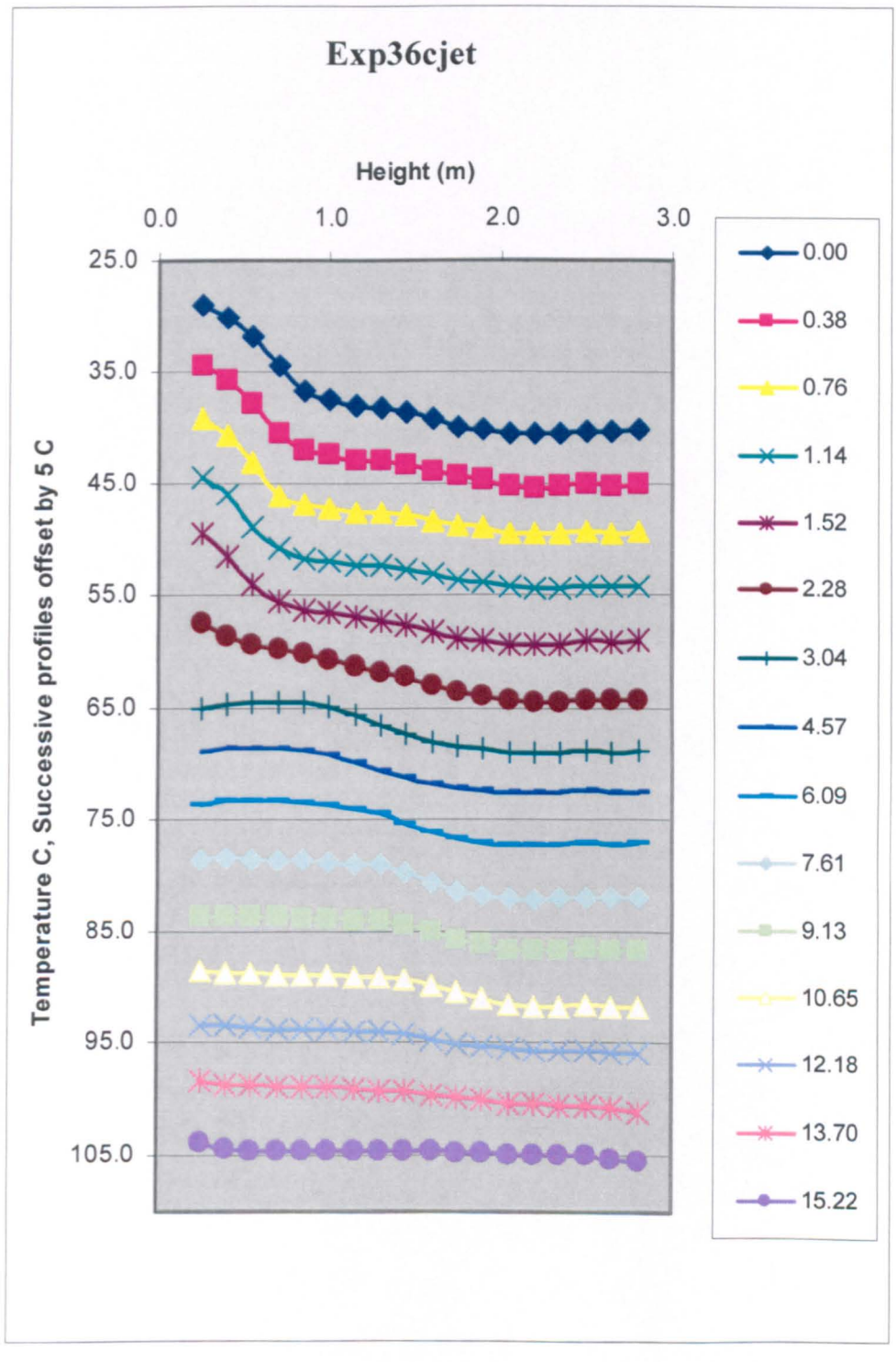

Figure A2.4.6: Illustrates vertical temperature profiles for various cold jet speeds. The flow was stratified at (Q_h = 3.0 m^3 / min) hot airflow rate and (Q_c = 6.0 m^3 / min) cold airflow rate at a locations of 2.0 and 1.5 m respectively at the centre of environmental chamber.

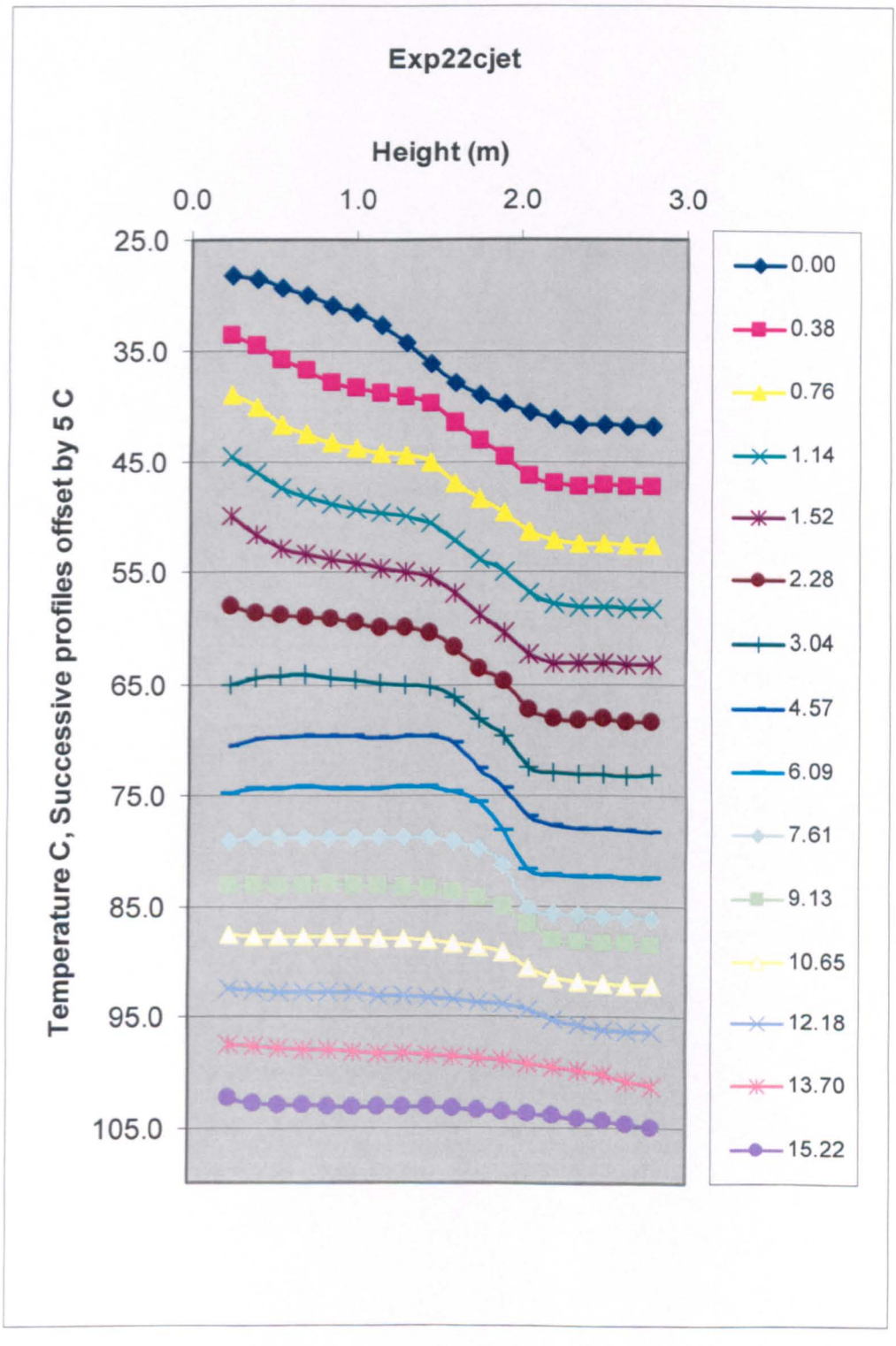

Figure A2.4.7: Illustrates vertical temperature profiles for various cold jet speeds. The flow was stratified at (Q_h = 2.0 m^3 / min) hot airflow rate and (Q_c = 2.0 m^3 / min) cold airflow rate at a location of 2.0 and 1.5 m respectively at the centre of environmental chamber.

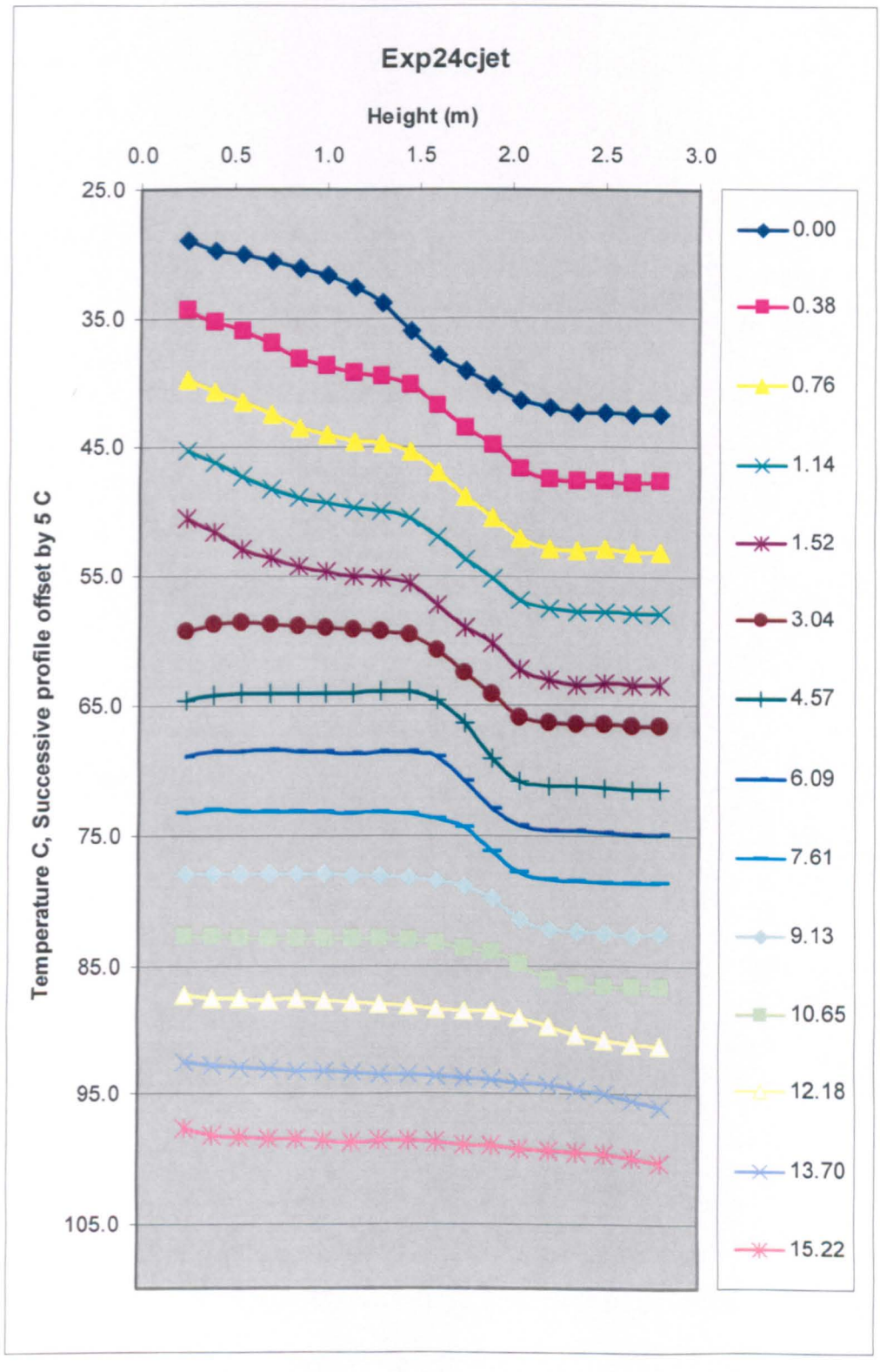

Figure A2.4.8: Illustrates vertical temperature profiles for various cold jet speeds. The flow was stratified at (Q_h = 2.0 m^3 / min) hot airflow rate and (Q_c = 4.0 m^3 / min) cold airflow rate at a locations of 2.0 and 1.5 m respectively at the centre of environmental chamber.

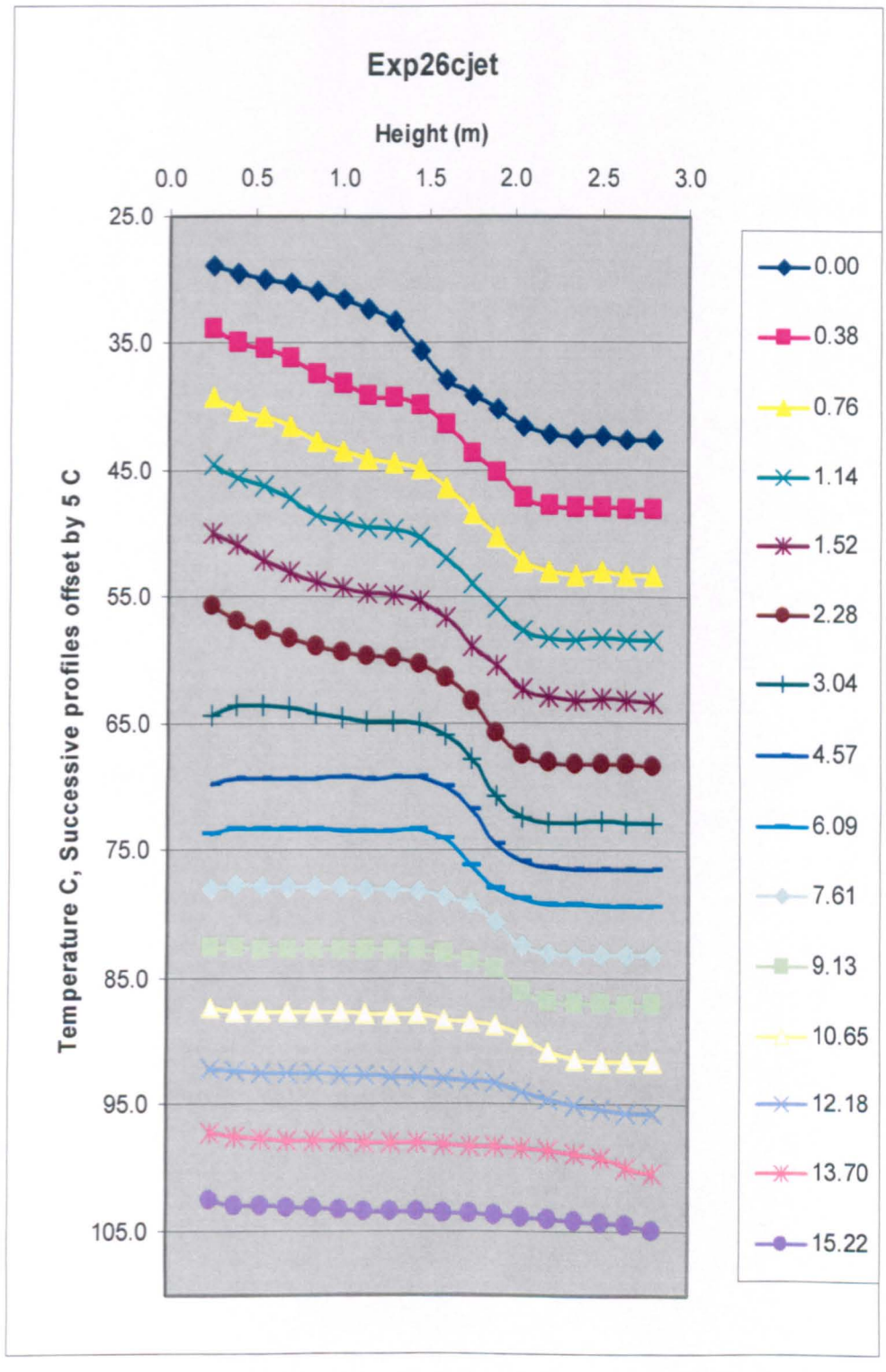

Figure A2.4.9: Illustrates vertical temperature profiles for various cold jet speeds. The flow was stratified at (Q_h = 2.0 m^3 / min) hot airflow rate and (Q_c = 6.0 m^3 / min) cold airflow rate at a location of 2.0 and 1.5 m respectively at the centre of environmental chamber.

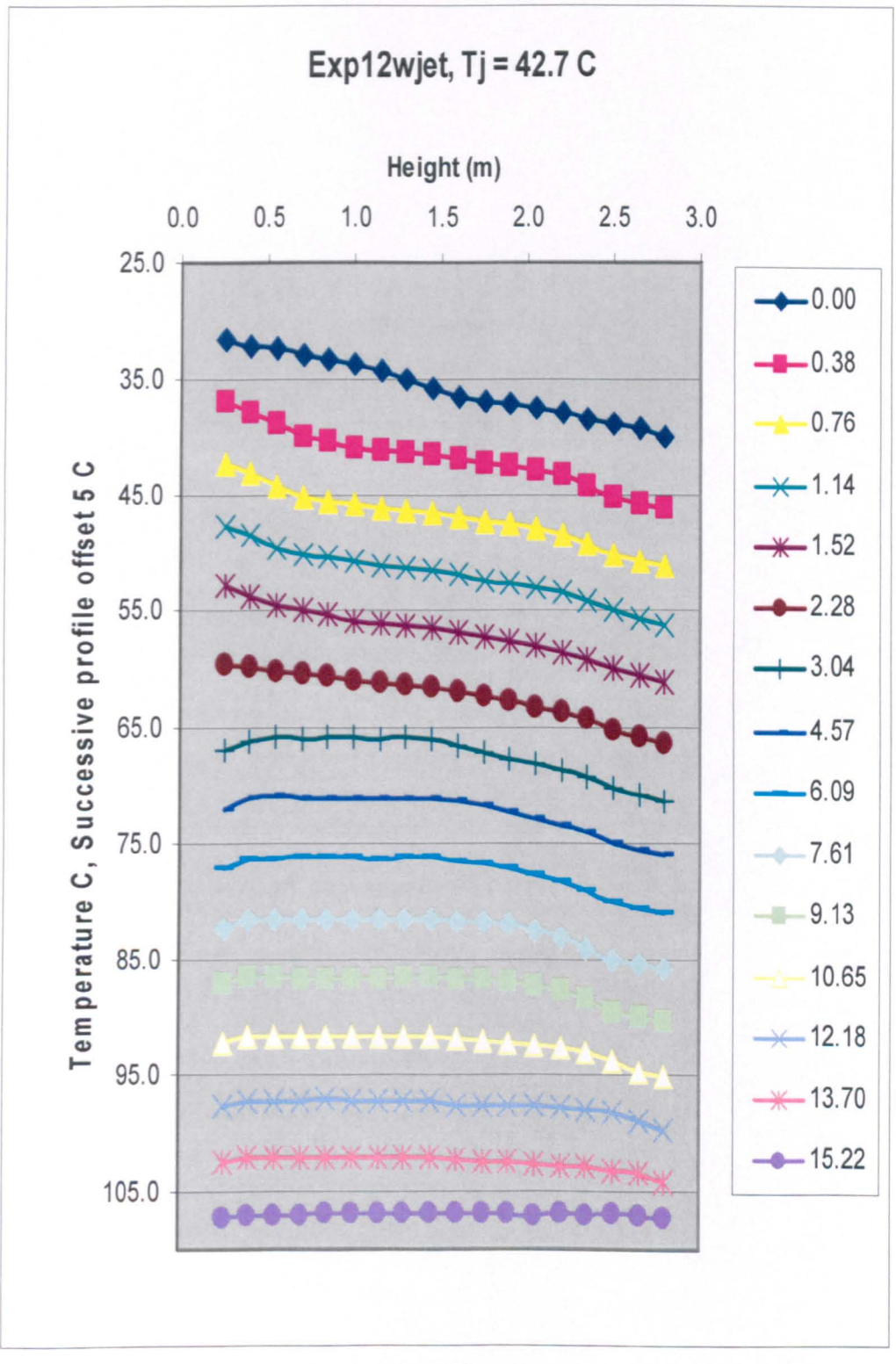

Figure A2.5.1: Illustrates vertical temperature profiles for various warm jet speeds. The flow was stratified at ($Q_h = 1.0\ m^3/min$) hot airflow rate and ($Q_c = 2.0\ m^3/min$) cold airflow rate at locations of 2.0 and 1.5 m respectively at the centre of environmental chamber.

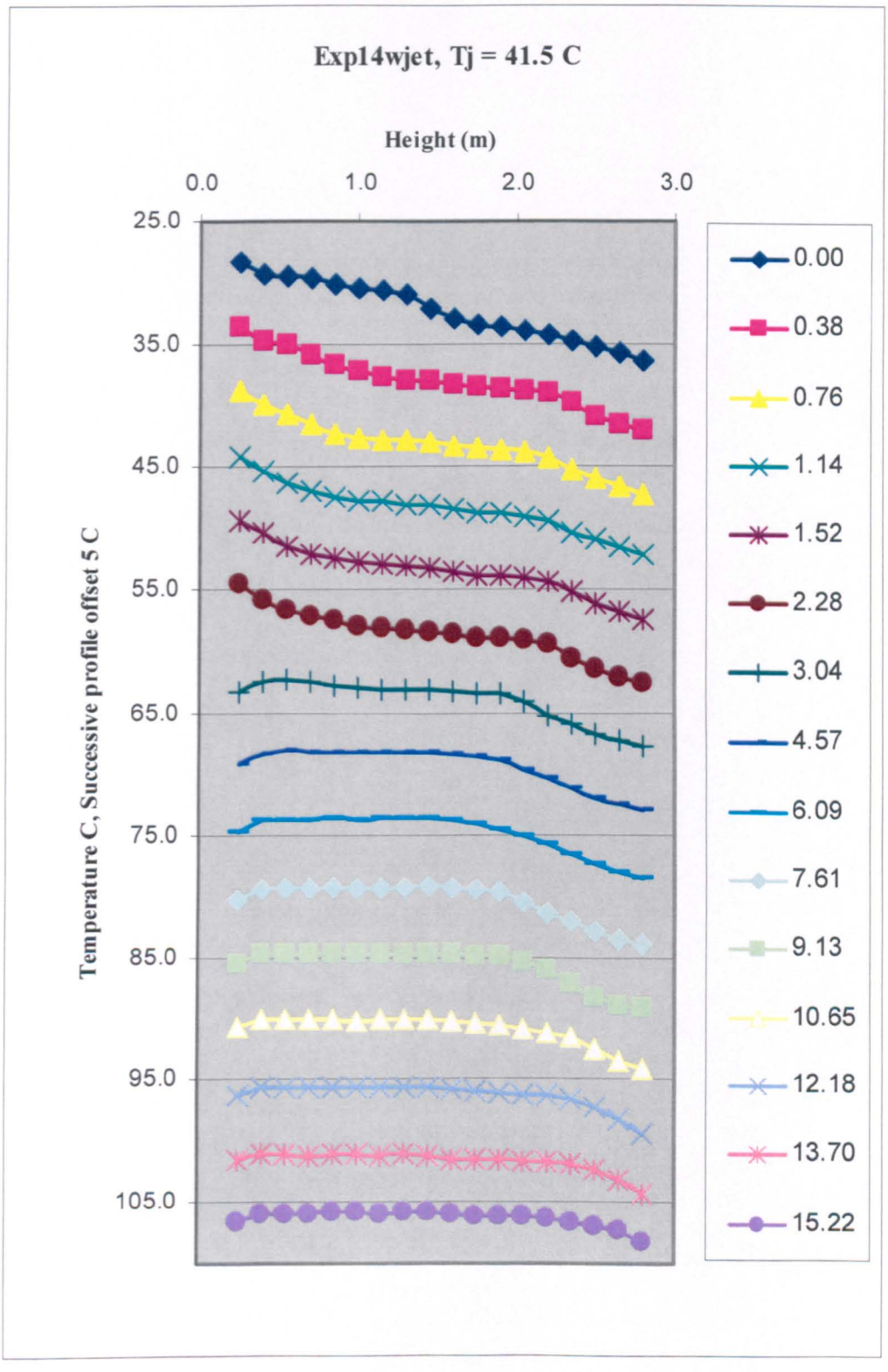

Figure A2.5.2: Illustrates vertical temperature profiles for various warm jet speeds. The flow was stratified at (Q_h = 1.0 m^3 / min) hot airflow rate and (Q_c = 4.0 m^3 / min) cold airflow rate at locations of 2.0 and 1.5 m respectively at the centre of environmental chamber.

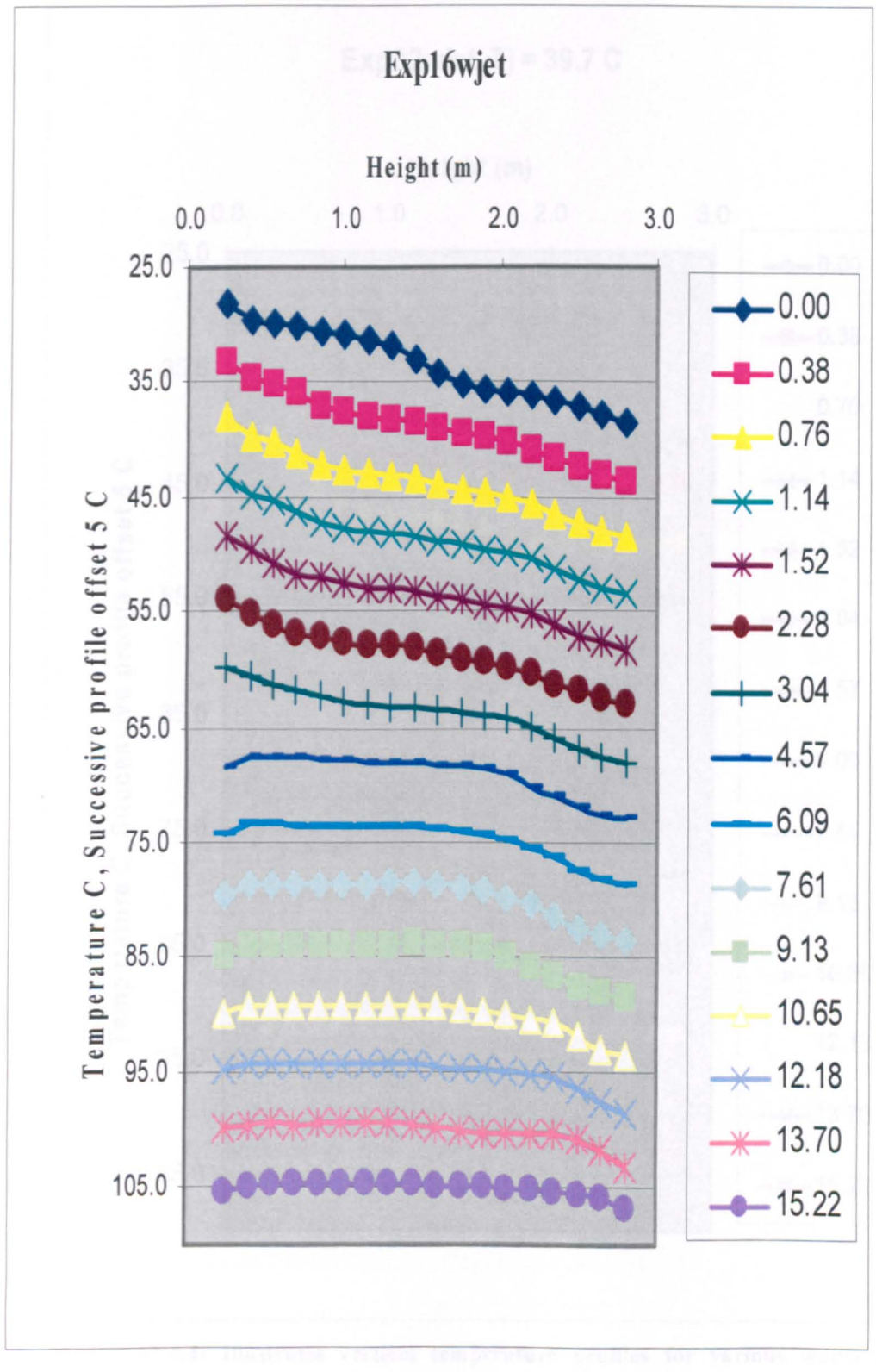

Figure A2.5.3: Illustrates vertical temperature profiles for various warm jet speeds. The flow was stratified at ($Q_h = 1.0\ m^3/min$) hot airflow rate and ($Q_c = 6.0\ m^3/min$) cold airflow rate at locations of 2.0 and 1.5 m respectively at the centre of environmental chamber.

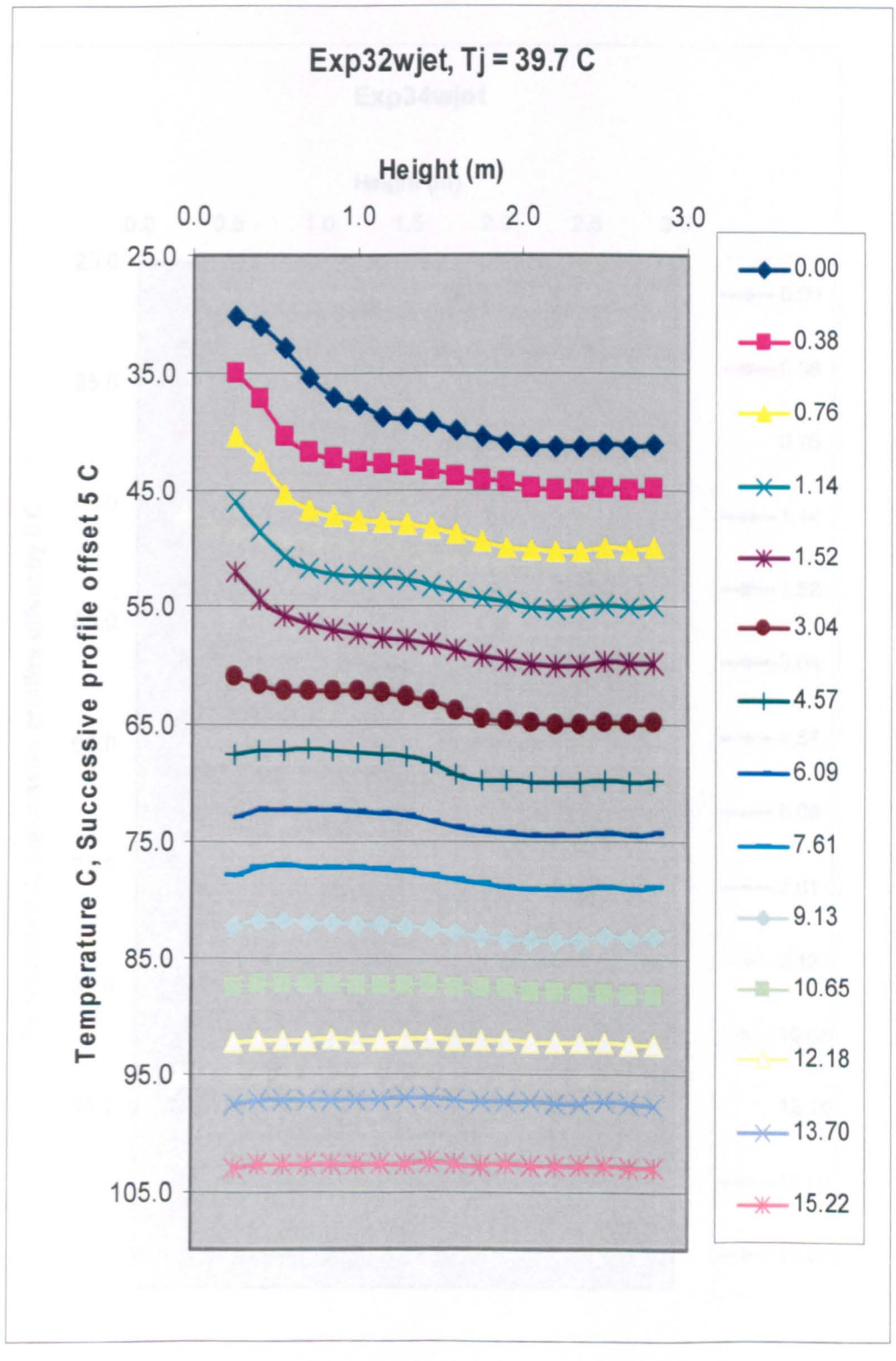

Figure A2.5.4: Illustrates vertical temperature profiles for various warm jet speeds. The flow was stratified at (Q_h = 3.0 m^3 / min) hot airflow rate and (Q_c = 2.0 m^3 / min) cold airflow rate at locations of 2.0 and 1.5 m respectively at the centre of environmental chamber

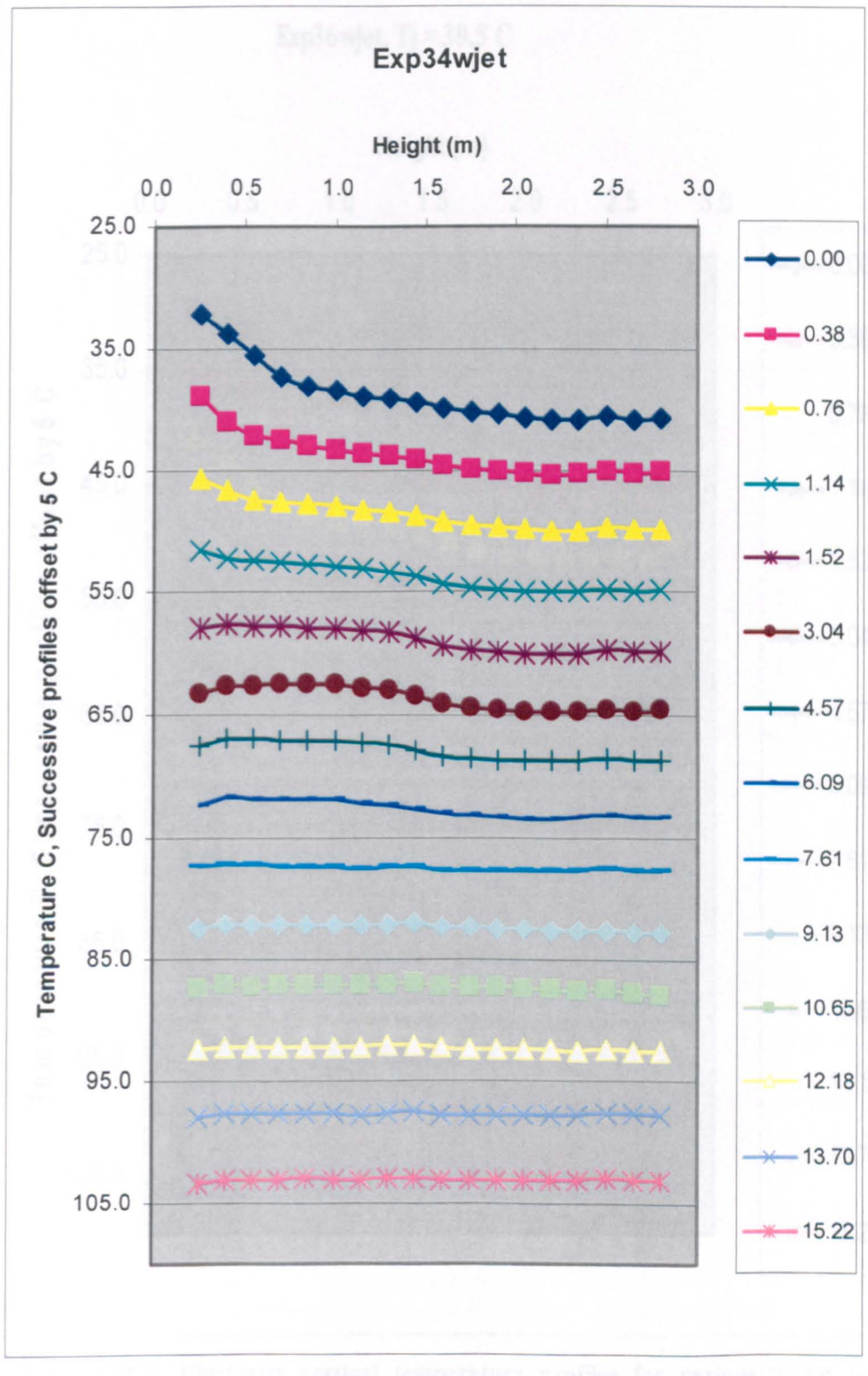

Figure A2.5..5: Illustrates vertical temperature profiles for various warm jet speeds. The flow was stratified at ($Q_h = 3.0\ m^3/min$) hot airflow rate and ($Q_c = 4.0\ \ m^3/min$) cold airflow rate at locations of 2.0 and 1.5 m respectively at the centre of environmental chamber.

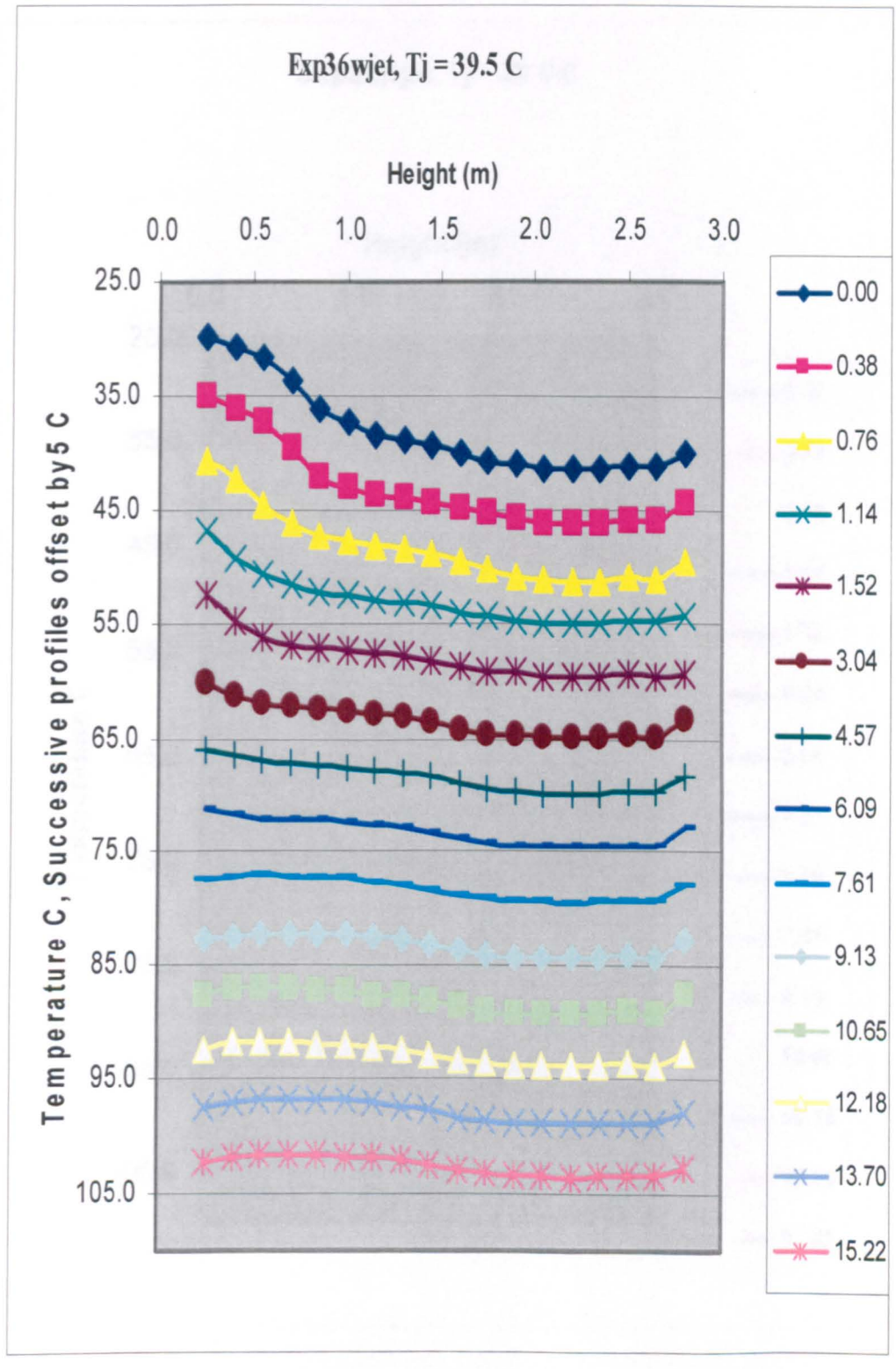

Figure A2.5.6: Illustrates vertical temperature profiles for various warm jet speeds. The flow was stratified at (Q_h = 3.0 m^3 / min) hot airflow rate and (Q_c = 6.0 m^3 / min) cold airflow rate at locations of 2.0 and 1.5 m respectively at the centre of environmental chamber

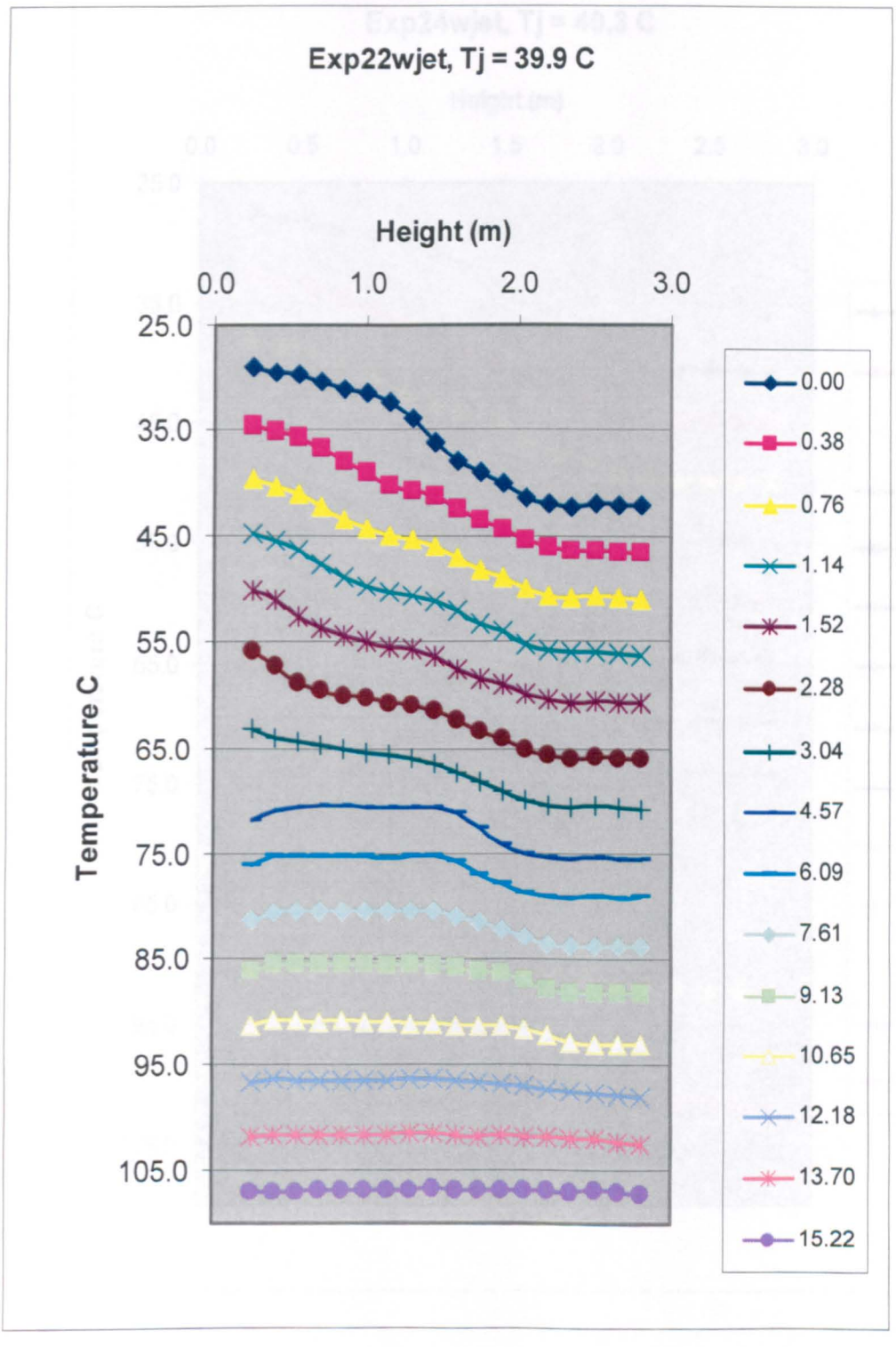

Figure A2.5.7: Illustrates vertical temperature profiles for various warm jet speeds. The flow was stratified at (Q_h = 2.0 m^3 / min) hot airflow rate and (Q_c = 2.0 m^3 / min) cold airflow rate at locations of 2.0 and 1.5 m respectively at the centre of environmental chamber.

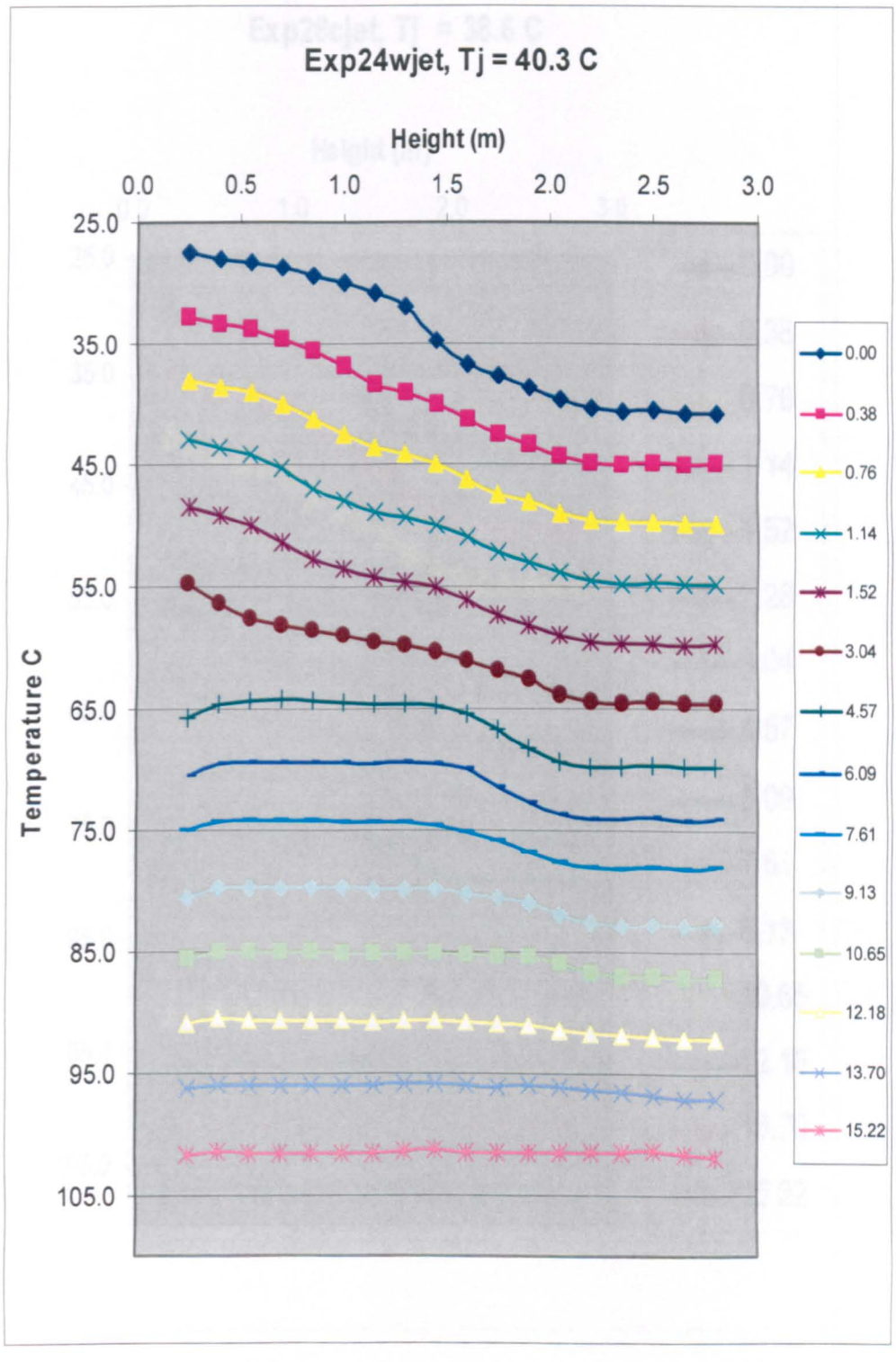

Figure A2.5.8: Illustrates vertical temperature profiles for various warm jet speeds. The flow was stratified at (Q_h = 2.0 m^3 / min) hot airflow rate and (Q_c = 4.0 m^3 / min) cold airflow rate at locations of 2.0 and 1.5 m respectively at the centre of environmental chamber.

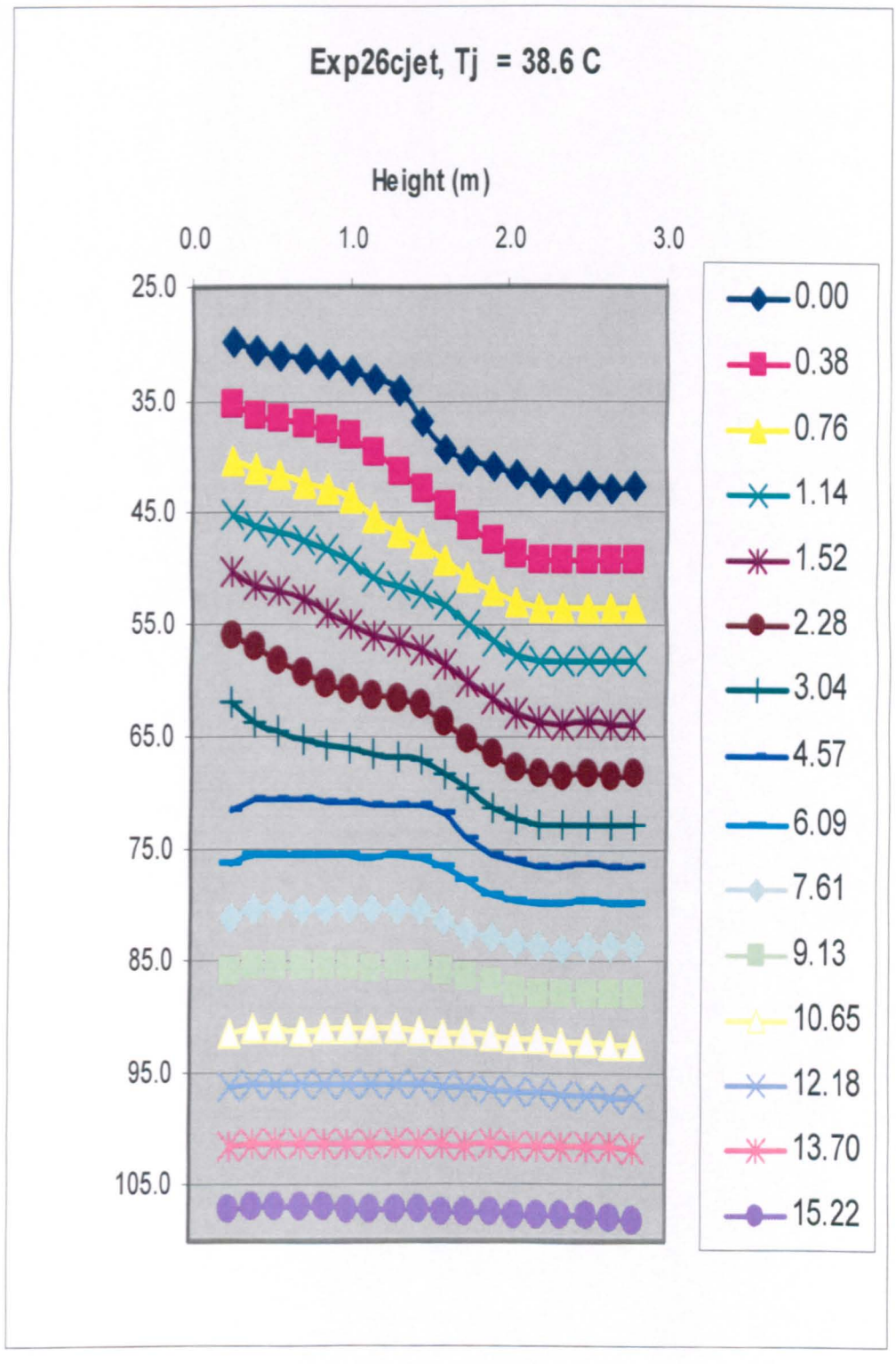

Figure A2.5.9: Illustrates vertical temperature profiles for various warm jet speeds. The flow was stratified at (Q_h = 2.0 m^3 / min) hot airflow rate and (Q_c = 6.0 m^3 / min) cold airflow rate at locations of 2.0 and 1.5 m respectively at the centre of environmental chamber.

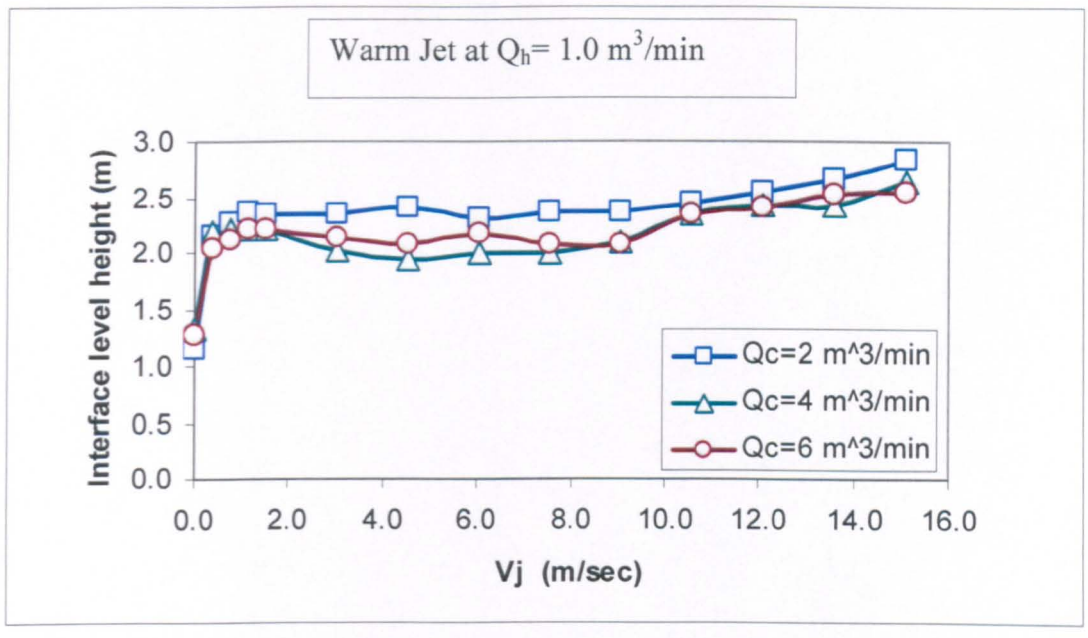

Figure A2.5.10: Comparison of interface level height with the jet speed, at hot airflow rate of Q_h = 1.0 m^3 / min and different cold airflow rates (Q_c = 2, 4 and 6 m^3 / min) in the environmental chamber.

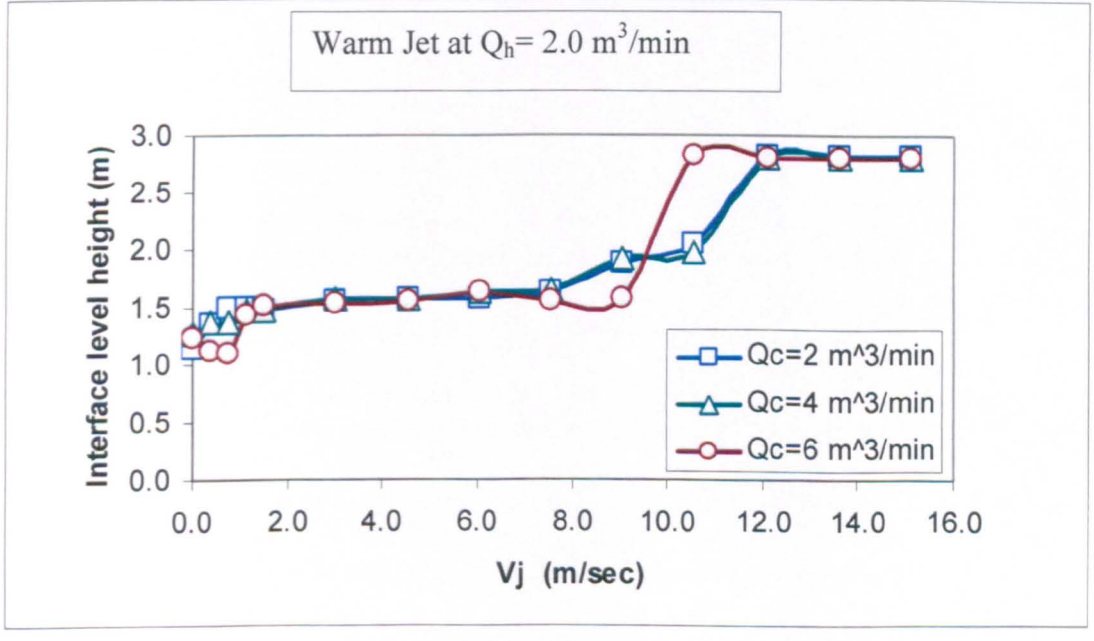

Figure A2.5.11: Comparison of interface level height with the jet speed, at hot airflow rate of Q_h = 2.0 m^3 / min and different cold airflow rates (Q_c = 2, 4 and 6 m^3 / min) in the environmental chamber.

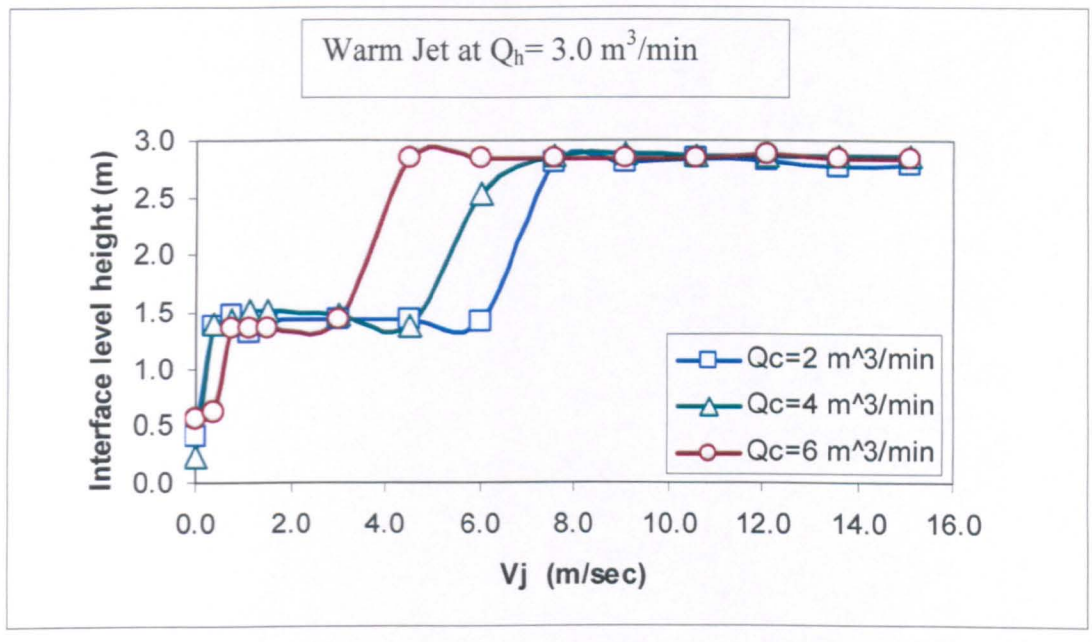

Figure A2.5.12: Comparison of interface level height with the jet speed, at hot airflow rate of Q_h = 3.0 m^3 / min and different cold airflow rates (Q_c = 2, 4 and 6 m^3 / min) in the environmental chamber.

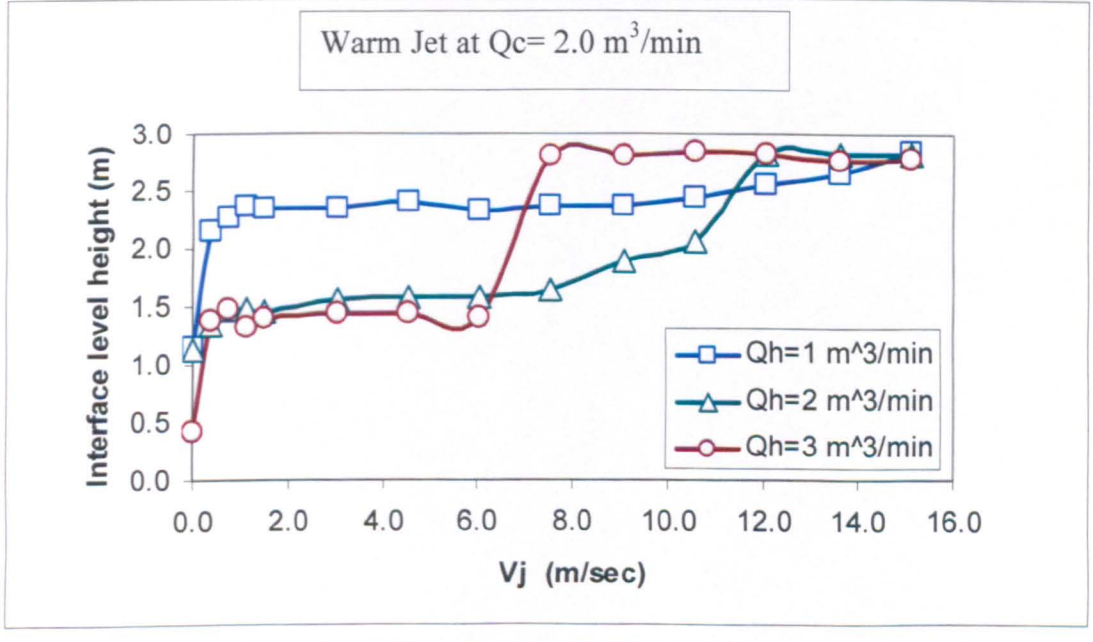

Figure A2.5.13: Comparison of interface level height with the jet speed, at cold airflow rate of Q_c = 2.0 m^3 / min and different hot airflow rates ()Q_h = 1, 2 and 3 m^3 / min in the environmental chamber.

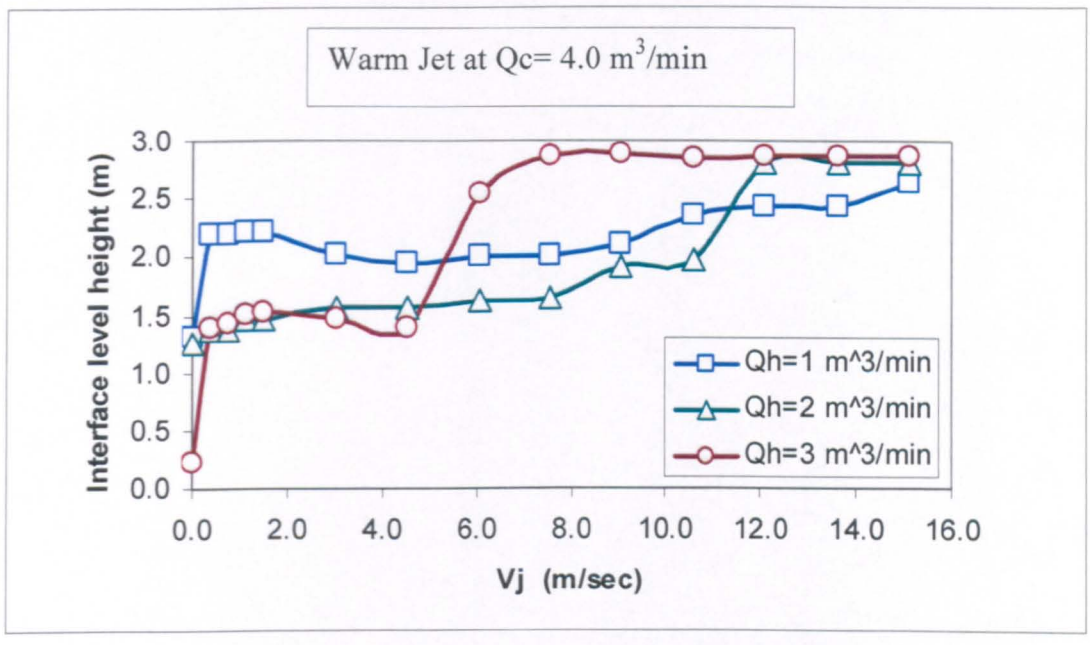

Figure A2.5.14: Comparison of interface level height with the jet speed, at cold airflow rate of $Q_c = 4.0\ m^3/min$ and different hot airflow rates ($Q_h = 1, 2$ and $3\ m^3/min$) in the environmental chamber.

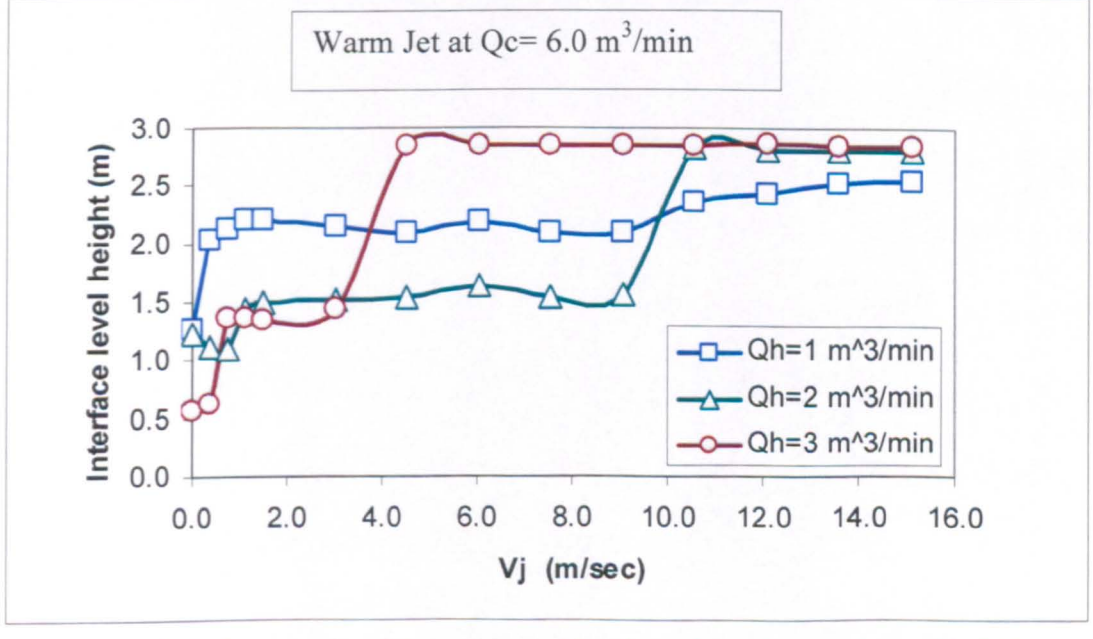

Figure A2.5.15: Comparison of interface level height with the jet speed, at cold airflow rate of $Q_c = 6.0\ m^3/min$ and different hot airflow rates ($Q_h = 1, 2$ and $3\ m^3/min$) in the environmental chamber.

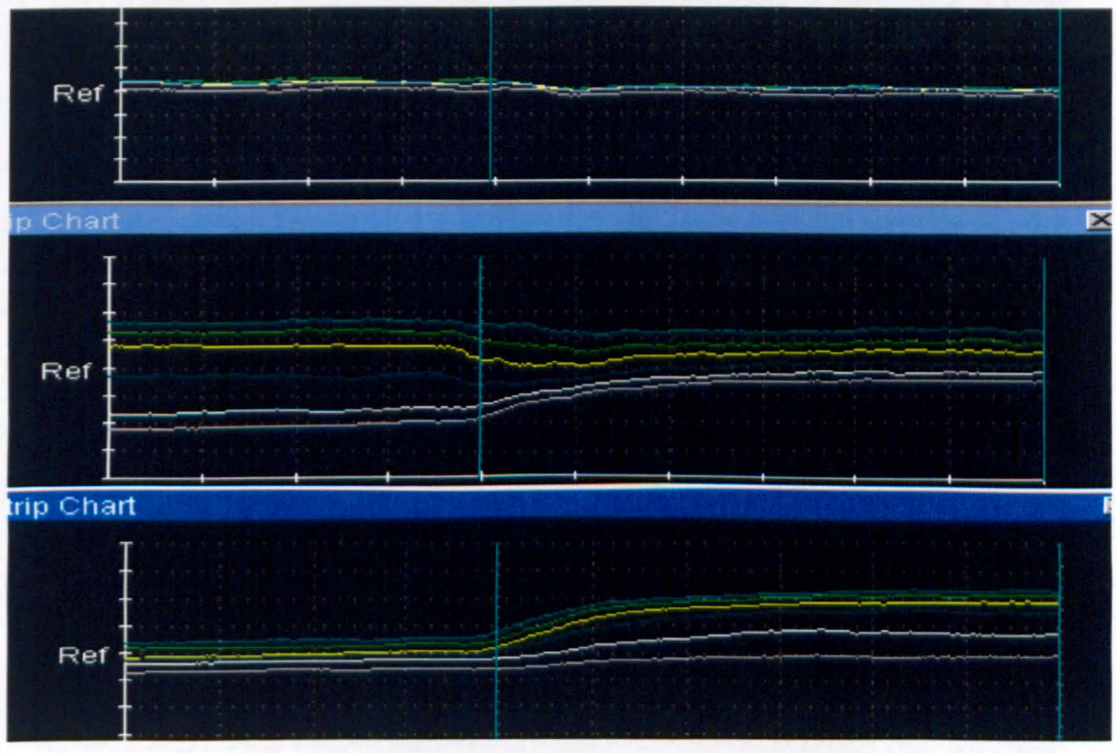

Figure A2.5.16: Temperature visualization showing the stratified flow with initial cold and hot airflow rates of 2 and $6\,m^3/min$, Richardson number of 2.0 and Reynolds number of 2008, and the effect of warm jet flow of ($V_j = 3.0\ m/sec$).

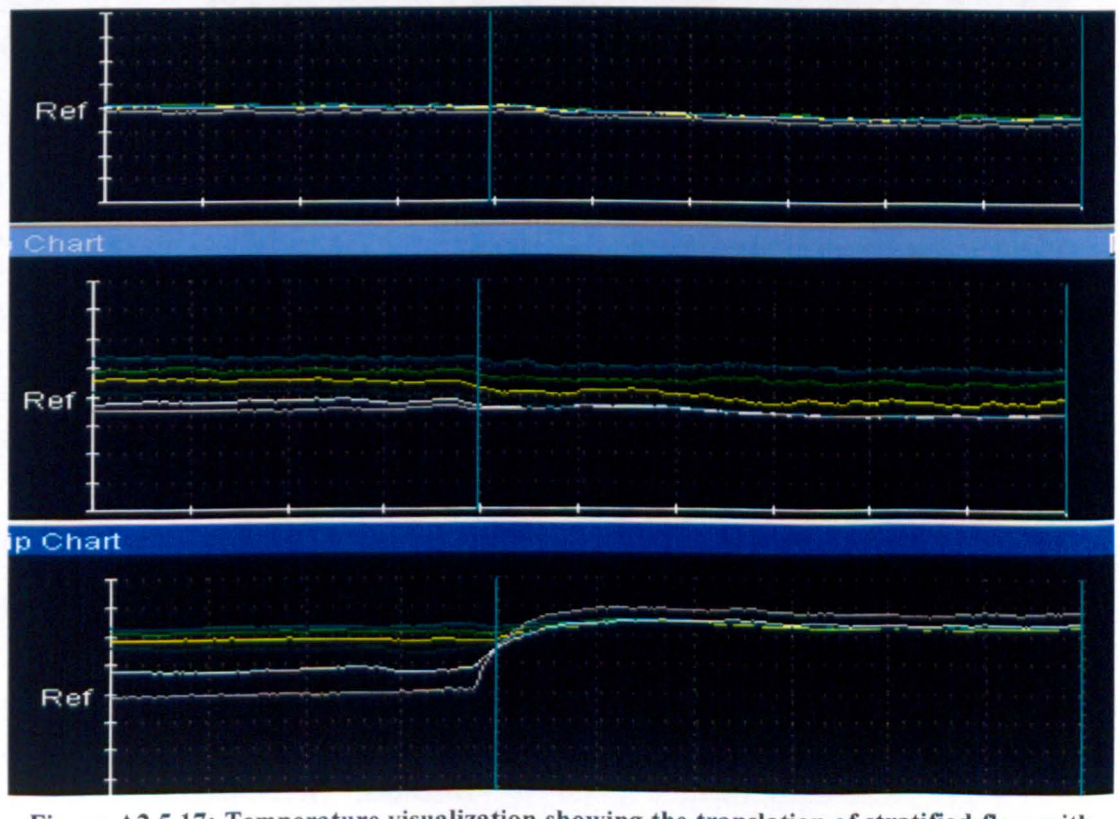

Figure A2.5.17: Temperature visualization showing the translation of stratified flow with (initial cold and hot airflow rates of 2 and $6\,m^3/min$, Ri of 2.0 and Reynolds number of 2008) from warm jet flow of ($V_j = 3.0\ m/sec$) to ($V_j = 6.0\ m/sec$).

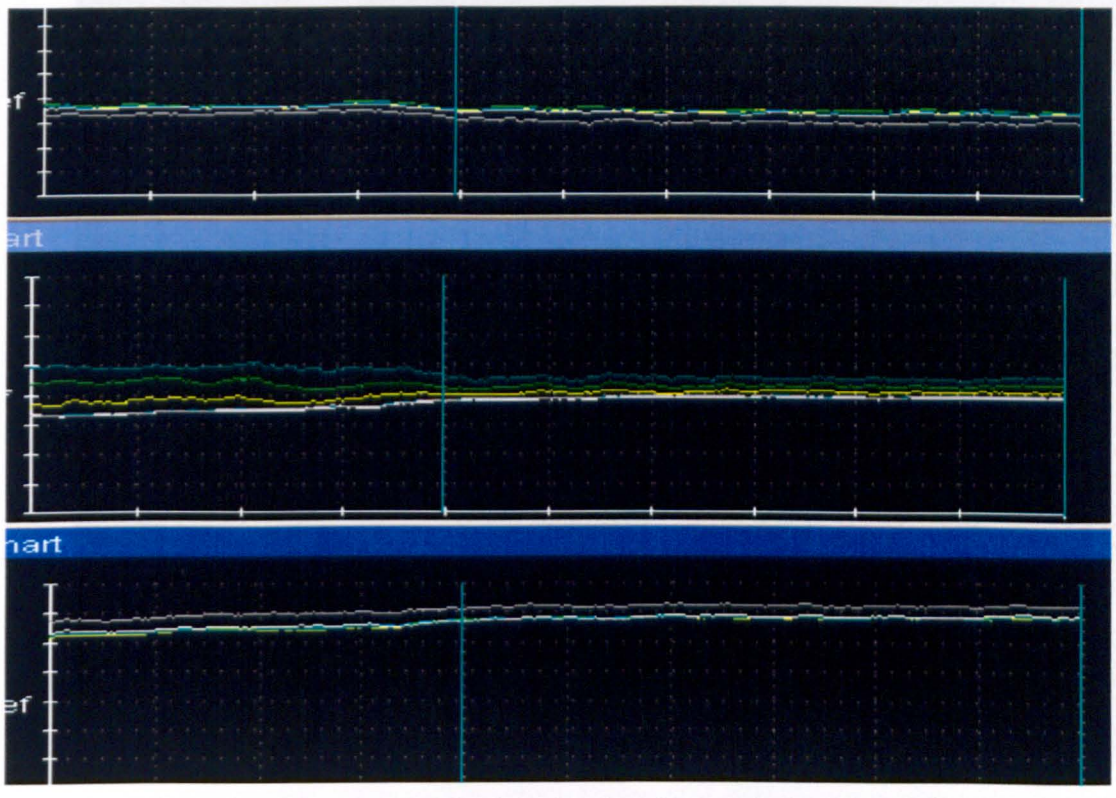

Figure A2.5.18: Temperature visualization showing the translation of stratified flow with (initial cold and hot airflow rates of 2 and $6\,m^3/min$, Ri of 2.0 and Reynolds number of 2008) from warm jet flow of ($V_j = 6.0\ m/sec$) to ($V_j = 9.0\ m/sec$).

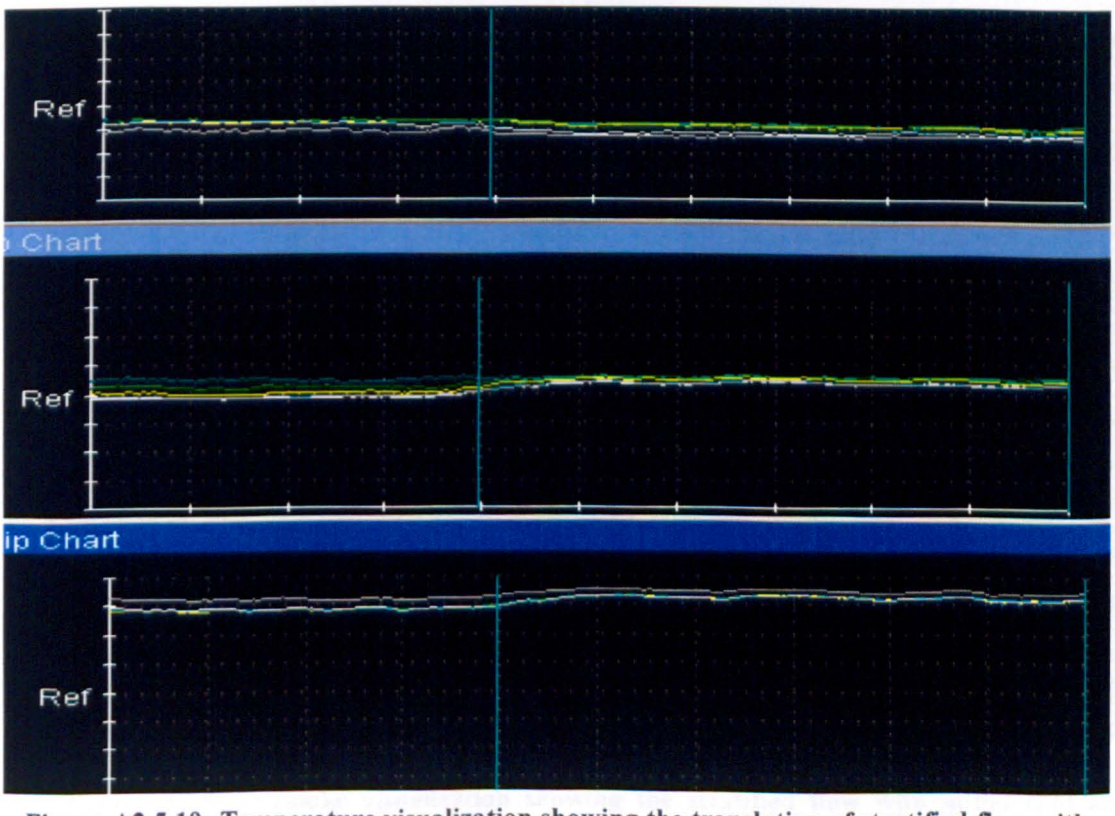

Figure A2.5.19: Temperature visualization showing the translation of stratified flow with (initial cold and hot airflow rates of 2.0 and $6.0\,m^3/min$, Ri of 2.0 and Reynolds number of 2008) from warm jet flow of ($V_i = 9.0\ m/sec$) to ($V_i = 12.0\ m/sec$).

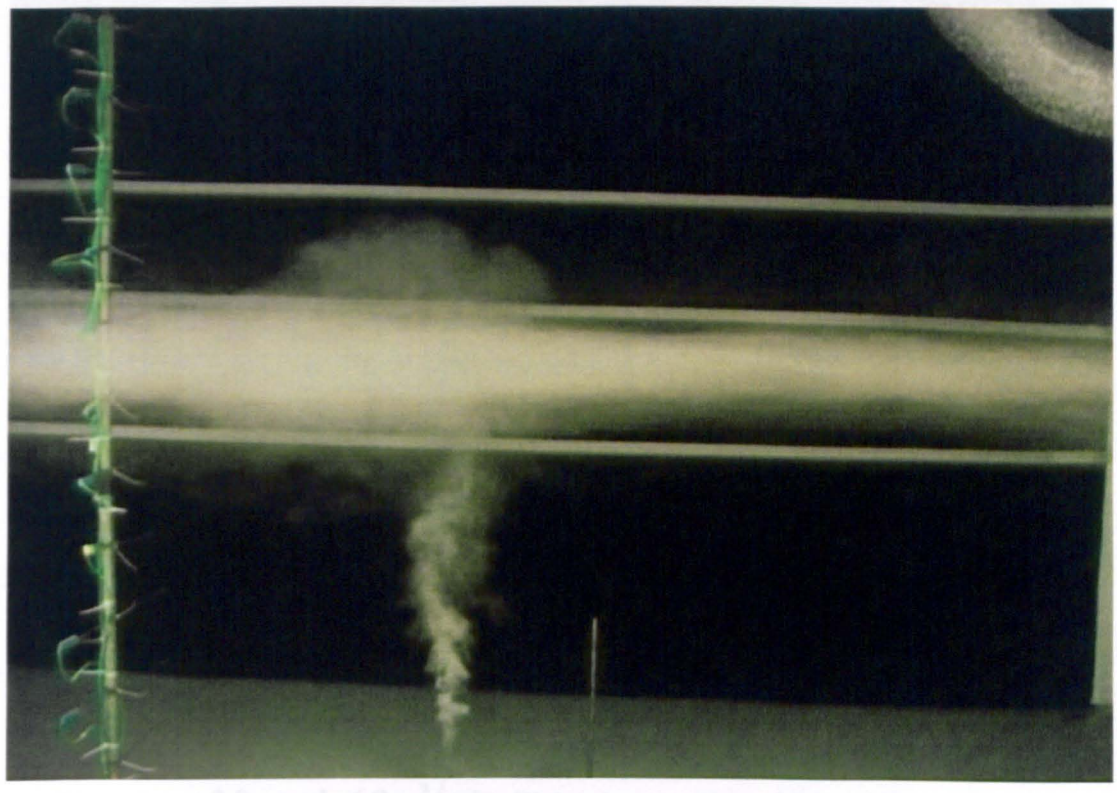

Figure A2.5.20: Smoke visualization showing the stratified flow with initial cold and hot airflow rates of 2.0 and $6.0\,m^3/min$, Richardson number of 2.0 and Reynolds number of 2008, and the effect of warm jet flow of ($V_j = 0.0\ m/sec$).

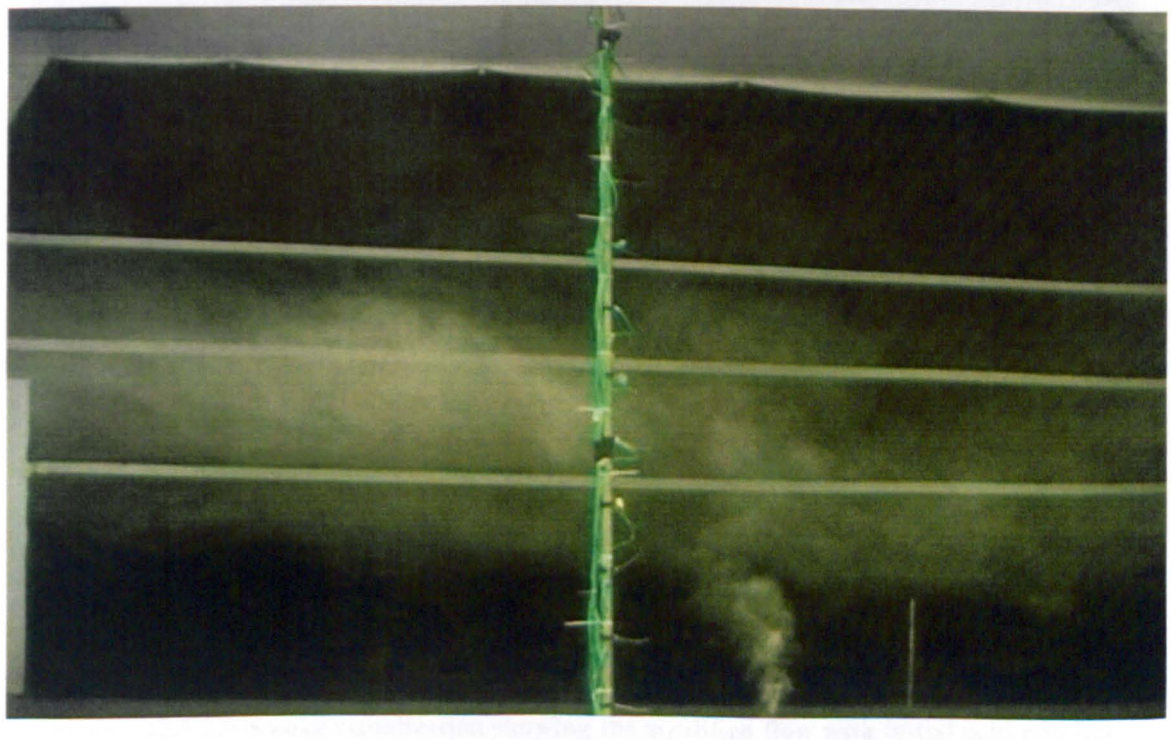

Figure A2.5.21: smoke visualization showing the stratified flow with initial cold and hot airflow rates of 2.0 and $6.0\,m^3/min$, Richardson number of 2.0 and Reynolds number of 2008, and the effect of warm jet flow of ($V_j = 3.0\ m/sec$).

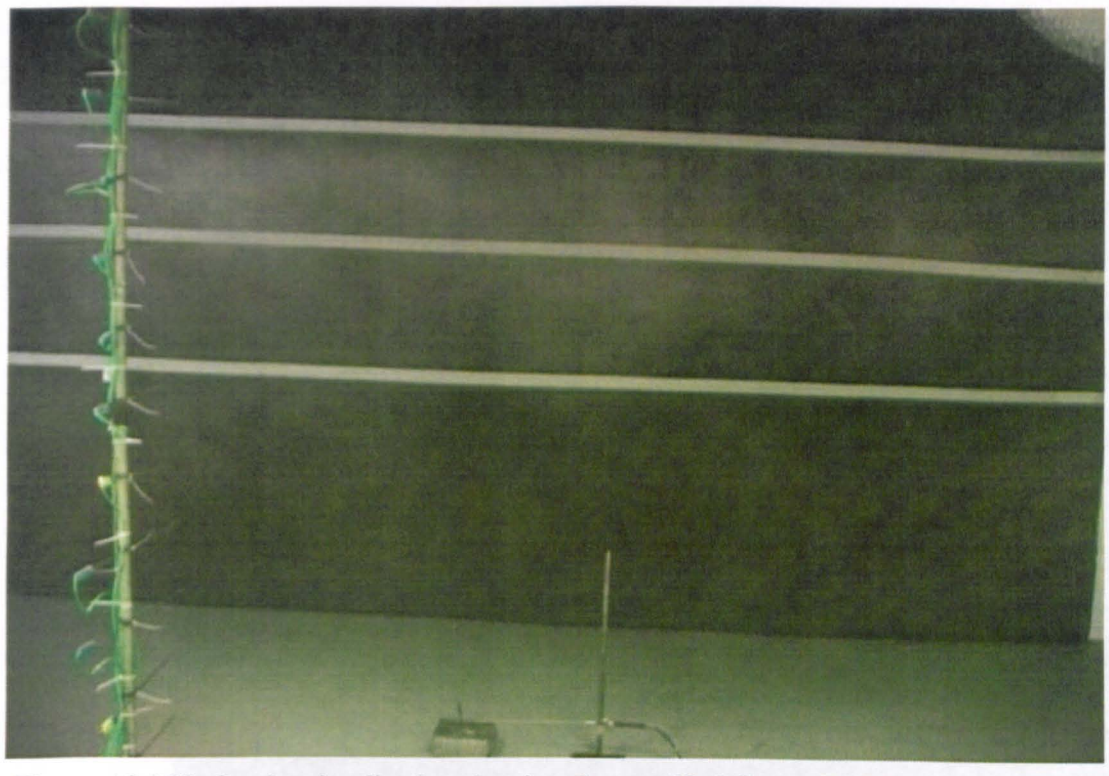

Figure A2.5.22: Smoke visualization showing the stratified flow with initial cold and hot airflow rates of 2.0 and $6.0\,m^3/min$, Richardson number of 2.0 and Reynolds number of 2008, and the effect of warm jet flow of ($V_j = 6.0$ m/sec).

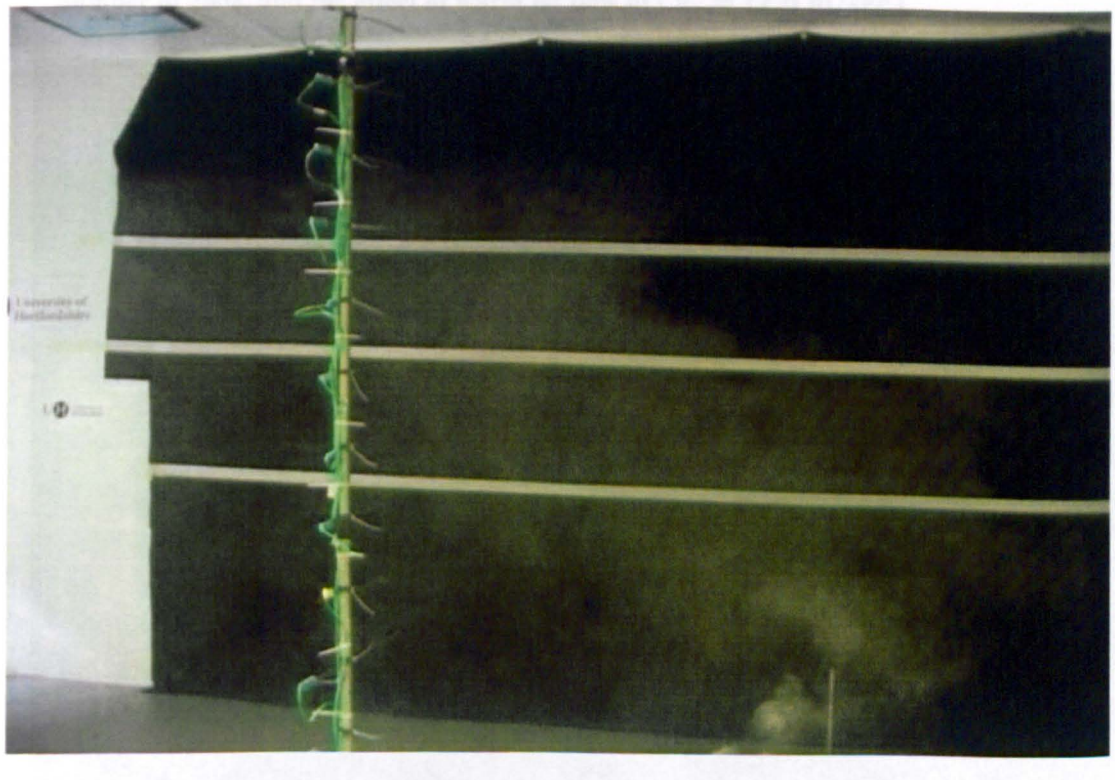

Figure A2.5.23: Smoke visualization showing the stratified flow with initial cold and hot airflow rates of 2.0 and $6.0\,m^3/min$, Richardson number of 2.0 and Reynolds number of 2008, and the effect of warm jet flow of ($V_j = 9.0$ m/sec).

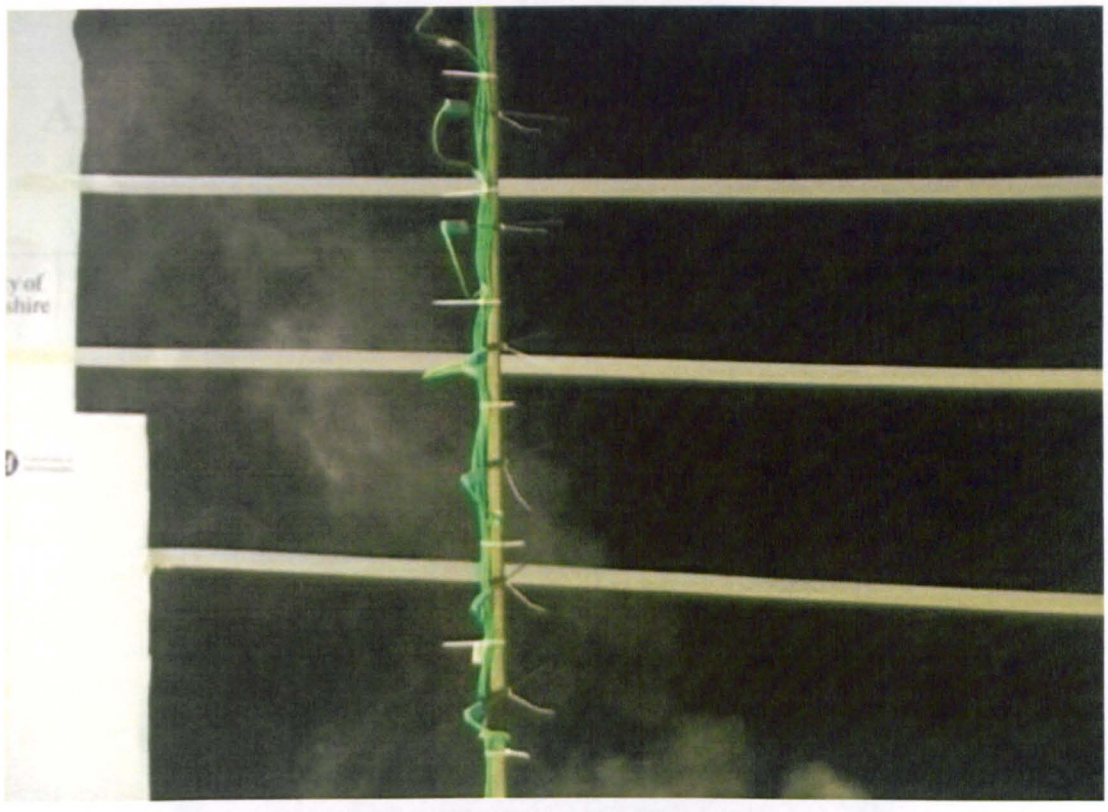

Figure A2.5.24: Smoke visualization showing the stratified flow with initial cold and hot airflow rates of 2.0 and $6.0\,m^3/min$, Richardson number of 2.0 and Reynolds number of 2008, and the effect of warm jet flow of ($V_j = 12.0\ m/sec$).

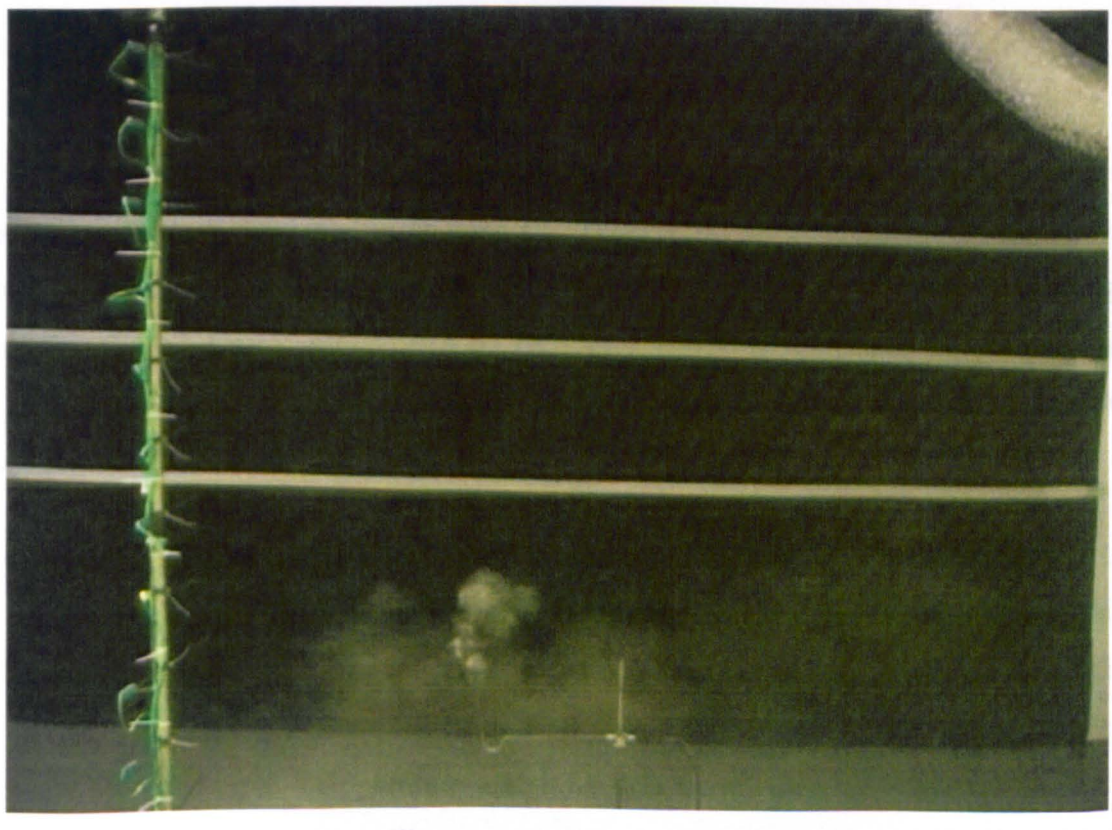

Figure A2.5.25: Smoke visualization showing the stratified flow with initial cold and hot airflow rates of 2.0 and $6.0\,m^3/min$, Richardson number of 2.0 and Reynolds number of 2008, and the effect of warm jet flow of ($V_j = 15.0\ m/sec$).

Appendix A3.1

Agilent 34970A Data Acquisition/Switch Unit

Agilent BenchLink 34970A Data Acquisition/Switch Unit

Eexperimental set-up described in chapter 3 consists of a data acquisition system and a personal computer. The data acquisition system used was the Agilent 34970A Data Acquisition/Switch Unit manufactured by Hewlett-Packard (Palo Alto, CA) (Appendix A3.1), connected to a personal computer, with the corresponding computer software entitled Agilent Benchlink Data Logger.

The Agilent data logger has 60 channels for data input. For this experiment, 20 channels were configured to type K thermocouples. The software allowed the data to be read and plotted in real time on the computer screen. An acquisition time of 10 and 60 seconds were chosen. The 20 channels used do not take data at the same instant in time, but rather one after the next. Temperature and time data could then be exported between tests to appropriate spreadsheet files on a personal computer using an RS232 60601 cable for more analysis.

Agilent 34970A
Data Acquisition/Switch Unit
Product Overview

Agilent performance at a fraction of the cost of other standalone data acquisition systems

Agilent Technologies
Innovating the HP Way

Table of Contents

Price and performance beyond compare

Go ahead and compare the Agilent Technologies 34970A Data Acquisition/Switch Unit with other DAC systems currently available. You'll find it hard to come up with a system that offers the powerful measurement performance, flexibility, and ease of use of the 34970A—even in systems costing three to five times as much.

How did we manage to pack so much performance into such a low-cost instrument? We borrowed technology developed for our top-of-the-line products and put it into a package that cuts assembly time, incorporates custom ICs to reduce parts count, and simplifies production testing. That means it costs us less to make. The results? You spend less without sacrificing quality or performance.

What can you expect from a data acquisition system that's this affordable?

Measurements you can trust

We took the measurement engine from our best-selling benchtop DMM and embedded it inside a 3-slot cardcage. You get the benefit of proven Agilent measurement performance, universal inputs with built-in signal conditioning, and modular flexibility, all in a low-cost, compact data acquisition package. The 34970A features 6½ digits (22 bits) of resolution, 0.004% basic dcV accuracy, and ultra-low reading noise. Combine that with scan rates of up to 250 channels/sec, and you've got the speed and accuracy you need to get the job done right the first time.

Powerful flexibility to get your job done

Whether you need to measure temperature, ac/dc volts, resistance, frequency, or current, the 34970A can handle it. The internal autoranging DMM directly measures 11 different functions, eliminating the need for expensive external signal conditioning. And our unique design allows complete per-channel configurability for maximum flexibility and quick, easy set up. It's like having an independent, high-performance DMM behind each channel.

Custom configurations that grow with you

Three module slots and eight switch/control modules allow you to customize the 34970A to meet your unique requirements. Buy only what you need—and add more modules later as your application grows.

Unequaled ease of use

From the simplified configuration procedures, to the self-guiding front panel interface, we put in extra time and energy to save yours. Simple things like on-module screw-terminal connectors, built-in thermocouple reference junctions, well-organized user documentation full of examples and hints, and a standard Getting Started kit that will have you making measurements 15 minutes out of the box all add up to increased productivity, whether you use the instrument every day or only now and then.

Free software to save you time and money

Now you don't have to spend your valuable time writing or configuring software. HP BenchLink Data Logger software gives you a familiar Microsoft Windows® interface for test configuration and real-time data display and analysis. Even better, this full-featured data logging application is included free with every standard Agilent 34970A.

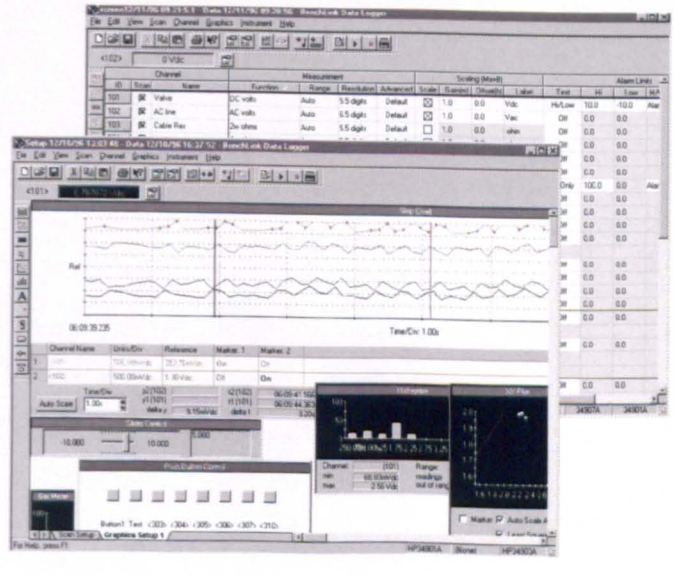

More power and flexibility than you ever imagined you could afford

Intuitive front panel: task-oriented, self-guiding menus

6½-digit (22-bit) internal DMM measures 11 functions without external signal conditioning

50k readings of non-volatile memory holds data when power is removed

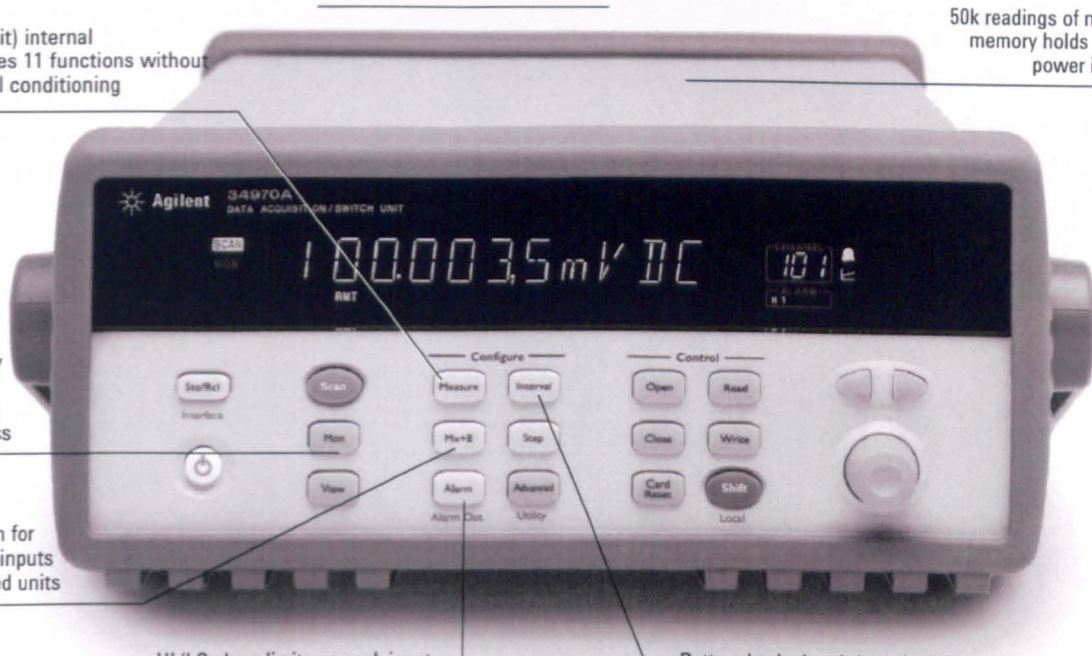

Monitor display mode lets you keep an eye on tests in progress

Scaling function for converting raw inputs into user-defined units

HI/LO alarm limits on each input channel, plus 4 TTL alarm outputs

Battery-backed real-time clock for pacing scans and timestamping readings

3-year warranty to protect your investment

3-slot mainframe offers up to 96 matrix crosspoints or 120 single-ended channels

HP BenchLink Data Logger software included; drivers available for Agilent VEE and National Instruments LabVIEW®

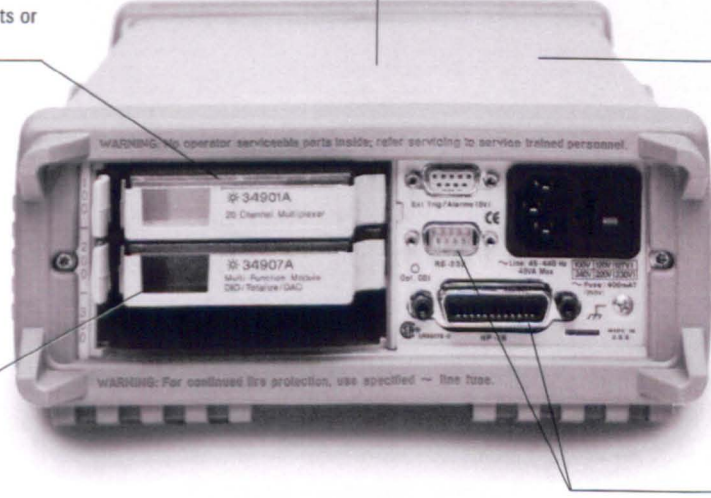

8 switch and control plug-in modules to choose from

Built-in GPIB and RS-232 interfaces

The Agilent 34970A offers unequaled versatility for your data acquisition applications

In the past, you had to make a choice. On the one hand, you could choose the simple operation and low cost of a data logger. On the other hand, you had the flexibility and higher performance of a modular data acquisition system. The Agilent 34970A Data Acquisition/Switch Unit gives you the best of both worlds: a simple user interface with low per-channel cost, modular flexibility, and impressive measurement performance.

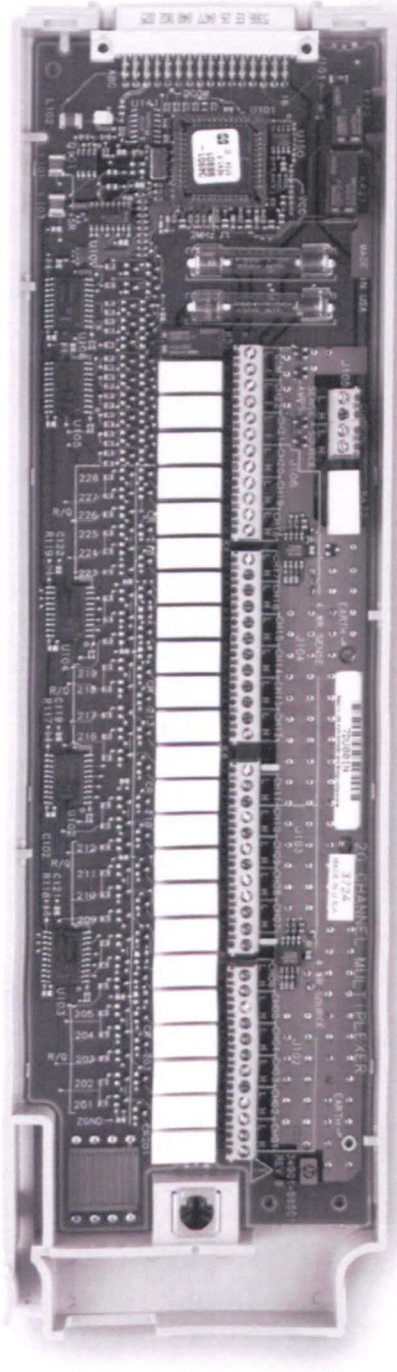

Whether you're an R&D engineer working on characterizing your latest design, or a manufacturing engineer building a test system or troubleshooting a process, the 34970A Data Acquisition/Switch Unit offers the best combination of price and measurement performance.

It's a data logger:
Configured with a 20-channel relay multiplexer, the 34970A becomes a powerful, low-cost data logger for simple characterization applications—one that's quick to set up and easy to run. For more information on using the 34970A for data logging applications, see page 6.

It's a data acquisition front-end:
The 34970A is an automated test system with excellent measurement performance—it's got the accuracy, resolution, and speed you need. See page 8 for application information.

It's a switch system:
Order the mainframe without the internal DMM and you've got an even lower cost, high-quality signal routing solution. See page 10 for details.

An easy-to-use data logger for monitoring and characterization applications

Data loggers are used to monitor multiple signals (temperature, voltage, etc.) over extended periods of time to identify irregularities. Example applications include environmental chamber monitoring, component inspection, benchtop testing, process troubleshooting, and temperature profiling.

The Agilent 34970A is easy to use for a multitude of data logging and monitoring applications, either stand-alone or with a computer. Its flexible, modular design makes it scalable from 20 to 120 channels, and lets you add actuator, digital I/O, and analog output channels for simple control. Its small size and ruggedized features make it perfect for portable applications, and its small footprint makes it ideal for cramped benchtop testing. Standard GPIB (IEEE 488) and RS-232 interfaces let you program the instrument if you wish to automate tests.

Better measurements with fewer hassles

Tired of putting up with the mediocre measurement performance you get with most data loggers or plug-in data acquisition boards? The 34970A offers 6½ digits of resolution and 0.004% basic 1-year dcV accuracy.

Simplify your data gathering with HP BenchLink Data Logger software

Do you want PC-based data logging capability, but don't want to spend hours programming? HP BenchLink Data Logger software is the answer. This Windows®-based application is designed to make it a snap to use your PC for gathering and analyzing measurements. Use it to set up your test, acquire and archive measurement data, and perform real-time display and analysis of the incoming measurements.

A familiar spreadsheet environment makes it easy to configure and control your tests. And a rich set of colorful graphics provides many options for analyzing and displaying your data–all with point-and-click ease. Set up multiple graphics using strip charts, histograms, X-Y scatter charts, alarm lights, and more. And of course you can use HP BenchLink Data Logger to easily move data to other applications for further analysis, or for inclusion in your presentations and reports.

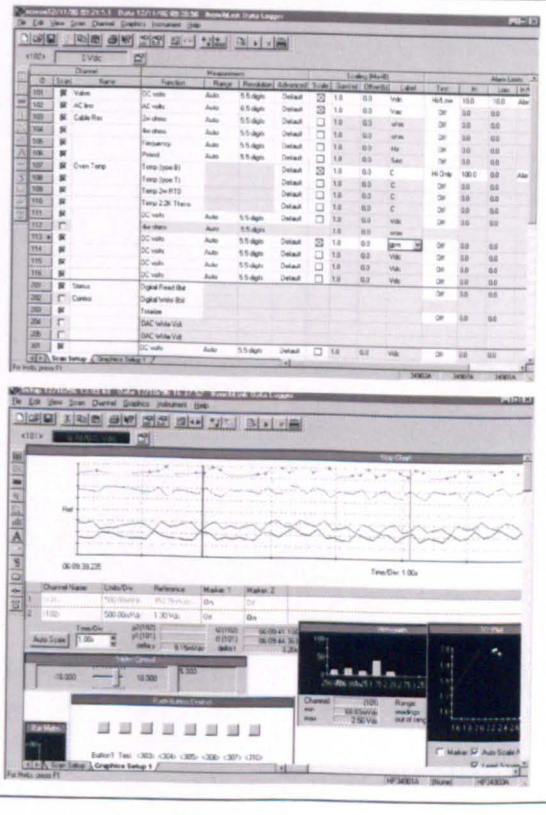

And the 34970A measures and converts 11 different input signals:

- temperature with thermocouples, RTDs, and thermistors
- dc and ac volts
- 2- and 4-wire resistance
- frequency and period
- dc and ac current

What's more, each channel is independently configurable. This means you can configure channel 1 for dcV, channel 2 for a K-type thermocouple, and channels 3 and 13 for a 4-wire RTD measurement–all on the same module, all in a single scan. For custom linear conversions, use the Mx+B scaling function on any channel. You can even display a custom 3-character engineering label like RPM or PSI to identify your measurement units.

Versatile alarms
Alarms are available on a per-channel basis as well. Enter a high limit, a low limit, or both. The 34970A compares each reading to its limits and flags any out-of-range measurements. You can assign one of four TTL alarm outputs to any input channel to trigger external alarm lights, sirens, or send a TTL pulse to your control system, all without a PC connected.

Scanning made simple
The 34970A automatically builds a scan list that includes all configured inputs (even digital inputs from the Agilent 34907A multifunction module) in ascending order by channel number. You can pace scans by setting the 34970A's internal timer for automatic scanning at a specific interval, by manually pressing a front-panel button, or by sending a software command or external TTL trigger pulse.

Monitor any input
A special display mode monitors a selected input channel, continuously updating the display with new readings—even during a scan. It's great for keeping an eye on a key input, or for troubleshooting your system before a test.

Nonvolatile memory adds convenience, portability
All readings are automatically time-stamped and stored in a nonvolatile 50,000-reading memory–enough memory to hold more than a week's worth of data (20 channels scanned every five minutes). The nonvolatile memory holds your data even after power is removed, so you can use the 34970A to collect data at a remote location for later uploading to a PC. And because the nonvolatile memory also holds your system configuration, if you lose power in the middle of a test, the 34970A resumes scanning when power is returned.

Data Logging Feature Checklist
- From 1 to 120 channels of analog input
- Measurements include dc volts, ac volts, thermocouple, thermistor and RTD temperature measurements, 2- and 4-wire Ohms, dc current, ac current, frequency, and period
- 6½ digits (22 bits) of resolution with 0.004% basic 1-year dcV accuracy
- 50k reading nonvolatile memory including timestamp
- Scaling and alarms available on each channel
- Full-featured front panel for stand-alone configuration, troubleshooting, and data viewing
- HP BenchLink Data Logger software for configuration and data analysis
- Nonvolatile storage for five complete instrument states

A powerful, flexible data acquisition system for automated test

The 34970A gives you the resolution, accuracy, repeatability, and speed you've come to expect from an Agilent data acquisition system. It provides the measurement muscle you need, along with signal routing and control capability, in a flexible, modular format that can grow and change to match your varied applications.

Powerful measurements

The internal 6½-digit DMM brings the power and performance of a world-class stand-alone DMM to the 34970A, but at a fraction of the cost and in a fraction of the space. It's as accurate as the best bench DMM available: 0.004% basic 1-year dcV accuracy, 0.06% basic 1-year acV accuracy, and 0.01% basic 1-year resistance accuracy. Our patented Multi-slope III A-D technology offers incredible linearity (2 ppm of reading +1 ppm of range) along with 22 bits of real resolution. And since it is an integrating A/D, it provides excellent noise rejection as well–a nice change from noisy PC plug-ins and sampling A/Ds. No more averaging lots of samples just to see the real data you wanted. And if you need high scan rates, the 34970A is capable of delivering fully converted measurements at speeds up to 250 ch/s.

The input section of the DMM is optically isolated and shielded from the 34970A's earth-referenced circuitry and computer interface, offering up to 300 V of input isolation. This is important for reducing ground loop and common mode voltage errors associated with long wiring runs and floating measurement sources.

Flexible functionality

The DMM is installed inside the chassis rather than in one of the slots, leaving all three mainframe slots free for switch and control modules. You can choose from eight different modules (see page 11) to get the precise functionality you need now–while giving you flexibility for future expansion.

The internal DMM gives you the flexibility to measure 11 types of inputs easily and inexpensively. The built-in signal conditioning and conversion routines turn raw inputs directly into real information. Each measurement channel is independently configurable, so you can set different measurement functions, scale factors and alarm limits, even on adjacent channels. Advanced measurement features such as offset compensation, variable integration time, and delay are also selectable on a per-channel basis.

Get better measurements with built-in signal conditioning

The Agilent 34970A architecture offers advantages over other data acquisition solutions which rely on external or plug-in signal conditioning modules for handling functions other than dcV:

- Minimizes external wiring and the resultant potential for noise and errors to enter your system
- Reduces hidden costs and overall system cost by avoiding unnecessary cables, breakout boxes and signal conditioning elements
- Simplifies your configuration–for faster, easier setup–with fewer connections and components
- Takes the guesswork out of error analysis. Measurement accuracies are specified to include all system-related errors
- Improves reliability, with fewer interconnects and fewer parts that can fail

Software drivers
Your months of test system software development time need not go to waste. Software drivers that support Agilent VEE and National Instruments LabView® are available for the 34970A to make integration into your test system easy. Standard RS-232 and GPIB interfaces and SCPI programming language make integration even easier.

ATE Feature Checklist

- 3-slot cardcage with 6½ digit (22 bit) internal DMM
- 0.004% basic 1-year dcV accuracy; 0.06% acV accuracy
- Up to 120 single-ended measurements or 96 matrix crosspoints in a 3½" high, half-rack instrument
- Eight switch and control modules include low-frequency and RF multiplexers, matrix and actuation switches, digital input and output, analog output, and event recording
- Scan rates up to 250 ch/s
- GPIB and 115 kbaud RS-232 interfaces standard
- Software drivers available to support Agilent VEE and National Instruments LabView®
- Relay maintenance feature for system maintenance
- 3-year warranty

Compact 60-channel data acquisition system

Low-cost, high-quality switching for automated test

If you don't need the built-in measurement capability of the 34970A, save money by ordering it without the DMM. What you end up with is the lowest-cost switch unit on the market. It's an ideal solution for routing test signals to and from your DUT and assorted instruments, including external DMMs, scopes, counters, and power supplies. Plus, you can add the DMM later if your needs change.

The functionality you need

We put a lot of thought into defining and designing the modules for the 34970A in order to cover a broad spectrum of switching and signal routing requirements with fewer modules. The result? Simplified ordering and easier configuration.

And while we were at it, we improved performance and density. The 34970A modules can switch from microvolts to 300 volts, dc to 2 GHz, and with densities as high as 120 single-ended channels or 96 matrix crosspoints per frame. Plus, simple control capabilities like analog outputs, open collector digital outputs, and isolated Form-C relays for controlling higher-powered devices are available.

Easy scanning

The 34970A can easily scan with external instruments. It builds a scan list that includes all enabled low-frequency multiplexer inputs. Scans are controlled with the external "channel advance" input, or with the front panel "Step" key.

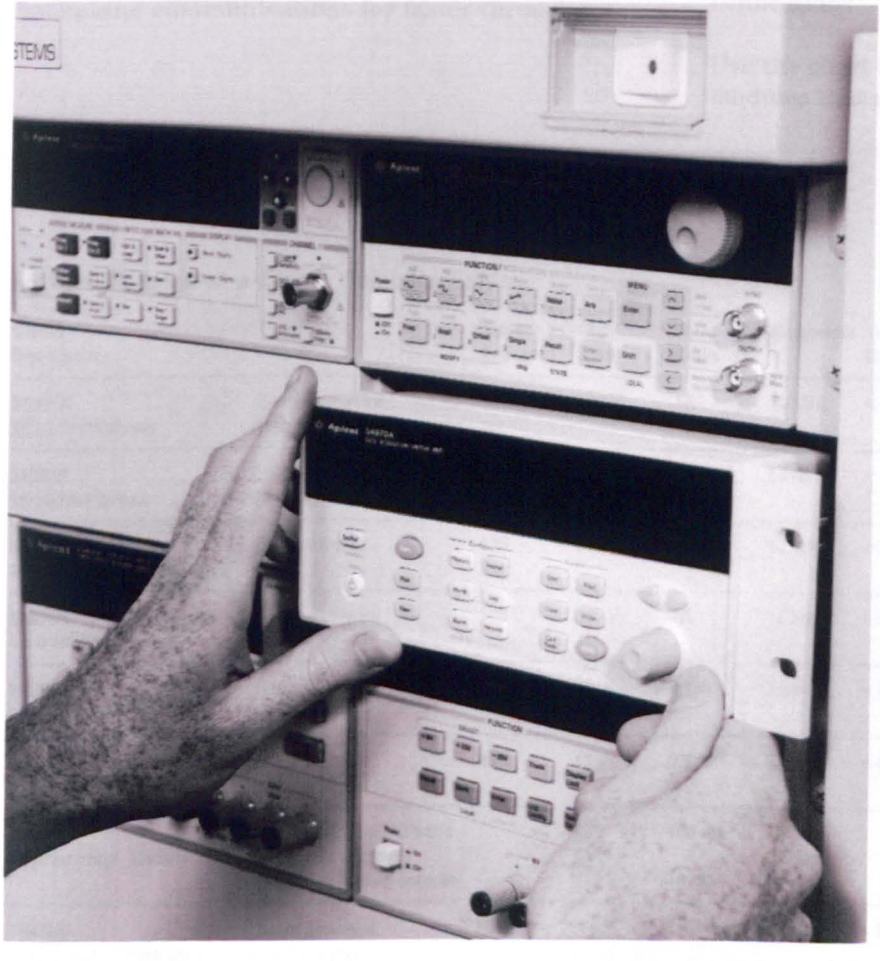

Low-cost switching system for automated testing

Customize your Agilent 34970A with plug-in modules

A complete selection of plug-in modules gives you high-quality measurement, switching, and control capabilities to choose from. Modules include both low-frequency and RF multiplexers, a matrix switch, a general-purpose switch, and a multifunction module that includes digital input/output, analog output, and totalizer capabilities. You can mix and match modules to get just the functionality you need right now—then change or add more channels later as your application grows.

Modules for the 34970A are designed to make your testing easier, faster, and more reliable. Here's how:

Higher throughput
Our unique architecture incorporates a high-performance microprocessor on each module, off-loading the mainframe processor and minimizing backplane communications for faster throughput.

More channels in less space
Surface mount construction and a highly integrated design minimize the space required for relay drive and interface circuitry. High density on-module connectors save both board and connector space normally required by a terminal block. We use the latest technology to squeeze the most out of the remaining board space, giving you up to 40 single-ended channels in roughly the same space used by many data acquisition system terminal blocks.

Convenient connections
On-module screw-terminal connectors make wiring more convenient. Built-in strain-relief cable routing and cable tie points keep your wiring secure and safe from accidental tugs and pulls. An internal analog bus routes signals from any of the low-frequency multiplexers directly to the internal DMM, without the need for external connections.

Use the chart below to help you pinpoint the modules that meet your needs.

Agilent Modules-at-a-Glance Selection Guide

Model Description	Type	Speed (ch/sec)	Max Volts	Max Amps	Bandwidth	Thermal Offset	Comments	Page
34901A **20 ch Multiplexer**	2-wire armature (4-wire selectable)	60	300 V	1A	10 MHz	< 3 µV	Built-in cold junction reference 2 additional current channels (22 total)	18
34902A **16 ch Multiplexer**	2-wire reed (4-wire selectable)	250	300 V	50 mA	10 MHz	< 6 µV	Built-in cold junction reference	19
34903A **20 ch Actuator/GP Switch**	SPDT/form C	120	300 V	1A	10 MHz	< 3 µV		20
34904A **4 x 8 Matrix**	2-wire armature	120	300 V	1A	10 MHz	< 3 µV		20
34905A **Dual 4 ch RF Mux 50Ω**	Common Low (unterminated)	60	42 V	0.7 A	2 GHz	< 6 µV	1 GHz bandwidth through BNC-to-SMB adapter cable	21
34906A **Dual 4 ch RF Mux 75Ω**	Common Low (unterminated)	60	42 V	0.7 A	2 GHz	< 6 µV	1 GHz bandwidth through BNC-to-SMB adapter cable	21
34907A **Multifunction Module**	Two 8-bit digital I/O ports 26-bit Event Counter Two 16-bit Analog outputs		42 V 42 V ±12 V	400 mA 10 mA	 100 KHz dc		Open drain Selectable input threshold Max 40 mA total output per frame	22
34908A **40 ch Single-Ended Mux**	1-wire armature (common low)	60	300 V	1A	10 MHz	< 3 µV	Built-in cold junction reference No four-wire measurements	19

A warranty worth reading

We know you can't afford instrument downtime due to hardware failures and unscheduled maintenance. That's why our engineers designed reliability into the 34970A: A rugged enclosure, state-of-the-art surface mount construction throughout, reduced parts counts, and rigorous and thorough testing on all aspects of the product. In fact, we are so confident of the quality and performance of the 34970A that we are offering a 3-year limited warranty on all hardware.

Take the guesswork out of relay maintenance

The 34970A uses our proprietary relay maintenance system to help you to predict relay end-of-life and avoid costly production-line downtime. It automatically counts every individual switch closure and stores it in nonvolatile memory on each module. You can query the total number of cycles on any individual channel so you can schedule maintenance and avoid erratic end-of-life failures.

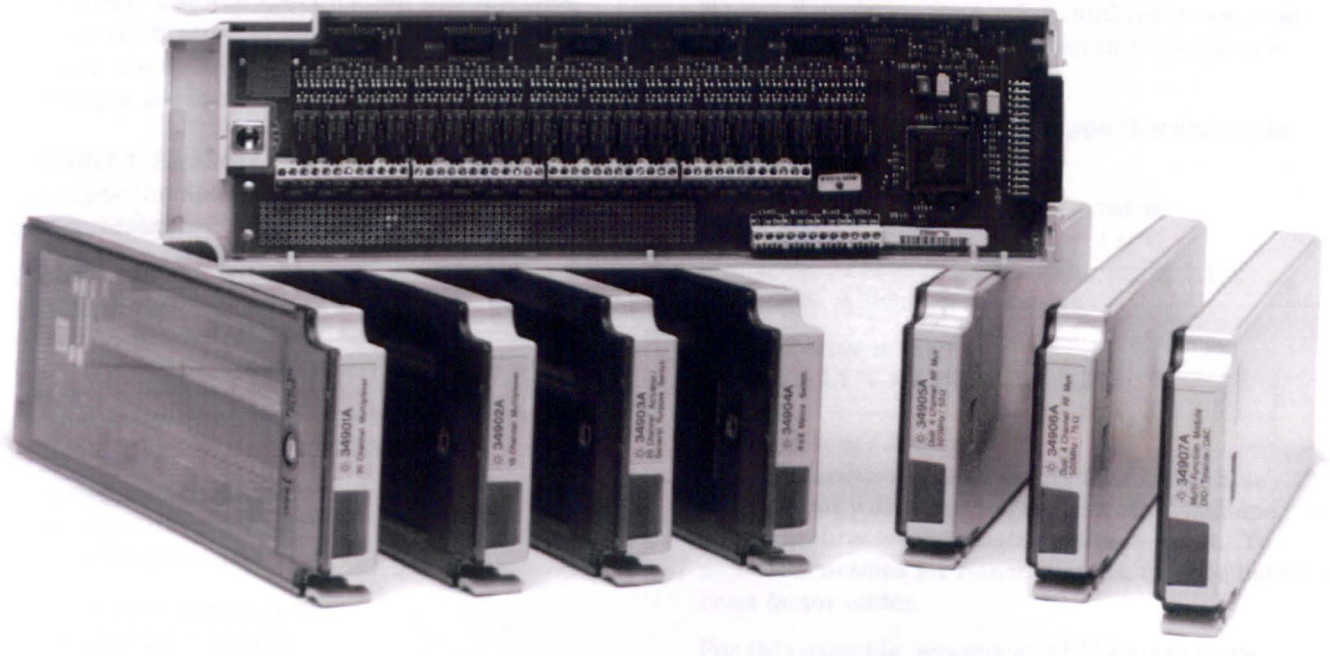

Spec Interpretation Guide

The following pages list the technical specifications for the Agilent 34970A Data Acquisition/Switch Unit and its modules. The explanations and examples below are helpful in understanding how to interpret these specifications:

- Measurement accuracy is specified as percent of reading plus percent of range, where reading is the actual measured value and range is the name of the scale (1V, 10V, etc.)—not the full scale value (1.2V, 12V, etc.).

- DMM measurement accuracies include all switching errors. Switching errors are also listed separately in the module specifications section. Temperature measurement accuracies include ITS-90 conversion errors. The thermocouple accuracies include the reference junction error as well.

- Accuracies are listed as either 24-hour, 90-day, or 1-year specifications. This refers to the length of time since the instrument's last calibration. Use the specification that matches your calibration cycle. The 24-hour specifications are useful for determining short-term relative performance.

EXAMPLE 1: Basic dcV accuracy

Calculate the accuracy of the following measurement:

9 V dc input
10 V dc range
1-year accuracy specifications
Normal operating temperature (18°C–28°C)

From the following page, the 1-year accuracy is:
0.0035% of reading + 0.0005% of range

Which translates into:
(0.0035/100 x 9 V)+
(0.0005/100 x 10 V) = 365µV

For a total accuracy of:
365 µV / 9 V = 0.0041%

EXAMPLE 2: Extreme operating temperature

When the 34970A is used outside of its 18°C–28°C temperature range, there are additional temperature drift errors to consider. Assume the same conditions in example 1, but at a 35°C operating temperature.

The basic accuracy is again:
0.0035% of reading + 0.0005% of range=365 µV.

Now, multiply the 10 V temperature coefficient from the following page by the number of degrees outside of operating range for additional error:
(0.0005% reading + 0.0001% range)
/°C x (35°C - 28°C) =
(0.0005% reading + 0.0001% range)
/°C x 7°C =
0.0035% reading + 0.0007% range = 385 µV

Total error is then:
365 µV + 385 µV = 750 µV or 0.008%

EXAMPLE 3: Thermocouple measurement accuracy

Calculating the total thermocouple reading error is easy with the 34970A–just add the listed measurement accuracy to the accuracy of your transducer. Switching, conversion, and reference junction errors are already included in the measurement specification.

For this example, assume a J-type thermocouple input reading 150°C.

From the following page, total error is:
Thermocouple probe accuracy + 1.0°C
The probe vendor specifies accuracy of 1.1°C or 0.4%, whichever is greater.

Total error is then:
1.0°C + 1.1 °C = 2.1°C total, or 1.4%

EXAMPLE 4: acV Accuracy

The acV function measures the true RMS value of the input waveform, regardless of waveshape. Listed accuracies assume a sinewave input. To adjust accuracies for non-sinusoids, use the listed crest factor adder.

For this example, assume a ±1 V square wave input with 50% duty cycle and a 1 kHz frequency.

Accuracy for 1 V, 1 kHz sinusoid is:
0.06% reading + 0.04% range
A 50% duty cycle squarewave has a crest factor of
Peak Value / RMS value = 1 V / 1 V = 1

From Crest Factor table, add:
0.05% of reading

The total accuracy is:
0.11% of reading + 0.04% of range = 1.5 mV or 0.15%

Accuracy Specifications ±(% of reading + % of range)[1]

Includes measurement error, switching error, and transducer conversion error

	Range[3]	Frequency, etc.	24 Hour[2] 23°C±1°C	90 Day 23°C±5°C	1 Year 23°C±5°C	Temperature Coefficient 0°C–18°C, 28°C–55°C
DC Voltage						
	100.0000 mV		0.0030 + 0.0035	0.0040 + 0.0040	0.0050 + 0.0040	0.0005 + 0.0005
	1.000000 V		0.0020 + 0.0006	0.0030 + 0.0007	0.0040 + 0.0007	0.0005 + 0.0001
	10.00000 V		**0.0015 + 0.0004**	**0.0020 + 0.0005**	**0.0035 + 0.0005**	**0.0005 + 0.0001**
	100.0000 V		0.0020 + 0.0006	0.0035 + 0.0006	0.0045 + 0.0006	0.0005 + 0.0001
	300.000 V		0.0020 + 0.0020	0.0035 + 0.0030	0.0045 + 0.0030	0.0005 + 0.0003
True RMS AC Voltage[4]						
	100.0000 mV	3 Hz–5 Hz	1.00 + 0.03	1.00 + 0.04	1.00 + 0.04	0.100 + 0.004
	to 100.0000V	5 Hz–10 Hz	0.35 + 0.03	0.35 + 0.04	0.35 + 0.04	0.035 + 0.004
		10 Hz–20 kHz	**0.04 + 0.03**	**0.05 + 0.04**	**0.06 + 0.04**	**0.005 + 0.004**
		20 kHz–50 kHz	0.10 + 0.05	0.11 + 0.05	0.12 + 0.05	0.011 + 0.005
		50 kHz–100 kHz	0.55 + 0.08	0.60 + 0.08	0.60 + 0.08	0.060 + 0.008
		100 kHz–300 kHz[5]	4.00 + 0.50	4.00 + 0.50	4.00 + 0.50	0.20 + 0.02
	300.0000V	3 Hz–5 Hz	1.00 + 0.05	1.00 + 0.08	1.00 + 0.08	0.100 + 0.008
		5 Hz–10 Hz	0.35 + 0.05	0.35 + 0.08	0.35 + 0.08	0.035 + 0.008
		10 Hz–20 kHz	0.04 + 0.05	0.05 + 0.08	0.06 + 0.08	0.005 + 0.008
		20 kHz–50 kHz	0.10 + 0.10	0.11 + 0.12	0.12 + 0.12	0.011 + 0.012
		50 kHz–100 kHz	0.55 + 0.20	0.60 + 0.20	0.60 + 0.20	0.060 + 0.020
		100 kHz–300 kHz[5]	4.00 + 1.25	4.00 + 1.25	4.00 + 1.25	0.20 + 0.05
Resistance[6]						
	100.0000Ω	1 mA current source	0.0030 + 0.0035	0.008 + 0.004	0.010 + 0.004	0.0006 + 0.0005
	1.000000 kΩ	1 mA	0.0020 + 0.0006	0.008 + 0.001	0.010 + 0.001	0.0006 + 0.0001
	10.00000 kΩ	**100 µA**	**0.0020 + 0.0005**	**0.008 + 0.001**	**0.010 + 0.001**	**0.0006 + 0.0001**
	100.0000 kΩ	10 µA	0.0020 + 0.0005	0.008 + 0.001	0.010 + 0.001	0.0006 + 0.0001
	1.000000 MΩ	5.0 µA	0.002 + 0.001	0.008 + 0.001	0.010 + 0.001	0.0010 + 0.0002
	10.00000 MΩ	500 nA	0.015 + 0.001	0.020 + 0.001	0.040 + 0.001	0.0030 + 0.0004
	100.0000 MΩ	500 nA/10 MΩ	0.300 + 0.010	0.800 + 0.010	0.800 + 0.010	0.1500 + 0.0002
Frequency and Period[7]						
	100 mV	3 Hz–5 Hz	0.10	0.10	0.10	0.005
	to 300 V	5 Hz–10 Hz	0.05	0.05	0.05	0.005
		10 Hz–40 Hz	0.03	0.03	0.03	0.001
		40 Hz–300 kHz	**0.006**	**0.01**	**0.01**	**0.001**
DC Current (34901A only)						
	10.00000 mA	<0.1 V burden	0.005 + 0.010	0.030 + 0.020	0.050 + 0.020	0.002+ 0.0020
	100.0000 mA	**<0.6 V**	**0.010 + 0.004**	**0.030 + 0.005**	**0.050 + 0.005**	**0.002 + 0.0005**
	1.000000 A	<2 V	0.050 + 0.006	0.080 + 0.010	0.100 + 0.010	0.005 + 0.0010
True RMS AC Current (34901A only)						
	10.00000 mA	3 Hz–5 Hz	1.00 + 0.04	1.00 + 0.04	1.00 + 0.04	0.100 + 0.006
	and[4] 1.000000 A	5 Hz–10 Hz	0.30 + 0.04	0.30 + 0.04	0.30 + 0.04	0.035 + 0.006
		10 Hz–5 kHz	**0.10 + 0.04**	**0.10 + 0.04**	**0.10 + 0.04**	**0.015 + 0.006**
	100.0000 mA[8]	3 Hz–5 Hz	1.00 + 0.5	1.00 + 0.5	1.00 + 0.5	0.100 + 0.06
		5 Hz–10 Hz	0.30 + 0.5	0.30 + 0.5	0.30 + 0.5	0.035 + 0.06
		10 Hz–5 kHz	0.10 + 0.5	0.10 + 0.5	0.10 + 0.5	0.015 + 0.06

Temperature	Type	1-Year Accuracy[9]		Extended Range 1-Year Accuracy[9]		
Thermocouple	B	1100°C to 1820°C	1.2°C	400°C to 1100°C	1.8°C	
	E	-150°C to 1000°C	1.0°C	-200°C to -150°C	1.5°C	
	J	**-150°C to 1200°C**	**1.0°C**	**-210°C to -150°C**	**1.2°C**	
	K	-100°C to 1200°C	1.0°C	-200°C to -100°C	1.5°C	0.03 °C
	N	-100°C to 1300°C	1.0°C	-200°C to -100°C	1.5°C	
	R	300°C to 1760°C	1.2°C	-50°C to 300°C	1.8°C	
	S	400°C to 1760°C	1.2°C	-50°C to 400°C	1.8°C	
	T	-100°C to 400°C	1.0°C	-200°C to -100°C	1.5°C	
RTD	R_0 from 49 Ω to 2.1 kΩ	-200°C to 600°C	0.06°C			0.003 °C
Thermistor	2.2 k, 5k, 10k	-80°C to 150°C	0.08°C			0.002 °C

[1] Specifications are for 1 hr warm-up and 6½ digits. Slow ac filter
[2] Relative to calibration standards
[3] 20% over range on all ranges except 300 Vdc and ac ranges and 1 Adc and ac current ranges
[4] For sinewave input > 5% of range. For inputs from 1% to 5% of range and < 50 kHz, add 0.1% of range additional error
[5] Typically 30% of reading error at 1 MHz, limited to 1 x 10^8 V Hz
[6] Specifications are for 4- wire ohms function or 2-wire ohms using Scaling to remove the offset. Without scaling, add 1 Ω additional error in 2-wire Ohms function
[7] Input > 100 mV. For 10 mV inputs multipy % of reading error x 10
[8] Specified only for inputs >10 mA
[9] For total measurement accuracy, add temperature probe error

Measurement Characteristics[8]

DC Voltage	
Measurement Method	Continuously Integrating Multi-slope III A-D Converter
A-D Linearity	0.0002% of reading + 0.0001 % of range
Input Resistance	
100 mV, 1 V, 10 V ranges	Selectable 10 MΩ or > 10,000 MΩ
100 V, 300 V ranges	10 MΩ ± 1%
Input Bias Current	< 30 pA at 25°C
Input Protection	300 V all ranges
True RMS AC Voltage	
Measurement Method	AC coupled True RMS — measures the AC component of the input with up to 300 Vdc of bias on any range
Crest Factor	Maximum of 5:1 at Full Scale
Additional Crest Factor Errors (non-sinewave)	Crest Factor 1-2 0.05 % of reading Crest Factor 2-3 0.15 % of reading Crest Factor 3-4 0.30 % of reading Crest Factor 4-5 0.40 % of reading
Input Impedance	1 MΩ ± 2% in parallel with 150 pF
Input Protection	300 Vrms all ranges
Resistance	
Measurement Method	Selectable 4-wire or 2-wire Ohms Current source referenced to LO input
Offset Compensation	Selectable on 100Ω, 1kΩ, 10kΩ ranges
Maximum Lead Resistance	10% of range per lead for 100 Ω and 1 kΩ ranges. 1 kΩ on all other ranges
Input Protection	300 V on all ranges
Frequency and Period	
Measurement Method	Reciprocal counting technique
Voltage Ranges	Same as AC Voltage function
Gate Time	1s, 100 ms, or 10 ms
Measurement Timeout	Selectable 3 Hz, 20 Hz, 200 Hz LF limit
DC Current	
Shunt Resistance	5 Ω for 10 mA, 100 mA; 0.1 Ω for 1 A
Input Protection	1A 250 V fuse on 34901A module
True RMS AC Current	
Measurement Method	Direct coupled to the fuse and shunt. AC coupled True RMS measurement (measures the ac component only)
Shunt Resistance	5 Ω for 10 mA; 0.1 Ω for 100 mA, 1 A
Input Protection	1A 250 V fuse on 34901A module
Thermocouple	
Conversion	ITS-90 software compensation
Reference Junction Type	Internal, Fixed, or External
Open thermocouple Check	Selectable per channel. Open >5kΩ
Thermistor	44004, 44007, 44006 series
RTD	α = 0.00385 (DIN) and α = 0.00392
Measurement Noise Rejection 60 (50) Hz[1]	
dc CMRR	140 dB
ac CMRR	70 dB
Integration Time	**Normal Mode Rejection[2]**
200 plc/3.33s (4s)	110 dB[3]
100 plc/1.67s (2s)	105 dB[3]
20 plc/333 ms (400 ms)	100 dB[3]
10 plc/167 ms (200 ms)	95 dB[3]
2 plc/33.3 ms (40 ms)	90 dB
1 plc/16.7 ms (20 ms)	60 dB
< 1 plc	0 dB

Operating Characteristics[4]

Single Channel Measurement Rates[5]

Function	Resolution[9]	reading/s
dcV, 2-wire Resistance	6½ digits (10 plc)	6 (5)
	5½ digits (1 plc)	57 (47)
	4½ digits (0.02 plc)	600
Thermocouple	0.1°C (1 plc)	57 (47)
	(0.02 plc)	220
RTD, Thermistor	0.01°C (10 plc)	6 (5)
	0.1°C (1 plc)	57 (47)
	1°C (0.02 plc)	220
acV	6½ Slow (3 Hz)	0.14
	6½ Med (20 Hz)	1
	6½ Fast (200 Hz)	8
	6½[6]	100
Frequency, Period	6½ digits (1s gate)	1
	5½ digits (100 ms)	9
	4½ digits (10 ms)	70

System Speeds[7]

INTO Memory	**ch/s**
single channel dcV	600
34902A scanning dcV	250
34907A scanning digital in	250
34902A scanning dcV with scaling & 1 alarm fail	220
34907A scanning totalize	170
34902A scanning temperature	160
34902A scanning acV[6]	100
34902A scanning dcV/Ohms on alternate channels	90
34901A/34908A scanning dcV	60
INTO and OUT of memory to GPIB or RS-232 (init, fetch)	
34902A scanning dcV	180
34902A scanning dcV with timestamp	150
OUT of memory to GPIB	
Readings	800
Readings with timestamp	450
Readings with all format options ON	310
OUT of memory to RS-232	
Readings	600
Readings with timestamp	320
Readings with all format options ON	230
DIRECT to GPIB or RS-232	
single channel dcV	440
34902A scanning dcV	200
single channel MEAS DCV 10 / MEAS DCV 1	25
single channel MEAS DCV/ MEAS OHMS	12

[1] For 1 KΩ unbalance in LO lead
[2] For power line frequency ±0.1%
[3] For power line frequency ±1% use 80 dB or ±3% use 60 dB
[4] Reading speeds for 60 Hz and (50 Hz) operation
[5] For fixed function and range, readings to memory, scaling and alarms off, AZERO OFF
[6] Maximum limit with default settling delays defeated
[7] Speeds are for 4½ digits, delay 0, display off, autozero off. Using 115 kbaud RS-232 setting
[8] Isolation voltage (ch - ch, ch - earth) 300 Vdc, ac rms
[9] 6½ digits = 22 bits, 5½ digits = 18 bits, 4½ digits = 15 bits

System Specifications

Scanning Inputs	
Analog	34901A, 34902A, and 34908A multiplexer channels
Digital	34907A digital in and totalize
Scan list	Scans channels in ascending order
Scan Triggering	
Source	Interval, external, button press, software, or on monitor channel alarm
Scan count	1 to 50,000 or continuous
Scan interval	0 to 99 hours; 1ms step size
Channel delay	0 to 60 seconds per channel; 1 ms step size
External trig delay	<2 ms. With monitor on <200 ms
External trig jitter	<2 ms
Alarms	
Analog inputs	Hi, Lo, or Hi + Lo evaluated each scan
Digital inputs	34907A digital in maskable pattern match or state change 34907A totalize: Hi limit only
Monitor channel	Alarm evaluated each reading
Alarm Outputs	4 TTL compatible Selectable TTL logic Hi or Lo on fail
Latency	5 ms (typical)
Memory	
	Battery backed, 4 year typical life[1]
Readings	50,000 with timestamp Readable during scan
States	5 instrument states with user label
Alarm Queue	Up to 20 events with channel number, reading, and timestamp
System Features	
Per-channel Math	Individual Mx + B scaling and Min/Max/Average calculated real time
Power Fail Recovery	Resumes scanning automatically
Relay maintenance	Counts each relay closure and stores on module User resettable
Real-time clock	Battery-backed, 4-year typical life[1]
General Specifications	
Power Supply	100V/120V/220V/240V ±10%
Power Line Frequency	45 Hz to 66 Hz automatically sensed
Power Consumption	12 W (25 VA peak)
Operating Environment	Full accuracy for 0°C to 55°C Full accuracy to 80% R.H. at 40°C
Storage Environment	-40°C to 70°C[1]
Weight	Net: 3.6 kg (8.0 lbs)
Safety	Conforms to CSA, UL-1244, IEC 1010 Cat I
RFI and ESD	CISPR 11, IEC 801/2/3/4
Warranty	3 years

Software

HP BenchLink Data Logger
(not included with Option 001)

System Requirements[2]	
PC Hardware	486, 66 MHz, 16 MB RAM, 12 MB disk space
Operating System	Windows® 3.1,Windows 95®, Windows NT 4.0®
Instrument Support	Single 34970A operation Single program window
Computer Interfaces[3]	
GPIB	82335B, 82340A/B/C, 82341A/B/C/D National Instruments AT-GPIB/TNT, PCI-GPIB, PC-MCIA
LAN-to-GPIB	E2050A (Windows 95 and NT only) RS-232 (Serial Port) PC COM 1-4
HP BenchLink Features	
Configuration	Spreadsheet-like setup page Upload and Download intrument setups Computed channels using + - */, dB, dBm, dBV, x^2, $\sqrt{x}$ and full, 1/2, or 1/4 bridge strain
Graphical Displays	Real-time and historical data displays Add, delete, size, and configure real time Strip chart with markers and alarm indication, X-Y chart with curve fit, Histogram with statistics, Bar meter, Digital meter, and Data table
Graphical Controls	Sliders, switches, buttons, and LED lights
Alarm / Limit testing	Start/Stop scanning on alarm condition Control 34903A relay state or 34907A digital output on alarm
Data	Real time streamed (saved) to disk Copy data or graphics to windows clipboard Export user-selected data to ASCII file, CSV, TSV
Event logging	Automatic entry of alarms and errors Enter user notes real time
Printing	Setup spreadsheet, all graphics, and event log entries
HP BenchLink Performance[4]	
Scan and save to disk	100 ch/s 2 strip charts displayed
Readings saved	Maximum 150M/file
Instrument Driver Support for Programming Languages	
Universal	Compatible with Windows 95 and NT
Instrument Driver[5]	Agilent VEE 3.2 or greater Visual Basic 4.0, LabWindows CVI 4.0, LabVIEW 4.0
Labview Driver (VI)	LabVIEW 4.0

[1] Storage at temperatures above 40°C will decrease battery life
[2] Software provided on CD-ROM and includes utility to create floppy disks for installation
[3] Interface and driver must be purchased and installed separately
[4] 90 MHz Pentium, 20 MB RAM
[5] Requires VISA command library for IEEE-488

Modules Specifications

The Agilent 34970A accuracy specifications already include the switching offset and reference junction errors shown below. These errors are listed separately for determining system error with external measurement devices.

Up to three modules, in any combination, can be inserted into a single mainframe. The 34970A's internal DMM connections are accessible only through the 34901A, 34902A, and 34908A low-frequency multiplexers.

On-module screw terminals accept wire sizes from 16 gage to 22 gage. Twenty-gage wire is recommended for high channel count applications. The 34905A and 34906A RF Multiplexers use SMB connectors. A standard set of (10) BNC-to-SMB adapter cables is provided with each RF module for convenient BNC connections.

		Multiplexer			Actuator	Matrix	RF Multiplexer		Multifunction
		34901A	34902A[1]	34908A	34903A	34904A	34905A	34906A	34907A
General									
Number of Channels		20 + 2	16	40	20	4 x 8	Dual 1 x 4		See page 22 for module specifications
		2/4 wire	2/4 wire	1 wire	SPDT	2 wire	50 Ω	75 Ω	
Connects to Internal DMM		•	•	•					
Scanning Speed		60 ch/s	250 ch/s	60 ch/s					
Open/Close Speed		120/s	120/s	70/s	120/s	120/s	60/s		
Input									
Voltage (dc, ac rms)[2]		300 V	300 V	300 V	300 V	300 V	42 V		
Current (dc, ac rms)		1A	50mA	1A	1A	1A	0.7A		
Power (W, VA)		50 W	2 W	50 W	50 W	50 W	20 W		
DC Characteristics									
Offset Voltage [3]		< 3uV	< 6uV	< 3uV	< 3uV	< 3uV	< 6uV		
Initial Closed Channel R [3]		< 1 Ω	< 1 Ω	< 1 Ω	< 0.2 Ω	< 1 Ω	< 0.5 Ω		
Isolation ch-ch, ch-earth		> 10 G Ω	> 10 G Ω	> 10 G Ω	> 10 G Ω	> 10 G Ω	> 1 G Ω		
AC Characteristics									
Bandwidth[4]		10 MHz	10 MHz	10 MHz	10 MHz	10 MHz	2 GHz [5]	2 GHz [5]	
Insertion Loss (dB)	10 MHz	—	—	—	—	—	-0.1	-0.1	
	100 MHz	—	—	—	—	—	-0.4	-0.4	
	500 MHz	—	—	—	—	—	-0.6	-0.5	
	1 GHz	—	—	—	—	—	-1	-1	
	1.5 GHz	—	—	—	—	—	-1.2	-1.5	
	2 GHz	—	—	—	—	—	-3	-2	
SWR	10 MHz	—	—	—	—	—	1.02	1.02	
	100 MHz	—	—	—	—	—	1.05	1.05	
	500 MHz	—	—	—	—	—	1.20	1.25	
	1 GHz	—	—	—	—	—	1.20	1.40	
	1.5 GHz	—	—	—	—	—	1.30	1.40	
	2 GHz	—	—	—	—	—	1.40	2.00	
ch-ch Cross Talk (dB)[4]	10 MHz	-45	-45	-18[6]	-45	-33	-100	-85	
	100 MHz	—	—	—	—	—	-85	-75	
	500 MHz	—	—	—	—	—	-65	-65	
	1 GHz	—	—	—	—	—	-55	-50	
	1.5 GHz	—	—	—	—	—	-45	-40	
	2 GHz	—	—	—	—	—	-35	-35	
Risetime							< 300 ps		
Signal Delay							< 3 ns		
Capacitance	HI - LO	< 50 pF	< 50 pF	< 50 pF	< 10 pF	< 50 pF	< 20 pF		
	LO - Earth	< 80 pF	< 80 pF	< 80 pF	< 80 pF	< 80 pF	—		
Volt-Hertz limit		10^8	10^8	10^8	10^8	10^8	10^{10}		
Other									
T/C Cold Junction Accuracy[3]									
	(typical)	0.8°C	0.8°C	0.8°C					
Switch Life	No Load (typical)	100M	100M	100M	100M	100M	5M	5M	
	Rated Load (typical)[7]	100k	100k	100k	100k	100k	100k	100k	

Temperature	Operating	all cards — 0°C to 55°C
	Storage	all cards — -20°C to 70°C
Humidity	(non-condensing)	all cards — 40°C/80% RH

[1] Not recommended for connection to ac line without external transient suppression
[2] Channel-to-channel or channel-to-earth
[3] Errors included in DMM measurement accuracy specifications
[4] 50Ω source, 50Ω load
[5] Bandwidth direct to card SMB connectors
[6] Isolation within channel 1 to 20 or 21 to 40 banks is -40 dB
[7] Applies to resistive loads only

Multiplexer Selection Guide

Choose between the broad functionality of the 34901A, the high speed scanning of the 34902A, or the single-ended density of the 34908A. These three modules are the only way to connect to the 34970A internal DMM. They can be used to scan with external instruments as well.

All multiplexer modules employ break-before-make scanning, ensuring only one closed channel (or channel pair) at a time. Multiple channel closures are allowed on the 34901A and 34902A modules when not configured for scanning.

The 34908A does not allow multiple channel closures at any time.

	34901A	34902A	34908A
Number of Channels	20 + 2	16	40
Max scan speed	60 ch/s	250 ch/s	60 ch/s
Number of contacts	2 or 4	2 or 4	1
Temperature			
Thermocouple	•	•	•
2-wire RTD	•	•	•
4-wire RTD	•	•	
Thermistor	•	•	•
dc Volts	•	•	•
ac Volts	•	•	•
2-wire Ohms	•	•	•
4-wire Ohms	•	•	
Frequency	•	•	•
Period	•	•	•
dc current	•		
ac current	•		

34901A

20-Channel General-Purpose Multiplexer

- 60 ch/s scanning
- Two- and four-wire scanning
- Built-in thermocouple reference junction
- 300 V switching

The Agilent 34901A is the most versatile multiplexer for general purpose scanning. It combines dense, multifunction switching with 60 channel/second scan rates to address a broad spectrum of data acquisition applications.

Two- and four-wire channels can be mixed on the same module. Two additional fused inputs (22 channels total) route up to 1A of current to the internal DMM, allowing ac and dc current measurements without the need for external shunt resistors.

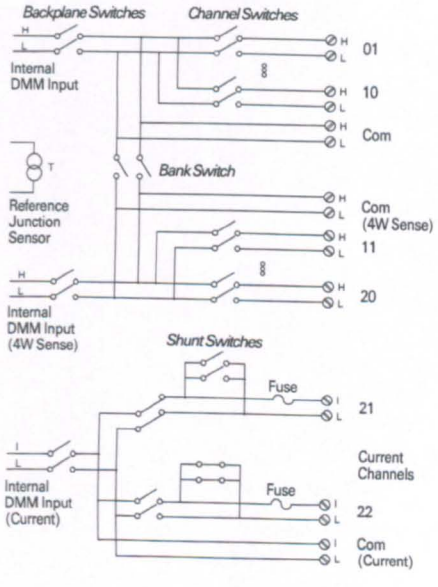

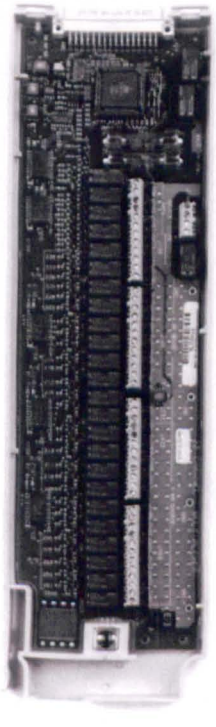

34902A

16-Channel High-Speed Multiplexer

- 250 ch/s scanning
- Two- and four-wire scanning
- Built-in thermocouple reference junction

The Agilent 34902A employs reed relays to achieve scan rates up to 250 channels per second. Use this module for high-throughput automated test applications as well as high-speed data logging and monitoring tasks.

Sixteen two-wire inputs switch up to 300 V. Two- and four-wire channels may be mixed on the same module. User provided shunt resistors are required for current measurements.

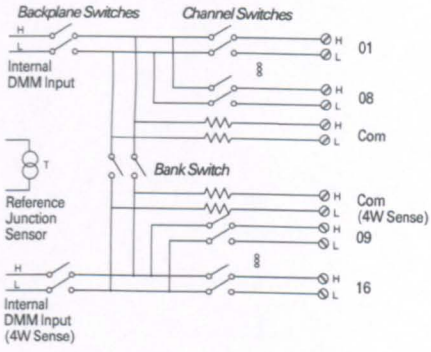

Note: Not recommended for connection to ac line without external transient suppression.

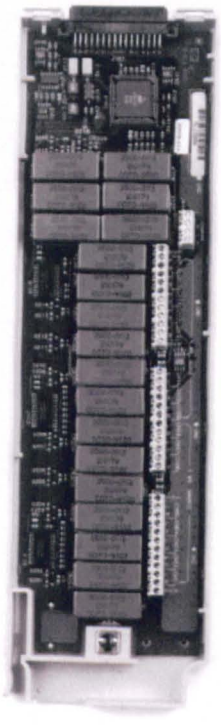

34908A

40-Channel Single-Ended Multiplexer

- 60 ch/s scanning
- Single-wire switching for common-low applications
- Built-in thermocouple reference junction

Use the Agilent 34908A for the greatest density in common-low applications, such as battery test, component characterization, and benchtop testing.

Each module switches 40 one-wire inputs. All two-wire internal measurements except current are supported. The module low connection is isolated from earth and can float up to 300 V.

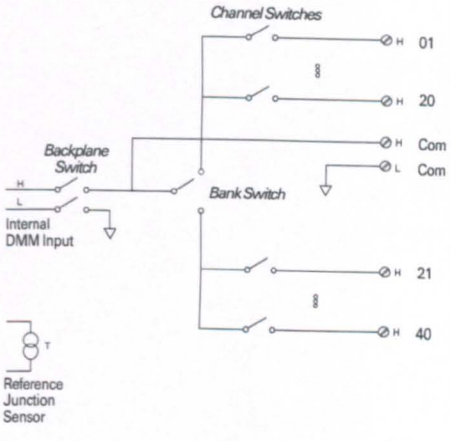

Note: Thermocouples must be electrically isolated from each other to avoid current loops and subsequent measurement errors.

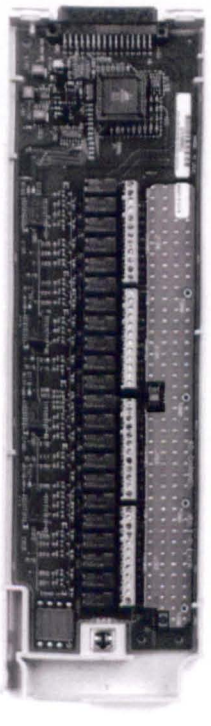

34903A

20-Channel Actuator/General Purpose Switch

- SPDT (Form C) latching relays
- 300 V, 1A actuation and control

This general-purpose switch module has 20 independent single-pole, double-throw (SPDT) relays. Use it to cycle power to products under test, control indicator and status lights, and to actuate external power relays and solenoids. Combine it with matrix and multiplexer modules to build custom switch systems. Its 300 V, 1A contacts can handle up to 50 W, enough for many power line switching applications.

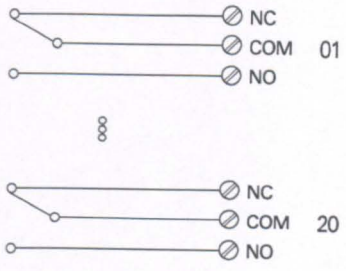

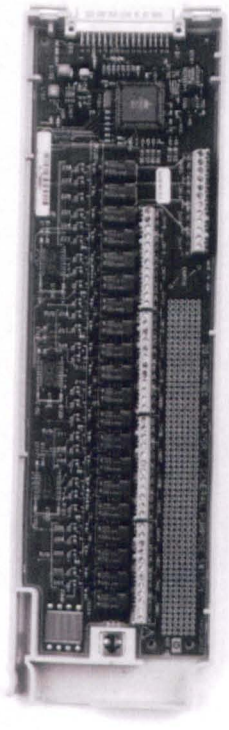

34904A

4x8 Two-wire Matrix Switch

- 32 two-wire crosspoints
- 300 V, 1A switching

The Agilent 34904A gives you the most flexible connection path between your device under test and your test equipment, allowing different instruments to be connected to multiple points on your DUT at the same time.

Rows or columns may be connected between multiple modules to build 8x8, 4x16 or larger matrices, with up to 96 crosspoints in a single frame.

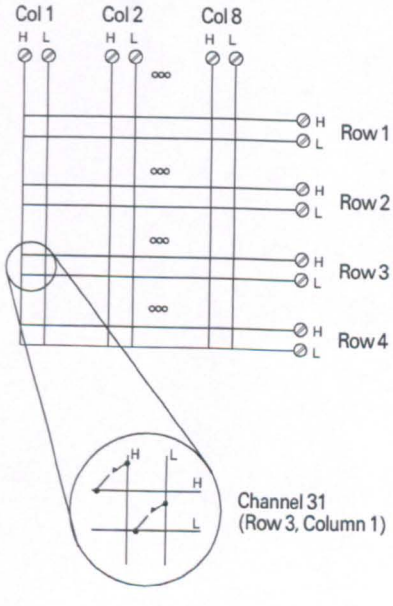

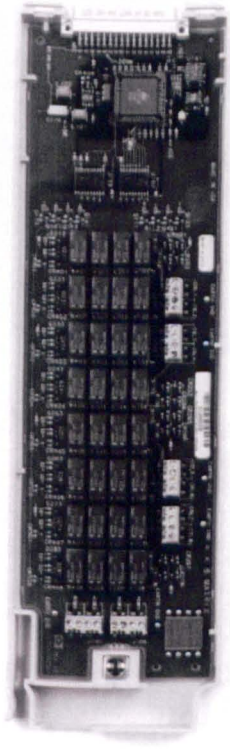

34905A 50Ω
34906A 75Ω

Dual 4-channel RF Multiplexers

- 2 GHz bandwidth
- BNC to SMB adapter cables included

The Agilent 34905A and 34906A RF multiplexers offer broadband switching capabilities for high-frequency and pulsed signals. Use them to route test signals between your device under test and your signal generator, oscilloscope, spectrum analyzer, or other instrumentation.

The RF multiplexers are arranged as two independent 1x4 multiplexers, each with a common shield and a switched center conductor. Connections can be made directly to SMB inputs with 2 GHz usable bandwidth, or to the BNC-to-SMB adapters provided with 1 GHz bandwidth. Multiple banks may be cascaded together for applications requiring even larger topologies—create a stubless 16:1 multiplexer in a single frame.

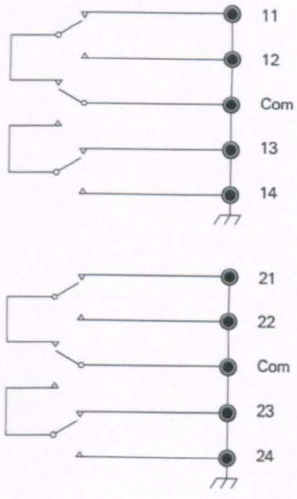

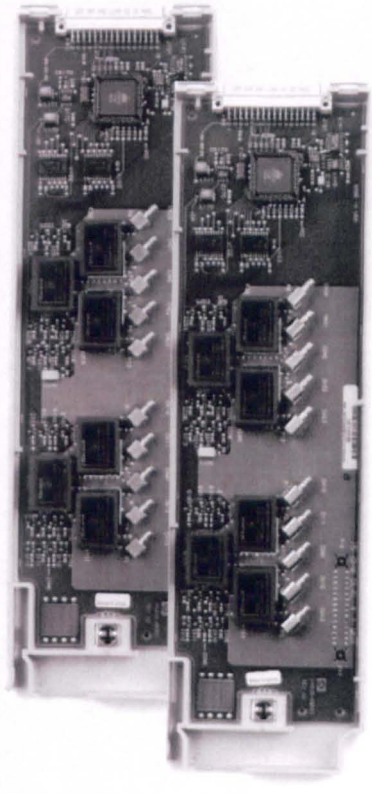

50Ω MUX Typical AC Performance Graphs

Insertion Loss

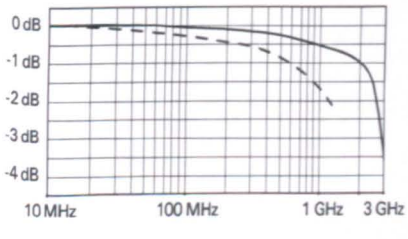

VSWR

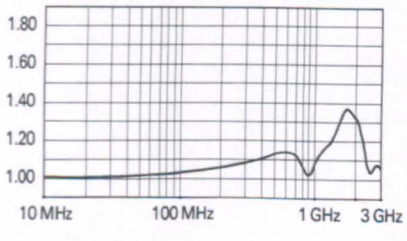

Crosstalk

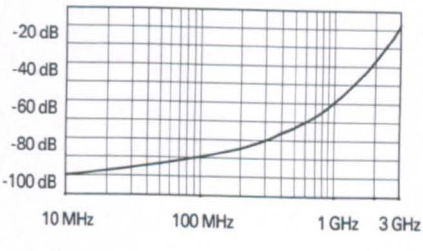

75Ω MUX Typical AC Performance Graphs

Insertion Loss

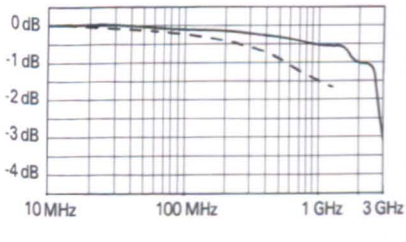

VSWR

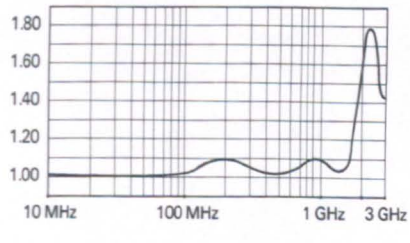

Crosstalk

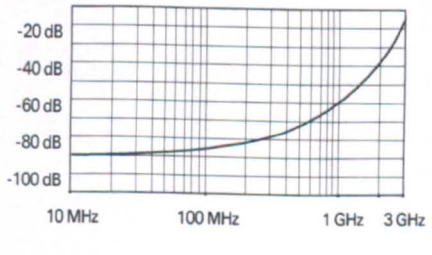

——— direct to card

- - - - - using provided adapter cables

34907A

Multifunction Module

- 16 bits of digital input and output
- 100 kHz totalizer input
- Two ±12V analog outputs

The Agilent 34907A allows great flexibility for a variety of sense and control applications. It combines two 8-bit ports of digital input and output, a 100 kHz gated totalizer, and two ±12V analog outputs—all on a single earth-referenced module. The digital inputs and totalizer input may be included in a scan. Alarm limits for the digital and event counter inputs are evaluated continuously, capturing and logging alarm conditions even between scans.

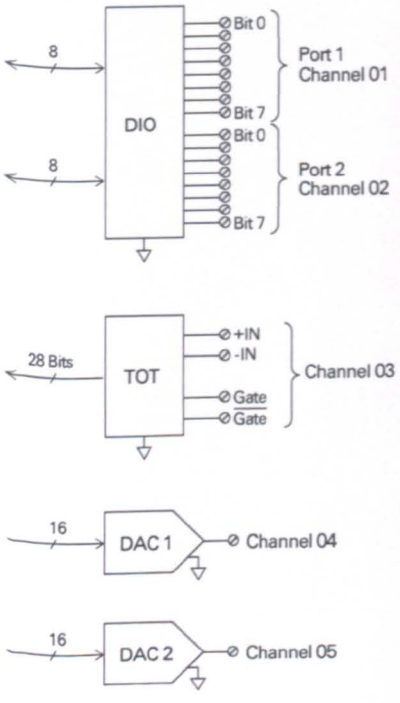

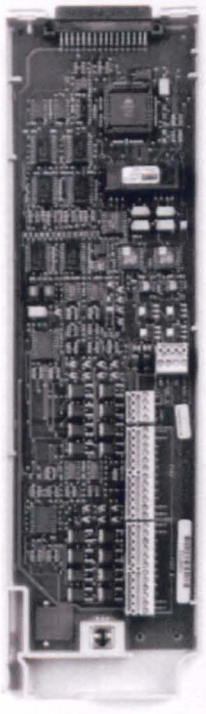

Digital Input/Ouput

Use the digital outputs with an external power supply to control microwave switches and attenuators, solenoids, power relays, indicators, and more. Use the digital inputs to sense limit switch and digital bus status. There are no complex handshake modes; reads and writes are initiated either from the front panel or the bus.

Digital Input/Output

Port 1, 2	8 bit, input or output, nonisolated
Vin(L)	< 0.8V (TTL)
Vin(H)	> 2.0V (TTL)
Vout(L)	< 0.8V @ Iout = -400 mA
Vout(H)	> 2.4V @ Iout = 1 mA
Vout(H) max	< 42V with external open drain pull-up
Alarming	Maskable pattern match or state change
Speed	4 ms (max) alarm sampling
Latency	5 ms (typical) to 34970A alarm output
Read/Write Speed	95/s

Totalize Input

Count events from devices like photo interrupters, limit switches, and Hall-effect sensors.

It keeps an updated total which can be read via the front panel or programmatically at any time. With 26 bits of resolution, it can count events at full speed for nearly 11 minutes without an overflow.

Totalize Input

Max Count	$2^{26} - 1$
Totalize Input	100 kHz (max) Rising or falling edge, programmable
Signal level	1 Vp-p (min) 42 Vpk (max)
Threshold	0V or TTL, jumper selectable
Gate Input	TTL-Hi, TTL-Lo, or none
Count Reset	Manual or Read + Reset
Read Speed	85/s

Analog Output

Use the two electronically calibrated analog outputs to source bias voltages to your device under test, to control your analog programmable power supplies, or use the outputs as setpoints for your control systems. The outputs are programmed directly in volts, either from the front panel or from the bus.

Analog Output

DAC 1, 2	± 12V, nonisolated
Resolution	1 mV
I_{OUT}	10 mA max
Settling time	1 ms to 0.01% of output
Accuracy	±(% of output + mV)
1 year ±5°C	0.25% + 20 mV
Temp. Coefficient	± (0.015% + 1 mV)/°C

Rack Mounting and Dimensions

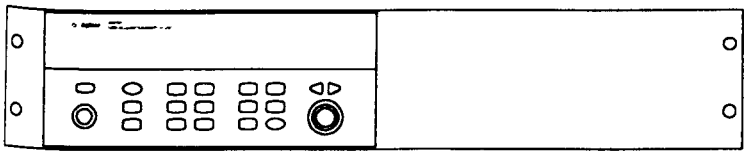

To rack mount a single instrument, order adapter kit 5063-9240 (Option 1CM).

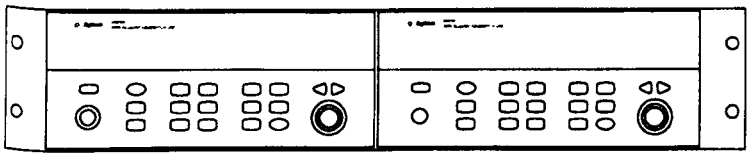

To rack mount two instruments side-by-side, order lock-link kit 5061-9694 and flange kit 5063-9212.

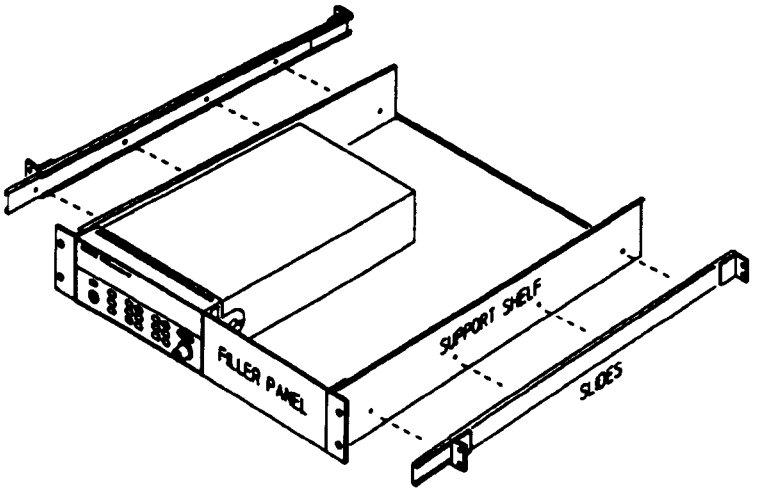

To install one or two instruments in a sliding support shelf, order shelf 5063-9255, and slide kit 1494-0015 (for single instrument, also order filler panel 5002-3999).

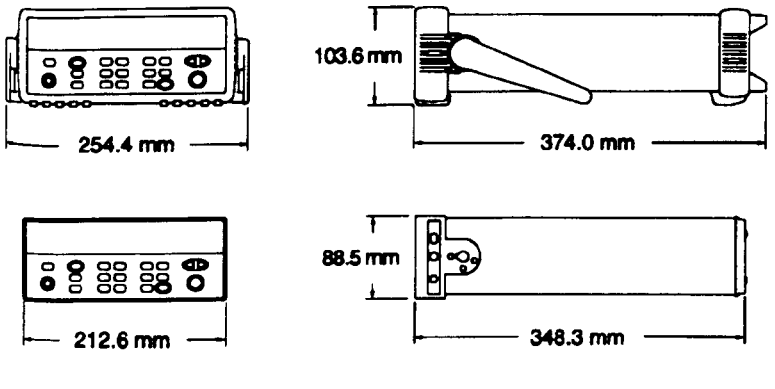

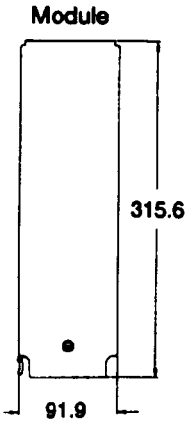

Ordering Information

Mainframe

34970A Data Acquisition/Switch Unit
Includes internal 6½ digit DMM, Operating and Service Manuals, Test Report, power cord, and Quick Start package (includes HP Benchlink Data Logger software, RS-232 cable, thermocouple, and screwdriver) Modules are purchased separately and are required to operate.
Option 001 Delete Internal DMM
Same as above but deletes DMM and Quick Start package. Order 34970-80010 to retrofit DMM at a later time.
Option 1CM Rack Mount Kit
Option 0B0 Delete Manual Set

Modules

34901A 20-Channel Armature Multiplexer
34902A 16-Channel Reed Multiplexer
34903A 20-Channel Actuator/General Purpose Switch
34904A 4 x 8 Two-Wire Matrix Switch
34905A Dual 4-Channel RF Multiplexer, 50 Ohms
34906A Dual 4-Channel RF Multiplexer, 75 Ohms
34907A Multifunction Module
34908A 40-Channel Single-Ended Multiplexer

Accessories

34307A 10-pack of J-type thermocouples
34308A 5-pack of 10 kΩ thermistors
34161A Accessory Pouch
34131A Hard Carrying Case (Transit Case)
34397A dc-to-ac Inverter
E2050A LAN/GPIB Gateway
34970-80010 DMM Field Installation Kit
Fully calibrated with Test Report and Quick Start Kit
34905-60001 Kit of 10 SMB-to-BNC adapter cables, 50Ω
34906-60001 Kit of 10 SMB-to-BNC adapter cables, 75Ω

Related Literature	Pub. number
Accessories for the 34970A Data Acquisition/Switch Unit, data sheet	5966-4443EN
Practical Temperature Measurements, application note	5965-7822E

Agilent Technologies' Test and Measurement Support, Services, and Assistance

Agilent Technologies aims to maximize the value you receive, while minimizing your risk and problems. We strive to ensure that you get the test and measurement capabilities you paid for and obtain the support you need. Our extensive support resources and services can help you choose the right Agilent products for your applications and apply them successfully. Every instrument and system we sell has a global warranty. Support is available for at least five years beyond the production life of the product. Two concepts underlie Agilent's overall support policy: "Our Promise" and "Your Advantage."

Our Promise

"Our Promise" means your Agilent test and measurement equipment will meet its advertised performance and functionality. When you are choosing new equipment, we will help you with product information, including realistic performance specifications and practical recommendations from experienced test engineers. When you use Agilent equipment, we can verify that it works properly, help with product operation, and provide basic measurement assistance for the use of specified capabilities, at no extra cost upon request. Many self-help tools are available.

Your Advantage

"Your Advantage" means that Agilent offers a wide range of additional expert test and measurement services, which you can purchase according to your unique technical and business needs. Solve problems efficiently and gain a competitive edge by contracting with us for calibration, extra-cost upgrades, out-of-warranty repairs, and on-site education and training, as well as design, system integration, project management, and other professional services. Experienced Agilent engineers and technicians worldwide can help you maximize your productivity, optimize the return on investment of your Agilent instruments and systems, and obtain dependable measurement accuracy for the life of those products.

Get assistance with all your test and measurement needs at:
www.agilent.com/find/assist

Printed in U.S.A. 4/00
5965-5290EN

Agilent Technologies
Innovating the HP Way

Appendix A3.2

Calibration of the Instrumentation used for the Flow and Temperature Measurements

---

A3.1 Introduction

This appendix presents the calibration of the experimental devices and uncertainty analysis for the validation of the present work. Accrediting the input of our experimental work includes refining these inputs for the use in the results and analysis get accurate measurements of flow conditions. The level of accuracy of the data is based on the measuring procedure, instrument errors and environmental conditions. Errors associated with the output of the flow measurements can be eliminated when each sensor is well calibrated accurately.

Therefore, a sequence of calibration procedures were performed and tested, whiles a series of analyses are provided to measure the influence of these measurements on flow parameters that estimated with some uncertainty

A3.2 Airflow Measurements

The air flow rate is determined from the flow velocity measured across a small tube diameter (i.e. 0.11 m) installed in the chamber in line with the supply input ducts. For more accuracy, the measurements were taken at the inputs of ducts locations. The airflow rate can be calculated from equation A3.2.1. The estimated uncertainty for the air flow rate measurement is ± 5.7%.

Since the input airflow rate is measured using velocity meter, the accuracy of the velocity meter is significant for the calculation of airflow rate. Hence, it is essential to pay a close attention to the manufacturers' published accuracies of the velocity meter to find out the errors of the input airflow calculated.

The air flow calculated is the reference for best measurement we expect from the sensors. However, the actual measurement will not so adequate as the theoretical ones, the output from the sensors will lead to some errors in the measured value for approximately of 5% according to the manufacturers' manuals. Figure A3.2.1 presents the velocity calibration for measurements using a rotating vane anemometer LC6000 (manufactured by airflow, 2001, approved to BS EN ISO 9001). Its standard accuracy at 20°C and 1013mb is around ±2% for the readings between 5-30 m/s, and ±0.1m/s for the readings between 0.25-4.99 m/s.

The airflow calculated is based on the ideal velocities in the catalogue data that is corresponding to the best measurement for the velocity of the inlet air. However, since the predictable error occurs for the velocity measured, there could be a deviation from the airflow rate calculated based on the ideal value. When the velocity is obtained, the airflow rate is calculated:

$$Q = 60\ V\frac{\pi d^2}{4} \qquad \text{(A3.2.1)}$$

Where Q (m^3/min) is the airflow rate, V (m/s) is the measuring velocity and d (m) is the tube diameter at designated plane. From equation A3.2.1, the error in airflow rate is 0.057m^3/min.

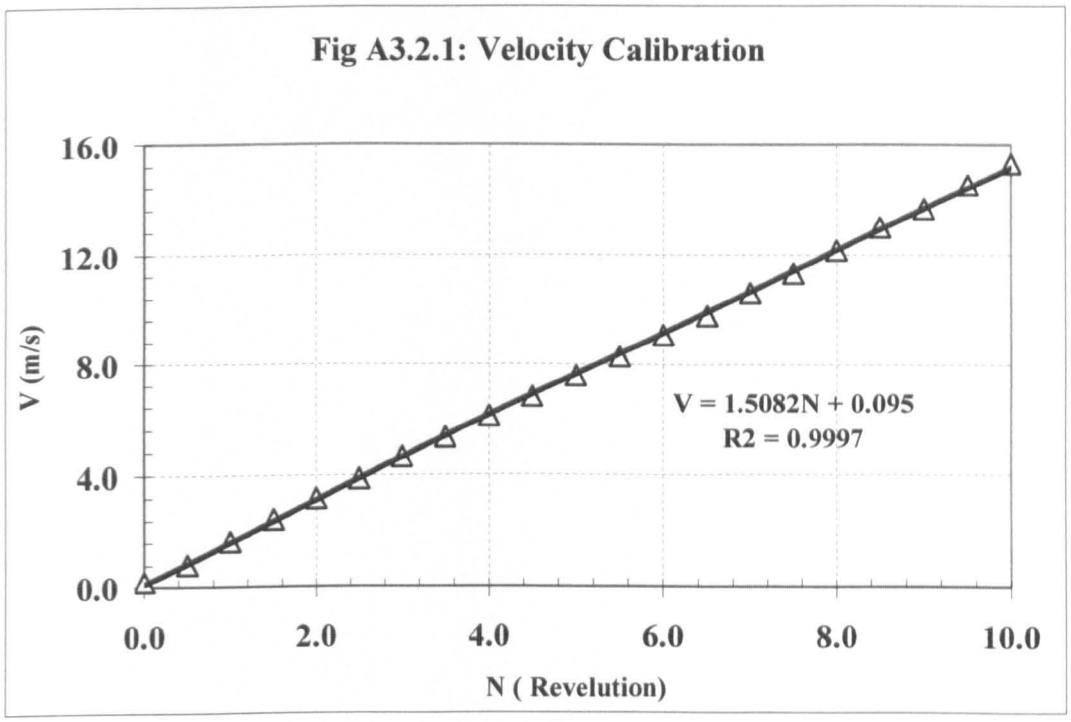

Figure A3.2.1 shows the calibration of airflow rate against a rotating vane anemometer LC6000.

A3.3 Temperature measurement

As the stratification phenomenon of air modeling technique is strongly depended on temperature gradient during heating or cooling process, monitoring of temperature is necessary throughout all experiments. However, in a built environment, temperature sensors were chosen to be sensitive to the small changes of temperature readings. Thermocouples type K is simple, rugged, prevalent and low cost contact sensors, where the temperature measuring units (HP pinch link data logger) is on hand.

A thermocouple is a temperature measurement device with two junctions. During temperature measurement, the two junctions are placed under different temperatures therefore a contact potential voltage is formed. The thermocouple signal is very small, normally a few mV, and often requires amplification for successive uses. The value of the potential depends on the types of the metals and the temperature of the junction.

Thermocouples K-type sensors are the most precise and accurate for measuring temperatures of stratification in built environment. They are simple, rugged, prevalent

and low cost contact sensors. They are also much simpler to deploy and easy service, as they are mounted on a single cable rather than dozens of cables. They connect to a single data logger channel (20 channels) on a low-cost logger providing an instantaneous picture of chamber temperature.

The thermocouples K-Type were calibrated by using a Platinum one. The medium was set to a particular temperature. Thermocouple voltage and Platinum readings were recorded continuously. When the temperature was steady for 20 minutes, the medium was adjusted for a new temperature and the temperature recording procedure repeated. These measurements were taken every 30 seconds while the temperature was increased from 10°C to 55°C.

The calibration factor, for the Aluminum /Constantan coaxial thermocouple, was taken as 39.6 μV/ °C. This value was supplied by the manufacturer. To verify this calibration factor, a number of points of temperature versus voltage output were measured and plotted in Figures A3.2.3 to A3.2.22 and listed in table A3.2.1. Calibration plot was made of thermocouple reading voltages against Platinum temperatures. The fitted equations have been found for each thermocouple probe using linear regression analysis tool in Excel software. The resulting linear fits shown in Figures A3.2.3 to A3.2.22 can be displayed saved and programmed on a personal computer to automatically adjust the temperature readings during data acquisition.

Thermocouples calibrations show that the relationship between the temperature and the voltage output of the thermocouples is nearly linear. The output voltage was from -1.0 mV to a value of +1.0 mV (for the temperature from 10 °C to 55 °C). The errors in temperature measurement were reported in table A3.2.1 and plotted in Figure A3.2.2. The slope of a linear fit through the data, revealed an overall average value of 40.26 μV/ °C with an overall standard deviation of 1.02 μV/ °C. This is very close to the value supplied by the manufacturers of the thermocouple (39.6 μV/ °C), with an overall average percentage error of 2.42 % and an overall standard deviation 1.67%. Most thermocouples do behave perfectly linearly for temperature ranges (10-55 °C) and this value might change for different temperature ranges. It is also noted that the model uncertainty discussed above is limited to the calibration ranges of certain temperatures and flow rates. If the temperatures and flow rates are considerably away from these ranges, the model errors are expected to be higher than what we have estimated.

Thermocouple No.	Slope µV/ ˚C	Offset	Error µV/ ˚C	Error%
1	42.10	1.1714	2.50	5.94
2	41.60	1.2265	2.00	4.81
3	39.90	1.1819	0.30	0.75
4	40.80	1.2032	1.20	2.94
5	38.50	1.1703	-1.10	2.86
6	40.90	1.2340	1.30	3.18
7	38.30	1.1802	-1.30	3.39
8	40.80	1.2435	1.20	2.94
9	40.90	1.2110	1.30	3.18
10	41.40	1.2552	1.80	4.35
11	39.20	1.2012	-0.40	1.02
12	40.00	0.0000	0.40	1.00
13	40.30	1.2153	0.70	1.74
14	41.90	1.2782	2.30	5.49
15	39.00	1.2026	-0.60	1.54
16	40.00	0.0000	0.40	1.00
17	39.80	0.1211	0.20	0.50
18	40.00	0.0000	0.40	1.00
19	40.00	0.0000	0.40	1.00
20	40.00	0.0000	0.40	1.00
21	40.00	0.0000	0.40	1.00
Average	40.26		0.66	2.41
STDEV	01.02		1.02	1.67

Table A3.2.1 shows a review of Figures A3.2.3 to A3.2.22 as well as the estimated error, overall average error and it standard deviation of the measured values.

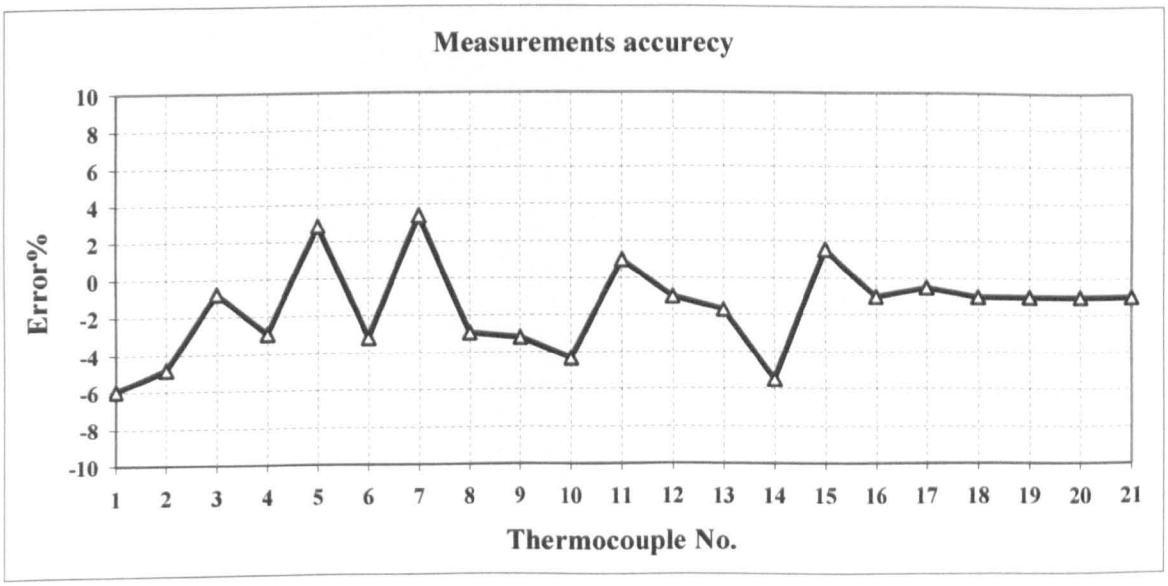

Figure A3.2.2 shows the percentage error estimated from Figures A3.3 to A3.2.23.

Figure A3.2.3: Calibration results for thermocouple no. 1

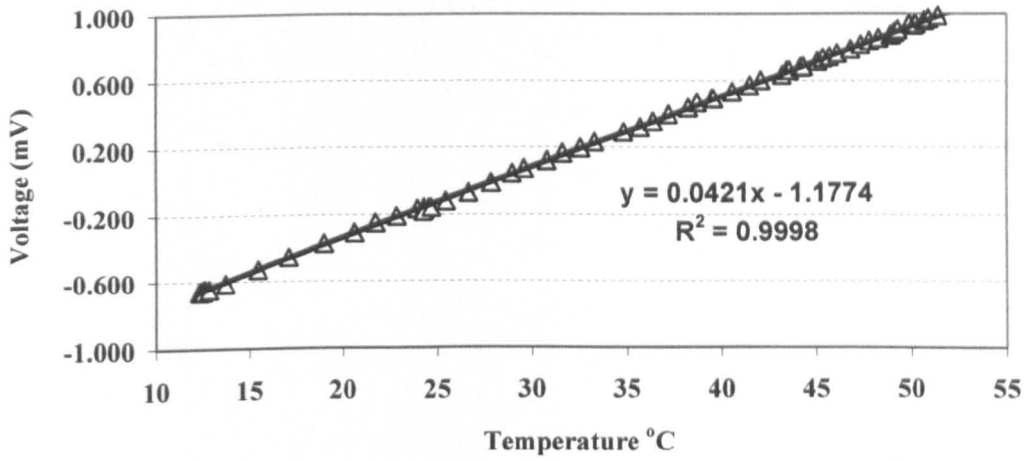

Figure A3.2.4 Calibration results for thermocouple no. 2

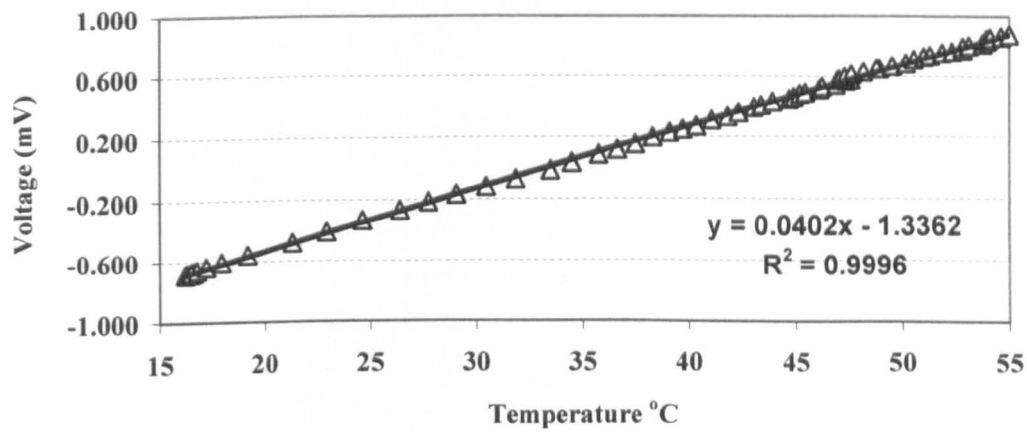

Figure A3.2.5 Calibration results for thermocouple no. 3

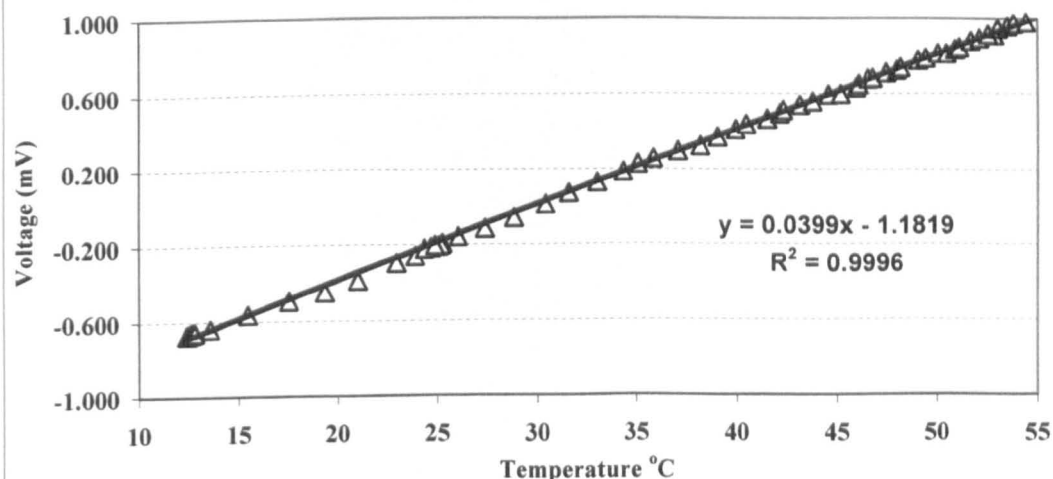

Figure A3.2.6 Calibration results for thermocouple no. 4

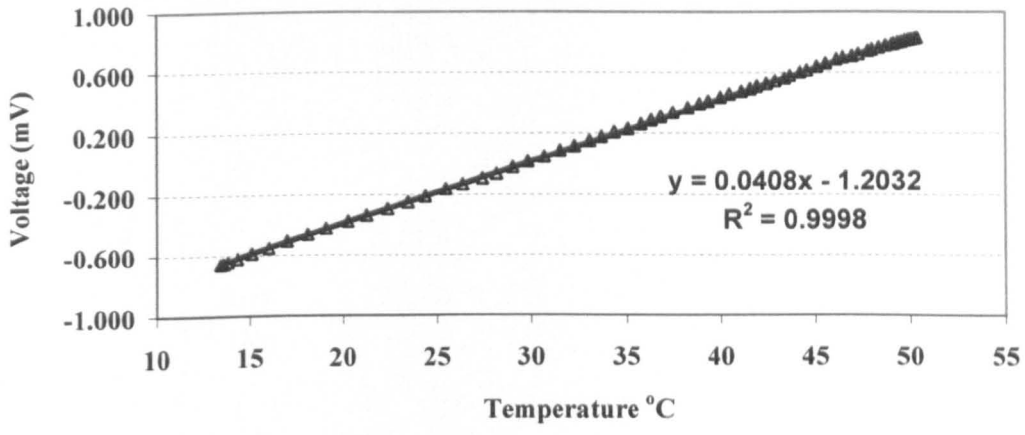

Figure A3.2.7 Calibration results for thermocouple no. 5

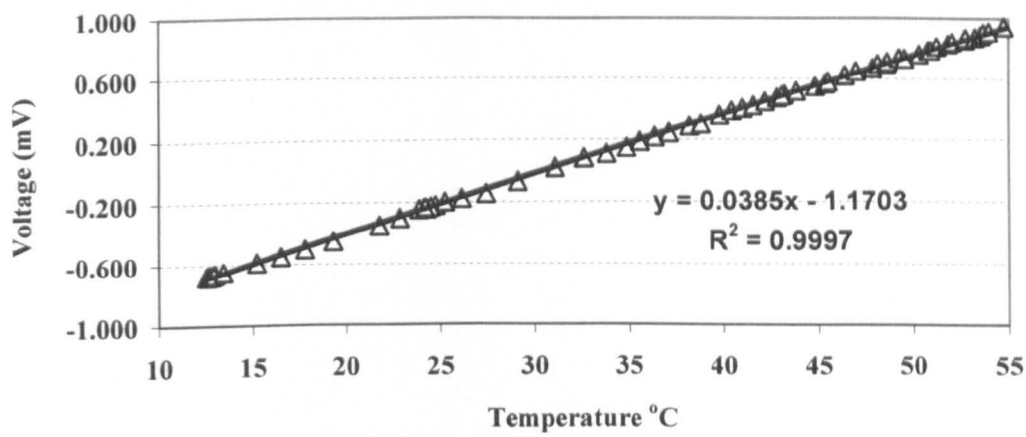

Figure A3.2.8 Calibration results for thermocouple no. 6

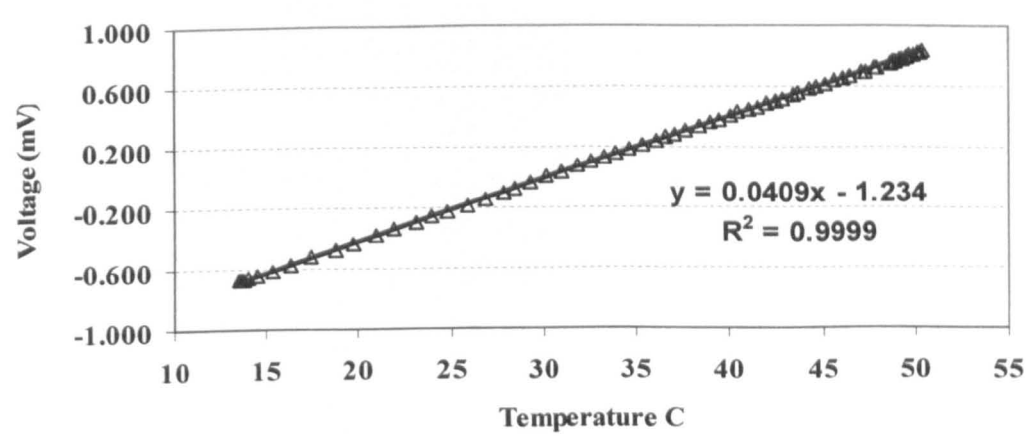

Figure A3.2.9 Calibration results for thermocouple no. 7

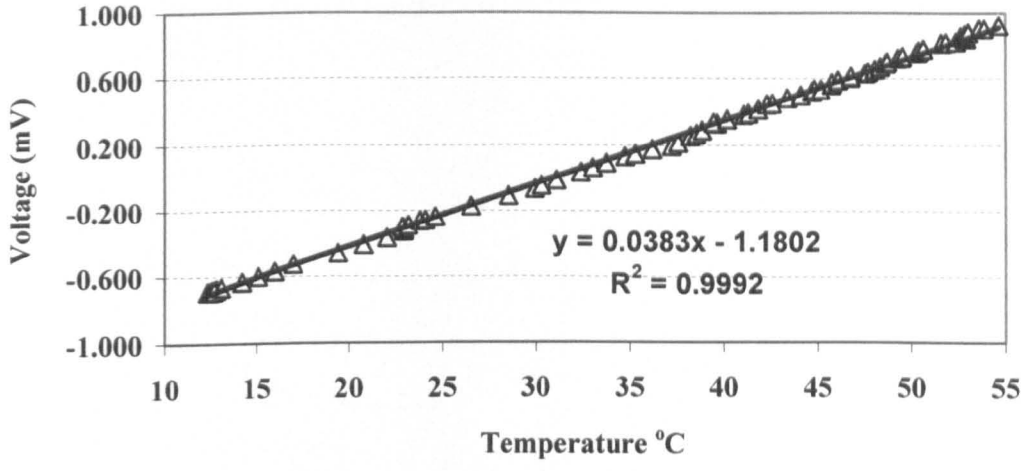

Figure A3.2.10 Calibration results for thermocouple no. 8

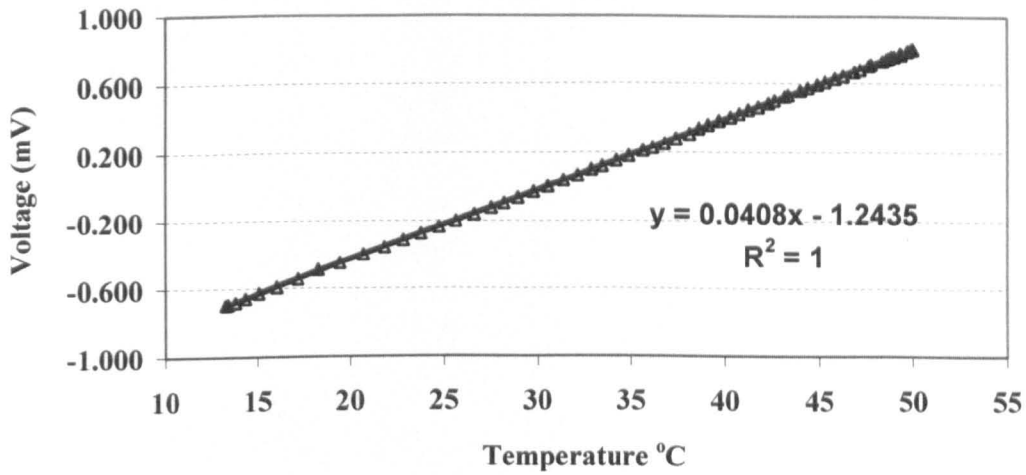

Figure A3.2.11 Calibration results for thermocouple no. 9

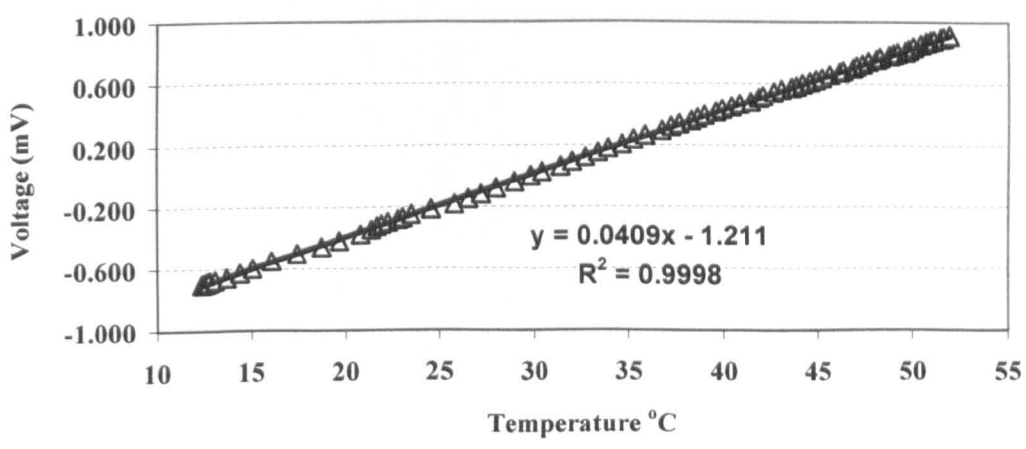

Figure A3.2.12 Calibration results for thermocouple no. 10

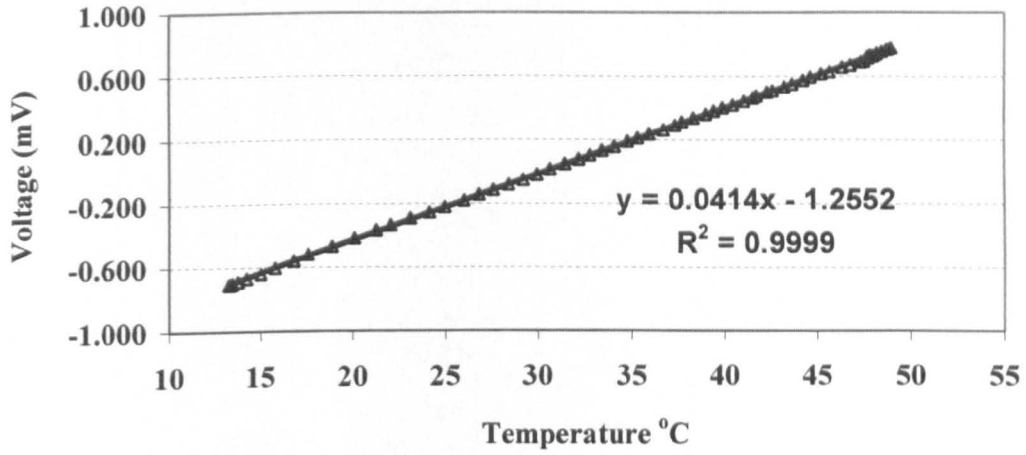

Figure A3.2.13 Calibration results for thermocouple no. 11

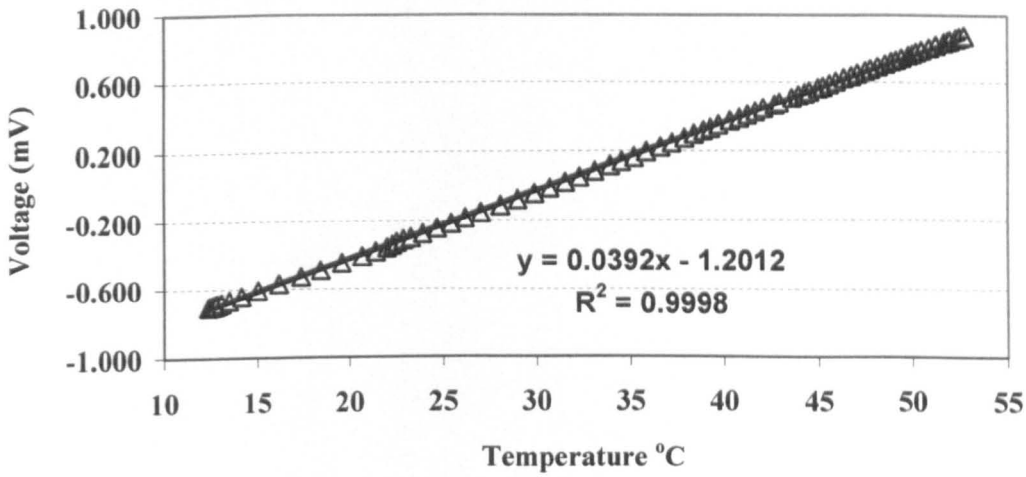

Figure A3.2.14 Calibration results for thermocouple no. 12

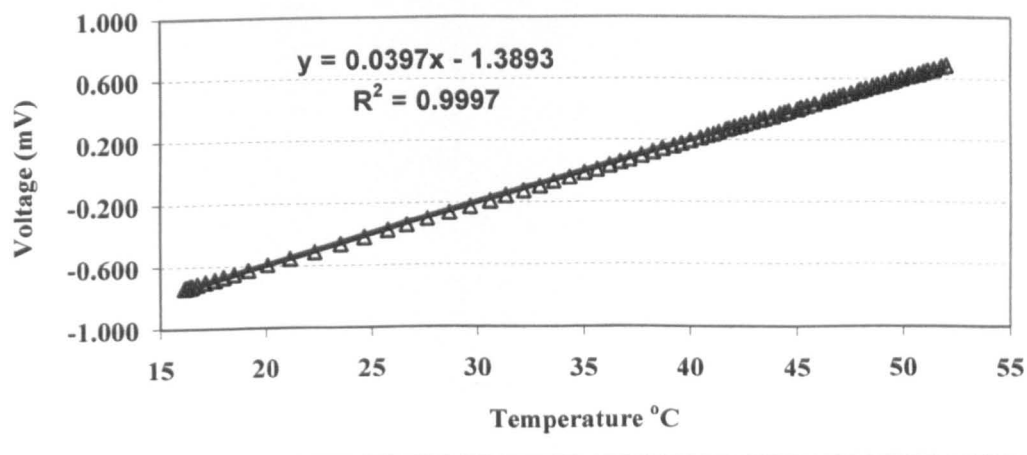

Figure A3.2.15 Calibration results for thermocouple no. 13

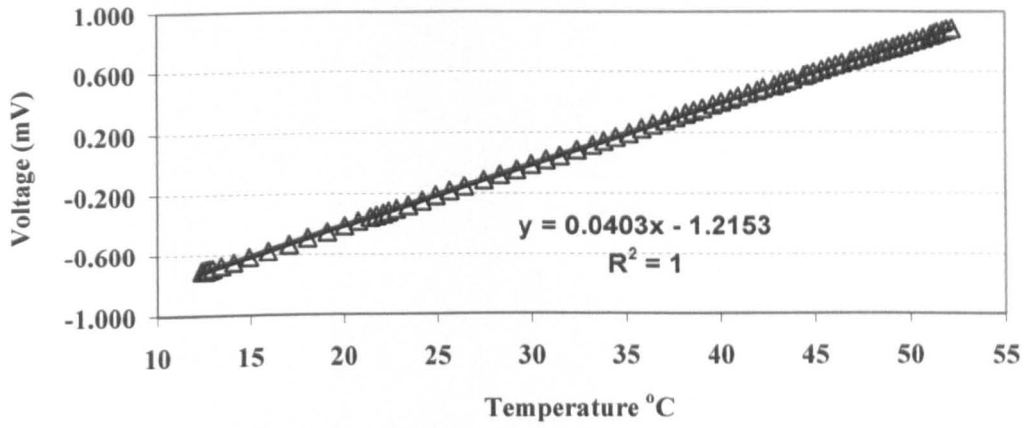

Figure A3.2.16 Calibration results for thermocouple no. 14

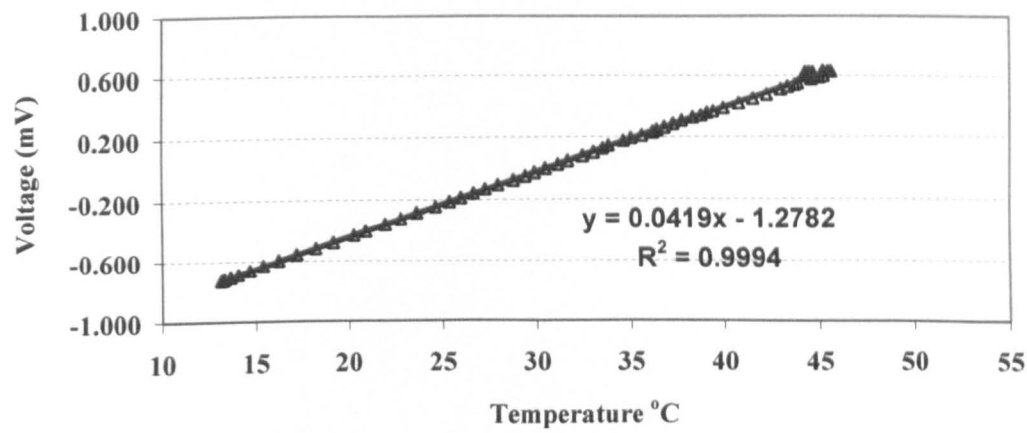

Figure A3.2.17 Calibration results for thermocouple no. 15

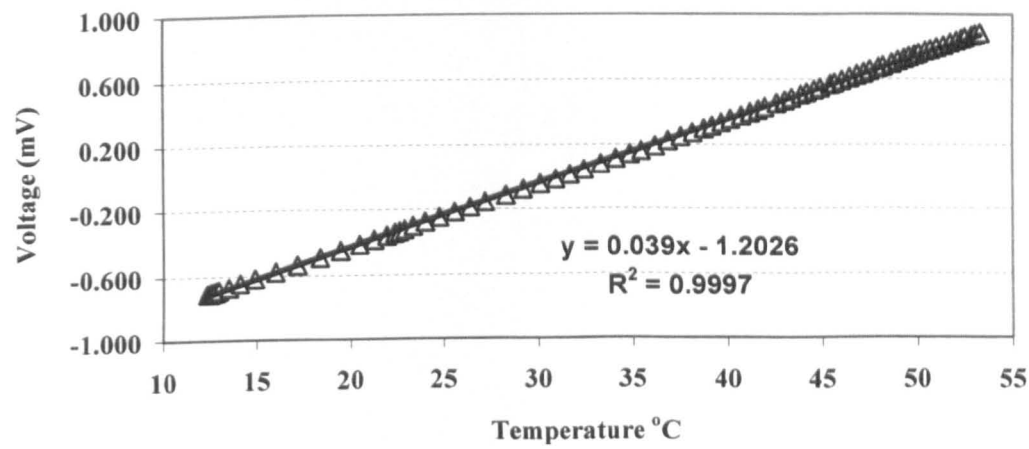

Figure A3.2.18 Calibration results for thermocouple no. 16

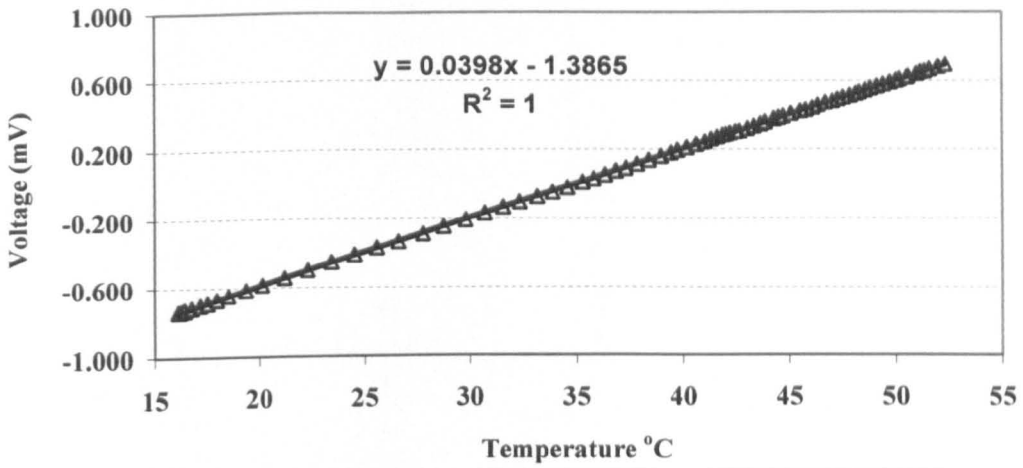

Figure A3.2.19 Calibration results for thermocouple no. 17

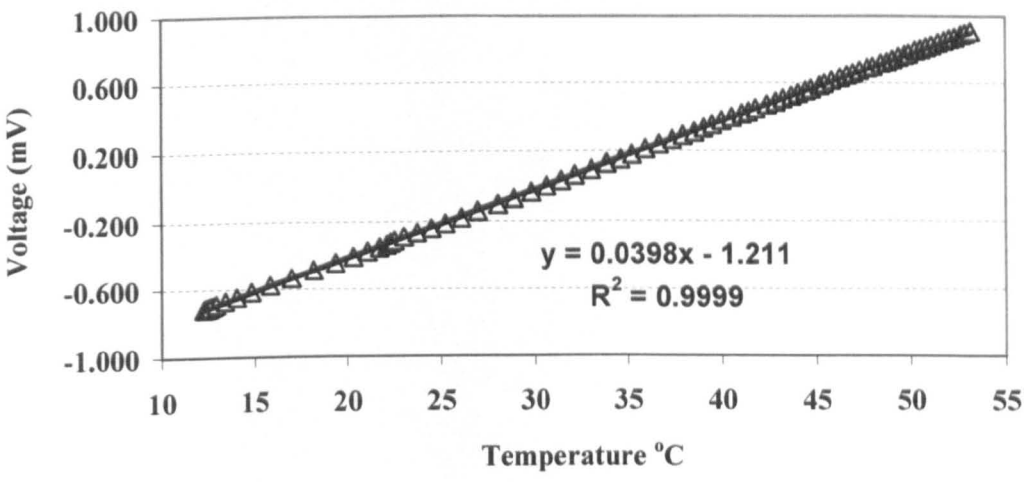

Figure A3.2.20 Calibration results for thermocouple no. 18

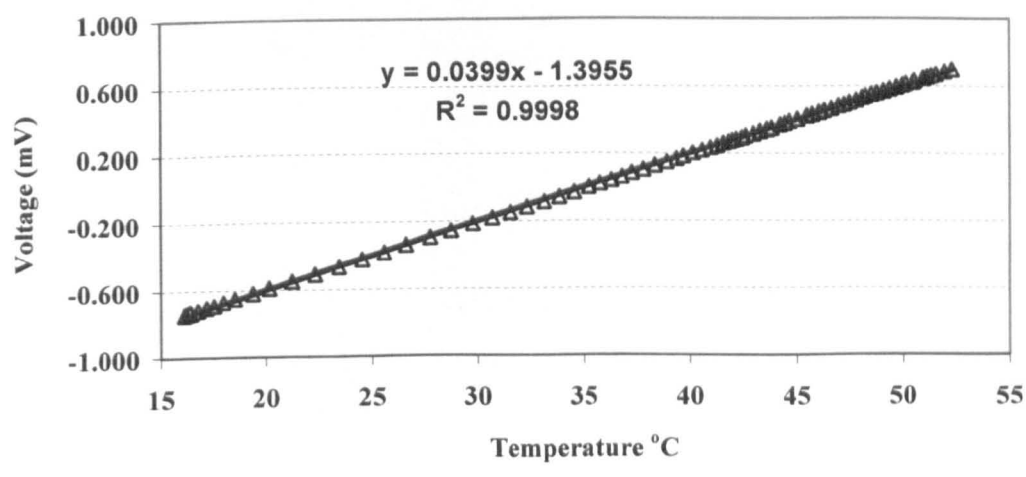

Figure A3.2.21 Calibration results for thermocouple no. 19

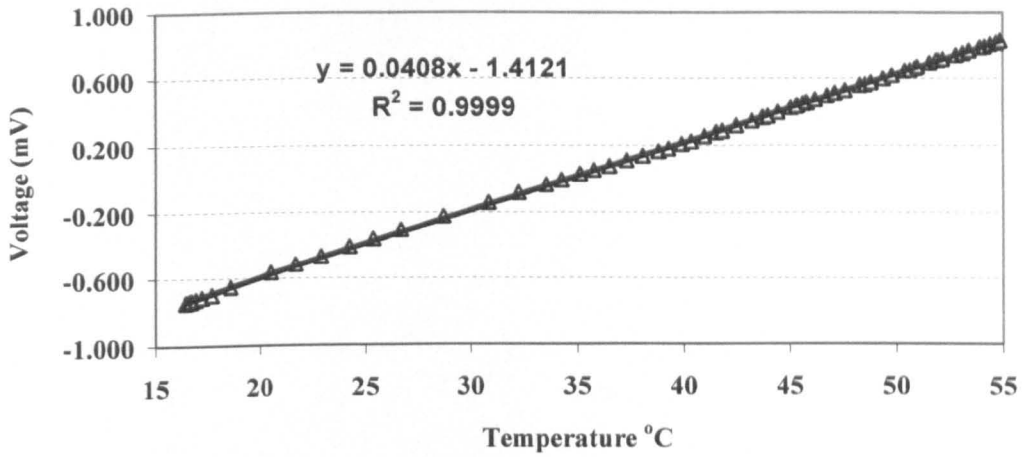

Figure A3.2.22 Calibration results for thermocouple no. 20

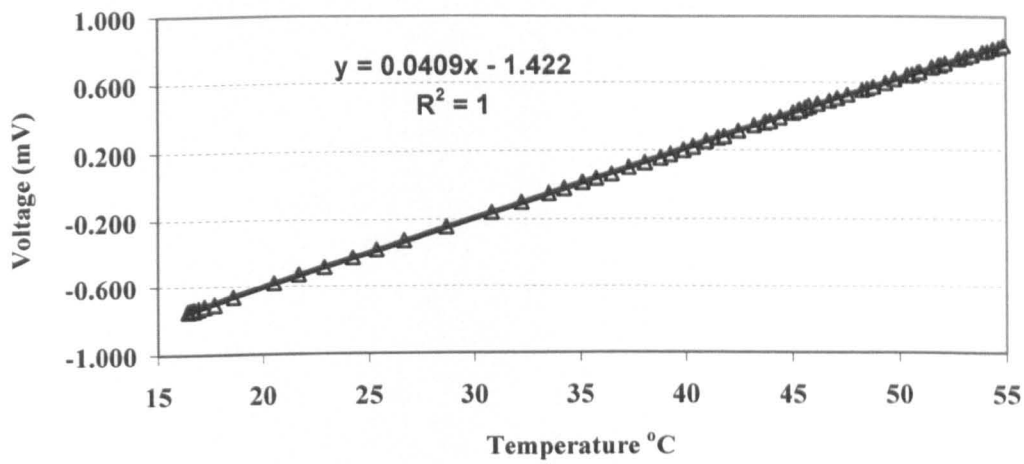

Appendix A3.3

Smoke Generator for Flow Visualization

Smoke generator for flow visualisation

Smoke generator unit was used for flow visualization. Smoke observations were done independently from temperature measurements. Vaporized Ondina EL oil (Shell, UK) from a lab-built smoke generator unit was introduced to provide a source of smoke at the center of environmental chamber. The recommended oil is medicinal quality white oil approved for use in environmental applications. The thermal and chemical specifications of the generator unit and the oil recommended are listed in the Appendix A3.3.

Specific Gravity	**0.86 at 20 °C.**
Viscosity	**14.3 centistokes at 40 °C**
Flash Point	**159 °C**
Auto-ignition Temp	**Above 250 °C**
Combustibility	**as for hydrocarbons with this flash point**
Extinguishing Media	**CO2, dry chemical powder or foam**

Aerotech

Aerodynamic Test Equipment

SMOKE GENERATOR SYSTEM

FOR FLOW VISUALISATION IN AIR

OPERATING INSTRUCTIONS

The equipment described in this publication must be used only in accordance with the instructions given herein. It should be operated by suitably qualified personnel, or under their supervision, taking care to observe such additional precautions as may be required under local health and safety regulations.

SMOKE GENERATOR SYSTEM SGS-90
OPERATING INSTRUCTIONS

PRELIMINARY PRECAUTIONS

Do not operate the Smoke Probe in a potentially explosive environment.

Never apply an electrical supply to the vaporiser unless oil is obviously present at the tip, and its flow is uninterrupted. Should the oil feed fail for any reason, the power should be switched off immediately to avoid overheating the vaporiser element and possibly burning it out.

Continued use of the probe with an oil flow insufficient for the operating conditions can result in the vaporiser's temperature rising above the ignition point of the oil. The approach of this situation is signalled by a rapid discolouration of the vaporiser through the metallic 'tempering' colours to a luminous cherry red. If, at this stage, a thin plume of bluish smoke appears, ignition is almost certain to follow immediately. This takes the form of a thin pencil of flame up to 15cm (6in) long but, providing the recommended oil has been used, there should be little risk of flash ignition or explosion spreading through the surrounding vapour loaded air. Nevertheless, the electrical and oil supplies should be turned off at once.

Provided that the electrical element remains intact and there are no significant carbon deposits, the vaporiser may still be usable after such ignition. However, if the performance is suspect, a replacement vaporiser should be fitted (see I.4).

Care should also be exercised when handling the vaporiser during use as temperatures in excess of 200°C are generated at the tip and will burn unprotected fingers.

MECHANICAL ARRANGEMENTS AND MOUNTING

The general appearance of the smoke probe and its screw-on vaporiser are shown in the illustrations.

The smoke probe may be attached to any convenient supporting structure by means of clamping the stainless steel body (12mm diameter) in a suitable rig. In most applications the exit orifice is fixed to a point downstream parallel to the local air flow but this may be modified to suit particular experimental conditions, subject to unavoidable deterioration in plume quality. Arrangements for mechanically traversing the probe or for hand held operation are best devised to suit individual requirements. Quotations for special probes with different dimensions and shapes to suit particular needs can be supplied on request.

EXTENSION HANDLES

If an extension handle has been supplied with this unit, it is not possible to ship the Probe and Handle as an assembly and must therefore be assembled by the user. To do this, unscrew the two blue plugs on the probe lead, attach the Oil Delivery Tube to the probe ensuring it is pushed well on to the small diameter stainless steel tube at the bottom. Thread the electrical cable by arranging blue plugs piggy back and oil pipe through the handle and secure the body of the probe to the handle with two M3 grub screws provided. Re-screw the plugs on the probe lead. The unit is now ready for use. If the cable needs to be extended - add to that existing - DO NOT attempt to replace the existing cable. Any 30V/3a capacity is sufficient.

OPERATION

1.0 INITIAL SETTING UP

1.1 First check the label on the rear of the unit and ensure that the voltage is correct for your local supply. Please also read "Preliminary Precautions" on the preceding pages of these instructions.

1.2 BEFORE CONNECTING TO MAINS SUPPLY - Turn "Heater Voltage" knob to "0" also "Oil Flow Rate" knob to "0". Place both pump and mains switches to OFF position.

1.3 Connect the oil delivery tube from the probe to the "Oil Feed" nipple on the front panel. Push fully home. Connect the two blue banana plugs from the probe lead to the 4mm "Heater Supply" sockets on the front panel. There is no preferred order of connection to these sockets since it is an AC supply which is isolated from both the unit chassis and the mains earth.

1.4 Screw one of the vaporisers supplied to the probe tip ensuring a reasonable "finger tight" fitting. Take care when fitting vaporisers that it is the right way round when introducing it to the probe tip: otherwise permanent damage may be caused to the fine heater element wire or its encompassing ceramic former.

1.5 Fill the oil reservoir bottle (white cap in unit cover) to about 2/3 full with SHELL ONDINA OIL EL and replace cap. Ensure that the bottle cap has a breather hole drilled into it - do not replace it with the similar cap to be

found on the spare oil bottles as supplied by AEROTECH without first drilling a minimum 2mm hole through it and its sealing washer.

1.6 Connect the mains lead to a suitable supply and switch on the mains on the front panel. Move the pump switch to DELIVER and increase the OIL FLOW RATE to its maximum position (10). The numbers around this knob are purely arbitrary and are only intended as a guide in setting up. Oil will begin to flow and will be evident at the tip of the vaporiser within 2-3 minutes of switch on.

When it appears that the vaporiser is fully wetted with oil reduce the flow rate to position 4 and turn the heater control knob to a position approximately at 20 - 25V. At this point the oil becomes less viscous and begins to drip from the vaporiser more quickly. Within a few seconds it will begin to vaporise and a fairly dense plume of smoke will appear.

WARNING - The vaporiser will now be very hot and will burn fingers!!!

1.7 The probe may now be introduced into the air stream (if it is not already) and the OIL FLOW RATE and HEATER VOLTAGE adjusted to suit prevailing conditions as necessary.

NOTE: No one air flow situation is the same as another, therefore AEROTECH cannot recommend ideal settings. It will be up to the individual operator to familiarise him/herself with the equipment and make adjustments accordingly. Please take note of the preliminary precautions preceding this section.

1.8 To discontinue use of the Smoke Generator - first reduce the heater voltage to zero and allow the pumped oil to flood the vaporiser for a few

seconds. This will reduce the possibility of carbon build up in the element. Next reduce the oil flow rate to zero and switch off the pump.

If it is not intended to use the unit again for some time, then switch the pump to DRAIN and increase the oil flow rate to maximum. The oil should fully drain from the probe and delivery tube within 2-3 minutes. Finally, switch off both the pump and the electrical mains.

1.9 For a short pause in operation there is no need to drain the system. Simply reduce the heater voltage and switch off the pump IN THAT ORDER. Since the pump speed has not been altered, reactivation is soon achieved by switching the pump to deliver and resetting the heater voltage to the previous operating setting.

2.0 FURTHER NOTES

2.1 USE IN MEDIUM AND HIGH SPEED AIR FLOWS

A filled reservoir contains sufficient oil for approximately six hours of normal operation of the equipment and during this time the smoke plume should remain sensibly constant. It is advisable, however, to check the oil level after every half to one hours running in case undetected leaks or accidental misadjustments have resulted in excessive loss which could result in the supply to the vaporiser becoming depleted.

2.2 USE IN NEAR ZERO AND LOW SPEED AIR FLOWS

As the smoke probe continues to function in still air it can be used to determine flow patterns in very low velocity air streams. Applications arise in heating, ventilating and extracting systems, and many other aspects of environmental control and simulation.

For maximum smoke emission under these conditions the heater voltage is best limited to 15 - 20 volts. The oil supply will have to be adjusted accordingly.

If, after a few seconds operation, oil is seen to drip or spit from the exit orifice, the flow must be reduced. On the other hand, if a transparent heat haze extends outwards for more than 12mm (0.5in) from the orifice before condensing into visible smoke, either increase the oil flow or reduce the heater voltage. If this extended heat haze is allowed to persist, there is danger of local ignition occurring (Preliminary Precautions).

Optimum conditions exist when the visible smoke plume starts no further than 3mm (1/8in) from the exit orifice.

As there is no entraining gas, the smoke exit velocity is due only to effects of thermal expansion. Although insignificant for most applications, this (and the inevitable thermal drift) may invalidate studies of very slow air currents.

2.3 VAPORISER: MAINTENANCE AND REPLACEMENT

After several hours of continuous use, the passage of oil over the element inevitably results in carbon build up. This cannot easily be removed and attempts to poke it out with a wire or needle almost always damages the element and its ceramic former. If the generator is to be used intensively, it is recommended that two vaporisers are used in rotation. After about 3 or 4 hours of smoke generation, the vaporiser should be removed, cleaned in a suitable organic solvent or degreasing agent and stored in a caustic soda solution (8g NaOH to 50ml H_2O) until required. Before refitting, rinse thoroughly in distilled water.

If a vaporiser becomes damaged, unscrew it from the stem of the smoke probe and screw on a replacement. Take care to ensure the vaporiser is held correctly so that attempts are not made to force the probe connection into the exit orifice, thus damaging the wire.

2.4 REPLACEMENT OF PERISTALTIC PUMP TUBING

The tubing used in the pump is high grade silicone rubber of 0.8mm bore and 1.6mm wall thickness. Whilst the oil delivery rate is governed by the tube bore and the pump speed and both may be adjusted to suit - the pump rollers are designed to operate with only one wall thickness tube (1.6mm) and therefore no other wall thickness should be used. Spare tubing can be obtained directly from "AEROTECH".

If, for any reason, the pump tubing should need replacing, proceed in the following manner:
Isolate the unit from the mains supply and remove the oil reservoir bottle cap. Remove 8 chrome screws securing the cover to the chassis and remove the cover.

Lift the perspex cover over the pump to expose the rollers and tubing. Unclip the pump tubing from the white retaining plastic clip on the INLET side of the pump body and pull upwards gently. At the same time rotate the pump roller mechanism by hand in a CLOCKWISE direction. The tubing will disengage itself from the rollers within 3/4 turn when the outlet end can be unclipped. Pull the silicone tubing off the stainless steel connectors. Remove any surplus oil from these connectors and ensure they are perfectly dry.

Cut a new piece of tubing 160mm in length and replace in the reverse order. Ensure that at least 20mm of tubing is pushed over the connectors and that the connectors are well seated in the white plastic clips. This will prevent the tube from becoming squashed in the clips and inhibiting oil flow. If the silicone tubing and the connectors are perfectly free from oil on assembly there will be no reason for these joints coming adrift in use. If however, these joints do come adrift then they can be sealed after assembly between tube and connector with Dow Corning "Silastic 732" silicone adhesive/sealant.

Finally, replace perspex cover and unit cover. Unit is now ready for re-use.

3.0 SMOKE GENERATOR OIL

The recommended oil is Shell "Ondina EL" (previously 'Ondina 17') or its exact equivalent. This is a medicinal quality white oil complying with USA and British pharmacopoeias. It is approved for use in pharmaceutical applications and for the lubrication of machinery and surfaces used in the manufacture of foodstuffs and confectionery.

Specific Gravity:	0.86 at 20°C.
Viscosity:	14.3 centistokes at 40°C.
Flash Point:	159°C.
Auto-ignition Temp:	above 250°C.
Combustibility:	as for hydrocarbons with this flash point.
Extinguishing Media:	CO_2, dry chemical powder or foam.
Boiling Point/Vapour Pressure:	not applicable as not volatile.

In accordance with the Health and Safety at Work Act 1974 Section 6(4)C, Shell UK Ltd state that this oil presents no health hazards from inhalation, skin absorption, skin contact, eye contact or ingestion, although prolonged over-exposure of the skin may cause some slight irritation.

Being a special solvent-refined hydrocarbon mineral oil, "Ondina EL" is classed as 'minimum risk' as far as carcinogenicity is concerned. Even this small risk is considered present only where contact is intimate, prolonged and continuous. At temperatures above about 300°C or higher (which can occur within the vaporiser, depending on operating conditions) some cracked products may form, including the possibility of a small proportion of polycyclic aromatic hydrocarbons. The latter are considered potentially carcinogenic but (to put this into reasonable perspective) so are comparable components in fumes from well-cooked meats and charring vegetable matter. When in doubt - ventilate adequately.

PROPYLENE GLYCOL

In addition to Shell 'Ondina Oil EL' Aerotech has included a 50:50 Propylene Glycol de-ionised water mix as an alternative. After initial tests Aerotech feel this may be more suitable for this particular application, due to the more rapid dispersal of the smoke. However, it is recommended that this medium is experimented with to assess suitability.

When changing between oil types, it is recommended that the existing oil be drained from the probe as detailed in section 1.8.

Specific Gravity:	1.0361 at 20°C.
Flash Point:	99°C.
Auto-ignition Temp:	above 371°C.
Combustibility:	can support combustion.
Extinguishing Media:	drychem, foam, water or CO^2

Effects: Extremely low oral toxicity. Unlikely to be hazardous by inhalation because of the low vapour pressure, however large concentration of mist may irritate the respiratory tract. Prolonged or repeated skin contact may cause irritation. Causes slight eye irritation by permanent damage is unlikely.

Appendix A3.4

Rotating Vane Anemometer LC6000

Rotating Vane Anemometer LC6000

The air flow rate is determined from the flow velocity measured across a small diameter (0.11 m) tube installed in a chamber in line with the supply input ducts. A rotating vane anemometer LC6000 (manufactured by airflow, 2001, approved to BS EN ISO 9001) was used. Its specification, operating manual and standard accuracy are listed in Appendix A3.4.

AIRFLOW™ 9020629/G/0103

SPECIALISTS IN AIR MOVEMENT TECHNOLOGY

LCA 30VT, LCA 30RVT and LCA 30VA

Operating Instructions

1. INTRODUCTION

Models from the LCA range which are described in these instructions are all rotating vane anemometers featuring digital display of Velocity (and Volume Flow rate on the LCA30VA) in metric or imperial units.

The LCA range has been designed for ease of operation with one operational control on the side of the handle. A slide switch is provided below the display to switch the unit On and Off, Metric and Imperial readout can be selected by means of a switch in the battery compartment.

The VA model also has an additional button on the front of the unit to scroll through the menu.

1.1 LCA30VT displays air velocity in Metric or Imperial units ranging from 0.25 to 30 m/s or 50 to 6000 ft/min. The instrument utilises a Microprocessor which enables the user to obtain a continually updated average of air velocity over extended periods.

1.2 The LCA30RVT is specially calibrated in reverse so that the display faces the operator when taking extract velocity measurements such as at the sash windows of fume cupboards or laminar flow safety cabinets. Calibration results are plotted for flows up to 5m/s to ensure accuracy for low extract velocity situations.

1.3 The LCA30VA displays air velocity or volume flow rate in Metric or Imperial units. Air velocity ranges from 0.25 to 30m/s, 50 to 6000ft/min whilst volume flow rate can be displayed from 0.01 to 3000m^3/s, 1 to 999999 l/s, 1 – 999999 m3/hr and 1.0 to 999.9E^3 cfm (Note; 999.9 x 10^3 displays as 999.9E3) with duct cross sectional areas programmable within the range of 0.00399 to 90.00m^2, 0.043 to 900.0 ft^2.

2. BATTERY INFORMATION

2.1 Instruments in the LCA range are supplied with a battery but this is not fitted into the instrument.

Due to the limited shelf life the battery is not covered by the Airflow standard warranty.

To fit the battery press firmly on the battery compartment cover and slide it in the direction of the arrow.

Carefully pull out the battery connector and flying lead and fit the battery to it. Place the battery and lead into the compartment and refit the cover and the screw if applicable. The instrument is now ready for use.

Do not leave a discharged battery in the instrument or the battery in place if the instrument is out of use for a long period of time.

2.2 **Type of Battery**

9V batteries type PP3 (IEC 6F22) or equivalent, standard, alkaline or rechargeable.

2.2.1 **To Remove a Battery.**

Remove the battery from the connector using a small screwdriver or similar tool. Do not disconnect it by pulling on the flying lead.

2.2.2 **Low Battery Indication**

If the battery voltage falls below a pre-determined level, the display will show "bat" in the top left hand corner. The instrument will still operate correctly but only for a limited time so the battery should be replaced as soon as possible.

3. Metric/Imperial Switch

All instruments in the range can display Metric or Imperial units. The metric/imperial switch is in the

battery compartment, See Fig 1.

Note: Unit must be off when changing from imperial to metric or vice versa.

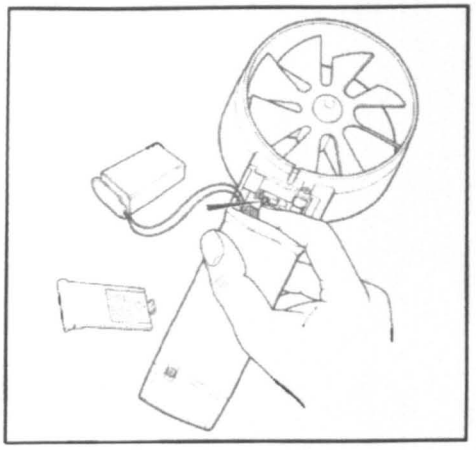

Figure 1

4. To Use the Instrument

4.1 LCA 30VT and LCA 30RVT:

Switch on the instrument using the on-off switch marked 0, 1 below the display. Hold the rotating vane in the airstream according to the direction of flow arrow on the side of the instrument. Allow the vane a few seconds in the airstream to enable it to reach a steady speed. The instrument may then be used in two modes:

4.1.1 A momentary push on the switchplate will display the average velocity over about a two second period.

4.1.2 Pushing and holding down the switchplate will display the average velocity over the period that it is depressed. During this time the instrument is programmed to display the current average reading about every two seconds. If the instrument is used in this mode for long periods, the memory will become full after about 12 minutes and the display will indicate 'FULL. The last valid reading will be displayed when the switchplate is released. This reading will continue to be displayed until the instrument is switched off. This erases the memory, extinguishes the display and makes the instrument ready for use again.

4.2 **Note:**

4.2.1 Incorrect readings may be displayed if the metal plate within the anemometer ring is touched whilst using the instrument.

4.3 LCA 30VA (See Figure 2 for Mode cycles)

4.3.1 Velocity Mode

Switch on instrument to 'VEL' using the Mode Button below the display. The instrument may then be used exactly as described for the LCA 30VT above (see sections 4.1 and 4.2).

4.3.2 Volume Flow Rate Mode

Before switching on the instrument determine the cross-sectional area of the duct, grille etc for which the volume flow rate is required. If working in Metric units, calculations must be in m^2. If working in Imperial units, calculations must be in ft^2. Switch the instrument to 'Area +' mode observe the area figure displayed from the memory. If the new area required is larger than the one displayed press the switchplate to increase the displayed area to the calculated figure. If the area is to be less than the figure displayed push the Mode Button to move to 'Area -' mode and press the switchplate to reduce the displayed area to the

calculated figure. When the correct area has been displayed use the Mode key to select the required 'Vol' mode.

Note: The last area value will be retained in the memory even when the instrument is switched off.

The instrument may then be used in two modes:

4.3.2.1 A momentary push on the switch plate will display the average volume flow rate over about a two second period.

4.3.2.2 Pushing and holding down the switchplate will display the average volume flow rate over the period that it is depressed. During this time the instrument is programmed to display the current average reading about every two seconds. If the instrument is used in this mode for long periods, the memory will become full after about 12 minutes and the display will indicate 'FULL'. The last valid reading will be displayed when the switchplate is released.

4.4 Notes:

4.4.1 Incorrect readings may be displayed if the metal plate within the anemometer ring is touched whilst using the instrument.

4.4.2 If a flow reading is above the displayable range: 'rAnGE' will be displayed and the mode button should be used to select a larger measurement unit if available.

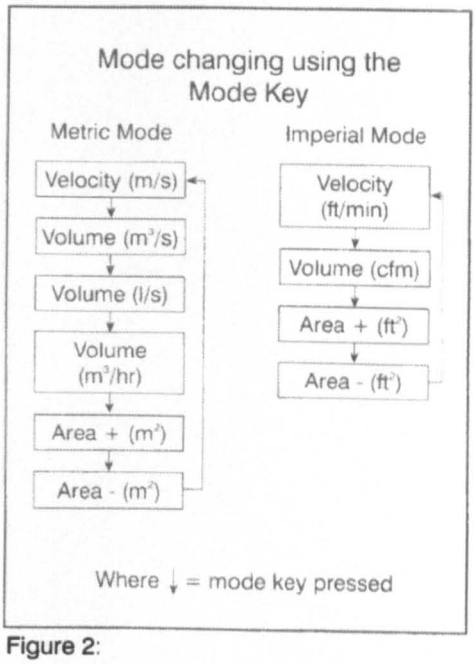

Figure 2:

5. Where to use the instrument.

5.1 Checking air velocity or volume flow rate in small areas.

The instrument will function satisfactorily in an angular position but should not be used in airstreams which are smaller than the entire face area of the measuring head (113mm diameter). The LCA range is calibrated for use in free air conditions. For smaller airstreams the Airflow TA type anemometers are recommended.

5.2 Checking air velocity or volume flow rate over larger areas.

When checking air velocity or volume flow rate over larger areas, a number of 'spot' readings should be taken and recorded as described in 4.1.1 or 4.3.2.1, to give coverage over the whole area.

Alternatively, the instrument will provide the mathematical average automatically, when steadily scanned across the whole area, if used as described in 4.1.2 or 4.3.22.

When taking 'spot' readings, it should be noted that quite large variations might be observed between individual readings. In general, the more readings taken, the more accurate the result will be. It does not matter if the positions of the readings overlap somewhat, so long as they are equally spread to cover the entire area.

6. Use on Grilles

Note: See Comments under section 8 'Possible sources of error'. Avoid intrusion of the hand, arm or handle of the instrument into the face area of the grille. The blockage effect created by this would cause artificially high velocity over the remainder of the grille, leading to additional errors.

Better measuring conditions can be obtained on grilles with adjustable direction vanes if the vanes on the grilles are temporarily straightened before making measurements. This should not significantly affect the flow rate so long as any built in dampers are not accidentally disturbed. It is advisable to use the aperture, not the surface area of the grille in any flow calculations.

The instrument is suitable for both supply and extract grilles, and the procedure for both is the same except that the measuring head must be rotated through 180° to align the direction arrow correctly.

Whilst it is acceptable to hold the anemometer head against the grille in extract it is usually recommended to hold it slightly away from the grille face on supply to avoid excessive turbulence and any vena-contracta effects.

7. Use in Airways

In Large airways the presence of the instrument will have a negligible effect, but in small airways the blockage caused by the instrument, hand and arm will cause the airstream to accelerate slightly as it passes the rotating vane. This effect is somewhat variable depending on the size of the airway and the distance from the duct walls. The error can be virtually eliminated by mathematical correction to allow for the reduction of free area caused by the obstruction. For this purpose the effective front area of the instrument (not including hand or arm) can be taken as $0.019m^2$ ($0.204ft^2$). The effect can be ignored completely if the duct exceeds about 500mm diameter (1' 9").

8. Possible sources of error

The above method ignores the effects of the reduced velocity at the duct walls. A more precise method is shown in BS 1042 Part 2.1 (ISO 3966) Log Tchebycheff method.

This procedure is satisfactory for use in ducts, and at unobstructed apertures.

Significant errors may occur if the aperture is covered by a grille, particularly if this is of the type having adjustable direction vanes and/or dampers. The airstream issuing from such a grille is invariably very disturbed, consisting of many small areas of high velocity

interspersed with areas of low velocity.

The transitions between these areas are highly turbulent, and there may even be some reversed flow. If maximum accuracy is required, it is advisable to make up a short length of test ducting which is just larger than the overall dimensions of the grille. This duct can be of any convenient rigid material (eg stiff cardboard) and should have a length about twice the diagonal measurement of the grille. The duct should be placed over the grille, and sealed to the wall with adhesive tape. Measurements of flow can now be conducted, as already described, at the unobstructed end of the test duct. Use the cross sectional area of the duct (not the grille) for the calculations.

It should be noted that using an LCA instrument as described in section 4.1.2 or 4.3.2.2 can result in an exaggerated velocity indication in applications where there is a significant variation in velocities across the test area. This is caused by the inability of the rotating vane to slow down quickly when being moved from a higher velocity area to a lower velocity area. It is quite common to experience situations where a factor of 0.9 would have to be applied although this varies considerably. For proportional balancing this does not matter but on quantitative measurement it should be taken into consideration.

9. Uncertainty of Measurement

Due to characteristics common to all rotating vane anemometers, the minute amount of bearing friction causes the head signal to depart from a linear signal/velocity relationship by an insignificant amount at high velocities but with progressively more effect below 2m/s (400 ft/mm). In the LCA range of instruments, means of compensation for this error is provided in the software enabling accuracy to be maintained to within: ±1% of reading: ±1 digit.

WARNING; ALTERING THE CALIBRATION WILL INVALIDATE AIRFLOW'S RESPONSIBILITY FOR CALIBRATION UNDER WARRANTY.

The unit will monitor each time the calibration is effected.

If the calibration routine is inadvertently entered then ABORT immediately by switching the instrument OFF and then retry.

10. SERVICE AND RECALIBRATION

If a fault or the instrument's calibration is suspected, it should be returned to Airflow Developments for repair or recalibration to original standards. In any event, it is good practice to have the instrument checked at least once a year. If an instrument is not working correctly or requires recalibration, contact your nearest Airflow agent or UK. Service Department on High Wycombe (01494) 525252 (International +44 1494 525252).

Airflow Developments operates an Instrument Hire Service for the convenience of customers having equipment repaired or recalibrated. If you intend to take advantage of this facility please contact the Service Department to make arrangements prior to returning your instrument.

11. CONTACTING AIRFLOW

Airflow Developments Ltd,
Lancaster Road
Cressex Business Park,
High Wycombe
Buckinghamshire. HP12 3QP.
England

Telephone (01494)
525252/443821.
Facsimile (01494) 461073

E-Mail: info@airflow.co.uk
WWW: http://www.airflow.co.uk

Airflow Lufttechnik GmbH,
Postfach 1208,
D53349, Rheinbach,
Germany.

Telefon: 02226-9205-0
Telefax 02226-9205-11

Airflow Technical Products Inc.
PO Box 372,
219 Route 206,
Andover,
NJ 07821 USA.

Telephone: 001-973-786-6386.
Fax: 001-973-786-7586

Airflow Lufttechnil GmbH,
o.s. Praha, Hostýnská 520,
108 00 Praha
10-Maleöice,
Czech Republic.

Telefon and Fax 02-77 22 30

12. SPECIFICATION

Parameter	Metric	Imperial
Velocity Range * Accuracy	0.25-30 m/sec Calibrated to better than +/- 1% of reading +/- 1 digit.	50-6000 ft/min Calibrated to better than +/- 1% of reading +/- 1 digit.
Volume Flow Ranges * Accuracy (VA only)	0.01 - 3000m^3/sec 1 - 999999 l/sec 1 - 999999 m^3/hr Calibrated to better than +/- 1% of reading +/- 1 digit.	1 - 999.9 x 10^3 ft^3/min Calibrated to better than +/- 1% of reading +/- 1 digit.
Air Flow Area - Ranges (VA only)	0.00399 - 90.00m^2	0.043 - 900ft^2
Maximum Averaging time.	12 Minutes	12 Minutes
Ambient Operating Environment	Barometric Pressure 500mb to 2 bar Temp -10 to +50°C	Barometric Pressure 15 in Hg to 60 in Hg Temp 14 to 122°F
Storage Temperature	-10 - +50°C	14 to +122°F
Dimensions of Instrument	268 x 113 x 43mm	10.55 x 4.44 x 1.69 in
Weight of Instrument (less battery)	280gms	0.62lbs
Battery Cells	One 9V battery type PP3 or equivalent (IEC ref 6F22) standard Alkaline or rechargeable	
Battery Life	Approximately 40 Hours using Alkaline battery cells	

*Accuracy is at ambient conditions of 20°C and 1013mb (68°F and 30in Hg.)

CE Marking: This unit complies with the EEC Directive on Electromagnetic Compatibility (EMC) 89/336/EEC.

Applied Harmonised Standards; EN50081-1 Radiated Emissions and EN50082-1 Radiated and ESD Immunities.

AIRFLOW™

QUALITY ASSURED TO ISO 9001

Airflow Developments Limited, Lancaster Road,
Cressex Business Park, High Wycombe,
Buckinghamshire HP12 3QP, England
Telephone: (01494) 525252/443821
Facsimile: (01494) 461073
E-mail: info@airflow.co.uk
WWW: http://www.airflow.co.uk

Certificate No FM00152
BS EN ISO 9001:1994

Appendix A4

Published Work

A4.1: Awad A. and Calay R., 2004, An Approximate analytical solution to flame length in a ventilated room, ASME, Vol. 485, No. 1, Pages, 65-72.

A4.2: Calay R, Awad A., 2004, A model to predict stratification in two-phase flow in horizontal pipes, ASME, Vol. 485, No. 1, Pages, 35-42.

A4.3: Awad A., Badran O., Calay R. and Holdo E, The effect of momentum jet air flow on the stratified layer characteristics. APCWE-6-The Sixth Asia-Pacific Conference on Wind Engineering, 12 - 14 September 2005, Seoul, Korea

A4.4: Awad A., Badran O., Calay R. and Holdo E., Experimental study of stratified flow in a built environment, Regional World Renewable Energy Conference-The 2nd International and Energy Conference, 22-24 January 2006, Tripoli-Libya.

A4.5: Awad A., Calay R., Holdo E. , and Badran O., The effect of input supply and flow rate on stratified flow characteristics inside enclosure, World Renewable Energy Congress-IX Programme, 19-25 August 2006, Florence-Italy.

A4.6: Jubran B., Hamdan M, and Awad A., 1994, "Prediction of transitional boundary layer over smooth and rough surfaces," Encyclopedia of Fluid Mechanics, Chapter 10, Pages, 139-163.*

A4.7: Awad A., Theoretical study of transitional boundary layer over smooth and rough surfaces, M.Sc. thesis, 1990, Amman Jordan.*

---

* Un-attached documents.

APPENDIX A1.1

An Approximate Analytical Solution

to

Flame Length in a Ventilated Room

The 12th Annual PVPD 2004
ASME Pressure Vessels and Piping Division Conference
July 25– 29, 2004, San Diego,
California, USA

Paper Number

AN APPROXIMATE ANALYTICAL SOLUTION TO FLAME LENGTH IN A VENTILATED ROOM

Ahmad Awad
Fluid Mechanics Research Group, University of Hertfordshire, College Lane, Hatfield, Herts, AL10 9AB, UK
Tel: +44(1707) 284942
Fax: +44(1707) 285086
a.awad@herts.ac.uk

Rajnish K Calay
Fluid Mechanics Research Group, University of Hertfordshire, College Lane, Hatfield, Herts, AL10 9AB, UK
Tel: +44(1707) 281098
Fax: +44(1707) 285086
r.k.calay@herts.ac.uk

ABSTRACT

An analytical study to investigate small fire in a ventilated room is presented. Most existing studies are either numerical or experimental and correlations for predicting characteristics of flame propagation such as temperature difference, flame (plume) length and terminal velocity are based on empirical data. A simple mathematical -from the first principles- is developed to predict these characteristics. The predictions are compared with the published experimental data and good agreement has been obtained. Such a simple model would be very useful to practicing engineers for fire control programs, designing fire detection mechanisms.

Keywords: Stratified flow, Plume length, Displacement ventilation

NOMENCLATURE

A	Cross-sectional area, m2
Cp	Specific heat (J $kg^{-1}K^{-1}$)
D	Flame diameter, m
g	Acceleration of gravity, ms^{-2}
K	Discharge coefficient
L	Flame length m
$\dot{m}$	Mass flow rate (kg s^{-1})
q	Flow rates of plume
$\dot{q}$	Heat output intensity (W)
$\dot{Q}$	Heat release (W)
T	Temperature K
t	Time (s)
Ri	Richardson Number
$\dot{V}_{ent}$	*Amount of air entrained*
U, V	Velocity vector, ms^{-1}
Z, H	Flame height
x, y, z	Descartes coordinates, m

Greek symbols

δ	Stratified layer thickness
ρ	Density kgm^{-3}
α	Plume entrainment constant
Φ_k	Convective heat output (W).

Subscripts

0	Ambient

1. INTRODUCTION

Preventing and managing accidental fires in buildings is a major safety concern. Detailed computational and experimental simulations and analyses of possible fire scenarios are performed in order to design effective safety programs and installation of fire prevention equipment. In case of fire flame, smoke and toxic pollutants from combustion rise upward to the ceiling due to buoyancy. For the removal of smoke and safe evacuation it is often desired that pollutants remain trapped in stable stratified layers near the ceiling

therefore it is useful to know interface i.e. the height to which smoke/flame would rise and other stability characteristics of the stratified layers. As the smoke is removed from the space fresh air enters near the floor level and displacement ventilation flow sets in, where essentially is very little mixing.

Most of these studies [1-8] are experimental or numerical, with little analytical work available in the literature. This is due to the complexities of the problem and the large number of parameters involved. Existing correlations are based on empirical data and their validity is problem specific, thus can not be employed. However simple mathematical models resulting from analytical analysis of the problem is of special significance for both scientists and engineers.

We assume similarity between small fire and strong buoyant plume for this analysis. Rooney and Linden [6] investigated the similarity between the small fire and buoyant plume. The similarity solutions for reduced gravity and plume velocity in the strong buoyant case were found to be consistent with experimental observations for centerline mean temperatures and velocities outside the burning region. However for plume entrainment constant, (α=0.083) poor fit to other parameters for experimental data of Thomas et al [2]. A range of entrainment constant $0.11 < \alpha < 0.15$ gave the optimum fit to the data of temperature difference vs. depth of hot layer. The reason of these poor fits seems to be related to the value of the discharge coefficient K = 0.6 which was chosen by Thomas et al [2] and Linden et al [3]. The best fit for temperature difference came from a value of the entrainment constant of α =0.13.Therefore Rooney and Linden found an optimum value of K =0.4 for α =0.13 to obtain the best fit.

It is the objective of the present work to analytically investigate the problem of small fire in a ventilated room to predict the temperature difference and flame length, terminal velocity at three different locations (or plume form a heat source).

2. THEORETICAL BACKGROUND

The concept of selective ventilation, which utilizes the principle of "selective withdrawal" presented by Calay et al [9], is depicted in Figure (1), which shows a general representation of withdrawal of a polluted layer of air at selected location.

Figure (1) shows the maximum height under the ceiling, before the flame start forming itself as a stratified layer.

Referring to Figure (1), using the thermodynamic definitions and laws, the net heat release within the control volume has been used to determine the temperature difference ΔT :

$$\dot{Q} = \dot{m} c_p \Delta T \tag{1}$$

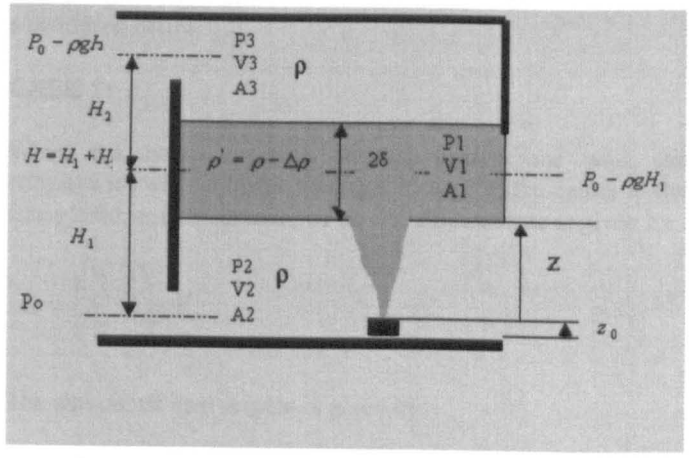

Figure (1): A schematic diagram illustrating the Selective withdrawal of polluted air in a manufacturing unit [9].

Where $\dot{Q}$ is the net heat release (kW), $\dot{m} = \rho V S$ is the mass flow rate, c_p is the specific heat capacity of air by constant pressure and V is the heat supply velocity..
Now

$$\dot{m} = \rho V A \tag{2}$$

Where, A is the horizontal cross sectional area of the flow. Equation (1) can be written as given below.

$$\Delta T = (T - T_0) = \frac{\dot{Q}}{\rho c_p A V} \tag{3}$$

Thus,

$$T = T_0 + \frac{\dot{Q}}{\rho c_p A V} \tag{4}$$

Applying thermodynamic internal energy equation at combustion point yields:

$$\dot{Q} = \dot{m} c_p T_0 \tag{5}$$

Thus the vertical velocity of the flame flow is given by:

$$V = \frac{\dot{Q}}{\rho c_p A T_0} \tag{6}$$

For linear motion in the gravitational field, the maximum height be reached when the terminal velocity:

$$V_z = V - gt = 0 \tag{7}$$

or

$$V = gt \tag{8}$$

Using, $t = \frac{H}{V}$, and multiplying equation (6) by (8) we get

$$V^3 = \frac{gH\dot{Q}}{\rho c_p A T_0} \tag{9}$$

Assume, $H = \sqrt{A}$, and by using the discharge coefficient K, equation (9) becomes:

$$V = K\left[\frac{g\dot{Q}}{\rho c_p H T_0}\right]^{\frac{1}{3}} \tag{10}$$

At the level of stratification, where the height z = H and $V_H = 0$, and by applying Bernoulli equation for this case:

$$V_H^2 = V^2 - 2gz = 0 \tag{11}$$

Substituting equation (10) into equation (11) yields the expression of stratified layer (or hot layer) hold-up

$$z - z_0 = \left[\frac{K^2}{2g}\right]^{\frac{3}{5}}\left[\frac{g\dot{Q}}{\rho c_p T_0}\right]^{\frac{2}{5}} \tag{12}$$

or

$$z = \left[\frac{K^2}{2g}\right]^{\frac{3}{5}}\left[\frac{g\dot{Q}}{\rho c_p T_0}\right]^{\frac{2}{5}} + z_0 \tag{13}$$

Substituting the values of constants in equation (13) gives:

$$z = 0.237\left[\frac{K^2}{2g}\right]^{\frac{3}{5}}\dot{Q}^{\frac{2}{5}} + z_0 \tag{14}$$

The hot or stratified layer hold-up can be evaluated using above relationship for different geometries and openings and different location of heat source. The discharge coefficient, K is the only empirical parameter in this relationship.

Cases with two different locations of heat sources are considered below.

CASE 1:

When the heat source is located against the wall, the entrainment will be lower than that located at the centre in the free plume, and the amount of air entrainment rate is given by

$$\dot{m} = \left(\frac{3}{4}A\right)\rho V \tag{15}$$

The amount of heat release is given by:

$$\dot{Q} = \frac{3}{4}\rho c_p A V T_0 \tag{16}$$

Using the discharge coefficient of $K = \frac{3}{4}K$, equation (13) becomes:

$$z = \left[\left(\frac{3}{4}\right)^2\frac{K^2}{2g}\right]^{\frac{3}{5}}\left[\frac{3}{4}\frac{g\dot{Q}}{\rho c_p T_0}\right]^{\frac{2}{5}} + z_0 \tag{17}$$

CASE 2:

When the heat source is located in the corner, the entrainment will be even lower. The amount of air entrainment rate is given by:

$$\dot{m} = \left(\frac{1}{2}A\right)\rho V \tag{18}$$

The amount of heat release is given by:

$$\dot{Q} = \frac{1}{2}\rho c_p A V T_0 \tag{19}$$

Using the discharge coefficient of $K = \frac{1}{2}K$, equation (13) becomes:

$$z = \left[\left(\frac{1}{2}\right)^2\frac{K^2}{2g}\right]^{\frac{3}{5}}\left[\frac{1}{2}\frac{g\dot{Q}}{\rho c_p T_0}\right]^{\frac{2}{5}} + z_0 \tag{20}$$

The ratio for plume flow rate, velocity and hot layer hold-up (maximum height of the flame) between the sources at centre location to that at the corner is constant.

$$\frac{q_{centre}}{q_{corner}} = \frac{V_{centre}}{V_{corner}} = \sqrt{\frac{(z-z_0)_{centre}}{(z-z_0)_{corner}}} = C \qquad (21)$$

From equations (11), (13), (17) and (20) the constant is calculated as: 1.74

Similarly the ratio of plume flow rate, velocity and the maximum height of the flame/plume located against the wall to that at the corner is constant and is given by:

$$\frac{q_{wall}}{q_{corner}} = \frac{V_{wall}}{V_{corner}} = \sqrt{\frac{(z-z_0)_{wall}}{(z-z_0)_{corner}}} = 1.38 \qquad (22)$$

These relationships can be used to calculate the temperature difference, the flame velocity and the stratified hold-up. The influence of the discharge coefficient on the predictions is also considered in the model.

3. RESULTS AND DISCUSSION

The mathematical model was used to solve the plume temperature difference, the flame terminal velocity and the stratified layer hold-up in a ventilated room. Equation (13) shows a good agreement for flame height calculations at K=0.4 with the following empirical equation for cylindrical flame column [10].

$$H_f = 0.23\dot{Q}^{\frac{2}{5}} - 1.02D_f \qquad (23)$$

Where, $D_f = \sqrt{\frac{4\dot{Q}}{\dot{q}\pi}}$ and H_f were the cylindrical flame column diameter and the height, while $\dot{Q}$ is the total heat release rate in (KW) and $\dot{q}$ is the heat output intensity (KW).

Figure 2 shows the predicted flame heights for various heat release values using a discharge coefficient of (K=0.443) for equation (13) and the results obtained from the empirical correlation of Rooney and Linden [6], for a fixed value of entrainment parameter α=0.13, and discharge coefficient K=0.4.

$$l = 0.015\dot{Q}^{\frac{2}{5}} - 1.02D \qquad (24)$$

Where, l is the flame length in (m), $\dot{Q}$ is the power output in W, and D is the source diameter in m.

When the heat source is located in the corner of the room Equation (20) at K=0.443 was used to predict the flame length. And the comparison was made with the data of Bjarne et al [11] who used the following correlation to fit their data.

$$l = 0.083\dot{Q}^{\frac{2}{5}} - 1.02D \qquad (25)$$

where $\dot{Q}$ the power output in kW.

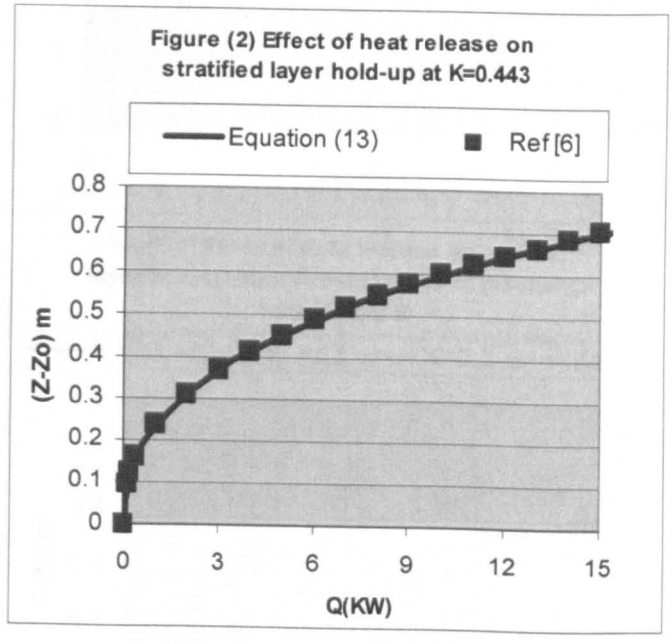

Figure 3 shows the comparison with the experimental data.

The amount of air entrained in the fire plume was calculated using following equation. The heat release rate was multiplied by a factor 4 since the fire is located in a corner [11]:

$$\dot{V}_{ent} = \frac{0.053(4\dot{Q})^{1/3}(z-z_0)^{5/3}}{4} \qquad (26)$$

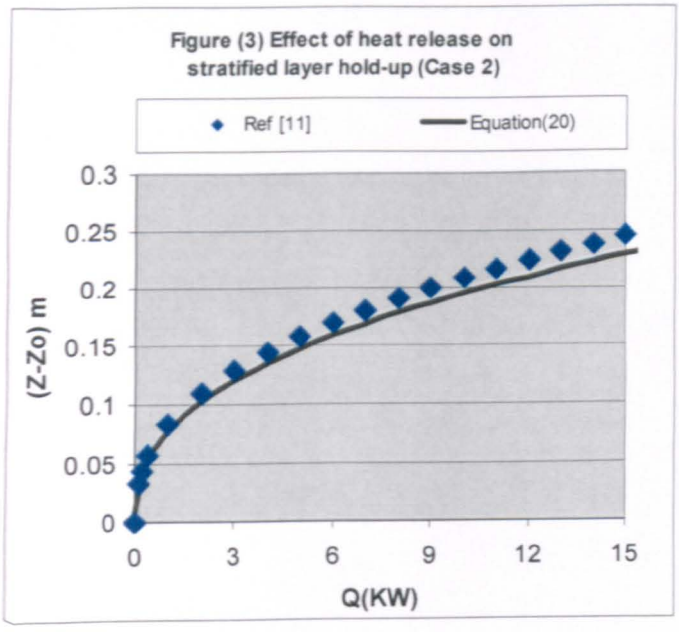

Figure (4) shows a comparison between the flame lengths for a plume located in the corner to that in the middle of the room. The amount of heat release and the amount of entrainment air will be less compared with that at the middle of the room. The predictions show a good agreement with the results of [6, 11].

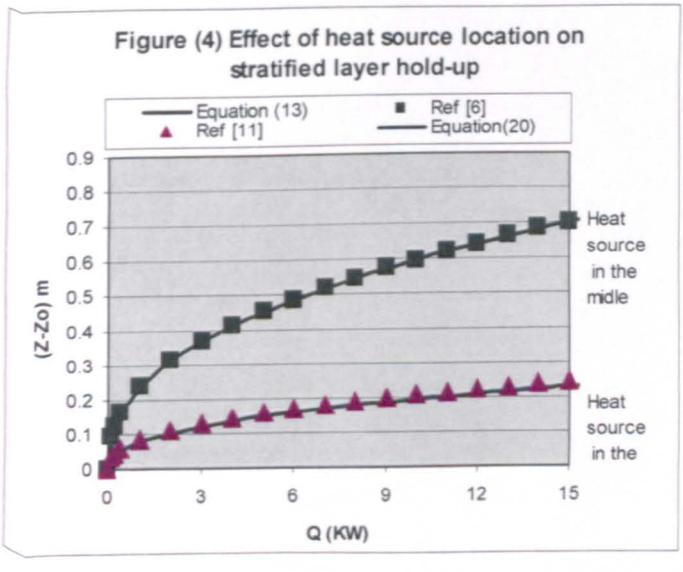

Both figures (5) and (6) show that; the terminal velocity and the length of the flame are not only a function of rate of heat release ($f(Q)$) but also a function of discharge coefficient ($f(K)$). Therefore discharge coefficient and the rate of heat release are the most relevant parameters of the problem, because they influence the momentum and buoyancy forces, and thus influencing the range of the plume velocity and the length of the flame.

The figures (5) and (6) also show that the effect of discharge coefficient is much greater than that of heat release after the flame reaches the steady state i.e. stratification.

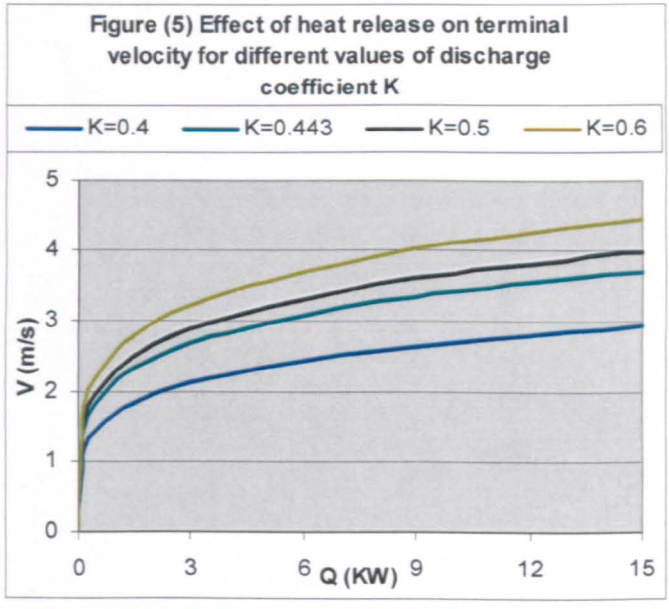

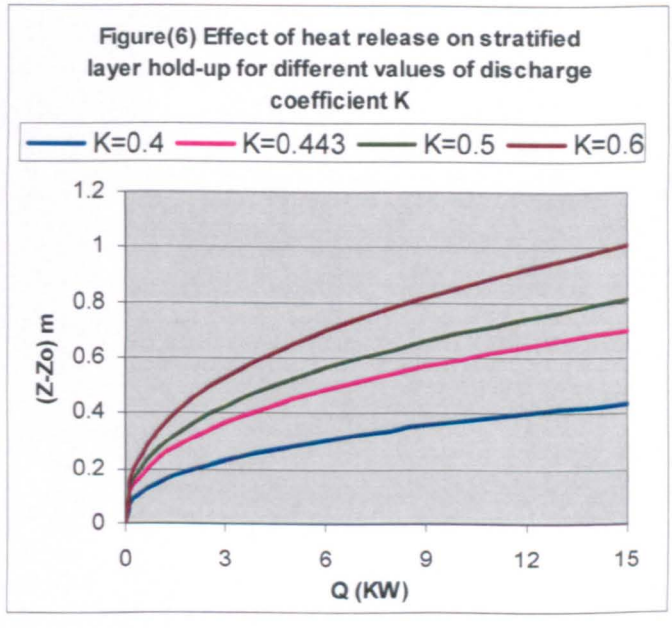

The effect of discharge coefficient on temperature difference ΔT, and so g' (the reduced gravity), when the flame reaches the maximum height (z) where the stratified layer starts to form is shown in Figure (7). The heat release has no effect on ΔT at the level of stratification, while the effect of discharge coefficient K is significant. The figure shows that ΔT increases with decreasing K, which can be controlled by appropriate geometry and designs of the openings. The geometry and location of the openings and heat source affect the heat losses and the amount of entrainment and thus the amount of heat in

the stratified layer, which leads to the stability parameter for the stratified layers i.e. the local or gradient Richardson number [8],

$$R_i = -\frac{g}{T}\frac{\partial T}{\partial y}\Big/\left(\frac{\partial u}{\partial y}\right)^2 \qquad (27)$$

At the lowest discharge coefficient, the local R_i would be the maximum introduced and so the strength of stratification. Whilst increasing the discharge coefficient leads to destabilize the layer, which is expected due to the large influence from convective currents and propagation of the momentum forces that leads to decrease the temperature difference and so the stability of stratified layers.

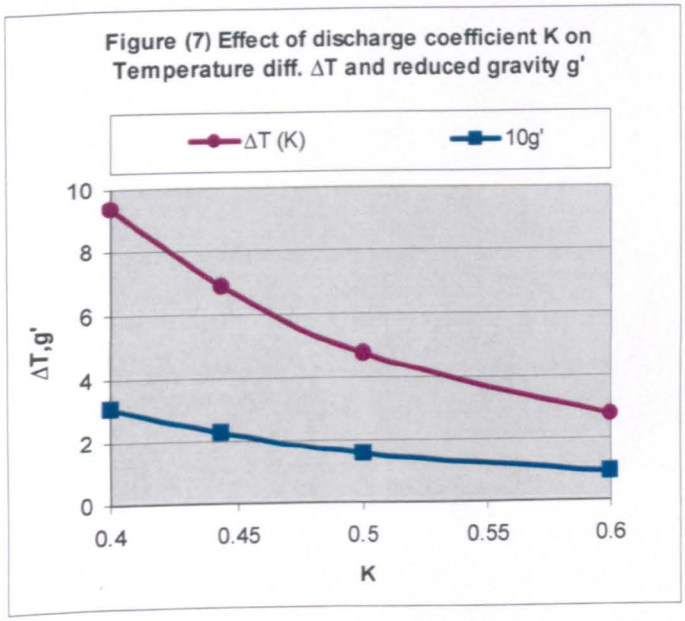

Figure (7) Effect of discharge coefficient K on Temperature diff. ΔT and reduced gravity g'

Equations (21) and (22) show that the location of the heat source influences the flow rate, velocity, heat release and layer hold up. The total flow rate for three similar plumes at different locations is a function of their locations.

$$q_{total} = q_{centre} + q_{wall} + q_{corner}$$
$$or = 2.36q_{centre} + 2.98q_{wall} + 4.12q_{corner} \qquad (28)$$

	q_{centre}	q_{wall}	q_{corner}
q_{centre}	**1.00**	**1.26**	**1.74**
q_{wall}	**0.79**	***1.00***	***1.38***
q_{corner}	**0.57**	***0.72***	***1.00***
q_{total}	**2.36**	**2.98**	**4.12**

Table (1): Calculated values of (location ratios) and total flow rate for a three similar plumes at different locations.

Equation (28) and Table (1) indicate how much influence the location of the heat source has on the flow and the heat release and the effectiveness of the heat source location near wall and corner related to that at the centre:

$$\frac{\dot{Q}_{wall}}{\dot{Q}_{centre}} = 0.79 \qquad (29)$$

and

$$\frac{\dot{Q}_{corner}}{\dot{Q}_{centre}} = 0.57 \qquad (30)$$

Xing and Awbi [12] formulated the flow rate at any height z for a line source of plume for that against the wall and that at the corner using following equations:

$$q_{wall} = 0.0032\ \Phi_k^{\frac{1}{3}}\left(z + z_0\right)^{\frac{5}{3}} \qquad (31)$$

$$q_{corner} = 0.002\ \Phi_k^{\frac{1}{3}}\left(z + z_0\right)^{\frac{5}{3}} \qquad (32)$$

Where, q_1 and q_2 are the flow rates of the plume against the wall and at the corner respectively, while Φ_k is the convective heat output (W). Using above relationships the ratio of flow rate at two locations i.e. at the wall to that at the corner can be estimated.

	q_{wall}	q_{corner}
q_{wall}	*1.00*	*1.60*
q_{corner}	*0.63*	*1.00*

Table (2): Calculates ratios for two locations (against the wall and at the corner using Equations (31) and (32).

The predictions of ratio of different locations using present analytical model (Table 1) are comparable with those obtained by empirical relationships of H. Xing and H. Awbi [12] (Table 2).

The location of the heat source influences the discharge coefficient, thus its effect must be considered in the value of discharge coefficient.

The results and discussion presented above shows that there is no unique constant value of the discharge coefficient K, which reflects the effect of aspect ratio, geometry and openings in the room, and the shape, size and location of the source. The correct value of discharge coefficient must be used for any analytical, numerical and experimental works in order to get good results.

Published empirical correlations have used different values of K ranging from 0.3 to 0.6 in conjunction with another empirical parameter entrainment constant α for values ranging from 0.083-0.2.

In the present analytical model there is only one parameter K, which needs to be optimized. More research is needed to obtain discharge coefficients for a range of room and openings geometries. K can also be introduced as a function of other measurable variables such as opening area and/or velocity.

5. CONCLUSIONS

A mathematical model based on first principles, to predict flow scenarios in the case of small fire in a naturally ventilated room is developed. The flow is essentially of displacement type flow leading to stratification. There is only one parameter, the discharge coefficient K, that depends on geometry of the openings and source location and needs to be obtained for different cases. Comparison of the present analytical model with the previous works shows that the model provides acceptable solutions for a whole range of ventilation scenarios when used appropriate value of discharge coefficients. Therefore future work will consist of obtaining values of discharge coefficients for a range of geometries and flow velocities.

1. The input heat release rate Q of a heat source in a ventilated room is not the only parameter that affects the plume regions and flame lengths, but also the discharge coefficient K.

2. The effect of discharge coefficient, which also indicates the momentum forces effect, on the flame length is significant when the flame reaches the steady state, thus the transition from stratified flow to mixed flow, so it must be taken into account in order to predict the flame length, and the other parameters.

3. The well-founded analytical solution can be used for the analysis and evaluation of the flame length. The model is applicable for all ranges of discharge coefficients. The good agreement of the present results with experimental data and the published correlations is for all values of discharge coefficients.

4. Heat release effect will disappear when the stratified layer forms (hot layer hold up or height of the interface), while the discharge coefficient has considerable effect on the layer stability and can be used to detect the flame/plume length independent of the rate of heat release.

5. The location of the heat source affects the flow rate parameters and must be taken into consideration for flow calculations.

6. In the light of the present analytical investigations, it can be concluded that additional theoretical and experimental information is required for a better understanding of the complex phenomena (fire) to develop and improve the future models.

ACKNOWLEDGEMENTS

The work was supported by a research studentship from the Al-Balq'a Applied University, Jordan.

REFERENCES

[1] Yasushi Oka and Graham T. Atkinson, Control of smoke flow in tunnel fires, Fire Safety Journal, Volume 25, Issue 4, November 1995, 305-322.

[2] Thomas, P.H., Hinkley, P.L., Theobald, C.R. & Simms, D.L, Investigations into the flow of hot gases in roof venting. Fire research technical paper (7), Fire research Station UK, 1963.

[3] Linden, P.F., laneSrff, G.F. & Smeed, D.A., Emptying filling boxes: the fluid mechanics of natural. J Fluid Mechanics, 212(1990), 153-76

[4] Y. Wu and M. Z. A. Bakar , Control of smoke flow in tunnel fires using longitudinal ventilation systems – a study of the critical velocity, Fire Safety Journal, Volume 35, Issue 4, November 2000, Pages 363-390.

[5] D. F. Fletcher, J. H. Kent V. B. Apte and A. R. Green, Numerical simulations of smoke movement from a pool fire in a ventilated tunnel, Fire Safety Journal, Volume 23, Issue 3, 1994, pp 305-325.

[6] G. G. Rooney and P. F. Linden, Strongly buoyant plume similarity and `small-fire' ventilation, Fire Safety Journal, Volume 29, Issue 4, November 1997, pp235-258.

[7] J. P. Kunsch, Critical velocity and range of a fire-gas plume in a ventilated tunnel, Atmospheric Environment, Volume 33, Issue 1, January 1998, Pages 13-24.

[8] Zhuman Fu and George Hadjisophocleous, A two-zone fire growth and smoke movement model for multi-compartment buildings, Fire Safety Journal, Volume 34, Issue 3, April 2000, Pages 257-285.

[9] R. K. Calay, B. A. Borresen and A. E. Holdø , Selective ventilation in large enclosures, Energy and Buildings, Volume 32, Issue 3, September 2000, pp 281-289.

[10] Yaping He, Jian Wang, Zhenkum Wu, Lu Hu, Yi Xiong and Weicheng Fan , Smoke venting and fire safety in an industrial warehouse, Fire Safety Journal, Volume 37, Issue 2, March 2002, Pages 191-215.

[11] Bjarne CHR. Hagen and James A. Milke The use of gaseous fire signatures as a mean to detect fires, Fire Safety Journal, Volume 34, Issue 1, 29 February 2000, Pages 55-67

[12] Huijuan Xing and H.B. Awbi Measurement and calculation of the neutral height in a room with displacement ventilation, Building and Environment, Volume 37, Issue 10, October 2002, Pages 961-967.

Appendix A1.2

A model to Predict Stratification

in

Two phase Flow in Horizontal Pipes

The 12th Annual PVPD 2004
ASME Pressure Vessels and Piping Division Conference
July 25– 29, 2004, San Diego,
California, USA

Paper Number

A MODEL TO PREDICT STRATIFICATION IN TWO PHASE FLOW IN HORIZONTAL PIPES

Rajnish K Calay
Fluid Mechanics Research Group, University of Hertfordshire, College Lane, Hatfield, Herts, AL10 9AB, UK
Tel: +44(1707) 281098
Fax: +44(1707) 285086
r.k.calay@herts.ac.uk

Ahmad Awad
Fluid Mechanics Research Group, University of Hertfordshire, College Lane, Hatfield, Herts, AL10 9EJ, UK
Tel: +44(1707) 284942
Fax: +44(1707) 285086
a.awad@herts.ac.uk

ABSTRACT

Stratified flow is encountered in many situations. The flow of hydrocarbons transported in horizontal pipes often gets stratified. The prediction of pressure drop and liquid hold-up is essential for reservoir and pipe management and optimizing the cost of transportation of constituents. The present paper presents a simple mathematical model to predict the pressure drop, water and oil hold up and stratified layer. A good agreement with the experimental data was found. The model will be further developed and incorporated within a numerical model in order to investigate the flow field characteristics and establish correlations for a wide range of parameters.

Keywords: Stratified flow, Two-phase flow, Oil-water flow, pressure drop.

NOMENCLATURE

A cross-sectional area, m2
c,n coefficients
D hydraulic diameter, m
f Damping function coefficients
g acceleration of gravity, ms_2
p pressure, Pa
Re Reynolds number
S Perimeter
u velocity in the x direction, ms_1
U,V velocity vector, ms_1
v velocity in the y direction, ms_1
w velocity in the z direction, ms_1
x, y, z Descartes coordinates, m
h_1 Water hold up
h_2 Oil hold up

Greek symbols
δ stratified layer depth
ρ density kg.m3
θ water volume fraction
ν kinematics viscosity, m2 s_1
μ dynamic viscosity
τ surface tension coefficient Nm_1

Subscripts
i,j integer number,1,2,3
1 for water
2 for stratified layer
3 for oil

1. INTRODUCTION

Most industrial flow systems involve multiphase flows. Even in single flow systems density difference due to temperature gradients such as water flow in reservoirs and atmospheric (air/cloud) flow, the flow characteristics resemble the multiphase flow systems.

In oil production oil and water are often produced together. Many reservoirs also contain sand, which is brought out together with the mixture of oil and water. In pipelines generally the mixture is transported over long distances. As the production period increases the amount of water in the well also increases up to over 90% water fraction. Sometimes water is added in controlled amounts to crude oil in order to reduce the pressure drop along the pipe-line and reduce the pumping power needed to transport oil over longer distances.

The greatest reduction in pressure drop is expected when the water, which is less viscous fluid, forms a uniform annulus along the pipe surface and oil phase flow within the annulus. In addition to this there is a need to separate different constituents during the production process. Two phase flow are subject to many kinds of instabilities which lead to different flow regimes. Figure 1 shows the schematic of various flow regimes. The accurate modelling of flow regimes is essential for the proper management of transportation of hydrocarbons. The stratified flow is one of the generic flow configurations in horizontal or inclined flow systems with a finite density gradient. Along the pipeline flow may tend to stratify due to density difference of the phases depending upon the local flow conditions.

Several investigations have been devoted to analyse the flow characteristics of two phase pipe flow. Hui et. al. [1] studded the stratified oil–water two-phase turbulent flow in a horizontal tube, by solving the momentum equation throughout the domain using a volume of fluid model. A time-dependent numerical simulation was performed to obtain the final solution that corresponded to steady-state flow conditions. The pressure loss, slip ratio, local phase fraction profile and the axial velocity profile were verified and correlations for pressure loss and oil hold-up were presented. It was concluded that the formulation was rather complex and demands on computational time were excessive.

G. H. Abdul-Majeed [2] conducted an experimental study to develop a data bank used for evaluation and improvement of the oil hold-up in a horizontal two-phase flow, using an air-kerosene mixture flowed through a test section of a horizontal pipe. He showed that the implicit model developed by Taitel and Dukler [3] can be accurately represented by a single explicit equation, and tends to underestimate the hold-up for stratified smooth flow and overestimate the hold-up for stratified wavy, slug and annular flows. M. Nadler and D. Meewes [4] investigated, experimentally, the flow of two immiscible liquids in a horizontal pipe, results were presented to show the effect of emulsification and phase inversion on the pressure drop for different flow regions of two phase oil water mixture. The measurements had been conducted for different oil viscosities, and no significant effect of temperature on the flow characteristics was observed. The results of these experimental investigations were presented to imply a good quality for the present work comparisons.

. Newton and Behnia [5] examined the use of stratified flow momentum balance for the deduction of interfacial velocities and liquid wall shear stresses. They used experimental measurements of gas pressure drop, liquid height and gas wall shear stress to develop empirical correlations for closure of the momentum equations. T. S. Ng et. al.[6] used the Boundary Element Method (BEM) to evaluate the integral and local flow properties of two-phase laminar–laminar stratified flow in a pipe for various interface shapes determined by exact solution of the Young–Laplace equation. They mentioned that "most important of integral flow properties, from the industrial and practical perspective, are the volumetric flow rates of the two liquids, which could be used to determine the optimal amount of water to be injected to minimise the energy requirements for oil transportation in pipelines. The computational time was very short, and the work could be used as a starting point for the analysis of such transitions.

M. Bonizzi and R. I. Issa [7] presented a mathematical model to simulate three-phase (liquid/liquid/gas) stratified and slug flows based on the one-dimensional transient two fluid models, in which the two-phases consist of the gas and the mixture of the two liquids. The equations were solved numerically using a previous developed finite volume methodology, and the study revealed that the slip between the two liquid phases plays a major role in determining the slug characteristics in three-phase flow.

Y. Taitel et al [8] calculated the gas/oil/water hold-ups for stratified three phase flow, as a first step, for analyzing the stability of stratified flow and developing the transition criteria. They mentioned that one can obtain three theoretical steady state configurations for stratified flow, but only the configuration with the thinnest total liquid layer is stable and can actually occur

In this paper we examined the formation of stratification in two-phase flow of oil and water flow in pipes. Depending on local flow velocity and pressure in pipe the oil and water mixture starts to separate into its constituents and stratifies. There exists a layer of water at the bottom and a layer of oil at the top with an interface where density of the mixture varies from oil to water. The purpose of this study is to present a simple model to investigate the conditions for stratified flow in horizontal pipes and to predict pressure drop and liquid hold up for two-phase flow. Locations and the thickness of the interface and stability considerations can then be studied.

The prediction with the developed mathematical model was conducted and comparison was made with experimental data from literature to present the similarities and differences between the experimental and analytical predictions.

2. MATHEMATICAL MODEL

2.1 *Geometrical equations*

The stratified two-phase three layers flow in a horizontal pipe as shown schematically in Fig.(1) is

considered, Geometrical equations for areas and perimeters can be written in terms of dimensionless heights of $\bar{h}_1, \bar{h}_2$ and δ.

$$S_1 = \frac{D}{2}\left[\pi + 2\sin^{-1}\left(2\bar{h}_1 - 1\right)\right] \quad (1)$$

$$S_3 = \frac{D}{2}\left[\pi + 2\sin^{-1}\left(2\bar{h}_2 - 1\right)\right] \quad (2)$$

$$S_2 = \pi D - \left(S_1 + S_3\right) \quad (3)$$

$$S_{12} = D\cos\left(\sin^{-1}\left(2\bar{h}_1 - 1\right)\right) \quad (4)$$

$$S_{23} = D\cos\left(\sin^{-1}\left(2\bar{h}_2 - 1\right)\right) \quad (5)$$

$$A_1 = \frac{D^2}{8}\left[\pi + 2\sin^{-1}\left(2\bar{h}_1 - 1\right)\right] + S_{12}D\left[2\bar{h}_1 - 1\right] \quad (6)$$

$$A_3 = \frac{D^2}{8}\left[\pi - 2\sin^{-1}\left(2\bar{h}_2 - 1\right)\right] - S_{23}D\left[2\bar{h}_2 - 1\right] \quad (7)$$

$$A_2 = \left[\frac{\pi D^2}{4} - \left(A_1 + A_3\right)\right] \quad (8)$$

Where the dimensionless parameters $\bar{h}_1, \bar{h}_2, \delta$ are given by:

$$\bar{h}_1 = \frac{h_1}{D}, \quad \bar{h}_2 = \frac{h_2}{D}, \text{ and } \delta = \frac{h_2 - h_1}{D} \quad (9)$$

2.2 Governing equations

Referring to the stratified two phase flow with three layers shown in Figure (1), and by applying the momentum balance for each these layer, the governing equations, which are dependent on volume fractions, velocity and layer dimensions can be written as:

$$\frac{\partial(\rho_1 U_1)}{\partial t} + \frac{\partial(\rho_1 U_1^2)}{\partial x} = \frac{-\partial p}{\partial x} - \frac{\tau_1 S_1}{A_1} + \frac{\tau_{12} S_{12}}{A_1} \quad (10)$$

$$\frac{\partial(\rho_2 U_2)}{\partial t} + \frac{\partial(\rho_2 U_2^2)}{\partial x} = \frac{-\partial p}{\partial x} - \frac{\tau_2 S_2}{A_2} - \frac{\tau_{12} S_{12}}{A_2} + \frac{\tau_{23} S_{23}}{A_2} \quad (11)$$

$$\frac{\partial(\rho_3 U_3)}{\partial t} + \frac{\partial(\rho_3 U_3^2)}{\partial x} = \frac{-\partial p}{\partial x} - \frac{\tau_3 S_3}{A_3} - \frac{\tau_{23} S_{23}}{A_3} \quad (12)$$

From equations (10) and (11):

$$\sum_{i=1}^{2} A_i\left[\frac{\partial(\rho_i U_i)}{\partial t} + \frac{\partial(\rho_i U_i^2)}{\partial x} + \frac{\partial p}{\partial x}\right] = -\sum_{i=1}^{2} \tau_i S_i + \tau_{23} S_{23} \quad (13)$$

And from equations (12) and (13)

$$\sum_{i=1}^{2} A_i\left[\frac{\partial(\rho_i U_i)}{\partial t} + \frac{\partial(\rho_i U_i^2)}{\partial x}\right] - \left(\sum_{i=1}^{2} A_i\right)\left[\left\{\frac{\partial(\rho_3 U_3)}{\partial t} + \frac{\partial(\rho_3 U_3^2}{\partial x} + \left\{\frac{\tau_3 S_3}{A_3} + \frac{\tau_{23} S_{23}}{A_3}\right\}\right]\right] = \tau_1 S_1 - \tau_2 S_2 + \tau_{23} S_{23} \quad (14)$$

Where, the shear stresses and friction factors correlations of Taitel et. al. [8], have been used with U as the average velocity of the fluid in the specific layer.

$$\tau_1 = f_1 \frac{\rho_1 U_1^2}{2}, \tau_2 = f_2 \frac{\rho_2 U_2^2}{2}, \tau_3 = f_3 \frac{\rho_3 U_3^2}{2},$$

$$\tau_{12} = f_{12} \frac{(U_2 - U_1)|U_2 - U_1|}{2}, \text{ and}$$

$$\tau_{23} = f_{23} \frac{(U_3 - U_2)|U_3 - U_2|}{2} \quad (15)$$

where, $f_i = c\,\mathrm{Re}_i^{-n}$, and $f_{i,j} = \max\begin{cases}0.014\\ f_j\end{cases}$

$$\mathrm{Re}_1 = \frac{4U_1 A_1 \rho_1}{(S_{12} + S_1)\mu_1}, \quad \mathrm{Re}_2 = \frac{4U_2 A_2 \rho_2}{(S_{12} + S_2 + S_{23})\mu_2},$$

$$\mathrm{Re}_3 = \frac{4U_3 A_3 \rho_3}{(S_{23} + S_3)\mu_1}$$

The coefficients c and n were taken as follows;

For turbulent flow, $\begin{cases} c = 0.046 \\ n = 0.2 \end{cases}$

and for laminar flow, $\begin{cases} c = 16 \\ n = 1 \end{cases}$

The density and the dynamic viscosity of the stratified layer were evaluated using the water volume fraction coefficient (θ) which was given by [1]:

$$\rho_2 = \theta\rho_1 + (1-\theta)\rho_3$$

and

$$\mu_2 = \theta\mu_1 + (1-\theta)\mu_3$$

The above equations (10 to 14) must be solved simultaneously to yield the levels $\bar{h}_1, \bar{h}_2$ and δ. The equations are not linear and can have multiple solutions [8]. In order to avoid this situation, the analytical solution can be obtained using the empirical correlation of Hui Gao et.al.[1] defined by the oil volume fraction parameter $\bar{h}_2$:

$$\bar{h}_2 = \left[\frac{1.3124\theta_o}{1+0.3124\theta_o}\right] \qquad (16)$$

where θ_o is the oil volume fraction coefficient can be given by: $\theta_o = (1-\theta)$.The above equation has been used to represent the upper layer flow hold-up, and after some arrangements it can be rewritten by:

$$\bar{h}_2 = 1 - \left[\frac{1.3124(1-\theta)}{1+0.3124(1-\theta)}\right] \qquad (17)$$

To evaluate the stratified and non stratified regimes, a correction factor C is related to the type of the flow regime [2]. Its values were greater than unity for stratified flow regimes and always smaller than unity for the others. The following correction factor is adopted here;

$$C = 0.528(V_{sg}V_{sw})^{-0.216121} \qquad (18)$$

where V_{sg} and V_{sw} are respectively the superficial velocities of oil and water..

Hui Gao et al. [1] results showed that the oil hold-up values were found to be dependent of the oil volume fraction coefficient θ_0 in the flow regime, and because the water hold-up values are to be dependent of water volume fraction coefficient θ, where θ_0 = (1-θ). It is necessary to correlate these values with the parameters that control the water hold-up in the flow regime. Fig (2) represents such data. The solid line is the best fit, which can be represented by the following empirical equation:

$$\bar{h}_1 = \theta \cdot e^{\theta-1} \qquad (19)$$

For incompressible fluid flow, where $\frac{\partial\rho}{\partial t} = 0$, and for constant mean stream velocity U.

The present prediction was applied for stratified two-phase three layers flow, and the results were obtained.

3. TEST CASES AND RESULTS

A stratified oil–water two-phase three layers turbulent flow, in a horizontal tube, has been investigated. Cases, of water volume fraction coefficients θ varying from 0 to 1 were assumed and the properties of oil were considered at various temperatures values for the mixture (18, 25, 30 °C). Pressure drop and oil and water hold-up for various layers were calculated. The comparison with the experimental data was made.

3.1. Pressure drop:

A comparison between the present predicted pressure drop, and experimental data of Nadler and Mewes [4] shows that the predicted results agree with the experimental data, for the whole water volume fraction and oil dynamic viscosities at temperatures of (18, 25 and 30 °C mixture temperature). The variation in temperature (density and viscosity) also influences the resulting flow regime (stratified flow or mixed flow). When the correction factor C defined by equation (18) is greater than unity the agreements are better. However, the great deviation appears, for the velocities where C is less than unity. This implies that the transformation of the flow from stratified three layers flow to a two phase mixed one takes place based on the limitation and assumptions of present work analysis.

Fig. (3) shows the comparison between predicted results and experimental data of [4] for oil temperature 18 °C, the results show a good agreement for that of U=0.3 m/s, and that of 0.9 m/s, it is observed from the figure that the predicted results are slightly over predicted compared to the experimental data when the water volume fraction θ is less than 0.56, and under-predicted than the experimental data, when the water volume fraction is more than 0.56. The absolute average error of 10% was observed between the

prediction and experimental results. The results are closely matched for that of 1.5 m/s, and the agreement appears in good quantitative for low velocities (C<1), and slightly agreement for high velocities, where (C>1).

Figure (4) and (5) show the comparison between predicted results and experimental data of [4] for oil temperature (25 and 30 °C), the results shows a good agreement for low correction factors and fluid temperature. At high correction factors (more than unity) or high temperature, where increasing temperature cause a decrease in oil viscosity which propagates the fluid into mixed flow regime the agreement is not good. The pressure drop becomes lower than the values predicted. This implies that the stratified model cant be applied in these cases. For low correction factors (stratified flow) the variations of pressure drop with water volume fraction is proportional to the decrease in the fluid temperature because of viscosity variations, and so the shear stresses.

3.2. Layers hold-up

Referring to Figure (2) it shows the agreement of the predicted dimensionless heights of $\bar{h}_2$ equation (16) with water volume fraction θ, and the experiment data of G.H. Abdul-Majeed [2]. The predicted results agree well with the experimental data for the whole water volume fraction θ and for all fluid temperatures of (18, 25 and 30 °C). The values have been used to represent the geometrical calculations data.

Figure (6) shows the variations of the predicted dimensionless heights of $\bar{h}_1, \bar{h}_2, \delta$ with water volume fraction θ for all fluid temperatures of (18, 25 and 30 °C). The values used to represent the geometrical calculations data, and show that the variation of the stratified layer thickness δ with the water volume fraction θ reaches the maximum value (maximum stratified layer thickness δ_{max}) at $\theta = 0.566$, which implies the ratio of $\frac{\rho_w}{\rho_w + \rho_o}$, so maximum stability of the stratified layer (the maximum stratification layer thickness) will represented when the volume fraction ratio is proportional to the density ratio,(when), $\frac{\theta_w}{\theta_o} \equiv \frac{\rho_w}{\rho_o}$ which implies the phase properties weighted ratios μ_m, ρ_m in the mixture.

4. CONCLUSIONS

The formulations of correlations for calculating pressure drop and layers hold up are based on experimental data. It can be used as guide lines for comparing the results from more complex and comprehensive numerical models. The following conclusions have been drawn in the present work:

1. Stratified two phase three layer flow in a horizontal tube is predicted, analytically, using the momentum equation for each layer and the empirical equations based on experimental data. To predict the pressure gradient the results has shown good quantitative agreement with the experimental data of M. Nädler and D. Mewes [4] for correction factors less than unity for all temperatures values. For low temperature values also acceptable agreement for correction factors greater than unity was achieved.

2. The predictions of water, oil and stratified layer hold-up was in a good agreement with the experimental data.

3. The stratified layer thickness δ reaches the maximum value when the water volume fraction θ is proportional to water density in the mixture.

References

[1] Hui Gao, Han-Yang Gu and Lie-Jin Guo, Numerical study of stratified oil–water two-phase turbulent flow in a horizontal tube, International Journal of Heat and Mass Transfer, Volume 46, Issue 4, February 2003, Pages 749-754.

[2] G.H. Abdul-Majeed, Liquid hold-up in horizontal two phase gas-liquid flow, International Journal of Multiphase Flow, Volume 23, Issue 7, December 1997, pages 70-71.

[3] Y. Taitel, A.E. Dukler, A model for predicting .ow regime transitions in horizontal and near horizontal Gas–liquid flow, AIChE J. 22 (1) (1976) 47–55.

[4] M. Nädler and D. Mewes, Flow induced emulsification in the flow of two immiscible liquids in horizontal pipes, International Journal of Multiphase Flow, Volume 23, Issue 1, February 1997, Pages 55-68.

[5] C. H. Newton and M. Behnia , On the use of the stratified momentum balance for the deduction of shear stress in horizontal gas–liquid pipe flow, International Journal of Multiphase Flow, Volume 24, Issue 8, December 1998, Pages 1407-1423.

[6] T. S. Ng, C. J. Lawrence and G. F. Hewitt Laminar stratified pipe flow, International Journal of Multiphase Flow, Volume 28, Issue 6, June 2002, Pages 963-996.

[7] M. Bonizzi and R. I. Issa, On the simulation of three-phase slug flow in nearly horizontal pipes using the multi-fluid model, International Journal of Multiphase Flow, Volume 29, Issue 11, November 2003, Pages 1719-1747.

[8] Y. Taitel, D. Barnea and J. P. Brill, Stratified three phase flow in pipes, International Journal of Multiphase Flow, Volume 21, Issue 1, January 1995, Pages 53-60.

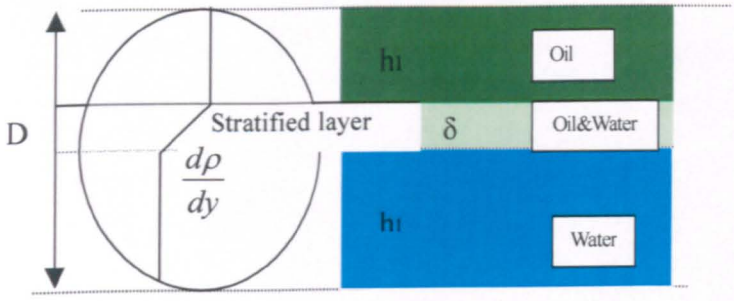

Figure 1 Schematic of oil-water flow in a pipe showing stratified layers

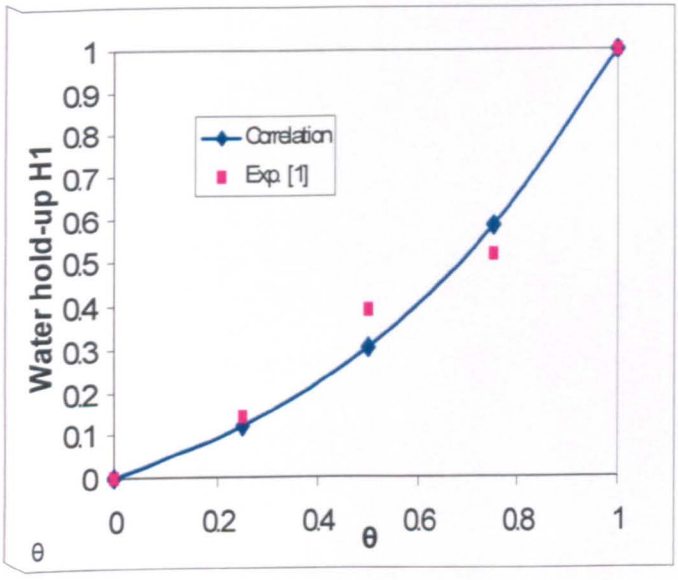

Figure 2 Comparison of water hold up (h1) using a correlation (Equation 19) with experimental data

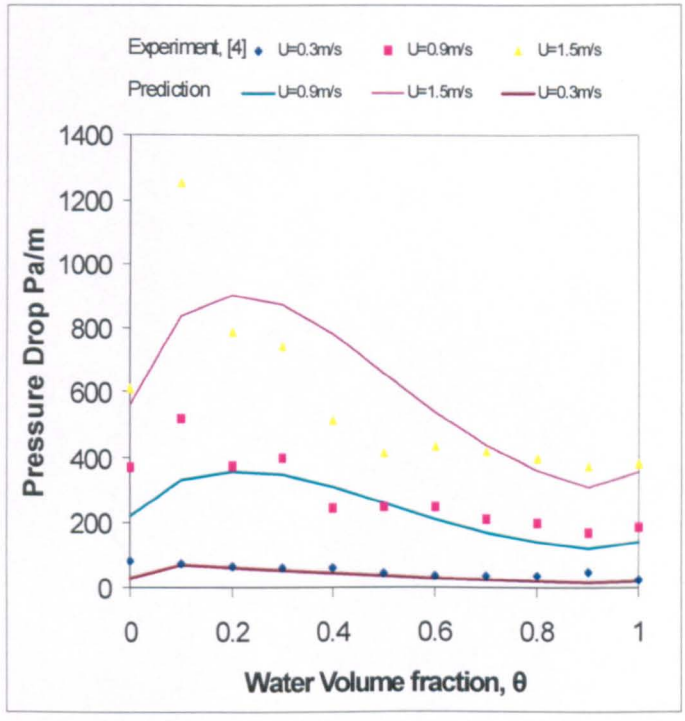

Figure 3 Comparison of predicted pressure drop with experimental data along the pipe at various velocities (mixture temperature 18° C)

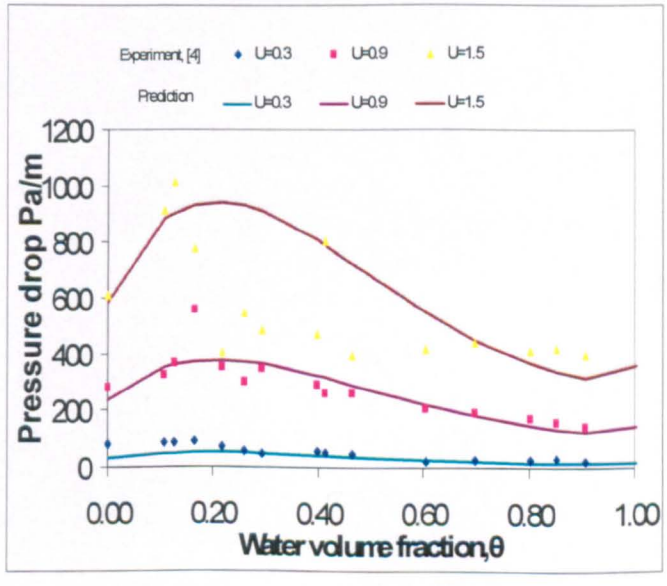

Figure 4 Comparison of predicted pressure drop with experimental data along the pipe at various velocities (mixture temperature 25° C)

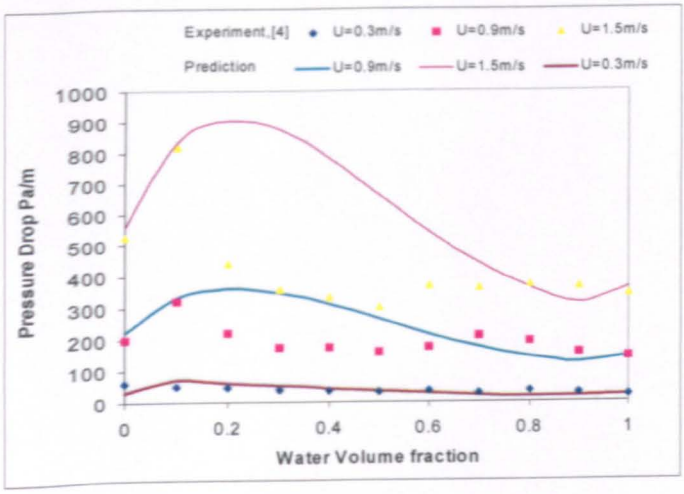

Figure 5 Comparison of predicted pressure drop with experimental data along the pipe at various velocities (mixture temperature 30° C)

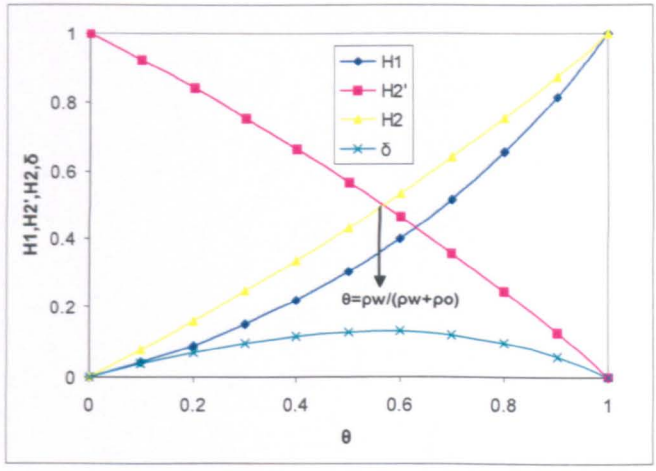

Figure 6 Predicted dimensionless heights of different constituents (h1, δ, h2) for a range of water volume fraction

The effect of momentum jet air flow on the stratified layer characteristics

Ahmad Awad[1] Omar Badran[2*] Arne Holdϕ[1] and Raj Calay[1]

[1] *Department of Aerospace, Automotive and Design Engineering, Faculty of Engineering and Information Science, University of Hertfordshire, Hatfield Campus, UK.*

[2] *Department of Mechanical Engineering, Faculty of Engineering Technology, Al-Balqa`*
Applied University, P.O.Box 330116, Amman 11134-Jordan,
O_badran@yahoo.com

ABSTRACT

An experimental work was carried out using ceiling jet to supply hot and cold air to a confined space, to investigate the effect of jet momentum in breaking and mixing the stratified layer. Also smoke visualization were conducted for comparison purposes. The flow of high buoyancy was supplied upward, while the flow of high momentum was supplied downward from the ceiling. The magnitude of momentum needed is depending on the degree of stratification, stratified layer interface level height and the stratification conditions. It can be seen that the jet momentum has significant influence on the mixing of the stratified flow characteristics. The results indicated that once the momentum was initiated a mixed flow grew in the occupied zone above the floor. The height of this zone is dependent on the stratified flow characteristics, and the temperature and momentum of the ceiling jet.

INTRODUCTION

Mixing ventilation is where air is supplied into the space with relatively high momentum flux, in order that, the air in the space will be mixed to a reasonably uniform temperature, yet satisfying the requirement for air speeds. Thus is usually achieved by supplying air at high level within the space. For low momentum jet, the flow unable to reach the floor due to the stronger stratification layer that generated in the lower zone Chow 1996.

Convection currents and thermal stratification dominate the flow pattern in a large enclosure. Stratification is very common in building with a single large open space. Warm air rises under the influence of buoyancy forces, which cause a positive temperature gradient between the floor and the ceiling. Activities such as heating and welding act as additional heat sources and contribute to already existing temperature gradients across the space.

However, in other buildings where indoor air quality load are important, stratification effects can be desirable. Cooling season stratification can reduce the cooling loads because warm stratified layer below the ceiling acts as an insulating buffer, which reduces the roof and lighting heat gain components. An additional reduction in cooling load is achieved by locating the extract at the height of stratification because heat extracted per unit of mass flow would be significantly higher than if the extract were positional below the stratified layer. There are many experimentalists and theoreticians investigated the effect of jets or plums on the stratified layer characteristics, (Redondo et al 1996, Cardoso et al 2001, Karimipanah 1999, Murakami et al 1996, Bloomfield and Kerr 1999, and Chen and Mahoney 2001).

Redondo et al 1996 used detailed flow visualization as well as density measurements in zero-mean-flow laboratory experiments involving grid-stirred turbulent mixing across a density interface and bubble-induced mixing. They found that the overall mixing efficiency of the processes depends on the local Richardson number as well as on the local vorticity.

Cardoso et al 2001 found from their experimental work that when small particles sediment from a surface current generated by an axisymmetric turbulent plume, the concentration of particles in the environment surrounding the plume is larger at higher levels than at lower levels. This distribution of particles in the environment results in unstable density stratification and as a result, convection in the environment may ensue.

Karimipanah 1999. Conducted measurements of the pressure along the perimeter of a slot ventilated room for different room sizes. He found that the momentum of the jet at the end of the room is decreased with increasing room length. He could not predict the corner flows by his CFD simulation using the linear eddy viscosity or standard stress models. However he suggested that these effects would be captured, by using a second moment closure turbulence model with a new near wall approach.

Murakami et al 1996 proposed a new k-ε model includes damping effect on vertical turbulent transport due to thermal stratification. They tested the model in two-dimensional thermally stratified flow fields (i.e. high and low Reynolds numbers flow field within an enclosure). They found that the proposed k-ε model is applicable to a flow field, which includes both turbulent area and pseudo-laminar area caused by thermal stratification. Chen and Mahoney 2001 suggested a simple multi-layer stratification model for displacement ventilation in a single-zone building driven by a heat source distributed uniformly over a vertical wall. Theoretical expressions were obtained for the stratification interface height and ventilation flow rate and compared with similar models. They used a recently

developed fine-bubble modelling technique. They concluded that their theoretical results were in good agreement with the experimental predictions.

Bloomfield and Kerr 1999 did an experimental and theoretical investigation of the flow and density distribution arising from the upward turbulent injection of a dense fluid into a stratified environment of finite extent. They found that as more dense fluid is added through either a point or line source, both fountain and the environment evolve with time. They have applied their results to two problems: the replenishment of magma chambers and the heating or cooling of a room.

The present study concentrated on the effect of momentum jet on mixing the stratified flow using a recently available experimental technique. Smoke visulization was used to validate the experimental work and to indicate the effect of air jet flow on the stratified flow chracteristics.

EXPERIMENTAL SET-UP

All tests were conducted in the test environmental chamber at the University of Hertfordshire. The physical dimensions of the chamber were large enough, so that the walls didn't affect the flow, and the height was sufficient to the build up of stratified layer. The dimensions of the identical rectangular chamber were (7.5m long, 3.6m wide and 3.0m height) with two windows (double glazed) isolated from an enclosed space. The walls of the test chamber were insulated. The walls as well as the roof were of 12.5 cm thick, with white polyester outer finish and polyurethane foam interior made. The floor was a layer of light grey colour of 10 cm thick concrete, and below it a layer of 10 cm thick Styrofoam.

Transient temperature distributions for the flow inside the chamber were measured using eighteen K-type thermocouples. The thermocouples stand was inserted vertically on a multidirectional movable base located at the centre of the chamber. The junctions of the thermocouples were located at the centres of eighteenth equal volumes of the fluid in the chamber. Three thermocouples were placed in the inlet hot airflow, inlet cold airflow and outlet. Another was located outside the chamber to measure the ambient temperature. All of these thermocouples were located to give continuously monitoring of all needed temperatures.

Concerning the measurements, the test chamber was equipped with sensors to determine the air temperatures (thermocouples), as well as, the input air velocities and flow rates (A rotating vane anemometer LC6000). A procedure was allowed by distributing the temperature sensors to cover the essential vertical and horizontal planes within the chamber. This was done by using thermocouple stand in the vertical direction, and by moving the base in both directions on the horizontal plane. As a result, the measurement points were represented at 15 cm grid in vertical plane, and 75 cm x 80 cm grid in each directions of investigated horizontal plane.

Velocity measurements:

1. A rotating vane anemometer was used to measure both cold and hot airflow rates. It was suitable for most applications where the air stream was large enough, and the air velocity was ranging from 0.25-30m/s. It is accuracy at 20°C and 1013mb is better than ±2% for the readings from 5-30 m/s, and ±0.1m/s for the readings between 0.25-4.99 m/s.

Measuring Stations:

1. At the middle of the environmental chamber, to measure the vertical temperature gradient from 0.2m to 2.8m above the floor (18 points in total). This was done to evaluate the stratified layer characteristics (interface level height, stratified layer thickness, temperature profiles and the degree of stratification).
2. At nine locations in the flow direction (x-axis) and six locations across flow direction. Each station measured the vertical temperature gradient from 0.2m to 2.8m above the floor (18 points in total). This was done to study the influence length, uniformity of the stratified layer.
3. At different inlet and outlet openings heights. Each station measured the vertical temperature gradient from 0.2m to 2.8m above the floor (18 points in total). The measurements were taken to evaluate the effect of these heights on stratified flow. It can be used to destratify the flow by supplying cold air from the top of the chamber and the hot air from the bottom.

The experiments were done to investigate the effect of jet flow on the stratified flow characteristics. The experiments were presented using both cold and warm air jet flow. The jet of 0.11m diameter was used to inject air vertically downward to destroy the stratified layer or flow through it. The injected momentum was increased gradually by increasing the jet speeds from (0.0 ~ 15.0m/s). The injected air has an efficient momentum to disturb the surrounding air, and hence the temperature distribution in the environmental chamber. With combined effects of buoyancy and momentum, the degree of stratification and the flow characteristics are being a complement of both the buoyancy and the momentum of injected flow. During the experiments the position of the interface and the motion through the layers were monitored visually. The jet is located at the center of the chamber, to minimize the effect of sidewalls on the determination of the amount of entrainment. A separate rotational fan was used to supply the jet with both hot and cold airflow rate. The 0.11 m diameter nozzle was directed vertically, and supplies the air with an adjustable flow rate. It is possible to go from the stratified case to the mixed case by changing jet airflow rate, thus the relative magnitudes of the buoyancy and momentum fluxes. The thermocouples were vertically distributed at the stand. The stand was located in the middle of the chamber in order to capture

the temperature gradients in the stratified region. A data logger was interfaced to a personal computer to collect the flow of temperature signals arriving from the test chamber. A video camera images were recorded onto videotape and simultaneously to computer hard disk.

To study the behavior of the stratified flow characteristics under the effect of jet momentum airflow, wide temperature and smoke visualization images were taken besides the quantitative and qualitative measurements for both stratified and mixed flow.

The experiments were performed according to the following procedure:

When a steady state is reached and a stratified layer is established between the upper and the clear lower zone. The source of momentum (the jet) located at the center of the chamber is turned on. The injected air is increasing, while the stratified layer is destroying or translating up or downward.

For the sequence of vertical jet experiments, the only parameter which was changed from one run to the next was the flow rate (stratified flow characteristics), while during the run jet speed was changed in the ranges of 0.0 – 15 m/s. The thermocouples readings were taken every 10 seconds. The criterion used to infer a steady state was based on a 0.2 °C variation during one hour in a reading of any thermocouple on the stand.

Table 1: Details of experimental tests using cold and warm jet flow to mix the stratified flow of hot and cold airflow rates as listed in the table. For each test, the jet speed was increased gradually from (0.0 ~ 15.0 m/s).

The Jet	$Q_{hot}(m^3/min)$	$Q_{cold}(m^3/min)$		
Cold Jet	1.0	2.0	4.0	6.0
=	2.0	2.0	4.0	6.0
=	3.0	2.0	4.0	6.0
Warm Jet	1.0	2.0	4.0	6.0
=	2.0	2.0	4.0	6.0
=	3.0	2.0	4.0	6.0

FLOW SPECIFICATIONS AND PRELIMINARY TESTS

The effect of cold jet momentum has been studied to evaluate the influence of cold momentum on the stratified flow characteristics. The jet speed and momentum were combined with the temperature profiles to provide the estimation of mixing in stratified flow. The momentum was introduced by injecting the cold air from the ceiling using a jet source. The temperature of the injected air was the ambient for cold jet flow and was the hot air temperature for the warm jet flow. The jet opening size was 0.11 m and the momentums were in the ranges of 0.0 to $2.17 m^4/s^2$. The flow specifications (velocity, volumetric flow rate and momentum) were listed in table 2.

From the preliminary tests, when the jet momentum is not large enough, or the temperature of air injected is less than that of the pre-stratified layer, the injected air cannot reach deep stratification heights. In this situation, the flow jet cannot activate the mixing in the domain and may stratify at certain levels above the floor. These levels of stratification depend on both the momentum and the temperature of injected air, and the stratified layer interface level height. The balance between momentum and buoyancy forces in injected air must be adjusted.

$V_j \ (m/s)$	$Q_j \ (m^3/\min)$	$M_j \ (m^4/s^2)$
0.000	0.000	0.000
0.378	0.215	0.001
0.756	0.431	0.005
1.133	0.646	0.012
1.511	0.862	0.022
2.267	1.292	0.049
3.022	1.723	0.087
4.533	2.585	0.195
6.044	3.446	0.347
7.555	4.308	0.542
9.066	5.169	0.781
10.577	6.031	1.063
12.088	6.893	1.389
13.599	7.754	1.757
15.110	8.616	2.170

Table 2: The jet speed (V_j), volumetric flow rate (Q_j) and momentum (M_j) used in the experiments.

RESULTS AND DISCUSSION

Mixing flow using cold jet

It is known that stratification will happen in the zones of comparatively high buoyancy flow. It should be noted that full mixing is assumed to happen for the zones of maximum momentum, and the maximum momentum in our case is caused by both cold and warm jet. Experimental results for a cold jet of 0.11 m diameter were done. It studied the effect of momentum in the mixing of stratified flow for a various air flow rates. The present data reveal the effect of various speeds of cold jet on the stratified flow characteristics. Comparisons of fifteen experimental temperature profiles in entire locations will be discussed. The temperature profiles appear to be a dependent of jet speed.

The flow stratifies at intermediate hot and cold airflow rates, and levels somewhere close to the exhaust height. In this case, the injected air can flow through the interface without destroying the stable layers. This type of flow has a high Ri, where the balance between buoyancy forces and momentum forces are the main parameters to control the flow.

For intermediate hot and cold airflow rate, the flow will stratify at levels near the mid height of the environmental chamber. In this case, the injected air will flow through the stratified layer or mix it depending on the amount of momentum. More increase in jet momentum will pick it up toward the ceiling before it destroys at high momentum, where the whole space becomes fully mixed.

Figures 1 to 3, show how the average temperatures profiles change with the change in momentum. In the lower zone, the temperature is increasing to reach the average temperature of the whole space, while it decreases in the upper zone. The temperature of the stratified layer is a complement of both temperatures in the lower and upper zones. The results reveal the effect of momentum on the flow temperature profiles. As the jet momentum increases, the average temperature in the upper zone is gradually decreasing due to the entrainment volume flux, while in the occupied zone the increasing is more rapidly due to the radiation heat gain into the lower zone.

Figures 4 to 6 show the effect of increasing jet speed on the temperature profiles. It illustrates that the growth and the vertical transport of the stratified layer interface level height with increasing jet momentum. As seen in the figures, the decrease in the temperature of the lower zone is initially faster due to the smaller thickness of the stratified layer, where the injected air can flow through without destroying the stable layers. With further increase in jet speed, thermal stratification decays and the stratified layer fades away until the temperature of the air becomes uniform, while the average temperature is decreasing steadily to approach the inlet ones. Also by increasing the airflow rates, comparisons indicated that since the momentum is higher, the layer becomes thicker and the

mixing in the lower zone becomes larger. It is similar to the results of Linden et al (1990) that small size of opening resulted in high amount of inflow that works as a jet caused the entrainment across the interface, and because of the greater density of the fluid above the interface, the interface descends faster. As the increase in jet speed continues the interface moves upward. It is owed to two reasons:

Firstly, it is due to the temperature difference. Since there is a much temperature difference through the interface, the cold air moves upward due to the heat transfer from the hotter region. Secondly, it is due to the circulation in the upper zone, while the air in the lower zone is static. In this case, the difference in velocity generate a shearing force through the interface, and tear out the cold air to the upper region, and increase mixing in the flow.

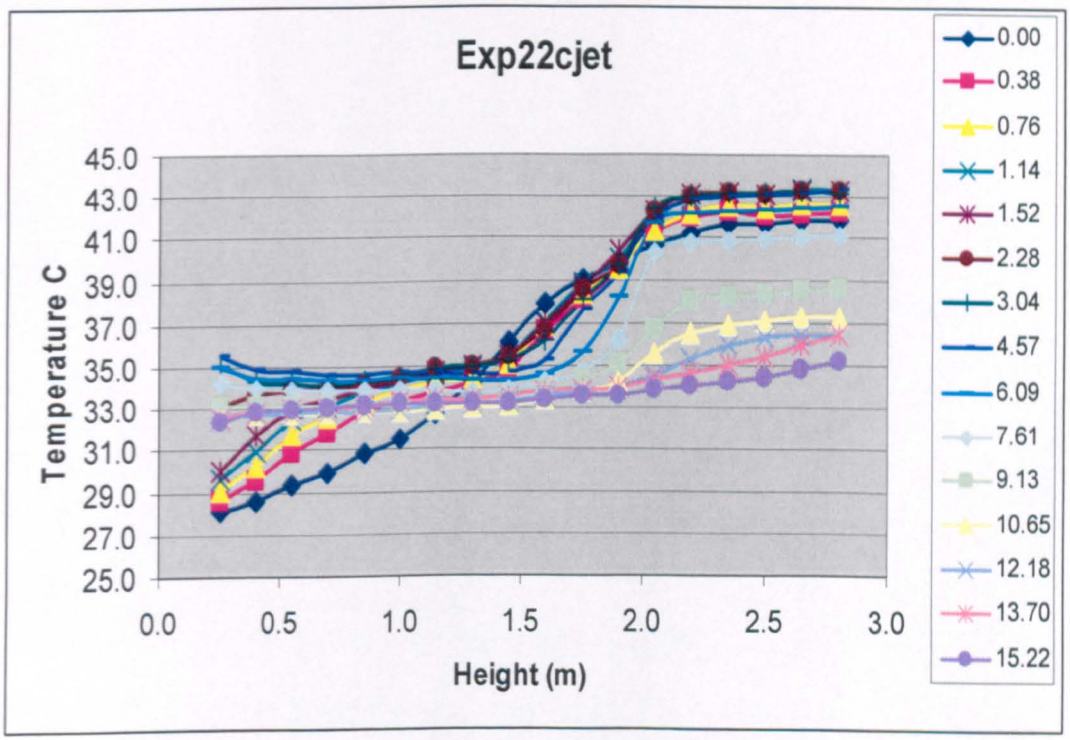

Fig. 1: Vertical temperature profiles for various cold jet speed of 0.11 m diameter, while the flow was stratified at ($Q_h = 2.0\ m^3/\min$) hot airflow rate and ($Q_c = 2.0\ \ m^3/\min$) cold airflow rate at a locations of 2.0 and 1.5 m respectively at

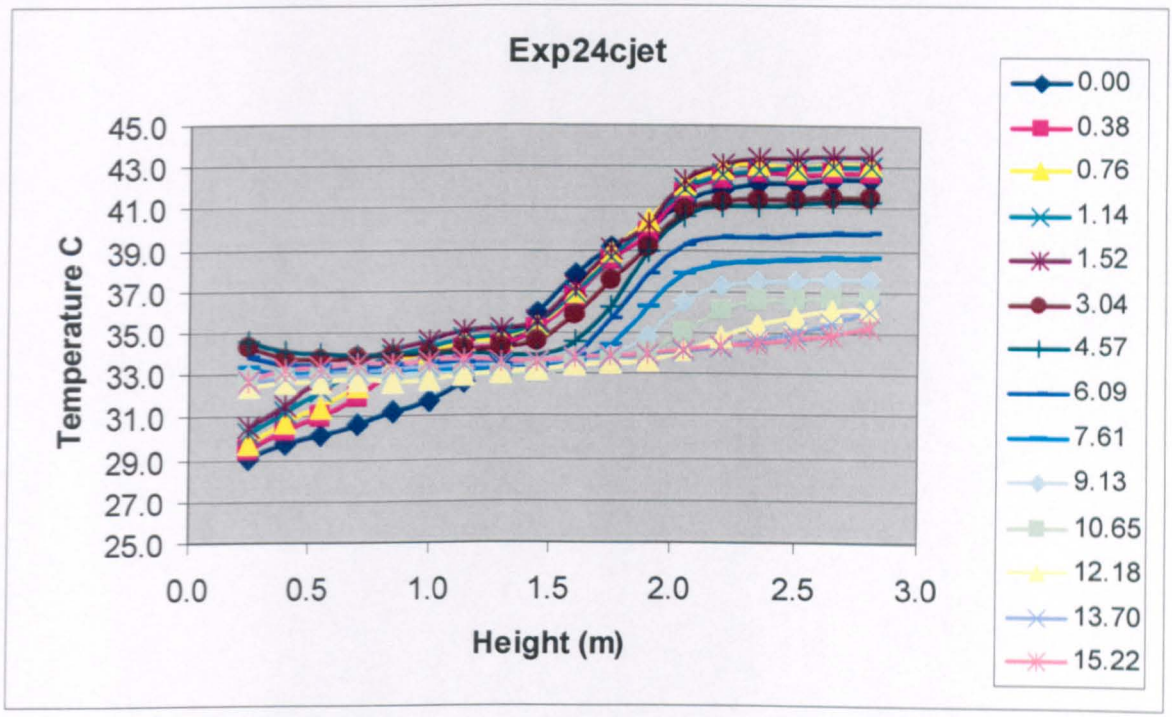

Fig. 2: Vertical temperature profiles for various cold jet speed of 0.11 m diameter, while the flow was stratified at (Q_h = 2.0 m^3 / min) hot airflow rate and (Q_c = 4.0 m^3 / min) cold airflow rate at a locations of 2.0 and 1.5 m respectively at the centre of environmental chamber.

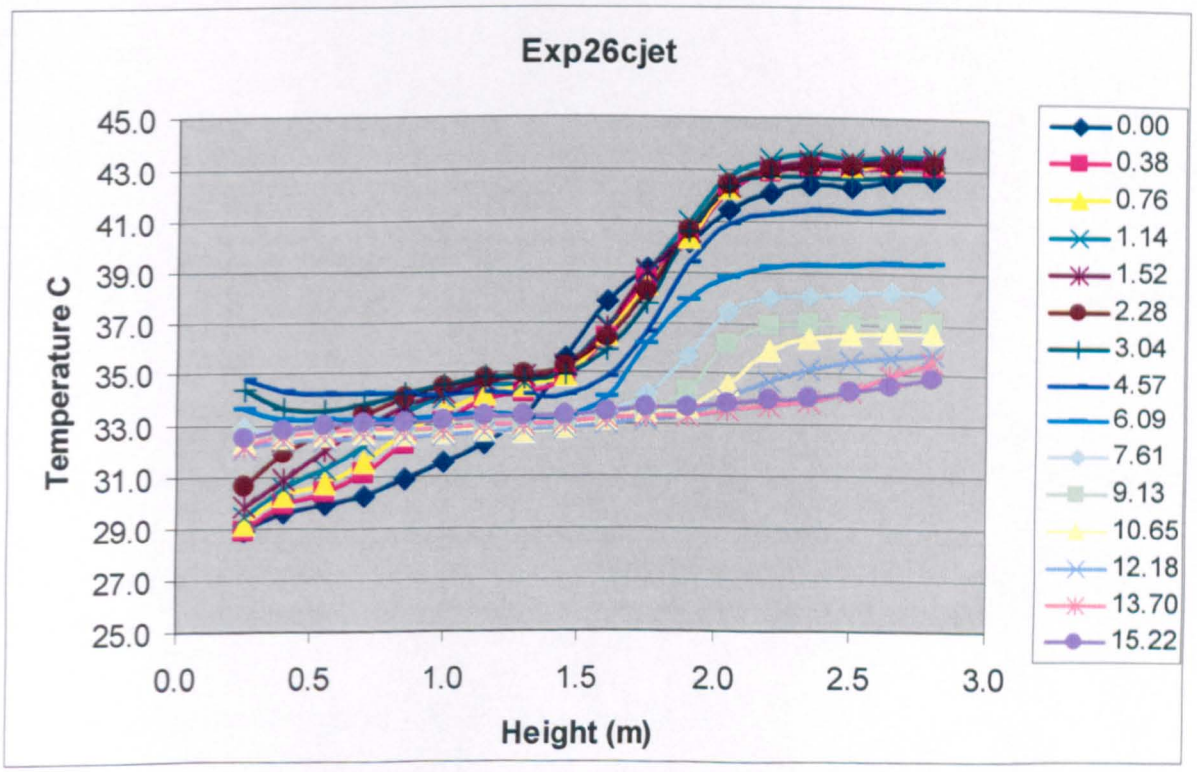

Fig. 3: Vertical temperature profiles for various cold jet speed of 0.11 m diameter, while the flow was stratified at (Q_h = 2.0 m^3 / min) hot airflow rate and (Q_c = 6.0 m^3 / min) cold airflow rate at a locations of 2.0 and 1.5 m respectively at the centre of environmental chamber.

Figures 4 to 6 illustrate the effect of momentum on the stratified flow characteristics for a case of Q_h = 2.0 m^3 / min with different cold air flow rates. With the increase in momentum, the temperature profiles indicated the decrease in the temperature difference and so the degree of stratification. It shows the translation of the stratified layer interface level height with the jet speed, while the stratified layer thickness is decreased.

Comparisons between these figures show no significant effect for the cold air flow rates on mixing flow. It is due to the insignificant effect of cold air flow rate on stratifying the flow and so on de-stratifying or mixing it. Also the mixing of a stratified flow is based on the stratified flow situation when the momentum jet starts to mix the flow rather than the initial conditions carried the flow to reach this situation.

The figures also show the decrease in temperature gradient by increasing the momentum until it reaches steep values. Therefore, the injected air is flowing direct toward the bottom of the chamber, which tends to circulate the flow in the lower zone. Since it has a negatively buoyant force relative to the chamber domain, the mixing of low momentum will established above the stratified layer pushing it downward. Increasing the momentum will increase the deep height of the injected air to flow through the stratified layer. More increase in momentum will increase buoyant forces in the lower zone under the stratified layer to pick it up until it reaches a stable stratification in the upper part of the chamber. This will be established with a relatively thin stratified layer separating the hot air in a small width layer between the ceiling and the occupied zone. A maximum increase in momentum will result in a fully mixed flow in the whole space.

Figures 4 to 6 give an indication for the design of working zones to be at certain height to increase ventilation efficiency, and the clear layer to be above the heads of people to escape in cases of smoke and fire hazards.

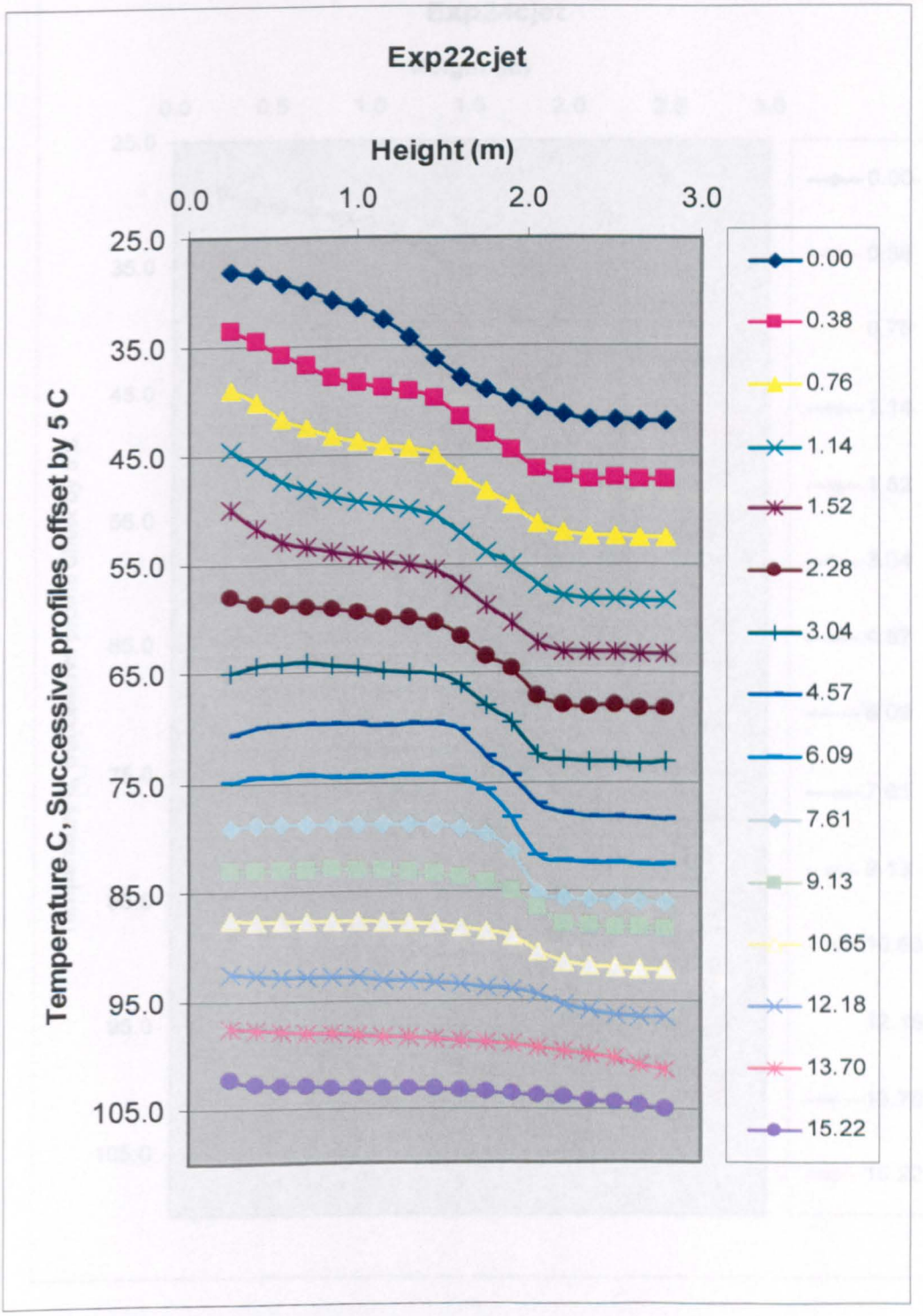

Fig. 4: Illustrates vertical temperature profiles for various cold jet speeds. The flow was stratified at ($Q_h = 2.0\ m^3/\min$) hot airflow rate and ($Q_c = 2.0\ \ m^3/\min$) cold airflow rate at a locations of 2.0 and 1.5 m respectively at the centre of environmental chamber.

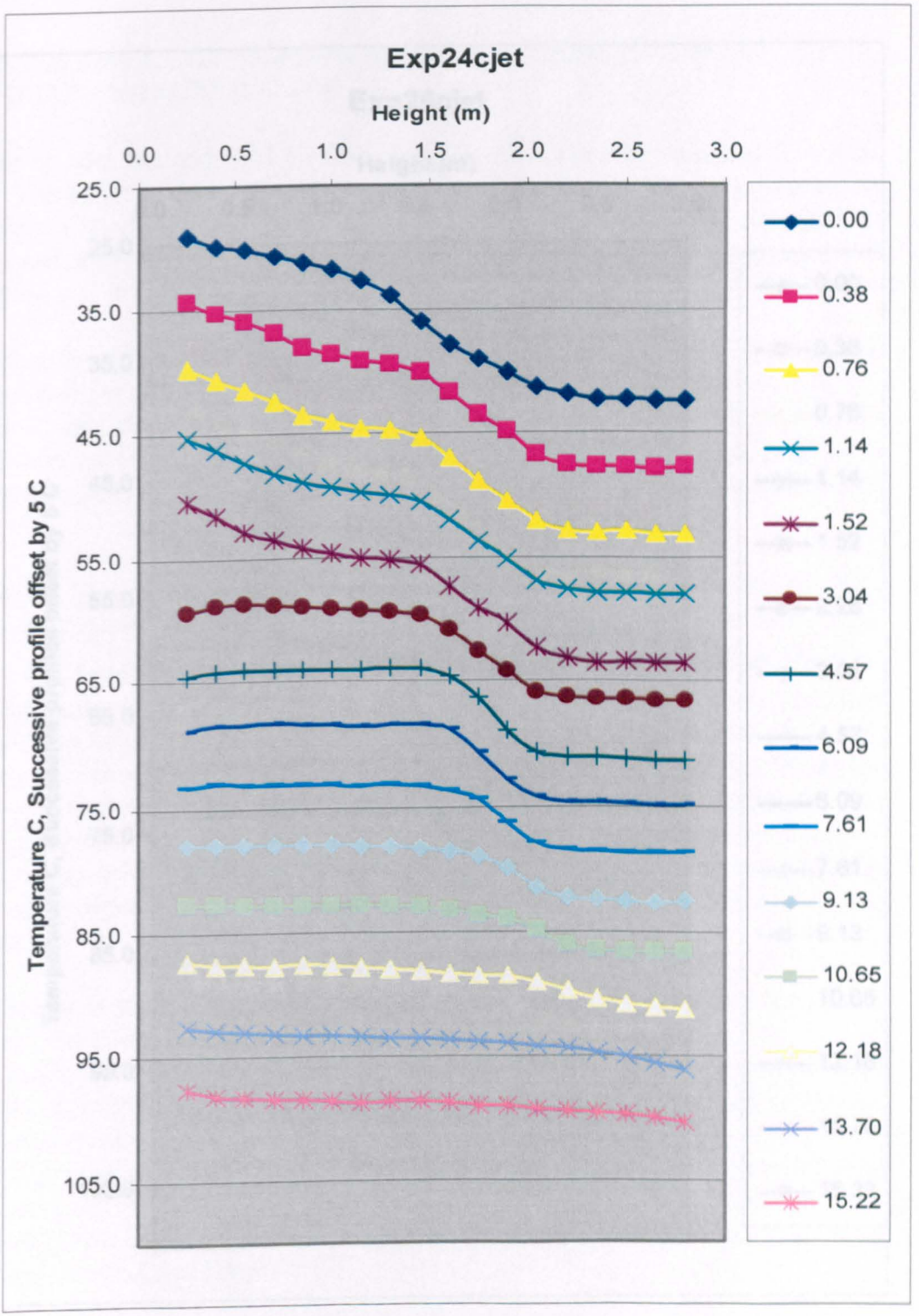

Fig. 5: Illustrates vertical temperature profiles for various cold jet speeds. The flow was stratified at (Q_h = 2.0 m^3 / min) hot airflow rate and (Q_c = 4.0 m^3 / min) cold airflow rate at a locations of 2.0 and 1.5 m respectively at the centre of environmental chamber.

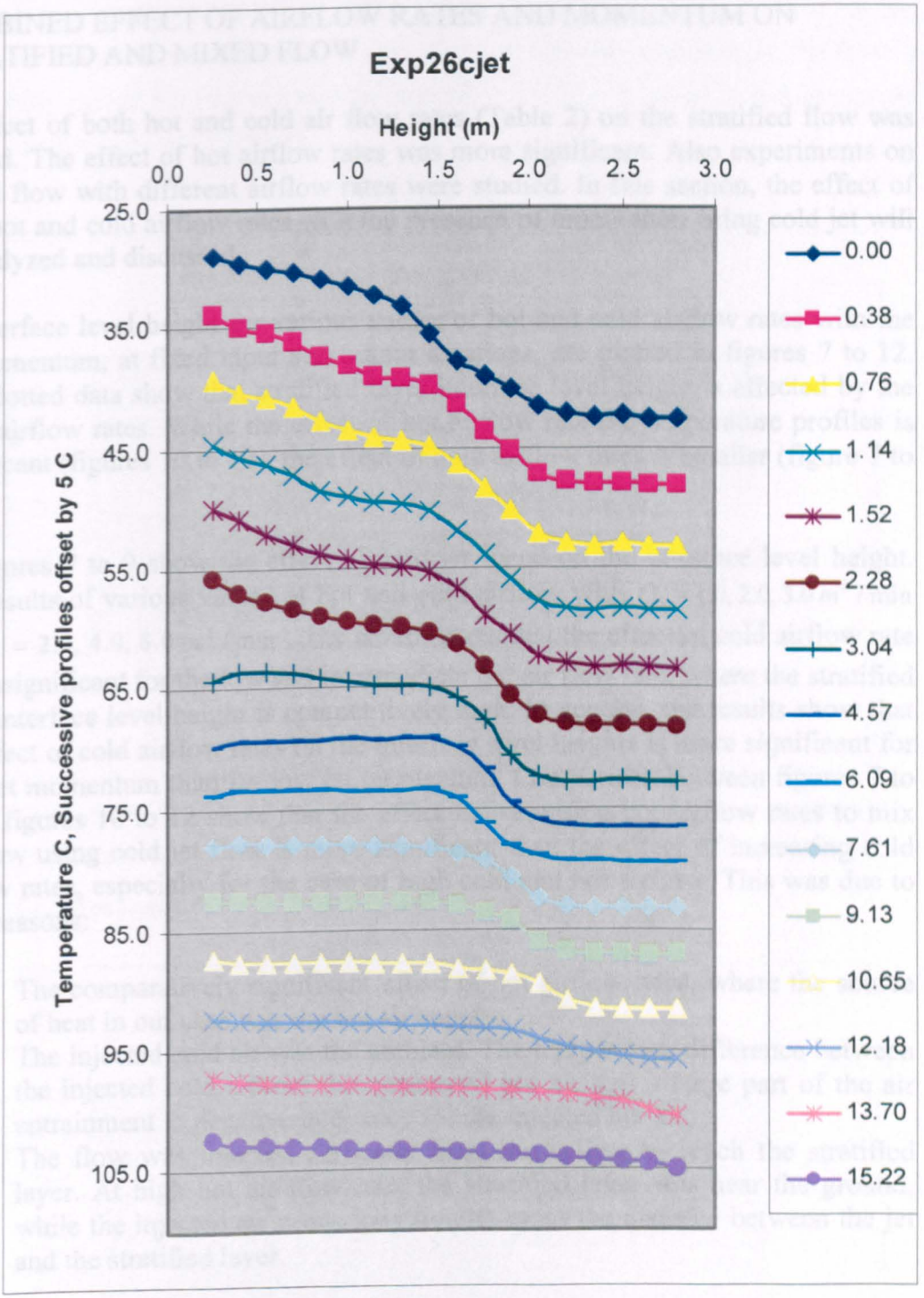

Fig. 6: Illustrates vertical temperature profiles for various cold jet speeds. The flow was stratified at ($Q_h = 2.0\ m^3/\min$) hot airflow rate and ($Q_c = 6.0\ \ m^3/\min$) cold airflow rate at a locations of 2.0 and 1.5 m respectively at the centre of environmental chamber.

COMBINED EFFECT OF AIRFLOW RATES AND MOMENTUM ON STRATIFIED AND MIXED FLOW

Effect of both hot and cold air flow rates (Table 2) on the stratified flow was studied. The effect of hot airflow rates was more significant. Also experiments on mixed flow with different airflow rates were studied. In this section, the effect of both hot and cold airflow rates with the presence of momentum using cold jet will be analyzed and discussed.

Interface level height for various values of hot and cold airflow rates with the jet momentum, at fixed input and output locations, are plotted in figures 7 to 12. The plotted data show that stratified layer interface level height is affected by the input airflow rates. While the effect of hot airflow rate on temperature profiles is significant (figures 10 to 12), the effect of cold airflow rates is smaller (figure 7 to 9).

Figures 7 to 9 show the effect of cold jet speed on the interface level height. The results of various values of hot and cold airflow with $Q_h = 1.0, 2.0, 3.0\, m^3/\min$ and $Q_c = 2.0, 4.0, 6.0\, m^3/\min$. The results show that the effect of cold airflow rate was insignificant for the low and intermediate hot air flow rate, where the stratified layer interface level height is competitively high. In general, the results show that the effect of cold airflow rates on the interface level heights is more significant for high jet momentum than for low jet momentum. Comparison between figures 7 to 9 and figures 10 to 12 show that the effect of increasing hot airflow rates to mix the flow using cold jet flow is more significant than the effect of increasing cold airflow rates, especially for the case of high cold and hot airflow. This was due to three reasons:

1. The comparatively significant effect of hot airflow rates, where the source of heat in our case was the hot air supply.
2. The injected cold air was the ambient. The temperature difference between the injected cold air and the penetrated hot air that a large part of the air entrainment to negative buoyancy for the injected hot air.
3. The flow was injected vertically from the ceiling to reach the stratified layer. At high hot air flow rate, the stratified layer was near the ground, while the injected air needs long time to cross the distance between the jet and the stratified layer.

Figure 9 shows that, at high hot airflow rate, the flow will be fully mixed at low momentum of ($0.5\, m^4/s^2$) for the cases of low and moderate cold airflow rates. On the contrary, the figure shows that to reach fully mixed of high cold airflow rate of ($6.0\, m^3/s$), more than triple times of this momentum will be needed ($1.75\, m^4/s^2$). Figures 10 and 11 show that, the flow will not fully mixed at hot airflow rates of ($1.0\ and\ 2.0\, m^3/s$) using low momentum jet of ($<0.5\, m^4/s^2$).

But the stratified layer interface level height go upward to reach 80% of the chamber height at a momentum of ($1.5\ m^4/s^2$). With more momentum, the flow is never fully mixed for low hot airflow rate of ($1.0\ m^3/s$), while it is fully mixed for hot airflow rate of ($2.0\ m^3/s$).

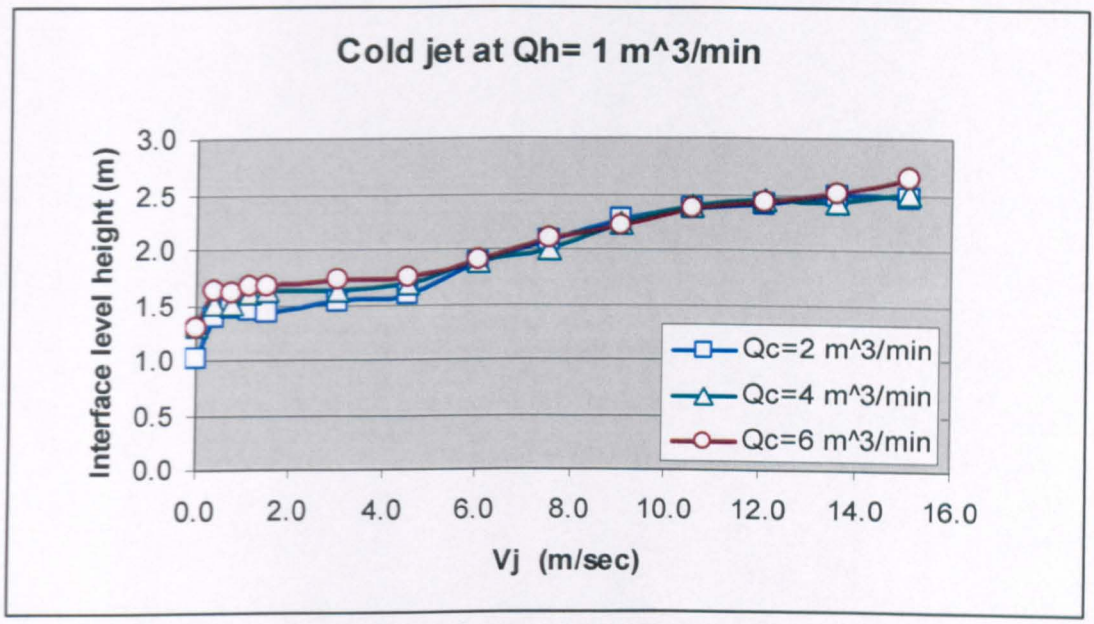

Fig. 7: Comparison of interface level height with the jet speed, at hot airflow rate of $Q_h = 1.0\ m^3/\min$ and different cold airflow rates ($Q_c = 2, 4$ *and* $6\ m^3/\min$) in the environmental chamber.

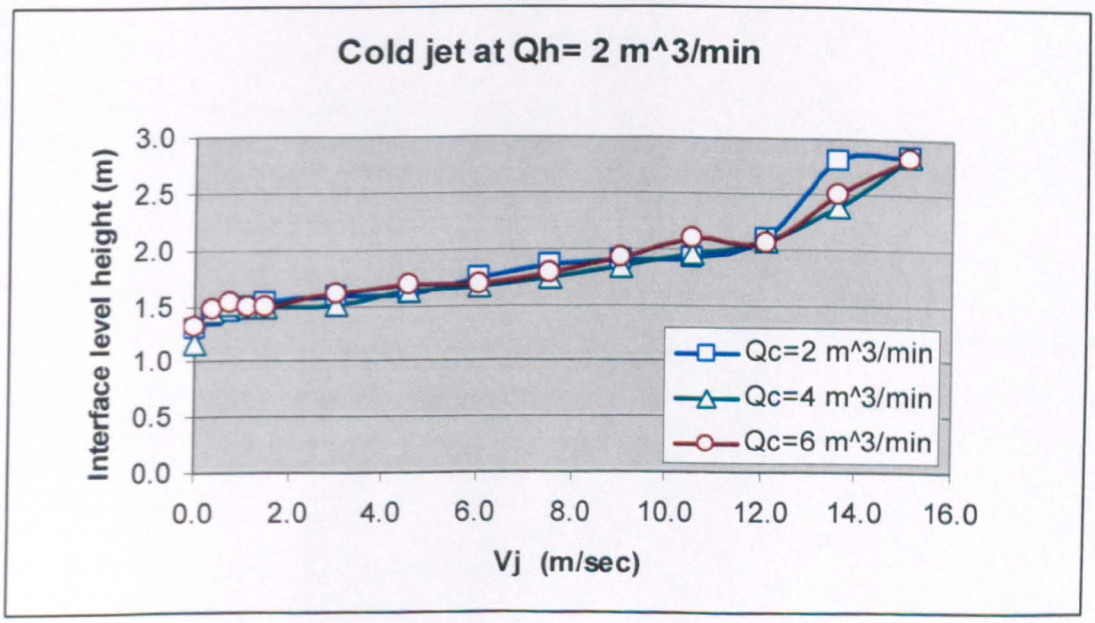

Fig. 8: Comparison of interface level height with the jet speed, at hot airflow rate of $Q_h = 2.0\ m^3/\min$ and different cold airflow rates ($Q_c = 2, 4$ *and* $6\ m^3/\min$) in the environmental chamber.

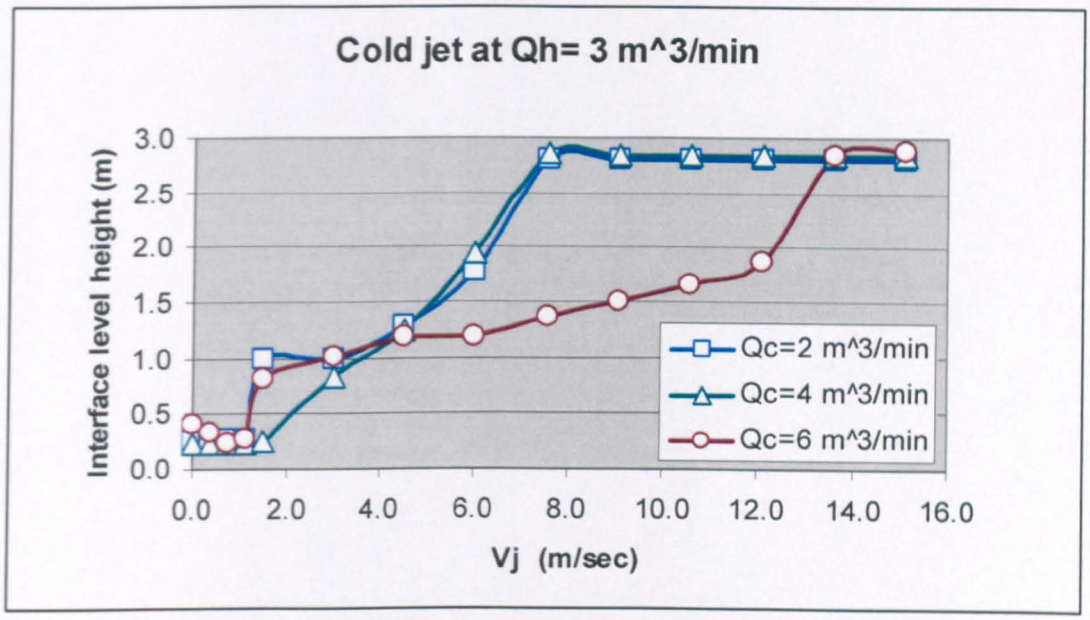

Fig. 9: Comparison of interface level height with the jet speed, at hot airflow rate of $Q_h = 3.0\ m^3/\min$ and different cold airflow rates ($Q_c = 2, 4\ and\ 6\ m^3/\min$) in the environmental chamber.

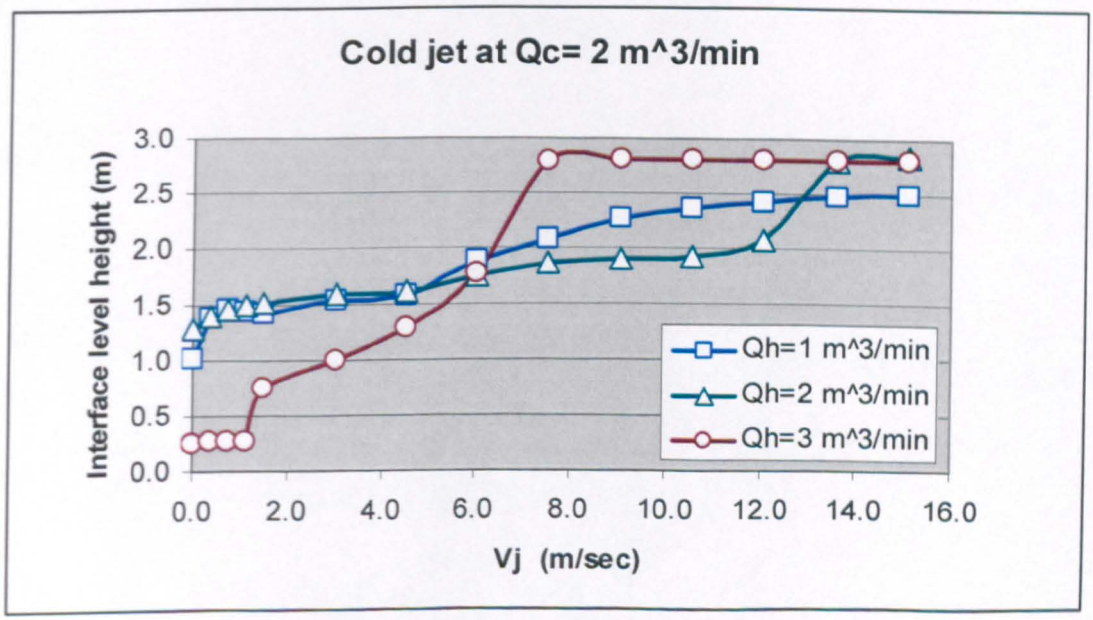

Fig. 10: Comparison of interface level height with the jet speed, at cold airflow rate of $Q_c = 2.0\ m^3/\min$ and different hot airflow rates ($Q_c = 1, 2\ and\ 3\ m^3/\min$) in the environmental chamber.

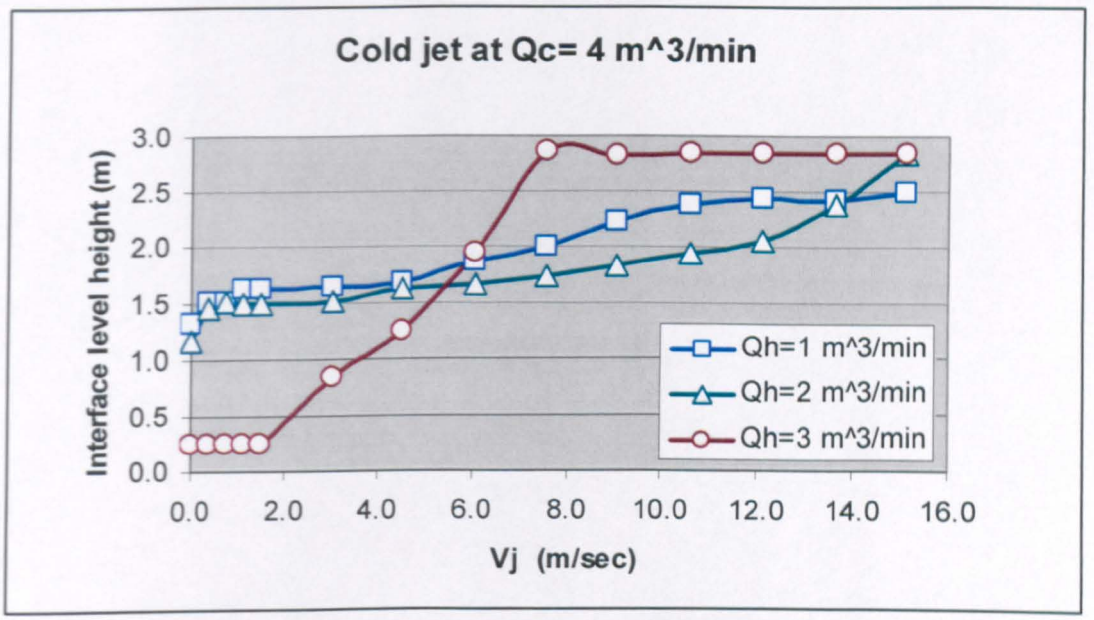

Fig. 11: Comparison of interface level height with the jet speed, at cold airflow rate of $Q_c = 4.0\ m^3/\min$ and different hot airflow rates ($Q_c = 1, 2\ and\ 3\ m^3/\min$) in the environmental chamber.

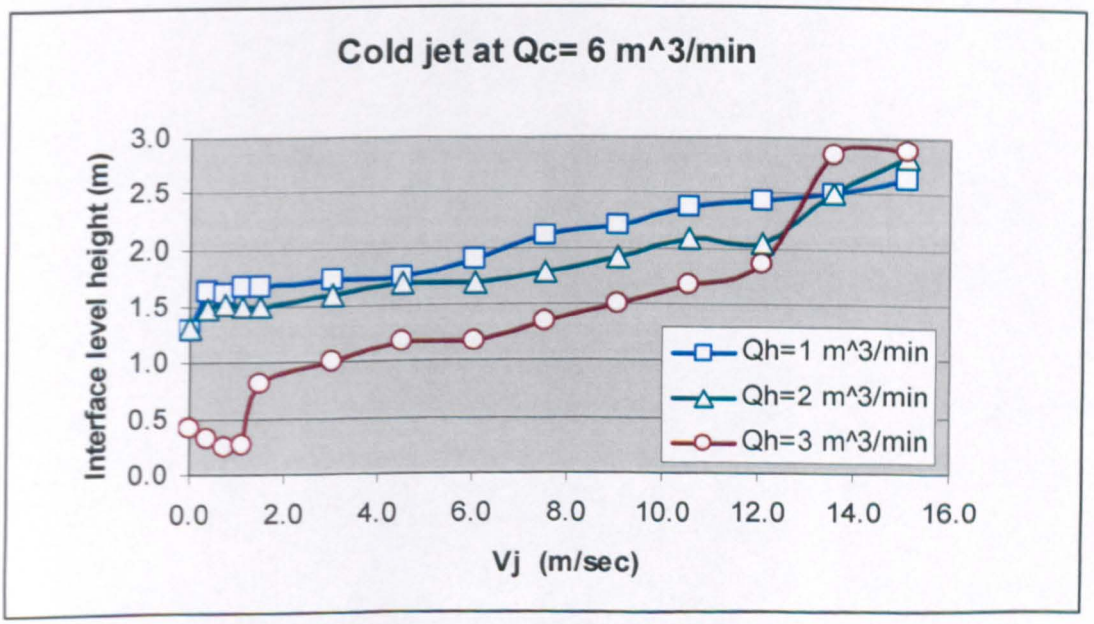

Fig. 12: Comparison of interface level height with the jet speed, at cold airflow rate of $Q_c = 6.0\ m^3/\min$ and different hot airflow rates ($Q_c = 1, 2\ and\ 3\ m^3/\min$) in the environmental chamber.

TEMPERATURE AND SMOKE VISUALIZATION

In this section smoke visualization is included for comparison with the experimental results. In general, the experimental and visualization results obtained in this work are in good agreement considering that different modeling technique, different surrounding conditions, complex flow patterns and turbulent dissipations in the domain were found in these experiments. While the discrepancies, between the experimental and visualized results are within the acceptable range of 2-5%.

Figures 13 to 18 are the momentum sequence photographs of a stratified and mixed flow with initial cold and hot airflow rates of (2 *and* $6 m^3/\text{min}$), Richardson number of 2.0 and Reynolds number of 2008. The flow has been mixed using a jet of 0.11m diameter. The injected air was in the range of ($V_j = 0.0$ *to* $15.0 m/\text{sec}$). The sequence in the figures shows the effect of cold jet flow on the stratified flow characteristics. The results represent the temperature visualization. Where sequences of smoke images are refer to different temperature distribution. Similar results were obtained with the temperature visualization.

Comparisons between the sequence figures illustrate the effect of momentum on the stratified flow characteristics. As the momentum is increasing, the smoke images indicate a more mixed flow in the lower zone and an upward translation of the stratified layer interface level height. More increase in momentum causes a fully mixed flow at $V_j = 15.0 m/\text{sec}$.

The results are so important to design ventilation systems considering the pollutants to be above the heads of people in the working zone, which will stuff the smoke layer at high level for that enable the people to escape in case of fire hazards to be safe from highest temperatures.

Unfortunately, it was difficult to get good-quality images for mixed cases of high momentum jet flows. At high jet flows, difficult flow phases, perturbations and fluctuations were introduced, while the flow is more mixed. For this case, the stratified layer is more dilute and the interface as well as the deviation of smoke refraction became so complicated to capture the images.

Fig. 13: Shadowgraph image showing the stratified flow with initial cold and hot airflow rates of 2 *and* $6 m^3/\min$, Richardson number of 2.0 and Reynolds number of 2008, with no jet flow ($V_j = 0.0\ m/\sec$).

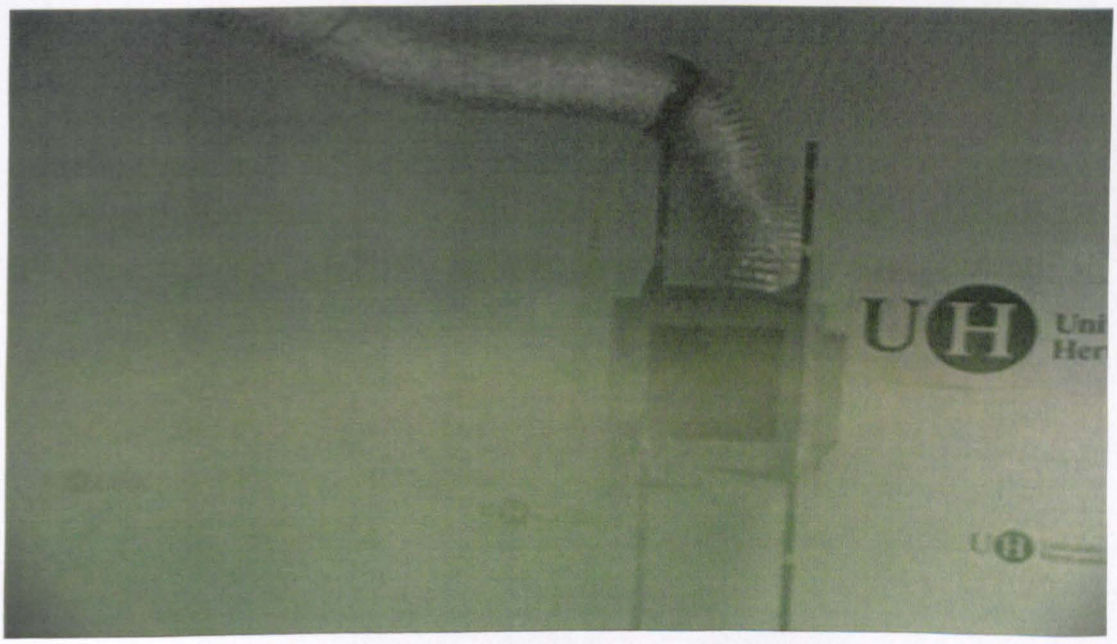

Fig. 14: Shadowgraph image showing the stratified flow with initial cold and hot airflow rates of 2 *and* $6 m^3/\min$, Richardson number of 2.0 and Reynolds number of 2008, with a jet flow of ($V_j = 3.0\ m/\sec$).

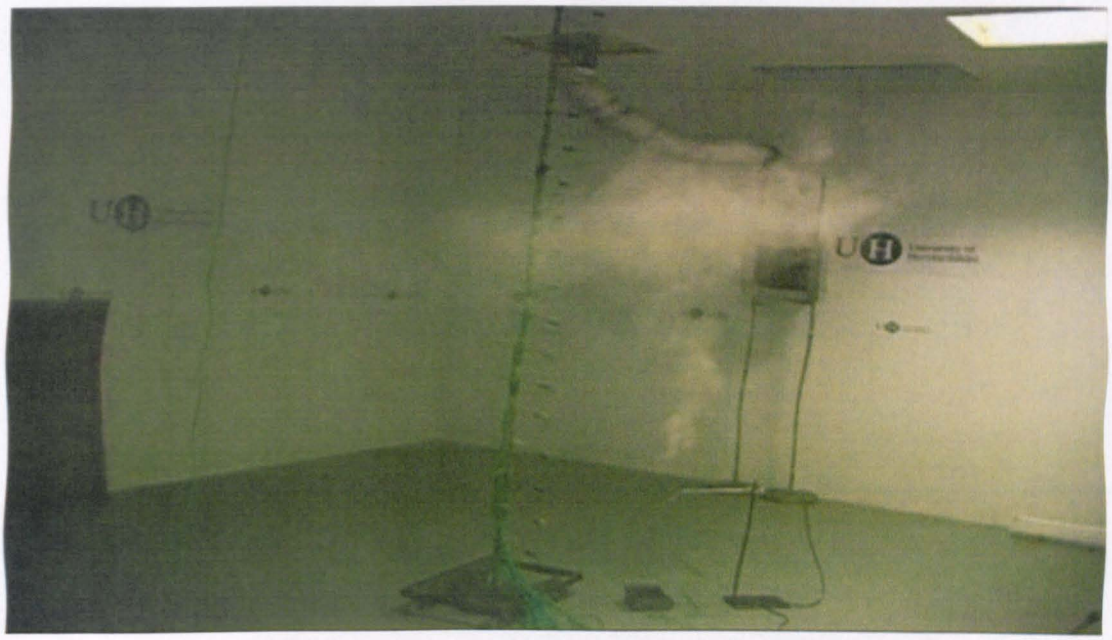

Fig. 15: Shadowgraph image showing the stratified flow with initial cold and hot airflow rates of 2 *and* $6 m^3/\min$, Richardson number of 2.0 and Reynolds number of 2008, with no jet flow ($V_j = 6.0\ m/\sec$).

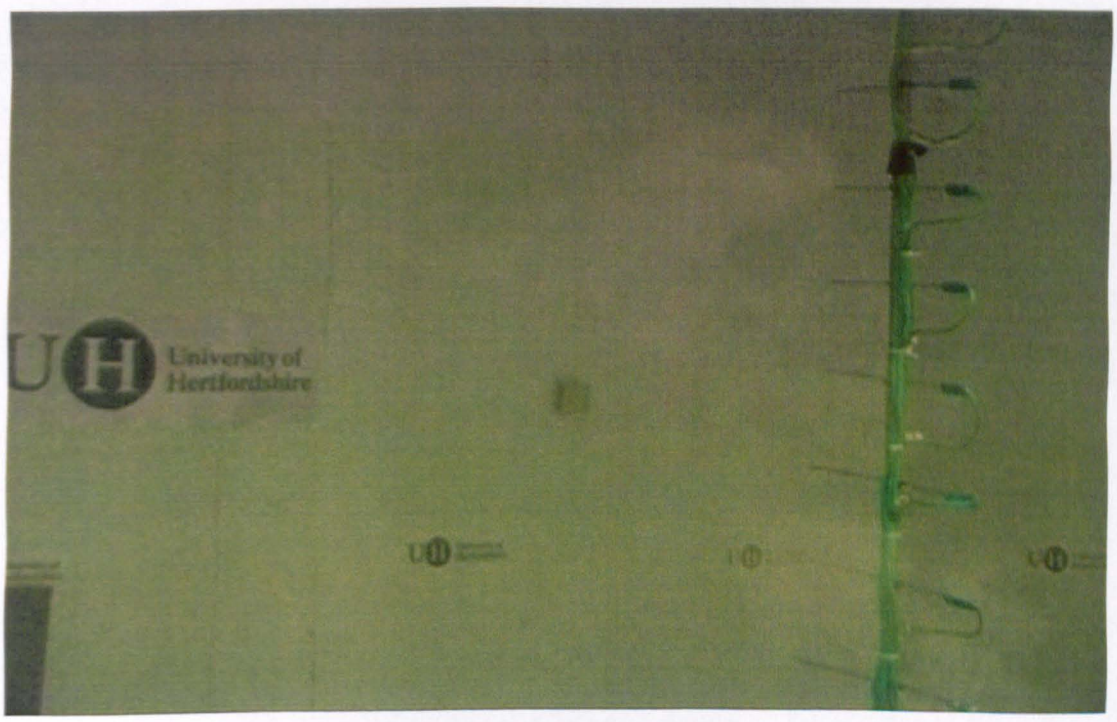

Fig. 16: Shadowgraph image showing the mixed flow with initial cold and hot airflow rates of 2 *and* $6 m^3/\min$, Richardson number of 2.0 and Reynolds number of 2008, with no jet flow ($V_j = 9.0\ m/\sec$).

Fig. 17: Shadowgraph image showing the mixed flow with initial cold and hot airflow rates of 2 *and* $6 m^3/\min$, **Richardson number of 2.0 and Reynolds number of 2008, with no jet flow (**$V_j = 12.0\ m/\sec$**).**

Fig. 18: Shadowgraph image showing the stratified flow with initial cold and hot airflow rates of 2 *and* $6 m^3/\min$, **Richardson number of 2.0 and Reynolds number of 2008, with no jet flow (**$V_j = 15.0\ m/\sec$**).**

CONCLUSIONS

The effect of momentum jet airflow on mixing the stratified flow was investigated by using experimental techniques. When a momentum of the cold jet is higher, a momentum turbulence gain from the momentum source to the lower zone increases, which results in change in the average temperature and in an increasing in the occupied zone by increasing the stratified layer level height. It can be concluded that the jet momentum has significant influence on the mixing of the flow and the stratified flow characteristics. The results indicated that once the momentum was initiated a mixed flow grew in the occupied zone above the floor. The height of this zone is a dependent of the stratified flow characteristics, and the temperature and momentum of the ceiling jet. Also the results showed that the stratified layer height is a function of the initial jet momentum over a wide range of flow rates. These results, despite of different types and values of jet flow, showed that the interface level height was approximately inversely proportional to the momentum in the case of cold jet, at least over the range of $0.22 - 2.17\ m^4/s^2$. Also it can be seen that increasing the momentum will increase the stratified layer interface level height, and more increase in jet momentum will increase the mixing in the lower zone and destroy the stratified layer before reaching the ceiling. Also it can be noted, that, the effect of hot airflow rate compare with cold airflow rate was much higher. For relatively cool jet injected air at high level from the ceiling, the entrainment volume flux from the upper zone is large enough. Also the hot air domain of penetration occurred in the upper zone.

REFERENCES

Bloomfield, L. and Kerr R. (1999). " Turbulent fountains in a confined stratified environment". J.Fluid mech. Vol.389, pp. 27-54.

Cardoso, S. S. and Zarrebini, S. (2001). " M. Convection driven by particle setting surrounding a turbulent plume. Chemical Engineering Science, Vol.56, pp.3365-3375.

Chen, Z.D. and Mahoney, L.J. (2001). "Natural ventilation in an enclosure induced by a heat source distributed uniformly over a vertical wall. Building and Environ, V 39, pp. 493-501.

Chow, WK. (1996). "Simulation of tunnel fires using a zone model". Tunnelling and Underground Space Technology, Volume 11, Issue 2, Pages 221-236.

Karimipanah, M.T. (1999). "Deflection of wall-jets in ventilated enclosures described by pressure distribution". Building and Environment, 34, pp. 329-333.

Linden P.F., Lane-Serff G.F. and, Smeed D.A. (1990). "Emptying filling boxes: the fluid mechanics of natural ventilation". Journal of Fluid Mechanics, Vol. 212, pp 309–335.

Murakami S., Kato S., Chikamoto T., Laurence D. and Blay D. Int.J. Heat Mass Transfer. 1996. Vol39. No.16, pp. 3483-3496.

Redondo, J.M. Sanchez, M.A. Cantalapiedra, I.R. (1996). " Turbulent mechanism in stratified fluids". Dynamics of Atmospheres and Oceans, 24, pp. 107-115.

The Effect of input and exhaust duct location on the stratified flow

A. S. Awad[1] O. O. Badran[2] A. E. Holdo[1] and R. K. Calay[1]

[1] *Department of Aerospace, Automotive and Design Engineering, Faculty of Engineering and Information Science, University of Hertfordshire, Hatfield Campus, UK.*

[2] *Department of Mechanical Engineering, Faculty of Engineering Technology, Al-Balqa` Applied University, P.O.Box 330116, Amman 11134-Jordan*

Abstract

This paper discusses the effect of input location (input height), exhaust location (exhaust height), airflow rates, on the stratified flow characteristics. The variations for both input and output locations and the variable openings of each condition to evaluate the effect of these parameters on the stratified flow characteristics were investigated. From the results it can be concluded that the input and exhaust locations reinforce each other, while the hot and cold airflow rates don't always reinforce each other, but in fact be against each other. The results can be used to obtain a good estimation of ventilation flows that aid in the design and applications of ventilation systems. The stratification interface level height and the ventilation flow rates are two main factors in the design of natural ventilation system.

Introduction:

A ventilation of air supply to both occupied and unoccupied spaces within buildings is necessary in order to replenish the oxygen supply; to act as a diluted to carbon dioxide, odours, process emissions; to prevent the build-up of potentially explosive vapour mixtures in the unoccupied plant spaces; to provide air movement, as a constituent part of comfort; and to control airborne contamination in industrial ventilation. Inside the enclosures, ventilation is used to remove pollutants, harmful gases and particulates from the multipurpose space, where different levels of pollutants are produced during different activities such as, welding, assembling and painting that take place side by side in one big hall, where ventilated air must conform to standards to ensure workers safety. It must be

supplied into the hall until the contaminants concentration decreases below the harmful levels. **Calay et al 2000**.

The configurations of building rooms and especially the location of inlet and outlet openings in relation to dominant wind direction at the site have major effects on the ventilation rates in buildings. Locating inlet openings near high-pressure surfaces of a building, and exit openings at low-pressure ones produces higher flow rates through windows. **Ayad (1999)**.

The thermal stratification generated by a localised source of heat at floor level in a confined space is of considerable interest to building ventilation. Many sources of heat generated in building may be regarded as being localised e.g. computers, occupants etc., and knowledge of the developing vertical temperature profile produced by these sources is required before air quality and occupant comfort levels can be determined. In general, these sources may be classified as either 'pure' buoyancy source, e.g. an electric fire or a radiator in a hot water heating system, or as' forced' buoyancy source which characterised by no-zero source momentum fluxes, e.g. in a heating system in which warm air is injected into space. **Hunt and Linden 1999.**.

Also during spray painting of objects, over spray and solvent vapours stratification layers are formed. These formed layers may cause an explosion and fire hazards. It may cause toxicity by absorption or inhalation of solvent vapours and fine over spray particles, in the place of work [**Wander (2002)**]. As a result, ventilation is used to remove particles of over spray to protect the texture of the surfaces already painted and those yet to be painted. This can be done, by removing over spray and solvent vapours by the ventilation stream to the external environment to be exhausted, **Wander (2003).**

Mundt (1994) found that the pollutants could be locked in at different levels (layers of pollutants). The distribution of pollutants is very sensitive to disturbances; that can cause a great decrease in the local ventilation effectiveness. "In spite of this, or perhaps because of this, a person can obtain a good air quality in the breathing zone, even if this zone is in a polluted layer. The convective plume around a body breaks through the polluted layers very rapidly".

The temperature gradient in the room is always positive and increasing up to the ceiling, while the contaminants concentration might have another form with maximum somewhere in the middle of the room. The temperature gradient is very much dependent on the ventilation flow rate and not so much on the position of the heat sources **[Mundt (1995)]**. The contaminant removal effectiveness, in displacement ventilation, was found to be related to the ventilation flow rate, and very sensitive to the level of the source and its position, **Mundt (2001)**. It was a function of both the location and the power of the sources; in relation to the supply and exhaust openings, **Hagstrom et al. (2000)**.

Wood et al. (2003) established a two-layer stratification and steady displacement flow in a room of turbulent plume originating from the top. The results showed that, the interface location is not only dependent of the opening geometry but also the source conditions, such as location and direction (upward or downward). Further series of computational and experimental studies were done by **Holford and Hunt (2003)** to provide a prediction for thermal stratification and airflow rates, by extending the theory of displacement flow developed by **Linden et al. (1990).** The experiments of **Holford and Hunt (2003)** were done on atrium buildings, using zones and field models. An atrium is a central feature of many modern naturally ventilated building designs.

Teitel and Tanny (1999) conducted a theoretical model to study the effect of openings height and wind speed in green houses. It was based on non-dimensional mass and energy conservation equations. The model was calibrated against experimental results. The results showed that ventilation, in greenhouses, was increased by increasing the height of the openings, the wind speed, and by decreasing the solar radiation. Mathematical and experimental analysis was done by **Hunt and Linden (1999)** to describe the natural ventilation using combined effects of buoyancy and wind. **Hunt and Linden (1999)** derived a mathematical model for stratified layer interface height based on wind speed and openings heights.

The position of neutral buoyancy, (the position where pressure in the room equals that in the exterior and the stratified layer is conformed), was investigated by **Andersen (2003),** and **Li et al. (2000).** Also **Fitzgerald and Woods (2004)** investigated the effects of thermal buoyancy, while **Li and Delsante (2001)** and **Chen and Li (2002)** investigated the effect of both wind and thermal buoyancy. With vents at multiple levels, using mass,

energy and momentum equations, it was found that the position of neutral buoyancy can be related to the ratio of the upper and lower vent areas depending on the nature of the heat source.

A relationship between neutral height, for air distribution, and ventilation load was investigated by **Xing and Awbi (2000).** The results of Xing and Awbi (2000) were obtained for a ventilated room, under several activities, using displacement ventilation. Also the neutral height above the heat source versus ventilation load based on mean temperature was investigated **Xing and Awbi (2000).**

In this study, the experimental modeling was used to test the effect of input and exhaust duct location parameters on stratified layer concentration and buoyancy. It is also highlighting the effects of various parameters (i.e. hot and cold airflow rates, height difference (between input and the exhaust heights) on stratified flow.

Experimental setup:

The experimental set-up used to support these models was presented. The flow parameters such as; input airflow, temperature, openings heights and other parameters were used to model the stratified flow patterns transactions.

Experimental Apparatus

All tests were conducted in the test environmental chamber at the University of Hertfordshire that is presented in figure1. The physical dimensions of the chamber were large enough, so that the walls didn't affect the flow, and the height was sufficient to the build up of stratified layer. The dimensions of the identical rectangular chamber were (7.5m long, 3.6m wide and 3.0m height) with two windows (double glazed) isolated from an enclosed space. The walls of the test chamber were insulated. The walls as well as the roof were of 12.5 cm thick, with white polyester outer finish and polyurethane foam interior made. The floor was a layer of light grey colour of 10 cm thick concrete, and below it a layer of 10 cm thick Styrofoam.

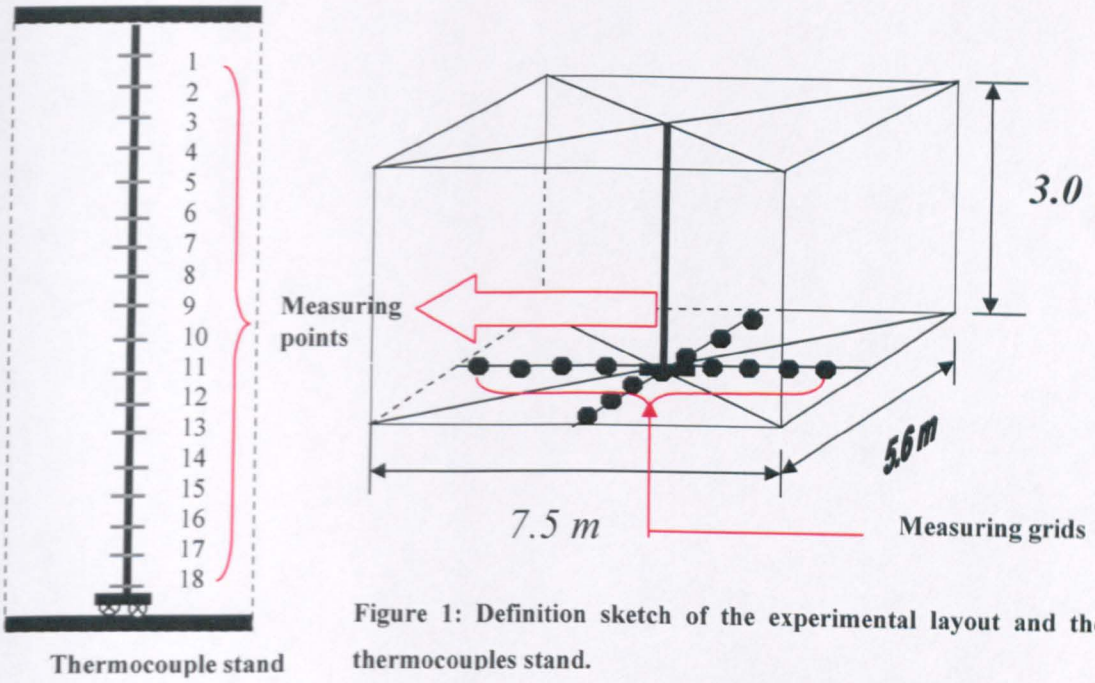

Figure 1: Definition sketch of the experimental layout and the thermocouples stand.

Environmental chamber flow variables were controlled by the means of airflow systems. The test chamber vent supply airflow up to $14\,m^3/min$ of hot air, and up to $12\,m^3/min$ of cold air. The hot air supply temperature was fixed at 45°C using the chamber heating and cooling system. The system can supply air at temperatures ranging from –40°C to +50°C. The cold air supply temperature was the ambient. It was varied according to the ambient temperatures and weather fluctuations. The chamber was insulated and the internal surfaces were painted white, so that the inside of the chamber was visible from the outside. The radiation heat transfer between the surfaces could be assumed insignificant, where the radiative heat transfer was between the walls of the chamber.

Transient temperature distributions for the flow inside the chamber were measured using eighteen K-type thermocouples. The thermocouples stand was inserted vertically on a multidirectional movable base located at the centre of the chamber as shown in figure 1. The junctions of the thermocouples were located at the centres of eighteenth equal volumes of the fluid in the chamber. Three thermocouples were placed in the inlet hot airflow, inlet cold airflow and outlet. Another was located outside the chamber to measure the ambient temperature. All of these thermocouples were located to give continuously monitoring of

all needed temperatures. The experimental results obtained will be used for the validity of both analytical and numerical models in the future work.

Concerning the measurements, the test chamber was equipped with sensors to determine the air temperatures (thermocouples), as well as, the input air velocities and flow rates (A rotating vane anemometer LC6000). A procedure was allowed by distributing the temperature sensors to cover the essential vertical and horizontal planes within the chamber. This was done by using thermocouple stand in the vertical direction, and by moving the base in both directions on the horizontal plane. As a result, the measurement points were represented at 15 cm grid in vertical plane, and 75 cm x 80 cm grid in each directions of investigated horizontal plane.

In conclusion, the experimental methodology has permitted us to obtain complete descriptions for the boundary conditions (supply air temperature and flow rate, inside temperatures and chamber boundaries), and all measurements were made under steady-state conditions.

The past theoretical and experimental studies have revealed that; the following variables can affect the stratified flow and flow characteristics in ventilated chamber:

- Heat loads and temperatures
- Input flow rates
- Ventilation openings.
- Opening heights (inlet and outlet)
- Geometric size and shape of the ventilated chamber.
- Thermal properties of the chamber boundaries.

Velocity Measurements:

A rotating vane anemometer LC6000 (manufactured by airflow, 2001, approved to BS EN ISO 9001) was used to measure both cold and hot airflow rates. It was suitable for most applications where the air stream was large enough, and the air velocity was ranging from 0.25-30m/s. It is accuracy at 20°C and 1013mb is better than ±2% for the readings from 5-30 m/s, and ±0.1m/s for the readings between 0.25-4.99 m/s.

Measuring Methods

The measuring methods used in this work were listed:

1. The temperature difference in the vertical direction was measured according to absolute difference between the temperatures in the top and the bottom of the chamber over the entire air column.
2. The temperature distribution in the vertical direction was measured at several stations along the vertical column (all stations were measured at the centre of the chamber between the inlet and the out let).
3. Input airflow rates for both cold and hot airflow were measured at the ducts entries.
4. The readings were taken at the centre of the environmental chamber, so that the walls would not have any significant effect on the measurements such as mixing and heat transfer.
5. The location of thermocouples stand was varied in both directions along and across the direction of the flow.

Measuring Stations:

1. At the middle of the environmental chamber, to measure the vertical temperature gradient from 0.2m to 2.8m above the floor (18 points in total). This was done to evaluate the stratified layer characteristics (interface level height, stratified layer thickness, temperature profiles and the degree of stratification).
2. At nine locations in the flow direction (x-axis) and six locations across flow direction. Each station measured the vertical temperature gradient from 0.2m to 2.8m above the floor (18 points in total). This was done to study the influence length, uniformity of the stratified layer and the validity of measurements in station1.
3. At different inlet and outlet openings heights. Each station measured the vertical temperature gradient from 0.2m to 2.8m above the floor (18 points in total). The measurements were taken to evaluate the effect of these heights on stratified flow. It can be used to destratify the flow by supplying cold air from the top of the chamber and the hot air from the bottom.

Measuring Procedure:

Based on the previous reported analytical, numerical and experimental observations in chapter 2, and preliminary experiments, we predicted the following:

- From the establishment of zones in stratified flow. Stratification takes place at a ranges of $0.1 \leq \bar{h} \leq 0.9$, otherwise, the flow may stratified but without zone establishment.

Where $\bar{h} = \frac{z}{H}$, z is the height of the temperature sensor (thermocouple) and H is the height of the chamber.

- From the definition of Richardson number, this is the ratio of potential energy to kinetic energy. The best stratification can be at large values of temperature difference ΔT and low values of momentum airflow.
- To study the stability of the flow, the flow rate values must cover the ranges of Richardson numbers based on the input conditions (airflow rates ant temperatures) ranging (from 0.08 to Max.), and indicate the stability and the type of the stratified flow.
- Stratification interface level height, stratified layer thickness and stability of the stratified flow must be studied at full ranges of openings heights ranging (from 0.5m to 2.0m).

According to the above specifications, following are the design sets of experiments. The technique used to evaluate the stratified flow characteristics was air modelling. Five sets of experiments were carried out. Both cold and hot airflow rates were entered at different inputs and outputs heights. Cold air was entered the bottom of the environmental chamber with five different values whiles the hot airflow was entered the top of the chamber with five different values. Both hot and cold airflow were supplied using rectangular diffusers of (0.5 x 0.5 m) for hot air and (1.0 x 0.5 m) for cold air. The diffusers help in admitting

the flow with minimum disturbances to establish the stratification in the flow and maintain on stratified layer. The experimental data must give the indication of the stratified flow characteristics such as stratified layer interface level height, stratified layer thickness, degree of stratification and stability.

The experiments were to study the effect of input hot airflow height on stratified flow. Both cold airflow and the exhaust heights were fixed, while the hot airflow height was varied. This was done for four different heights (1.0, 1.5, 2.0, 2.5). The hot air supply was then activated to produce stratification. These experiments were carried out for hot airflow rates of (1, 2, 3, 4, 5 m^3/min) at 45°C, and cold airflow rates of (0, 2, 4, 6, 8 m^3/min) at the ambient temperature. The purposes of this set of experiments were:

- To study the effect of both hot and cold airflow rates on the stratified flow characteristics with various input heights.
- To study the effect of input height on the stratified flow characteristics.
- To study the effect of input height difference (between hot and cold airflow rates) on the stratified flow characteristics.
- To study the flow transformation from stratified to destratified flow.

The fourth set of experiments was to study the effect of exhaust height on stratified flow. It was similar to the previuos set, except that both hot and the cold airflow heights were fixed at certain heights, while the exhaust height was varied for five different heights (0.5, 1.0, 1.5, 2.0 2.5 m). The hot air temperature for this case was 45°C and the experiments were carried out for hot airflow rates of (1,2,3,4,5 m^3/min). The cold inflow temperature for this case was the ambient and the experiments were carried out for cold airflow rates of (0, 2, 4, 6, 8 m^3/min). The purposes of this set of experiments were:

- To study the effect of both hot and cold airflow rates on the stratified flow at various exhaust heights.
- To study the effect of exhaust height on the stratified flow characteristics and contaminant removing.
- To study the effect of height difference (between input and the exhaust heights) on the stratified flow.

- To predict the best exhaust height be used in designs and applications of ventilation systems.

The last set of experiments was to investigate the mixing process that takes place inside the environmental chamber, the growth of the mixed layers, and how to destratify the flow. This was done by changing the hot air temperature to be less than the ambient. In this case, the hot airflow was the ambient temperature and supply the bottom of the chamber, while the cold airflow be fixed at 10°C and supply the top of the chamber. This type of experiments was done after complete stratified flow to investigate the effect of changing suppliers on stratified flow. The experiments were carried out for (0, 2, 4, 6, 8 m^3/min) hot airflow rates and (1, 2, 3, 4, 5 m^3/min) cold airflow rates. The preliminary test illustrates that rapid destratification was occurred. The purposes of this set of experiments were:

- To study the instability and how to destratified the flow.
- To study the effect of layers overturns on stratified flow.
- To study the time needed to destratify already stratified flow as time scale affects flow energy.

A total numbers of 21 thermocouples were used (18 on the stand and 2 at the inlets and one at the outlet). The thermocouples were vertically distributed at the stand. The stand was located in the middle of the chamber in order to capture the temperature gradients in the stratified region. Thermocouples that placed at the inlets and outlets were used for monitoring the inflow and outflow temperatures. A data logger was interfaced to a personal computer to collect the flow of temperature signals arriving from the test chamber.

The thermocouples were calibrated against a platinum resistance thermometer. The accuracy of the measured temperatures (using a K-type thermocouple) was within 1.0 °C. The inflow rate was measured using a rotating vane anemometer (the accuracy being, approximately, within $0.1 m^3/min$. The overall accuracy was a function of the over all parameters that affect the flow and the instruments used at certain boundaries and the experimental conditions.

Smoke Visualization

Smoke visualization was used as an easy method to display the results in simple form being to the human observer. Smoke, as a form of pollutant source was present by introducing the smoke into the environmental chamber using a smoking machine. Photographic flow visualization records were also prepared using digital camera. A series of visualization tests were conducted using Aero-tech smoking machine. The tests were to study the stratification flow characteristics such as thickness, interface level height, and degree of stratification.

The smoke, initially, was penetrated with high momentum and turbulent mixing. It mixes with the air through the lower zone at the centre of the environmental chamber. On reaching the interface level height, the smoke starts to spread out steadily along the interface in the stratified region, where it was seen easily in this case.

From Figure 2 it can be seen that the smoke was ascending and staying in stratified region to form a layer of certain thickens. This thickness was a dependent of flow parameters. After that the smoke started to evacuate through the exhaust opening,

Figure 2 shadowgraph image of stratified flow induced by smoke rise at steady state conditions in the environmental chamber.

Results and Discussion

Effect of Input location

Noting that, for our case, the input location was the source of heat release in the chamber where hot air was penetrated. This location was considered as an effective parameter to be investigated. Various input locations were tested, experimentally, along with several flow parameters inside the chamber. The studied locations were (1.0, 1.5, 2.0 m). The experiments were done for different ranges of flow rates of hot and cold air corresponding to different ranges of Ri > 0.08. The temperature profiles for various values of cold airflow rates ($Q_c = 0.0 - 8.0 m^3/min$) and input locations, at fixed exhaust location (1.5 m) and at comparatively low hot airflow rate $Q_h = 2.0 m^3/min$, are plotted in both figures 1 and 2 respectively. The results were in terms of the dimensionless temperature $(T - T_1)/(T_2 - T_1)$ with the dimensionless height z/H, where T_1 and T_2 being respectively the temperatures at the bottom and the top of the chamber, and H is the total height of the chamber.

For both cases shown in figures 3 and 4, it is observed that the temperature distribution is affected by both the input location and the cold airflow rate. While the effect of input location on temperature profiles is significant, the effect of cold airflow rates is smaller, especially for input location of 1.5 m. The effect of cold airflow rate was much stronger for the 2.0 m input location than that of 1.5 m.

Comparison between figures 3 and 4 shows the effect of increasing the location of hot airflow rate from 1.5 m to 2.0 m (i.e. 30% height increase) on the stratified flow characteristics while the hot airflow rate was fixed.

With increasing of input location, the following observations can be made:

1. It increases the stratified layer interface level height.
2. It increases the variations of flow characteristics in the upper zone.
3. It amplifies the effect of cold airflow rates on the stratified flow characteristics.

Firstly, the higher of the input location yields a higher interface level height; the effects were due to the height shift of hot air flow rate that shifted the stratified layer upward in

response to the change in elevation of the supply diffuser, so the interface level height. From the figures, the increase in stratified layer level height was more than the height shift, which is due to both: the height shift and the height difference between hot and cold airflow rates that decrease the amount of heat transfer between the zones and the amount of mixing and so propagates the flow to stratify.

Secondly, as input location increases, larger circulation flows are generated in the upper region, whereas; smaller ones are formed for low input location. This change of flow fields was related to plume strength, which results in different levels of stratification. **[Hee-Jin and Dale (2001)]**. When input location is located at 1:0 m, no visible stratification level is observed. It is because of the hot airflow that directed into the floor before it yields a stratified layer, where the spread of hot air beneath the low input location is dependent on the input location, as one would expect. Because the penetration distance is decreased then the small height is sufficient to prevent hot air reaching the ground. In this case it can also be observed that the flow is completely mixed where the penetration distance and the interface level height are both found to decrease with decreasing input location. **[Abdulkarim and Yogesh (1996)]**.

Thirdly, the cold airflow rates have a wide domain to affect the flow, especially in both the stratified layer and the upper zone.

From the figures 3 and 4, it can be seen that, when input location is reduced by 25% (1.5 m), the shape of temperature profile showed less sensitivity to the change in cold airflow rate than the (2.0 m) input location. It also can be seen that, the decrease of input location of hot airflow rate affects the flow to stratify at lower height while the interface level height descends to attain the ground.

It can be noted that, in the stratified layer, the temperature profiles is more mixed close to the upper zone than that close to the lower zone, while it is more mixed in lower zone than that in the upper zone. However, as the input location increases or the amount of cold airflow rates increases, the interface tends upwards towards the ceiling of the chamber, and therefore extends the stratified layer thickness. As a result, the flow becomes more dilute and the stratified layer more diffuses.

As a heat source supply, the results showed that the input location has a significant influence on the flow characteristics. Figures 3 to 6 illustrates that as the hot airflow rate increases, the amount of heat in the upper zone, and the interface level height migrates downwards from the top of the chamber to reach the ground, even though the input location is increasing. It also showed that the interface level height seen to increase with an increase in the location of hot supply, and to decrease with an increase in the hot airflow rate.

The results show that higher input location offer a stable stratified flow in which the layer is built up and becomes strong enough to overcome mixing forces. For this case, increasing the hot airflow rates will increase the temperature in the upper zone, and then the hot air in the upper region pushes the stratified layer downward. More increase in rate will make the layer to lose its buoyancy. In this case, only one type of flow would be observed in whole space. It is deduced that when the source is at low location, a large circulation is created yielding a lower stratification level. The reverse is applied to the case of higher locations of the heat source where momentum based stratification is to form at a higher level.

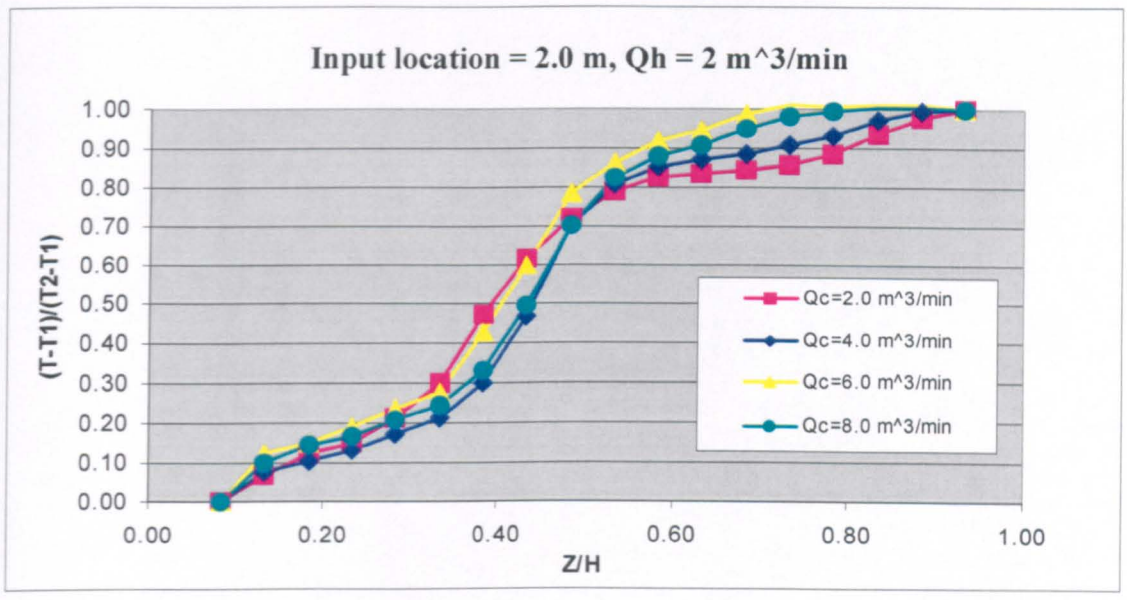

Figure 3: Comparison of dimensionless temperature profile along vertical centreline with dimensionless height across the chamber at a fixed axial location of (3.75, 2.8) m and fixed hot air flow rate ($Q_h = 2.0 m^3/min$) for different cold flow rates ($Q_h = 0,2,4,6,8 m^3/min$) in the environmental chamber for 2.0 m input location.

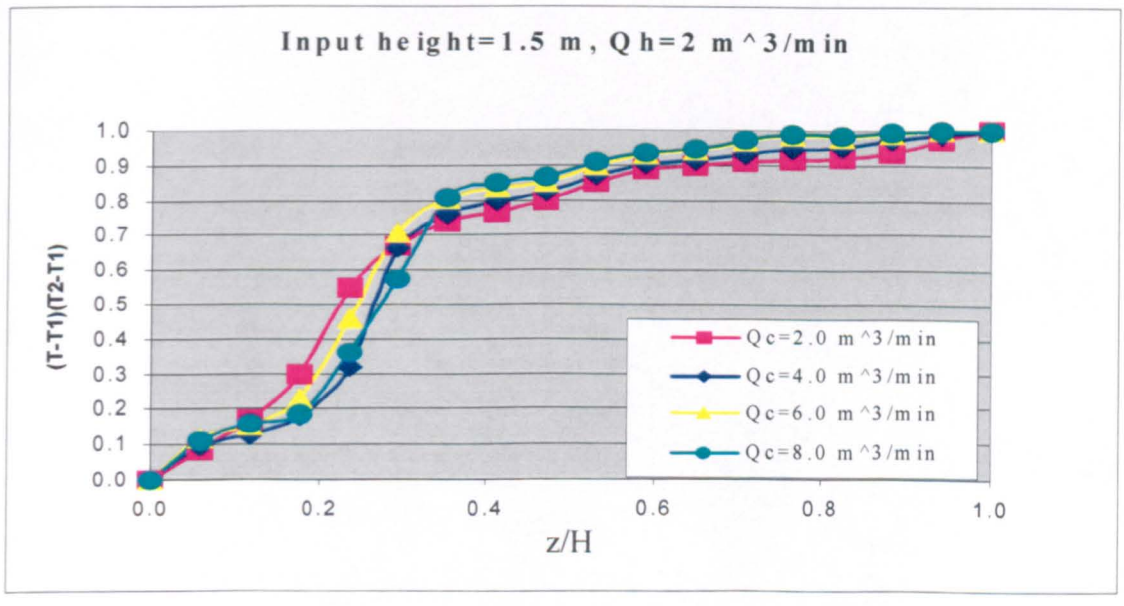

Figure 4: Comparison of dimensionless temperature profile along vertical centreline with dimensionless height across the chamber at a fixed axial location of (3.75,2.8) m and fixed hot air flow rate ($Q_h = 2.0 m^3/min$) for different cold flow rates ($Q_h = 0,2,4,6,8 m^3/min$) in the environmental chamber for 1.5 m input location.

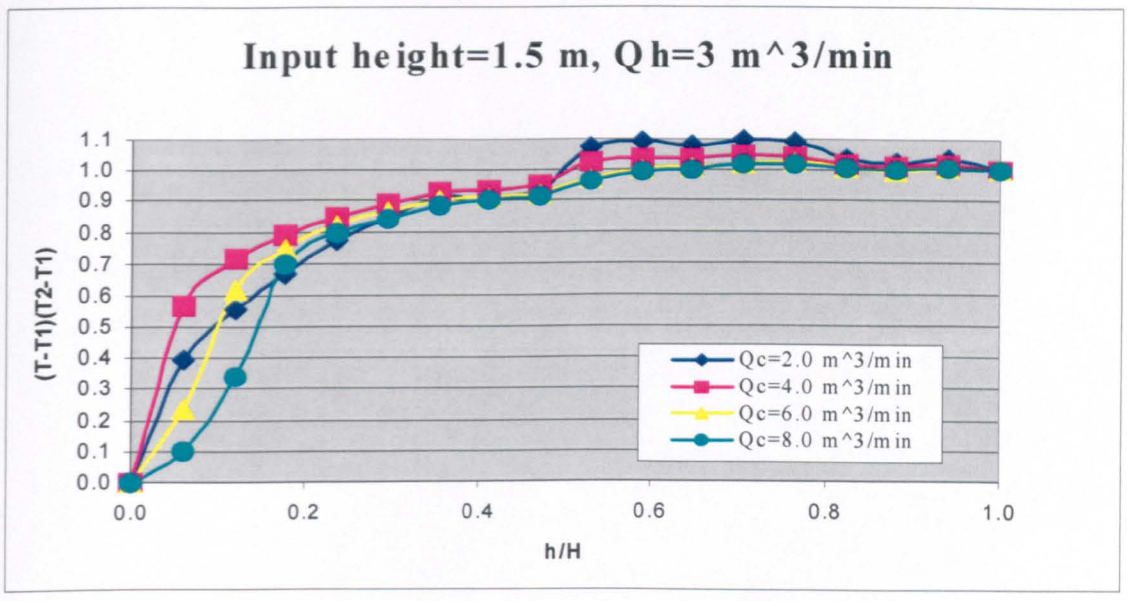

Figure 5: Comparison of dimensionless temperature profile along vertical centreline with dimensionless height across the chamber at a fixed axial location of (3.75,2.8) m and fixed hot air flow rate ($Q_h = 2.0 m^3/min$) for different cold flow rates ($Q_h = 0,2,4,6,8 m^3/min$) in the environmental chamber for 1.5 m input location.

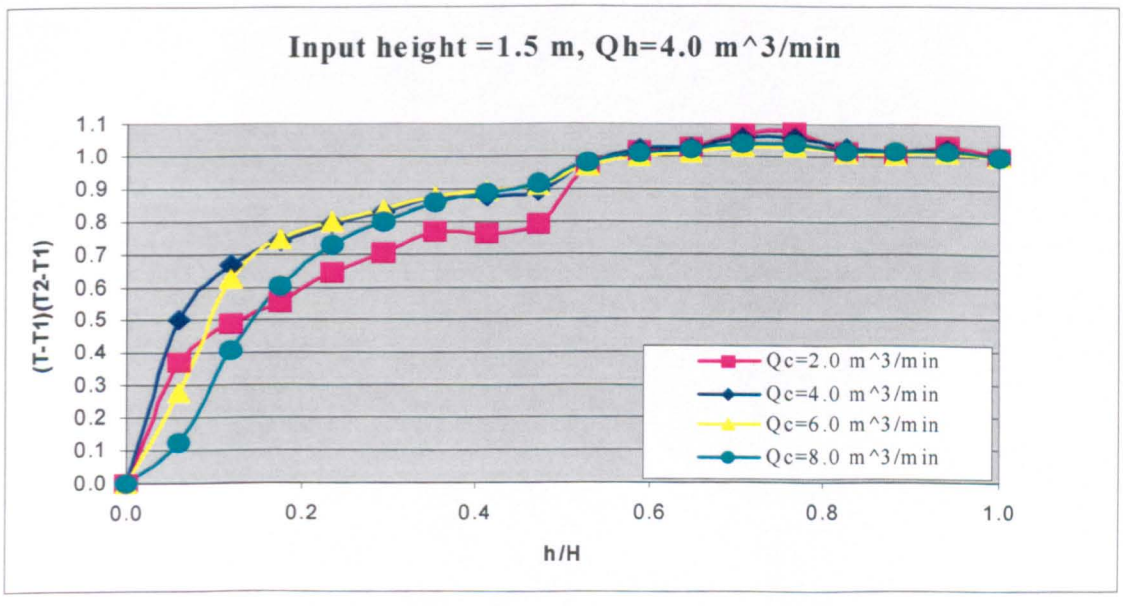

Figure 6: Comparison of dimensionless temperature profile along vertical centreline with dimensionless height across the chamber at a fixed axial location of (3.75,2.8) m and fixed hot air flow rate ($Q_h = 2.0 m^3/min$) for different cold flow rates ($Q_h = 0,2,4,6,8 m^3/min$) in the environmental chamber for 1.5 m input location.

Typical temperature profiles are shown in Figures. 7 and 8 for input location of heights 1.0, 1.5 and 2.0 m. It was for various modes of flow rates. The temperature distributions were for cases of mixing flow. The figures show the flow was fully mixed for both modes of low and high airflow rates.

Figure 7 show the input locations of no significant effect on temperature profile for a fixed mode of flow rates, whiles mode airflow rates has a significant effect on temperature difference. At low airflow rates, the flow hasn't sufficient buoyancy forces required to stratify the flow, while at high airflow rates the flow has a maximum momentum which it is sufficient to break the stratified layer and mix the flow.

Figure 8 shows the temperature profiles for moderate airflow rates, with a significant effect of input locations. When the input location gets higher, a larger temperature gradient is created (compared to lower location) in the lower zone. The flow was stratified in different degrees of stratifications. This amount of stratification was increasing by increasing the input location. It was due to two reasons:

1. There is an increase in buoyancy forces propagate the flow to stratify compare with low airflow rate. On the other hand, there is a decrease in momentum forces that break the stratified layer and mix the flow compare with high airflow rate.
2. As the hot air goes downward, the volumetric flow rate is increased by entrainment of surrounding air, and a circulation flow is formed in the region under the input location. It is observed that when the input location is low both hot and cold air will mix together, which increase the temperature in the lower zone. When the input location is higher, the hot air is circulated in the upper region, while the cold air is circulated in the lower region yielding a stratified layer in between.

From the analysis, the input location is not only affects the yielding of the stratified layer but also the flow characteristics. Therefore, the strength and size of those circulation flows are main factors in characterizing the stratification level [**Hee-Jin and Dale (2001)**].

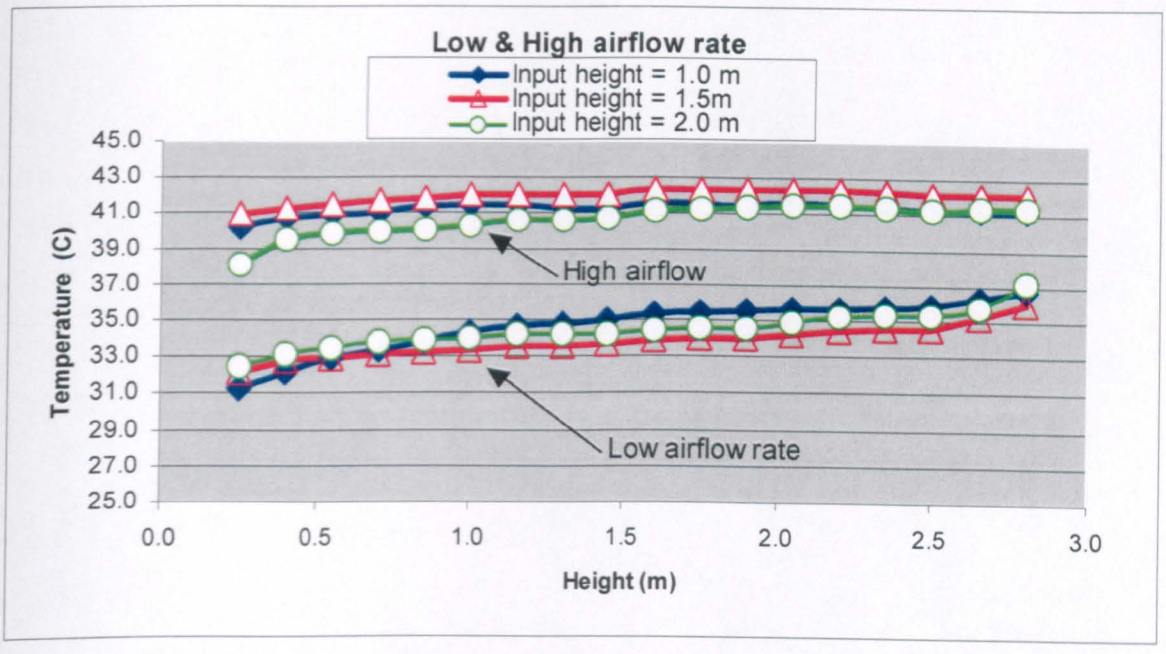

Figure 7: Comparison of temperature profile along vertical centreline with chamber height at low and high air flow rates in the environmental chamber for different input locations

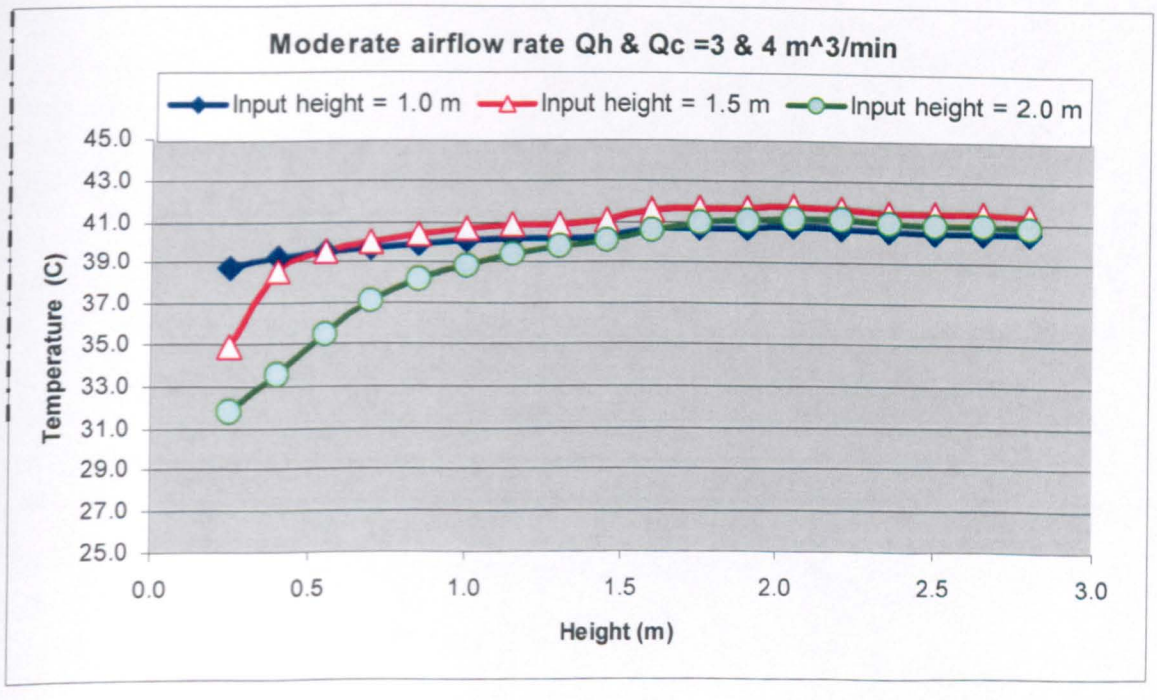

Figure 8: Comparison of temperature profile along vertical centreline with chamber height at intermediate airflow rates in the environmental chamber for different input locations.

Effect of exhaust location

Exhaust location was another parameter that has been investigated to find if there were visible effects on the flow characteristics. Compared with the previous results for the effect of input location, the flow characteristics are affected considerably by the exhaust location as seen from the results. The dimensionless temperature profiles for various values of hot and cold airflow rates, at fixed input location and large values of exhaust locations were plotted in figures 7 to 10. The figures show that at exhaust location 2.5m, the temperature distribution was affected by the input airflow rates with significant values for hot airflow rates, and in smaller values for cold airflow rates.

These figures also show that the exhaust location does not alter the position of the interface level height. It could be in the location above or below the interface level height. Note that the exhaust location does influence the flow rate and the level of the interface. In order to improve the effectiveness of ventilation and to save heating energy costs, the exhaust location must be where "the exhaust temperature should not exceed the temperature in the occupied zone" **[Hagstrom et al. (2000)]**.

Comparisons between figures 9 to 12 show that the flow can stratify at certain heights below the exhaust location depending on the flow boundary conditions. For this the opening geometries must be designed to overcome the phenomenon and exhausted the contaminants and unneeded gases with high removing efficiency. However, when the exhaust location is not at the stratified layer height, but at some way below or above, the removing efficiency becomes low. In other words, fixed exhaust location is ineffective to exhaust the contaminant rather than the fresh air from the occupied zone, when it designed without taking in consideration the stratified flow characteristics. These three flow modes will be discussed individually:

1. The exhaust location is below the stratified layer height. In this case, the cold air flows out through the exhaust opening, while the stratified interface level height immigrates toward the ground.
2. The exhaust location is at the stratified layer position. In this case, the stratified flow is not established and the transition to mixing flow is observed. This was due to the airflows from the stratified layer through the exhaust opening.

3. The exhaust location is above the stratified layer. In this case, the hot air flows out through the exhaust opening while the stratified interface level height immigrates to reach the top of the chamber.

It is seen that the degree of stratification for case 1 is considerably higher than that for case 3. Where a higher exhaust location will tends to higher level of stratification. On the other hand, a lower location may result in lower levels of stratification. For these three cases, the stratified interface level height will move up and down to maintain on the stratified layer. It could be fixed by distributing the exhaust location vertically.

From the figures, it can be seen that, the exhaust location is a key factor in stratification phenomenon and so in ventilation process. It is important in the evaluation of the flow characteristics in ventilated rooms. When the exhaust location is situated in the upper zone, the exhausting of fresh air is large and the concentration of contaminants in the lower zone is too high. On the contrary, when the exhaust location is situated in the lower zone or close to the stratified layer interface, the contaminant removal effectiveness is larger. Very similar suggestion was obtained by **Mundt (2001)** that the source of contaminant must be in the upper zone to be exhausted at large effectiveness.

The increase in hot air flow rates increases the degree of stratification, but further increases in hot air flow rate produce little further increase in degree of stratification. Whatever the explanation for these observations, the results of figures 9 to 12 could provide a useful indication for this case.

From the results, while the input and exhaust locations reinforce each other, there are hot and cold airflow rates are in evidence that they don't always reinforce each other, but in fact be against each other, as found clearly from the results.

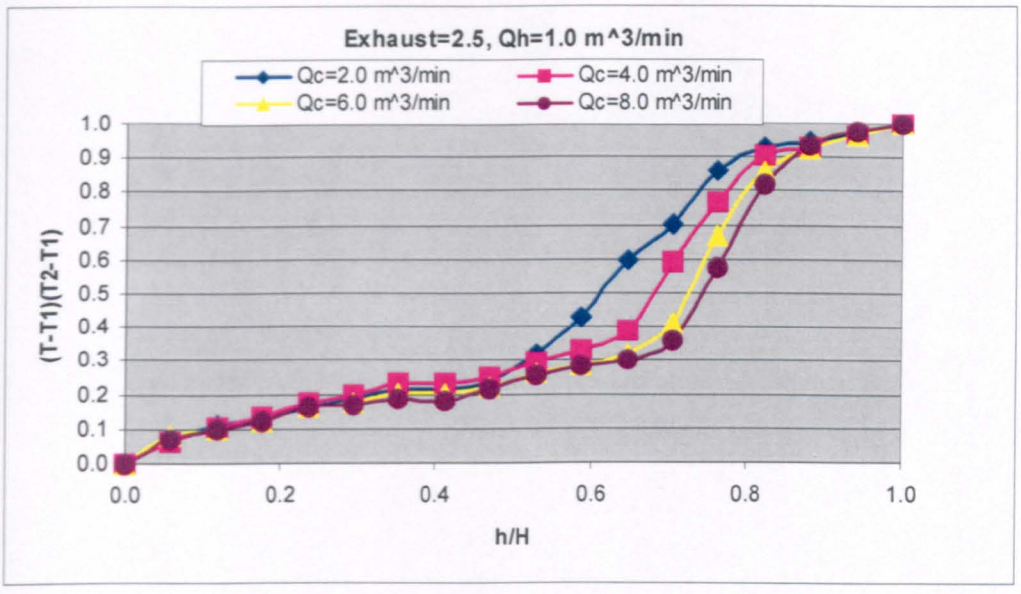

Figure 9: Comparison of dimensionless temperature profile along vertical centreline with dimensionless height across the chamber at a fixed axial location of (3.75,2.8) m and fixed hot air flow rate ($Q_h = 2.0 m^3/min$) for different cold flow rates ($Q_h = 0,2,4,6,8 m^3/min$) in the environmental chamber for 1.5 m input location.

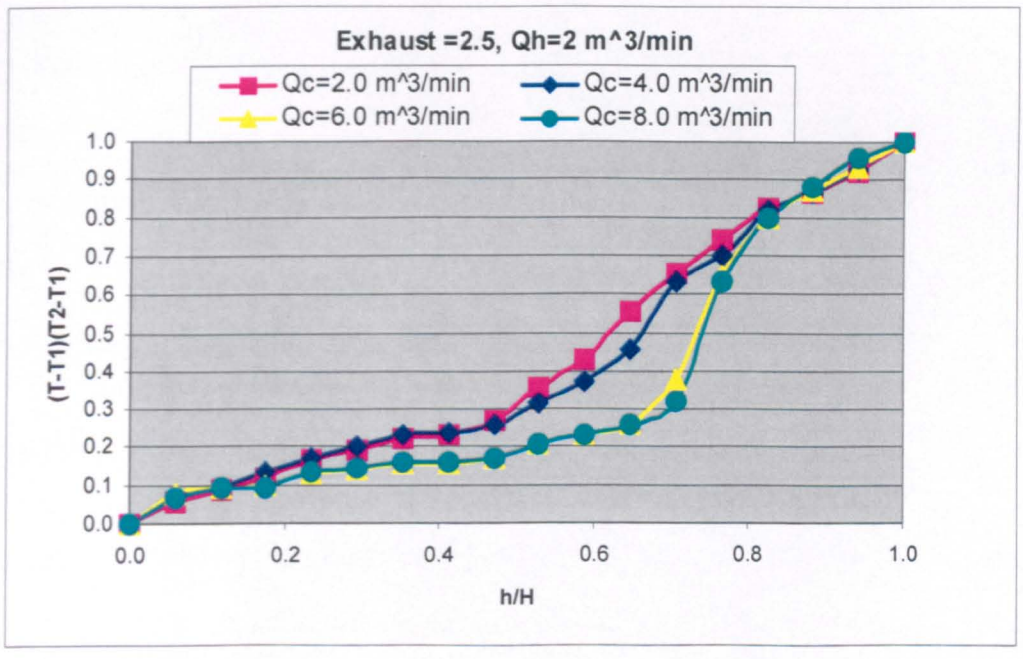

Figure 10: Comparison of dimensionless temperature profile along vertical centreline with dimensionless height across the chamber at a fixed axial location of (3.75,2.8) m and fixed hot air flow rate ($Q_h = 2.0 m^3/min$) for different cold flow rates ($Q_h = 0,2,4,6,8 m^3/min$) in the environmental chamber for 1.5 m input location.

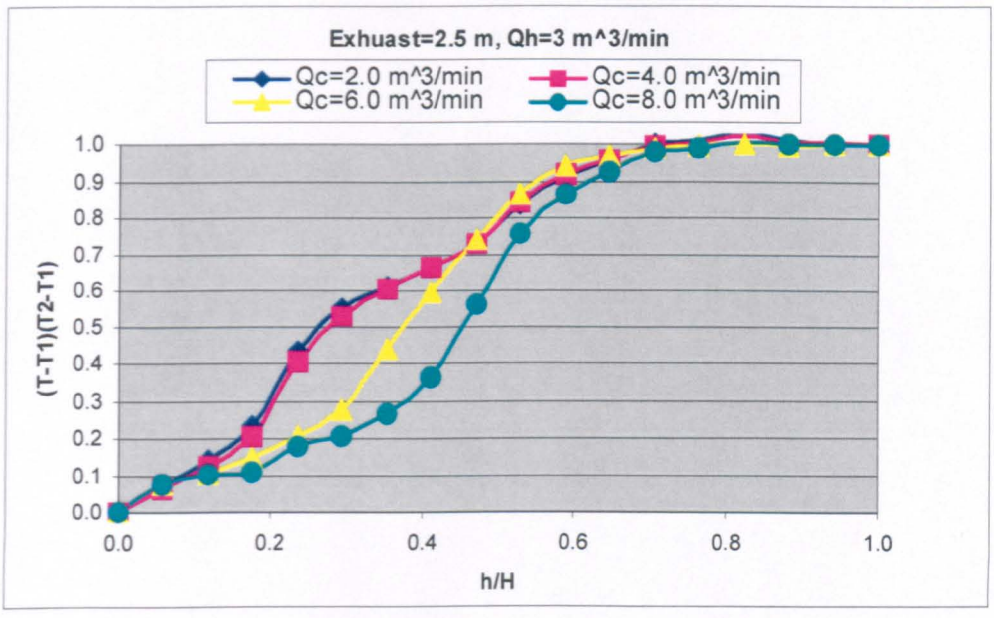

Figure 11: Comparison of dimensionless temperature profile along vertical centreline with dimensionless height across the chamber at a fixed axial location of (3.75,2.8) m and fixed hot air flow rate ($Q_h = 2.0 m^3/min$) for different cold flow rates ($Q_h = 0,2,4,6,8 m^3/min$) in the environmental chamber for 1.5 m input location.

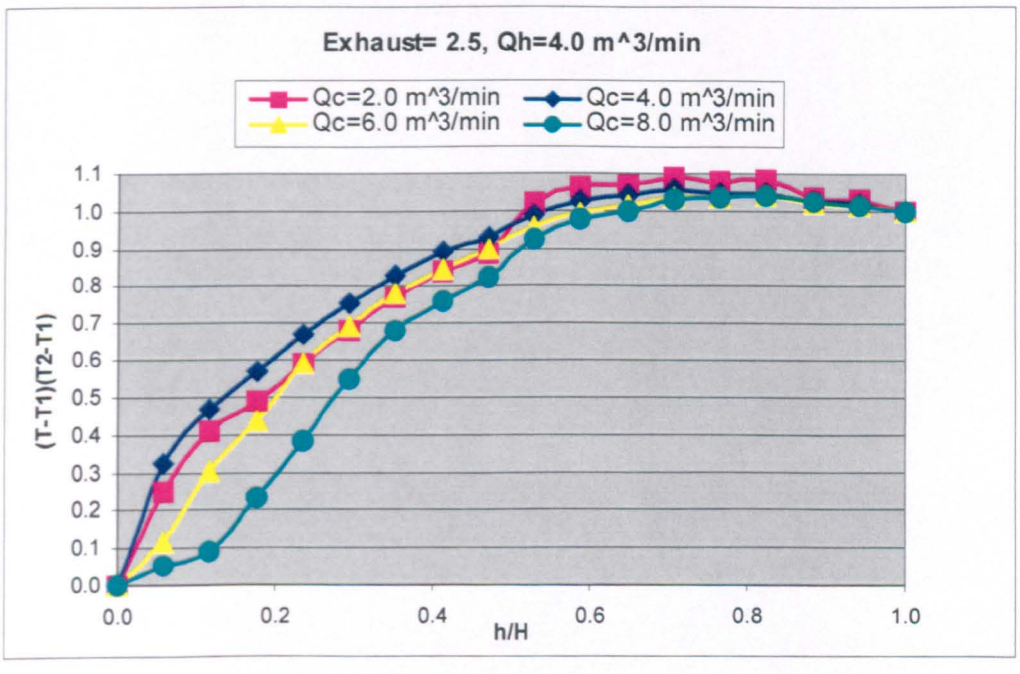

Figure 12: Comparison of dimensionless temperature profile along vertical centreline with dimensionless height across the chamber at a fixed axial location of (3.75,2.8) m and fixed hot air flow rate ($Q_h = 2.0 m^3/min$) for different cold flow rates ($Q_h = 0,2,4,6,8 m^3/min$) in the environmental chamber for 1.5 m input location.

Comparison between figures 13 and 14, show the effect of increasing exhaust location on the stratified flow characteristics. However, for this case:

1. It increases the stratified layer height, due to the height shift, and decreases the temperature difference and so the degree of stratification due to the evacuation of fresh hot air from the upper zone.
2. It increases the significant effect of cold airflow rate due to the wide domain in the lower zone where both the mixing and the influence length will increase.

In the analysis above it has been seen that increasing the exhaust location was resulting in an extended stratified region with less temperature difference and so the degree of stratification, which tends to destratify the flow, which it is similar to the results obtained by **Linden et al. (1990),** using filling boxes, that when the output location some where down the ceiling, the amount of mixing was so greater and the interface was diffused.

Figures 13 and 14 show how the dimensionless temperature distribution varies depending on various exhaust locations. The figure show that the temperature does not vary linearly over the chamber height and it can be divided into three zones. While the height of the lower zone is changing with the source location, the upper zone is well fixed for various source locations. While temperature remains constant in the lower and upper zones, (except at 2 m case) temperature in the stratified zone changes linearly.

Figure 14 shows temperature distribution according to the change of exhaust locations when a low airflow rate is used; by the change of exhaust location without changing input location the degree of stratification show a visible change. The results show the effect of increasing exhaust location. When the exhaust location increases the degree of stratification becomes better.

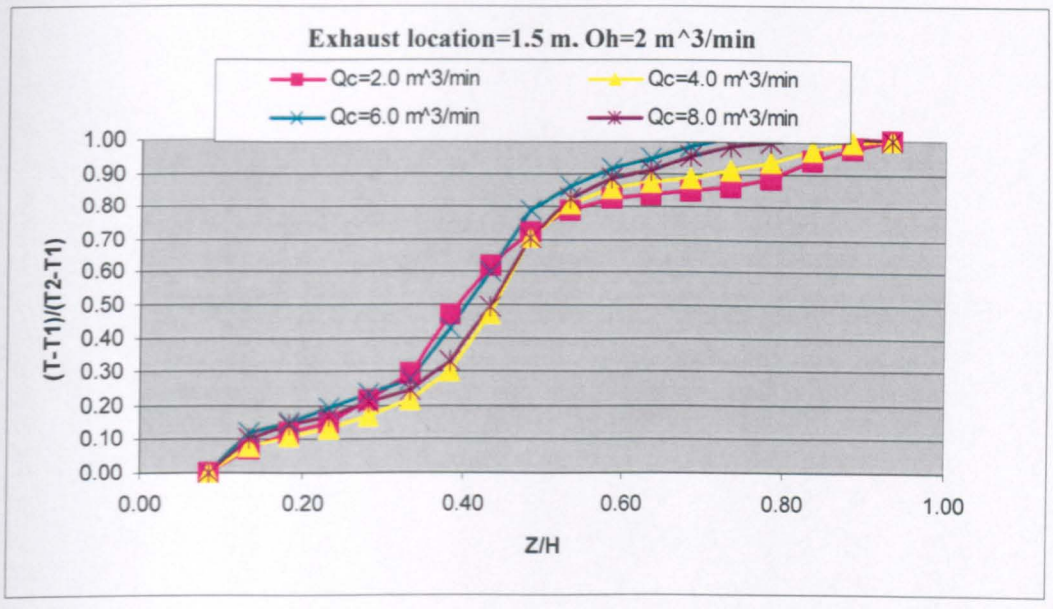

Figure 13: Comparison of dimensionless temperature profile along vertical centreline with dimensionless height across the chamber at a fixed axial location of (3.75,2.8) m and fixed hot air flow rate ($Q_h = 2.0 m^3/min$) for different cold flow rates ($Q_h = 0,2,4,6,8 m^3/min$) in the environmental chamber for 2.0 m input location.

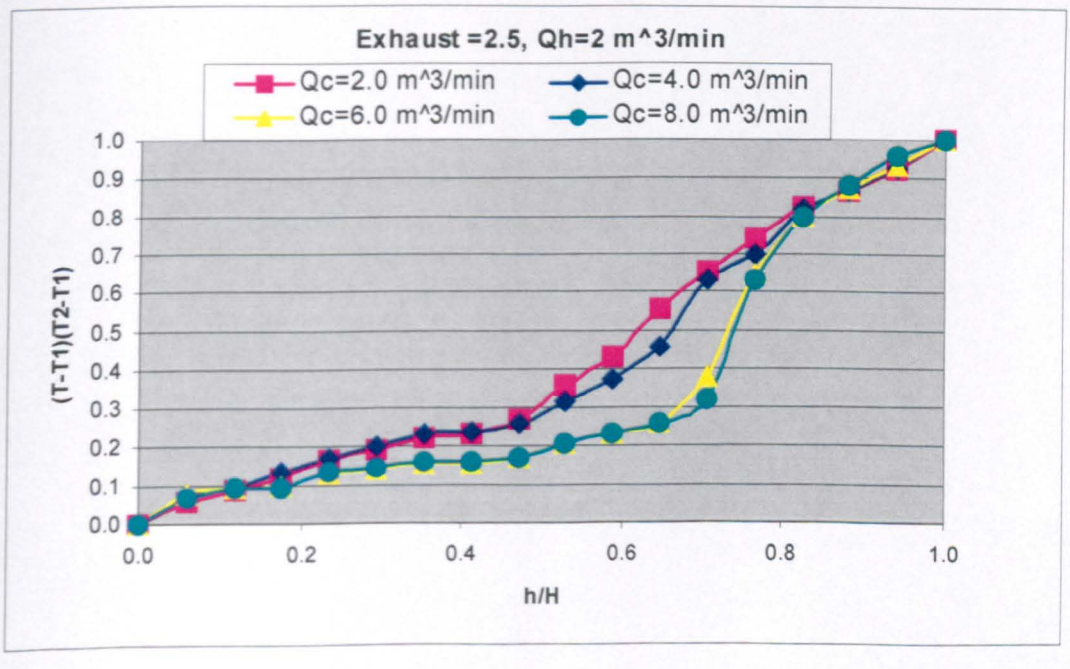

Figure 14: Comparison of dimensionless temperature profile along vertical centreline with dimensionless height across the chamber at a fixed axial location of (3.75,2.8) m and fixed hot air flow rate ($Q_h = 2.0 m^3/min$) for different cold flow rates ($Q_h = 0,2,4,6,8 m^3/min$) in the environmental chamber for 2.0 m input location.

Smoke Visualization of exhaust locations

smoke visulization was also used to evalute the stratified flow characteristics with variable exhaust locations. The results of temperature profiles and smoke visulization show that both models can give the same indications for the flow characterstics of various values of exhaust locations. The results of smoke visulization were shown in the figures 16 to 21.

In figures 15 and 16, it is seen that when the exhaust height was low, the smoke penetrates and emerges in the stratified layer. There are two reasons for this:

- Firstly, when the stratified layer interface level height is low enough then the smoke will emerge in the stratified layer under the effect of high upward buoyant forces, where smoke is still warm compare with the relatively cool lower zone, cross temperature differences did, however, provide a source of potential energy which drive the smoke to rotate downward.
- Secondly, when the stratified interface level height is low, the entrainment air from the lower zone to the smoke plume will be at minimum, for this case, the smoke velocity will be high enough to reach the maximum height at an elevation above the interface level height. However, if the exhaust is in the upper zone, then the velocity reaches its minimum value at an elevation below the exhaust location as seen in figures 17 and 19.

Figure 18 show a very thin interface layer between the upper hot and lower cold zones. As shown in the figure, the temperature gradient is very high in the stratified layer, due to the high mixing in the upper hot and lower cold zones, whiles the mixing betwween these layers is very limitted.

A combined effect of high exhaust location and high cold airflow rate is shown in figure 20. The results show how they reinforce each other and the flow is stratified near the ceiling. It is interesting to note that when the location of the source gets higher, a larger temperature gradient is created (compared to lower source location) in the region above the heat source.

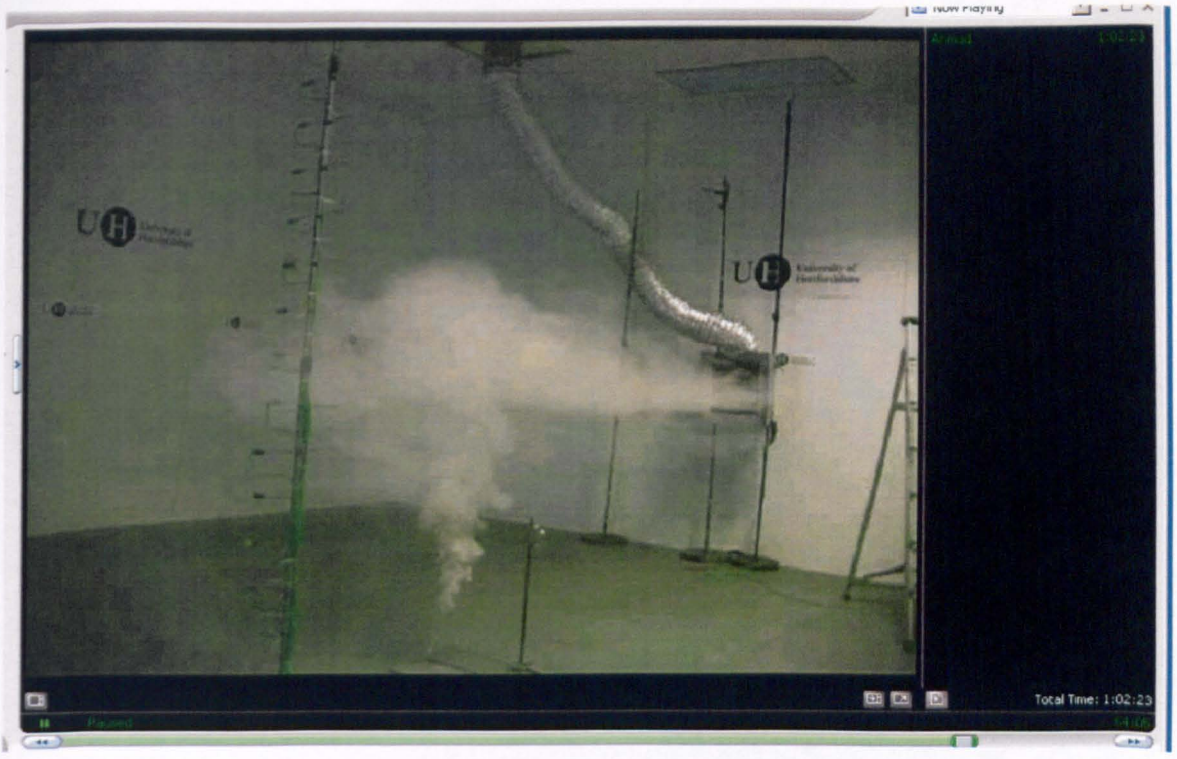

Figure 15: A shadowgraph image showing stratification induced by smoke visualization, at steady state, for $H_h = 2.0\text{m}$, $H_{ext} = 1.0m$, $Q_h = 1.0m^3/\text{min}$ **and** $Q_c = 6.0m^3/\text{min}$.

Figure 16: A shadowgraph image showing stratification induced by smoke visualization, at steady state, for $H_h = 2.0\text{m}$, $H_{ext} = 1.0m$, $Q_h = 1.0m^3/\text{min}$ **and** $Q_c = 6.0m^3/\text{min}$.

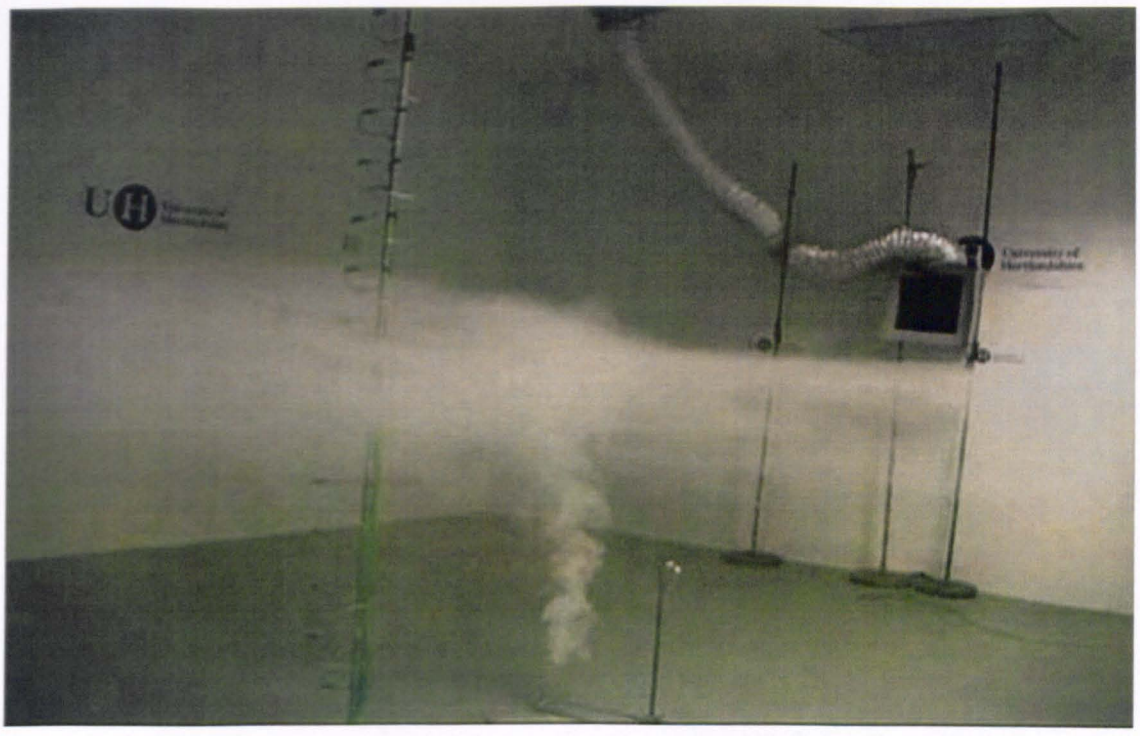

Figure 17: A shadowgraph image showing stratification induced by smoke visualization, at steady state, for $H_h = 2.0m$, $H_{ext} = 1.5m$, $Q_h = 2.0m^3/min$ and $Q_c = 8.0m^3/min$.

Figure 18: A shadowgraph image showing stratification induced by smoke visualization, at steady state, for $H_h = 2.0\,m$, $H_{ext} = 2.0\,m$, $Q_h = 1.0\,m^3/min$ and $Q_c = 8.0\,m^3/min$.

Figure 19: A shadowgraph image showing stratification induced by smoke visualization, at steady state, for $H_h = 2.0\,m$, $H_{ext} = 2.0\,m$, $Q_h = 1.0\,m^3/\min$ and $Q_c = 8.0\,m^3/\min$.

Figure 20: A shadowgraph image showing stratification induced by smoke visualization, at steady state, for $H_h = 2.0\,m$, $H_{ext} = 2.0\,m$, $Q_h = 1.0\,m^3/\min$ and $Q_c = 8.0\,m^3/\min$.

Conclusions

The effects of both input and exhaust locations on the stratified flow characteristics were investigated. When a location of input location is higher, the buoyancy forces is increased with a sufficient amount to stratify the flow, whiles for the decreasing of input location, the interface level height is decreasing downward to reach the ground, yielding a mixed flow in both zones. The temperature distribution in the upper zone is somewhat independent of the location of input location unlike the lower zone. The results also show that the level of stratification is affected by the exhaust location,

From the results it can be seen that the input and exhaust locations reinforce each other, while the hot and cold airflow rates don't always reinforce each other, but in fact be against each other.

It can be concluded that the stratified flow characteristics are dependent upon the flow parameters and the geometry of the space (opening locations). The designing of opening heights can be used for controlling the flow characteristics such as mixing or maintaining the flow of the stratified layer.

References

Calay R.K., Borresen B.A. and Holdø E., Selective ventilation in large enclosures, Energy and Buildings, Volume 32, Issue 3, September 2000, Pages 281-289.

Ayad, S. S. Computational study of natural ventilation. J. Wind Eng. Ind. Aero. Vol.82 1999, pp 49-68.

Hunt G.R. and Linden P.F., The fluid mechanics of natural ventilation—displacement ventilation by buoyancy-driven flows assisted by wind, Building and Environment, Volume 34, Issue 6, November 1999, Pages 707-720.

Wander, J. D., Cost-effective ventilation for large spray-painting 0perations, Metal Finishing, Volume 100, Issue 3, March 2002, Pages 23-24.

Mundt E., Contamination distribution in displacement ventilation—influence of disturbances, Building and Environment, Volume 29, Issue 3, July 1994, Pages 311-317.

Mundt El., Displacement Ventilation Systems- Convection Flow and Temperature Gradients, Building and Environment, Volume 30, Issue 1, 1995, Pages 129-133.

Mundt E., Non-buoyant pollutant sources and particles in displacement ventilation, Building and Environment, Volume 36, Issue 7, August 2001, Pages 829-836.

Hagström K., Sandberg E., Koskela H. and Hautalampi T., Classification for the room air conditioning strategies, Building and Environment, Volume 35, Issue 8, 1 November 2000, Pages 699-707.

Wood A.W., Caulfield C.P., Phillips J.C., Blocked Natural Ventilation: The effect of a Source mass flux, J. Fluid Mech., 2003, Volume 495, pp 119 – 133.

Holford J.M. and Hunt G.R., Fundamental atrium design for natural ventilation, Building and Environment, Volume 38, Issue 3, March 2003, Pages 409-426.

Linden P.F., Lane-Serff G.F. and, Smeed D.A., Emptying filling boxes: the fluid mechanics of natural ventilation. Journal of Fluid Mechanics, Vol. 212, 1990, pp 309–335.

Teitel M. and Tanny J., Natural ventilation of greenhouses: experiments and model[*1], Agricultural and Forest Meteorology, Volume 96, Issues 1-3, 30 August 1999, Pages 59-70.

Andersen K.T., Theory for natural ventilation by thermal buoyancy in one zone with uniform temperature, Building and Environment, Volume 38, Issue 11, November 2003, Pages 1281-1289.

Li Y., Delsante A. and Symons J., Prediction of natural ventilation in buildings with large openings, Building and Environment, Volume 35, Issue 3, April 2000, Pages 191-206.

Fitzgerald Sh.D. and Woods A.W., Natural ventilation of a room with vents at multiple levels, Building and Environment, Volume 39, Issue 5, May 2004, Pages 505-521.

Li Y. and Delsante A., Natural ventilation induced by combined wind and thermal forces[*1], Building and Environment, Volume 36, Issue 1, 1 January 2001, Pages 59-71.

Chen Z.D. and Li Y., Buoyancy-driven displacement natural ventilation in a single-zone building with three-level openings, Building and Environment, Volume 37, Issue 3, March 2002, Pages 295-303.

Xing H. and Awbi H.B., Measurement and calculation of the neutral height in a room with displacement ventilation, Building and Environment, Volume 37, Issue 10, October 2002, pp 961-967.

The effect of input supply location and flow rate on stratified flow characteristics inside enclosures

A. S. Awad[1], R. K. Calay[1], A. E. Holdo[1] and O. O. Badran[2]

[1] Department of Aerospace, Automotive and Design Engineering, Faculty of Engineering and Information Science, University of Hertfordshire, Hatfield Campus, UK.

[2] Department of Mechanical Engineering, Faculty of Engineering Technology, Al-Balqa` Applied University, P.O.Box 330116, Amman 11134-Jordan

Abstract

This paper presents an experimental investigation of flow scenarios that lead to stratification within the ventilated enclosures. The effect of supply terminal at various airflow rates on the flow characteristics is experimentally investigated. It has been found that relative influence of inertia and buoyancy forces resolves the stratified flow characteristics. The stratification interface level height and the ventilation flow rates are two main factors in the design of natural ventilation system. The results can be used to obtain a good estimation of the effectiveness of a ventilation system at design stage.

Keywords: Stratified flow, Natural ventilation, Temperature distribution

Introduction

Thermal stratification is often dominant feature of the flow characteristics within ventilated buildings. There may be many heat sources such as occupants and equipment within a room that acts like heat sources and thermal plume develop around them resulting into a vertical temperature gradient. These sources may develop pure buoyancy driven plumes or mixed convection jets as in the supply of hot air in mechanical heating systems. Generally such jets or plumes propagate entraining air from ambient to a height where the temperature within the jets becomes equal to the ambient temperature. At this height flow becomes stratified and there may be a zone above or below the stratified zone where flow is mixed i.e. the temperature profile is uniform.

It has been shown that the flow region is usually divided into zones characterised by temperature gradient. The temperature gradient within the enclosure is influenced by ventilation flow rate and not so much by the position of the heat sources. Thus contaminant removal effectiveness, in displacement ventilation, is influenced by the ventilation flow rate and also sensitive to the level of the source and its position [1, 2]. The vertical position of the interface is also related to the ratio of the upper and lower vent areas depending on the nature of the heat source as shown by Fitzgerald and Woods [3].

For maintaining air quality and thermal comfort any ventilation system must ensure that (1) the interface between the thermally stratified zone and clear zone is adequately high to keep the working zone at a desirable temperature and clear of any pollutants and (2) the thickness of the stratified zones are

large enough to contain all the pollutants within. Therefore the understanding of the mechanisms of the flow patterns leading to stratification is particularly important for displacement ventilation systems and naturally ventilated buildings.

Various experiments have been reported on the study of the flow characteristics for displacement and natural ventilation and information is available on plume development due to single and multiple heat sources and the development of zones within confined spaces [5, 6, and 7]. Most experiments by Linden et al were performed using scale models and salt-bath technique [5]. However, it is not always possible to maintain similarity for both momentum and heat transfer in the model due to differences in the properties of air and water. The current experimental study investigates the flow characteristics within enclosures due to the temperature and momentum differential across the enclosure. In particular the focus is on studying the effect of positioning of the inlet and outlets and the flow rates on the vertical temperature profiles in order to evaluate the characteristics of stratification namely height of the interface, the thickness and the stability of stratified layers.

Experimental setup:

All tests were conducted in the environmental chamber at the University of Hertfordshire (Figure1). The test chamber (enclosed by another room) was 7.5m long, 3.6m wide and 3.0m in height. The walls floor and ceiling were well insulated by polyurethane foam. During the tests the temperature in outer space was also maintained close to the inside temperature to minimise the heat transfer from the test room to the surroundings.

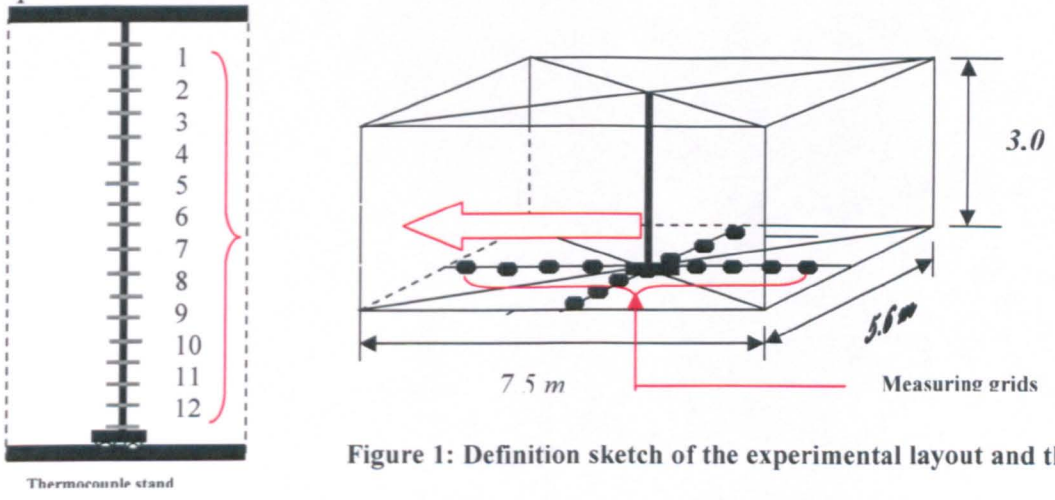

Figure 1: Definition sketch of the experimental layout and the

The inflow parameters were controlled by the environmental control systems. The air treatment plant consisting of heating batteries and a cooling unit, can supply airflow up to 14m^3/min. The system can supply air at temperatures ranging from –40°C to +50°C. The supply and extract locations can be positioned at any position within the room. The vertical temperature measurements within the chamber were made using a vertical array of eighteen K-type thermocouples ~15cm apart as shown in Figure 1. Supply and extract flow rates and velocities were also monitored using a rotating vane anemometer was used to measure airflow rates at the supply inlets. The accuracy of the velocity measurements was ±2% for the readings from 5-30 m/s, and ±0.1m/s for the readings between 0.25-4.99 m/s.

Experimental Procedure

Preliminary experiments were performed by adjusting the supply air flow rates and temperatures to set up zones of stratified

flow within the enclosures. The input location for cold and hot air supply was at different heights. The hot and cold air was supplied into the chamber to create a temperature differential across the height of the enclosure so that stratified flow is established. Initially cold air was entered at the bottom of the environmental chamber and the hot air was near the top of the chamber. Flow visualisation was done using an oil-based smoke machine in order to study flow characteristics identifying the location of the interface and stratification layer thickness. To study the characteristics of the stratification of the flow vertical temperature measurements were taken at the centre of the environmental chamber, where walls would not have any significant effect on the measurements. Measurements were also made at other locations in the horizontal plane in the flow direction (x-axis) and across the flow (z-axis) to study the temperature variation within the wider space and to estimate the influence of the momentum source on the interface height. The experiments studied the effect of the location and flow rate of in flow of hot air and cold air on the stratified flow characteristics. The air inflow rate was varied from (1-5m^3/min). The tests allowed us to study the effect of both hot and cold air in flow rates and locations of the supply ports on the stratified flow.

Results and Discussion

Flow visualization

The flow visualisation using smoke provides the qualitative information of the flow characteristics within the room. Figure 2 shows a typical photograph of the three flow zones.

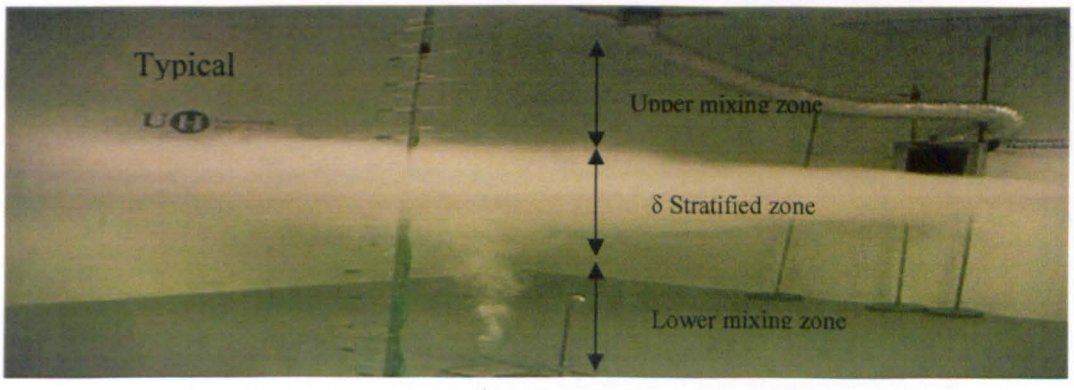

Figure 2 Typical visualisation of flow patterns showing three distinct zones

Smoke penetrates the lower mixed zone and spreads horizontally at certain height and stay within this region to form a layer of certain thickness where the flow direction is only in the horizontal plane. In this case flow is driven by the extract and moves in the direction of the exhaust opening. The interface between the stratified and mixed zones is also clearly visible. The thickness of the stratified layers and the location of the interface depend upon flow parameters. Generally there is always an increase in temperature with the height and flow stratifies from the floor to the ceiling without zone establishment. However, when designing displacement ventilation installation it is important that there is stable stratified zone located above the working zone. Thus vertical temperature gradients are presented to study the conditions that lead flow to form into distinct zones. From these the interface location, stratified layer thickness and degree of stratification can be estimated. Temperature profiles are plotted in terms of the dimensionless temperature $(T-T_c)/(T_h-T_c)$ along a vertical height with

T_h and T_c being respectively the temperatures at the ceiling and the floor of the chamber and versus dimensionless height z/H. Figures 3a and 3b show the non-dimensional vertical temperature variation with respect to the non-dimensional height for two different cases. The hot air input location is fixed at 1.5m for both cases. The flow is divided into three zones (Figure 3a), whereas there are only two flow regimes as shown in the Figure 3b. Flow is stratified starting from the floor to some height (z/H~0.2) and then temperature gradient becomes smoother in the upper region. In this case the hot air flow rate was increased from $2m^3$/min to $3m^3$/min, which not only resulted in higher momentum but there was slight increase in the heat input into the enclosure. Initial momentum is increased which resulted in better heat transfer due to mixing and the higher temperatures are extended further down towards the floor. The stable stratified layers are also pushed towards the floor. Although the flow parameters were estimated using the overall dimensions of the enclosure in order to investigate the combined effect of different mechanisms within the room, the change in parameters (Re) is due to change in the hot-air supply, thereby the change in the flow characteristics is more apparent in the upper region which is more affected by these changes. Figure 4 shows the vertical temperature profiles for a changed position of the hot air supply for the same range of flow parameters as in Figure 3a. Despite a shift from 1.5m to 2m the temperature profiles are similar and the flow region is divided into three zones. It is obvious from the figures (Figure 3a and Figure 4) that for the same flow parameters by changing the location of hot air supply from 1.5 m to 2.0 m there is no change in the thickness of the stratified layer. However there is a shift in the location of the interface which depends linearly on the shift in the vertical location of the hot supply terminal. In both cases flow is divided into three zones; two mixed zones divided by a clear stably stratified layers. The temperature profile also varies from a mild gradient in mixed zone to a sharp gradient within the stratified layers. The Richardson number (Ri) is large enough for flow to be stratified. However, as the input location shifts upward the interface also moves upwards towards the ceiling of the chamber. When the input height is at 1.5m the lower zone also show some stratification as the local Ri number is approximately 0.15. The thickness of stably stratified region (for local Ri >0.25) is similar in both cases. The effect of buoyancy is more significant than the momentum forces in this case. The overall effect of various mechanisms that influence the flow characteristics within the enclosures are defined by Re and Ri. Figures 5 and 6 show the dimensionless temperature profiles for various values of global flow parameters controlled by the flow rates of cold and hot air. For both cases shown in Figure 5, Ri is of the same order and the profile shows stable stratification and the interface forms. However, due to the difference in the momentum forces i.e. Re number, the location of interface is not the same. For a higher Re number which was achieved by increasing the momentum of air supply at the floor level, the interface is shifted towards the floor and is below the exhaust level. For weak momentum (Re=9700) the interface is at the exhaust location. Increase in momentum also results in decrease in global temperature difference. The flow is stratified right from the floor level to the exhaust location for both cases shown in Figure 6. The location of interface is below the exhaust location for both cases but very different to on another. As shown in the temperature distribution i.e. the position of the interface and the level of stratification is both affected by the momentum and buoyancy forces.

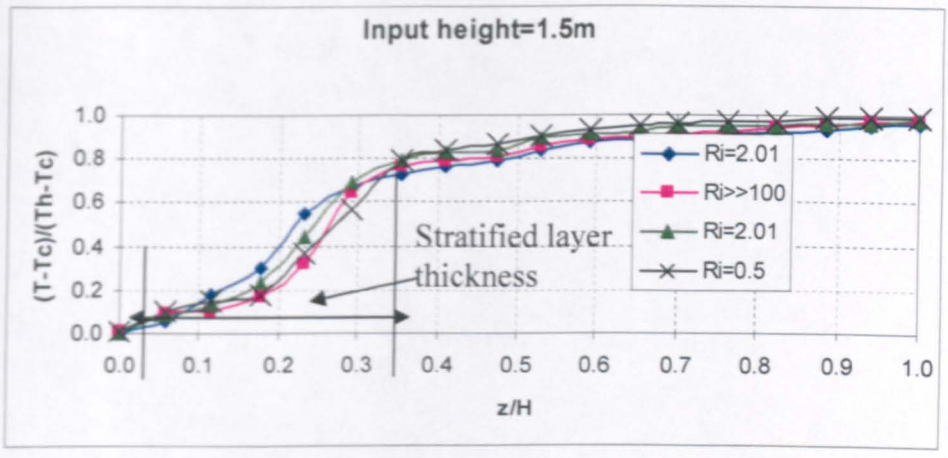

Figure 3a Vertical temperature profile at the mid plane (Re: 9710-19430)

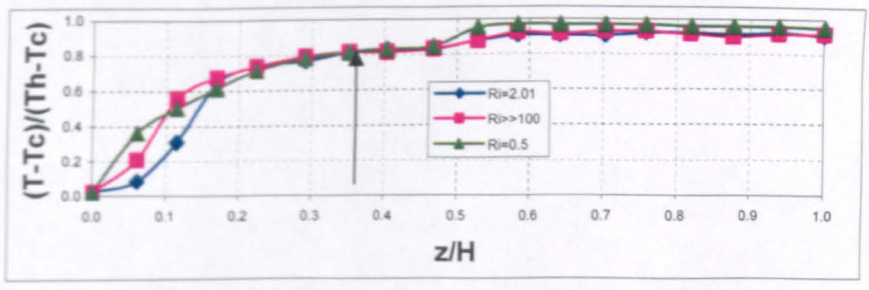

Figure 3b Vertical temperature profile at the mid plane (Re varies from ~1300-25000)

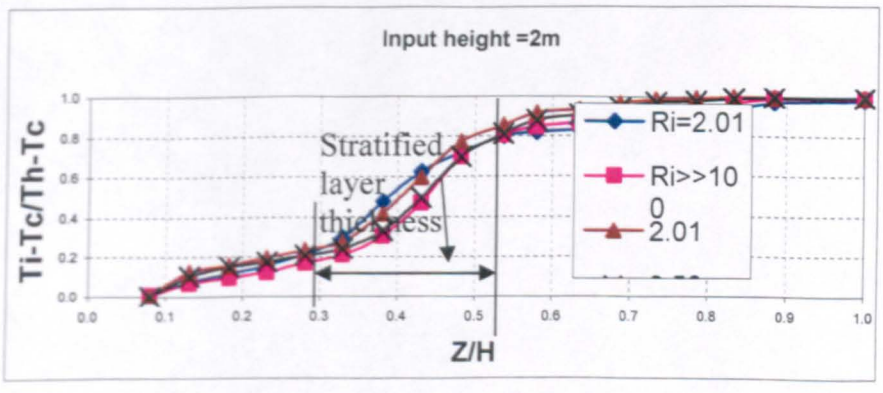

Figure 4 Vertical temperature profile at the mid plane (Re varies from 9710-19430)

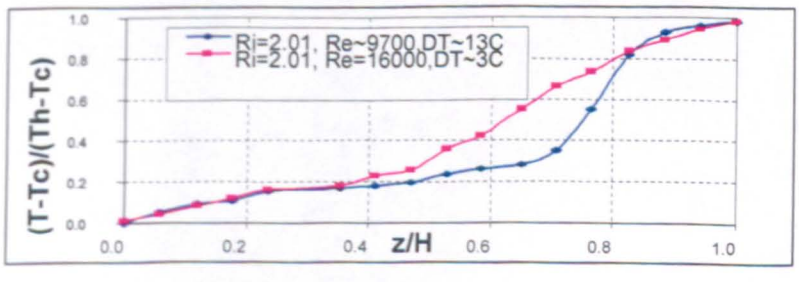

Figure 5 Vertical temperature profiles at the mid plane for different flow rates that yield same degree of stratification (same Ri) but interface level is different due to different Re number

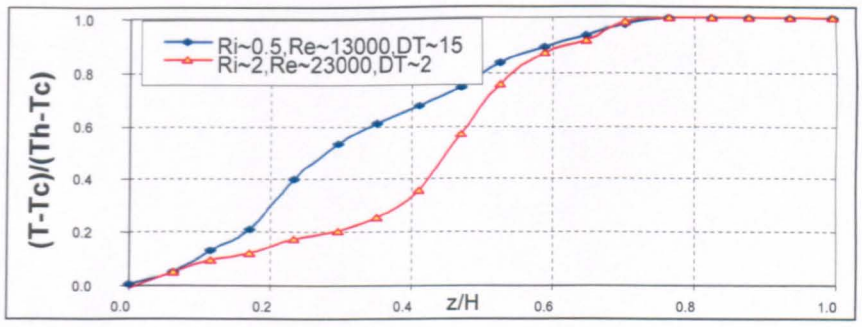

Figure 6 Vertical temperature profiles at the mid plane for different flow rates and heat input i.e. Re and Ri both are different

Conclusions

The effects of input location on the stratified flow characteristics were investigated. When a location of hot air input terminal is high towards the ceiling, supply is in terms negatively buoyant jet. The ratio of momentum and buoyancy forces is such that sufficient flow stratifies across the height of the room and the flow region shows a clear stratified zone with an interface, while for a low level input location, the interface level moves downward yielding unstable stratified flow leading to mixed flow in both zones. The temperature distribution in the upper zone is somewhat independent of the location of input location unlike the lower zone. Although air supply at high momentum tends to de-stratify the flow, leading to vertical uniform temperature profiles and high temperature differences lead to stratification of the flow, it is the relative influence of inertial and buoyancy forces that determine the position of the interface and degree of stratification.

References

[1] Awad A. S., Badran, O.O., Holdo, A.E. and Calay R.K., Experimental study of stratified flow in a built environment. Proceeding of World Renewable Energy and Environment Conference (WREEC2006), Tripoli-Libya.

[2] Mundt E., Non-buoyant pollutant sources and particles in displacement ventilation, Building and Environment, Volume 36, Issue 7, August 2001, Pages 829-836.

[3] Fitzgerald Sh.D. and Woods A.W., Natural ventilation of a room with vents at multiple levels, Building and Environment, Volume 39, Issue 5, May 2004, Pages 505-521.

[4] Calay R.K., Borresen B.A. and Holdø E., Selective ventilation in large enclosures, Energy and Buildings, Volume 32, Issue 3, September 2000, Pages 281-289.

[5] Linden P.F., Lane-Serff G.F. and, Smeed D.A., Emptying filling boxes: the fluid mechanics of natural ventilation. Journal of Fluid Mechanics, Vol. 212, 1990, pp 309–335.

[6] Mundt E., Displacement Ventilation Systems- Convection Flow and Temperature Gradients, Building and Environment, Volume 30, Issue 1, 1995, Pages 129-133.

[7] Hunt G.R. and Linden P.F., The fluid mechanics of natural ventilation—displacement ventilation by buoyancy-driven flows assisted by wind, Building and Environment, Volume 34, Issue 6, November 1999, Pages 707-720.